TG

FOURTEENTH TRANSDUCER WORKSHOP

16-18 JUNE 1987

COLORADO SPRINGS, COLORADO

TELEMETRY GROUP

RANGE COMMANDERS COUNCIL

WHITE SANDS MISSILE RANGE
KWAJALEIN ATOLL
YUMA PROVING GROUND

PACIFIC MISSILE TEST CENTER
NAVAL WEAPONS CENTER
ATLANTIC FLEET WEAPONS TRAINING FACILITY
NAVAL AIR TEST CENTER

EASTERN SPACE AND MISSILE CENTER
ARMAMENT DIVISION
WESTERN SPACE AND MISSILE CENTER
AIR FORCE SATELLITE CONTROL FACILITY
AIR FORCE FLIGHT TEST CENTER
AIR FORCE TACTICAL FIGHTER WEAPONS CENTER

FOURTEENTH TRANSDUCER WORKSHOP

16-18 JUNE 1987

COLORADO SPRINGS, COLORADO

TRANSDUCER COMMITTEE
TELEMETRY GROUP
RANGE COMMANDERS COUNCIL

Published and Distributed by

Secretariat
Range Commanders Council
White Sands Missile Range,
New Mexico 88002

DISCLAIMER

This document has been published for information purposes only. The material contained here does not necessarily represent the position or conclusions of the Range Commanders Council (RCC).

TABLE OF CONTENTS

TELEMETRY GROUP COMMITTEES

Chairman, Phillip D. Sharp (WSMR)
Vice Chairman, J. W. Rymer

Data Multiplex
RF Systems
Recorder/Reproducer
Vehicular Instrumentation/Transducer

MEMBERS OF THE VEHICULAR INSTRUMENTATION/TRANSDUCER COMMITTEE

LeRoy Bates
NSWSES - Code 4250
Port Hueneme, CA 93043

Richard Hasbrouck
Lawrence Livermore National Laboratories
P.O. Box 808, L154
Livermore, CA 94550

William A. Xavier
EG&E Energy Measurements, Inc.
P.O. Box 9051
Pleasanton, CA 94566

Lawrence Sires
NWC - Code 6213
China Lake, CA 93555

Raymond Faulstich
NATC
Range Directorate (RD42)
Patuxent River, MD 20670-5304

Larry Rollingson
NWC - Code 6421
China Lake, CA 93555-6001

Steve Kuehn
Sandia National Laboratories
P.O. Box 5800, Div. 7545
Albuquerque, NM 87185

John Ach
AFWAL/FIBGA
Wright-Patterson AFB, OH 45433

Dennis Henry
Physical Science Laboratory
New Mexico State University
P.O. Box 3548
Las Cruces, NM 88003

Richard Krizan
ESMC/RSL
Patrick AFB, FL 32925-5532

TRANSDUCER COMMITTEE OBJECTIVES

This committee apprises the Telemetry Group (TG) of significant progress in the field of telemetry transducers; maintains any necessary liaison between the TG and the National Bureau of Standards and their transducers' program or any other related telemetry transducer efforts; coordinates TG activities with other professional technical groups; collects and passes on information on techniques of measurement, evaluation, reliability, calibration, reporting and manufacturing; and recommends uniform practices for calibration, testing and evaluation of telemetry transducers.

TRANSDUCER WORKSHOP SUMMARY

Workshop Number	Date	Host	General Chairman	Number Attendees	RCC TG Transducer Chairman
1	March 1960	Albuquerque, NM			
2	25-26 July 1961	Holloman AFB Alamogordo, NM	W. M. Sanders Holloman AFB, NM	46	Paul Polishuk Wright-Patterson Dayton, OH
3	21-23 June 1962	NBS Washington, D.C.	Arnold Wexler NBS Washington, D.C.	106	Paul Polishuk Wright-Patterson Dayton, OH
4	18-19 June 1964	Wright-Patterson Dayton, OH	Jack Lynch NATC Patuxent River, MD	53	Jack Lynch NATC Patuxent River, MD
5	3-4 October 1967	NBS Gaithersburg, MD	Loyt L. Lathrop Sandia Labs Albuquerque, NM	106	Loyt L. Lathrop Sandia Labs Albuquerque, NM
6	22-24 October 1969	Langley Research Ctr. NASA Hampton, VA	Paul Lederer NBS Washington, D.C.	49	Loyt L. Lathrop Sandia Labs Albuquerque, NM
7	4-6 April 1972	Sandia Labs Albuquerque, NM	W. G. James AEFDL Wright-Patterson Dayton, OH	111	Pat Walter Sandia Labs First Manufacturers' Panel Boo-Boos
8	22-24 April 1975	Wright-Patterson Dayton, OH	Pierre F. Fuselier Lawrence Livermore Labs Livermore, CA	74	Pat Walter Sandia Labs

Workshop Number	Date	Host	General Chairman	Number Attendees	RCC TG Transducer Chairman
9	26-28 April 1977	Fort Walton Beach Eglin AFB, FL	Kenny Cox NWC China Lake, CA	100	William Anderson Patuxent River, MD
10	12-14 June 1979	Colorado Springs Colorado North American Air Defense Command	Richard Hasbrouck Lawrence Livermore Labs Livermore, CA	106	William Anderson Patuxent River, MD
11	2-4 June 1981	Seattle, WA, Air Force Plant Representative Office, Det. 9	LeRoy Bates NSWSES Port Hueneme, CA	95	William Anderson Patuxent River, MD
12	7-9 June 1983	Melbourne, FL Patrick AFB, FL	Kenneth D. Cox NWC China Lake, CA		William Anderson Patuxent River, MD
13	4-6 June 1985	Monterey, CA	Richard Krizan Patrick AFB, FL		LeRoy Bates NSWSES Port Hueneme, CA
14	16-18 June 1987	Colorado Springs, CO Air Force Academy	Stephen F. Kuehn Sandia National Labs Albuquerque, NM	118	LeRoy Bates NSWSES Port Hueneme, CA

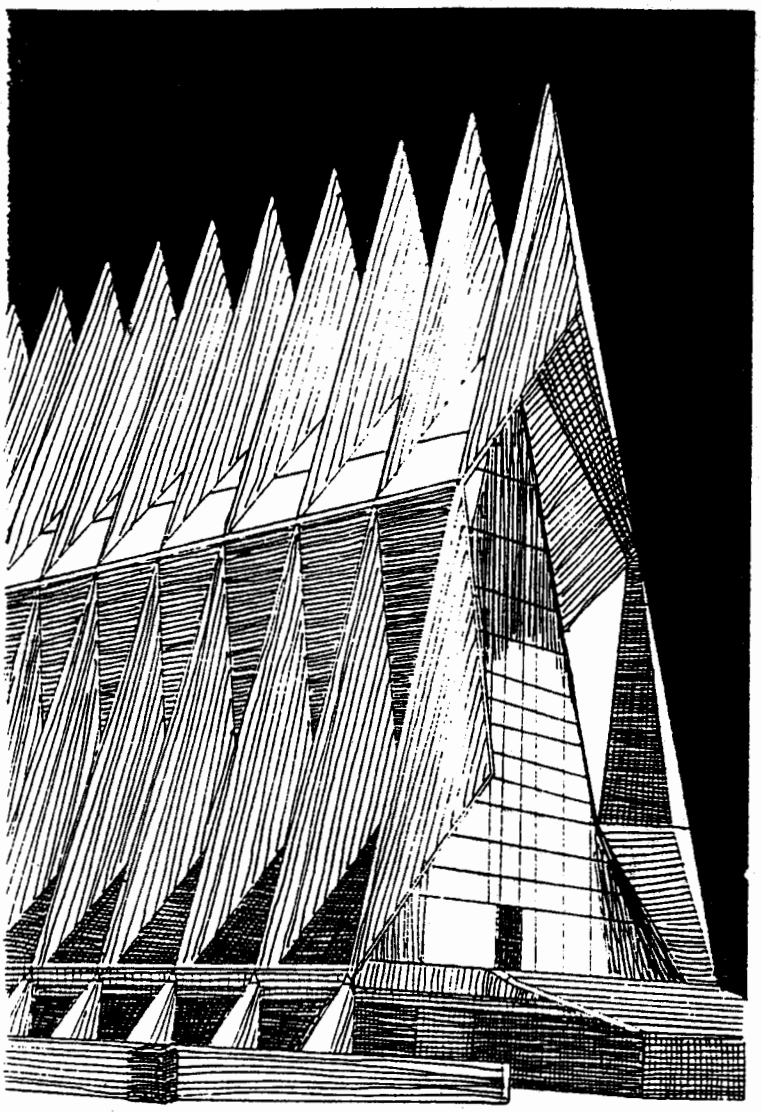

FOURTEENTH TRANSDUCER WORKSHOP

Colorado Springs, Colorado

June 16 - 18, 1987

Sponsored by
Vehicular Instrumentation/
Transducer Committee of
Range Commanders Council
Telemetry Group

Participating Society

ISA Test Measurement Division

DEFINITION OF THE TRANSDUCER WORKSHOP

History:

The Workshop is sponsored by the Vehicular Instrumentation/Transducer Committee, Telemetry Group of the Range Commanders Council. This committee is tasked to provide IRIG documents for transducer applications. The thirteen previous workshops, beginning in 1960, were held at two year intervals at, or near various U. S. Government installations around the country.

Attendees:

Attendees are working-level people who must solve real-life hardware problems and are strongly oriented to the practical approach. Their field is making measurements of physical parameters using transducers. Test and project people who attend will benefit from exposure to the true complexity of transducer evaluation, selection , and application.

Subjects:

Practical problems involving transducers, signal conditioners, and readout devices will be considered as separate components and in systems. Engineering tests, laboratory calibrations, transducer developments and evaluations represent potential applications of the ideas presented. Measurands include force, pressure, flow, acceleration, velocity, displacement, temperature and others.

Emphasis:

1. A practical approach to the solution of measurement problems.
2. Strong focus on transducers and related instrumentation used in measurements engineering.
3. High ratio of discussion to presentation of papers.
4. Open discussion and problem solving through the sharing of knowledge and experience. Session chairmen will encourage questions from the audience after each presentation.

Goals:

To bring together those people who use transducers to identify problems and suggest some solutions; to identify areas of common interest; and to provide a communication channel within the community of transducer users. Some examples are:

1. Improve the coordination of information regarding transducer standards, test techniques, evaluations, and application practices among the national test ranges, range users, range contractors, other transducer users, and transducer manufacturers.
2. Encourage the establishment of special sessions so that attendees with measurement problems in specific areas can form subgroups and remain to discuss these problems after the workshop concludes.
3. Solicit suggestions and comments on past, present, and future Vehicular Instrumentation/Transducer Committee efforts.

General Chairman:
Stephen F. Kuehn
Sandia National Laboratories
Organization 7544
Albuquerque, New Mexico 87185-5800
(505) 844-5195

PROGRAM

MONDAY, JUNE 15, 1987

2000 Social Hour, at the Clarion Hotel, courtesy of the Vehicular Instrumentation/Transducer Committee
All attendees welcome

TUESDAY, JUNE 16, 1987

0730 Registration
0800 STEPHEN F. KUEHN, General Chairman
Fourteenth Transducer Workshop
Welcome: USAF Academy Representative
Introductions: LEROY BATES, Chairman Vehicular Instrumentation/ Transducer Committee, RCC/TG
0900 **Session 1: Performance Evaluation**
Chairman: WILLIAM A. XAVIER, EG&G/LLNL
Paper Presentations (15 - 20 minutes each):
- **"A Self Monitoring and Reporting Transducer"** JOHN W. GIERER and ROBERT L. GRANT, McDonnell-Douglas
- **"The Development, Performance & Application of a New Ruggedized Mass Air Flow Transducer"** THOMAS C. RAMEY, Kurz Instruments, Inc.
- **"Self-Check Development for Lithium Niobate Explosive Monitors"** STEPHEN F. KUEHN, Sandia National Laboratories

1015 **BREAK**
1030
- **"Accelerometer Evaluation - Problems & Special Measurements"** TORBEN LICHT, Bruel & Kjaer Instruments, Inc.
- **"Recent Developments in Piezoelectric Polymer Stress Gages"** R. P. REED, Sandia National Laboratories
- **"BRL's Approach to Calibration of Ballistic Pressure Transducers"** CHARLES BULLOCK Aberdeen Proving Ground

1200 **LUNCH**
1330 **Session 2: Applications**
Chairman: R. P. REED, Sandia National Laboratories
Paper Presentations (15 - 20 minutes each):
- **"Dynamic Strain Measurement on Track Pins of Tracked Vehicles"** BOBBY E. REED and C. W. BOBBITT, Waterways Experiment Station and Mississippi State University
- **"Solid Propellant Strain Measurement Transducer Considerations"** E. C. FRANCIS, S. PERKINS, and L. VINCENT, United Technologies
- **"Digital Quartz Pressure Transducer"** DONALD W. BUSSE and CURTIS YOUNG, Paroscientific, Inc.

1500 **BREAK**
1515
- **"Intelligent Digital Pressure Transmitter for Aerospace Applications"** DONALD W. BUSSE and RICHARD B. WEARN, Paroscientific, Inc.
- **"Aircraft Ground Speed Measurements using Landing Gear Video"** DAVID BANASZAK, Air Force Wright Aeronautical Laboratories
- **"A Temperature Controlled Pressure Transducer for Measuring Engine Inlet Pressure"** E. N. KOCHMAN, JR. and JOHN HAYER, McDonnell-Douglas and Kulite Semiconcuctor
- **"Ballistics Preasure Transducers and Their Application"** URS ROESLI and JOHN M. KUBLER, Kistler Instrument Corporation

WEDNESDAY, JUNE 17, 1987

0830 **Session 3: Calibration Techniques**
Chairman: WILLIAM D. ANDERSON,
Naval Air Test Center
Paper Presentations (15 - 20 minutes each):

- **"Problems with Frequency Creation in Nonlinear Measurement Systems"**
  PATRICK L. WALTER
  Sandia National Laboratories
- **"An Application of Parameter Estimation Theory in Low Frequency Accelerometer Calibration"**
  B. F. PAYNE and M. R. SERBYN
  National Bureau of Standards
- **"Calibration Anomalies of a Sub-miniature Dynamic Pressure Sensor"**
  MARTHA PIERCE WILLIS, Rocketdyne
- **"Software Design for Compensated Dead-Weight Testing"**
  PAUL A. KLEVGARD,
  Sandia National Laboratories, Livermore

1015 **BREAK**

1030
- **"Low Frequency Performance Verification of Piezoelectric Accelerometers"**
  ERNST SCHONTHAL,
  Bruel & Kjaer Instruments, Inc.
- **"Characterization of Accelerometer Mountings in Shock Environments"**
  V. I. BATEMAN and O. M. SOLOMON, JR.
  Sandia National Laboratories
- **"A Microprocessor Based Digital Pressure Transducer"**
  GORDON E. MILLS, Paine Corporation

1200 **LUNCH**

1330 Tour of Air Force Academy

1830 No-host social hour at hotel

1930 Banquet at hotel

THURSDAY, JUNE 18, 1987

0830 **Session 4: Manufacturer Presentations**
Chairman: LARRY ROLLINGSON,
Naval Weapons Center
Presentations by:

AVL North American, Inc.	John Terrell
DJ Instruments, Inc.	David J. First
Kaman Instrumentation	William T. Zeri

1030 **BREAK**

1045 **SESSION 5: Minipaper Presentations**
(5 to 10 minutes each)
Chairman: PATRICK L. WALTER
Sandia National Laboratories

- **"Improved Techniques for Measurement of Velocities with Piezoelectric Transducer Pins"**
  PAUL V. WHALEN, Eglin AFB
- **"An Inexpensive Millitorr (Gage) Pressure Source"**
  WILLIAM B. LEISHER,
  Sandia National Laboratories
- **"Design and Applications of a Highly Stable Miniature Pressure Transducer"**
  RONALD POFF, Endevco
- **"The 155mm Ballistic Rail Gun Characterization of the Acceleration/ Deceleration Vector"**
  JOHN R. ZIMMERMAN & MICHAEL J. PADUANC
  U. S. Army Armament Research, Development and Engineering Center
- **"Miniature Silicon Temperature Sensor with High Output Voltage, Hi-Reliability and Fast Response"**
  HERBERT CHELNER, Micron Instruments, Inc.
- **"I. R. Temperature Measurement of Metal Parts During Vacuum Coating Process"** C. AVALLE and D. ROACH,
  Lawrence Livermore National Laboratory

1215 **LUNCH**

1330 **Session 6: Data Acquisition**
Chairman: DAVID BANASZAK
Air Force Wright Aeronautical Laboratories
Paper Presentations (15 - 20 minutes each):

- **"Modular Automated Recording System (MARS)"** MICHAEL T. LYNCH and ROBERT TAYLOR, Air Force Wright Aeronautical Lab.
- **"A Full-Motion Compressed Digital TV Link"** JAMES L. RIEGER,
  Naval Weapons Center
- **"STRUCTCEL - A New Instrumentation System"** MICHAEL J. LALLY,
  University of Cincinnati

1500 **BREAK**

1515
- **"Computerized Testing of High-Speed Data Acquisition Systems Downhole"**
  JOE R. COSTANEA, Kaman Sciences Corp.
- **"Semi-Hardened, Non-Multiplexed Digital Data Acquisition System",**
  GORDON B. DEAN, Pacific Instruments, Inc.

- **"Integrating the Lecroy 6880 Waveform Digitizer into an Existing Instrumentation System"** JOHN R. CARREL
  EG&G Energy Measurements
- **"Implementation of Digital Signal Processing Functions in a CAMAC Module"** THOMAS S. POUNDS
  EG&G Energy Measurements

1715 Closing Remarks - Workship Chairman
1730 **WORKSHOP CONCLUDES**

GENERAL INFORMATION

This Fourteenth Transducer Workshop will be held June 16 - 19, 1987 at the Clarion Hotel in Colorado Springs, Colorado. The hosting agency is the United States Air Force Academy.

Registration

The registration consists of two parts: a written "Murphyism" of one page or less and a fee of $60.00.

A "Murphyism" can describe any measurement attempt that went astray with the objective of learning from our errors and keeping our feet on the ground. It should be something generic rather than common human oversight; something from which we can learn. The tone should be anonymous to not embarrass any person, organization , or company. While a "Murphyism" is not a mandatory requirement, submissions are strongly encouraged and the best will be included in the program.

Advance registration is desirable. Please use the enclosed registration form, include a check or money order for $60.00 payable to the Fourteenth Transducer Workshop, and mail to the Workshop Treasurer by May 17, 1987. (Note: Purchase orders are not acceptable.)

The registration fee covers the cost of coffee, tea, soft drinks, doughnuts, an evening banquet, and a tour. A copy of the minutes of the workshop is supplied to all attendees. Late registration will be provided at the Workshop registration desk in the hotel.

Hotel Accommodations

The official hotel for the Workshop is the Clarion Hotel, 2886 S. Circle Drive, Colorado Springs, Colorado, 80906. A fixed block of rooms has been reserved at the special rates indicated on the enclosed hotel registration card. Early hotel reservations are strongly encouraged. Hotel registrations must be received by May 15, 1987.

No formal program will be provided for spouses or guests. However, they will be most welcome at the Social Hour on Monday and the banquet on Wednesday ($20.00 additional per guest for the dinner). Note: Final count for the banquet must be known by 11 am, June 15th.

Tour - Wednesday Afternoon

A three hour tour of the Air Force Academy is planned for Wednesday, June 17, 1987. Please indicate on the registration form if you will be accompanied by guests so that adequate transportation may be provided.

Format and Background

Workshops are just what the name implies: everyone should come prepared to contribute something from his knowledge and experience. In a workshop the attendees become the program in the sense that the extent and enthusiasm of their participation determines the success of the workshop.

Participants will have the opportunity to hear what their colleagues have been doing and how it went: to explore areas of common interest and common problems; to offer ideas and suggestions about what's needed in transducers, techniques, and applications. A few manufacturers, selected to represent a sampling of transduction methods and measurands, have been invited to give presentations.

Additional Information

May be obtained from the General Chairman or,

Proceedings Chairman and Treasurer
LEROY BATES
NSWSES Code 4R13
Port Hueneme, CA 93043
(805) 982-5030
(Autovon) 360-5030

Facilities Chairman
RICHARD T. HASBROUCK
Lawrence Livermore National Laboratory
P. O. Box 808, L-154
Livermore, CA 94550
(415) 422-1256
(FTS) 532-1256

Paper Chairman
JOHN T. ACH
AFWAL/FIBGA
Wright-Patterson AFB, OH 45433
(513) 255-6622
(Autovon) 785-6622

LIST OF ATTENDEES

Lt. Paul V. Whalen
3246 TESTW/TZFT
Eglin AFB, FL 32542

Vern E. Bean
National Bureau of Standards
A56 MET
Garthersburg, MD 20899

James Rieger
Naval Weapons Center
Code 6406
China Lake, CA 93555-6001

Charles F. Grabenstein
Grabenstien Industries, Inc.
50 Maple Street
Bradford, CT 06406

Art Gilbert
Endevco
30700 Rancho Viejo Road
San Juan Capistrano, CA 92675

Gordon B. Dean
Pacific Instrument
215 Mason Circle
Concord, CA 94520

Herbert Chelner
Micron Instruments
4509 Runway Street
Simi Valley, CA 93063

Richard T. Hasbrouck
Lawrence Livermore National Lab.
P.O. Box 808, L-154
Livermore, CA 94550

Vesta I. Batemen
Sandia National Labs.
Organization 7544
Albuquerque, NM 87185-5800

Errol P. Eernisse
Quartztronics/Quartex
1020 Atherton Dr., Bldg C
Salt Lake City, UT 84123

Jim Lally
PCB Piezotronics, Inc.
3425 Walden Avenue
Depew, NY 14043

Ben A. Granath
PCB Piezotronics, Inc.
305 Farm Lane
Aberdeen, MD 21001

Harvey Weiss
Grumman Aircraft Systems
Flight Test Center, M/S F05-07
Calverton, NY 11933

John T. Ach
Air Force Wright Aeronational Lab.
AFWAL/FIBG
Wright-Patterson AFB, OH 45385

Ronald B. Tussing
Naval Surface Weapons Center
White Oak Laboratory
Silver Spring, MD 20910

Paul A Klevgard
Sandia National Labs.
P.O. Box 969
Livermore, CA 94550

Dr. John R. Zimmerman
U.S. Army Armament Research
Development & Engineering Center
SMCAR-AEC-TL
Dover, NJ 07801

Roger P. Noyes
EG&G Energy Measurements, Inc.
P.O. Box 1912, N-28
Las Vegas, NV 89125

Charles H. Forbes
Naval Weapons Center
Code 3354
Ridgecrest, CA 93555

Nick D. Change, Jr.
Dytran Instruments, Inc.
21592 Marilla Street
Chatsworth, CA 91311

Don P. Kramer
Pacific Missile Test Center
Code 1063
Point Mugu, CA 93042

Daniel E. Cook
Proportion-Air, Inc.
P.O. Box 147
McCordsville, IN 46055

Thomas J. Naughton
Dresser Industries
250 East Main Street
Stratford, CT 06497

John Kalinowski
EG&G Energy Measurements, Inc.
P.O. Box 9051
Pleasanton, CA 94566

Dennis Reid
EG&G Energy Measurements, Inc.
5667 Gibralter Drive
P.O. Box 9051
Pleasanton, CA 94566

Ken Pearce
EG&G Energy Measurements, Inc.
5667 Gibralter Drive
P.O. Box 9051
Pleasanton, CA 94566

Charles Simkins
EG&G Energy Measurements, Inc.
5667 Gibralter Drive
P.O. Box 9051
Pleasanton, CA 94566

Melton Hatch
EG&G Energy Measurements, Inc.
5667 Gibralter Drive
P.O. Box 9051
Pleasanton, CA 94566

Donald W. Busse
Paroscientific, Inc.
4500 148th Avenue, NE
Redmond, WA 98052

Willixm A. Xavier
EG&G Energy Measurements, Inc.
P.O. Box 9051
Pleasanton, CA 94566

Lawrence A. Smith
Pacific Missile Test Center
Code 1032
Point Mugu, CA 93042

John E. Terrell
AVL North America, Inc.
Box 36438
Tucson, AZ 85740

Friedrich Ruckenbauer
AVL LIST GmbH
Klieiststrasse 48
A-8020 Graz, Austria

Gerhard Resch
AVL LIST GmbH
Klieiststrasse 48
A-8020 Graz, Austria

Walter R. Kitchen
EG&G Energy Measurements, Inc.
P.O. Box 1912, M/S S-06
Las Vegas, NV 89125

Louis F. Green
EG&G Energy Measurements, Inc.
2621 Losee Road, M/S S-06
North Las Vegas, NV 89030

Thomas S. Pounds
EG&G Energy Measurements, Inc.
P.O. Box 1912, M/S S-06
Las Vegas, NV 89125

Jack R. Carrel
EG&G Energy Measurements, Inc.
P.O. Box 1912, M/S S-05
Las Vegas, NV 89125

David L. Banaszak
U.S. Air Force
AFWAL/FIBG
Wright-Patterson AFB, OH 45433

William M. Shay
Lawrence Livermore National Lab.
P.O. Box 808, L-145
Livermore, CA 94550

Robert M. Howard
NASA/Kennedy
Code DL-ESS-32
Kenneay Space Center, FL 32899

David First
D-J Instruments
18 Republic Road
N. Billerica, MA 01862

Charles R. Belensky
Grumman Aerospace Corp
M/S T01-06
Bethpage, NY 11714

Charles H. Griffin
NASA/Kennedy
Code DL-ESS-31
Kennedy Space Center, FL 32899

Peter Stein
Stein Engineering Service, Inc.
5602 E. Monte Rosa
Phoenix, AZ 85018

Marshall M. Scott
NASA/Kennedy
Code DL-ESS-32
Kennedy Space Center, FL 38299

Lawrence A. Rempert
Allison Gas Turbine
Box 420
Indianapolis, IN 46206

Patrick L. Walter
Sandia National Labs.
Organization 7532
Albuquerque, NM 87185-5800

Martha P. Willis
Rockwell International
6633 Canoga Avenue, M/S SS11
Canaga Park, CA 91303

William Cardwell
General Electric Company
1 Neumann Way, Box 156301
Cincinnati, OH 45211-6301

Robert M. Whittier
Endevco
30700 Rancho Viejo Road
San Juan Capistrano, CA 92675

Ron Poff
Endevco
30700 Rancho Viejo Road
San Juan Capistrano, CA 92675

Alex Karolys
Endevco
30700 Rancho Viejo Road
San Juan Capistrano, CA 92675

W. Ben Ham
Endevco
9004 Menaul, NE, #20
Albuquerque, NM 87112

Robert F. Clark
Endevco
1717 S. State College Blvd.
Suite 180
Anaheim, CA 92806

Barry J. Birnhak
Planning Research Corp.
PRC 5100
Kennedy Space Center, FL 32899

B. F. Payne
National Bureau of Standards
Bldg 233, Room A147
Gaithersburg, MD 20899

Joe R. Costanza
Kaman Sciences Corp.
1500 Garden of the Gods Road
Colorado Springs, CO 80907

Mike Lally
University of Cincinnati
3425 Walden Avenue
Depew, NY 14043

Roberta A. Pizarro
General Dynamics
1675 W. Mission Blvd.
P.O. Box 2507
Pomona. CA 91769-2507

Michael Lynch
Kaman Sciences Corp.
1500 Garden of the Gods Road
Colorado Springs, CO 80907

Glenn Roark
Kaman Sciences Corp.
P.O. Box 7463
Colorado Springs, CO 80933-7463

Eldine L. Cole
Kaman Sciences Corp.
P.O. Box 7463
Colorado Springs, CO 80933-7463

Mark Misplon
General Electric/Neutron Device
P.O. Box 290, MD 001
Largo, FL 34294-2908

Bob J. Temes
Bourns Instruments, Inc.
6135 Magnolia Avenue
Riverside, CA 92506

Edward N. Kachman, Jr.
McDonnell Douglas Corp.
P.O. Box 516
St. Louis, MO 63166

Bill W. Bellow
EG&G Energy Measurements, Inc.
P.O. Box 1912, M/S N-28
Las Vegas, NV 89125

Jerry R. Horner
EG&G Energy Measurements, Inc.
2621 Lossee Road, M/S L-01
North Las Vegas, NV 89030

John W. Gierer
McDonnell Douglas Corp.
P.O. Box 516, Bldg 065
St. Louis, MO 63166

John M. Kubler
Kistler Instrument Corp.
75 John Kubler
Amherst, NY 14120

C. W. Bobbitt
Mississippi State University
Drawer A
Mississippi State, MS 39762

Donald H. Rapp
Hydrologic Instrumentation Fac.
U. S. Geological Survey
Bldg 2111
NSTL, MS 39529

Daniel C. Larson
Structures Instrumentation
P.O. Box 3707, M/S 47-06
Seattle, WA 98124-2207

Charlie A. Leach
Sverdrup Technology, Inc.
M/S 470
Arnold AFS, TN 37389-5000

Edward E. Hartman
Caterpillar, Inc.
100 NE Adams St., TC-L
Peoria, IL 61629

Joseph R. Mallon, Jr.
NovaSensor
1055 Mission Court
Freemont, CA 94539

John Gates
NASA/PRC
2907 N. Indian River Road
Cocoa, FL 32922

T. Stubbs
EG&G Energy Measurements, Inc.
P.O. Box 1912
Las Vegas, NV 89125

Richard Talmadge
UASF, AFWAL/FIBA
Wright-Patterson AFB, OH 45433

William Anderson
Naval Air Test Center
Range Directorate, Code RD40
Patuxent River, MD 20670-5304

Gordon E. Mills
Paine Corporation
2401 South Bayview Street
Seattle, WA 98144

J. R. Miller
U.S. Army
AMXTM-SP
Redstone Arsenal, AL 35808

Richard W. Krizan
ESMC/DVEC
Patrick AFB, FL 32925-5532

Raymond Faulstich
Naval Air Test Center
Range Directorate, RD43
Patuxent River, MD 20670-5304

Paul Urtiew
Lawrence Livermore National Lab.
P.O. Box 808
Livermore, CA 94550

Charles D. Bullock
Ballistic Reasearch Laboratory
DRDAR-BLT
Aberdeen Proving Ground, MD
21005-5066

Dr. R. Maglic
Honeywell, Inc.
1150 E. Cheyenne Mount Blvd.
Colorado Springs, CO 80903

Dieter Eckhart
AVL LIST GmbH
Klieiststrasse 48
A-8020 Garz, Austria

Bill Webb
EG&G Energy Measurement, Inc.
7695 South Hinson
Las Vegas, NV 89118

Steven Perkins
Chemical Systems Division, UTC
P.O. Box 50015
San Jose, CA 95150-0015

Eunwhan Kim
Statham Transducers
2230 Statham Blvd.
Oxnard, CA 93033

Lawrence Sires
Naval Weapons Center
Code 6213
China Lake, CA 93555

Clifford Hawkins
Ruska Instruments
3601 Dunvale
Houston, TX 77063

Torben Licht
Bruel & Kjaer Instruments
18 Naerum Havedgarde
Denmark DK 2850 Naerum

Wiley E. Dunn
Fairchild Weston Systems
P.O. Box 3041
Sarasota, FL 33578

Bill Butler
Colorado State
1600 W. Plum, 24-F
Fort Collins, CO 80521

Wayne A. Charlie
Colorado State University
Dept. Civil Engineering - CSV
Fort Collins, CO 80523

Jack R. Thompson
Naval Weapons Center
Code 3244
China Lake, CA 93555

Robert A. Gould
Naval Weapons Center
Code 3244
China Lake, CA 93555

Bobby E. Reed
U.S. Army Corps Engineers
Waterways Exp Sta.
P.O. Box 6x 631, WES-JD
Vicksburg, MS 39180-0631

Ray P. Reed
Sandia National Labs.
Organization 7116
Albuquerque, NM 87185-5800

Steven Chen
PCB Piezotronics
3425 Walden Avenue
Depew, NY 14043

William P. Russell
Naval Air Test Center
Range Directorate
Patuxent River, MD 20670

Randy De Brine
Grumman Corp.
M/S J06-43
Great River, NY 11739

Charles W. Motte, Jr.
Naval Weapons Center
Code 3145
China Lake, CA 93555-6001

Steven K. Motte
Naval Weapons Center
Code 6421
China Lake, CA 93555

Todd A. Kjormoe
EG&G Energy Measurements, Inc.
P.O. Box 1912
Las Vegas, NV 89125

Tom Ramey
Kurz Instruments
2411 Garden Road
Monterey, CA 93940

Mark A. Santor
Kaman Sciences Corp.
1500 Garden of the Gods Road
Colorado Springs, CO 80970

Billy E. Todd, WX-11
Los Alamos National Labs.
P.O. Box 1663, M/S C931
Los Alamos, NM 87545

Dennis G. Henry
PSL/NMSU
P.O. Box 3548
Las Cruces, NM 88003

LeRoy Bates
NSWSES
Code 4R13
Port Hueneme, CA 93043-5007

Steven Kuehn
Sandia National Labs.
Organization 7544
Albuquerque, NM 87185-5800

Harold G. Quillen (Civ)
U.S. Army
USAA BNSOTBD
Fort Bragg, NC 28307-5000

Larry Rollingson
Naval Weapons Center
Code 3521
China Lake, CA 93555

Dr. Henry F. Bunch
Air Force Flight Test Center
6521 Range Squadron/ENRS
Edwards AFB, CA 93523

William B. Leisher
Sandia National Labs.
Organization 7241
Albuquerque, NM 87185-5800

Frank Benedict
Endevco
3436 Carolina Street
San Pedro, CA 90731

SESSION 1

PERFORMANCE EVALUATION

SELF MONITORING AND REPORTING TRANSDUCERS

John W. Gierer
Robert L. Grant
McDonnell Aircraft Company (MCAIR)
McDonnell Douglas Corporation

ABSTRACT

Flight test instrumentation should provide a reliable tool to acquire information on a new weapons system. It should not interfere with the development and evaluation of the new system. Instrumentation complexity and capability is increasing to keep pace with the more capable weapons systems. Supportability, in the form of mean time to find a problem and complete repairs, is an important feature of the data acquisition system. Built-in-test (BIT) can provide the key to a supportable system. A transducer with BIT will improve system supportability since it alone can provide an end to end assessment of a data channel.

INTRODUCTION

Development of a new aircraft requires a complex and capable instrumentation system. F/A-18A development tests required as many as 700 analog measurands on a single aircraft. The data acquisition system did not have the capacity to accommodate all of the measurands at the same time. Only those needed on the next series of flights were activated. This is not the best situation since faulty instrumentation is not discovered until needed and costly delays are encountered while repairs are made. Failed equipment should be identified during the normal assessment operations so that maintenance action can be taken when the aircraft is being serviced for other purposes.

Future data acquisition systems will include BIT to enchance the supportability of the instrumentation system. The transducer is the ideal device to include a BIT since it can result in an end to end evaluation of a data channel. The Digital Data Acquisition System (DDAS) developed by MCAIR includes a BIT in each of the hardware modules. The combination of BIT in the transducer and the DDAS modules can identify the item that requires service and minimize the trial and error approach to maintaining the aircraft. A Self Monitoring and Reporting Transducer (SMART) is one that can convert physical phenomena to an electrical signal and also provide BIT.

Calibration functions were included in flight test data systems of the 1950's and 1960's. These functions were necessary to allow set up of the strip chart recorders, and they also provided a BIT capability. With the arrival of the magnetic tape recorder and more repeatable sensors and electronic circuitry the need for R-CAL/Z-CAL was diminished. Since a rather large amount of hardware was needed to implement the function the built-in-test was not used by MCAIR during the 1970's.

However during the period we encounter situations where the BIT feature would have been beneficial. We found that transducers that have no output, when the aircraft is at rest, are difficult to verify during a preflight test. In some cases wiring errors resulted in the incorrect identification of test points on the aircraft. The piezoelectric vibration sensors were involved in some of these situations and therefore it was chosen as our first candidate for a BIT capability. A vibration sensor is desired that can provide the following features:

- Identify the transducer by serial number
- Identify the channel gain setting
- Identify the orientation

In 1984 McDonnell Douglas commissioned a study by the University of Cincinnati to investigate vibration sensors that could provide these features. No self identifying transducers were found although a number of self calibrating concepts were discovered in the literature. This study concluded that it is feasible to develop transducers with the desired features. Techniques for fabricating mechanical structures in silicon are being developed so that in the future a single silicon chip could provide both the sensor and electronics (Reference 1,2,3). In the interim period hybrid devices using more than one chip could be developed.

This paper identifies approaches for integrating a transducer BIT into a digital data acquisition system and reviews our experimental activity to incorporate the capability into an FM data acquisition.

THE TRANSDUCER

A flight test instrumentation system usually has access to information that could allow the vibration transducer BIT to be simplified. The identification of accelerometer orientation could be obtained by comparing the accelerometer output to the aircraft attitude during a set of phasing maneuvers performed by the pilot prior to a data run. Figure 1 indicates the result of laboratory tests to check the response of an Endevco 2250 piezoelectric sensor. These tests indicated that a usable output is obtained during a 36 degree per second aircraft roll phasing maneuver. This corresponds to a frequency of 0.1 Hz. A gyro rate table, tipped over on its side, was used to simulate the roll input to the accelerometer. In a real world situation aircraft vibration would be present that could mask the low frequency phasing signal. Signal processing would be needed to recover the phasing signal from the accelerometer output.

The serial number reporting feature can be implemented with integrated circuit chips. An Application Specific Integrated Circuit (ASIC) could contain both memory and electronics and would be included in the transducer case to provide the self identification feature. This is illustrated in the hybrid circuit of Figure 2a. The manufacturers part and serial number would be imbedded in the device memory during manufacture. The user would extract the information by energizing a command line which would cause the transducer to transmit the code over the signal wires. If the amplitude was also an indication of the transducer integrity the BIT data would provide assessment.

Figure 2b illustrates a further simplification of the transducer BIT. The ASIC is deleted and the end to end test of the channel is obtained by applying a known amplitude signal to the test input. This does not provide the desired self identifying feature but it is expected to provide a low cost initial step for a transducer with a BIT capability.

Our investigation indicated that different requirements are encountered for incorporating these features in FM and digital data acquisition systems.

INTEGRATION INTO AN FM ENCODING SYSTEM

The dynamic range of FM encoding system is not sufficient to cover the vibration acceleration range encountered on an aircraft. It is necessary to provide an adjustable gain amplifier ahead of the FM encoder to scale the signal to the range of interest. This factor complicates the orientation check and BIT.

A signal conditioner that provides adjustable gain, orientation evaluation, and BIT was developed in 1986 and is currently being evaluated. In order to capture the phasing maneuver signal it is necessary to switch the channel filter characteristic and the channel gain. A low pass filter is required so that the small amplitude phasing maneuver signal can be detected in the presence of normal aircraft vibrations. It is necessary to return the filter and gain to the correct setting for the actual signal following the phasing manuever.

During the BIT a high level sinusoidal signal is used for the self identifying code. The binary information is transmitted as a series of sinusoidal bursts.

In order to evaluate the gain of the data channel a sinusoidal signal with an amplitude that increases as a series of stair steps was used. One or more of the steps provides an on scale signal so that the channel gain can be identified. A strip chart recorder is used to display the output and allow a manual interpretation of the BIT results.

INTEGRATION INTO A DIGITAL ENCODING SYSTEM

The desired features are more easily incorporated into a digital data acquisition system. If the digital encoder has sufficient dynamic rante it is not necessary to change the channel gain or the filter setup needed for the actual signal. Low pass filtering necessary to extract the phasing maneuver signal can be done in the ground based data processing system. The evaluation of the test signals can be automated to assure consistency of the evaluation and reduce manpower cost. Autorange digital encoding techniques available in the DDAS can provide the dynamic range needed for this task.

To simplify the evaluation of the response code it is necessary to synchronize the transducer BIT with the digital data system. The pulse code modulation (PCM) frame sync can be used for this purpose. A code format is suggested in Figure 3. The signal amplitude is held constant during the PCM frame so that a signal bit of code information is transmitted for each frame. A BIT status word in the PCM frame indicates to the ground processing system that the identification and test of the transducer is in progress. The data points for that measurand would indicate the 'one' or 'zero' binary bit value.

CONCLUSION

Transducers used in complex test operations can facilitate supportability of the instrumentation system by providing a built-in-test that evaluates the end to end performance of a data channel. Digital systems designed to acquire dynamic data can accommodate the special features needed to support a SMART transducer.

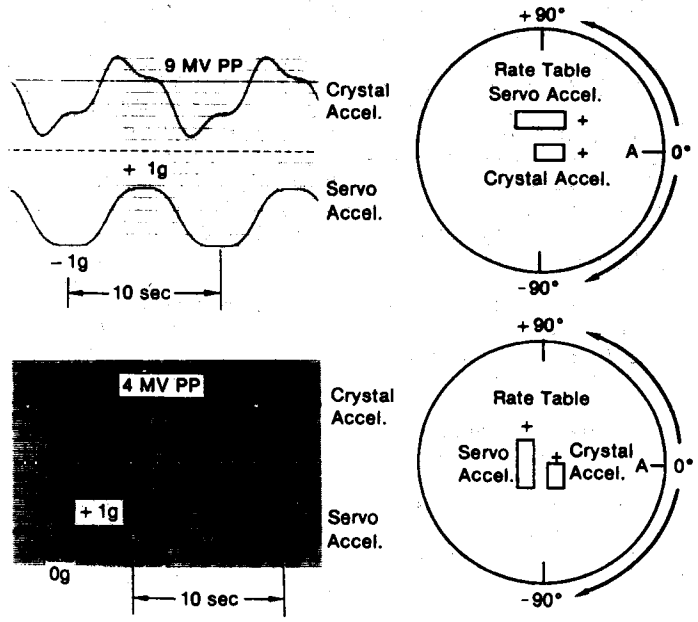

Notes:

1) Crystal Accelerometer - Endevco 2,250 AMI-10 SNAJ92
2) Rate Table - Contravis Goetz Model 811
   Servo Controller Model 404D
3) Servo Accelerometer - Sunstrand Model 303B SN212
4) Rate Table Motion: Point A moves through the arc from 0° to +90° to 0° to −90° to 0° to simulate an aircraft roll phasing maneuver of 36° per second.

GP71-0319-30

Fig. 1 Phasing Maneuver Laborstory Test

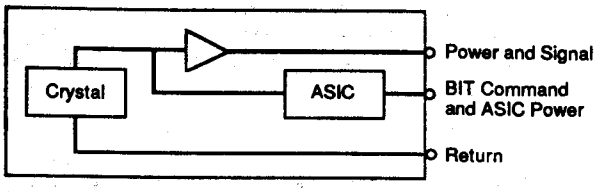

Fig. 2A BIT Provides for Self Identification and Channel Test

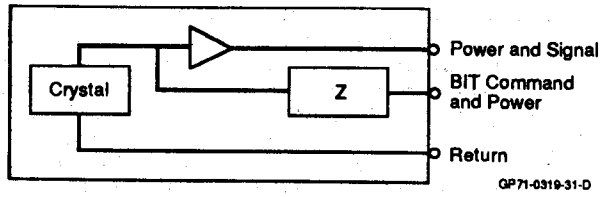

GP71-0319-31-D

Fig. 2B BIT Provides for Channel Test

Fig. 2 Self Monitoring and Reporting Transducer

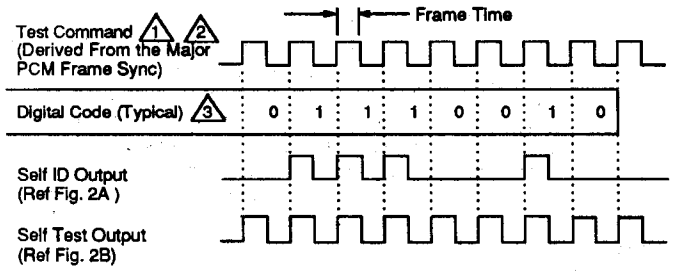

Notes:

1. A status word in each PCM minor frame indicates the activation of BIT.
2. The major PCM frame sync is divided by 2 to provide the signal used during the BIT period. This signal is compatible with both self identification and channel test only devices.
3. The value of the parameter during each frame is used to determine the binary value.

GP71-0319-32-D

Fig. 3 Signal Coding

REFERENCES

(1) Roylance, Lynn M. and Angell, James B., "A Batch Fabricated Silicon Accelerometer", IEEE Transaction on electronic devices, Vol. ED-26, No. 12, 1979, p. 1911.

(2) Rudolf, F., "A Micromechanical Capacitive Accelerometer With A Two-point Inertial Mass Suspension", Sensors and Actuators, Vol. 4, 1983, p. 191.

(3) Petersen, K., "Micromechanical Accelerometer Integrated with MOS Detection Circuitry", IEEE Transactions on Electron Devices, Vol. ED-29, 1982, p. 23.

A SELF MONITORING AND REPORTING TRANSDUCERS

Q: Dr. R. Maglic (Honeywell, Colorado Springs): When you talked about orientation, I got the impression you have one accelerometer. Is that enough to determine orientation? I think it would be confusing to know only one axis of rotation.

A: John W. Gierer (McDonnell Douglas Corp.): We are interested in knowing the orientation and polarity of all the accelerometers on board. We have additional information the aircraft gives us relative to what it is doing. From the INS System, we know the roll rates and the roll angles the aircraft is going through. In using this technique with lower frequency type accelerometers, these signals are used as the basis. The INS System tells us what the aircraft is doing, then you can look at the output of the transducers and make a judgment as to its orientation.

Q: Peter Stein (Stein Engineering Service, Inc.): At what stage do you program the SMART box with the serial number of the transducer? Is a particular transducer then calibrated with that particular channel or is that handled differently?

A: John Gierer: One way would be to have the transducer manufacturer permanently code the transducer where changes could not be made by the user. Consequently if you could read that code you would be able to pin down that transducer. I said serial number, but provisions might be made for the manufacturer's identification code.

Q: Harvey Weiss (Grumman Aircraft Systems): I'm still not clear, John, as to what the excitation is to the transducer under the bit test. I think you said something about audio pulses or some sort of sonics. If we are using an accelerometer, are we, in fact, imparting some sort of acceleration for the bit, or is it something else?

A: John Gierer: That was one of the techniques identified by the University of Cincinnati, so I don't have the answer to that question. I am looking for the capability to put into a data system. During the course of the University of Cincinnati's study, Dr. Brown indicated that the output impedance of the transducer would be a good indicator of the health of the device. So perhaps the bit test on a piezoelectric device might involve the output impedance of the crystal. If that output impedance hasn't undergone any drastic change, the amplitude of the signal coming back to you would be what you expected, and you would assume everything is correct. But now the transducer designers have other good things that they could put into the device to do that test.

Q: Harvey Weiss: In this area of polarization orientation, couldn't the transducer manufacturer, by some specification by the user, be responsible for delivering an accelerometer with a specific polarization, based on a configuration you requested, based on his Q.C. and all these devices that when you installed it a certain way, with a positive acceleration, you would get a positive acceleration output?

A: John Gierer: That is correct. Our own specifications now contain that provision. In general, our specifications do have that requirement in it. If there is a slip-up, I think our shop people may have mounted it upside down.

Q: Roger P. Noyes (EG&G Energy Measurements, Inc.): I have two questions: Why did you select piezoelectric in the first place? Second, is there any manufacturer making these commercially and are they available?

A: John Gierer: We selected a piezoelectric device initially for our work because it was the one device that we had a very difficult time with during the preflight operation, deciding whether it was any good. When the aircraft is on the ramp and is at rest, the transducer gives no output, which is also true if the wires are cut. As a result, we were finding it quite difficult to assess that kind of a parameter in a 15-minute preflight operation with automatic equipment. And to answer the other question you asked: No, I am not aware of any manufacturer producing such a device. We would like to see that capability in all the transducers in the system; at least those that are technically feasible to do it.

THE DEVELOPMENT, PERFORMANCE, AND APPLICATION OF A NEW RUGGEDIZED MASS AIR FLOW TRANSDUCER

Thomas C. Ramey
Marketing Manager
Kurz Instruments Incorporated
Monterey, California

ABSTRACT

This paper details the development begun in 1984 of a new generation of ruggedized metalclad thermal air velocity and mass flow sensors, and briefly summarizes the underlying theory of the sensor. Designed to measure air velocities as low as 10 feet per minute, these sensors function in hostile environments of high temperature, corrosive flows, and particulate-laden gases. Data from performance tests showing temperature and pressure compensation characteristics are presented, and calibration methods are discussed.

Brief examples are given of applications of the ruggedized sensors in aerospace, conventional and nuclear power plants, chemical plants, defense waste handling facilities, pulp and paper mills, etc.

INTRODUCTION

This paper details the development of a new generation of thermal mass flow sensors designed to be extremely sensitive and accurate while simultaneously exhibiting extraordinary ruggedness and ability to function in hostile environments of high temperature, corrosive flows, and particulate-laden gases. While this same sensor can be used in liquids such as water, oil, paint, and fuel, our discussion today will be limited to its applicability to and performance in gases. Historically, thermal anemometers developed out of turn-of-the-century hot-wire research. In the 1960's they were further refined by wrapping platinum on ceramic mandrels and glass-enamel coating the assembly.

FUNDAMENTAL IDEA

The fundamental idea behind any thermal flow sensor is this: The velocity of any fluid capable of absorbing heat--be it air, a gas, or a liquid--can be inferred from the heat transferred or carried away from a well-defined, well-understood, heated element.

Such a heated element can be constructed and operated as a constant-temperature thermal anemometer by using two temperature-sensitive resistance temperature detectors (RTDs).

A light-duty sensor can be constructed of reference-grade platinum (such as grade 385) on a hard, stable, high-density ceramic mandrel. The resulting thermal anemometer is then virtually identical to a National Bureau of Standards platinum RTD temperature standard.

What does a thermal flow sensor measure? Because of the equations of heat transfer, the output of any thermal anemometer is related to mass flow rate, NOT volume flow rate. Therefore, the effect of density is automatically compensated for.

Because a thermal anemometer measures the unit-area mass flow, it can be said to measure mass velocity. In other words, it measures the true velocity, weighted by the density of the flowing gas.

Mass velocity can also be viewed as Standard Cubic Feet per Minute per square foot ($SCFM/ft^2$). If you look at the unit of this term, you find that it is equivalent to Standard Feet per Minute (SFPM), a term coined by Kurz Instruments to describe what our sensors actually measure.

But how are mass flow and SCFM related? Standard Cubic Feet per Minute is a measure of cubic feet per minute referenced to standard conditions. Kurz Instruments uses standard conditions of 25 degrees C and 29.92 inches Hg. Once standard conditions are defined, density is defined, and, because of the laws of thermo-dynamics and the properties of gases, SCFM also indicates a mass flow rate. Let's define mass flow rate:

Equation 1

$$\dot{m} = \rho_a \times V_a A$$

where

$\dot{m}$ = mass flow rate (lb/min)

ρ_a = gas density (lb/ft^3)

V_a = actual velocity of gas (FPM)

A = area of flowing gas (ft^2)

But we usually define mass flow rate in terms of SCFM. How are SCFM and mass flow rate (lb/min) related? The mass of one cubic foot of air varies according to its density. Density is dependent upon temperature and pressure. One standard cubic foot of air has a mass identical to one actual cubic foot of air at a temperature of 25 degrees C and at atmospheric pressure of 29.92 inches of mercury. SCFM is, therefore, a unit of mass flow, just as surely as is lb/min. Increase or decrease SCFM by n%, and you increase or decrease lb/min by the same percentage. Therefore,

Equation 2

$$\dot{m}_s = \dot{m}_a$$

where

$\dot{m}_s$ = standard mass flow rate (lb/min)

$\dot{m}_a$ = actual flow rate (lb/min)

But from Equation 1, it follows that

Equation 3

$$\dot{m}_s = \rho_s \times V_s \times A$$

and

Equation 4

$$\dot{m}_a = \rho_a \times V_a \times A$$

where

ρ_s = gas density at standard conditions

ρ_a = gas density at actual conditions

V_s = velocity referenced to standard conditions (SFPM)

V_a = actual velocity (FPM)

Therefore, using equations 2, 3, and 4, we find that

Equation 5

$$\rho_s V_s A = \rho_a V_a A$$

Since the area (A) is the same for both conditions, we can also write

Equation 6

$$\rho_s V_s = \rho_a V_a$$

Now we can define standard velocity in terms of actual velocity, actual density, and standard density:

Equation 7

$$V_s = \frac{\rho_a \times V_a}{\rho_s} \text{ (SCFM)}$$

This is what thermal flow sensors measure.

Because such sensors measure SFPM directly, it follows that they do not need to be corrected for temperature or pressure, as do most other types of air velocity instruments. It also follows that thermal sensor technology is ideally suited to measure total mass flow, because no correction is required.

If the actual velocity is desired--in order, for example, to compare it to readings obtained from a pitot tube--Equation 7 can be used to obtain the desired information, because actual density (ρ_a) is available, and ρ_s is known (pitot tube data must be corrected for ρ_s and ρ_a).

Let's assume that we have measured the velocity in a duct and have obtained the average. The total mass flow rate (SCFM) is easily determined by simply multiplying the average SFPM (V_s) by the area (A) of the duct; therefore:

Equation 8

$$SCFM = V_s A$$

To convert SCFM to units of mass such as lb/min or kg/min, it is necessary only to know the numerical value of the standard density of the gas in question. For example, ρ_s for air = 0.074 lb/ft^3.

To obtain the proper mass flow units in terms of lb/min, use the following equation:

Equation 9

$$lb/min = \rho_s \times SCFM$$

Obviously, similar arguments apply for other units of mass flow.

THERMAL FLOW SENSORS BASED ON THE WHEATSTONE BRIDGE

The sensor technology employed by Kurz Instruments uses two RTD windings of different sizes as legs of a balanced Wheatstone bridge circuit. The larger winding is used to measure the ambient temperature of the flow in which the sensor is inserted. The bridge circuit is adjusted to supply sufficient power to the smaller winding to maintain a constant temperature differential between the two windings. The greater the velocity of the flow passing over the sensor, the greater the power and voltage required to maintain the temperature differential. The system produces as its output a voltage that is proportional to the heat transfer between the heated winding and the gas stream. This heat transfer is proportional to the velocity of the flow.

Figure 1 shows two Wheatstone bridge circuits employed by Kurz. The top illustration is a direct or "voltage mode" bridge; the bottom illustration is the standard "two-wire" bridge.

Figure 1. Wheatstone Bridge Circuits

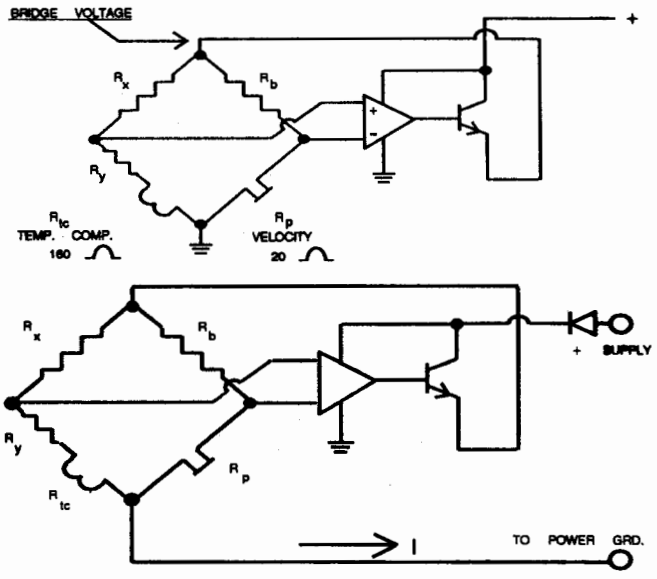

None of the technology detailed so far is entirely unique to the sensors developed by Kurz Instruments. What differentiates those sensors from competitive products based on the same principles are the following characteristics:

- Larger diameter for greater resistance to particulate contamination
- Stainless steel sheath for greater ruggedness and easier cleaning
- Extreme sensitivity at low flow rates
- Operation at relatively low power levels

The larger diameter of the sensor is worth discussing further. Why is it an advantage? At first blush, you might suppose that a larger sensor would represent a larger target, and would therefore more often be hit by particles in the gas flow than would a smaller sensor.

In fact, just the reverse is true. A small, hot-wire type sensor creates very little upstream disturbance in the gas flow. Therefore, a particle bearing down on such a sensor is not likely to be carried around the sensor by that flow. Instead, the particle will hit, and very likely stick to, the smaller sensor. Moreover, because the small sensor has a correspondingly small surface area, the adhesion of relatively few particles can significantly alter the heat-transfer characteristics of the sensor and thereby degrade its accuracy.

In contrast, the larger sensors developed by Kurz Instruments create a significantly greater upstream flow disturbance. Most particles are therefore diverted around the sensor. And any particles that do hit and adhere to the sensor do not significantly change the sensor's thermal transfer characteristics because of its much larger surface area.

RUGGEDIZED SENSOR CONSTRUCTION

Construction of the metalclad sensors developed by Kurz is considerably more difficult and expensive than the construction of the ceramic sensors discussed in general terms earlier. A 316 Stainless Steel sheath is tig welded, and the wrapped ceramic mandrel is potted into it. The sensor is then baked to remove any residual moisture, and the tip is welded shut. Both windings of the dual-prong sensor are constructed similarly.

SENSOR PERFORMANCE

TEMPERATURE COMPENSATION

All heat transfer results from a difference in temperature between the heated winding and the gas stream. Kurz maintains the difference constant by using a unique Wheatstone bridge temperature compensation circuit, as described earlier. The ability of that circuit to compensate for changes in ambient temperature is graphically illustrated in Figure 2.

Figure 2. Temperature Change vs Signal Fluctuation

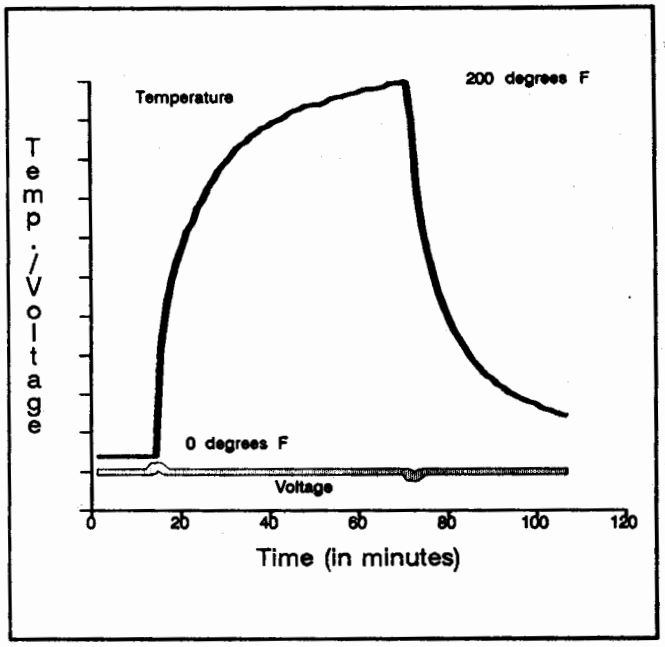

Note that the onset of sudden increases and decreases in temperature cause only a small (about 1 volt) and short-lived (about two-minute) fluctuation in the sensor's signal.

PRESSURE COMPENSATION

The Kurz thermal sensor, because it responds to the amount of heat being carried away by molecules, inherently and automatically compensates for pressure (more pressure means more molecules, which means more mass flow). Table 1 shows the performance of a single sensor operating over turndowns of approximately 25 to 1 over both velocity and pressure.

Table 1. Effects of Pressure on Non-Linear Output

Pressure	15*	29.92*	15	30	45	75	100	175	300	500	600	800	1000
SFPM	Non-Linear Bridge Voltages												
0	3.59	3.55	3.623	3.71	3.77	3.89	3.97	4.2	4.54	4.80	4.97	5.20	5.42
250	5.05	5.04	5.04	5.04	5.05	5.05	5.06	5.08	5.08	5.15	5.36	5.54	5.76
500	5.60	5.60	5.59	5.60	5.61	5.61	5.62	5.62	5.64	5.73	5.84	5.89	6.00
750	5.87	5.868	5.868	5.87	5.87	5.87	5.88	5.88	5.93	5.99	6.10	6.15	6.23
1000	6.11	6.111	6.08	6.09	6.09	6.09	6.11	6.11	6.15	6.25	6.35	6.38	6.41
2000	6.77	6.79	6.79	6.78	6.78	6.79	6.80	6.80	6.82	6.89	6.90	6.93	7.00
3000	7.29	7.285	7.28	7.28	7.27	7.28	7.28	7.26	7.26	7.32	7.35	7.35	7.40
4000	7.67	7.67	7.67	7.65	7.65	7.67	7.67	7.64	7.64	7.65	7.65	7.69	7.75
5000	7.97	7.97	7.97	7.95	7.95	7.95	7.95	7.95	7.95	7.96	7.96	7.98	8.00
6000	8.24	8.238	8.24	8.22	8.23	8.23	8.23	8.23	8.23	8.23	8.23	8.24	8.24
7000	8.52	8.51	8.52	8.48	8.48	8.48	8.48	8.48	8.48	8.48	8.48	8.48	8.49
8000	8.80	8.80	8.80	8.72	8.74	8.72	8.72	8.72	8.72	8.72	8.72	8.72	8.73
9000	9.03	9.03	9.04	8.95	8.96	8.96	8.95	8.95	8.95	8.95	8.95	8.95	8.96
10,000	9.27	9.27	9.28	9.15	9.16	9.15	9.15	9.15	9.15	9.15	9.16	9.16	9.17
11,000	9.46	9.46	9.47	9.35	9.36	9.35	9.35	9.35	9.35	9.35	9.35	9.36	9.37
12,000	9.66	9.65	9.69	9.50	9.49	9.49	9.48	9.48	9.50	9.51	9.51	9.52	9.53

* These pressures are in inches of mercury. All other pressures are given in PSIG.

All readings are for air at 25 degrees C.

The data in Table 1 characterize sensor performance at 13 different pressures ranging from 15 inches of mercury to 1,000 psi and at 16 flow rates ranging from 0 to 12,000 SFPM. These data demonstrate that pressure is a significant issue only at very low rates of flow.

At 0 SFPM, for example, output voltages range from 3.59 volts at 15 inches of mercury to 5.42 volts at 1,000 psi, a differential of approximately 50%.

At 1,000 SFPM, however, output voltages range from 6.11 volts to 6.41 volts over the same range of pressures, a differential of less than 5%.

And at 5,000 SFPM, output voltages range from 7.97 volts to 8.00 volts, a differential of less than four tenths of one per cent.

TIME RESPONSE

Because the surface temperature is maintained constant by a very fast electronic circuit, and the ceramic mandrel upon which the platinum wire is wound and the metal cladding are already at the same temperature as the winding, our sensors have a much faster response to changes in flow than one would normally expect. As shown in Figure 3, when flow over the metalclad sensor is instantaneously boosted from 0 to 6,000 SFPM, the sensor's output is 90% of actual flow within 3.2 seconds. Within 18 seconds, sensor output is at 100% of actual flow.

Figure 3. Time Response of MetalClad Sensor

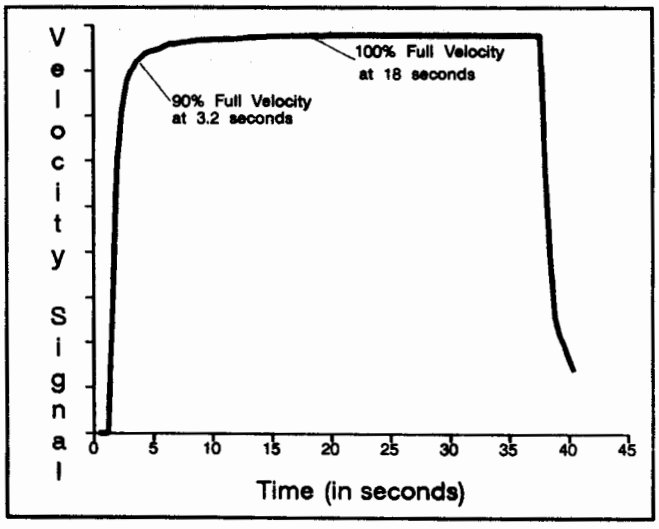

REPEATABILITY

Repeatability is one of the strongest features of a thermal anemometer with platinum construction. Excellent repeatability on the order of 1/4% or better is due to the inherent stability and minimal change in resistance over temperature of all grades, but especially of the reference grade 385 Platinum used in Kurz sensors.

SIGNAL

With thermal sensors and accompanying Wheatstone bridge, the circuit develops a raw output signal from the bridge of typically 3 Vdc to 8Vdc. This healthy amount of DC voltage output means there is plenty of sensitivity in our sensors to detect velocity differences of only a few feet-per-minute.

SENSOR ORIENTATION: ROTATION AND YAW

Kurz-designed metalclad sensors are calibrated while oriented as follows relative to the gas flow: The sensor is inserted into the flow at a 90-degree angle, and the two sensor elements are aligned parallel to the flow, with the shorter temperature-compensation winding upstream of the longer velocity winding. Ideally, the sensor's orientation during actual use should be the same as its orientation during calibration. In fact, the metalclad sensor can tolerate significant deviations from the ideal orientation as to both rotation and yaw.

Rotation refers to deviations from parallel in the alignment of the sensor elements with the gas flow. Yaw refers to deviations in the angle of the sensor's insertion into the flow.

As shown in Figure 4, rotational deviations of +/- 10 degrees result in a measurement error of only 1%. Yaw of +/- 10 degrees results in a measurement error of only 2.7%.

Figure 4. Measurement Error: Rotation and Yaw

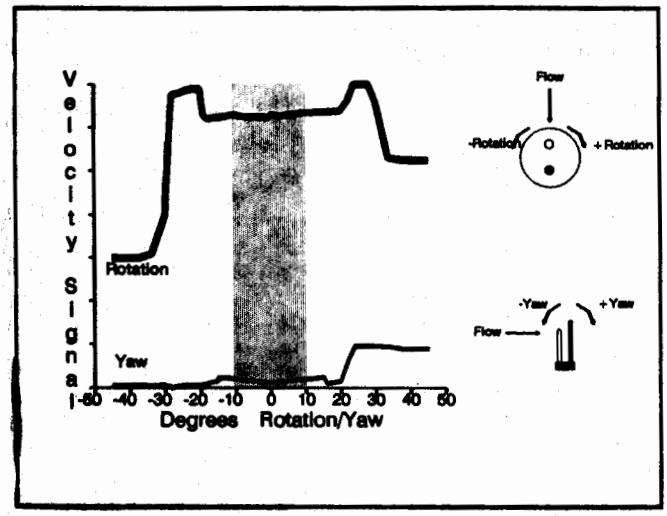

ZERO

Another important feature of the Kurz-developed sensors is the fact that they actively zero. That is, they exhibit a raw output of around 3 Vdc at no flow. Thus, during calibration we can fix a zero or no-flow data point. Many other types of flow devices such as differential pressure devices (Pitot tubes and orifice plates), as well as turbine meters and vortex shedders, yield no interpretable signal when they are within even several hundred feet-per-minute of zero or no flow conditions.

FAILURE MODES

A sensor is either working or not working. A bad sensor almost always fails by a short occurring in one of the windings. Sensors can be tested and verified by measuring the ohmage of the two windings. They should be about 20 ohms and 200 ohms respectively.

CALIBRATION METHODS

Sensors are calibrated in enclosed wind tunnels using inclined water manometers. The sensor is inserted in a flow with a very flat velocity profile provided by a section of honeycomb flow conditioner. Flow rate is determined by the differential pressure drop across the honeycomb. Local temperature and barometric pressure are measured, and correction factors are applied to correct to standard temperature and pressure (25 degrees C and 29.92 inches of mercury, respectively). The nonlinear output curve of each instrument is plotted, and eleven points on that curve are selected as breakpoints to be used in linearizing the signal.

An NBS-traceable calibration certificate is provided with each instrument.

For sensors used in flow-metering applications, calibration involves inserting the sensor in a line between a cylinder of the specified gas and a volume prover.

GASES IN WHICH SENSORS CAN BE USED

Kurz-designed sensors can handle virtually any gas. Sensors are available sheathed in 316 stainless steel, titanium, Hastelloy[1], and Monel[2] to resist even the most corrosive of gases.

LINEARIZING THE NONLINEAR SIGNAL

Heat transfer is a nonlinear function of velocity or flow rate. Because flow pulsations and large-scale turbulence may occur at rapid rates, we have designed a fast linearizer circuit to accomplish proper signal averaging. (Note: The average of a non-linear, time-varying signal representing air velocity does not yield the current average air velocity!)

Many Kurz products use our EPROM board for signal linearization. The EPROM board consists fundamentally of three components: a 10-bit analog-to-digital converter, a 2K EPROM, and a digital-to-analog converter. The 10-bit analog-to-digital converter uses the nonlinear voltage output of the sensor as its input and converts the voltage into a 10-bit binary value. This 10-bit binary value represents numbers up to 1,024. These numbers are used as addresses for 1 kilobyte of EPROM memory. At each of these 1,024 addresses is stored an 8-bit word or byte. This 8-bit word represents a number between 0 and 255. The 8-bit value or number is converted back to an analog voltage--now the linear output signal--by a digital-to-analog converter.

The linearizing takes place in the EPROM. A calibration technician takes voltage vs. flow data at a number of data points (500, 1000, 1500, 2000, 2500, and 3000 SFPM, for instance) and plugs this data into a software program that runs on an IBM PC or compatible computer. The software performs a curve fit and derives the numbers to get a linear curve. The software then graphically plots the data on the screen so the technician can make a quick visual check that the curve fit data results in an approximately linear curve plot. The software then automatically programs and verifies an EPROM. The EPROM is a 2K 2716, so it can hold two curves, one for each of the two ranges available on some Kurz products.

The 10-bit analog-to-digital converter is used so that there is more accurate addressing of the EPROM. There are 256 steps in the output curve, but those 256 steps are selected by 1,024 addresses. For the output to be off 1 bit, the 10-bit analog-to-digital converter would have to be off by 4 bits.

The EPROM linearizer employed by Kurz operates at 20 KHz.

The EPROM linearizer uses ten or eleven straight-line segments to closely approximate the smooth calibration curve. The circuit is highly accurate, repeatable, easy to set up, and relatively inexpensive compared to other techniques. In addition, we have recently improved the circuit to follow the inflection point near zero flow. This means that under all conditions we produce a zero output voltage at zero flow and follow the calibration curve very well at all points. (By the way, many of our competitors who use pitot tubes with averaging manifolds suffer greatly from the fact that their equipment obtains the average pressure, which is not the average velocity, because of the quadratic nature of the relationship between velocity, density, and pressure.)

APPLICATION EXAMPLES

General Dynamics of San Diego, CA uses a Kurz 7500 flow-control system built for mass flow control of cruise missile cooling air for a ground-based test stand. The 7500 system incorporates the metalclad sensor, which is used in conjunction with a flow-control valve.

General Dynamics, San Diego, CA. uses a Kurz sensor for measuring airflow in a pipe approximately one inch in diameter. The pipe is a ducting section for the electronic cooling airflow on cruise missiles. The sensor was mounted in the pipe at a 30-degree intercept angle. Kurz electronics included a DC/DC power converter to operate on 28 Vdc. A special 5-point linearizer board was included in a small 2" x 2" can or housing, and it sat on top of the bridge/DC/DC converter board. Then the whole assembly was potted and sealed. The sensor also included an additional winding serving as a Platinum RTD for temperature measurement.

1 Hastelloy is a trademark of the Cabot Corporation.

2 Monel is a trademark of the International Nickel Corporation.

McDonnell Douglas, St. Louis, MO. uses Kurz sensors to measure oxygen flow through the pilot's breathing tube on the Harrier jet that McDonnell Douglas is building in the USA under license from British Aerospace. McDonnell Douglas insisted on designing the circuit boards and enclosures, and Kurz technicians discovered they (McDonnel Douglas) had made several fundamental mistakes on circuitry. After new boards were provided, Kurz calibrated the systems to very stringent and rigorous specifications.

Boeing Seattle, WA uses a EVA 4000 multipoint velocity averaging system to measure exhaust airflow from a free electron laser research project for the Strategic Defense Initiative ("Star Wars").

Monsanto, Cincinnati, OH is installing a 3-point IK-EVA isokinetic sampling system to sample uranium nucleotides in a 9 ft. stack. This Monsanto site manufactures small nuclear power generators for satellites and other spaceborne applications.

Fisher Controls is doing a boiler rebuild for Minnesota Power. They are using EVA 4000s with K-BAR12 probes for forced draft (feed air) as well as for the overfire air. Eight systems with a total of 26 sensors are being installed.

Hope Creek Nuclear Generating Station, Public Service Electric & Gas (New Jersey). EVA systems were installed there as part of a GA Technologies radiation monitoring system which samples plant vents or stacks. One of these EVA systems was supplied as a qualified nuclear safety related system. Qualification data is being supplied through Bechtel Power. The EVA systems were integrated with Kurz 7500 flow control systems to control the sample flow and provide auto-isokinetic sampling using the customer's pre-existing sample nozzles.

Niagara Mohawk's Nine Mile Point Plant. This is an SAI system that uses our new EVA multipoint velocity array sensors for stack and duct flow measurement. The system was recently installed in Niagara Mohawk's Nine Mile Point Plant in NY. This system samples for airborne radioactive particulate, iodine and noble gases. It is a true isokinetic system and includes the addition of a noble gas monitor that looks for krypton and zenons. A multipoint EVA system is installed in a circular stack 28 ft. in diameter for measuring airflow. SAI fabricated their own sample withdrawal "rake" consisting of multiple nozzles co-located with the EVA sensors. The EVA's provide a highly accurate signal of the average airflow across the stack. Controlling to this signal, sample pumps and flow controllers pull a sample out through the sampling rake. The sample is routed to filter cartridges, iodine and noble gas detectors, and then returned to the stack just downstream of the sample withdrawal rake to continue on its way.

Mobay Chemical, Pitts, WV, for a flue gas application had a theortical flow calculation of 6,000 SCFM in the duct they intended to instrument. A duct traverse was performed after the EVA 4000 system was installed. Results of the traverse also showed a flow of 6,000 SCFM, + or - 300. When personnel walked down to the control room shortly thereafter, the digital displays showed the EVA system to be reading 6,150 SCFM. Mobay engineers were elated to have all three measurements agree within 5%. Although the working fluid is flue gas, the EVA 4000's were shipped with a straight air calibration, and this was found to be completely satisfactory.

At Mobay, the EVA 4000 installation consisted of two KBAR 24 probes with 3 sensors on one, and 2 sensors on the other. Since the duct was round (5 ft. I.D.) the bars were installed in the cross configuration. The EVA array is installed only 5 ft. downstream from a 90-degree bend. Mobay uses the EVA signal for process control. They take two signals: the EVA signal and a direct reading O^2 analyzer to trim combustion in a reformmer (natural gas fired boiler). Recently, Mobay purchased a duplicate EVA to use elsewhere in the plant.

Savannah River Plant (Defense Waste Processing Facility). E.I. DuPont is using a complete IK-EVA 4200 Isokinetic Sampling system for characterization and determination of isokinetic sampling requirements. DuPont anticipates a facility-wide requirement for isokinetic sampling systems.

Kerr-McGee, West Chicago, nuclear plant de-commissioning application. A 1275 is installed in an incinerator stack to sample emissions. The allowable amount of material burned in any one month is based on emissions.

International Paper, Naches, MS, is using an EVA 4000 with 3 probes, each with 3 sensors. Originally, International Paper used an EVA 4100 system, but found they needed the ruggedness of the all-metal velocity sensors of the EVA 4000, and had their system upgraded to metal sensors.

Tampa Waste Management Energy Systems has 12 EVA 4000 systems that are being used on four identical boilers. Each boiler uses three EVA systems: two measure primary combustion air, one measures flue gas. Tampa Waste also uses 455-08's, seven on each boiler, to measure secondary air. The primary air blows underneath the grate the garbage is on, the secondary air blows into the combustion area above the "trashpile". The Tampa plant justs dumps whole mixed garbage into the boiler.

BIBLIOGRAPHY

"Electronic Velocity Sensors," Mechanical Engineering, May 1986, pg. 29.

"Mass Flow Measurements in Nuclear Applications," Sensors, May 1986, pg. 20.

"Thermal Mass Flow Technology," Measurements & Control, April 1986, pg. 164.

"Sensing Thermal Mass Flow for Gas Velocity," Control & Instrumentation, June 1986, pg. 91.

THE DEVELOPMENT, PERFORMANCE AND APPLICATION OF A RUGGEDIZED MASS AIR FLOW TRANSDUCER

Q: Randy DeBrine (Grumman Corp, Great River, N.Y.): Could you describe how the unit compensates for the temperature of the air flowing?

A: Thomas C. Ramey (Kurz Instruments, Inc., Monterey, CA): You basically have two sensors. One sensor measures the ambient temperature all the time; it's one side of a basic, classical whetstone bridge. It's that ambient temperature protection that sets the temperature of the heated winding; the heated winding is where you are measuring the flow. If temperature goes up, the resistance changes in the whetstone bridge; it rebalances. The temperature goes up in what we call R_p the heated winding. The temperature differences remain constant. If the flow doesn't change the velocity sensor, its temperature will rise. With no flow change, it won't draw any more current. But, if flow increases, it will draw more current and we measure the flow by measuring the amount of current that the heated sensor is drawing.

Q: Randy DeBrine: As the temperature of the air rises, so then does the temperature of the probe. Now isn't it drawing more current?

A: Thomas C. Ramey: No. It should be using more voltage changes because it is run as a constant temperature bridge. There are two ways of running the bridge: constant power and constant temperature. This one is run as a constant temperature bridge. The key word is overheat; however, overheat is maintained the same regardless of the ambient temperature.

Q: Lawrence A. Rempert (Allison Gas Turbine, Indianapolis, IN): Is there a commercial transducer available for fuel and oil measurement?

A: Thomas C. Ramey: Yes, but we don't talk about it, and it's not in our advertising literature. We take a number of applications for liquid application, diesel oil, and fuel. What we have worked on most recently is General Motors paint flow meters. Paints are very difficult because they are all different. They have different solvents, pigments and emulsifiers, and are very difficult to measure accurately. Call me or Jerry Kurz for more information.

Q: Dr. R. Maglic: I have not seen the errors estimated in your measurements. Do you think that a micro bridge made of silicon is comparable to yours?

A: Thomas C Ramey: Yes, I would expect a silicon bridge to be pretty stable and be comparable to our bridge. Basically, we build a bridge in a very simple, classical fashion. We use the finest resistors we can get. Each sensor goes through a process call Timcon, where additional resistors are put on the bridge to fine tune them, and to balance them. So, I would expect it could be powered by a smaller silicon device and, perhaps, use less power that way. In terms of temperature effect, the air is about 0.4 of 1 percent. There is pressure compensation of 0.6 of 1 percent. Repeatability is 0.25 of 1 percent. Overall accuracy, of course, depends on your wind tunnel setup, and on whether you have 5-1/2 DVM that you are keeping in calibration every six months. We use a two percent reading accuracy as good rule of thumb. That percent reading improves as you go down and is different from percent full scale.

SELF-CHECK DEVELOPMENT FOR LITHIUM NIOBATE EXPLOSIVE MONITORS

S. F. Kuehn
Sandia National Laboratories
Albuquerque, New Mexico 87185-5800

ABSTRACT

This paper reports on the design criteria and experimental results associated with the development of a self-check scheme in lithium niobate explosive monitors. These monitors have been developed at Sandia National Laboratories and a patent is pending. This monitor was developed to measure timing of explosive detonations with sub-microsecond resolution. Because the monitor is usually non-recoverable and undergoes catastrophic damage, its condition has to be ascertained prior to explosive detonation. The verification of its condition was the motivation for this development.

The paper will discuss the various self-check methods investigated and their practicality. The discussion will then focus on one method that uses an undesirable characteristic of piezoelectric crystals to perform a useful function: the pyroelectric self-check.

1. INTRODUCTION

The DOE Albuquerque office provided funding to General Electric Neutron Devices in Largo, Florida, for a lithium niobate production facility. Since May 1984, GEND has been supplying Division 7545 with self-check feasibility hardware.

Two dedicated assembly and testing labs at GEND are shown in Figures 1 and 2. In these labs lithium niobate crystals were cut and polished, then assembled into the transducer housings. Figure 3 shows the tester used to evaluate the explosive response. The tester consisted of a boom box within a temperature chamber, the Tektronix 7912AD digitizers, and data processing capability. An ultrasonic testing unit was incorporated into this tester to perform a nondestructive test before the transducer was inserted in the boom box and the explosive was fired.

One version of the monitor is illustrated in Figure 4. Note the 125 by 16.5 mil crystal, its attendant guard ring for electrical isolation between the center electrode and negative crystal face, and the 500 Ω resistor used as a preassembly continuity check. Figure 5 shows the transducer response observed. The electrical characteristics of prime importance are the amplitude specified to be 12±2 A, the rise time measured from the 25% to 75% level specified (10±5 ns), and the pulsewidth at the 4-A level (30±10 ns).

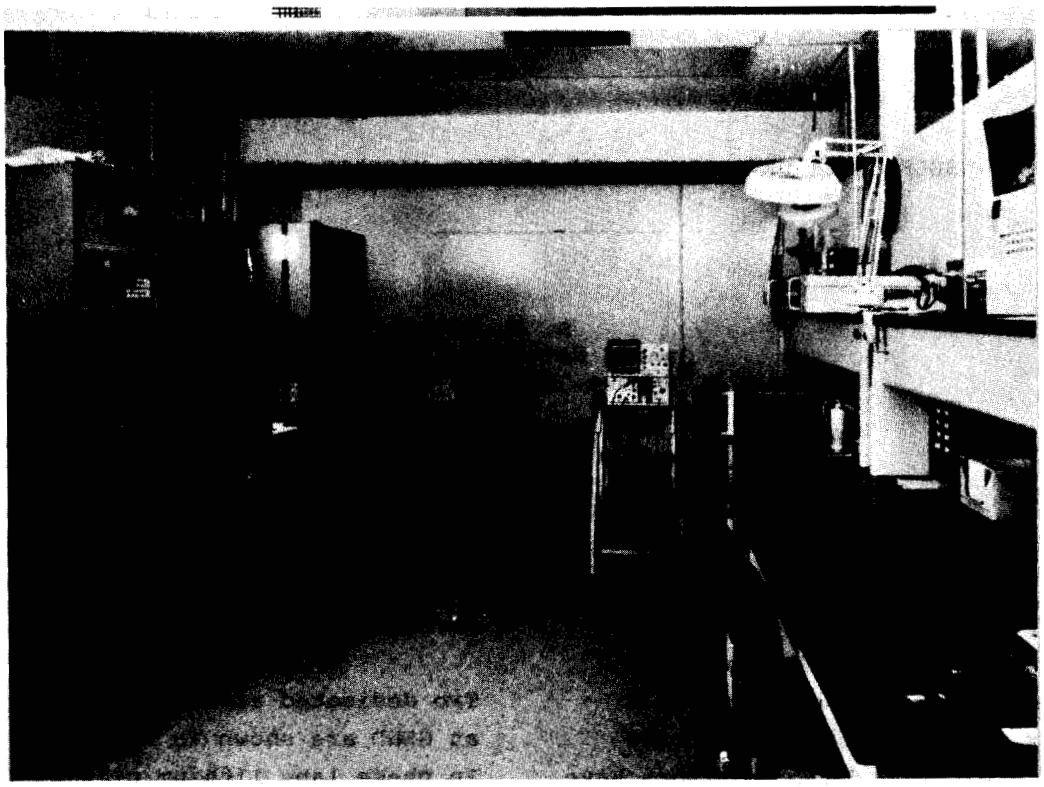

Figure 1. GEND Environmental Testing Laboratory

Figure 2. GEND Assembly Area

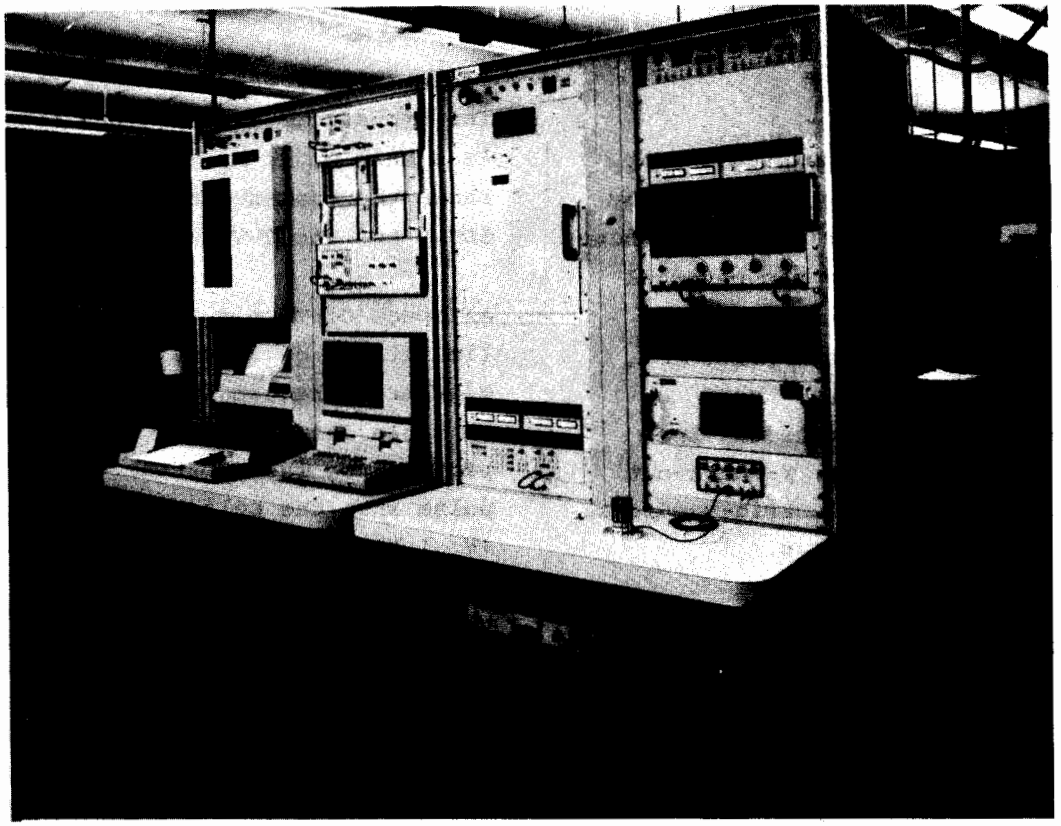

Figure 3. Product Tester

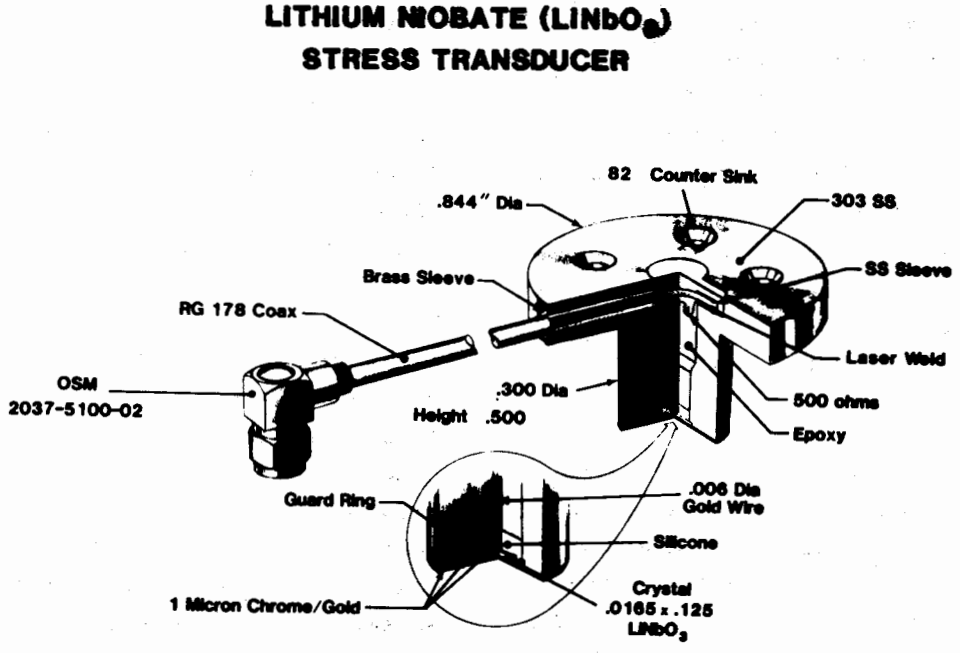

Figure 4. Artist Conception

2. SELF-CHECK CAPABILITY

Lithium niobate can (conceptually, at least) be stimulated for self-check by many methods. The practicality of these methods is determined by the physical properties of the lithium niobate crystal. The first method presented, continuity loop, shows how the connections could be verified. The other methods--biannular, Y-cut/Z-cut back-to-back, and pyroelectric--address the crystal integrity issue.

2.1 CONTINUITY LOOP

Lithium niobate is a "frozen-in" ferroelectric for which electric field and pressure do not appear to cause domain reorientations inside the crystal. This quality (as well as the crystal's high passive resistance) made the continuity concept practical. Two circuit configurations were investigated (Figure 6). Concept B in Figure 6 is the preferred method, but Concept A provided insight to the practical limitations. In Concept A, the current pulse I_{test} induced current to flow in R_T and through the output current-viewing transformer (CVT). The minimum value of R_T was determined by the transmission line characteristics of the current loop and the CVT. During explosive activation, the inductive impedance in the loop required that the minimum value of R_T be high enough to prevent excessive signal current (>5%) from shunting through R_T.

Alternatively, R_T was kept as low as possible to allow for the largest self-check pulse at V_o. Division 7545 lab tests showed that a maximum V_o of 28mV was achieved when R_T was $\geq$300 Ω, the CVT gain resistor (R) was 1000 Ω, and the cable (RG178) was no longer than 3 ft. The transducer response was attenuated less than 5% if R_T was $\geq$500 Ω. Figure 7 shows the transducer response with R_T = 500 Ω and the CVT gain resistor of 50 Ω.

Although Concept B had the same general limitations of inductive impedance at gigahertz frequencies and an upper limit on cable length, its self-check performance was substantially better. A pulse into the self-check drive line (V_{sc}) turned the FET Q1 on. The current generated from the discharge of the 0.1 μF capacitor C1 induced a higher current into the secondary of the stepdown pulse transformer T1. The current generated by the pulse transformer flowed through the 1N3070 diode and the MC2822 CVT. The CVT then generated a voltage pulse proportional to the current flow. With C1 charged to 15V, a current as high as 1.5 A could be observed through 30 in. in RG178 cable. As expected, Figure 8 shows a slightly higher self-check amplitude, 1.75 A, when the cable length is only 5 in. The concept B circuit reacted to the cable load very much as a true current source since a 600% increase in cable length produced only a 15% decrease in the self-check current amplitude. The transducer response (Figure 9) was not substantially affected while the secondary of transformer T1 was present in the loop.

The response rise time was <10 ns, the pulse width at the 3.5-A level was >30 ns, and the peak amplitude was a nominal 10 A through a 5-in. RG178 cable. A comparison of these values with the values of a crystal without the continuity check showed that this unit had no increase in rise time and no appreciable decrease in either the pulse width or amplitude.

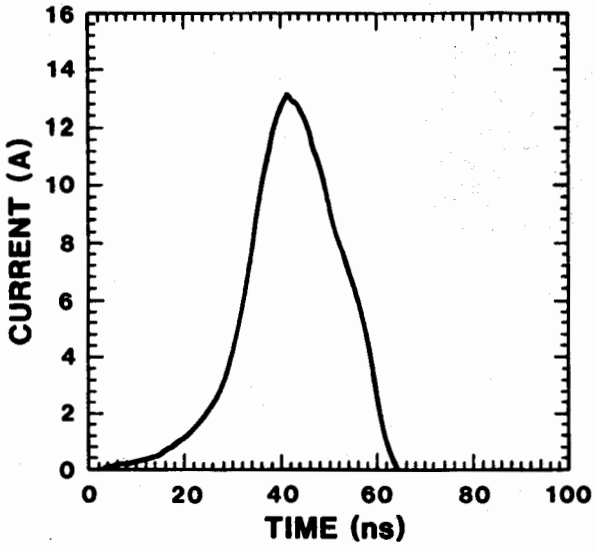

SERIAL NO.: 8521061
TEST DATE: 8-5-85
WIDTH (@ 4 A): 30.08 ns
PULSE WIDTH (@ 50%): 22.51 ns
RISE TIME (25% - 75%): 7.97 ns
PEAK AMPLITUDE: 13.453 A
TEST TEMP: 24° C

Figure 5. Transducer Response

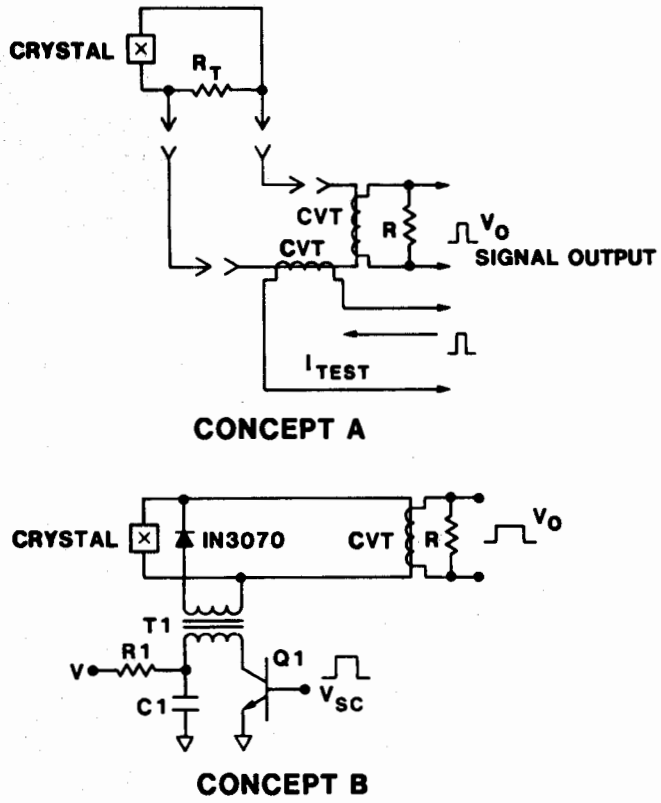

Figure 6. Continuity Loop Self-Check Concepts

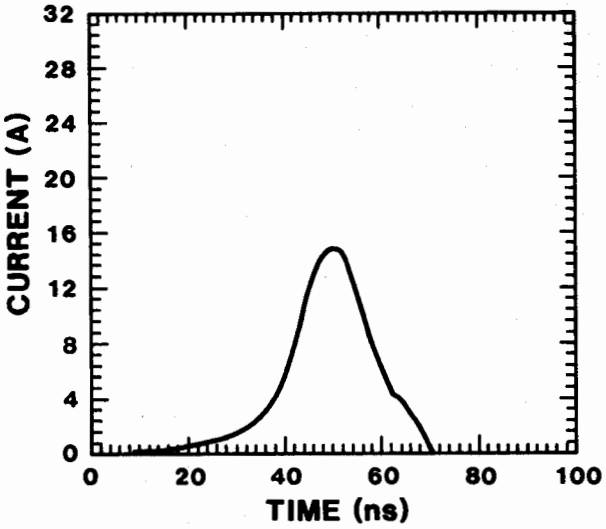

CRYSTAL DIAMETER: 125 MILS
CRYSTAL THICKNESS: 16.5 MILS
ELECTRODE DIAMETER: 95 MILS

CABLE LENGTH: 30 IN.

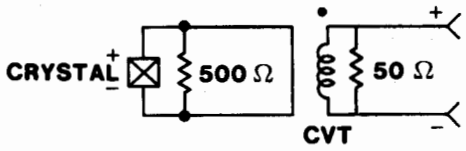

SERIAL NO.: X34
TEST DATE: 12-12-84
WIDTH (@ 3.5A): 27.7 ns
PULSE WIDTH (@ 50%): 16.8 ns
RISE TIME (25% - 75%): 7.2 ns
PEAK AMPLITUDE: 14.76 A (CVT)

Figure 7. Transducer Response with Resistive Continuity Loop

Figure 8. Self-Check Pulse from Diode Continuity Loop

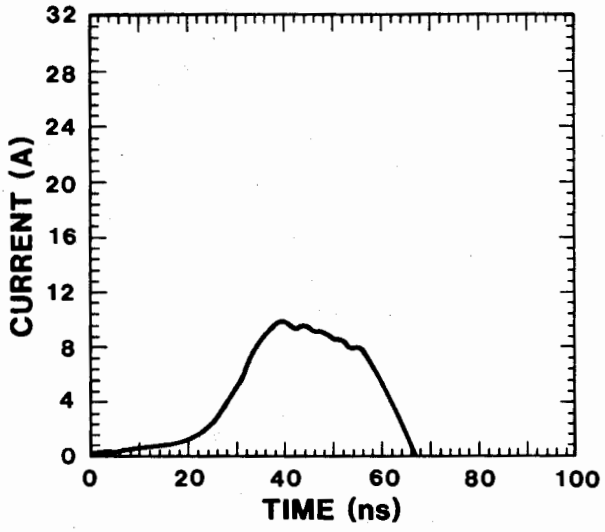

CRYSTAL DIAMETER: 175 MILS
CRYSTAL THICKNESS: 16.5 MILS
ELECTRODE DIAMETER: 95 MILS

CABLE LENGTH: 5 IN.

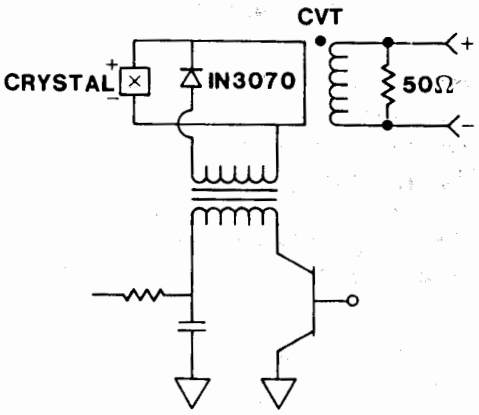

SERIAL NO.: X112
TEST DATE: 4-3-85
PULSE WIDTH (@3.5 A): 35.2 ns
PULSE WIDTH (@50%) : 30.7 ns
RISE TIME (25% - 75%): 8.6 ns
PEAK AMPLITUDE: 10.01 A (CVT)
TEST TEMP: 25 °C

Figure 9. Transducer Response with Diode Continuity Self-Check

A. BI-ANNULAR

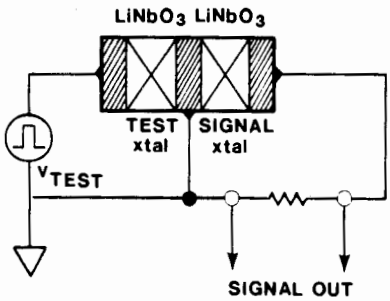

B. BACK-TO-BACK

C. LITHIUM NIOBATE ($LiNbO_3$)

Figure 10. Bi-Annular and Back-to-Back Approaches

2.2 BI-ANNULAR AND Y-CUT/Z-CUT BACK-TO-BACK APPROACHES

These methods are shown in Figure 10A and 10B. A "cut" is defined as the orientation of the lithium niobate crystal when it was removed from its parent boule (Figure 10C). (As is obvious from the rounded appearance of the boule, lithium niobate is not a naturally grown crystal.) Lithium niobate seemed to be ideal for this kind of self-check because its piezoelectric output is high--4 to 12 times greater than that of quartz. Both the bi-annular and the Y-cut/Z-cut options pulse a test crystal. The mechanical energy generated from the deformation was to be coupled into the signal crystal and reconverted by the reverse nature of the piezoelectric effect into an electrical pulse to indicate the functionality of the signal crystal. The back-to-back approach had the advantage of using a Y-cut test crystal with 100 times the electrical output of the Z-cut signal crystal. The bi-annular option had the advantage of using independent concentric crystals on a single homogeneous slab of lithium niobate. It was hoped that this would eliminate manufacturing problems associated with the back-to-back configuration and increase the mechanical coupling between the crystals. Unfortunately, the drawback to good mechanical coupling was a high capacitive coupling, which masked the piezoelectric effect generated in the bi-annular approach. Figure 11 shows two test fixtures used to evaluate the bi-annular piezoelectric response. In the one on the right, a lithium niobate crystal was used; in the other, a sapphire crystal was used. The piezoelectric properties of sapphire are virtually nil compared to those of lithium niobate. In both cases, only capacitive coupling was observed when a 200-V, 1-ms pulse was applied to the test crystal. Other tests with the back-to-back configuration yielded similar results.

2.3 PYROELECTRIC EFFECT

The fourth option was the pyroelectric self-check. This method looked promising and, oddly enough, gave a "back door" approach to generating the piezoelectric effect wanted in the bi-annular and back-to-back configurations.

The following crystal theory is presented in order to explain the lab tests. Figure 12 shows how different crystal cuts are removed from a lithium niobate boule. Quartz is not a ferroelectric crystal and has no pyroelectric properties, but is shown here for comparison only. Both quartz and lithium niobate belong to the trigonal system. Of the 20 piezoelectric crystal classes, 10 are characterized by their unique polar axis; that is, an axis that shows properties at one end different from those at the other. Lithium niobate belongs to one such class (Class 19, Ditrigonal Polar, C_{3v}); quartz does not (1). Lithium niobate's unique polar axis is the Z-axis. Crystals in these classes are called "polar" because they are permanently polarized. Generally, this permanent polarization cannot be detected by charges on the surface of the crystal because the charges have been compensated through external or internal conductivity. Uniform temperature is critical to the value of permanent polarization. Temperature fluctuations in the crystal change the polarization, and electric charges can be observed on the crystal faces

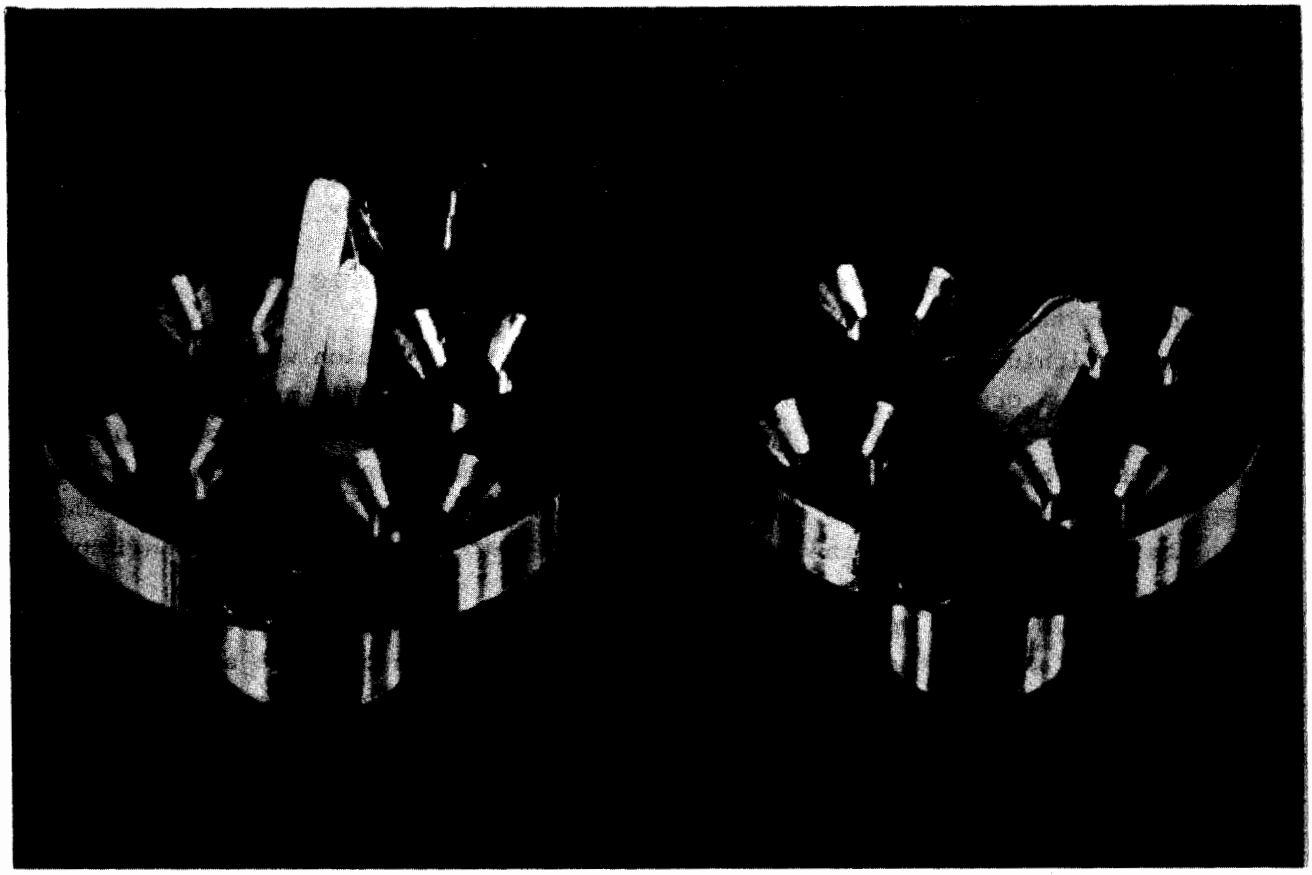

Figure 11. Bi-Annular Test Fixtures

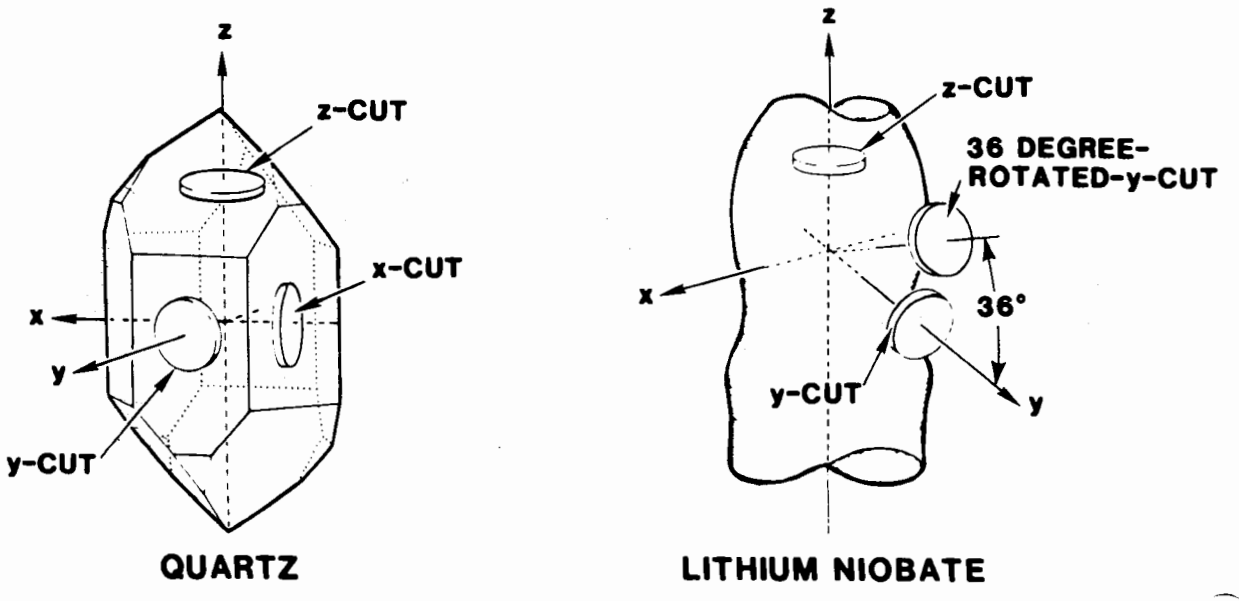

Figure 12. Crystalline Structure

perpendicular to the polar axis, a condition known as the pyroelectric effect. An estimate of the charge generated by the pyroelectric effect alone is not difficult. However, every pyroelectric crystal is also piezoelectric, which means that temperature changes cause mechanical deformation of the crystal faces, producing a secondary polarization that is superimposed on the pyroelectric effect. Because this complication can result in a "false" pyroelectric effect that could dominate and yield an invalid estimate, it is not a trivial matter. Whatever the source of polarization, however, if it is a true indication of the crystal's integrity, the pyroelectric method is a viable self-check.

The first experiments to quantify the pyroelectric pulse used the apparatus in Figure 13. A description of the hardware can be found in Reference 2. Essentially, the lithium niobate crystal (125 mils in diameter by 16.5 mils thick) was uniformly heated by a flashbulb located 7 cm from the crystal. The charge generated by the radiant heat was collected on the 95-mil-diameter electrode and input to a charge amplifier. The output was stored on an oscilloscope. The charge amplifier was an inverting type (Model 504A Kistler), which provided good zero stability and variable gain. The frequency response was flat within 5% from near dc to 100 kHz. This device permitted selection of the input resistance to allow for drift-free dynamic operation. The extra cable shown on the transducer housing was a means of thermally exciting the crystal internally (explained later).

The basic physics of these experiments is summarized in Figure 14. At the 7-cm distance, 1.8 joules/cm^2 was deposited on the chromium gold layer. Taking the crystal area into account, the heat energy was only 0.08 J. The bulb temperature was $\cong 3300^{\circ}C$ and emitted (according to the Wein Law) its maximum energy at $\cong$8000 Å. Only 4% of the normal incident radiation was absorbed by the gold. Since the transmission of gold was essentially 0% for these wavelengths, the maximum energy available for charge generation in the lithium niobate was 0.0032 J (0.007 calories). Assuming that the specific heat capacity was constant over a small temperature interval, ΔT was $\cong 15^{\circ}C$. The pyroelectric charge generated was estimated to be $\cong$242 pC. The quantity of energy per unit time that was emitted from the bulb filament is shown in Figure 15, and the charge signature of the crystal's temperature gradient is given in Figure 16. The leading edge was crystal produced; the trailing edge depended on instrumentation time constants. The overall response pulse width was $\cong$50 ms. The amplitude of 210 pC compared well to the 242 pC calculated. Keep in mind that this experiment was ideal in keeping thermal stresses to a minimum.

A better method of controlling the applied heat energy was an arc lamp (Figure 17). The Oriel, Inc., 150-W xenon lamp used in the experiment had prominent output spectral peaks between 7500 and 9000 Å. The lamp housing allowed radiant energy to be focused on the crystal. At a 1-s exposure, the arc lamp test apparatus could provide a range of energy inputs (0.02J to 0.1J). The electronic shutter controlled total exposure time and allowed the energy input to be quantified. Figure 18 shows the transducer housing in its iris diaphragm fixture, which provided

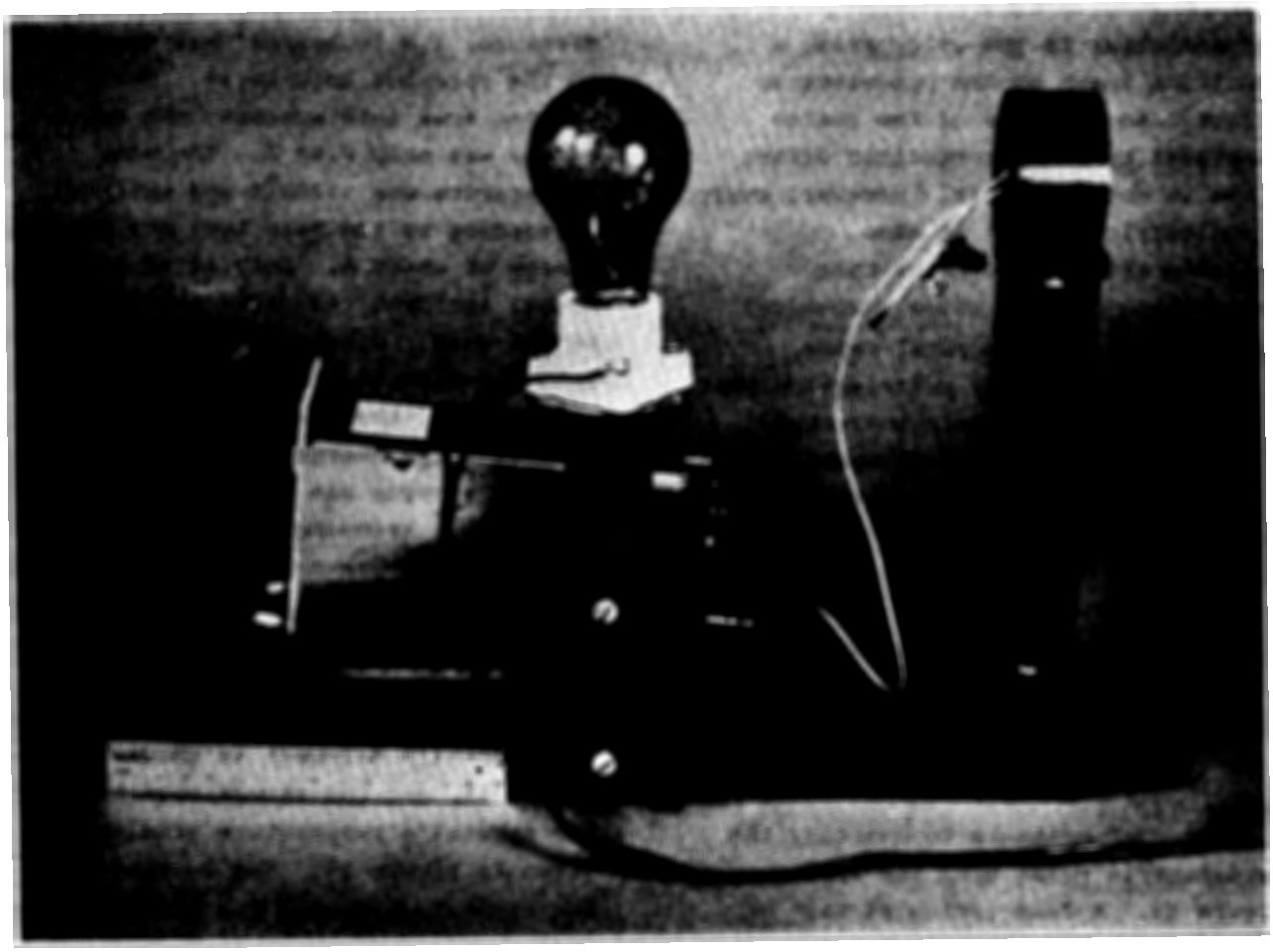

Figure 13. Radiant Heat Apparatus

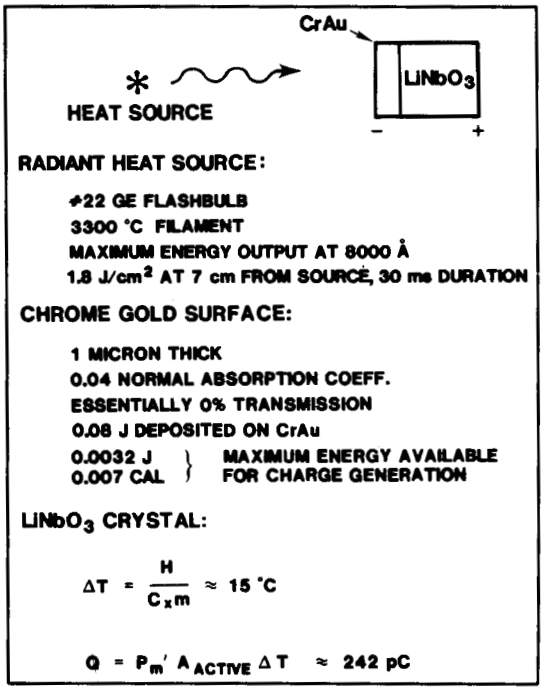

Figure 14. Radiant Heat Calculations

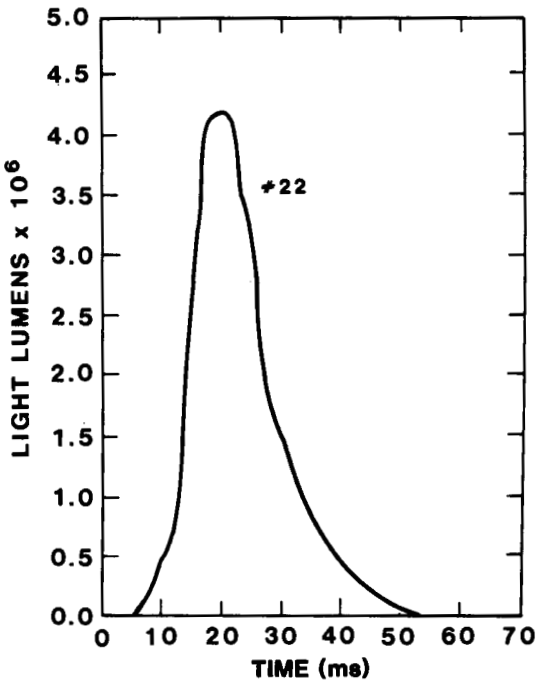

Figure 15. Radiant Heat Input

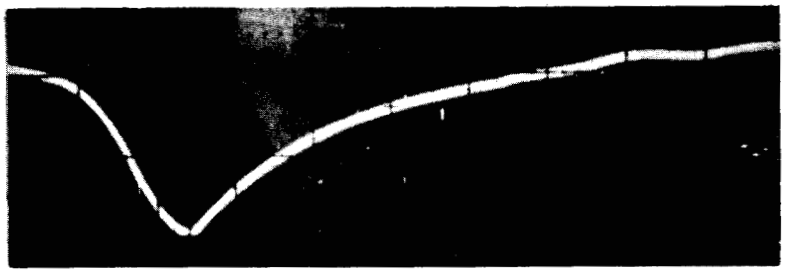

Figure 16. Pyroelectric Response — Flashbulb

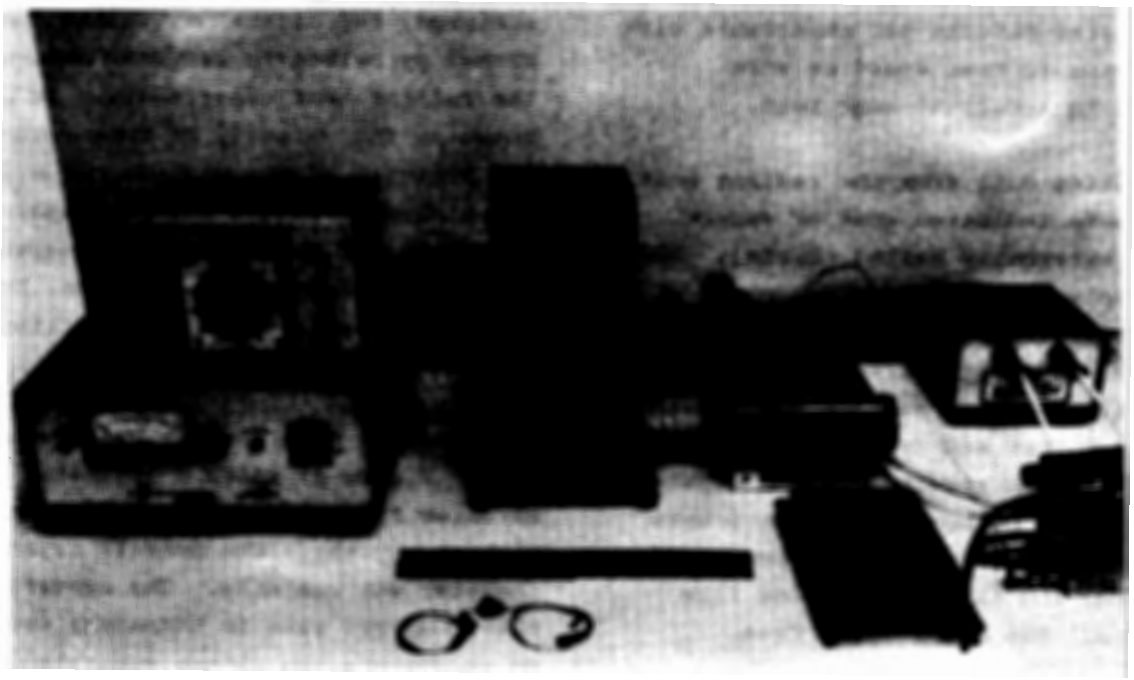

Figure 17. Arc Lamp Apparatus

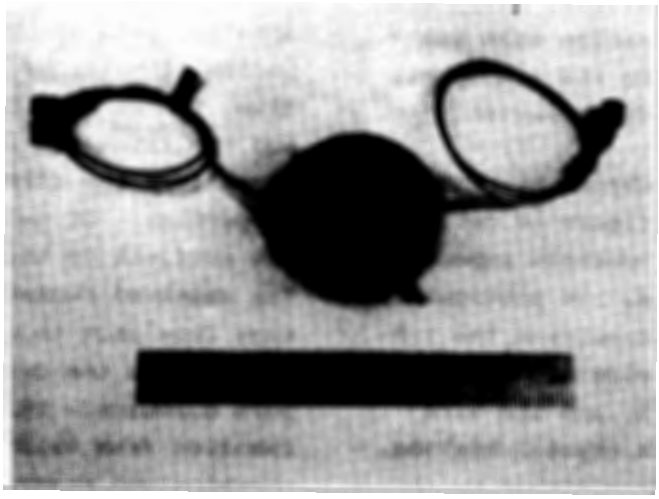

Figure 18. Iris Diaphragm Fixture

aperture size control. The arc lamp was calibrated within 2% by means of a laser power meter (Scientech, Inc., Model 36) for a fixed geometry from the xenon lamp. The response (Figure 19) had a peak value of 4.3 pC with an energy input of 0.02J. The energy generated by the arc lamp was approximately 10^4 to 10^5 times greater than the ultrasonic nondestructive test currently used in the product tester. Because the energy input was much higher, it is believed that crystal defects not observable with the ultrasonic test would be more apparent in a radiant heat test.

The baseline data from the radiant heat experiments indicated what to expect from an externally heated crystal. The next step was to evaluate the pyroelectric response from heat generated inside the transducer. Figure 20 shows two cables exiting the housing--one for output and one connected to a heating element attached to the crystal. Various types of heating elements were evaluated; nichrome wire, chromium film resistors, and tantalum nitride film resistors. The progression from nichrome to chromium evolved from assembly difficulties and the improved thermal conductivity to the crystal provided by the film resistor. Tantalum nitride was evaluated because it is more stable in terms of oxidation than the chromium when exposed to the atmosphere and because it had a higher resistivity.

Figure 21 shows the nichrome heating element concept. The figure is not drawn to scale because certain aspects needed to be emphasized. In particular, an epoxy was sandwiched between the 1.5-mil-diameter nichrome wire and the lithium niobate crystal, and the wire did not provide uniform crystal heating. Figure 22 shows the pyroelectric response of unit P5 when a 28-V, 1-ms voltage pulse was applied to the nichrome wire (resistance 47.6Ω). This output was different from the charge signature generated by radiant heat methods. The capacitive coupling first observed had the same width as the input pulse. It is believed that the crystal's rising stress response superimposed on the capacitive coupling caused the coupling's rise. After the peak positive stress response was achieved, the crystal exhibited the normal pyroelectric response observed in the radiant heat experiments. As a check on the validity of this result, the polarity of the voltage pulse into the nichrome element was reversed. As expected, the polarity of the capacitive coupling changed also. However, the crystal response after the coupling was finished was identical.

The chromium film concept was evaluated next. Figure 23 shows a sputtered chromium film resistor on a lithium niobate crystal. The overall crystal diameter was 225 mils. The center electrode (95 mils in diameter) was used to accumulate the charge generated by the heat pulse as well as the explosive monitor signal. The dark annular area was chromium with gold pads for soldering. The total resistance was the parallel path of the annulus. The inside diameter of the film was 120 mils, the outside diameter was 205 mils, and the thickness was 3000 Å. Figure 24 summarizes the film's basic physical properties. Of particular interest was the estimate of the parallel resistance. The observed resistance was found to vary from unit to unit and was always higher than the calculated value for pure chromium. This higher resistance resulted from oxidation when the chromium was exposed to the atmosphere.

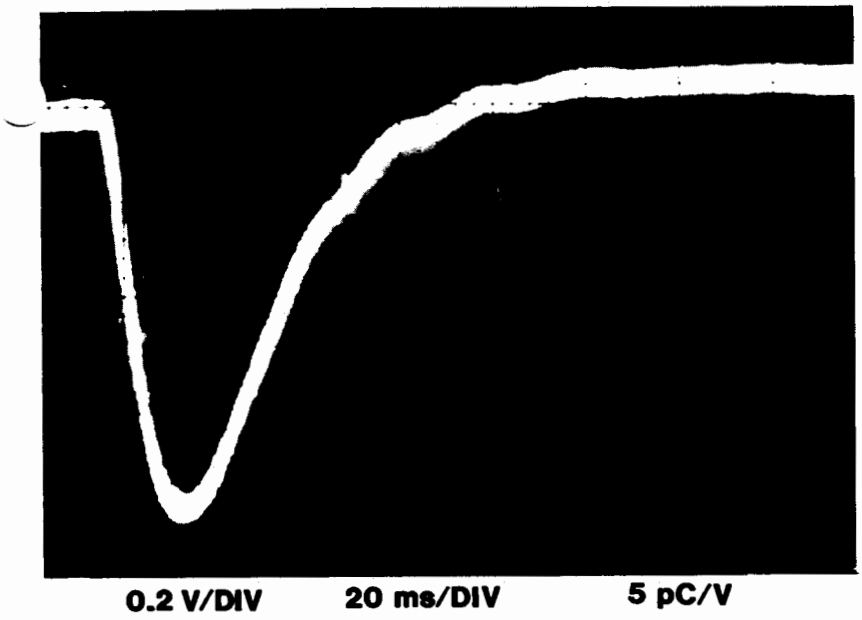

Figure 19. Pyroelectric Response — Arc Lamp

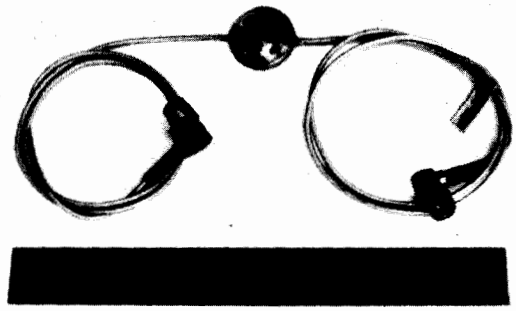

Figure 20. Transducer Housing with Self-Check

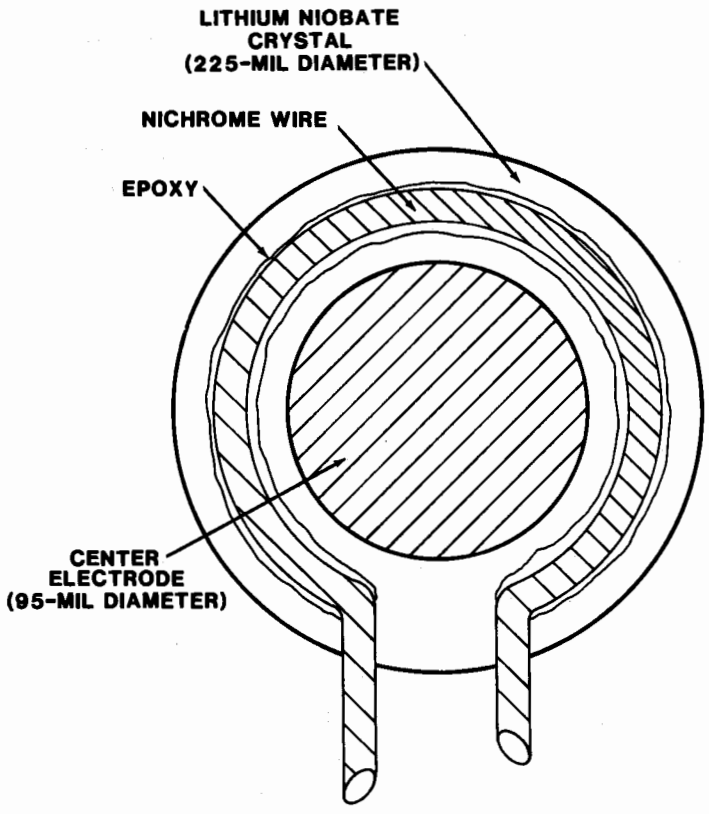

Figure 21. Pyroelectric Self Check — Nichrome

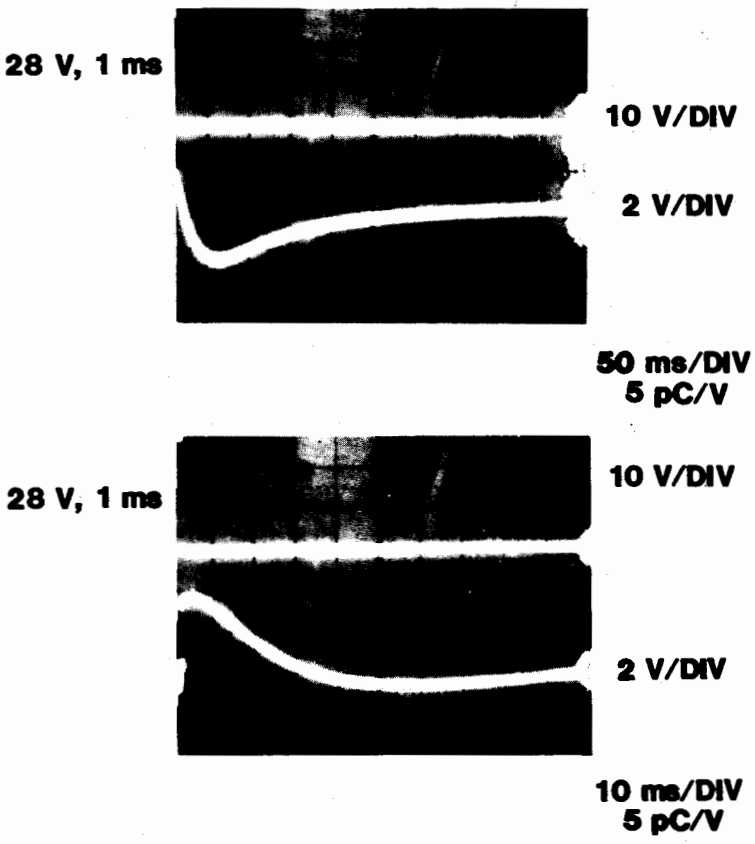

Figure 22. Pyroelectric Response — Nichrome

When a 100-μs, 28-V pulse was applied to the film (Figure 25, top trace), the response characteristic of the film (lower trace) was substantially different from the charge signature using the arc lamp. Presumably, this was because thermal stresses were no longer insignificant and apparently predominated for much of the pulse. As before, the part of the output that ramped and corresponded to the 100-μs input represented the capacitive coupling through the charge amplifier with the rising stress response superimposed on it. The peak positive charge was 41.2 pC and the pulse duration was 10 ms. Lab tests have shown that it is possible to minimize (and perhaps cancel) the capacitive coupling by applying bipolar complementary pulses to each end of the film resistor. Figure 26 is a plot of charge versus voltage input and shows how the charge generated for low voltages is proportional to the square of the voltage or power input. At higher voltages, the points deviated because the temperature coefficient of resistance became significant and increased the film's overall resistance. This in effect lowered the amount of power actually applied to the lithium niobate. An estimate of the change of temperature on the film with a 45-V, 100 μs input pulse was 300°C. Although this temperature was not enough to depole the crystal, it generated large strains that could account for the drastic sign change in the response.

An inherent characteristic of the pyroelectric self-check was that the self-check signal (charge in picocoulombs) is fundamentally different from the transducer monitor signal (current in amperes). Each required different kinds of circuitry for detection (charge amplifier versus CVT). As a further complication, the telemetry system required that the self-check be done without elaborate switching that could reduce the overall reliability of the system. Figure 27 shows one possible solution. The key element is the diode which prevented the CVT from interfering with the pyroelectric self-check. The charge generated by the crystal could not forward-bias the diode. Also, when the explosive was fired, the diode easily conducted the high current to the CVT. The charge amplifier was designed to have a high enough input impedance to minimize its loading effect on the detonator response. Division 7545 lab tests determined the specific diode required (FDH300), and subsequent tests have shown this concept works during explosive actuation. Figure 28 shows the transducer response with the self-check circuit load. Note that the rise time was <10 ns, the pulse width was >30 ns, and the correct amplitude (given below the plot) was above the 10-A level. The plot itself was the raw data without appropriate correction factors. Figure 29 is an artist's conception of the transducer showing the details of the chromium film resistor and its output without the charge amplifier load.

The tantalum nitride (T_aN_2) film evaluation yielded no surprises. Tantalum nitride avoided the oxidation problem of chromium when exposed to the atmosphere and possessed a higher resistivity. The higher resistivity could be useful in determining "fact of occurrence" at explosive actuation. Figure 30 shows a 240-mil-diameter by 10-mil-thick lithium niobate crystal with the 430-Å-thick tantalum nitride film resistor. The gold-center

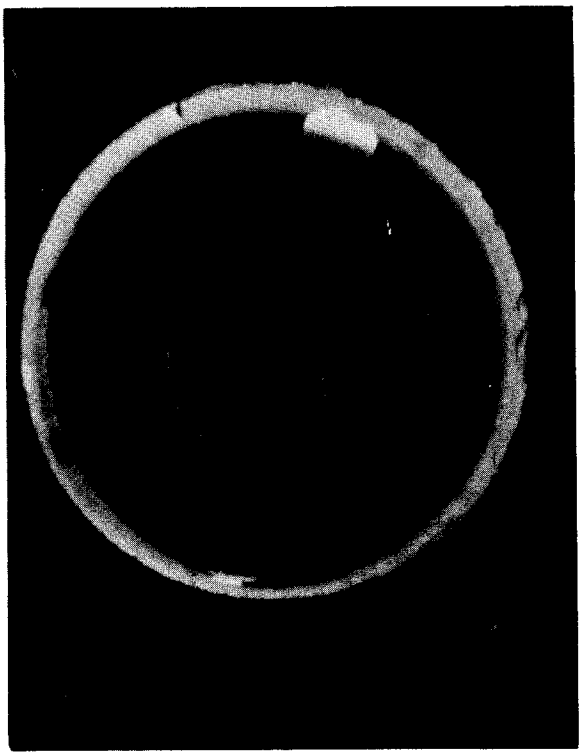

Figure 23. Chromium Film Resistor

PHYSICAL CONSTANTS

MATERIAL:	PURE CHROMIUM
DENSITY:	7.20 gm/cm^3
SPECIFIC HEAT:	0.448 J/gm °C
RESISTIVITY:	12.9 $\mu\Omega \cdot$ cm
MELTING POINT:	1857 °C

DIMENSIONS

FILM I. D. :	0.120 INCHES
FILM O. D. :	0.205 INCHES
THICKNESS :	3000 ANGSTROMS

CALCULATED PARAMETERS

VOLUME :	3.73 μ(cm^3)
MASS :	26.9 μgm
RESISTANCE OF PARALLEL COMBINATION :	PURE - 2.6 Ω OXIDIZED - 16.1 Ω

OBSERVED RESISTANCE

16 TO 63 Ω

Figure 24. Chromium Film Properties

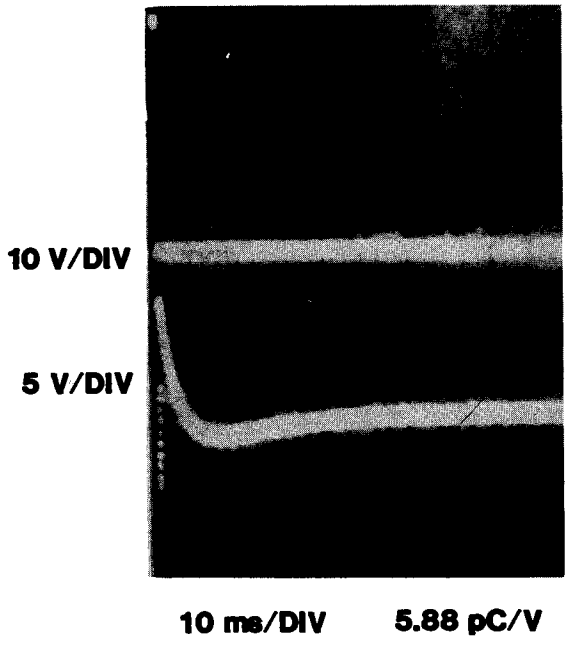

Figure 25. Pyroelectric Response — Chrome Film

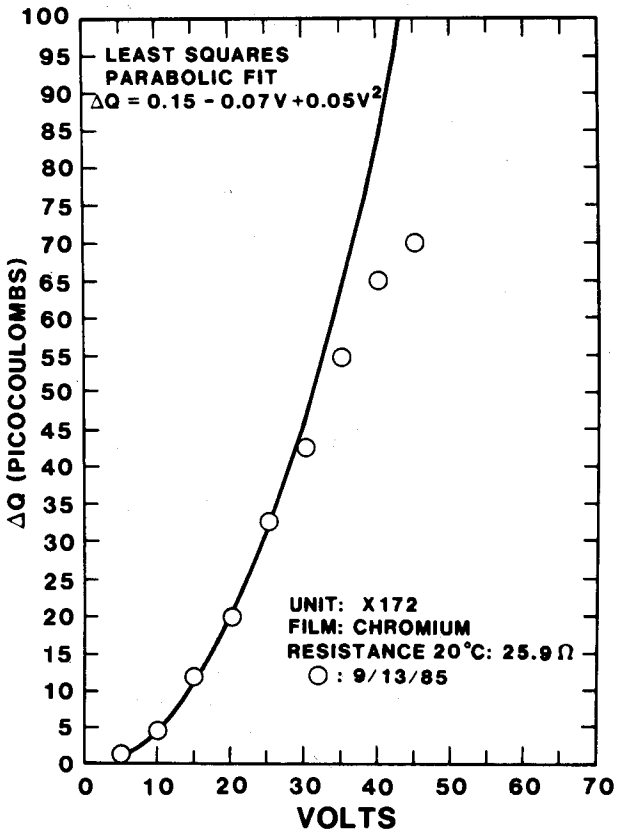

Figure 26. Charge Response Curve

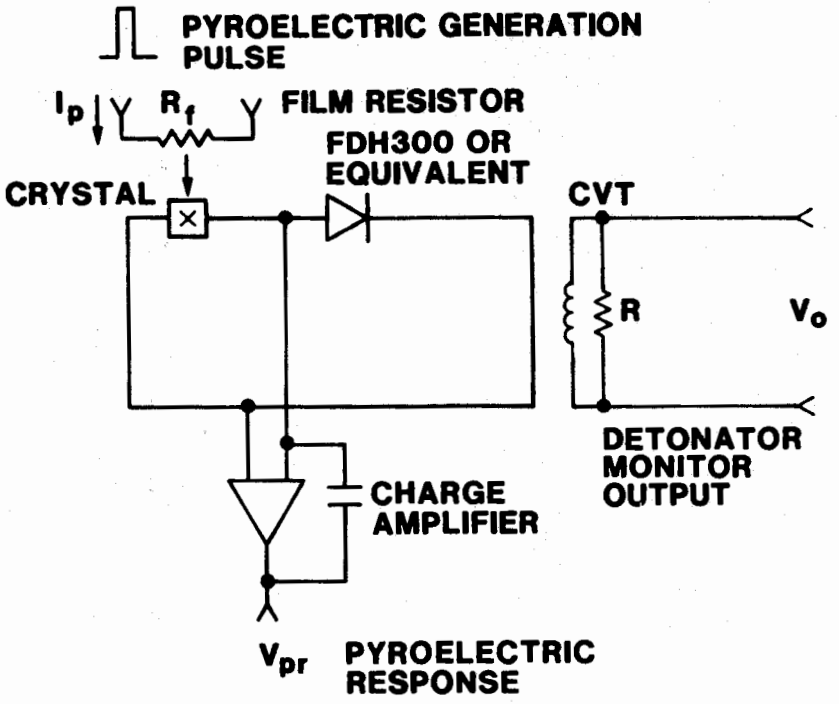

Figure 27. Pyroelectric Implementation

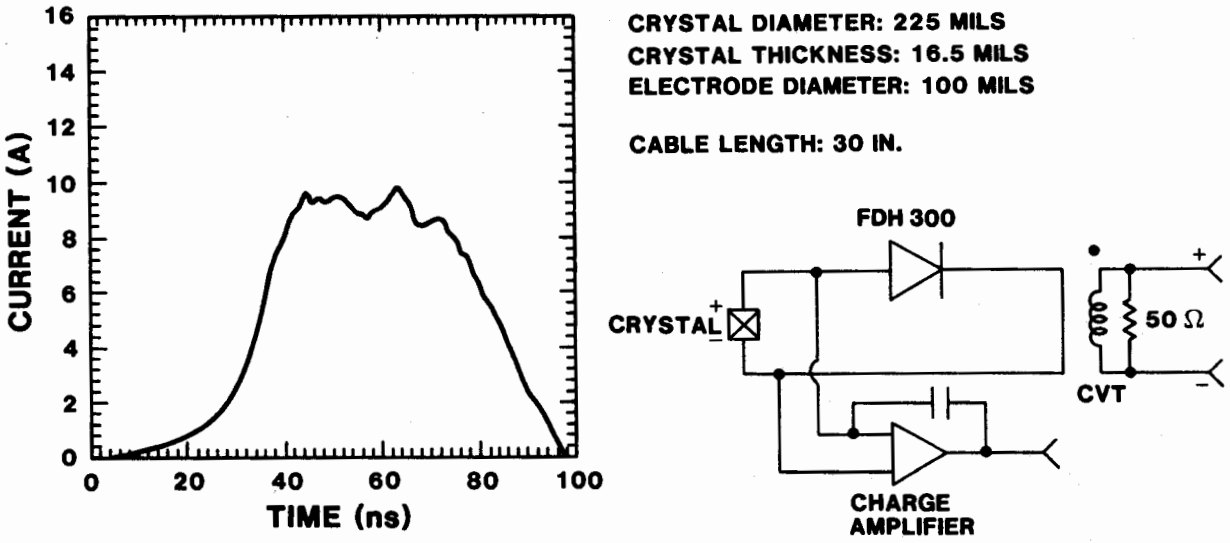

SERIAL NO.: X171
TEST DATE: 9-3-85
PULSE WIDTH (@ 4 A): 55.07 ns
PULSE WIDTH (@ 50%): 50.50 ns
RISE TIME (25% - 75%): 8.75 ns
PEAK AMPLITUDE: 10.356 A
TEST TEMP: 24 °C

Figure 28. Transducer Response with Pyroelectric Self-Check Circuit Load

electrode was 95 mils in diameter. Figure 31 shows the crystal's response when a 28-V, 100-μs pulse was applied. Note the shape similarity to the chromium response and the reduction in amplitude (0.4pC). This particular unit had a film resistance of 1227 Ω. With a resistance this high and the same input pulse, less energy was actually available for charge generation within the crystal. Figure 32 shows the response when the explosive was fired. The rise time, pulse width, and amplitude all met specifications. This response was observed with the self-check circuit load in place. In comparison to Figure 28, the rise time was 34% shorter and the amplitude was 35% higher. The reason for this difference appears to be the fact that the crystal was more than 50% thinner. The transducers mechanically shocked in three axes at 2000 g's, 1 ms (haversine) successfully performed the pyroelectric self-check and explosive monitor response. The schematic in Figure 33 shows the charge amplifier used during the tests. In this configuration, resistor R1 in the charge input was added to the design used for the chromium film tests in order to increase the input impedance.

CONCLUSION

This report has described two self-check schemes: the continuity loop concept and the pyroelectric effect. The continuity loop self-check can exercise a data acquisition system. However, this does not check the integrity of the crystal. As an alternative, the pyroelectric self-check verifies the crystal state-of-health as well as its connections. This particular method uses a crystal property usually considered detrimental to a piezoelectric transducer. In summary, the lithium niobate explosive monitor is a useful device for varied measurements in which the temporal resolution must be at least an order of magnitude better than that of the measurand expected. The explosive industry which manufactures aerospace and aircraft systems for initiation, separation, thrust termination, and time delay could use this device to quantify shaped explosive charges. Since explosive testing of such systems is usually expensive, a transducer self-check capability is a valuable tool in determining system functionality prior to explosive detonation.

ACKNOWLEDGMENTS

The author thanks R. W. Bruner and C. H. Bundy at General Electric Neutron Devices in Largo, Florida, for their assistance during this study. In addition, he thanks the following Sandia Personnel who provided support: R. A. Graham, 1131; D. J. Sharp, 1831; W. R. Conley, 7471; R. G. Sharrer, 5145, who suggested that the diode be used in the self-check system; and M. S. Rogers, R. R. Precit, and W. D. Fisher, 7545.

REFERENCES

1. Walter G. Cady, Piezoelectricity: An Introduction to the Theory and Applications of Electromechanical Phenomena in Crystals (New York: McGraw-Hill Book Company, 1946), pp 16-38, pp 200-225.

2. Hilten, Vezzetti, Mayo-Wells, and Lederer, A Test Method for Determining the Effect of Thermal Transients on Pressure-Transducer Response. National Bureau of Standards Report NBS TN-905, SD Cat. No. C13.46:905

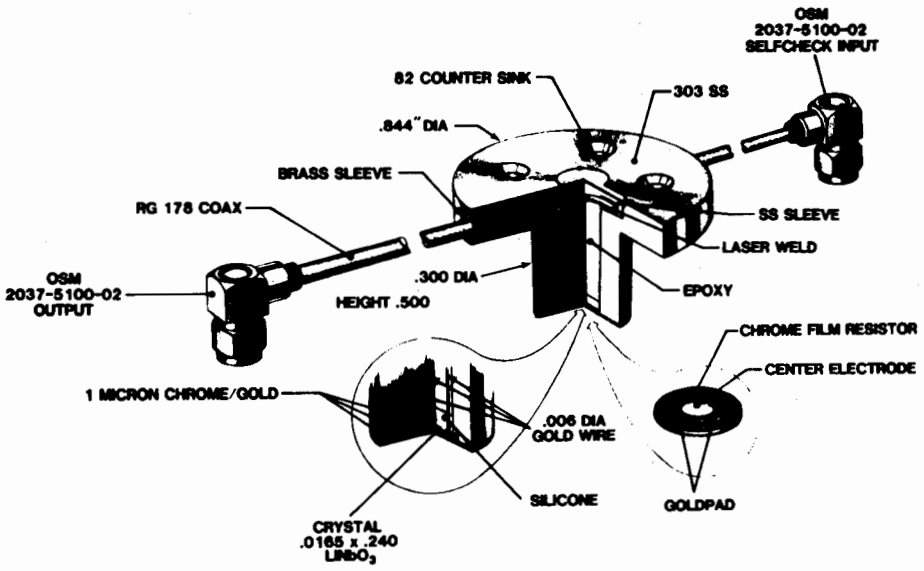

Figure 29. Artist Conception

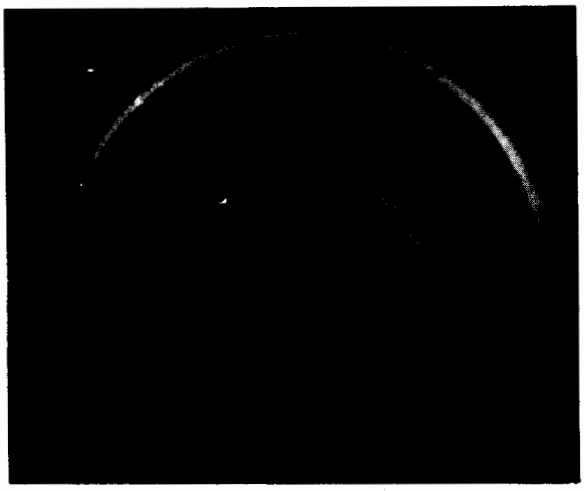

Figure 30. Pyroelectric Self-Check — Tantalum Nitride

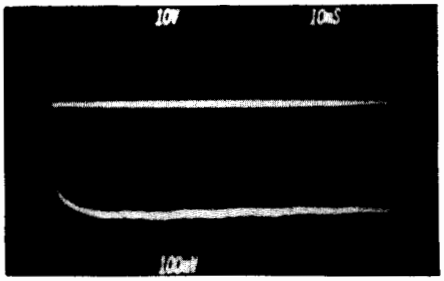

Figure 31. Pyroelectric Response — Tantalum Nitride

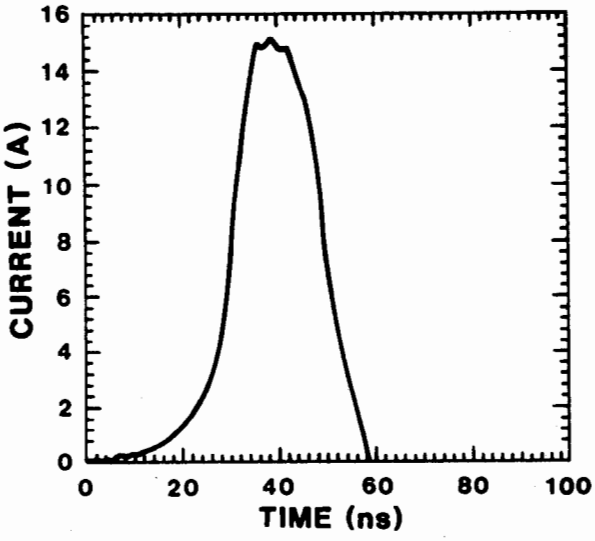

CRYSTAL DIAMETER: 240 MILS
CRYSTAL THICKNESS: 7.93 MILS
ELECTRODE DIAMETER: 100 MILS

CABLE LENGTH: 30 IN.

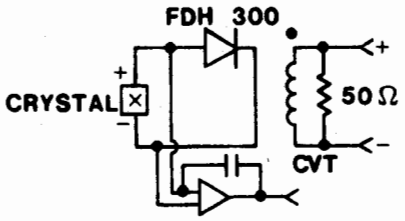

SERIAL NO.: X196
TEST DATE: 10-31-85
PULSE WIDTH (@ 4 A): 27.60 ns
PULSE WIDTH (@50%): 20.80 ns
RISE TIME (25% - 75%) : 5.60 ns

PEAK AMPLITUDE: 15.849 A
TEST TEMP: 25° C

Figure 32. Transducer Response with Pyroelectric Self-Check Circuit Load

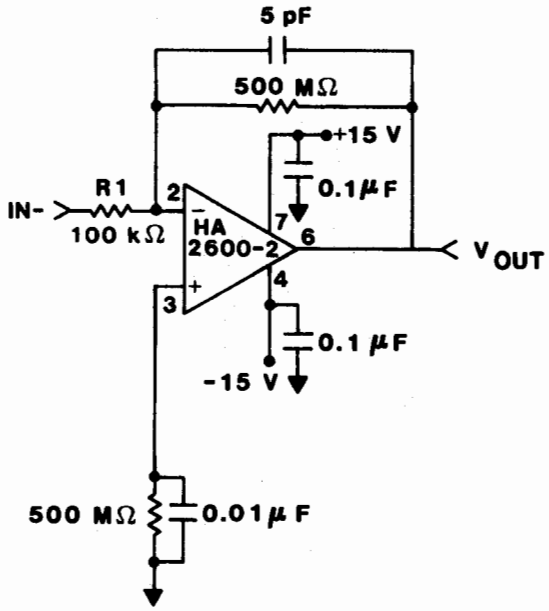

Figure 33. HA2600-2 Charge Amplifier Design

Q: Dr. R. Maglic: What is the crystal orientation of the lithium niobate? I would think that you would have two temperature responses because of heat conductivity in the pryroelectric region. There will be two time responses: one to the temperature flow and one to the dipole reorientation. And that would be theoretic. Do you feel it is fast enough to record what you want it to see? What is the effect and what is the instrument capability and maximum frequency?

A: Steve Kuehn (Sandia National Laboratories, Albuquerque, NM): We are talking about the time effects on this device. The orientation of the crystal is a Z-cut crystal.

Q: Dr. R. Maglic: Is it a 111?

A: Steve Kuehn: Yes.

Q: Dr. R. Maglic: How are those two time constants optimized? You have propagation of heat and you have reorientation of a dipole. These are totally different physical phenomenon.

A: Steve Kuehn: The question is whether or not we optimized the two time constants you are talking about? No, we did not. The idea was simply to verify that the crystal was functioning in some way. Further research at GEND probably yields that sort of optimization. At this point in the development of the device, the idea was did we get a charge signature, and does it indicate how well that the crystal is functioning. What we are looking at is a method to verify the crystal integrity. We did not optimize certain parameters of the temperature coefficients, for example.

Q: Dr. R. Maglic: What's the Curie temperature of the lithium niobate?

A: Steve Kuehn: 1500°C.

Q: Ronald B. Tussing (Naval Surface Weapons Center): As I understand, your measuring arrival time is your shock wave, and so just to clarify this in my mind, you are using a pyroelectric effect to check it. I take it the unit disappears before the pyroelectric effect from the explosion itself. Is that correct?

A: Steve Kuehn: Are you asking about the time from when we do the pyroelectric effect to when we actually fire the explosive?

Q: Ronald Tussing: No. Does the explosive itself contribute to what the unit would see or give a pyroelectric effect output from the explosive itself? Unless that's behind the shock waves, the unit would disappear before you get two pulses. Is that correct?

A: Steve Kuehn: No. Your question is when do we see an output pulse and is the pyroelectric pulse generated by the explosive that we use? The explosive is so fast that it destroys the unit before a pyroelectric pulse can be generated.

Q: Ronald Tussing: That's what I was asking: it disappears before you get any pyroelectric effect from the explosion.

A: Steve Kuehn: Correct.

A: Ronald Tussing: Thank you. I had another use in mind for that.

Q: Torben Licht (Bruel & Kjaer Instruments): You are distinguishing between charge and current in some strange way. To my knowledge the current is charged per second. What was the difference between the two things?

A: Steve Kuehn: The difference between charge and current in this application was because of the time involved. We did not want to measure, in a charge mode, an explosive detonation. There was no time especially when you are talking about nanosecond rise times. That is why I made the distinction. Certainly, physically there is an relationship there. One is the derivative of the other. In this particular device, there are two separate, different kinds of instrumentation and that was the distinction that I was trying to make.

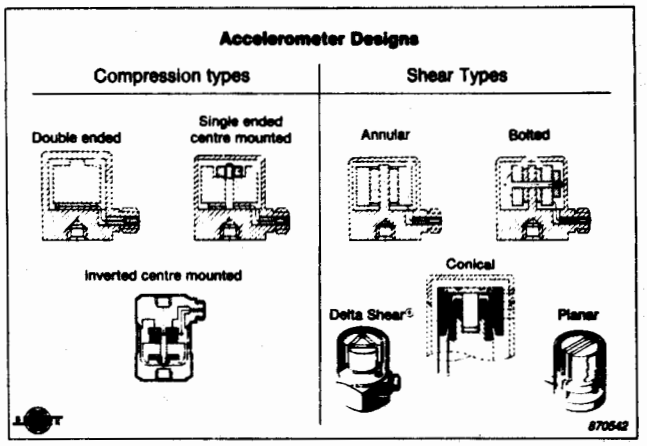

Fig. 3. Compression and Shear Type accelerometers

While the basic parameters for a piezoelectric accelerometer are independent of the specific design, the ability of the accelerometer to suppress the influence from unwanted environmental effects is a matter of design. Thus, the shear designs have some intrinsic advantages compared to compression designs. These advantages are inherent in the basic design of the sensing element.

BASE BENDING

When vibration is present, so too is bending of the vibrating surface and, provided that the accelerometer is properly mounted, the bending will be transmitted to the accelerometer base.

As indicated in Fig. 4, the forces resulting from the bending of the base will, for the compression design, act directly on the piezoelectric element and therefore a non-vibration related output will be generated. It should be noted that this output will appear at the frequency of the vibration and it cannot therefore be filtered out. In contrast, as also indicated in Fig. 4, for the shear design, base bending will not introduce shear forces on the piezoelectric element and no output will be generated.

It should be noted that even when a beryllium disc is inserted between the base and the piezoelectric element or when special designs of the base are made the compression-type accelerometer cannot match the shear design with respect to reducing base bending effects.

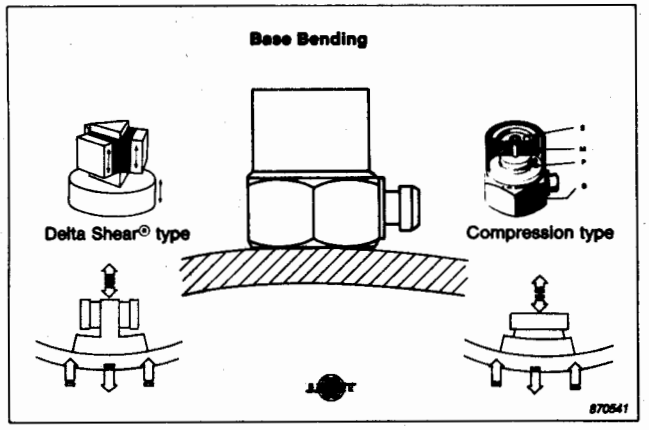

Fig. 4. Sensitivity of Shear and Compression type accelerometer to Base Bending

BASE BENDING TEST RESULTS

The standard method for measurements of base strain sensitivity (described in ISO/DIS 5347 and ANSI S 2.11-1969 and originally in ANSI Z 24.21-1957) is to use a steel beam with dimensions of 3″ × 0,5″ × 57″ or 76 × 12,5 × 1240 mm^3 clamped at one end. The accelerometer under test and a set of strain-gauges are placed at a distance of 1,5″ or 40 mm from the clamp. The beam is excited by hand. At a strain level of 250 $\mu\epsilon$ peak, the corresponding peak output from the accelerometer is measured.

An improved method was used to obtain more detailed information. The excitation was applied by a Brüel & Kjær Vibration Exciter Type 4805/4814 driven by a Brüel & Kjær Frequency Analyzer Type 2032/34. This was also used to analyze the outputs from the transducers and the strain-gauges. Examples of the outputs are shown in Figs. 5, 6 and 7.

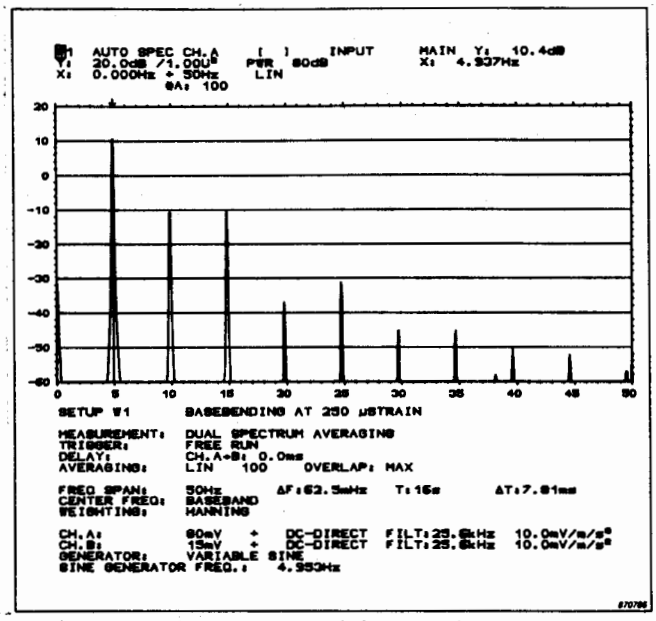

Fig. 5. Base Bending output signal from Brüel & Kjær Type 4371 Delta Shear® Accelerometer at 250 $\mu\epsilon$. Frequency range 0 – 50 Hz

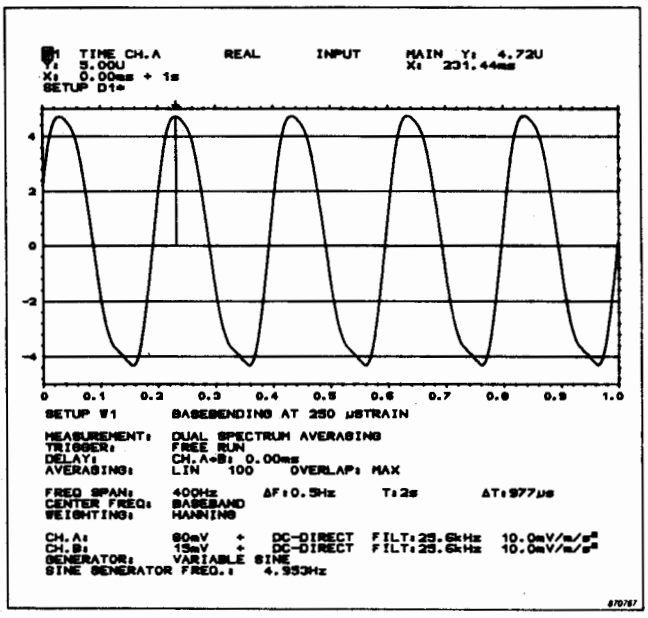

Fig. 6. Base Bending output signal from Brüel & Kjær Type 4371 Delta Shear® Accelerometer at 250 $\mu\epsilon$. 1 second time record

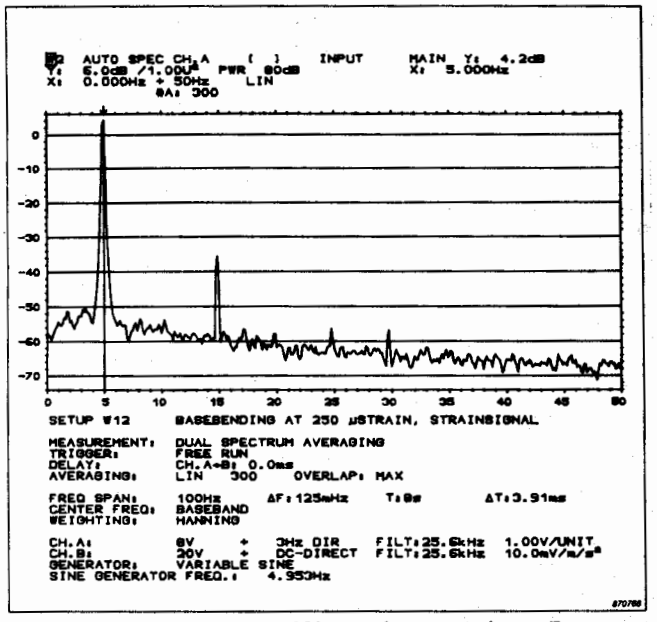

Fig. 7. Strain gauge output at 250 με on base strain beam. Frequency range 0 – 50 Hz

A number of measurements at strain levels from 10 με to 250 με were made to investigate the content of harmonics in the signals and the linearity of the Delta Shear® accelerometer Type 4371, with respect to this type of excitation.

The results are shown in Fig. 8 as the change in dB of the ratios between the accelerometer output and the strain input taken at the excitation frequency and at the 3rd harmonic.

It is seen that a reasonably good linearity exists up to about 100με, but then the transducer signal starts to be distorted, which gives lower output at the excitation frequency and higher distortion.

This example shows that perhaps the choice of 250 με peak as the proper excitation level does not always lead to useful results, especially because strains of that magnitude normally do not occur.

Furthermore the sensitivity at the third harmonic seems to be twice the sensitivity at the fundamental frequency of 4,75 Hz, i.e. the 3rd harmonic generated in the transducer is always bigger than the signal generated from strain at this frequency.

A number of different transducer designs were tested. An old Brüel & Kjær compression type was found to be more than 40 dB (100 times) more sensitive than the Delta Shear® accelerometer Type 4371.

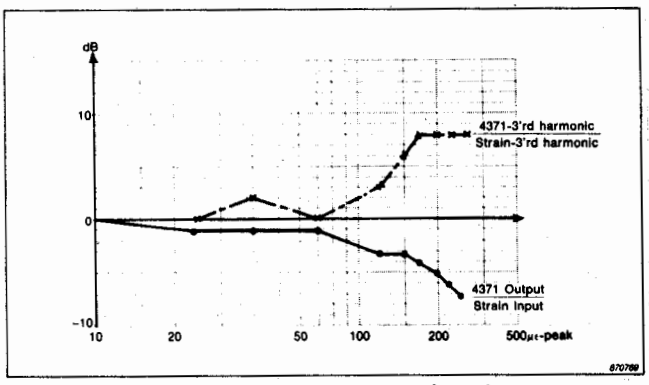

Fig. 8. Brüel & Kjær Type 4371 Delta Shear® Accelerometer output linearity for base strain 10 – 250 με

Different commonly used compression designs and some bolted, conical and annular shear types were tested. Base strain output levels 18 dB (8 times) to 33 dB (45 times) higher than the output from Type 4371 were found – which underline the efficiency of the Delta Shear® design.

TEMPERATURE TRANSIENTS

Generally, compression type accelerometers are much more sensitive to temperature transients than shear type accelerometers.

When exposing a piezoelectric accelerometer to temperature fluctuations, it will, due to pyroelectric effects and non-uniform thermal expansion/contraction of the sensing element, generate a non-vibration-related output.

When exposed to temperature fluctuations, all polarized piezoelectric materials will generate a charge on the surfaces perpendicular to the polarization direction. As seen from Fig. 9 in the compression design, these surfaces are the same as the ones from which the charge generated by the vibration is picked up.

Therefore accelerometers of compression design will give a non-vibration-related output due to pyroelectric effects when they are exposed to temperature fluctuations or transients.

In contrast the pyroelectric charge generation will, in the shear design, not show up on the surfaces where the charge generated by the vibration is picked up. Consequently the suppression of temperature transient effects is an inherent advantage of employing the piezoelectric element in "shear mode".

For the compression design, thermal expansion/contraction of the sensing element due to exposure to temperature transients will cause compression/tension forces to act on the piezoelectric element. As a result of this, a non-vibration related output will add to the pyroelectric effect. Again, in contrast to this, the shear design is highly insensitive to these effects.

Often compression design accelerometers employ quartz as the piezoelectric element as this material shows no pyroelectric effect. Still, the thermal expansion/contraction effects are so severe that these accelerometers have a temperature transient sensitivity which is much higher than the sensitivity of shear type accelerometers employing piezoelectric ceramics.

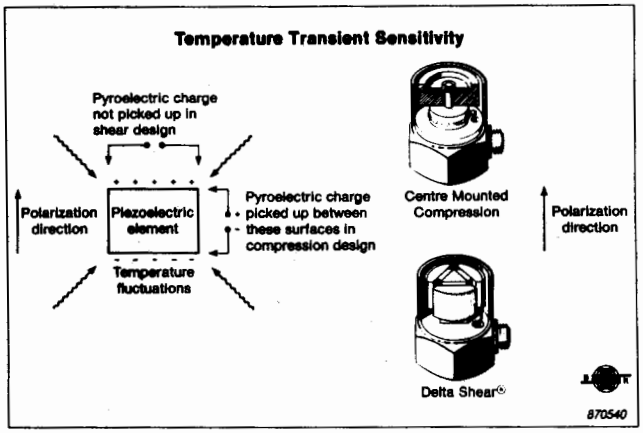

Fig. 9. Sensitivity of Shear and Compression type accelerometer to temperature transients

TEMPERATURE TRANSIENT TEST RESULTS

Three methods were used to measure the temperature transient sensitivity of the accelerometers under test.

A test method where the test accelerometer base is mounted on a heater element was employed to simulate effects from temperature changes of a structure (the ambient temperature being constant). To

simulate how an accelerometer responds to changes in the ambient temperature, the test accelerometer was mounted on a 5 kg aluminium block and hot air was blown on the accelerometer. The third method employed followed the guidelines given in ISO 5347. Here the accelerometer is mounted on an aluminium block. The block and transducer is then immersed into water with a temperature of approximately 50°F above the ambient temperature.

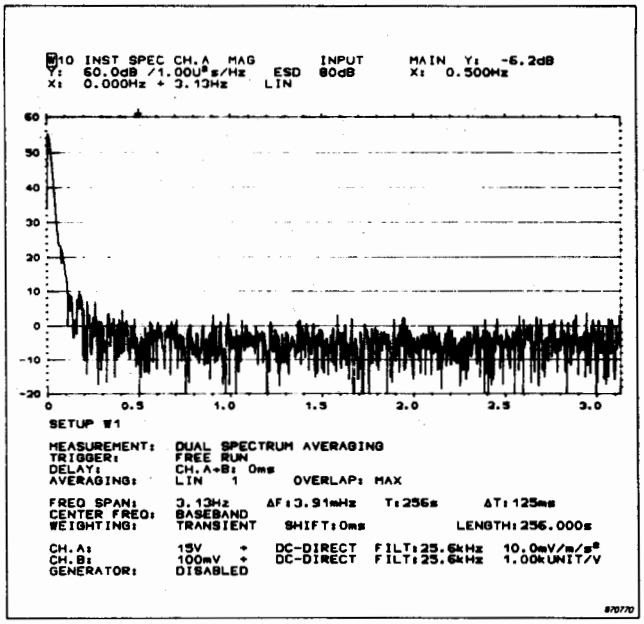

Fig. 10. Temperature transient response for Brüel & Kjær Type 4371 Delta Shear® accelerometer, heating of base

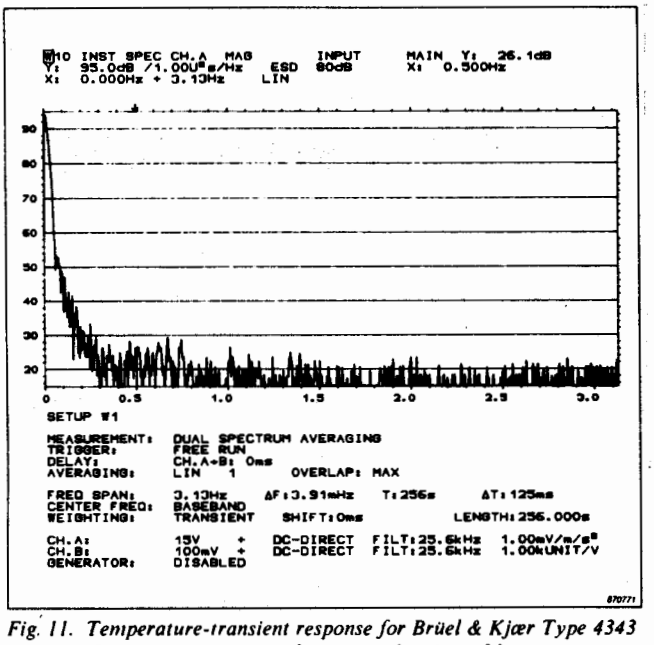

Fig. 11. Temperature-transient response for Brüel & Kjær Type 4343 Compression type accelerometer, heating of base

The temperature transient effects were measured in the time and frequency domain with a Brüel & Kjær Dual Channel Signal Analyzer Type 2032/34. The settings on the Brüel & Kjær accelerometer preamplifier used were LLF: 0,2 Hz ULF: 0,1 kHz.

The transducers tested were a Brüel & Kjær Type 4371 Delta Shear® accelerometer, an old Brüel & Kjær compression type accelerometer together with various other compression designs and some bolted, conical and annular shear accelerometer designs made by other manufacturers.

In general, significant peaks in the frequency spectra from temperature transient effects are found in a range below 0,5 - 2 Hz.

Also with respect to temperature transient characteristics, the measurements underlined the efficiency of the Delta Shear® design. Thus, for the Delta Shear® design, the maximum output from the temperature transient, when the base of the accelerometer was heated was 50 dB above the noise while the level for all other accelerometers was 70 dB or more above the noise. (See Fig. 10, 11 and 12). Thus as a 0,2 Hz LLF (one pole 20 dB/decade) was the setting used on the preamplifier, the LLF should be 60 Hz when using the Delta Shear® accelerometer and at least 600 Hz for all the other accelerometers in order not to lose dynamic range.

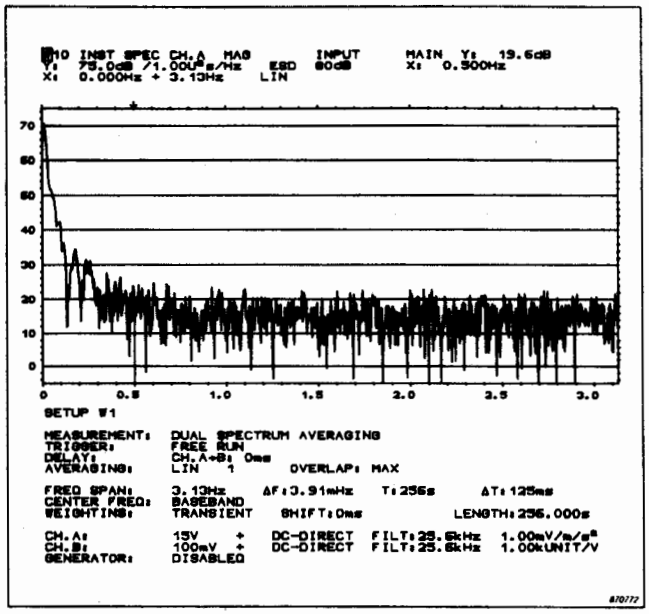

Fig. 12. Temperature-transient response for annular shear accelerometer, heating of base

The measurements have demonstrated that for low-level measurements and especially for low-level low-frequency measurements, the effects from temperature transients must be considered a very important noise source. The only way to cope with the noise is to try to limit the temperature fluctuation or to use an accelerometer like the Delta Shear® which has a low sensitivity to temperature transients.

One of the designs under test, a line drive compression type employing quartz as the piezoelectric element, showed a significant change in temperature transient sensitivity depending on how the transient was applied. For this accelerometer Fig. 13 and 14 show a difference of 10 times between the peaks in the spectra obtained by heating the base and blowing hot air onto the housing. The same thermal inputs gave two nearly identical peaks in the spectra from the Brüel & Kjær Type 4371 Delta Shear® accelerometer shown in Fig. 15 and 16.

The data given for this compression accelerometer seem to be obtained by only heating the base. Therefore, in practical use, where changes in the ambient temperature are the predominant form of exposure it is likely that the measurement error will be bigger than expected from the manufacturers specifications.

The two spectra in Figs. 13 and 14 illustrate yet another problem. To avoid overloading of the preamplifier, the gain is reduced by a factor of

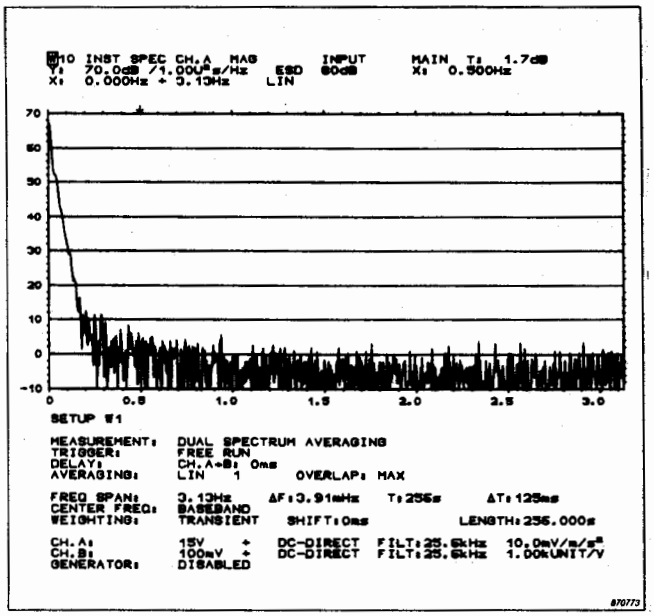

Fig. 13. Temperature-transient response of compression type accelerometer with built-in electronics, piezoelectric elements made of quartz, heating of base

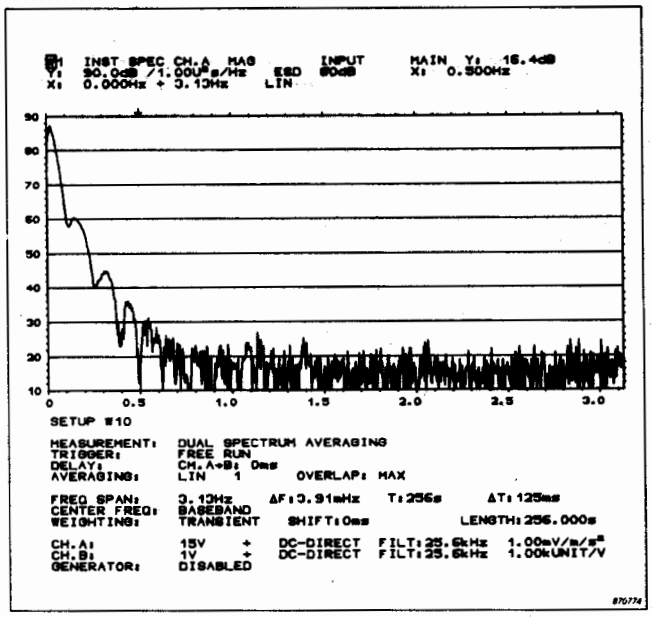

Fig. 14. Temperature-transient response of compression type accelerometer shown in Fig. 13. The only difference is that the temperature transient has been applied to the housing of the accelerometer

10 in Fig. 14, which gives a preamplifier noise floor corresponding to a ten times higher vibration. Thus if very high cut-off frequencies cannot be used, a significant reduction in the capability of the transducers to measure low level low frequency signals is the result. This could not be predicted from the manufacturers specifications.

ISO 5347 seems to give a good simulation of temperature transient effects as being a combined thermal exposure to base and housing.

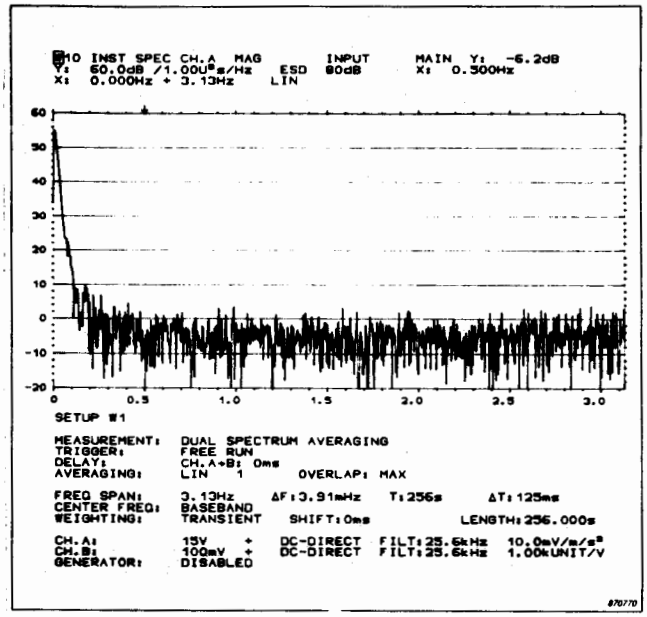

Fig. 15. Temperature transient response of Brüel & Kjær Type 4371 Delta Shear® accelerometer, heating of base

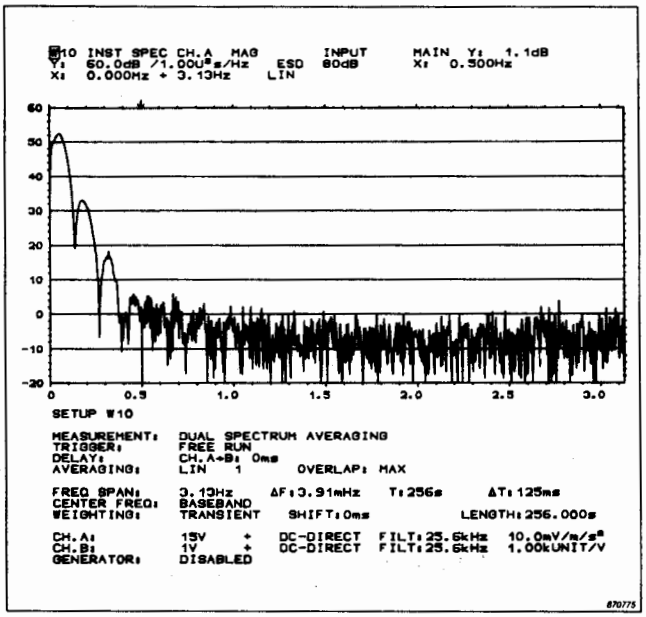

Fig. 16. Temperature transient response of Brüel & Kjær Type 4371 Delta Shear® accelerometer, heating of housing

CONCLUSION

The measurements made demonstrated that a proper accelerometer design is of great importance if good vibration data are required.

The measurements also demonstrated that a single value is generally not sufficient to give a proper evaluation of a transducer sensitivity to environmental effects. Not only the transducer time signal generated by the environmental exposure but also the frequency spectrum of this signal is necessary to reveal the overall behaviour of the transducer.

The measurements of base strain sensitivities in accordance with the standards indicated that measurements at lower strain levels give better

information. Thus at lower strain levels than prescribed in the standards 3 times higher base strain sensitivities were found.

Furthermore, the content of harmonics only 10–20 dB lower than the fundamental at higher strain levels is important information when possible sources of measurement errors are investigated.

The efficiency of the Brüel & Kjær Delta Shear® Design compared to a number of other constructions is proved by differences from 18 to 33 dB in the base strain sensitivities.

Measurements on temperature transient effects showed that these are generally characterized as having a very high amplitude in the low frequency region from 0 to 2 Hz.

The Brüel & Kjær Delta Shear® Accelerometer Type 4371 showed a peak level 20 dB lower than others when exposed to a temperature transient. This means Brüel & Kjær, with this design, has extended the frequency range one decade down compared to the other piezoelectric accelerometer designs.

The measurements also indicated that some designs, here a compression type accelerometer with built-in electronics, showed a significant variation of the sensitivity to temperature transients, depending on how the transient is applied. To ensure that the users are properly informed, the measurements made indicated that if the manufacturers follow the guidelines in ISO 5347 the data given will give a good estimate of the worst-case temperature-transient sensitivity.

Q: Jim Lally (PCB): Comments and questions to Mr Licht at B&K. On the acceleration strain sensitivity I would agree it's certainly an important consideration. Whether it's a problem or not, in a specific application depends a great deal on the nature of the structure, thickness or thinness of the mounting walls.

The transient thermal sensitivity can be handled in several ways. One way is by internal accelerometer mechanical design. Another way is by inexpensive insulating materials like RTV boots or by high-pass filters, which may or may not be practical in the application depending on the low frequency required.

Regarding accelerometer designs, you differentiated between the shear designs by mentioning planer, annular and delta shear. But there was a tendency to lump the compression designs under one somewhat negative heading. Like the sheer designs, there are several compression designs. There are upright compression, inverted compression, single and multiple crystal designs, a column array compression design which exhibits low strain, and low thermal sensitivity which is comparable to the shear mode designs.

I guess what confuses me is that it is my understanding that the B&K calibration standard is a quartz inverted design, which is cited in your literature for highest accuracy, low strain, low thermal sensitivity and long term stability. This seems to be somewhat in conflict with your promotion of merits of the shear mode and the compression designs. I wonder if you could elaborate on that a little bit for me?

A: Mr Licht: That was quite a long talk but let me try and say a few words more. It is very difficult to classify all the different designs of transducers. I've tried to make a very crude distinction between different designs. Basically you will have a compression design. For whatever you do, you'll have to do a pre-loading thing of some kind. It can be made in many different ways, but you'll have to make a pre-loading even if you use quartz. You'll have to try to match expansion coefficients of that pre-loading thing. Thermal effects, which are impossiable to avoid, will give some output even though the quartz itself doesn't give an output if you have uniform heating. Apart from that you will have non-uniform heating which will also create output because of the tertiary pyroelectric effect of quartz. That's why I tried to distinguish between the compression type and the shear types. In the shear, basically you have pre-loading perpendicular to the direction where you are having your sensitive direction.

I'm not quite sure I followed all your types of transducers in compression, but let me try to answer the last part you tried to pinpoint. We're using a compression design transducer as a reference. That's true for many different reasons. The first reason is that we made that transducer back in 1970, and you do not change such a transducer because of a very long historical record. You do not throw that away overnight. Apart from that, you have a controlled

environment and know pretty much how it is going to be used. It doesn't present exactly the same problems as when you are using a transducer in many different applications and many different structures. You will not normally mount it on a structure with a big base and you will normally have very low temperature variations over it. It is still a good design for a very stable and reliable reference transducer. Looking at what exists today, I think Kistler has a reference transducer which is also a compression design, using quartz. I think the Endevco 2270 is also a compression design using ceramic. I think the basic reason not to change is that we do not want to change until we are certain we have something much better. It has to pay off; you don't sell thousands of reference transducers per year.

RECENT DEVELOPMENTS IN PIEZOELECTRIC POLYMER STRESS GAUGES

R. P. Reed
Sandia National Laboratories
Albuquerque, NM 87185

ABSTRACT

Piezoelectric polymer stress gauges of polyvinylidene fluoride (PVF2) now allow the accurate measurement of shock and stress waves of more than 20GPa amplitude and time resolution generally of tens of ns but in special circumstances of a few ns. Among the many benefits of this gauge type are fidelity, high sensitivity, small size, simple signal conditioning, design versatility, flexibility, and adaptability to use in the radiation environment. Reliability and accuracy of PVF2 measurement transducers has been made possible only by the availability of well controlled material and development of special procedures for electrically poling the material. This paper describes the measurement principle and application of the piezoelectric polymer material as well as some benefits and limitations of this class of stress gauge that is under development at Sandia National Laboratories.

INTRODUCTION

Significant piezoelectric activity was recognized in some polymers as early as 1950 [1]. A one to two order of magnitude increase in piezoelectric activity over those materials was observed in the study of the polymer, polyvinylidene fluoride, by Kawai in 1969 [1]. Investigators at Sandia began to study the material following that announcement. Pyroelectric behavior of PVF2 was first announced by Bergman in 1971 [2].

The strong ferroelectric nature of the PVF2 material immediately suggested its use as a transducer to convert acoustic, mechanical, and thermal energy to electrical form. The possibility of using PVF2 for casual measurement was also immediately apparent. However, the application of the obviously complex and unreproducible plastic material for the accurate measurement of extreme shock stresses seemed somewhat less plausible at that time. Indeed, a casual examination of much of the research literature of the intervening two decades and up to the present would not offer obvious promise for a reproducible piezoelectric polymer transducer material. Reasonably, the material has been lightly considered and abandoned for precision measurement by several serious experimenters. However, recent developments have served to reinstate the class of piezoelectric polymers generally and PVF2 in particular as appropriate and unique materials for shock stress and other sensors.

Shock stress sensors are destroyed in use. They must be characterized as a class. They cannot be individually calibrated under the conditions of actual use. Therefore the characteristics of each sensor must accurately reflect the same properties as the entire group. Demonstrated and reliable reproducibility of behavior is a critical issue, particularly for polymer materials where the sensing property is not intrinsic but must be achieved by careful processing. Extensive industrial and laboratory development of the process technology for the production of the film of high quality and, notably, several years [3,4] of careful work by Bauer in developing special electrical polarizing techniques necessary to obtain reproducible sensors adequate for shock stress work, has made accurate shock stress measurement feasible with this material at very high stresses. The first cooperative effort between François Bauer of the Institut Franco-Allemand de Recherches de Saint-Louis, France (ISL) and Sandia was initiated in 1979. The early work of Bauer on commercial grade material clearly demonstrated that reproducibility of polarization was a major obstacle to precision measurement. It is for that reason that development of precision shock sensors of PVF2 has been considered seriously only recently at Sandia. Special PVF2 material and poling procedures developed by Bauer can now produce transducer elements that not only are reproducible, but also address an exceptionally broad range of applications.

Gauges furnished by Bauer have been used by Sandia Laboratories and Ktech Corporation to measure accurately the stress waves generated by varied sources including laser beam, electron beam, exploding bridgewire-HE detonator, light-initiated explosive, and nuclear and chemical explosive, as well as precision gas gun impact in the laboratory.

Sandia is presently developing a standardized sensing element of PVF2, in cooperation with Bauer, using the patented [5,6] Bauer procedure and specially produced material. Development is intended to produce a transducing element that is well characterized as are the classical Sandia quartz and lithium niobate shock stress gauges [7]

but with an extended range and versatility of application.

The present paper reviews some issues involved in the processing, characterization, and application of a particular PVF2 film for use in stress transducing elements of specialized gauges primarily relating to stress wave and other dynamic mechanical phenomena. This paper describes some of the technical issues with which a prospective user should be familiar.

SPECIAL FEATURES OF PVF2 GAUGES

In its simplest form, the piezoelectric polymer stress gauge appears to be nothing more than a pair of broad shiny crossed leads on a flimsy plastic film, Fig.1 . To the contrary, the technology that makes the novel sensor available and the physics of its behavior are both very complex. Measurement transducers made from piezoelectric polymer materials are similar in many ways to other piezoelectric gauges made from quartz, lithium niobate, or PZT [7]. Yet, because they are very thin they have many distinctive features that distinguish them from their relatives in the way they are applied, recorded and analysed. Compared to more familiar sensors, they have a number of potential advantages and disadvantages. Many of both the favorable and unfavorable characteristics result from the use of the gauge in the uncommon stress-rate sensing mode.

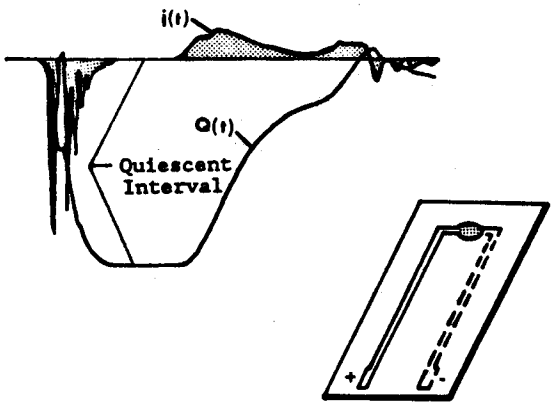

Fig. 1. Stepped Pulse of Stress from PVF2 Stress gauge as recorded in the Direct-Stress (Charge) Mode and in the Indirect-Stress Derivative (Current) Mode. A Bauer ISL PVF2 shock stress gauge is shown. [3]

As described by Bauer and later in this paper, the favored mode of application records the time derivative of stress rather than the stress itself. Figure 1 shows a comparison of a simple experimental stepped "square pulse" of stress as recorded in the direct charge mode of recording and in the indirect current mode. Subtle structure in the wave front that is indistinct in the charge mode is prominent in the current mode record. Both records accurately represent the same stress wave [4]. The ISL gauge shown is of the circular active area type initially used by Bauer [3].

Favorable Characteristics

Fidelity — Wave shape reproduction in loading is excellent and in unloading appears unusually good.

Stress range — While quartz and lithium niobate gauges are limited to less than 2.5 to 4GPa stress [7], PVF2 is usable to more than 20GPa [8]. In contrast to manganin, the high sensitivity of PVF2 also allows its use at very low stress levels. It is especially well adapted to resolving subtle low stress features in the presence of large stresses.

Sensitivity — The signal level from PVF2 gauges is substantially greater than for a given size sensor of manganin, ytterbium, quartz, or lithium niobate.

Time resolution — PVF2 gauges can observe prolonged record wave structure to tens of nanoseconds resolution. Resolution to a few ns in the special circumstance where the wave front rises in less than the 5 to 40ns transit time of PVF2 film gages is possible in a "thick" gauge mode in a manner analogous to the thick piezoelectric quartz and lithium nibate shock stress gauges [7,8].

Reproducibility — Proper processing allows accurate calibration by class and also matching of multiple sensors as for triaxial applications.

Linearity — From the limited calibration data reported by Bauer, the charge response appears to be exceptionally linear and remain large over the broad stress range from about 3GPa to more than 12GPa (although the material is very nonlinear for smaller stresses). No discontinuities in sensitivity have been evident in calibrations to date.

Thickness — The sensing elements are thin, typically 25μm. This reduces "ring-up time", allows fine time resolution, and reduces the perturbation of stress field by embedded gauges. Gauges can be less than 10μm thick if necessary for special situations.

Area — High sensitivity allows the gauge to be made with a sensing area of 1mm^2 or less so that stress measurements can be highly localized. Tilted or nonplanar wavefronts can be observed with reduced distortion. Small stress sources such as detonators can be readily instrumented. Conversely, where stresses should be averaged over broad regions the gauge can be made to areas of 100cm^2 or larger.

Shape — The sensing area can be of arbitrary shape and can be made to conform to curved developable or even domed surfaces.

Flexibility — The polymer is not brittle as are crystalline ceramic or single crystal piezoelectric materials. This improves survivability.

Signal conditioning — For current-mode recording only a terminating resistor is required. Long signal lines can be used if bandwidth needs allow.

Radiation tolerance — Constituents can all be of low atomic number to minimize pulsed heating. While the radiation effects on PVF2 have not been extensively studied some materials have appeared to survive practically significant x-ray and neutron exposure [9,10] and gamma exposure below 50Mrad has been reported to improve elevated temperature stability [11].

Embeddability — Allows the measurement of stresses within a body, such as an explosive.

Stress rate sensing — PVF2 can be used to observe the history of either stress or rate of stress change.

Self Generating — No power supply nor extra excitation leads are required.

Producibility — The gauge is well adapted to quantity production.

Cost — Apart from development costs, if produced in quantity, PVF2 gauges could be less expensive to produce than any present shock stress sensor.

Noise Rejection — Used in the stress differentiating current mode, the signal does not include low frequency drift from temperature, pressure or static stresses imposed before the transient stress event; the signal does not drift off scale (However, the sensitivity of the sensor may be affected by any unrecognized pressure or temperature shifts away from the boundary conditions of calibration).

Unfavorable Characteristics

No gauge is uniformly good. Some of the potential benefits compromise convenience or even the measurement function in particular circumstances. Most of the following disadvantages are associated with the same current mode recording that produces a number of benefits.

Familiarity — The manner of use is different from more familiar gauge techniques.

Availability — Commercial gauges with a track record in shock stress measurement have not been available. But, commercial gauges are coming to market and are now available for critical evaluation.

Nonlinearity — From the limited published calibration data of Bauer it appears that the PVF2 calibration is strongly nonlinear in the stress range up to about 3GPa, however, the nonlinearity appears to be unusually small in the important high stress region from 3 to 20GPa.

Directness of Indication — Where the application requires recording in the current-mode, the waveform is the derivative of the actual wave shape. The record is an indirect, though accurate, representation of the stress waveform. Direct interpretation is often difficult. Data must be reduced before use. Rather than scaling by a simple constant, data must be integrated by computer. Special software must be written for data reduction (Beneficially, this property might reduce the incidence of spurious "quick-look" interpretations).

Signal conditioning — To observe the waveform directly as stress the signal may be recorded by high input impedance recorders, voltage follower or charge amplifiers, or else hardware in-line integration may be used. All of these are less common signal conditioning techniques.

Charge mode — For direct recording of waveform charge mode operation is necessary. Recording with open-circuit termination is recognized as being noise-prone (However, the high signal output available has proved to produce records with large signal to noise ratio under adverse field conditions as is the case with lithium niobate gauges [12]).

Aggravated bandwidth requirement — Where current mode recording is used, the derivative nature of the waveform doubles the required recording bandwidth.

Obscured Break Points — In current mode recordings of typical waveforms the differentiated-stress record is so richly structured that distinct breaks that would be evident in the stress waveform are obscured; subtle inflections in the stress wave appear as major breaks in the record. This mode complicates direct time-of-arrival or event interpretation.

Aggravated Noise — Because current mode recorded signals must be integrated, any noise mixed with signal is exaggerated by the data reduction. Noise filtering is more difficult.

Recorder Setup — To select recorder settings for current mode recording a reasonably detailed prediction of expected stress waveform is required. Subtle structure in an actual waveform can cause large amplitude excursions in the recorded stress derivative. Clipped peak amplitudes introduce substantial error in integrating for stress.

Measurand Noise — Both temperature and extraneous stress loading may present significant noise sources in some situations.

PIEZOELECTRIC POLYMERS

Sources of Piezoelectric Polymer Materials

Manufacturers of nominal PVF2 material are in commercial production in several countries. These include the Pennwalt Chemicals Company (United States), Rhône-Poulenc Films and also Thompson-CSF (France), Kureha Chemical Industries (Japan), and Solvay et Cie (Belgium). PVF2 is produced in commercial quantity for a variety of piezoelectric applications of industrial significance such as microphones, headphones, speakers, igniters, and capacitors. It has also found use in pyroelectric detectors and thermal imaging devices. Yet, unfortunately, the commercial market is not now so large as to suggest that a desirable diversity of materials with measurement grade properties will likely become available. Ordinary industrial grade materials and poling processes now suitable for noncritical application are not adequate for the demanding shock measurement application.

The Nature of Piezoelectric Polymers

A piezoelectric polymer is a plastic material that has groups of some of its molecules linked as orderly crystallites. Polar crystallites can be oriented so that they produce a net electrical charge on surface electrodes when stressed. Such crystallites also produce charge when subjected to temperature change; that is, they are inherently pyroelectric as well as piezoelectric. The crystallites form in an amorphous matrix of the chemically similar but differently structured material. Broadhurst has described the structure as crystalline lamella arranged in a spherulitic arrangement with amorphous material interspersed [13]. Polymers can be produced in bulk form [14] but they are commonly used in stress transducers in the form of thin flexible films of less than 100μm thickness.

The relative population of crystallites strongly affects the piezoelectric behavior. Ionic or metallic impurities and space charge introduced during processing may enhance the charge production from stress but degrade the fidelity and reproduciblity. These factors differentiate quality between different polymer materials. Unfortunately, it is not possible to distinguish the performance capability of a material by visual inspection or even by measurement of simple low stress piezoelectric parameters of poled samples.

Polyvinylidene Fluoride

The nominal designation polyvinylidene fluoride (PVF2 or PVDF) is applied to a class of materials that are chemically the same, based on the monomer $[- CH_2- CF_2 -]_n$, but they may differ markedly in piezoelectric characteristics. A general PVF2 material contains an amorphous phase that accounts for half or more of the film volume but it also contains crystallites of one or more of four distinct phases [14]. The α phase, alternately termed Form II, is antipolar and makes no piezoelectric contribution. A modified α phase denoted as α_p, δ, or Form IV is polar. The uncommon γ phase (Form III) is also polar. Form I, the β phase is the polar crystallite of greatest piezoelectric activity. It is the β phase only that is intended to be utilized in the piezoelectric stress transducers [4]. Reproducible high sensitivity PVF2 stress gauges are based on materials processed to have a uniform high volume fraction of β phase crystallites and relatively few crystallites of other phases.

Polyvinylidene fluoride is the most prominent piezoelectric polymer material. This complex material has been extensively investigated by many workers worldwide over a period of almost two decades. Yet, many of its important characteristics remain to be explored. No single material or process has been studied thoroughly. Nevertheless, the generic class of homopolymer, PVF2 is the most fully studied of the piezoelectric polymers. It is this popular material that is being used for stress gauge development and measurement by Sandia. Much of the developmental work of Bauer has been done with material of this general type. A summary of typical properties of PVF2 materials is given in Table 1

Matrix Piezoelectric Properties of PVF2

In general application of any stress transducer it is necessary to be conscious of the directional responses of the sensor to arbitrary loading. Rarely is such general response really well known for any shock transducer element. Most transducer elements have significant transverse sensitivity [12]. For PVF2, only a limited amount of general information is presently available to describe the full sensitivity to a general tensor stress. That general information does not usually represent material at hand.

Table 1. REPRESENTATIVE PHYSICAL PROPERTIES OF POLYVINYLIDENE FLUORIDE FILMS (Ambient Conditions)

Transition Temperatures:		
Melting point, Tm	°C	165 to 190
Glass temperature, Tg	°C	-50 to -40
Poling temperature, Tp	°C	-40 to 160
Depoling temperature, Td	°C	Tp to 160
Thermal conductivity	W/m.K	0.13
Specific Heat	J/m^3K	2.5e6
Thermal Expansion Coefficient	K^{-1}	0.1 to 1.5e-4 *
Density	gm/cc	1.7 to 1.9
Sound Speed	km/s	2.2 to 2.4
Acoustic Impedance	kg/m^2s	3.7 to 4.6e6
Poisson's Ratio		.39 t0 .45
Young's Modulus	Pa	1.5 to 2.5e9
Bulk Modulus	Pa	3.8e9
Volume resistivity	ΩM	10e13
Dielectric Permittivity		12
Dielectric Strength	V/M	150 to 200e6
Pyroelectric Modulus	C/m^2K	-1.25 to -2.74e-5
Piezoelectric Modulus, d_h	C/N	-4 to 10e-12

* Suffix e-x denotes $X10^{-x}$

Kawai [1] noted that his uniaxially stretched PVF2 material, being predominantly of rhombohedral form β phase, was effectively of the crystal class mm2 which distinguished it from prior polymers that showed little piezoelectric activity because they were of class $\infty 2$ having only d_{14} and d_{24} piezoelectric coefficients as active parameters.

Fukada and Takashita [16] confirmed for Kawai's material that effectively the matrix of active

piezoelectric coefficients for the polycrystalline PVF2 was:

$$d_{ij} = \begin{vmatrix} 0 & 0 & 0 & 0 & d_{15} & 0 \\ 0 & 0 & 0 & d_{24} & 0 & 0 \\ d_{31} & d_{32} & d_{33} & 0 & 0 & 0 \end{vmatrix}, \quad (1)$$

using the convention for a unixaxial stretched film that the 1 axis is in the direction of stretching, 2 is the transverse direction in the surface of the film, and 3 is normal to the film. That matrix form is characteristic of one of two noncentrosymmetrical subclasses of orthorhombic crystals. The other form is active only with regard to shear stresses. In the present paper, following the precedent of Kepler [16], for biaxially stretched film, extruded or rolled, 1 will be taken in the direction of rolling or extrusion, the 2 axis transverse to that direction

The significance of the array of active piezoelectric coefficients for β-phase film is that the material should be piezoelectrically responsive to stress in the directions normal (d_{33}) and transverse (d_{31}, d_{32}) to the plane of the film. As the material is electroded in the thickness direction, this matrix suggests that the charge output should not be affected by shear components of stress.

In single crystal piezoelectrics like quartz and lithium niobate, d_{31} and d_{32} have well related values but in uni- or biaxially stretched piezoelectric polymer containing more than one species of crystallite, it is neither expected nor observed that the effective d_{32} is the same as the d_{31} coefficient although both should have the same positive sign. The sign of d_{33} and d_h are negative. It has been reported that for some PVF2 materials $|d_{33}/d_{31}|$ is typically in the range from 1.3 to 1.5; i.e., both transverse and hydrostatic response is significant.

Table 2. TYPICAL PIEZO- AND PYROELECTRIC COEFFICIENTS OF POLED PVF2 POLYMERS

Material	d_{33}	d_{32}	d_{31}	d_h	p
	pC/N	pC/N	pC/N	pC/N	$\mu C/m^2K$
PVF2 Mono[4]	14	4	6		
PVF2 BiAx[4]	-30	4	24		
PVF2 Mono[16]	-12.4	4.36	4.34	-9.6	-27.4
PVF2 BiAx[16]	-31.5	2.3	21.4	-4.8	-12.5
PVF2 Mono[1]			10-20		
PVF2 Mono[15]		6.6	11		

While several investigators have reported studies of the set d_{31}, d_{32}, d_{33}, d_h, and their variation with temperature, or pressure, or stress, the values reported are useful in measurement only for describing trends as there is no agreement at a level useful for measurement. Different material samples and different poling methods produce significantly different piezoelectric characteristics. Parameter values for uncoordinated materials and poling from the research literature cannot be generally applied to piezoelectric polymers as they can for single crystal materials such as quartz and lithium niobate piezoelectrics. Without a common research material, standard parameter values cannot evolve by refinement. To be specifically useful, information must be developed for a standardized and reproducible piezoelectric polymer.

Copolymers and Composites

Basic chemical units or "mers" like CH_2 and CF_2, as a linked pair, form a chemical "monomer" unit "building block" or repeat unit as in [-CH_2 - CF_2 -] (vinylidene fluoride) that join together with like or different monomers. The resulting polymer chain is called "homopolymer" if the monomers are all of the same kind or "copolymer" if more than one kind of monomer are linked. Monomers may link head-to-tail, head-to-head or tail-to-tail. polymers possess properties different from any of the monomers.

Since 1963, piezoelectric activity has been discovered in several other homopolymers such as vinylidene fluoride (VDF), trifluorethelene (TFE), vinylidene cyanide (VC), and vinyl acetate (VA). Mixtures of such polymers with PVF2 or other polymers have produced active copolymers that have a range of useful properties. A copolymer of current interest is VDF/TFE.

There is the additional prospect of composites of ceramic and fluoropolymer piezoelectrics to combine the benefits of both kinds of material [18].

Many polymers such as polycarbonate (Lexan), Polytetrafluoroethelene (PTFE), Polyethylene, Polypropylene, and Polyvinyl chloride (PVC) have low or negligible piezoelectric activity so that they can cautiously be used as insulating materials at high stresses [1,19]. Other polymers, such as poly(ethylene teraphthalate) (PET or Mylar) and poly(pyromelittilite) (PMMI or Kapton) become actively polarized under severe shock loading so have restricted usefulness as insulators in high stress shock applications [19].

Further development of these advanced copolymer and composite materials may suggest their preferred use in stress transducers should they eventually offer higher attainable polarization, improved stability, extended stress range, lower glass transition temperature or higher crystal transition, softening, and melting point temperatures, or other beneficial characteristics.

For the present, the outstanding properties of PVF2 are adequate to justify its development in the stress gauge application. Practical considerations have lead Sandia Laboratories to focus on the use of the one material, the single piezoelectric

homopolymer material PVF2, for stress gauge development to allow thorough characterization as a shock stress transducing material.

Production of Piezoelectric Polymer Film

PVF2 raw stock can be polymerized and produced from emulsion or suspension [20]. Powders of the resin contain a population of crystallites of relative abundance and type that results from the temperature and pressure of the process [20]. When cooled from a melt, the normal crystallite form is nonpolar α-phase [20]. The raw material can be fabricated in bulk or film form by casting, pressing, rolling, or extrusion [20]. Crystallites in the formed material, though individually polar, are not aligned in a way that results in a net external polarization. Typically, a processed film contains up to about 50 volume percent of crystallites but the volume fraction of crystallites can be much lower. The reason for the commonplace 50% limitation is not well understood. Polymer films can vary broadly in the types and relative abundance of crystallites. In films with a crystallinity of 50 percent the fraction of the crystallites that are of the desirable β phase as received can range from near zero to near 100 percent [20,21]. The crystallite population can change during processing. For example, crystallites of α type can be converted to polar α or β type [22]. It has also been demonstrated that the crystallinity or proportion of crystallites can change reversibly with temperature or electric field [23].

The crystallites are caused to be aligned with their polar axis normal to the film surface by stretching the film to 4 to 6 times the original dimension [24]. The film is stretched in one direction or in two orthogonal directions. Each stretching further increases the degree of alignment and nature of the crystallites as well as the crystallinity [24]. The stretching process reduces the film thickness as it aligns crystallites. The film thickness may vary with location because of variations in extrusion, pressing, or rolling and the subsequent stretching process. The amount of stretching will differ in the two directions and with location in the film. For reproducible polarization and accurate measurement the uniformity of stretching and of thickness must be considered both in poling and in analysis.

Thus, the magnitude, homogeneity, and anisotropy of polarization of a film is critically dependent on the stretching process. Just as materials formed from impure resins with undesired crystallite populations may have significantly different properties, so materials produced from identical pure raw materials may have substantially different properties due to the stretching process.

POLARIZING POLYMER FILMS

As the film is stretched, the crystallites, though somewhat aligned, are oriented in random polarity so that any net polarization is small, coincidental, and uncontrolled. For piezoelectric application, strong polarization is induced by applying an electrical field across the thickness of the film. The crystallite dipoles tend to align parallel with the applied field [16,23]. Poling rotates crystallites around the crystallographic c-axis. The b-axis is aligned normal to the film surface. These treatments produce an orderly lamellar array of crystallites with coordinated polarity.

The electric field can be applied in many ways that differ in electric field magnitude, polarity, frequency, duration, and repetition. The film can also be exposed to different stress states and temperature schedules during poling process. Each combination of poling parameters leads to a polarized film with distinctive piezoelectric characteristics [4].

DC Poling

In the simplest poling, a constant dc poling potential is applied through leads connected to electrodes on opposite faces of the film. Only the region of the film between opposing electrodes is polarized by this method. Regions of the film beyond the electrodes maintain a net polarization that is insignificant.

Discharge Poling

A poling field can be applied to large areas of film without the use of contacting electrodes by plasma, glow, or corona discharge [24,25]. In this method, broad areas of the film are polarized. Such discharge exposure has also been used to stabilize film properties.

For piezoelectric application, electrodes are added to opposite surfaces, possibly after poling. In this procedure, it is intended that the charge be collected from the stressed film only in the region defined by the electrodes. However, charge is generated wherever the film is stressed. The corona discharge method of poling is well suited to quantity production of voltage generating devices not intended for measurement. It has been shown to result in a crystallite population different from contact electrical field poling [25]. It can result in exceptionally high piezoelectric activity because it allows the application of higher poling fields without dielectric breakdown through the film [25].

Films polarized in these simple ways by dc or discharge fields will readily produce a strong piezoelectric charge under stress but polarization created in this way is suspect for measurement because such poling for industrial applications usually introduces or leaves uncontrolled extraneous charge producing mechanisms such as surface charge, internal space charge, and mobile ions [4,24]. These can produce superposed signals that mix with the purely piezoelectric output to confound the data and to preclude accurate measurement or even reliable interpretation. The nonsystematic character of charge generation by shock stress from such materials cannot be reliably anticipated by simple measure of the low stress values of the piezoelectric parameters.

The Bauer Poling Process

To avoid these demonstrated spurious effects that can seriously degrade accuracy a special poling

technique has been developed over a period of several years of careful investigation by Bauer [3,4]. The proprietary poling process is the subject of both U. S. and French patents [5,6]. To the present, the essential process has been fully employed only in the laboratories of ISL in France. Gauge elements made by this process are to be commercially offered in France and the fabrication process is now being implemented in the United States by Sandia and a private laboratory [27] under contract to Sandia National Laboratories, Albuquerque under those patents.

As described in the patents and in the public literature, the process involves the following approach:

Polymer film, with overlapping electrodes sputtered on opposite faces of the film, is clamped under a mechanical load of about 2MPa. At ambient or elevated temperature, an electrical field is imposed via the electrodes across the film only over the area where the electrodes overlap. The magnitude of the electric field is progressively increased with time, cycling between positive and negative polarity, sinusoidally, at a frequency of 0.001 to 1Hz . The cyclic amplitude of the field is increased by schedule at a rate of about 0.05MV/cm/min over many cycles from an initial small value until a maximum field amplitude of about 1MV/cm is attained. In this process, only the local portion of the film over the region in the effective vicinity between the electrodes is poled.

The Bauer poling procedure is specifically tailored to create a transducing element that produces charge under stress only from the piezoelectric effect and under temperature change only from the pyroelectric effect. The process – homogeneously throughout the poled region – aligns crystallites, orients dipoles, and migrates out of the film via the electrodes ions and space charges that have been resident in the pre-poled material.

The Bauer process has been shown to be capable of producing poled piezoelectric polymer transducing elements that have the homogeneity, stability, and reproducibility essential for accurate shock stress measurement [4,8,9,28-31]. Preliminary indications suggest that the stability and reproducibility of polarization can exceed that of polycrystalline ceramic piezoelectrics and may eventually approach that of classic single crystal materials like synthetic quartz and lithium niobate [8].

As in other piezoelectric sensors, the piezoelectric and pyroelectric responses are interrelated and inseparable in the gauge element. In transient measurement, an ambiguous charge response must be avoided by experiment and gauge package design.

MEASURES OF PIEZOELECTRIC ACTIVITY

Three measures of polarization are particularly useful for characterizing the material as a transducer for shock stress measurement. Two low-stress measures are the remanent polarization, P_r, and piezoelectric d_{33} coefficient. The third is the corresponding stress dependence of polarization over a broad stress range. The first two are used in production quality control, the latter is necessary for data reduction in stress wave measurement.

Remanent Polarization

During the polarization process, as the varying electric field is applied a current through the gauge element is observed. The observed current includes capacitive and resistive current contributions as well as the polarizing current. The total current observed in poling is [9]:

$$i(t) = \frac{dP}{dt} + \epsilon \frac{dE}{dt} + \frac{E}{R} \quad . \qquad (2)$$

Here, P is the instantaneous Poplarization, E is the applied field, ϵ is the relative dielectric permitivity, and R is ,effectively, the large dielectric resistance of the element. By numerically subtracting the resistive and capacitive current components from the recorded current of a poling cycle, the poling current is obtained as a function of poling field. The current is integrated to yield the polarization loop P(E) for the poling cycle. As for other ferroelectric materials, the plot of this specific charge versus electric field appears as a sigmoidal hysteresis loop. The coercive field, E_c, is the half width of the hysteresis loop at null current, the remanent polarization, P_r, is the magnitude of polarization as the field is reduced to zero.

The poling process is terminated just as the field is reduced to zero from a positive maximum. Thus, the residual polarization and gauge polarity are determined by the final poling cycle. The remanent polarization, as a terminal measure is available only at the end of the poling process and it reflects the state of the poled device at the instant of termination. The measurement cannot be repeated after poling is complete.

The d_{33} Piezoelectric Modulus

For the determination of pyroelectric properties of bulk ceramic materials there have long been available accurate resonance methods. Because of the very high frequencies required, they are less adaptable to very thin polymer films. The most readily available technique uses a commercial instrument, the "Berlincourt piezo-meter"(Model CPDT 3300-FGR) [32]. This device directly measures d_{33} and it can be adapted to measure d_{31} as well. In this method, for d_{33}, the poled piezoelectric film is lightly clamped, with a bias force of less than one Newton, between electrodes that both apply force and collect charge from the specimen. A 0.3 Newton oscillating force of low frequency, typically 100 Hz, is superposed on the bias force. The time varying charge generated by the fluctuating force is compared to the corresponding output of a stabilized standard PZT 53/47 reference transducer. As the stressed area and charge collecting area are, by this means made to be identical, the specific size of the area is unimportant and the ratio of the force to the charge is a measure of the piezoelectric coefficient. The value is directly indicated by a digital indicator that is graduated in units of coulombs per

Newton. By calibrating against standardized specimens, a stated accuracy of 10 percent is routinely attained. Special precautions and the use of a dial indicator to precisely set the load allow the precision of readings to be improved to better than 3%.

The Berlincourt tester provides an essential means to observe the stability of d_{33} with time at ambient temperature or with thermal cycling. The low stress Berlincourt measurement cannot be used to calibrate the gauge for measurement under stress wave loading but it is the most direct way to compare the relative sensitivity between gauges, to establish control of the poling process, and to observe the response of a single gauge to a variety of environmental exposures. The measure is required for studies of polarization stability for which the other methods are inappropriate.

Under the conditions of measurement, the simultaneous remanent polarization and d_{33} coefficient are related by the corresponding Young's modulus. The remanent polarization measured during the last poling cycle and the d_{33} measured promptly after poling should reflect this constant relationship [3]. There can be some immediate decay in polarization following poling [1]. The slightly time dependent d_{33} should therefore be measured promptly after poling and at appropriate standard intervals for a period after poling. It has been reported that well poled materials exhibit little decay of polarization over tens of months while poorly poled materials show prompt and prolonged decay of polarization [1]. The statistics of the determination of these quantities distinguishes whether the fabrication process is under control and may suggest the degree of reproducibility of stress measurement.

Polarization versus σ_{33} Stress

Because PVF2 stress gauges may be used to measure transient stress amplitudes exceeding 20GPA accurate characterization for high amplitude stress wave measurement must be accomplished by very well controlled mechanical impact tests. The most common calibration is performed by gas gun impact between an impacter and a PVF2 gauge on the face of a target of very well known physical characteristics. This experiment exposes the gauge to a square pulse of stress loading in a one-dimensional strain state along the 3 axis while charge is collected in the same direction. Using the Sandia 25m gas gun especially adapted to this characterization, shock stress pulses of 2ns risetime and amplitudes to 20GPa have been imposed on Bauer gauges [8].

Quartz or sapphire materials have been used in this determination. The gauge is dynamically loaded in a state of normal one-dimensional strain in the plane of impact between the impacter and target. The stress history imposed is very well defined and accurately established. Because the gauge is capable of resolution of stress features of duration shorter than 5ns risetime, accurate characterization of the gauge requires the use of a facility capable of imposing impacts of less than 5ns risetime and recording features to less than 1ns resolution.

This normal impact characterization is accurate and complete for gauges that are to be used under corresponding boundary conditions. However, it provides only a portion of the calibration required for more general use. Complete characterization for arbitrary boundary conditions may also require other special tests such as hydrostatic or transverse loading that address the general response to full tensor loading. Such calibrations are more difficult to perform dynamically to the necessary stress levels.

The calibration necessary for shockwave measurement is destructive of each gauge calibrated. Calibration by gas gun is expensive and time consuming. Thus, calibration of the gauge is by type and confirmation of calibration is by lot sample rather than by individual certification. Accuracy of the individual gauge cannot be improved by separate calibration under the actual conditions of use. Therefore, as with most other shock wave transducers, the accuracy with which the gauge can be used depends as much on the reproducibility of production run gauges as on the calibration proper.

In alternate forms of loading, structured stress waves that combine linear loading and unloading ramps with abrupt shocks in both loading and unloading [8,33] and other multiple loading histories have been used to confirm fidelity of waveform measurement under precisely controlled laboratory conditions [8]. Such structured loading provides calibration over a range of stress in one experiment

Calibration relations for ISL gauges of three particular PVF2 materials obtained by projectile impact have been reported by Bauer [3,4] as:

$$\frac{Q}{A} = 0.248\ \sigma^{0.637} \quad \text{(biax stretched, 23}\mu\text{m)}, \qquad (3)$$

$$\frac{Q}{A} = 0.248\ \sigma^{0.583} \quad \text{(uniax stretched, 35}\mu\text{m)}, \qquad (4)$$

and

$$\frac{Q}{A} = 0.342\ \sigma^{0.583} \quad \text{(uniax stretched, 40}\mu\text{m)}. \qquad (5)$$

or, generally

$$\frac{Q}{A} = a\ \sigma^{b} \qquad (6)$$

where σ is the normal stress, in kbar, on the electrode in the one-dimensional strain state that is characteristic of the initial phase of plate impact experiments, Q is liberated charge, microcoulombs, A is electrode area, cm^2, and a and b are experimental constants. For data reduction, for the same one-dimensional strain conditions, to determine σ from measured Q, the inverse relation is:

$$\sigma = \left(\frac{Q}{a\,A} \right)^{1/b} \qquad (7)$$

These relations for ISL PVF2 gauges were found to apply for compressive stress magnitudes up to 12GPa. The functional form is empirical rather than physically based. The calibrations apply specifically to particular materials processed in the Bauer manner. The apparent dependence on thickness is incidental as the films have been produced in different ways. The relations do not necessarily pertain to other gauges of like thickness nor to PVF2 materials in general, even to those that have the same stretching.

The corresponding relation for the gauges under development at Sandia has not yet been established. Because the materials, design, sputtering, and poling conditions are not identical to the ISL gauges, the relation is expected to have different values of parameters. It may be of similar form over the same stress range.

REPRODUCIBILITY

Batches of gauge elements produced by Bauer under informal laboratory conditions and used by Sandia have been reproducible in the d_{33} coefficient, measured with a Berlincourt piezo-meter, with a sample standard relative deviation of about 2-3 percent. Prototype gauges of PVF2 material produced for Sandia in establishing control of the process have had a typical percent sample standard deviation of about 5-8 percent that improves progressively as process control is established. Some of the deviation is representative of the gauge samples; some of it is due to the control measurement technique itself.

A variation is also seen in the remanent polarization, P_r, at the end of the poling cycle for conditions of fixed maximum poling potential. The standard deviation of least squares fit to a power relation between charge and stress for Bauer gauges is apparently about 5 percent.

These values are encouraging and are expected to improve as both the gauge reproducibility and the means of monitoring it are improved. The Sandia PVF2 gauge produced by the Bauer process shows specific promise of developing into a reliable tool for shock stress measurement.

SANDIA PVF2 POLYMER MATERIAL

The special material being used by Sandia for shock stress gauges was produced with special control for measurement application. This material appears to be of exceptionally good quality. While, nominally, this material is a PVF2 homopolymer, it differs significantly in quality and fabrication from commercial grade materials of the same name routinely available from other industrial sources.

Source

To justify the considerable expenditure demanded by material shock stress characterization, an adequate quantity of high quality, stable, homogeneous transducer grade material must be available. In January 1984, R. A. Graham of Sandia negotiated with the research staff of Rhône-Poulenc for the production of two custom batches of high grade polyvinylidene fluoride film to be produced especially for Sandia. The product was specified to be:

> " 23 micron Bi-oriented and 35 micron Mono-oriented PVF2 Film "of stress gauge quality as defined by Dr. François Bauer of ISL." [34]

The material was produced under the scrutiny of Dr. Bauer and was judged by him to be of exceptional quality [35]. The material appears to have homogeneity of property and thickness acceptable for shock stress transducers. The thickness of sampled coupons of the material as delivered measured 26±2 and 35±2μm, respectively. The material is essentially pinhole-free. Further detailed characterization of the physical properties of the material will be performed in the course of development of transducer elements.

Standard Designations for Sandia PVF2

Materials from these two particular batches will henceforth be formally denoted as "SNLA26" and "SNLA35" PVF2 materials, respectively. They are informally referred to as "Sandia Master Batch PVF2". To allow thorough characterization as a shock stress transducing material it is expected that, for the foreseeable future, the characterization of Sandia standardized PVF2 shock stress gauges will be on this biaxially stretched SNLA26 material.

STRESS GAUGE IMPLEMENTATIONS

Gauges of nominal PVF2 material have been made by several organizations for their own use in a variety of special geometries. A few are already commercially available [36-39]. Though the name of the PVF2 polymer material is the same for all these gauges, there may be significant differences in the measurement characteristics and integrity of gauges from materials of various types and from different sources because of variations in material purity, fabrication, electroding, poling, and intended application. None of these commercial gauges are produced by the Bauer process so they should be different in characteristics from ISL gauges whose calibration has been reported.

The physical appearance of a gauge is not a reliable indicator of quality and measurement integrity. Neither is the clean appearance and plausibility of stress indication from a PVF2 gauge any guarantee of correctness. Even a superficial agreement of peak amplitude within some percentage of an expected value provides no assurance of general accuracy of form. The material, improperly implemented, is capable of specious results faulty in both wave structure and magnitude.

Indeed, early results from improperly made gauges and misinterpreted data has clouded the reputation of PVF2 material as a class. The cautious user will independently confirm the validity and relevance of calibration data on gauges custom made or received

from others. Where independent verification under the conditions of use is not possible, it is appropriate to inquire in detail about the specifics of gauge characteristics and calibrations received from others.

Careful independent characterization at Sandia of some gauges produced in the Bauer manner has confirmed that proper PVF2 material properly poled is, indeed, capable of accurate reproducible stress measurement. Please note that it is not claimed nor presumed that the fabrication process reported by Bauer is necessarily unique in its result. But, it has been confirmed that the Bauer process is adequate to produce accurate stress gauges. It is for that reason and for expedience that stress gauge development at Sandia is employing the demonstrated Bauer technique. However, the conclusion that the Bauer process can produce reproducible gauges of PVF2 is not generally applied to arbitrary PVF2 material arbitrarily poled.

THE STANDARDIZED SANDIA PIEZOELECTRIC POLYMER STRESS TRANSDUCING ELEMENT

It is customary to refer to the piezoelectric sensing element as a shock stress gauge. That convenient colloquial usage has been followed here. There is, however, a non trivial and very practical distinction between a transducing element and a measuring gauge that must be recognized by the potential user.

A measurement transducing element is a component that converts, for measurement, a physical boundary condition measurand imposed on it to an analogous measurable quantity such as charge, current, or voltage. The element is only the sensing part of a gauge assembly.

Usually, the transducing element is not directly exposed to the physical measurand of which a measure is intended. Rather, the transducing element must be packaged in a complementary measurement assembly. Depending on circumstance and application, the packaging of the element may be very simple, or it may be complex.

A measurement gauge is an assembly that incorporates a measuring transducing element, relays to the element the relevant boundary conditions of the measurand, isolates the element from irrelevant boundary conditions, protects the element from environmental conditions, provides for convenient handling and installation, and connects the signal from the element to the balance of the measuring system.

In the present instance, the PVF2 element that is being standardized and characterized reponds to many different primary boundary conditions — three significant tensor stress components and a scalar temperature change — yet, it can produce only a single measurable output, a change in polarization.

The sensing property, change of polarization, is indirectly and significantly affected by a host of incidental environmental variables. Each of these can have a substantial effect on a recorded result. Peter Stein has referred to this collection of measurement noise sources as "COMETMAN", an acronym for Chemical, Optical, Mechanical, Electrical, Thermal, Magnetic, Acoustic, and Nuclear [40]. The transducing element is not useful as a measuring device in any circumstance where all undesired boundary conditions imposed on the transducing element, except the relevant ones, cannot adequately be isolated or controlled [40].

To be practical and specific, the element that will now be described is a transducing element not a gauge in the measurement sense. It will be carefully characterized and made reproducible regarding material, process, geometry, and application so that it can be employed as the sensing element in gauges adapted to a variety of applications. Its initial and primary use is expected to be in a shock stress gauge. Alternate uses might include free field stress or pressure gauges, accelerometers, or even transient thermometers.

In many ways, the laboratory shock stress application, though extremely demanding in stress range and time resolution, is its simplest and best application requiring so little of formal packaging as a gauge that the distinction between gauge and element may not even be recognized. Simplicity of gauge design is possible in this demanding application only because control of boundary conditions is done by experiment design rather than by gauge design. The experiment conditions are designed to be tractable by both experimental and theoretical methods. The laboratory technology does not translate directly into measurement under adverse field conditions.

The point made is practical. The transducing element loosely referred to as a "PVF2 gauge" cannot be used successfully to measure an arbitrary measurand without first carefully developing a gauge package for the transducing element and an experiment design suited to that measurement. Unfortunately, it can, however, be used with very little thought and effort as an effective experimental generator of nebulous time-varying voltage and a stimulator of creative experiment interpretation.

Because PVF2 does offer a transducer with a unique combination of measurement properties Sandia has undertaken to implement the Bauer process in the fabrication of transducing elements for use in diverse stress wave measurements. Elements made to Sandia design, specification, and quality control from special PVF2 material are being fabricated in-house and in a contract facility. Many prototype elements have been made by the Bauer process in establishing the control of process necessary to justify expensive calibration.

Detailed characterization will require some time. Meanwhile, preliminary fieldings and applications are being conducted to establish usability and to discover problems that may arise in specific environments and situations. Unusually high accuracy in arbitrary applications is not yet claimed for this Sandia sensing element. While the ISL Bauer gauge has demonstrated its practicality in specific laboratory situations, the Sandia implementation is yet a developmental protype.

Features of a Standardized
Sandia PVF2 Stress Transducing Element

Slightly different in design detail from gauges that have been reported by Bauer and others, The generic Sandia implementation has the following characteristics controlled to attain the necessary reproducibility:

1. The general configuration of the element is shown schematically in Fig. 2.

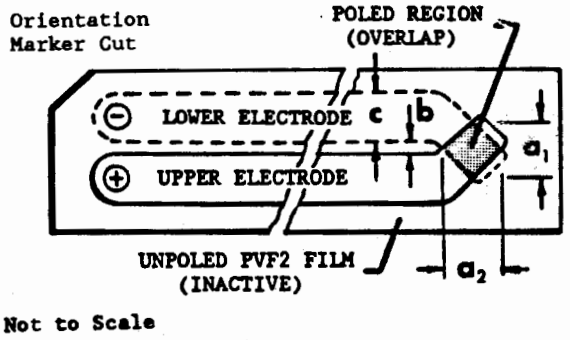

Fig. 2. Sandia Standardized Piezoelectric Polymer Stress Transducing Element (Schematic)

2. Gauges follow a uniform design protocol that allows for calibration by class and interpolation of characteristics. The element is scaled systematically from this geometry to different applications.

3. The piezoelectrically active region of the film element is defined by the overlap of conducting electrodes on opposite surfaces of the film. The electrodes are electrically separated by the thickness of the film. The active electrode area is generally square in profile. The area can be less than 1 sq. mm or arbitrarily large as required by the application.

4. The polymer element is piezoelectrically inactive except in the region of electrode overlap. The net polarization apart from the localized active area is uniformly negligible in the thickness and the lateral directions.

5. The transverse separation between leads is as small as allowed by poling and circuit parameter considerations.

6. Electrodes are deposited by sputtering.

7. Electrodes and leads are of aluminum or of gold over platinum. The leads are approximately 3000 Å in overall thickness.

8. The piezoelectric polymer is from one particular batch of material custom fabricated by Rhône-Poulenc for Sandia in 1984. This material is designated as "SNLA26" PVF2.

9. The material was extruded and biaxially stretched about equally in both directions to a nominal thickness of 26um.

10. Polarization is by the ISL Bauer procedure as described by U. S. and French patents and by the underlying technology.

11. Polarization is by application of a high voltage electrical potential applied via electrodes.

12. Conventions, illustrated in Fig. 3, are established to assure that position and orientation dependent factors for the film, recognized or obscure, that may affect reproducibility or behavior are traceable throughout development and application.

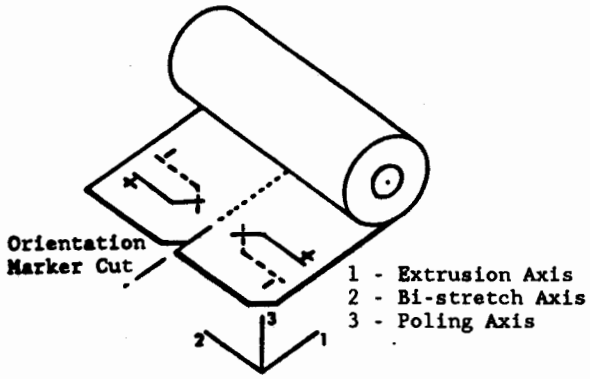

Fig. 3. Gauge Orientation Conventions for the Sandia Standardized Piezoelectric Polymer Stress Transducing Element and Film

13. Orientation of each specimen of the film throughout fabrication is identified by an oblique corner cut across the near right corner of the film segment as it is withdrawn from the bottom while facing the roll, Fig. 3. The 1 film axis is positive in the direction in which the film was extruded. It is also the direction of stretching for uniaxially stretched film. It is the primary stretching direction for biaxially stretched film. Axis 2 is the secondary direction of stretching for biaxially stretched film. The orthogonal 3 axis is positive in a right handed coordinate system.

14. The leads are aligned transverse to the extruded length of the spooled film. The charge collecting polarized area is positioned toward the center of the film roll away from the film edges.

15. The electrode marked positive is on the film surface toward the inside of the roll as spooled. The negative electrode is on the opposite surface of the film.

16. The electrode marked positive presents a positive charge when the element is compressed in the thickness direction. As the d_{33} coefficient is of negative sign, the negative electrode is the electrode that last experienced a positive field on the poling cycle.

17. For shock measurement, the transducing element is applied with the negative-marked electrode nearest the source of a stress front to be measured. The wave front advances in the direction of the positive 3 axis.

18. As appropriate to the application, electrodes may be insulated by thin films of PTFE or other materials that do not produce significant charge or conduct excessively under stress as do Poly(pyromellitimide) (PPMI or Kapton) film and other plastics with complex monomers that have been shown to be strong generators of shock induced polarization and subject to conduction at high stresses within the range of usefulness of PVF2 [19].

19. Electrical connections to robust leads are made through foil conductors using low melting point solder or conducting epoxy for joining.

20. Conventions and nomenclature of ANSI/IEEE Standards 176 and 180 will be followed, where applicable, in description of the elements [41,42].

The sensing element is intended to be incorporated into gauge assemblies specialized for particular classes of measurement. These general design definitions will be augmented and supplemented as characterization progresses.

GEOMETRIC INFLUENCES ON ACCURACY

Electrode Area

The effective area of the active electrode affects the ultimate accuracy of measurement in several ways. In the electrode configuration utilized in the Sandia stress gauge the area of the active electrode is determined by the area of overlap between the two electrodes deposited on opposite faces of the film. The area is measured by observing under high magnification, using a Leitz optical profilometer, the dimensions across the two diagonals of the, nominally square, diamond shaped area. As the crossing electrodes are essentially perpendicular, the area is simply the product of the two diagonal dimensions. Two sources of stress measurement error relate to the measurement of effective electrode area. An error in area measurement is reflected directly as a corresponding error in stress measurement.

The platinum and gold electrode materials are conductive even in thicknesses at which they are optically transparent. Edges, if graduated in thickness, cannot be accurately located. For accurate gauge characterization the electrode edges must be very sharply delineated in deposition. In prototype production, the reproducibility of area readings of sharply delineated electrodes has been within 1% where areas were of the order of $10mm^2$. For fuzzy edged electrodes, the area was undefined to the extent of 5%. The percentage variation increases as the electrodes are reduced in area.

Also, the electrical polarization extends for an undetermined distance beyond the visually evident electrodes due to field fringing. The extent of this fringe area has not yet been fully determined but is expected to be much less than 1% of the active area for $10mm^2$ electrodes.

It is customary to report polarization normalized to electrode area. Reported polarization is effected directly by the accuracy of area determination.

Film Thickness

Film thickness does not appear explicitly in any of the relations for data reduction. Nevertheless, the accuracy of film thickness, h, affects the accuracy of measurement in two significant ways.

In poling the film, the degree of polarization is dependent on the electric field, E (i.e.,V/h) ; but, it is the electric potential, V, alone, that is actually electrically controlled in poling. Therefore, the electric field is affected by the thickness of the film during poling. As the film is only about $26\mu m$(1 mil) thick, a thickness uncertainty of only $2.5\mu m$ can change the field value by 10 percent. The polarization changes accordingly. This directly affects the reproducibility of polarization of gauges within a set and so the accuracy of measurement.

In the measurement of very sharp shocks, the thickness of an embedded gauge affects the time resolution. Embedded gauges are usually of a shock impedance different from the host material. Consequently, an abrupt wavefront reverberates across the gauge thickness to attain equilibrium. The transit time of a reverberation across the thickness of a $26\mu m$ thick PVF2 gauge is approximately 10ns. Experiments performed for calibration at Sandia resolve the detail of this "ring-up" process [8]. Thinner gauges of PVF2 or copolymers may be feasible but are not usually required.

USE OF THE PVF2 STRESS TRANSDUCER

The Equivalent Measuring Circuit

The piezoelectric polymer stress gauge, as a typical piezo- or pyroelectric device shares with the Sandia quartz and lithium niobate shock stress gauges the simplified equivalent circuit of Fig. 4. Adequate to illustrate a point, the circuit is descriptive only of simple low frequency applications with the source and recorder in close proximity. The gauge element has a very small capacitance, C_g, and a very high resistance R_g. The gauge is loaded by terminating impedances C_1 and R_1.

The resistive or capacitive load may be of arbitrary magnitude depending on application. Under appropriate conditions the terminating capacitor or resistor can be chosen to scale the voltage output but possibly with an unacceptable effect on on the transient response. The simple circuit demonstrates that the physical measurand significance of the

dynamic response is effectively defined by the terminating impedances at the recorder or signal conditioner input.

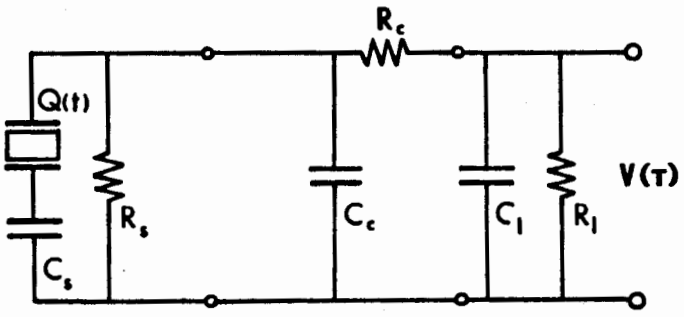

Fig. 4. Simplified equivalent circuit for recording a general piezo- or pyroelectric charge source element.

For measurement of extremely sharp rising stress pulses, inclusion of inductances is necessary. In many practical instances, the source will be separated from the recorder by an extended transmission line of 50 to 120 ohm characteristic impedance as much as several hundred kilometers in length. Capacitive loading by the cable must be considered in data analysis. In such extreme instances, special signal conditioning may be required [12].

For the elementary circuit used as illustration, the charge generated in the gauge is observed as a voltage at the recorder. The transient voltage behavior resulting from any general charge source is expressed by the equation:

$$\frac{1}{C}\frac{dQ}{dt} = \frac{dV}{dt} + \frac{V}{R\,C} \qquad (8)$$

The two extreme conditions of gauge electrical loading are of interest, "open-circuit" termination and "short-circuit" termination.

Short-Circuit Termination
Where the load impedance presented to the gauge is very small (circuit RC time constant small or current-mode recording), the first term becomes negligible, relatively. The voltage varies as the time rate of change of charge:

$$V(t) = R_c \frac{dQ(t)}{dt}, \text{ or} \qquad (9)$$

$$i(t) = dQ/dt. \qquad (10)$$

The voltage resulting from the charge is directly proportional to the circuit resistance. Simple resistive scaling of output is possible.

Inversely, from the recorded current,

$$Q(t) = \int_0^t i(t)\,dt \qquad (11)$$

Open-Circuit Termination
At the other extreme, if the resistance is very large (large time constant or charge-mode recording) then the response is:

$$V(t) = \frac{1}{C}\int_0^t dQ = \frac{Q(t)}{C}, \qquad (12)$$

where C is the lumped capacitance of the circuit. At this extreme, the voltage variation is directly proportional to the change of the charge. Here, the scaling is effected by the capacitance. An indeliberate change of circuit capacitance, as from cable heating or motion directly affects the indicated value.

Except at the two extremes, the relation between charge and voltage is an indefinite mix of the two forms of response and is not useful for measurement. The user must be conscious of the effect of circuit parameters on the physical significance of the measurement with piezoelectric sensors. Here, the circuit response overrides any intended measurand meaning of gauge response. This consideration is additional to, but distinct from, the usual concern for transient response fidelity of the signal conditioning, circuit, and recorder.

Both forms of recording have areas of usefulness. The general significance of Eqn(8) is that the relation applies to all forms of piezoelectric elements and to all sources of charge. Distinctions between different implementations stem from the nature of the forcing function and its local interaction with the gauge element. Local charge response to stress of the very thin film PVF2 gauge is directly analogous to that of the "thin" and "thick" quartz gauges. For stress pulses with risetime of nanosecond order the behavior of the PVF2 gauge is analogous to the behavior of the Sandia Quartz Gauge for the brief period of the first wave transit of the film. Any piezoelectric element responds in either mode as controlled by the circuit and the physical measurand. The appropriate behavior must be attained by proper matching of the transducer element to the experiment.

Generation of Charge

Considering the general self-generating PVF2 sensing element, the charge per unit area of electrode generated by arbitrary stress and temperature exposure with no imposed electric field is:

$$Q/A = d_{31}\,\sigma_{11} + d_{32}\,\sigma_{22} + d_{33}\,\sigma_{33} + p\,\theta \qquad (13)$$

It is this relationship in four different variables, normal streses, σ_{ii}, and temperature change, θ, that produces a single observable voltage. The shock stress gauge is intended to measure only σ_{33}, the normal compressive stress component. Clearly, for accurate measurement, it is essential that the

transverse stresses and temperature variation be isolated from the gauge during the interval of measurement as the other piezo- and pyroelectric coefficients are significant. In the state of one-dimensional strain imposed for a period during gas gun driven projectile loading of a gauged specimen in the laboratory, as during calibration, and under conditions where the contribution from shock heating is insignificant the condition is fulfilled, and

$$\frac{Q}{A} = q\,\sigma_{33} \,. \qquad (14)$$

Here, q is different from d_{33} because it is measured in a one-dimensional strain state where σ_{11} and σ_{22} are not zero. Alternately, where isothermal measurement of a hydrostatic pressure loading is desired, the normal stresses are equal and the Equation simplifies to:

$$\frac{Q}{A} = d_h\,\sigma_h, \qquad (15)$$

where $\sigma_h = (\sigma_{11}+\sigma_{22}+\sigma_{33})/3$ and $d_h = (d_{31}+d_{32}+d_{33})$. This relation applies, for example, where the element is to be used in a fluid coupled stress gauge.

In the final instance, where the gauge element is isolated from stresses and only temperature change, θ, is imposed, the pyroelectric charge resulting from temperature is:

$$\frac{Q}{A} = p\,\theta \qquad (16)$$

Equations (10) through (13) illustrate the mechanics of the stress measurement. They show, for example, as in Eqn(8) that:

$$d_{33}(\sigma,N) = \frac{1}{A}\left(\frac{\partial Q}{\partial \sigma_{33}}\right)_N \qquad (17)$$

emphasizing that d_{33} measured in the absence of σ_{11} and σ_{22} and is a strong function not only of the normal stress component but also of temperature, and other incidental "COMETMAN" [40] variables, collectively indicated by N , that are presumed to be constant during measurement. Under specific boundary conditions, q represents the local slope of the Q/A versus σ_{33} calibration curve. It is that empirical $Q(\sigma)$ relation as expressed for example by Eqn(6), that is actually used for data reduction.

Under appropriate boundary conditions, the same self-generating polarized sensing element can be used, alternately, to measure accurately either the normal shock stress, or transverse planar stress, or pressure, or temperature.

In principle, sets of three or four closely matched triaxially oriented gauges can be used as a group to eliminate the ambiguity caused by multi-dimensional loading [43].

Under any other combination of imposed conditions, the charge is an ambiguous measure of a desired quantity with the other physical inputs producing measurement noise that may confound or entirely obscure the intended signal and preclude meaningful interpretation. It is the responsibility of the user to assure that only one of the five particular conditions is imposed on the gauge element(s) by the experiment.

Equation (13) appears to provide the means to evaluate the possible effect of extraneous loading. If the temperature history of a gauge were well known, it seems that the effect of charge variation due to temperature during a stress measurement could be corrected. It should be noted, however, that as both the pyro- and piezoelectric coefficients are strongly nonlinear functions of temperature [44,45], stress [44], and confining pressure [45-47] this is possible only for small deviations from an initial boundary condition. Moreover, the nonlinear relations are characteristic of specific kinds of PVF2, not of PVF2 in general. Dependencies reported in the literature do not likely correspond well to those of an arbitrary sensor. The values of coefficients as they depend on relevant variables over the range of application must be developed for a specific PVF2 material.

One interesting possibility exists. In a circumstance where the pyroelectric coefficient is directly proportional to the d_{33} coefficient, and the temperature change, θ, is proportional to the stress, then

$$\frac{Q}{A} = (1+k_p k_\theta)\, d_{33}\, \sigma_{33} \,. \qquad (18)$$

The temperature change would act as a simple scaling constant to modify the apparent sensitivity of the gauge. In one PVF2 material, the pyroelectric coefficient was demonstrated to be experimentally a linear function of the d_{33} coefficient [13]. Kepler showed that the pyroelectric effect in PVF2 is principally a secondary effect indirectly resulting from piezoelectric response and a temperature change in crystallinity [17]. Calibrations performed in only a few materials have shown no overt temperature dependence. This is an issue requiring study. From the simplistic Eqn(18), shock experiments performed at the same stress level in two different host materials would produce a different charge due to the pyroelectric contribution.

Shock heating varies with the host material. At high stress levels the temperature behind the shock front can attain more than 1000K. Remarkably, though the ambient melting temperature of PVF2 is less than 200 °C, the PVF2 material sustains a piezoelectric and pyroelectric activity well above 200kB. This apparently is due to the strong pressure and rate dependence of melting point [48].
Where temperature change occurs through diffusion temperature isolation is accomplished by thermal time delay. In the measurement of strong shocks, however, the heating may be significant and immediate within the shock front. Isolation by spatial thermal delay is not possible. The effect of temperature on stress measurement must be considered. Accurate knowledge of the pressure and temperature dependence of the parameters is not yet available.

DATA ANALYSIS

The conversion of voltage records to the analogous physical quantity that they measure is accomplished in the usual fashion by application of either Eqn(10) or Eqn(11) together with the calibration of Q/A versus the physical measurand. For shock stress using, for example, the Bauer form, Eqn(6), this yields:

current mode

$$\sigma = \left(\frac{1}{a\ A\ R} \int_0^t V(t)\ dt \right)^{1/b}, \text{ and} \qquad (19)$$

charge mode

$$\sigma = \left(\frac{C}{a\ A} V(t) \right)^{1/b} \qquad (20)$$

Corresponding equations hold for use of the same transducing element for transient temperature measurement using the pyroelectric coefficient calibration, $Q(\theta)$, or for pressure the calibration, $Q(\sigma_h)$.

SUMMARY AND CONCLUSION

Special methods of poling and the availability of measurement quality PVF2 film has made possible the development of stress sensors with a remarkable range of beneficial characteristics. Essential among these are reproducibility and stability that allows calibration to be performed on surrogate subjects that are truly representative of a class of sensors. After a long history of development, properly prepared piezoelectric polymer materials can now be used as the basis for precision stress sensors. No endorsement of product is expressed by this paper that asserts only that polyvinylidene fluoride polymer film, if of suitable quality and properly processed, can be used to reliably measure stresses in shock waves. However, the paper further cautions that PVF2 sensors made from readily available material and by arbitrary poling should be used with particular vigilance.

ACKNOWLEDGEMENT

François Bauer had the tenacity to develop the material technology to the point of credibility and the willingness to share his scientific insights. Robert Graham had the perception to recognize the significance and authenticity of Bauer's work and the initiative to convince others, including me. I appreciate his comments on this paper. Several colleagues at Sandia and at Ktech preceded me in the development work and in being convinced. I am pleased to reflect their influence in this paper. S. P. Breeze and J. I. Greenwoll both have been of great assistance in my own work with PVF2.

* This work was supported by US DOE contract #DC04-76-00089.

REFERENCES

[1] Kawai, H, "The Piezoelectricity of Poly(vinylidene Fluoride)," Jap. J. Appl. Phys., 8, 975-976, 1969.

[2] Bergman, J. G., et al, "Pyroelectricity and Optical Second Harmonic Generation in Polyvinylidene Fluoride Films," Appl. Phys. Lett., 18, 203-205, 1971.

[3] Bauer, F., "Behavior of Ferroelectric Ceramics and PVF2 Polymers Under Shock Loading," Shock Waves in Condensed Matter, W. J. Nellis, L. Seaman, and RE. A. Graham,(Eds), American Institute of Physics, 1981.

[4] Bauer, F., "Properties and High Pressure Shock Loading Response of Poled Ferroelectric PVF2 Polymer Gauges," ASME 1987 Summer Meeting, Symposium on Techniques and Theory of Stress Measurements for Shock Wave Applications, Cincinnati, OH, June 1987.

[5] Bauer, F., "Method and Device for Polarizing Ferroelectric Materials," United States Patent 4611260, September 9, 1986.

[6] Bauer, F., "Procede et Dispositif Pour Polariser des Materiaux Ferroelectriques (Process and Device for Polarizing Ferroelectric Materials), Republic of France, National Institute of Industrial Property, 82 210215, November 4, 1986.

[7] Graham, R. A. and R. P. Reed (Eds.), "Selected Papers on Piezoelectricity and Impulsive 'Pressure' Measurement," Sandia National Laboratories, SAND78-1911,1978.

[8] Graham, R. A., Personal communication.

[9] Bauer, F., "Piezoelectric and Pyroelectric Polymers," Polymers as Synthetic Metals Conference, London, May 1983.

[10] Reed, R. P., Experimental neutron exposure data to be reported.

[11] Wang, T. T., "Properties of Piezoelectric Poly(Vinylidene Fluoride) Films Irradiated by γ-Rays," Piezoelectricity, Gordon and Breach, Science Publishers, New York, 1985.

[12] Reed, R. P.,"A System for Measurement of Free-Field Stress Waves using Lithium Niobate Piezoelectric Transducers," RCC 9th Transducer Workshop, April,1977.

[13] Broadhurst, M. G., et al, "Piezoelectricity and Pyroelectricity in Polyvinylidene Fluoride--- A Model," J. Appl. Phys., 49, 4992-4997, 1978.

[14] Pae, K. D., et al,"Mechanical and Physical Properties of Poly(vinylidene Fluoride) at High Pressures and Temperatures," Ferroelectrics, 57, 249-265, 1984.

[15] Nakamura, K., et al,"Rotation of Polar Axis of β-form Poly(vinylidene Fluoride) under High Electric Field," Ferroelectrics, 57, 139-149, 1984.

[16] Fukada, E., and S. Takashita,"Piezoelectric Effect in Polarized Poly(vinylidene Fluoride)," Jap. J. Appl. Phys., 8, 960, 1969.

[17] Kepler, R. G. and R. A. Anderson-,"Piezoelectricity and Pyroelectricity in Polyvinylidene Fluoride," J. Appl. Phys, 49, 4490 ,1978.

[18] Miyata,S., Panel Discussion, Ferroelectrics, 57, 1984.

[19] Graham, R. A., "Shock Induced Electrical Activity in Polymeric Solids. A Mechanically Induced Bond Scission Model," J. Phys. Chem., 83, 3048-3056, 1979.

[20] Prest, W. M., Jr., and D. J. Luca, "The Formation of the γ-phase from the α and β Polymorphs of Polyvinylidene Fluoride," J. Appl. Phys.,49, 5042-5047, 1978.

[21] Latour, M. and H. A. Dorra,"Study of Phase Transitions in Piezoelectric Polyvinylidene Fluoride," Rev. Phys. Appl., 20, 137-142,1985.

[22] Kepler, R. G., et al,"Electric Field Dependence of Crystallinity in Polyvinylidene Fluoride," Phys. Rev. Lett.,48,1274-1277,1982.

[23] Kepler, R. G.and R. A. Anderson, J. Appl. Phys.,49, 1232-123 ,1978.

[24] Davis, G. T., et al,"Hysteresis in Copolymers of Vinylidene Fluoride and Trifluoroethelene," Ferroelectrics,57, 73-84, 1984

[25] Hayashi,K. and Kubo,U.,"Pyroelectricity and Space Charge in Polyvinylidene-Fluoride." Jpn. J. Appl. Phys., 21, 1379-1380, 1982.

[26] Davis, G. T., et al, "Electric-Field-Induced Changes in Poly(vinylidene Fluoride)," J. Appl. Phys., 49, 4998-5002, 1978.

[27] Sandia Development Contract Number 02-9875 to Ktech Corporation, Albuquerque,NM.

[28] Fogelson, D. J., L. M. Lee, D. W. Gilbert, W. R. Conley, R. A. Graham, R. P. Reed, and F. Bauer-."Fabrication of Standardized Piezoelectric PVF2 Shock Gauges by the Bauer Method," APS 1987 Topical Conference on Shock Waves in Condensed Matter, Monterey, CA, July 1987.

[29] Lee, L. M., D. J. Fogelson, and W. D. Williams, "Dynamic Stress Transducer Qualification," Shock Waves in Condensed Matter, Elsevier, 1984.

[30] Lee, L. M., et al,"Studies of the Bauer Piezoelectric Polymer Gauge (PVF2) under Impact Loading," Shock Waves in Condensed Matter, Elsevier, 1986.

[31] Lee, L. M., R. A. Graham, and F. Bauer," Bauer Piezoelectric Polymer Gauge (PVF2) Stress Wave Response to Shock Loading," APS 1987 Topical Conference on Shock Waves in Condensed Matter, July 1987.

[32] Germano, C.P., "Development of Specialized Equipment to Measure the Piezoelectric Coefficients of Polymer Piezoelectric Materials," Channel Products,Inc., Chesterland, OH 44026, 1980.

[33] Setchell, R. E.,"Response of Polyvinylidene Fluoride (PVF2) Gauges to Structured Waveforms," APS 1987 Topical Conference on Shock Waves in Condensed Matter, Monterey, CA, July 1987.

[34] Williams, W. D., Sandia National Laboratories, Albuquerque, NM, Purchase Order 58-8220, 3/16/84.

[35] Bauer, F., Personal communication,1986.

[36] Dynasen, Inc., Arnold Place, Goleta, CA 93117

[37] Charest, J. A. and D. B. Larson, "Comparison of Stress Response Repeatability and Hysteresis for Three Polyvinylfluoride Films," 1987 ASME Summer Meeting, Cincinnati, OH, June 1987.

[38] Pennwalt Corporation, 900 First Avenue, P.O. Box C, King of Prussia, PA 19406-0018.

[39] Chatigny, J. V., "Piezo Film Yields Novel Transducers," Electronics Week, August 6, 1984.

[40] Stein, P. K., Measurement Engineering, Vol. I, Basic Principles, Stein Engineering Services, Phoenix, AZ, 1970.

[41] Anon., IEEE Standard Definitions of Primary Ferroelectric Terms, ANSI/IEEE Standard 180-1986, The Institute of Electrical and Electronics Engineers, New York, 1986.

[42] Anon., IEEE Standard on Piezoelectricity, IEEE Standard 176-1978, The Institute of Electrical and Electronics Engineers, New York, 1978.

[43] Reed, R. P.,"Triaxial Measurement of Stress Waves in the Free-Field," RCC 10th Transducer Workshop, June,1979.

[44] Wada, Y.,"Theoretical Analysis of Temperature Dependence of Complex Piezoelectric Constant and Pyroelectric Constant of Poly(vinylidene Fluoride)," Ferroelectrics,57,343-351,1984.

[45] Destruel, P., et al,"Pressure and Temperature Dependence of the Electromechanical Properties of Polarized Polyvinylidene Fluoride films," J. Appl. Phys.,56, 3298-3303, 1984.

[46] Takemura, T.,"Piezo- and Pyroelectric Properties of Poly(vinylidene Fluoride) under High Pressure," Ferroelectrics,57,243-248,1984

[47] Gookin, D. M., et al, "Correlation of Ferroelectric Hysteresis with 33 Ferroelastic Hysteresis in Polyvinylidene Fluoride," Ferroelectrics, 57, 89-98, 1984.

[48] Samara, G. A., "Pressure Studies of Polyvinylidene Fluoride (PVF2) and Copolymers," APS 1987 Topical Conference on Shock Waves in Condensed Matter, Monterey, CA, July 1987.

BRL CALIBRATION PROCEDURES FOR BALLISTIC PRESSURE TRANSDUCERS

Charles D. Bullock and Arpad A. Juhasz
US Army Ballistic Research Laboratory
Aberdeen Proving Ground, MD

ABSTRACT

Current procedures used for the calibration of ballistic pressure transducers at BRL are described. Checks include evaluation of continuity, hysteresis, and zero return characteristics as well as calibration against a dead weight system. Static versus dynamic response behavior is evaluated with the aid of a high pressure dynamic positive step calibrator. For the most exacting measurements, adapters are used permitting calibration of transducers in the same mechanical environment as during measurement. Recommended recalibration intervals are indicated.

INTRODUCTION

The mission of the Interior Ballistic Division of BRL includes research on novel ballistic concepts, charge design methodology and advancing the state of the art in interior ballistic computations. These efforts are supported by a variety of combustion, interior ballistic and ballistic simulator firings. Central to all these experiments is the measurement of pressure. Pressures may range from a few hundred pounds per square inch (Psi) to a hundred thousand Psi full scale depending on the experiment. The quality of the measured pressures, in large scale, is dependent upon the methodology, care and accuracy of the calibration process.

The primary function of the calibration procedures is to determine transducer response characteristics and to act as a screening tool to help weed out problem transducers before they can do damage. A secondary but vital function is to help solve measurement related problems and assure that the devices perform as required under the conditions of service. The purpose of this paper is to discuss the procedures which have evolved over the past twenty five years at BRL for the calibration, selection and use of high pressure transducers for ballistic applications. It will include a discussion of the most important characteristics of high pressure transducers, BRL's calibration and evaluation procedures and a look at potential problem areas.

DISCUSSION

Transducers Used.

Ballistic pressure transducers in routine use at BRL fall into two categories, piezoelectric element and single arm strain sensors. The commonly used piezoelectric transducers (gages) are obtained commercially. The strain sensor transducers are made privately for BRL. All of the above are used daily to measure pressures up to 100,000 Psi. The gages have a fast response (10-90 per-cent response times on the order of 10 microseconds). The events measured range from the sub-millisecond to several hundred millisecond time frames.

High pressure transducers can, with adequate care in calibration and use, be successfully employed to make measurements under 1000 Psi. This requires special calibration procedures, however, which will be discussed later. In addition to high pressure transducers, good low pressure, fast response transducers are also commercially available and find applications in ignition simulators and the like. At the other end of the spectrum, a current development effort is aimed at providing a ballistic pressure transducer capable of measuring pressures to 200,000 Psi.

Calibration Procedures

The purpose of pressure calibration is to determine the response of the transducers to known pressures, to verify the response specified by the manufacturer, and to show repeatability. During the calibration procedure for a given transducer the following questions are considered:

* is the response continuous
* does it suffer from hysteresis
* does it return to zero
* is response linear or at least well-behaved

* is there a difference between first and subsequent cycles
* are static and dynamic characteristics the same
* have response characteristics changed with use

Initial Screening.

Calibration typically begins with an examination of the continuity, hysteresis and zero return properties of a transducer over the pressure range of intended use. A schematic of the main calibration system in use at BRL is given in Figure 1. The output of the test transducer is plotted (Y- axis) against the output of a stable reference strain gage transducer of known characteristics (X- axis) while the system is pressurized and depressurized over the desired pressure range. Pressurization is accomplished using the air pump/intensifier portions of the system. The response curve of the transducer is used as an indicator of its overall quality.

Continuity. Examples of "good" and "bad" continuity response are given in Figure 2. In this case, both plots were obtained from the same transducer but at different times, indicating degradation in performance as a function of use. Normally, when discontinuities of this type are encountered, the transducer is retired.

Hysteresis. Examples of "good" and "bad" hysteresis characteristics are shown in Figure 3. In the plot on the left the ascending and descending portions of the curve coincide. In the plot on the right the transducer appears to take a "set" on depressurization. Normally, a maximum hysteresis level of 1-2 per-cent of full scale is thought to be acceptable. Excessive hysteresis would make interpretation of the up

Flow Chart of BRL Static Deadweight Calibration System

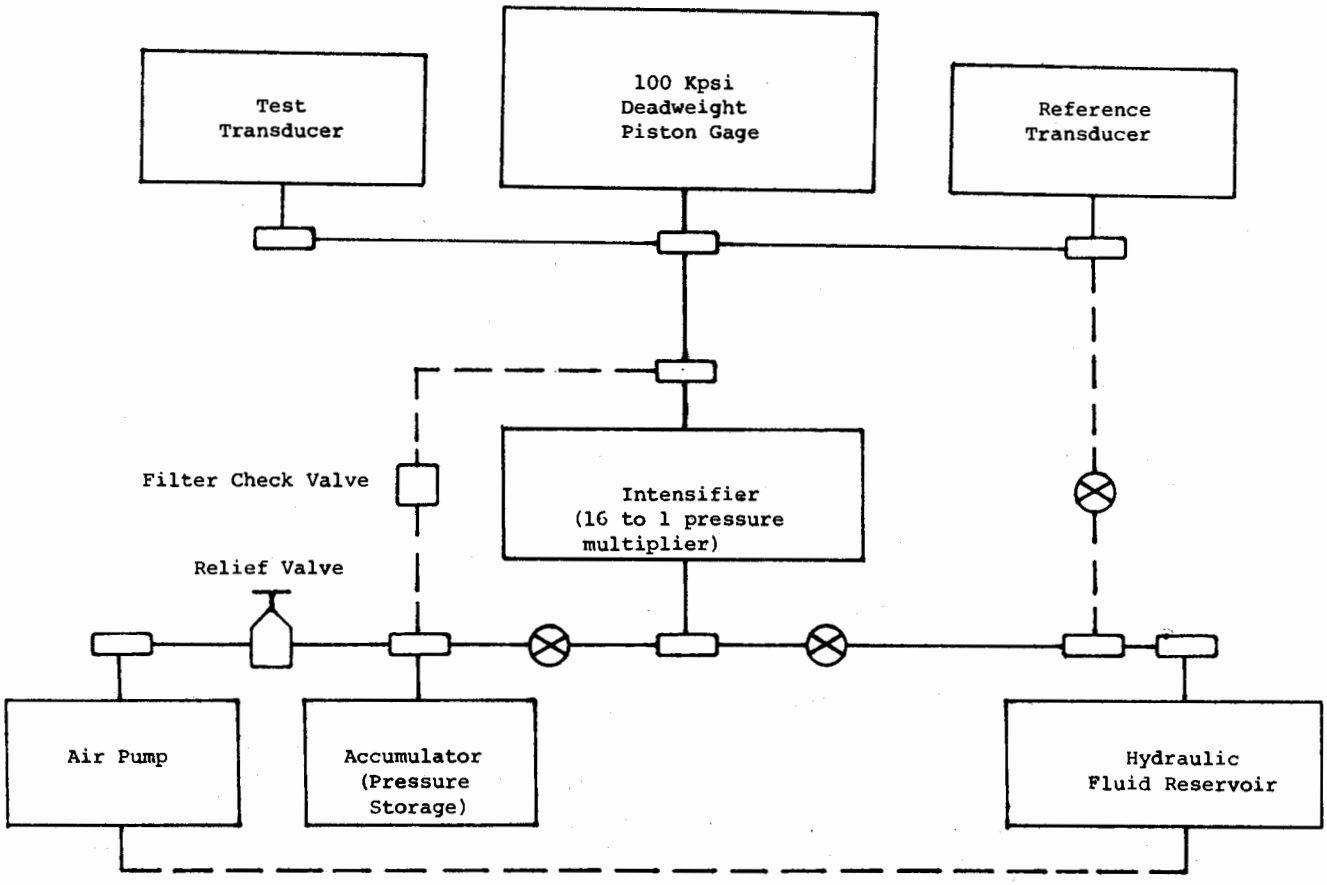

Figure 1. Schematic of the Main Deadweight Calibration System in Use at BRL

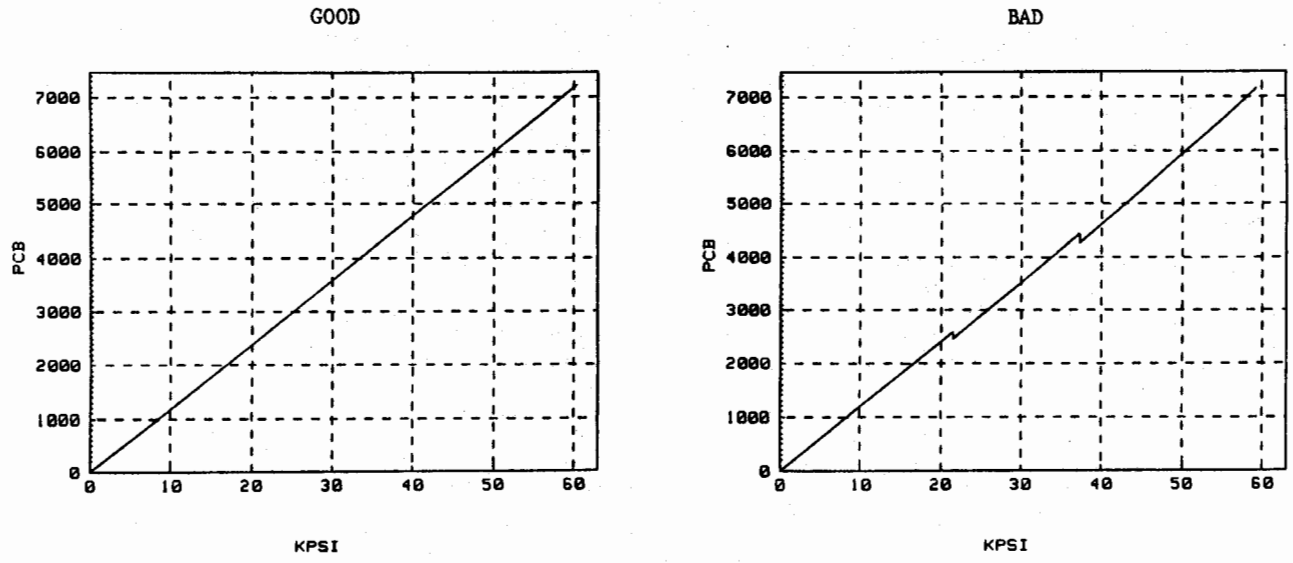

Figure 2. Examples of Good and Poor Continuity of Response.
(In This Use Response for the Bad Gage Deteriorates with Use).

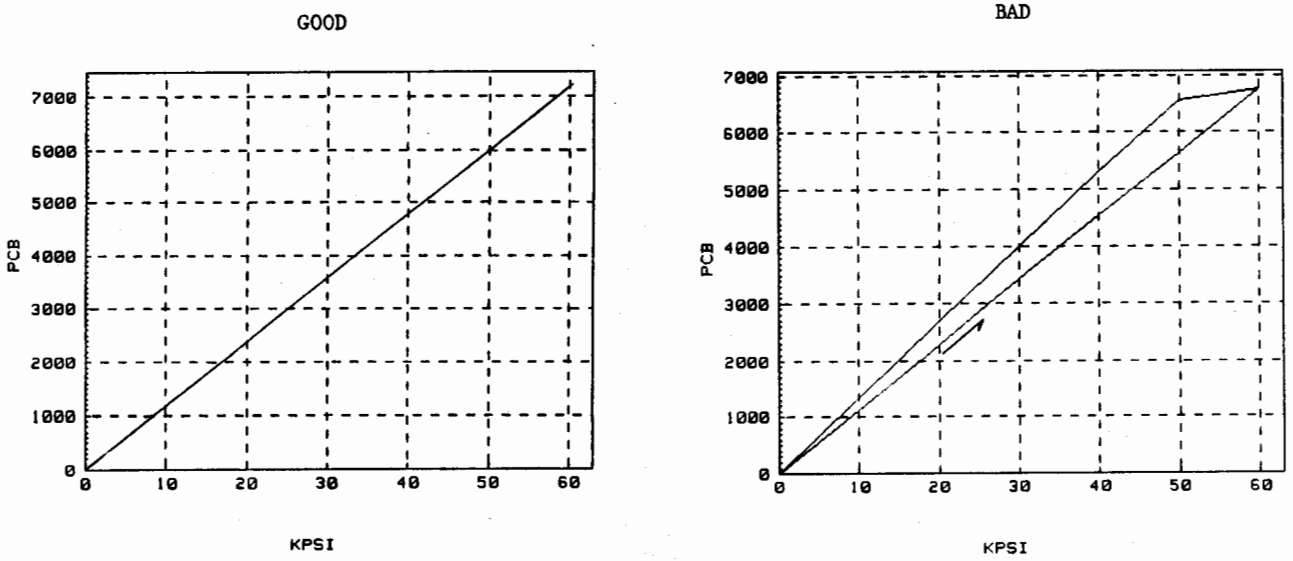

Figure 3. Examples of Good and Bad Hysteresis Behavior.

and down slope portions of ballistic data difficult to interpret.

Zero return. Examples of "good" and "poor" zero return properties of a transducer are given in Figure 4. In this case, the transducer exhibits a residual output after the pressure loading is removed. Normally, the maximum error in zero return deemed acceptable is one per-cent of full scale.

A final characterization made at this point involves a comparison of the first and subsequent cycles of transducer output. With certain transducers, response characteristics change between the first and subsequent pressurizations for a given installation. This could lead to serious problems in measurements, especially in cases involving cyclic events such as multi-shot bursts. Examples of "good and "bad" first vs second cycle output are given in

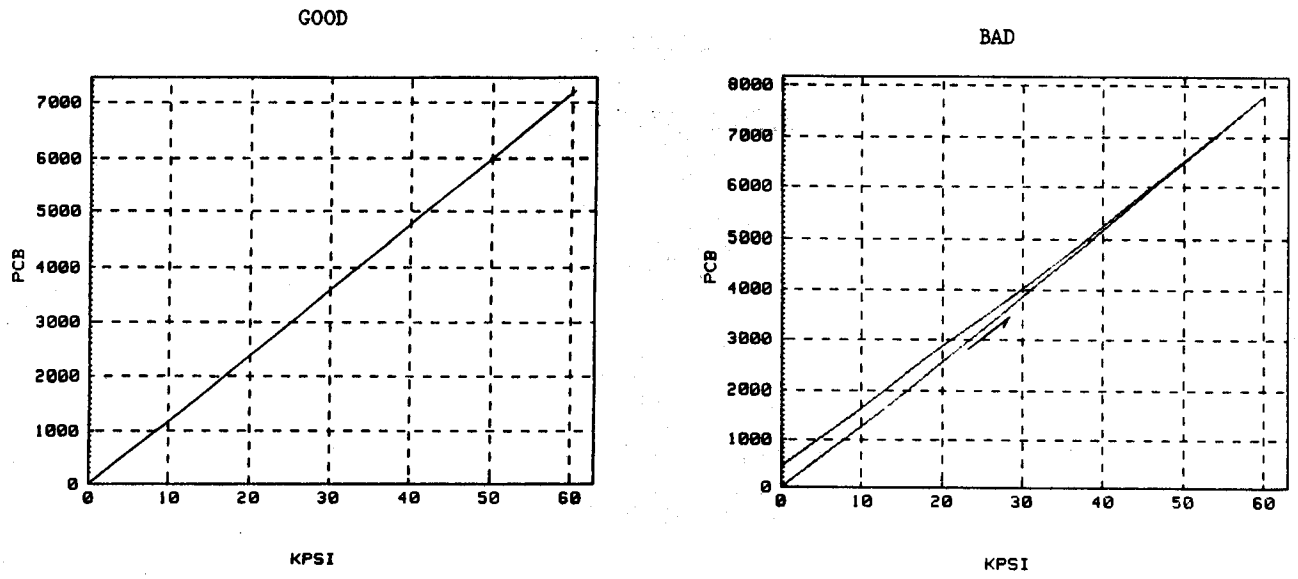

Figure 4. Example of Good and Poor Zero-Return Characteristics

Figure 5. Normally, a difference of less than one per-cent full scale variation of cyclic output is found to be acceptable.

is, where the mass/ piston combination is exactly balanced by pressure in the fluid, the hydrostatic pressure throughout the fluid may be

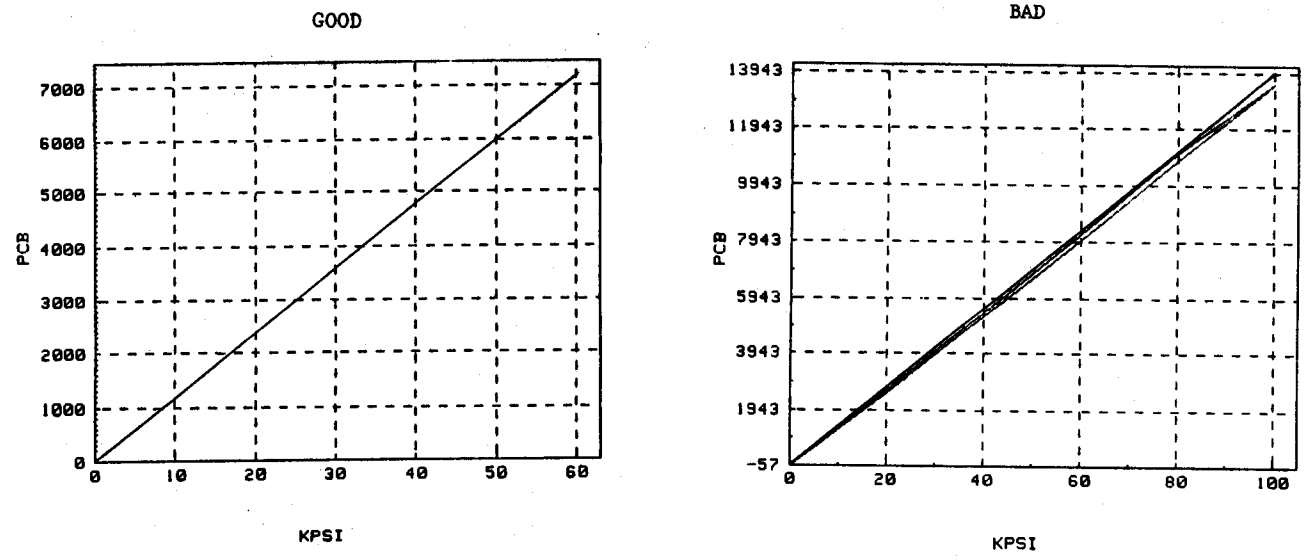

Figure 5. Examples of Good and Poor First vs Subsequent Cycle Response

Quantitative Procedures.

Quantitative transducer response characteristics are obtained using a dead weight system. A simplified schematic of a dead weight system is given in Figure 6. The principle of operation is simple. At the point of equillibrium, that

calculated by dividing the total mass ("weight" plus piston) by the piston area. The output of the test transducer is measured at a series of float points corresponding to various mass loadings. The static dead weight calibration method has both advantages and disadvantages; it is the most accurate and repeatable source of

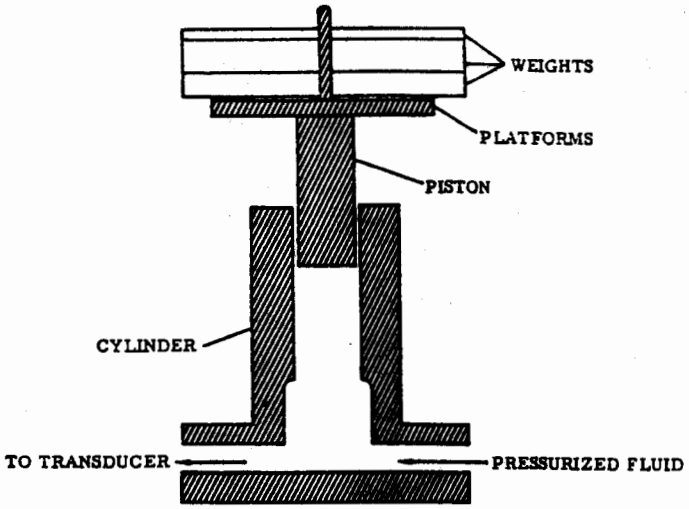

Figure 6. Simplified Schematic of a Deadweight System

calibration pressures. Its principal disadvantage for ballistic applications is that it needs dynamic verification.

The dead weight calibrator used at BRL is a 100 KPsi Astra model D-100KS.[1] In this device the pressurizing fluid balances the force of a series of calibrated masses transmitted through a piston of precisely known area. A thin film of hydraulic fluid separates the piston from the cylinder wall and the piston is oscillated about its axis to reduce the effects of static friction. Various combinations of masses permit the generation of pressures at intervals as small as 100 Psi up to a maximum pressure of 100,000 Psi. In the "at-rest" position, all the masses are loaded onto the yoke. A series of air operated lifters is used to download respective masses to yield the desired pressures. The tare pressure (due to the weight of the yoke alone) is three thousand Psi, representing the minimum pressure attainable with this system. Common calibration intervals are 5 KPsi and above.

For the most accurate work with deadweight calibrators, corrections need to be made for the effects of gravity, bouyancy of air, and effective piston area of the calibration system.[2] The maximum error from all these sources for our facility is less than 0.25 per-cent, as measured by cross-floating our device against a Harwood controlled clearance deadweight calibrator. The precision of the

Astra gage as used is 0.15 per-cent. Our data analysis program is currently being revised to include the bouyancy and gravity corrections. Once this is complete, the accuracy of the system is expected to move closer to its precision.

The dead weight device as used in our main calibration station is given in Figure 1. The pressure generating source is an hydraulic intensifier (pressure multiplier) of 16:1 ratio, capable of producing over 100 KPsi. The low pressure side is driven by a 10 KPsi air pump. The normal high pressure medium is plexol 201 (now Monoplex), a synthetic lubricant. A check valve, relief valve, additional valving and hydraulic reservoir complete the system.

Transducers are calibrated over the range at which they will be used. Typically, if the expected maximum pressure for an experiment is 100 KPsi, a series of points at 20 KPsi intervals is chosen for calibration. For a test series with an expected maximum pressure of 25 KPsi, 5 KPsi intervals are used. Output values from both the upward and downward portions of the calibration cycle are included, giving typically 11 points for curve fitting purposes. Table 1. The values Y1, Y2 and Y3 are voltage readings representing transducer output which are averaged (Y) and converted to gage output units (PCB), in this case picocoulombs. The data are fitted via a least squares method to a first degree equation (with intercept) and a second degree equation. Curve fitting is done both in terms of transducer response vs pressure and pressure vs transducer response (which is used in computerized data reduction programs). Due to the slight curvature in even "good" pressure transducers, users generally prefer the second order fit for computerized data analysis purposes. For the sake of simplicity, however, they prefer the

TABLE 1. Gage Calibration Record

GAGE: PIEZO

PT	KPSI	Y1	Y2	Y3	Y	PCB
1	0	0.0000	0.0000	0.0000	0.0000	0.0
2	20	.2673	.2673	.2673	.2673	2673.0
3	40	.5399	.5399	.5399	.5399	5399.0
4	60	.8183	.8183	.8183	.8183	8183.0
5	80	1.1069	1.1069	1.1069	1.1069	11069.0
6	100	1.4010	1.4010	1.4010	1.4010	14010.0
7	80	1.1090	1.1090	1.1090	1.1090	11090.0
8	60	.8219	.8219	.8219	.8219	8219.0
9	40	.5435	.5435	.5435	.5435	5435.0
10	30	.2700	.2700	.2700	.2700	2700.0
11	0	.0006	.0006	.0006	.0006	0006.0

FIRST DEGREE FITS

PCB = 8.6081E+01 1.3946E-01 * PSI
PSI = -6.3059E+02 7.1683E+00 * PCB
MPA = -4.3489E+00 4.9436E-02 * PCB

CORRELATION COEFFICIENT = .99985

SECOND DEGREE FIT

PSI = -4.6285E+02 7.5573E+00 * PCB -2.9739E-05 * PCB 2
MPA = -3.1921E-01 5.2119E-02 * PCB -2.0510E-07 * PCB 2

CORRELATION COEFFICIENT = .99999

first order fits to make amplifier settings.

When high pressure transducers are to be used in low pressure measurements, special precautions are needed. Certain makes and models of high pressure transducers appear to have superior low pressure linearity and torque sensitivity properties. These transducers are first pre-screened using the conventional technique. The best of these units are calibrated against a 10 KPsi dead weight system using the negative going pressure step method. That is, the deadweight system is floated at a given pressure against the gage and the pressure is released to zero. (The signal generated is equal to but opposite in sign to the output during actual pressure measurement). The amplifier is zeroed just prior to the pressure step, the whole process taking approximately one second. This fast procedure helps to reduce the effect of drift which can be a significant problem in using high pressure transducers at their low end. For calibrations under 0.15 KPsi a commercial air operated dynamic calibrator is used.

Problem areas and solutions.

Among the practical transducer problems of interest to ballisticians are changes in response characteristics as a function of use, poor dynamic performance, response changes with calibration range, difficulties involving concentricity and depth tolerances in gage ports, and differential pressure measurements. The purpose of this section is to highlight some of these areas and to point out procedures which may help to prevent difficulties before they occur.

Change of response characteristics with use. It is normal for transducer sensitivity to change with use. Typically, gage response decreases, and linearity and hysteresis properties may be adversely affected. Presumably this is due to a gradual degradation of the sensing element. This need not be a problem, however. Regularly scheduled recalibration is used to keep track of these changes, users changing calibration constants as appropriate. For high pressure firings (90-100 KPsi) recalibrations are recommended at 5-10 round intervals. At lower pressures, say 60 KPsi, recalibration after 25 - 50 rounds is recommended. In extreme cases, degradation can be sufficient to affect the continuity of response of the transducer (see Figure 2). In such cases the device is immediately retired. In other cases gages are retained until they fall outside of acceptable hysteresis or zero return characteristics.

Dynamic performance. Questions of the dynamic vs static response behavior of ballistic pressure transducers have concerned ballisticians for some time. In an effort to address this problem, BRL in conjunction with

the Harwood Engineering Company has developed a 150 KPsi positive step calibrator.[3] The device has been used to assess transducer dynamic performance properties. In most cases static and dynamic properties have agreed quite well. Occasionally, however, problems have occurred. Figure 7 illustrates examples of "good" and "bad" dynamic response behavior. In the bad response case the signal from the transducer is showing an upward creep over many milliseconds. Similar, but shorter term, instances have also been observed where the 10-90 per-cent response appears to be normal but the last 10 per cent of the response curve takes several milliseconds. It is thought that seal movement and air bubbles under the strain patch may have caused some of these problems. Other cases where dynamic response problems have occurred have involved eccentric loading of gages due to mismatch between transducer and mounting cavity, see below.

Mounting problems. Figures 8 and 9 present two common problems in transducer/mounting cavity interactions. A lack of concentricity in either the transducer or the mounting hole can result in eccentric loading. The curves may look "normal" but the response may be far out of line. Similar results can be noted if the sensing element touches the bottom of the mounting cavity. In the case of one popular commercial transducer, for instance, seal rings of two thicknesses, steel (.010 in) or copper (.020 in), are available. The cavities are dimensioned according to the intended seal thickness. Substitution of the thinner steel seal for the originally intended copper, for instance, can cause the transducer to "bottom" giving false, often high, readings. While this may seem, on the surface, trivial, such problems are often hard to track down in practice due to the depth and inaccessability of gage cavities. A related problem where tolerances

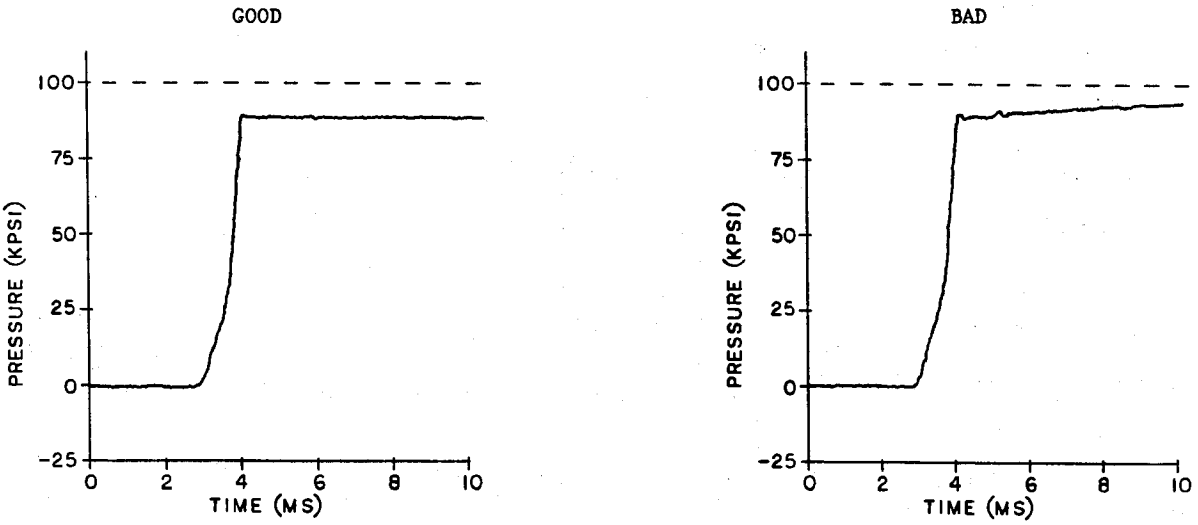

Figure 7. Examples of Good and Bad Dynamic Response

Calibration over the wrong range. A common error among project engineers is to use calibration data obtained over one range in analyzing the results of experiments over a significantly different pressure range. Table 2 illustrates this point. The gage in question was calibrated to 100,000 Psi and the calibration data fitted to a first and a second order equation. The error columns indicate the difference between the fitted equation and the measured calibration points. The greatest deviation from the curves comes at the low pressure end. Use of this calibration data for measurements made over the 0-20 KPsi range, for instance, could introduce as much as six to seven per-cent error in the interpreted data. This error can be dramatically reduced by recalibrating the transducer over the 0-20 KPsi range, see Table 3.

are close is the flexing of the fixture in such a way as to introduce transient mechanical loading on the transducer. Some mounting problems may indicate their presence during installation. If the "feel" of the transducer being screwed into the cavity is "too tight" chances are that there is a concentricity problem. Alternately, recording electronics may be connected to the gage prior to installation to see if excessive signals are generated during the mounting procedure.

Differential pressure measurements. One of the most exacting pressure measurement problems in gun ballistics involves so called differential pressure measurements. Typically, the objective is to measure pressure differences between the fore and aft ends of the breech section in the early portion of the ballistic cycle to detect

TABLE 2. Examples of Potential Errors Introduced at the Low Pressure and in Calibration Over a Wide Pressure Range.

PT	PSI	PCB	1ST	ERROR %	2ND	ERROR %
2	20000	2673.000	19160.83	4.20	19988.22	.06
3	40000	5399.000	38701.59	3.25	39935.09	.16
4	60000	8183.000	58658.10	2.24	59850.15	.25
5	80000	11069.000	79345.78	.82	80008.23	.01
6	100000	14010.000	100427.72	.43	100040.83	.04
7	80000	11090.000	79496.32	.63	80153.10	.19
8	60000	8219.000	58916.16	1.81	60104.66	.17
9	40000	5435.000	38959.65	2.60	40195.55	.49
10	20000	2700.000	19354.38	3.23	20187.96	.94

Table 3. Example of Improvement in Error Levels Due to Calibration Over the Range of Test Pressure.

PT	PSI	PCB	1ST	ERROR %	2ND	ERROR %
2	5000	651.000	4902.81	1.94	4969.78	.60
3	10000	1311.000	9873.40	1.27	9979.62	.20
4	15000	1975.000	14874.11	.84	14990.72	.06
5	20000	2642.000	19897.42	.51	19995.06	.02
6	25000	3313.000	24950.86	.20	24999.70	.00
7	30000	3990.000	30049.48	.16	30018.87	.06
8	25000	3320.000	25003.57	.01	25051.75	.21
9	20000	2651.000	19965.20	.17	20062.39	.31
10	15000	1986.000	14956.96	.29	15073.49	.49
11	10000	1322.000	9956.24	.44	10062.87	.63
12	5000	662.000	4985.65	.29	5053.51	1.07

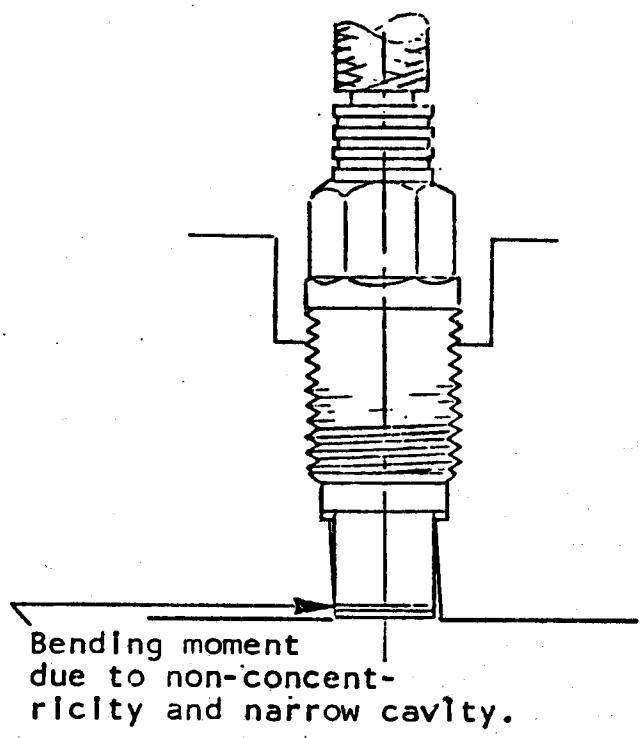

Figure 8. Concentricity Problems in Gage/Mount Installations

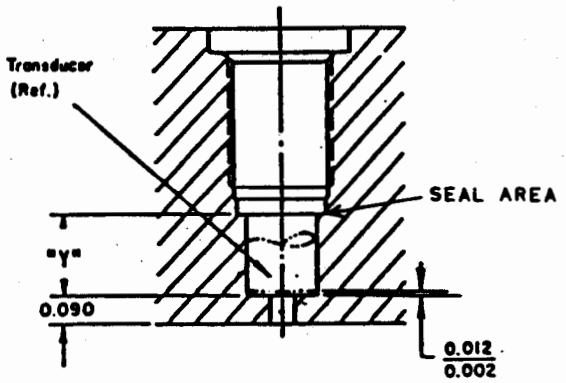

"Y" = .235 ± .002 when used with 600E42 seal
"Y" = .245 ± .002 when used with 600A10 seal

Figure 9. Example of Potential Gage "Bottoming" Due to Use of Seal Ring of Improper Thickness

the formation of pressure waves which may have ill effects on gun performance. The problem is that whereas the event may have a maximum pressure of 80-90 KPsi, the region critical to pressure wave formation is often below 10 KPsi. The pressure differencing needs to be accurate at the low end of the range, where gage errors are greatest. For these measurements, transducers are preselected for the best linearity and hysteresis characteristics. In addition, two and sometimes three sets of calibrations data are used for the same transducer depending on the pressure range being probed. For instance, calibration data for 10 KPsi maximum may be used to interpret the low pressure end of the data while calibration data for 100 KPsi maximum are used to interpret the overall character of the full pressure-time curve. An additional technique used to obtain quality pressure difference data involves the use of mounting adapters, see below.

Mounting adapters. One effective way of minimizing mounting problems is by use of an adapter. A typical example appears in Figure 10. The small size of the adapter permits easier machining and quality checks of the cavity dimensions. A further advantage is that calibration can be done in the adapter, making transducer remounting unnecessary. The adapter, in effect, protects the transducer from mounting strains in the fixture. If necessary, the measurement system, gage and amplifier, can be calibrated together, further refining the data. This can result in excellent performance and repeatability. Figure 11 shows the response behavior of a transducer in its adapter over three calibration cycles. The lines are indistinguishable. The impressive fact about this data is that the transducer had been used to make measurements between the calibration cycles.

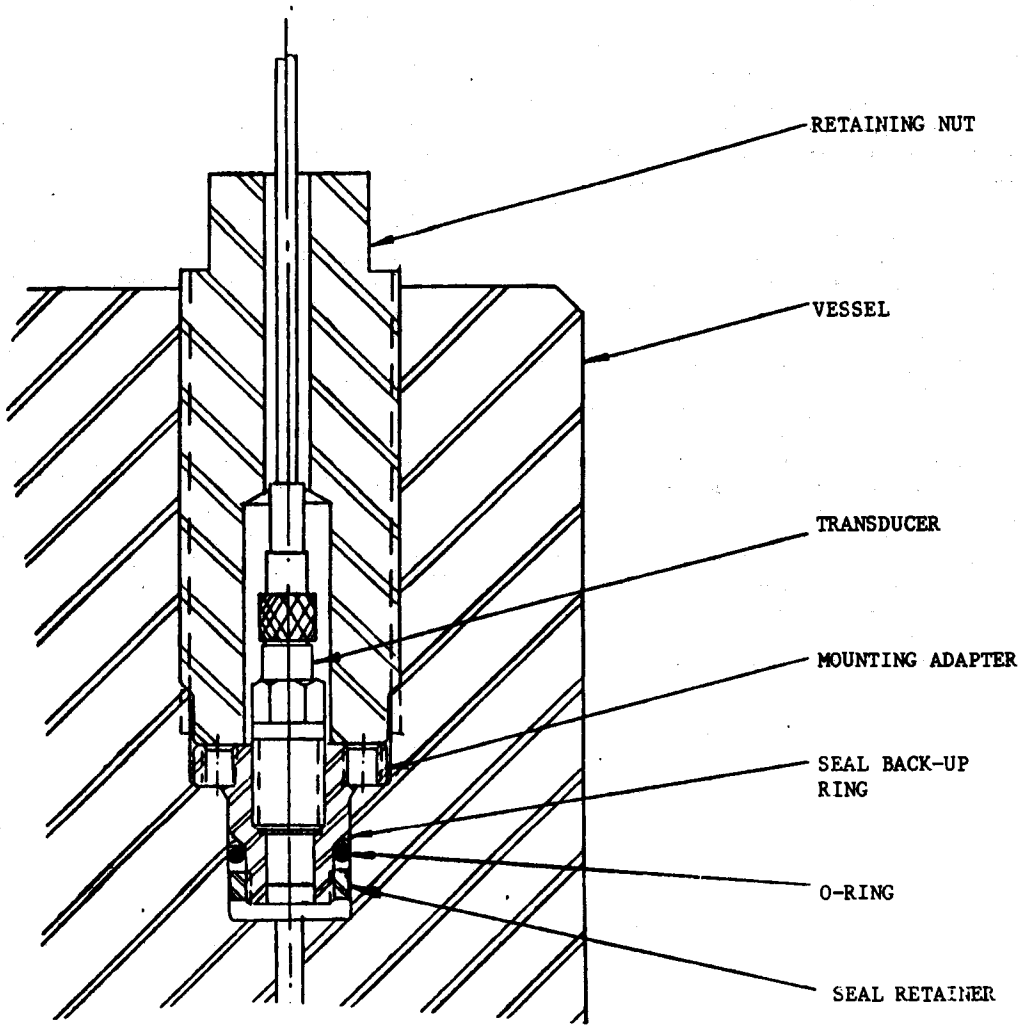

Figure 10. Schematic of a Gage Mounting Adapter

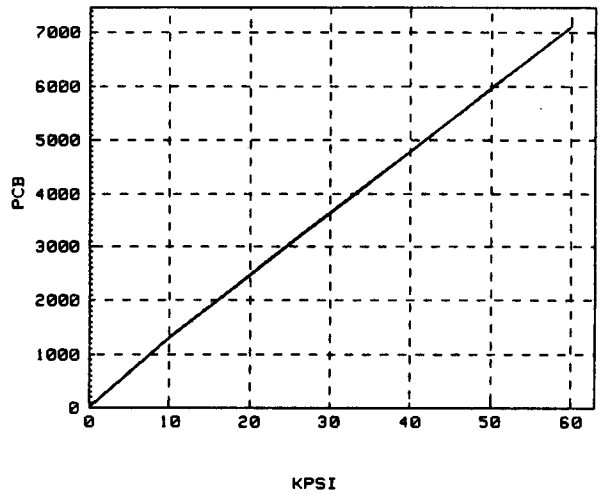

Figure 11. Three Superimposed Calibration Cycles for a Gage in a Mounting Adapter

SUMMARY AND CONCLUSIONS

The procedures in use at BRL are aimed at preventing problem transducers from entering the system and weeding out those whose useful life is past. Continuity, linearity, hysteresis and repeatability characteristics are evaluated for new transducers and for transducers submitted for recalibration. Numerical data are derived using a dead weight calibration system. Static vs dynamic performance differences, when suspected, are evaluated using a high pressure, dynamic positive step calibration system. Calibrations are recommended at 5-10 round intervals when pressures in the range of 90-100 KPsi are to be measured. For pressures in the 60 KPsi regime recalibration is recommended at 25-50 round intervals. Calibration of transducers for the expected pressure range is strongly recommended, since needless large errors may be introduced at the low pressure end by the fitted curve. Mounting adapters not only help to eliminate undesirable mounting effects on the measurements but permit calibration of the transducer in the mechanical environment of the actual measurement. This procedure has been especially useful in exacting measurement applications such as differential pressure measurements.

ACKNOWLEDGEMENTS

We wish to thank Mr. D. Dykstra, mentor to one of us (CDB), who was responsible for setting up the original calibration system. Further thanks go to Harwood Engineering Co., for their assistance with the controlled clearance measurements and the dynamic positive step calibrator. Final appreciation goes to R. Tompkins and J. Newberry for their assistance with this report.

REFERENCES

1. Thirteenth Transducer Workshop, Monterey, CA
2. The Piston Gage as a Precise Pressure Measuring Instrument; Harwood Engineering Company, Walpole, MA.
3. Astron Gage Manual; Pressure Products Industries, Warminster, PA.
4. Handbook of Transducers for Electronic Measuring Systems; Harz N. Norton, Prentice Hall Inc., Englewood Cliffs, NJ.

SESSION 2

APPLICATIONS

DYNAMIC STRAIN MEASUREMENT ON TRACK PINS OF TRACKED VEHICLES

Bobby E. Reed
Chief, Design & Development Branch
Instrumentation Services Division
USAE Waterways Experiment Station
Vicksburg, Mississippi

Charles W. Bobbitt
Associate Professor of
Engineering Mechanics
Aerospace Engineering
Department
Mississippi State University
Mississippi State, Mississippi

Abstract

The severe loading conditions placed on the track-shoe connector pins of tracked vehicles such as the M1 Battle Tank lead to pin failures which seriously limit service life. A necessary step in extending life is a determination of the load description in an operational situation, which requires the measurement of pin strains on a vehicle as it traverses a test track. A system is described which continuously and simultaneously measures six variables on the Ml tank track by means of transducers and associated electronics mounted directly on the track. The signals are telemetered to the tank hull where they are recorded on magnetic tape and/or retransmitted to a data acquisition van. The variables are strain measurements at four axial stations on a track pin, transverse acceleration of the track, and battery power supply output voltage. The current system has evolved to successfully overcome noise problems and the difficult geometery and hostile environment of the tank track.

Introduction

The US Army maintains a number of combat and service vehicles which best accomplish their design purposes by traveling on tracks rather than on rubber tires. Tracks can better support very heavy vehicles and can provide a type and degree of cross-country maneuverability not found in ordinary wheeled vehicles (Figure 1). These desirable characteristics, however, come at the expense of a relative short service life of the tracks, which is costly both in terms of operational capability and dollars expended. For example, the current annual expenditure for maintenance and replacement of tracks is approximately $150 million and by 1990 is projected to be in excess of $200 million (1). It is evident, then, that an effort which contributes to extended service life is much to be desired.

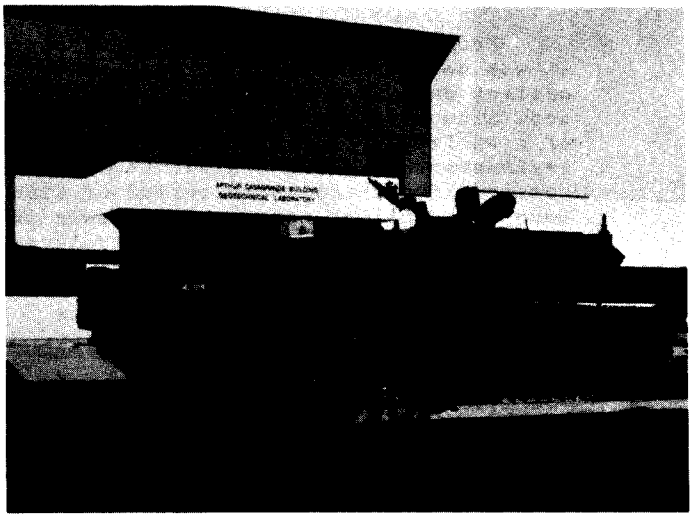

Fig. 1. Ml Tank

The Army's new main battle tank is the Ml which weighs over 65 tons and has a top speed in excess of 40 miles per hour. In traversing all types of terrain, this extreme weight, in a dynamic operating mode, places a variety of severe loading conditions on the track shoes and on the pins which connect them. The pins, in particular, are frequently subjected to combined loads of torsion, shear, and bending, such that direct failures or relatively low cycle fatigue failures occur at an unacceptable rate. To counter this growing problem, the US Army Tank Automotive Command (TACOM) supports several related studies aimed at solving existing problems and, at the same time, developing design tools for future generations of tracked vehicles. One such study, conducted by the US Army Engineer Waterways Experiment Station (WES) and others (2), has the goal of developing a family of computer codes which completely describe and analyze

track dynamics, pin stresses, and other areas of interest in relation to specified input conditions. In order to verify these codes, it is necessary to obtain, under actual operating conditions, experimental data points which give reliable values to such quantities as total track tension and stress distribution over the track pin.

The work described in this paper was performed by the Instrumentation Services Division (ISD) to develop a measurement method to provide the data required by the Mobility Systems Divison (MSD), Geotechnical Laboratory, WES.

Overview

From the beginning of this effort, it was deemed necessary to be able to collect data from a moving vehicle in a test situation which could represent any of a variety of operating environments. Thus, a given test could continue for an extended period of time (and distance) at rather high speeds and require the acquisition of a very large amount of data. These conditions ruled out the possibility of using a data acquisition vehicle connected to the test vehicle by an umbilical, and of using "on-track" data loggers for storing the data during the test. The former would put too great a restriction on the mobility of the test vehicle, and the latter would limit the amount of data which could be obtained in a given test as well as eliminate the possibility of immediate examination of data during an ongoing test. The remaining choice was to telemeter the data from the track to a receiver and appropriate recording equipment in the tank hull, and optionally, to permanent recording and output devices in a suitably equipped instrumentation van.

Based on work done in this direction by Battelle Laboratories and others (3) it was judged that a reliable system based on telemetry could be developed, in spite of severe space constraints and an extremely hostile environment. The remainder of this paper will describe the development and calibration of the measurement system and present the results of selected tests.

Measurement System

In order to obtain a reasonable estimate of the loads applied to the track pin, it was necessary to have as many strain gages as possible along the length of the pin, since many loading situations can produce the same strain at a given point. Moreover, significant loads occur in both the direction of the track (tangential) and perpendicular to it (normal). At the same time, each strain gage location corresponds to a channel of information to be telemetered, which places a practical limit on the number of locations. In the configuration reported here, four strain locations are simultaneously monitored. This is the maximum number of bridges that can be accommodated by the prototype system. In choosing the locations for the gages, theoretical stress distributions along the pins under typical loading conditions were examined to determine points of significant stress activity. The theoretical stresses were computed by the MSD of the Geotechnical Laboratory at WES, using codes developed especially for track dynamics. As a result, the gages were placed symmetrically on the pin, two immediately adjacent to the center connector, and two just inboard from the end connectors. At each position, gage pairs were mounted for tangential as well as normal strain measurement. In addition to these four channels, a fifth channel is provided to measure track acceleration in the transverse (normal) direction, and a sixth channel monitors the battery power supply voltage.

To transmit these signals to receiving equipment in the tank hull, each signal feeds its own voltage-controlled oscillator (VCO) and the resulting signals are then mixed in the frequency multiplexer and fed to the S-band transmitter (2.2-2.3 GHz) for transmission to the hull instrumentation. At the hull, the received signal is demultiplexed and discriminated to recover the analog signal, then is properly conditioned and stored on magnetic tape. Along with these six signals, four additional signals from chassis mounted transducers are recorded, giving track position, pad position, vehicle speed, and vehicle distance.

Optionally, these data can be fed to an on-board transmitter for retransmission to the instrumentation van. Figure 2 shows block diagrams of both the track-mounted instrumentation and hull-mounted instrumentation.

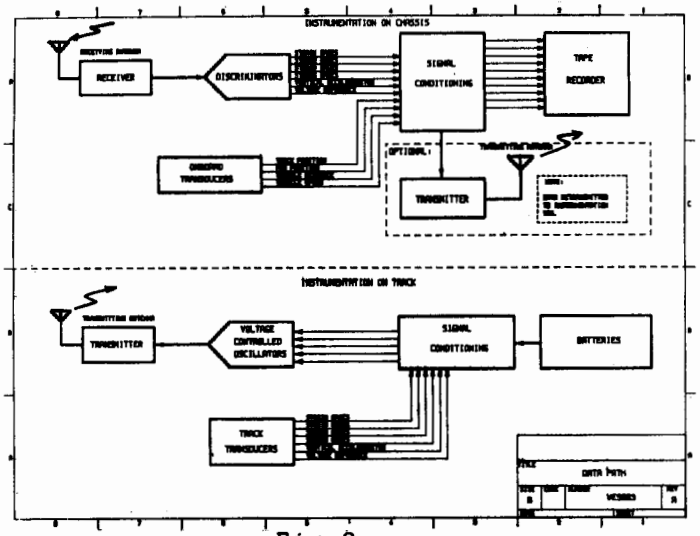

Fig 2.
Track/Hull Mounted Instrumentation

Strain Gage Installation

The attachment of the strain gages to the track pin presented some rather formidable problems. A typical track pin is pictured in Figure 3, where it is noted that the pin is a thick-walled steel cylinder with flats at either end to facilitate connection of adjacent track shoes. The pin has an outside diameter of 1.375 inches, and a bore of 0.75 inch. The pin is connected to the track shoe by slipping it into a binocular tube in the shoe. Rubber bushings are used to avoid metal-to-metal contact. The bushings consist of a series of rubber "donuts" vulcanized to the pin's outer surface, and as the pin is pressed into the shoe tube, the incompressible rubber deforms to completely fill the annular space. Subsequent relative angular motion between the pin and shoe is through shear deformation of the rubber.

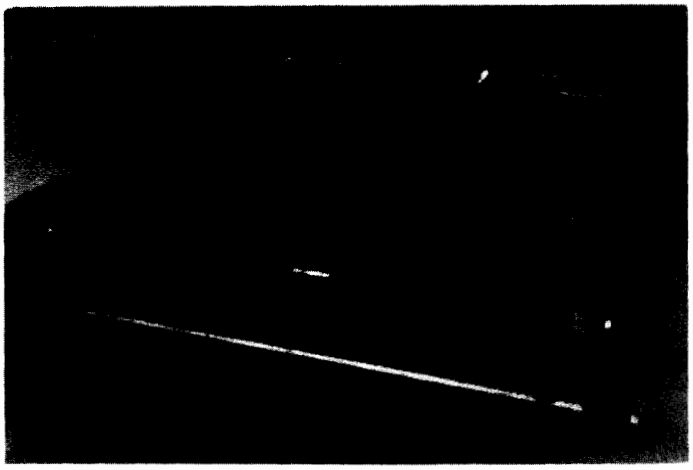

Fig. 3
Track Pin, Pin with Rubber Bonded, and Shoe Assembly

The original gage attachment plan was to place the gages on the outside of the bare track pin at four axial stations, then vulcanize the rubber over these gages. Lead wires would pass through the bore via small holes drilled in the pins adjacent to the strain gage tabs, and the pins would then be pressed into the track tubes. This plan was ultimately rejected because of the likelihood that the gages would not survive the installation process and because the lead-wire holes would alter the strain field which the gages were to measure.

The alternative to the original plan was to mount the gages inside the bore, a task in some respects more formidable than the original. Gages had to be satisfactorily bonded to a surface at a location as much as 12 inches deep in a 3/4-inch bore. At each axial station within the bore, four gages were to be bonded at equally spaced circumferential locations, so that one opposing pair could be used as a half-bridge to measure normal bending strain and the other pair to measure tangential bending strain. The half-bridge configuration would have the usual advantage of minimizing temperature and non-bending strain effects.

The necessity for mounting the gages in the bore led WES technical personnel to design a special tool for this purpose. This ingenious device consisted of a long shaft with four "fingers" at one end which could be opened or closed from the other end. The device is pictured in Figure 4 in "fingers open" position. In use, the four strain gages are attached to the fingers by double-sided tape and the exposed surfaces coated with adhesive. The pre-soldered lead wires are fixed to a long central shaft which can slide axially through the installation tool body. These features are shown in Figure 5. Gage location is set by an adjustable collar which can index the gages to any desired axial and circumferential position. A typical installation procedure is illustrated in Figure 6. After the adhesive has cured, the installation tool is retracted and the gages are protected by filling the pin bore with a suitable potting compound. The size 36 AWG insulated lead wires, thirty-two in number, are brought outside the bore through a small drilled hole (with rounded, tapered edges) approximately midway between axial strain gage locations. These wires are soldered to a multi-pin connector attached to the track shoe underneath an instrumentation module. This connector can be seen at the left

end of the track shoe in Figure 10. The signals are then distributed to the strain gage amplifiers and connected to produce the desired output readings.

Fig. 4
Strain Gage Installation Tool

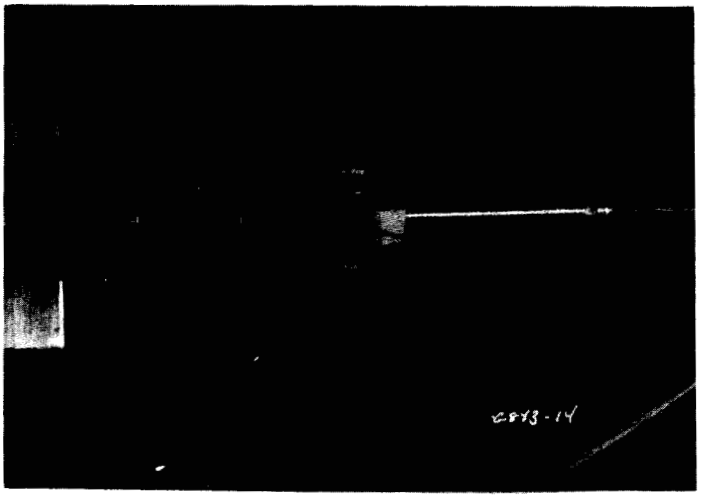

Fig. 5
Gages Mounted for Installation

Strain Gage Calibration

The strain gage signals can also be diverted away from the system instrumentation to external calibration instrumentation so that known applied loads can be related to bridge outputs at each axial station, in both normal and tangential directions.

In establishing acceptable calibration procedures, several methods were employed. Two gaged pins were assembled in a track shoe and tested at the TACOM facility at Warren, Michigan. Available test equipment included a track tension machine and a six degree-of-freedom machine. These machines are pictured in Figures 7 and 8. The major result from these tests was the observation that loads applied

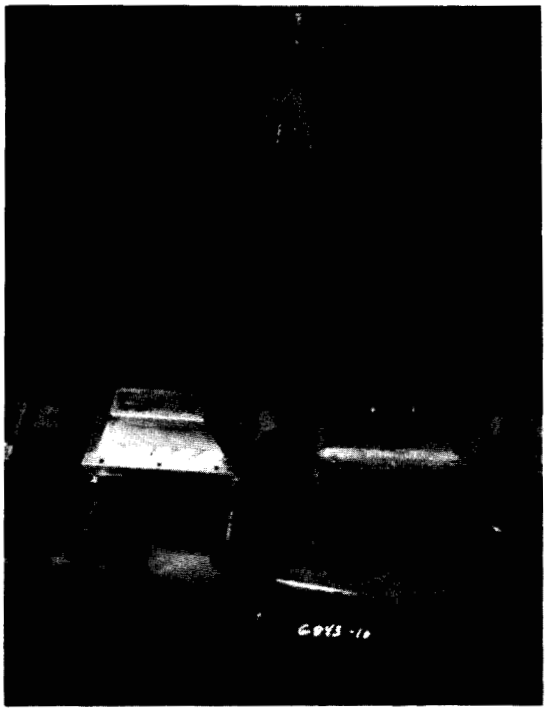

Fig. 6
Gage Installation

to one pin in a track shoe were distributed in significant amount to the other pin through deformation of the shoe itself. Another result was the observation of a failure mode through an unexpected overload of the system. Figure 9 shows a deformed center connector stemming from the overload, compared to an undeformed connector.

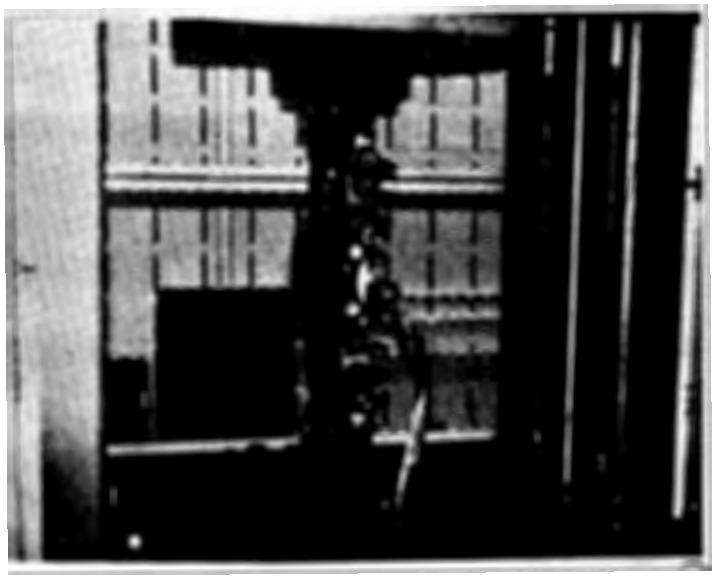

Fig. 7
Tensile Test Machine

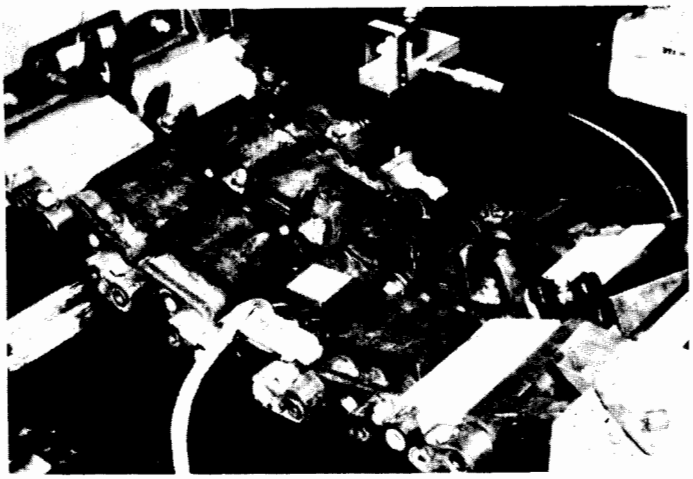

Fig. 8
Six Degree Freedom Loading Machine

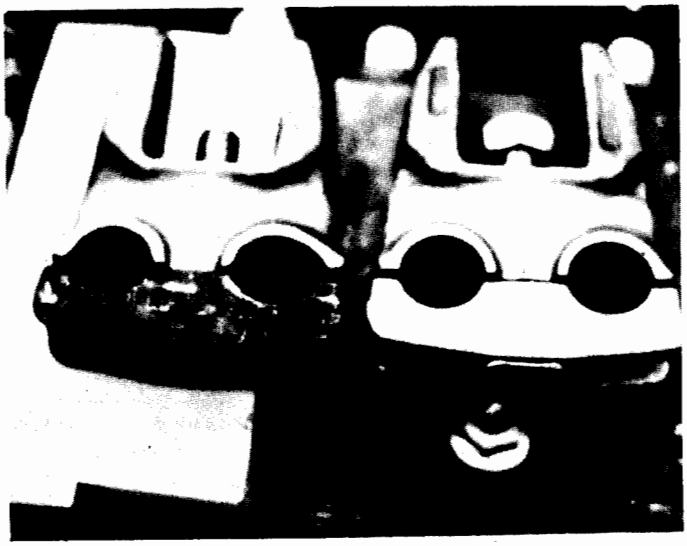

Fig. 9
Deformed Center Connector (Lt)

As a result of the TACOM tests, additional calibration systems and techniques were devised at WES. One system is pictured in Figure 10, which shows how a symmetric load of pure bending is applied to the track shoe/track pin assembly for the purpose of calibrating the normal gages. The device not only eliminates cross-coupling between the pin loads, but also rotates each pin relative to the track shoe so that the gages will be in the true normal configuration. Notice that bending force (bending moment) is applied by means of a turnbuckle acting through a load cell. To calibrate the tangential gages, the load arms on one pin are rotated ninety degrees, and the arms on the other pin are removed. In this procedure, it is clear that the track shoe couples the load from one pin to the other, but this is the desired effect since it corresponds more closely to the operating configuration.

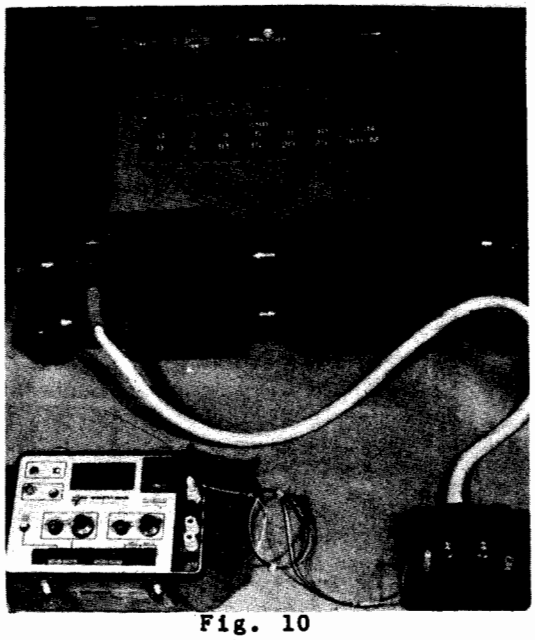

Fig. 10
Bending Test Fixture

A second calibration system was devised with a view toward obtaining a single number which would be indicative of track tension under various operating conditions and at all positions of the gaged pin relative to the drive sprocket as it executes a cycle around the track. This number is required for verification of computer codes representing tank performance. The determination of this data point is complicated by the change in loading of the pin as the gaged track shoe engages the drive sprocket. During this process, the distribution of load between end connectors and center connector changes significantly, and the output of a single strain gage bridge cannot be taken as representative of track tension. To meet this difficulty, a loading system was devised to simulate track tension at a point off the drive sprocket, and upon demand to simulate the drive sprocket load. This system is shown in Figure 11. Notice that load is transmitted from leading to trailing pin in a given track shoe through the shoe proper, and from one track shoe to another through the end connectors and center connector. A typical output of the tangential gage system is shown in Figure 12. First the tensile load in the track is applied by lifting the system with the overhead crane at a more-or-less constant rate, and continued lifting engages the simulated sprocket load. By a trial-and-error manipulation of all the tangential gage outputs, it was found that an average of all gage outputs gave the best indication of track tension. This can be seen in Figure 13, which shows load cell output and strain gage bridge outputs for a typical loading process.

When the outputs of all the gages are added and calibrated, the result is a very good measure of the total load (tension plus sprocket load) even though the individual gage outputs do not qualitatively indicate total load.

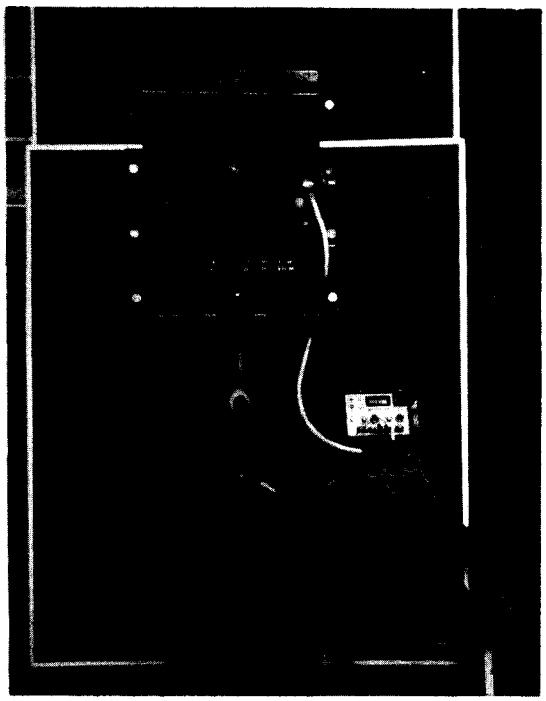

Fig. 11
Simulated Track Tension

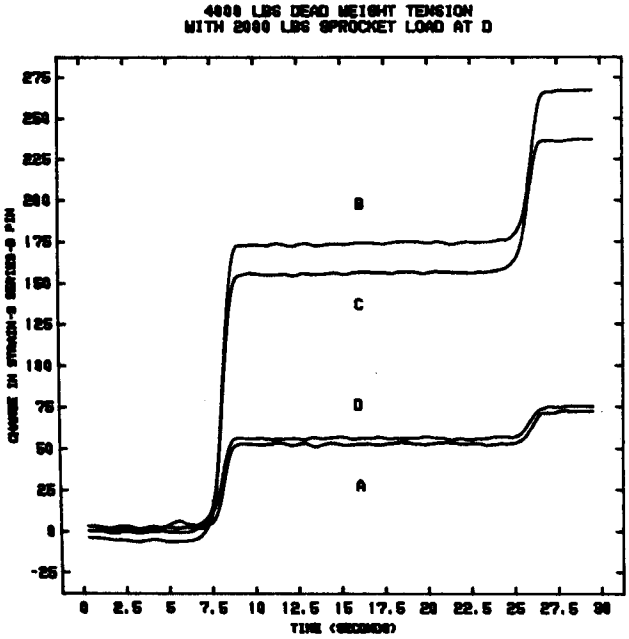

Fig. 12
Track Tension Test

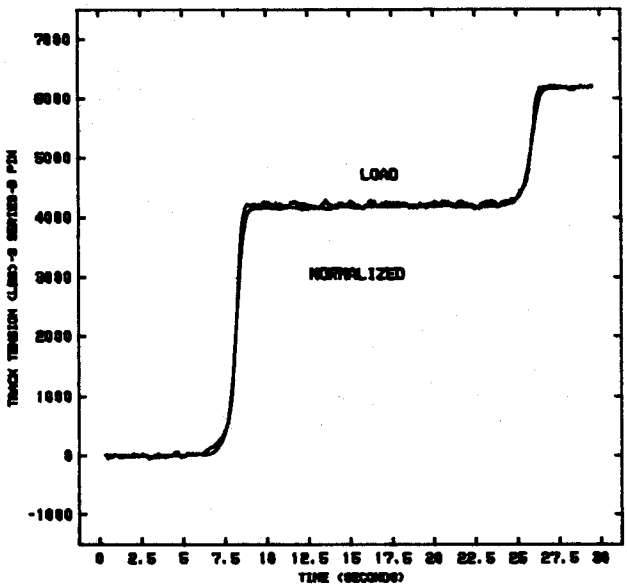

Fig. 13
Tension Summed

The Electronic System Packaging

Having established the integrity of the strain gage transducer, the next task was to fit the electronic signal processing circuitry to the tank track environment. A number of separate modules were required to hold the electronic packages and the printed circuit (PC) boards necessary to connect them. The modules were of two-piece design. The lower piece was attached to the track shoe with machine screws and the top piece, which housed the electronics, was fastened to the bottom with cap screws. Because the track is subject to some lateral motion relative to the sprocket and road wheels, it was necessary to size the modules for proper clearances. Two test modules of different sizes were fabricated and covered with a thick layer of styrofoam. These modules were mounted on the track such that subsequent operation of the tank caused some styrofoam to be scraped off at the points of maximum interference. In this way, the total module volume for containing the electronics was maximized. Figure 14 shows two styrofoam covered modules of different sizes before and after operation.

In the final configuration, the electronic components were contained in eight modules, four of which held the power supply in the form of nickel-cadium batteries connected to provide 28 VDC, nominal. These modules can be seen mounted on the tank track (front, bottom) in Figure 1 and on a section of track with covers removed in Figure 15. Close-up views of the major components are shown in Figures 16-21.

Fig. 14
Clearance Test Module

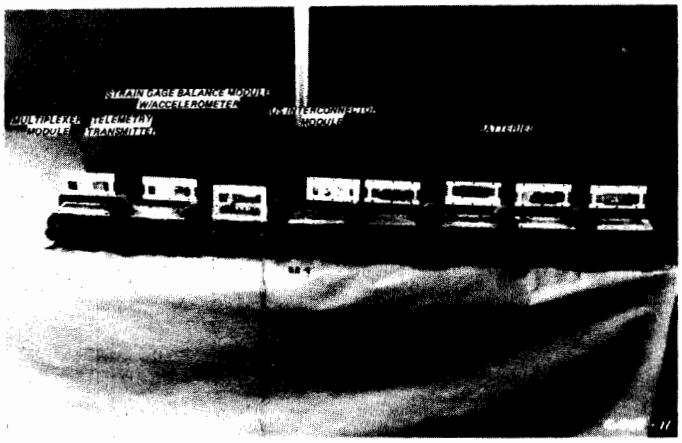

Fig. 15
Track Mounted Instrumentation System

Notice that the components are connected by a twenty-conductor ribbon cable bus system which allows the modules to be tightly sealed from the environment.

Figure 16 shows one of the four modules containing three batteries each to make up the power supply. The batteries provide the capacitiy for extended testing before recharging is required. The battery power switches, battery charger connector, and calibrator-monitor connector are shown in Figure 17. The module pictured in Figure 18 contains the strain gage power supply ((DC-DC converter), balance potentiometer for the strain gage/Wheatstone bridges, a 250g accelerometer, and the accelerometer calibration switch. (As a matter of interest, all the PC boards used in the system were made in the WES/ISD facility.) Figure 19 shows the track telemetry transmitter removed from the housing while Figure 20 shows the top of the transmitter module with the S-band dipole slot antenna in place. The last module (Figure 21) contains the differential amplifiers and subcarrier oscillators for the strain gage bridges, the mixer, and a micromount for the components.

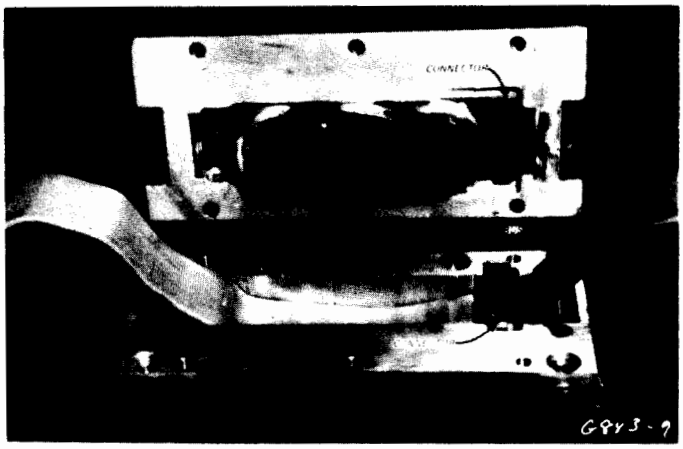

Fig. 16
1 of 4 Battery Modules

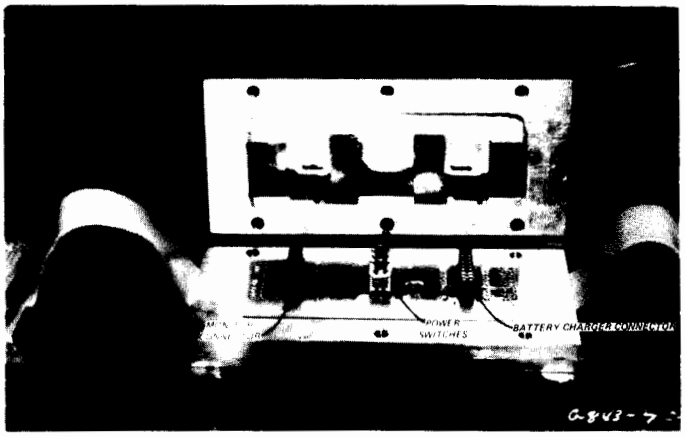

Fig. 17
Power Distribution/Bus Monitor Module

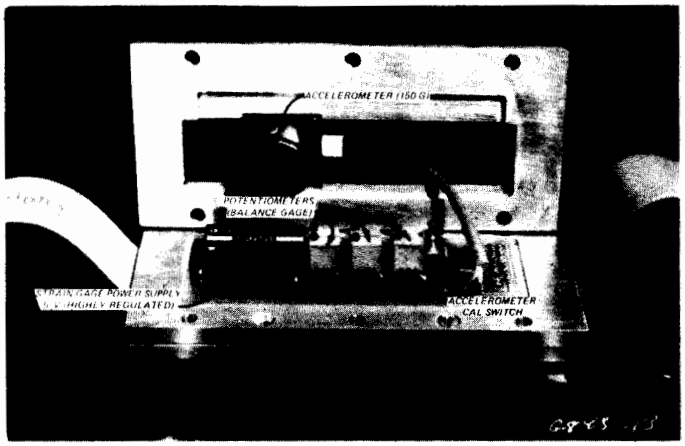

Fig. 18
Strain Gage Interface Module

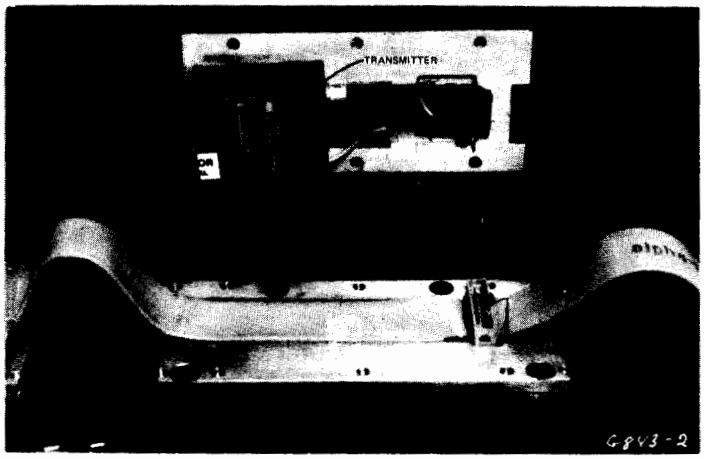

Fig. 19
Telemetry Transmitter Module

The multiplexed signal sent from the track is received by hull-mounted equipment. The major items are the quarter-wave stub antenna and receiving unit containing receiver, demultiplexer, discriminators, and power supply (Figure 22), the WES constructed signal conditioning unit (Figure 23), and the 21 channel tape recorder (Figure 24). Additional equipment is provided to retransmit the signals to an instrumentation van for immediate hard-copy if desired.

In addition to the instrumentation described, the tank chassis carries a fifth wheel for vehicle speed and distance information (Figure 1), and a magnetic pickup which senses track pad position relative to drive sprocket.

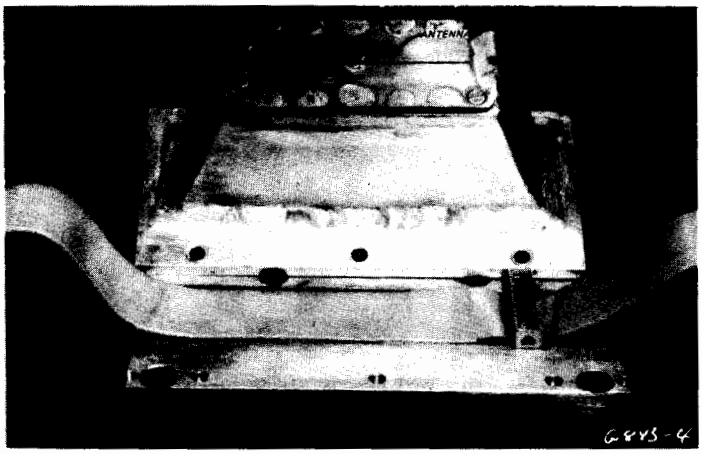

Fig. 20
Transmitting Antenna

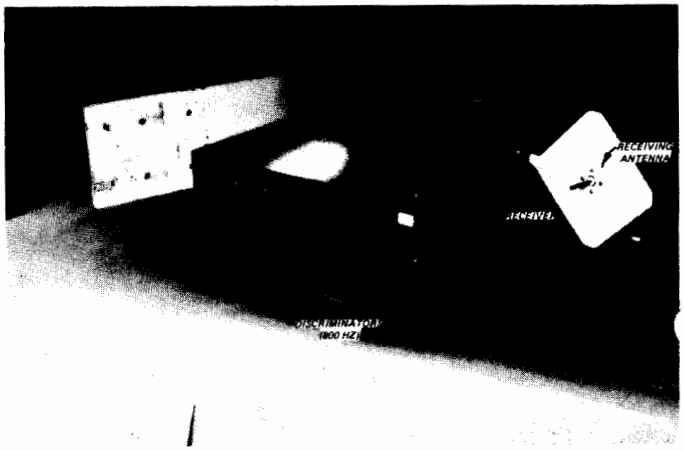

Fig. 22
Receiver/De-multiplexer

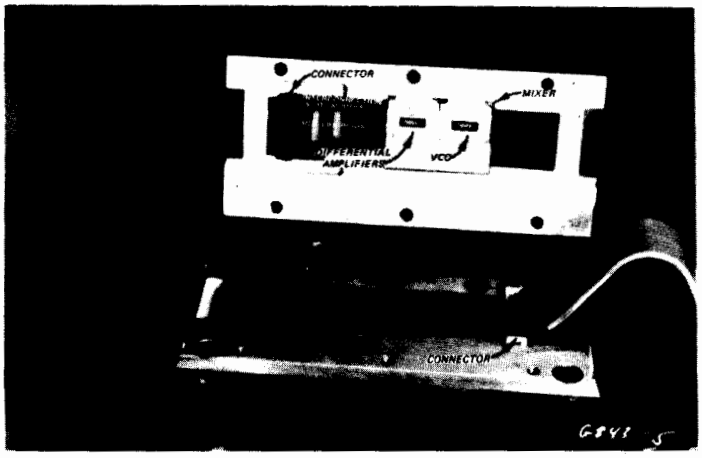

Fig. 21
Multiplexer Module

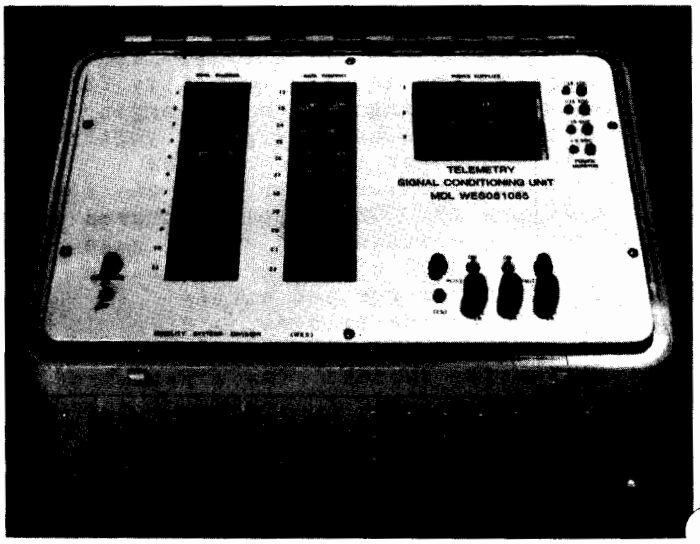

Fig. 23
Signal Conditioning Unit

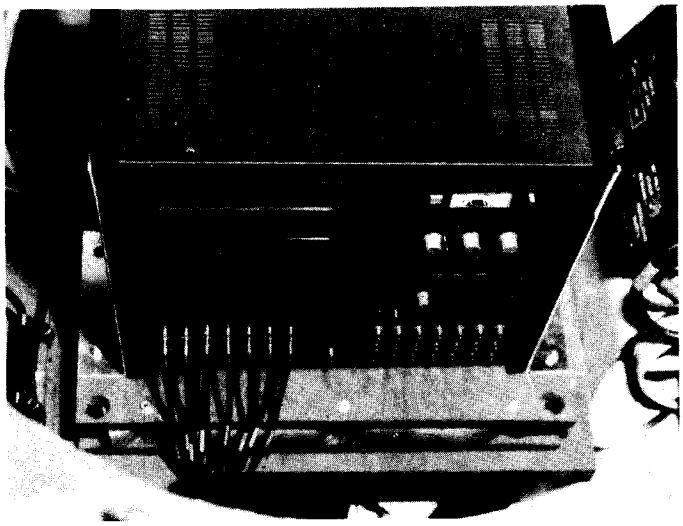

Fig. 24
Analog Tape Recorder

System Performance

Although a substantial amount of testing has been done, the primary purpose of this paper is to describe the development of the system and indicate its effectiveness in measuring the quantities of interest. Consequently, only a few test results will be presented to show the quality of the data. It is also necessary to be familiar with the test vehicle in examining and interpreting the data. For example, the track tension, set to a nominal preload by an adjustment cylinder, varies significantly in its sojourn around the drive and suspension components of the vehicle. Moreover, the track shoes and pins are subject to a variety of loading conditions governed by the terrain and the successive passage of the road wheel over the track section on the ground. Figure 25 shows the output of a typical track pin strain gage bridge as the vehicle moves at constant speed over a smooth, level path. Note the quality of the signal and the sensitivity to load variations as the gaged track pin passes over the idler wheel, the individual road wheels, and the drive sprocket. The track and terrain geometery govern the distribution of bending moment along the length of the track pin, so the output of the four bridges will vary appreciably in any specific test mode. The results of other tests (not pictured) show clearly that the gage outputs can be used to identify maneuvers such as turns and accelerations. A correlation of gage outputs with a variety of test conditions is one objective of ongoing tests and development.

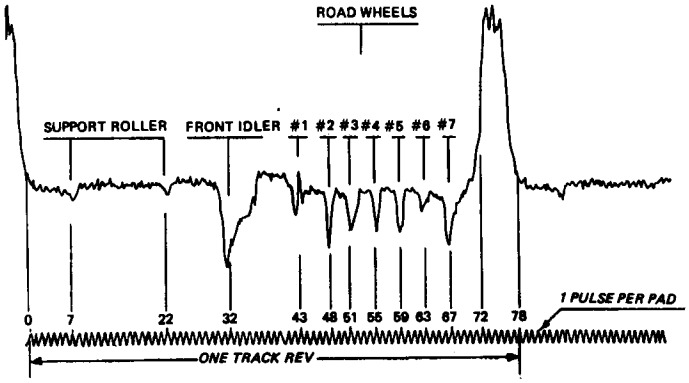

Fig. 25
Constant Speed on Level Surface

Finally, Figure 26 presents a time history of a quasi-static test designed to place maximum bending load on the track pin. Two 4 x 4 timbers were placed in a parallel position and spaced the track width apart so that the vehicle could be driven upon them in such a way as to be supported by the track pin end connectors only. The pins thus became (nominally) simply-supported beams loaded symmetrically between supports. The figure shows how the outboard (A) and inboard (B) bridge outputs differ, both in mean value, and in instantaneous variation as the road wheels pass over the pin.

To produce these last two figures, the analog signal was digitized and stored on a floppy disk. In this form, the information is put in a computer where it can be manipulated in ways to produce the most usable outputs. For example, this procedure led to the observation that the algebraic sum of all the outputs was the best indicator of track tension under all loading conditions.

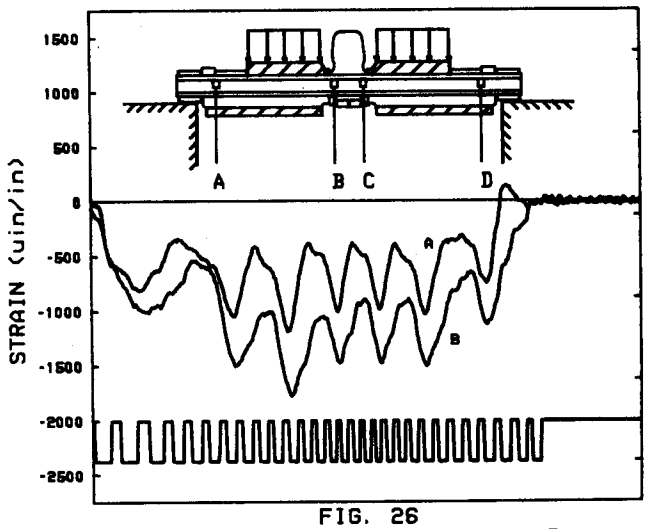

FIG. 26
SIMPLY-SUPPORTED TRACK TEST

Conclusion

This experimental activity proved to be unique in a number of ways, in terms of the problems encountered and in the solutions to them. Many of the problems could not have been anticipated and certainly could not have been overcome without experimental development and creative engineering. It is evident that problems still exist, especially in the area of correlating transducer output with track loads under arbitrary conditions. Continued development efforts hold promise for significant rewards. It is desirable to gage track pins at as many as eight to ten axial stations in order to refine the load determinations. This will require correspondingly more telemetered output channels. In using this additional output, procedures and methods for correlating output to load must be developed for use as routine track design tools.

As a final observation, the methods developed for track measurement can be applied to a variety of other experimental situations. For example, the strain gage application tool has already been used to place gages inside pipe and tubing for use in concrete strain measurements. Any test requirement involving a hostile environment and close space demands would be well served by the kind of system described herein.

Acknowledgment

The authors express their appreciation to the Track and Suspension Division, Directorate for Tank Automotive Technology, Research, Development and Engineering Center at the US Army Tank Automotive Command for sponsoring this program, and to the Mobility Systems Division, Geotechnical Laboratory, US Army Engineer Waterways Experiment Station, for supporting this effort. Approval for the presentation has been granted by Office, Chief of Engineers.

References

1. Kaifesh, M.; Chief, Track and Suspension Division, US Army Tank Automotive Command, Warren, Michigan; Telephone Communication to Mr. Newell Murphy, April 1987.

2. Murphy, Newell R., Bobby E. Reed, and Allan S. Lessem; "Initial Field and Simulation Studies," TR GL-87-7, US Army Engineer Waterways Experiment Station, January 1987.

3. Rodman, Charles W. and Howard C. Meacham; Battelle Columbus Laboratories; "Laboratory and Field Checkout of T-142 Track Telemetry System", TR 13089, Research and Development Center, US Army Tank Automotive Command, Warren, Michigan, May 1985.

Q: Rogers P. Noyes (EG&G Energy Measurements, Inc., Las Vegas): What, if anything, did you do about the varying ambient temperature, assuming that you ran hot and cold?

Q: Bobby E. Reed: Are you talking about strain gages?

A: Roger P. Noyes: The whole system.

A: Bobby E. Reed: Most of the electronics in the system were of the type that would withstand the temperature extremes that we operated under.

Q: Edward E. Hartman (Caterpillar, Inc.): We do some of the same testing. I have a question for you on your connectors and your ribbon cable. Evidently, your environment is as not severe as ours because we have had little or no success with that. Do you have any problems with the ribbon cables and the type of connectors you use?

A: Bobby E. Reed: We didn't have a problem with the cable, but we did have a problem with the connectors. The main thing is to make sure that the connectors interface rigidly and are not loosened by vibration. If we got vibration, we would periodically lose signal.

CLIP GAGE STABILITY*

United Technologies, Chemical Systems Division
San Jose, CA
E. C. Francis
S. Perkins
S. Heerema

ABSTRACT

Clip gages have been used to measure solid propellant bore and slot strains for over twenty-five years. When one compares analytically predicted or mechanical measured strains with the clip gage measured strains a significant difference has been noted. This measurement uncertainty has been attributed to attach problems and gage instability. This paper addresses the instability factor and how one can rapidly determine this instability and also reduce this factor using good gage manufacturing procedures.

BACKGROUND

Solid propellant motor instrumentation has been utilized for measuring stress and strain for many years. Early stress gages have displayed instability both in the motor environment and in laboratory bench tests. Clip gages have not been evaluated to the same degree, but reported motor strain data has shown a poor correlation with predicted strains. CSD has routinely used spring loaded strain measurement devices without this problem, but bonded or pinned clip gages have certain application features which make their use desirable. CSD has conducted a series of clip gage tests in the 1984-1986 period which showed that clip sensor stability problems can invalidate their use unless the devices pass rigid screening tests. The best way to develop stable clip gages is to use the applicable manufacturing procedures developed for stable stress gages[1]. This paper will show some of the stability data which identified the clip gage problem and how to screen stable foil and semiconductor strain gage displacement transducers.

EARLY STABILITY TESTING

Clip gage configurtions used for 1984 tests were designed for both slot width and bore strain measurements (Figure 1). Gages were manufactured by CSD using Micro-Measurements: strain gages, adhesives, and bonding procedures. Initial designs used MA-06-031CE-350 strain gages and AE-15 epoxy. Later designs incorporated NK-06-5022H-50C strain gages and M-bond 600 epoxy. The micro-measurements recommended bonding process was followed with close attention paid to surface preparation, clamping, cure time, and temperature.

*This work conducted on Contract F04611-85-C-0081 for Air Force Rocket Propulsion Laboratory, Edwards, CA 93523. Approved for public release; distribution is unlimited.

EARLY TESTING

Early clip gage calibration tests were short time tests which did not include evaluation of time dependency of gage outputs. These gages were used on bulk uniaxial propellant test samples. These tests showed a surprising amount of discrepancy between clip gage readings and optical (cathetometer) readings and changed with test time. As a result these clip gages were returned to the calibration fixture and monitored at various displacements and over reasonable time increments. Analysis of this data showed an excessive amount of clip gage creep which reached 10% for one of the displacement transducers.

To expedite collection of gage creep data, the test conditions were reduced to a single displacement from nominal zero displacement to nominal full scale displacement. Test time at full scale displacement was standardized to 30 minutes. This became the basis for comparing creep screening test data.

A variety of factors were studied using the 30 minute creep test. Among these were:

- Strain Level at Full Scale Displacement
- Power Level - Excitation
- Foil Strain Gage Configurations
- Gage Coatings
- Temperature

STRAIN LEVEL EFFECT

Strain level effects on the sensors were studied by conducting tests at two strain levels (500 vs 2300uε). These tests were performed on the same gage. To minimize the effects of the previous strain histories, the gage was allowed to relax at 160^{0}F for 2 hours followed by 22 hours at ambient before the next test was run. Results in Figure 3 show that the lower strain level of 500uε showed a 1.5% creep in 30 minutes. The 2300uε test showed 3% creep in 30 minutes. Creep is related, though not proportional to induced strain. Strain gage manufacturers recommend that sensors be designed to operate in the 1000uε or less region to avoid instability problems. However, the 500uε test sample showed that even at reduced strains the creep was still excessive.

POWER LEVEL

Tests were conducted at sensor excitation levels of 5 volts and 0.1 volts. Results in Figure 4 show that over 3% creep was experienced for both

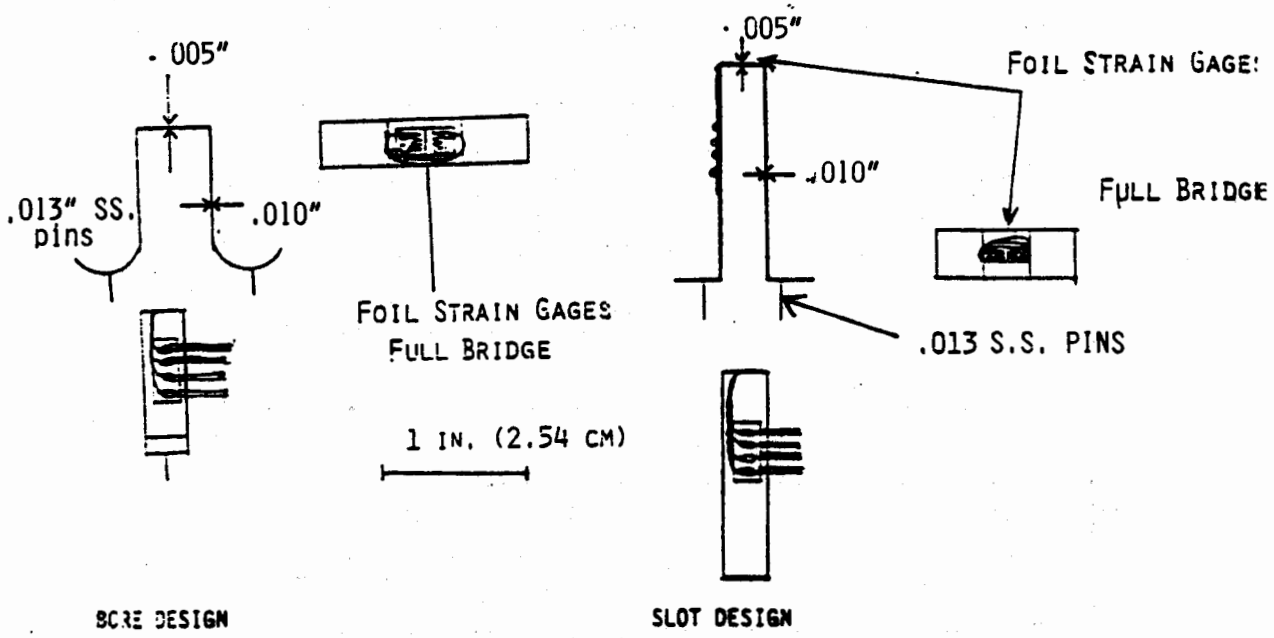

Material: 302 Stainless Steel
Strain Gages: Micro Measurements MA-06-031CE-350
Strain Gage Adhesive: Micro Measurements AE15

Figure 1. Bore Surface and Slot Clip Gage Designs

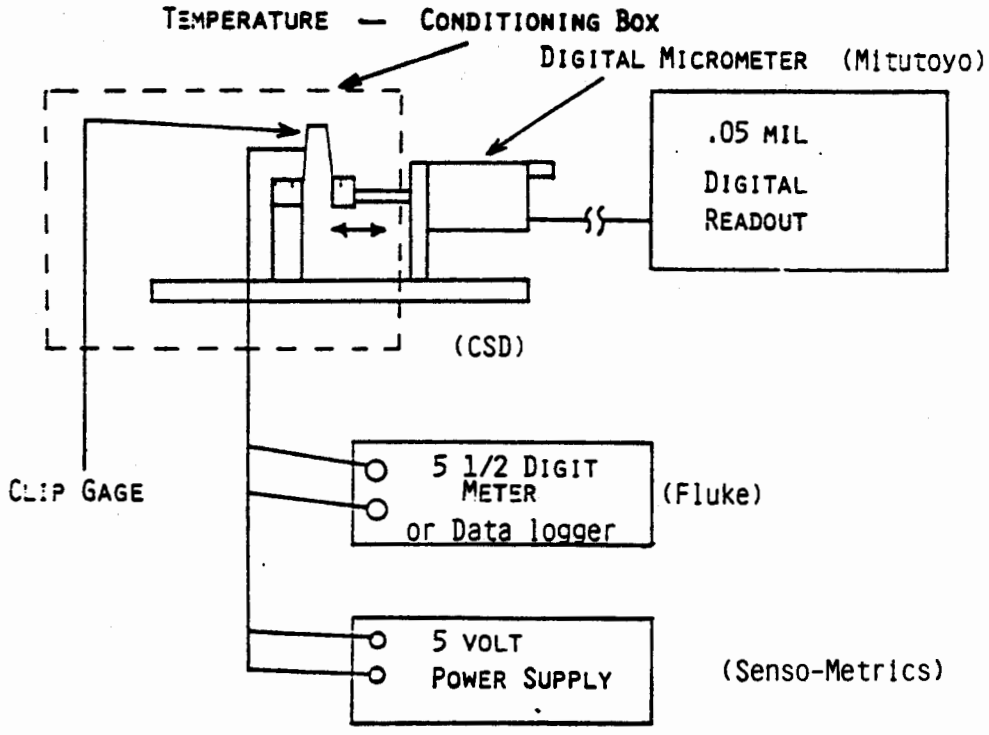

Figure 2. Clip Gage Creep Test Equipment Schematic

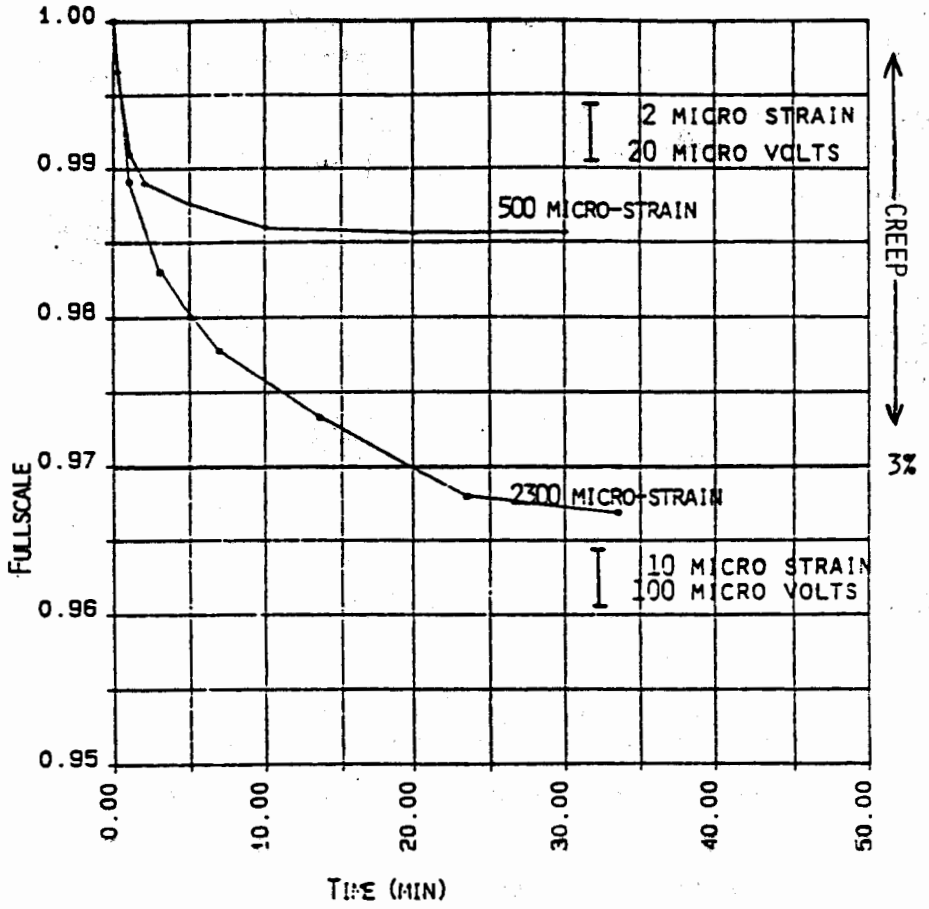

Figure 3. Clip Gage Creep versus Micro-Strain Levels

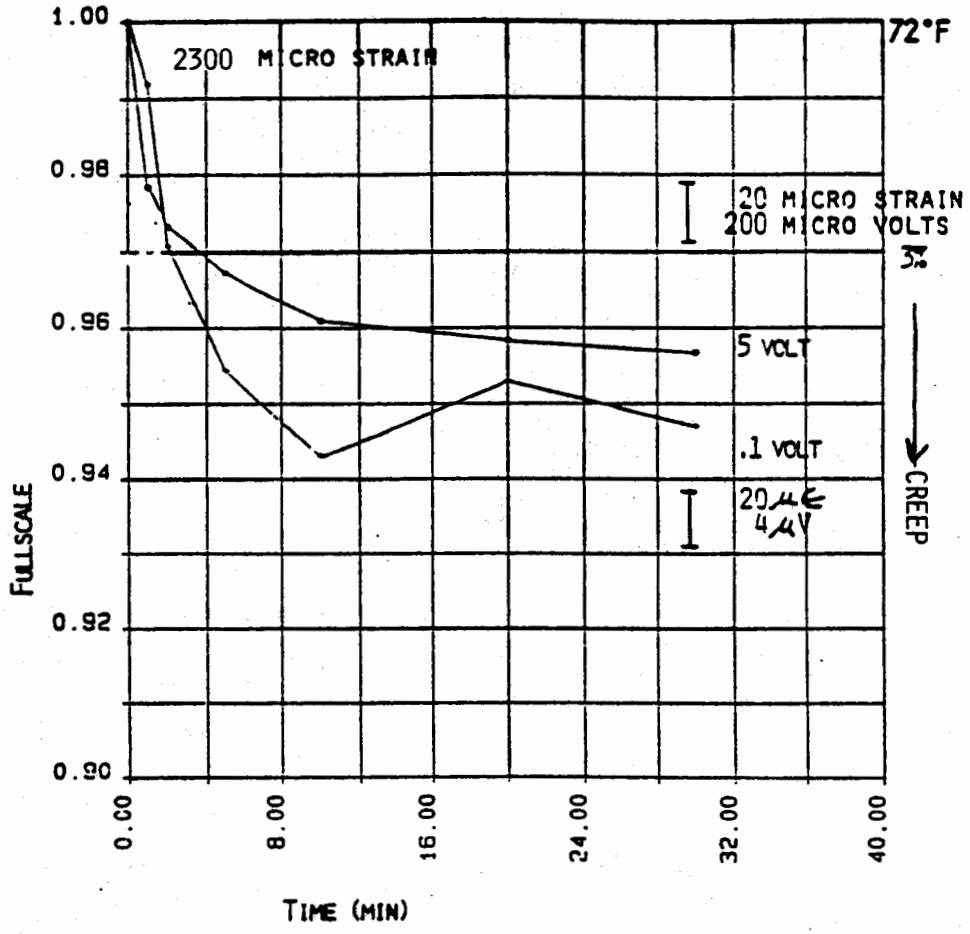

Figure 4. Clip Gage Creep vs Excitation (Power Level)

tests. Power level had no effect on the creep behavior. Low power levels however, reduced signal to noise ratios making accurate measurements difficult. This is evidenced by data scatter in the 0.1 volt excitation test.

FOIL STRAIN GAGE CONFIGURATION

Both MA-06-031CE-350 and NK-06-5022H-5000 strain gage sensors were tested at 500u to determine if the gage type would alter the creep response. Changing strain gages required changing other test variables. Among these were gage element material, gage backing, gage size, bonding adhesive and resistance. Test results (Figure 5) show that both gage configurations exhibited approximately 3% creep in 30 minutes. Greatly alterning foil strain gage configurations and other parameters did not have an appreciable effect on creep behavior. This would indicate that a major contributor to creep may be the common metal structure used for the gage.

GAGE COATING

Moisture protection was provided by a coating (M-coat D) over the gages. Test results in Figure 6 showed that the coating did not significantly alter the measured creep behavior.

TEMPERATURE

Data for a variety of sensor tests from 62^{o}F to 90^{o}F was collected and presented in Figure 7. The results are scattered, but do tend to show increased drift for the higher test temperatures as expected. This could indicate both conventional epoxy or metal creep could contribute to gage instability.

IMPROVED GAGE TESTING

None of the factors evaluated could be isolated as the prime cause of the clip gage creep. Therefore a review was conducted of the stress gage creep problem which showed that three variables could be drivers[2].

THREE CREEP SOURCES

(1) Metal Instability
(2) Epoxy Creep
(3) Excessive Induced Strain

The 302 stainless steel is not as stable as 17-4 or 17-7[3]. Machining and bending stresses are induced during manufacturing so a metal conditioning process[4] is required to eliminate these residual stresses.

Epoxy creep was reduced on the stress gage program by using a filled epoxy which was filtered to remove large filler particles and agglomerates. The epoxy thickness was also reduced to less than 0.0005" using special manufacturing procedures[4]. These same procedures would now be used for clip gage manufacturing.

Excessive strains could be avoided by designing the gage structure to operate at lower strain levels. Improved strain designs were developed to stay in the 750 to 850u region at full scale displacement.

In order to manufacture gages with the listed improvement, the process was conducted at Senso-Metrics which also manufactures stress transducers. Both foil and semi-conductor strain gages were considered in these improved clip gages.

Concurrent with the improved gage manufacturing some testing changes were conducted to standardize the creep test equipment and test procedures.

SCREENING TEST IMPROVEMENTS

- Installed rigid pin clamping mechanism
- Installed micrometer adjustment of displacement rather than as a readout
- Procedure controls pre-strain condition and strain ramping and unloading
- Installed creep test equipment in a light tight environmental box
- Control test temperature to 70^{o}F

The screening test consists of straining each gage from a nominal zero-microstrain to the gages desired full scale displacement. Gage output is monitored and recorded for 30 minutes. This data was tabulated to determine the instability of each clip gage over the 30 minute test interval. Pre and post test creep is also monitored for 30 minutes to establish a consistent test reference and as a secondary creep measure (Figure 8).

Complete data for a few test samples is presented in Figure 9 and 10 to illustrate the the measured response.

CLIP GAGE SCREENING TEST DATA

Both the older and some new clip gages were evaluated using the improved thirty minute screening test. Results are shown in figure 11 and 12. The new clip gages used 17-4 and 17-7 stainless steel, a metal stabilization process, and an improved bonding procedure such as used for stable stress transducers. The improved process clip gages were consistently more stable than the older types. However, even one of these new gages showed excessive creep and would have been rejected based on the screening test data. Both foil and semiconductor gages showed improved stability over previous designs. While the strain sensitivity for the semiconductor devices are much higher, the light and temperature sensitivity of the foil gages is much lower.

DISCUSSION AND RESULTS

All strain gaged clip or slot gages experienced some instability in electrical readout when structurally loaded. This drift can be significantly reduced by using the most stable metal, a metal stabilization procedure, and

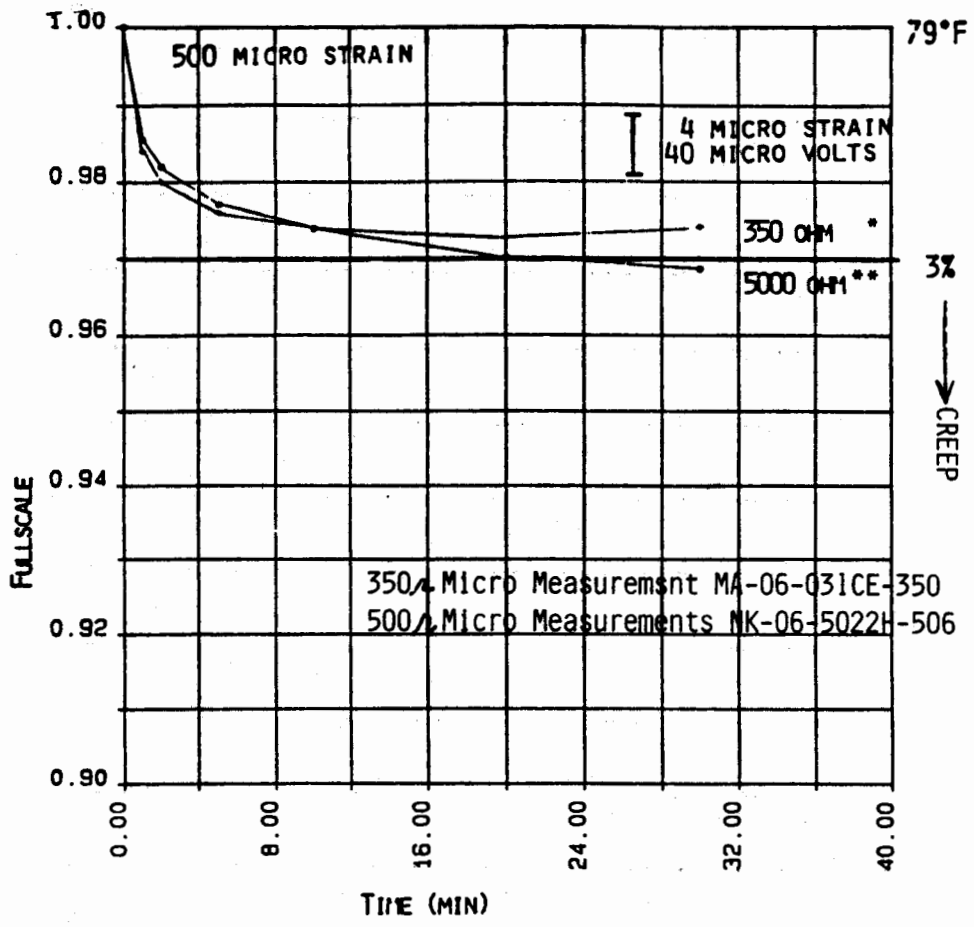

Figure 5. Clip Gage Creep for Different Foil Strain Gages

Figure 6
CREEP -- COATED VS UNCOATED STRAIN GAGES

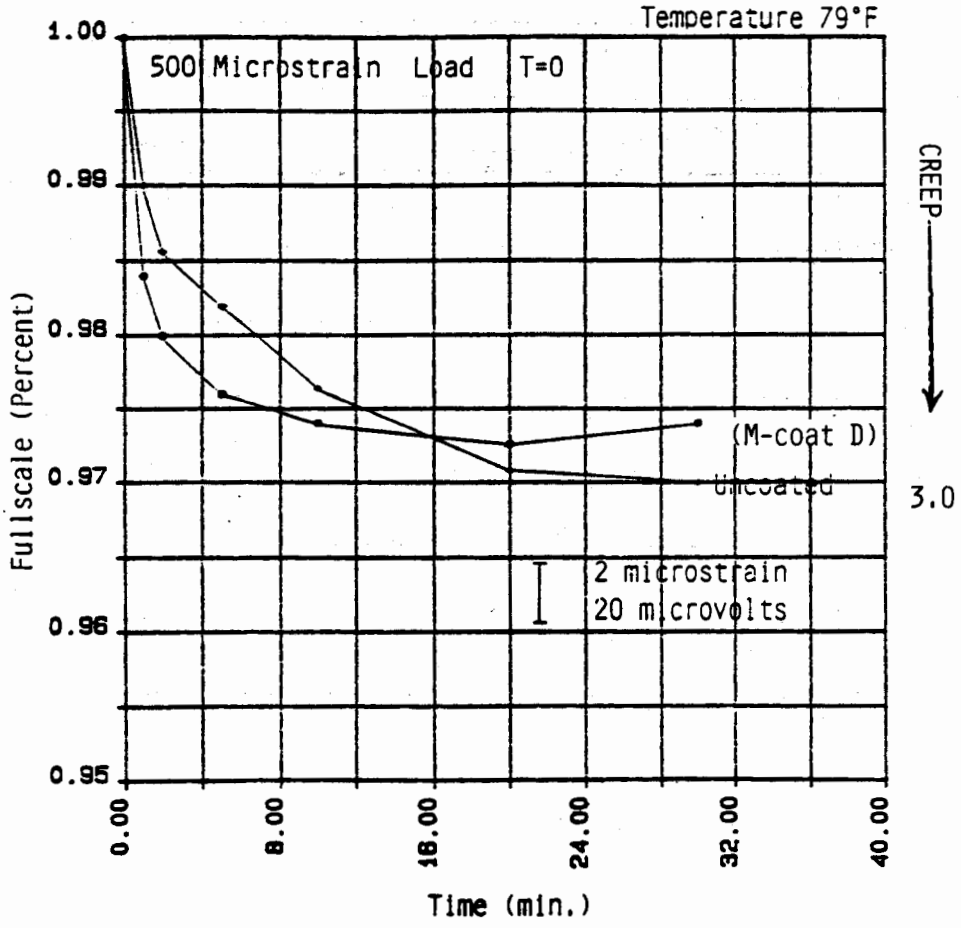

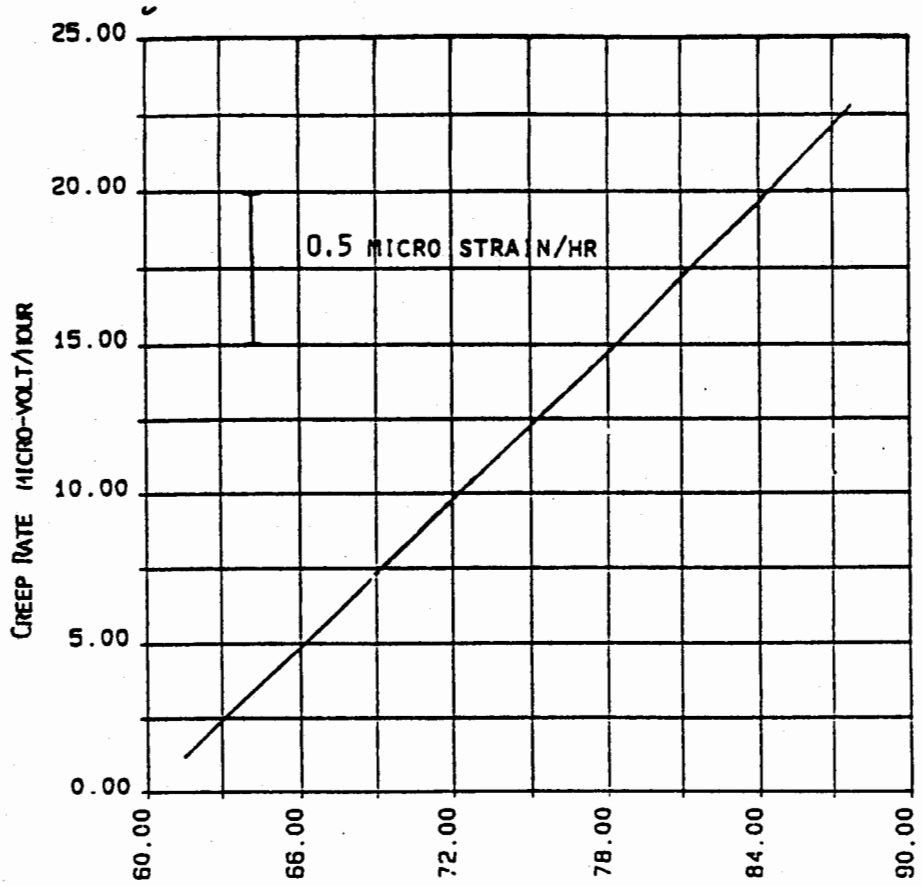

Figure 7. Clip Gage Creep Rate vs Temperature

$$\text{CREEP \%} = \frac{\Delta\epsilon}{\epsilon} \times 100 = \frac{\Delta V}{V} \times 100$$

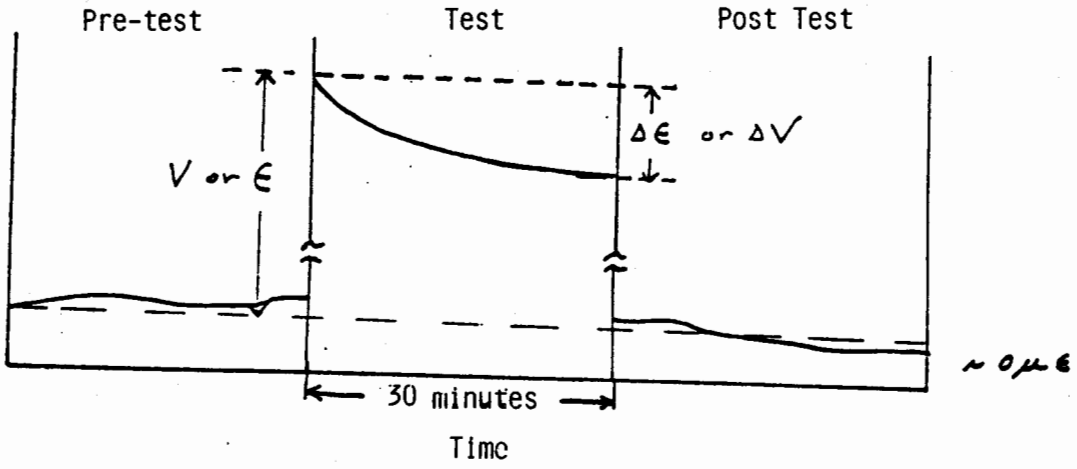

Figure 8. Creep Test Behavior

Figure 9. 30 Minute Creep Data for Clip Gage #2

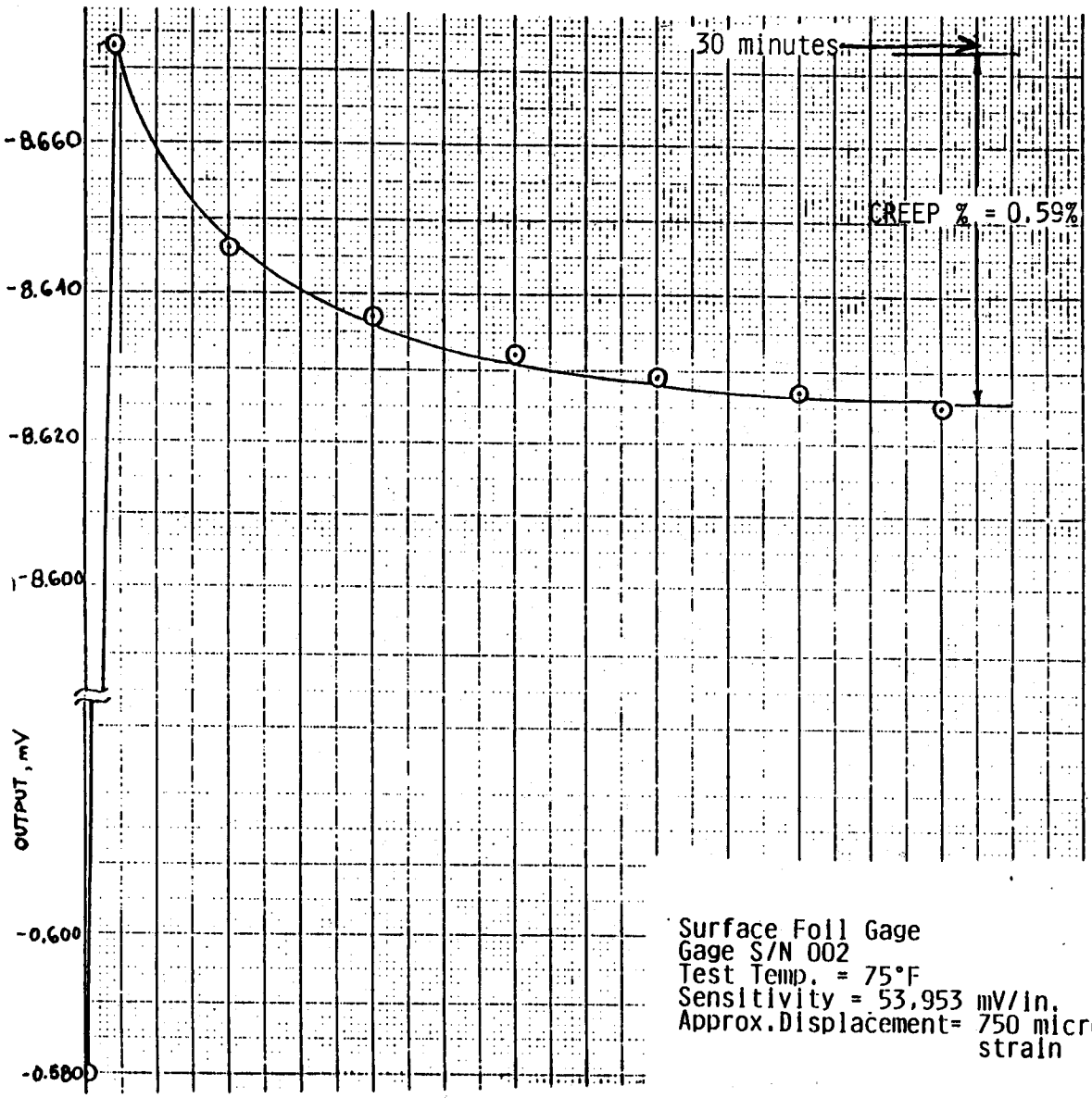

Figure 10. 30 Minute Creep Data for Clip Gage #4

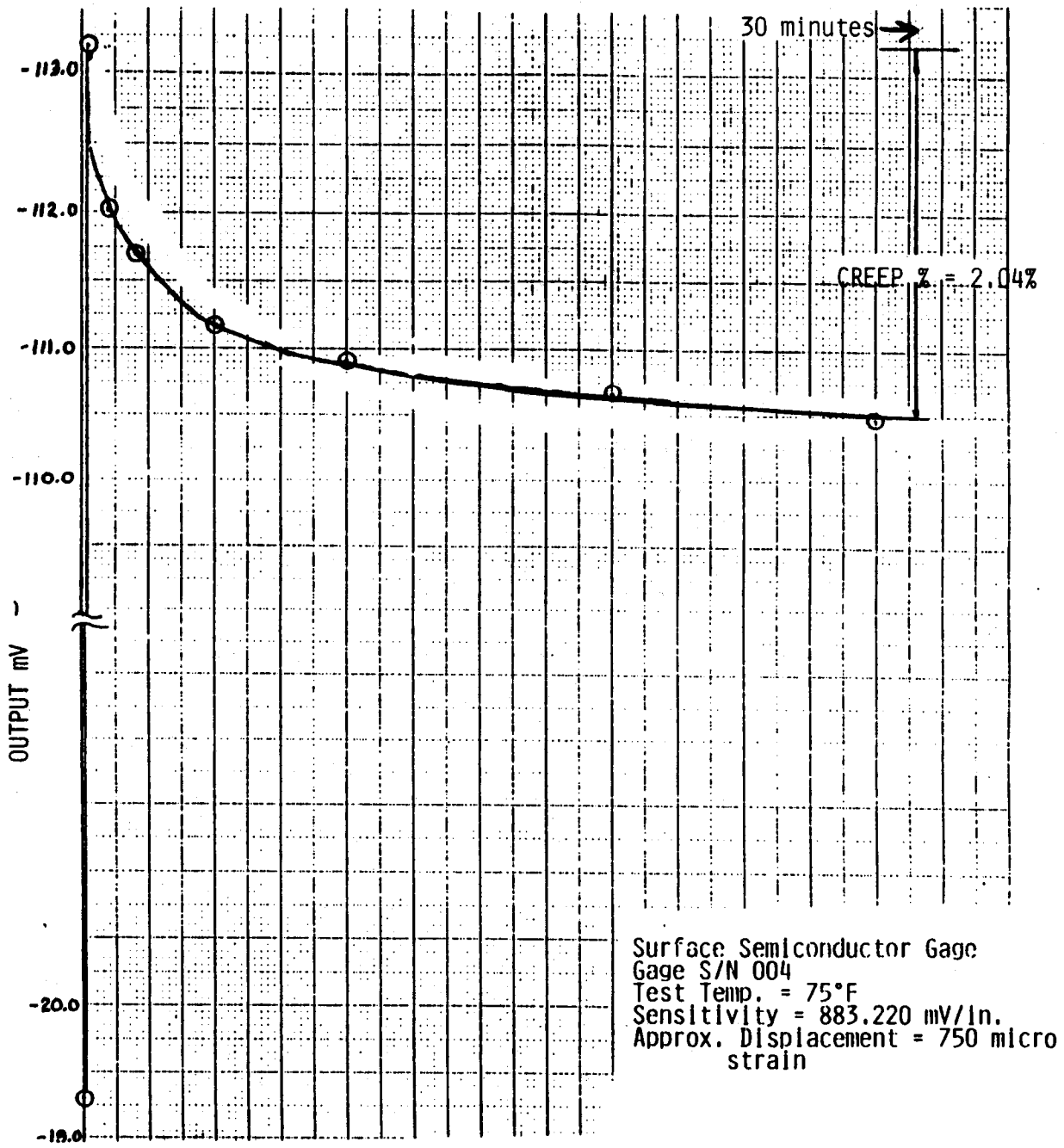

Slot Clip Gage Screening Data

ID #	Strain Gage Type	Sensitivity (mV/μ)	30 min Creep %
1	Foil 350	35.566	3.20
2	Foil 350	62.450	1.44
3	Foil 350	62.667	1.37
4	Foil 350	62.444	1.07
5	Foil 350	61.750	1.21
6	Foil 350	64.460	.90
7	Foil 350	66.212	2.23
8	Foil 350	59.200	1.76
9A	Foil 5000	64.414	2.16
10A	Foil 350	69.008	3.71

All structures are 302 Stainless Steel
Bonding Process - Micro Measurements
Strain Applied ~2500με

Surface Clip Gage Summary Data

ID #	Strain Gage Type	Sensitivity (mV/μ)	30 min. Creep %
	Foil 350	68.780	3.13
1	Foil 350	70.381	1.75
2	Foil 350	66.524	1.72
3	Foil 350	71.282	1.97
4	Foil 350	68.427	1.75
5	Foil 350	72.429	2.66
6	Foil 350	69.821	1.78
7	Foil 350	66.841	1.37
8			

All structures are 302 stainless steel
Bonding Process - Micro Measurements
Strain Applied ~ 2000με

Figure 11. Retest Data for Older Clip Gages with Improved Equipment & Procedures

SURFACE CLIP GAGE SUMMARY

S/N	Bonding Process	Metal	Strain Gages	Sensitivity (mV/in.)	30 min. Creep %
1	SM *	17-4 SS	Foil 5000	50.287	.49
2	SM	17-4 SS	Foil 5000	53.953	.59
4	SM	17-7 SS	Semiconductor	883.220	2.04

SLOT CLIP GAGE SUMMARY

S/N	Bonding Process	Metal	Strain Gages	Sensitivity (mV/in.)	30 min. Creep %
1	SM	17-4 SS	Foil 5000	20.756	.79
2	SM	17-4 SS	Foil 5000	20.267	.91
3	SM	17-4 SS	Foil 5000	19.123	.94
1	SM	17-7 SS	Semiconductor	327.437	.95
2	SM	17-7 SS	Semiconductor	347.060	.95

Strain Applied between 750-850$\mu\epsilon$

*SM = Senso Metrics, Inc.

Figure 12. Stability Screening Data for Improved Clip Gages

optimized gage bonding techniques. Even with these features some manufacturing variability should be expected. Short time creep screening is desirable to insure that the gages used for propellant testing are acceptable for long time measurements. CSD has developed manufacturing and test procedures that provide acceptable clip and slot gages. The short time screening process is now used to screen all strain gage type displacement sensors used for propellant tests at CSD.

REFERENCES

(1) Francis, E. C., R. E. Thompson and W. E. Briggs, "The Development of Improved Normal Stress Transducers for Propellant Grains" (Final Report), AFRPL-TR-79-34, June 1979

(2) Francis, E.C. and R. E. Thompson, "Age Stability of a Semiconductor Stress Transducer", 26th International Instrumentation Symposium, Instrument Society of America, Seattle, Washington, May 1980

(3) Maringer, R.E., et. al "Material Properties Pertinent to the ISUS Sensor Block" Final Report, Battelle Memorial Institute, Apr 1968

(4) Francis, E. C. and H. Chelner, "Design of a High Stability Stress Transducer", 23rd International Instrument Society of America, Las Vegas, Nevada, May 1977.

CLIP GAGE STABILITY

Q: John Kalinowski (EG&G Energy Measurements, Inc., Pleasanton, CA): What is the modulus of your propellant material?

A: E. C. Francis: The modulus of the propellant material varies greatly with the temperature. It can be anywhere from 500 to 5,000 psi.

Q: John Kalinowski: Have you considered looking at the modulus of your strain gage and comparing the two? They might be controlling your measurement.

A: E. C. Francis: Yes, we have. That's the whole idea of the clip gages. You couldn't put strain gages directly on the propellant surface because the modulus of the propellants is so low. It strains the propellant and the strain gage will just tear loose. That's why the clip gage itself was designed to transmit the much larger strain from the propellant to the strain of the clip gage.

One of the things that we do analysis on is the interaction between the clip gage and propellant. These have to be designed with very thin beam members. Typically, we have spring constants on the order of 10, 20, 30 grams force per inch to minimize the interaction with propellant. On the first test we did with the bulk uniaxial sample, a large amount of that error was because of the interaction, but it could later be factored out. The creep we were looking at here was actually observed in a very stable metal fixture.

Q: Peter Stein (Stein Engineering Service, Inc.): One of your conclusions is really a very sound, excellent one. "Creepy" transducers are bad transducers. A 304 SS is not a particularly good material, as I think you, yourself, found when you changed to the 17-Ph stainless. But one variable appeared to be missing from your test, and that's the operator. Now it is considered reasonably good practice to take not a clip gage, for example not the transducer you are going to instrument, but just a plain old straight little beam that you can clamp as a cantilever to evaluate the mounting techniques themselves. This practice is not necessarily to check the technician but rather the mounting techniques themselves. In addition, it is to studies the creep behavior of a very simple titanium or other well-characterized material to see now the operator does. Did you have any opportunity to do that?

A: E. C. Francis: In addition to the clip gages, we had a third design which was a mounted cantilever beam configuration for measuring bore diameters. Those particular beams in the strain gage area were about 5 mils thick, whereas the others were much stiffer, more on the order of 20-25 mils thick. The creep response of those were much better, even though we used the same techniques for mounting the strain gages. So one of the things it could be is higher shear gradient in the thinner metal sections. Percentage wise, when you put the gage on top of the metal, you are a much farther percentage distance from the neutral axis than you are with a thicker beam.

DIGITAL QUARTZ PRESSURE TRANSDUCER

Donald W. Busse
Curtis Young
Paroscientific, Inc.

APRIL, 1987

INTRODUCTION

Most precision measurement instruments have one thing in common; they are inherently sensitive to temperature. We have all heard the old saw "it makes a better thermometer than a transducer", but unfortunately that is frequently the case when we develop new precision instruments. Naturally, we can't get away from the effects of thermal expansion, modulus changes, crystal anisotropy, resistance effects, or other physical phenomena which affect most transducers.

In some cases the transducers can be desensitized by clever compensation mechanisms within the transducer itself. Usually such compensation utilizes counteractive elements that are designed to balance known and predictable effects, leaving only residual differences or higher order nonlinearities. Seldom are we lucky enough for the accurate compensation mechanisms to be exact or even accurate across a wide temperature range. While we usually know exactly what compensation we want, we frequently can't find the exact means to provide this compensation by counteractive methods.

Now, with the pervasive microchip, the knowledge of <u>what</u> temperature effect we want to compensate is all that is needed to do the job. We don't have to be as concerned with <u>how</u> to compensate. The microprocessor can do that rapidly and with great precision after the raw transducer measurement has been made. The transducer output can contain the full uncompensated effect of temperature as long as we know what the effect is and what algorithm describes the effect. The microprocessor can remove the modeled thermal effects to provide temperature compensated output. Of course, the smaller the initial thermal effect the better that final compensation can be. So, it is still advantageous for the instrument designer to provide as much inherent compensation as practical economics allow.

Most precision pressure measurement systems now contain computers or microprocessors to handle the measurements and process or store the data. With only a slight increase in processing time, the computer can also perform the necessary compensation for modelable error sources such as temperature.

With the foregoing in mind, Paroscientific, Inc. has developed a series of high precision digital pressure transducers from its standard Digiquartz® line which are easily interfaced to digital systems and are readily modelable across a wide range of temperature. Now, this is nothing new to the community of instrumentation engineers, but normally thermal modelability is achieved through the use of some temperature readout (usually, analog), such as a thermistor, resistance element or active current device. These methods generally require analog to digital conversion, algorithmic conversion of the digital information to temperature, then finally another algorithmic compensation of coefficients or addition of corrective errors to achieve an output.

This new series of Digiquartz® pressure transducers, identified as the "T" Series to denote Temperature compensation, uses a somewhat different approach to the problem to eliminate the steps of analog to digital conversion and calculation of temperature. The "T" Series transducers utilize a force sensitive quartz crystal beam oscillator for sensing pressure induced stress and a similar temperature sensitive quartz crystal oscillator for sensing temperature. The two output frequencies are then used together in a unique algorithm not involving temperature per se to achieve true temperature compensation of pressure output which is free of analog to digital conversion errors and truncation errors in traversing through units of temperature.

BACKGROUND

The Paroscientific, Inc. Digiquartz® pressure transducers use a crystal quartz beam or double ended tuning fork (DETF) resonator operating in a compressive or tensile mode to measure the pressure induced stress that is applied by either a bellows or a bourdon tube. Crystalline quartz was specifically chosen for these applications because of its piezoelectric properties and highly stable frequency characteristics.

The particular crystallographic cut of quartz used for the pressure sensor yields small temperature effects and precisely modelable frequency characteristics resulting in a transducer that can be characterized across a broad range of environmental conditions. The cut of quartz used for the temperature sensor provides high temperature sensitivity.

PRESSURE MECHANISM

Bellows or Bourdon tube pressure mechanisms are used to convert input pressure to an axial force applied to the crystal resonator. Both types are shown in Figure 1. Combinations of different bellows and Bourdon tube sizing with either single beam or DETF crystals allow full scale pressure sensor designs from one atmosphere to over a thousand atmospheres of pressure. Both mechanisms use a sealed internal chamber to provide a vacuum environment for crystal operation as well as a zero reference pressure for the bellows or Bourdon tube, allowing measurement of absolute pressure.

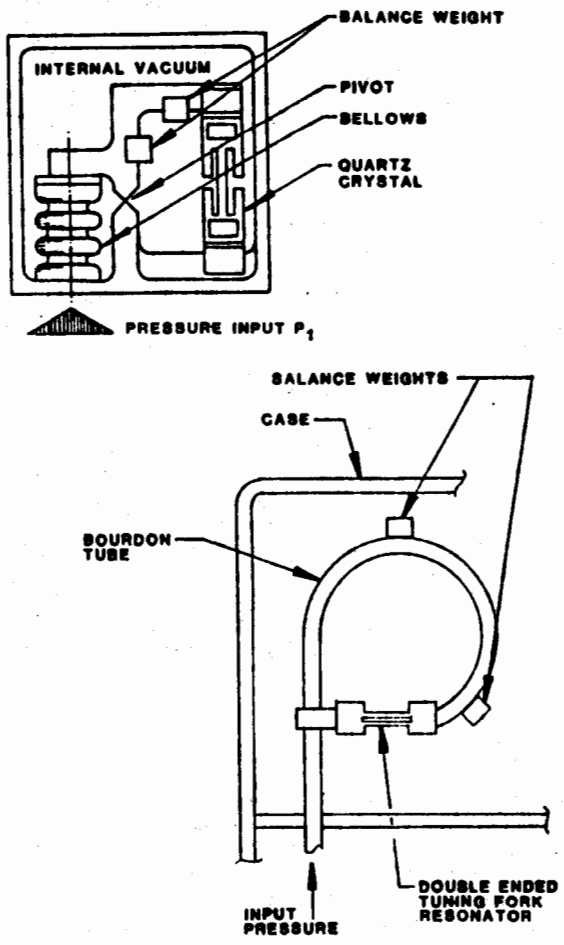

Figure 1
Pressure Transducer Mechanisms

In the absolute pressure sensor configuration, the bellows develops a force upward on the lever arm. This force is the product of absolute applied pressure and the bellows effective area. The force thus generated develops a torque about the pivot that is counteracted by the rigid crystal. This imposed axial compressive stress in the crystal resonator beam decreases the resonant frequency of oscillation providing a means of pressure measurement. By changing the size and position of the bellows relative to the lever arm pivot, the ratio of bellows force to crystal stress can be adjusted over a wide range. This allows various pressure range transducers to be fabricated with minimal change in components. Differential pressure transducers can be fabricated by opposing another bellows on the other side of the lever arm. With one bellows counteracting the other, only the difference in the two bellows pressures is transmitted to the crystal resonator.

The second type of pressure mechanism is illustrated by a single turn Bourdon tube constrained by the crystal resonator. In this case, the Bourdon tube tends to uncoil under application of pressure placing the resonator crystal under tension thus increasing the resonant frequency. Although the bellows mechanism develops decreasing frequency with applied pressure and the Bourdon tube mechanism develops increasing frequency, the relative change in frequency follows the same physical principals and therefore is subject to the same algorithm in converting frequency to pressure reading.

Both types of mechanisms contain an integral temperature sensitive crystal for thermal compensation. Also, both types can be balanced against acceleration forces by means of small movable masses which are adjusted so that inertial torques and forces about the effective pivot or center of rotation are made to be zero. This makes the transducers insensitive to linear acceleration and vibration.

QUARTZ RESONATOR

The sensitive element of the Digiquartz® pressure transducer is a quartz crystal resonator whose frequency of oscillation changes with applied axial force. This element is essentially a precision oscillator similar to the crystal oscillators used in frequency standards or clocks and watches which can attain long term accuracy on the order of 1 part in 10 million.

There are two basic types of resonator elements used in Digiquartz® pressure transducers. The first type shown in Figure 2 is a single beam design which is mechanically isolated from its mounting pads by means of a novel set of low pass mechanical filters on either end of the beam. These mechanical filters allow the single beam to oscillate in a high frequency flexural mode

without coupling energy to the pads. This means that mechanical energy loss is virtually eliminated, resulting in an extremely high operating Q that contributes to the accuracy and stability of the transducer.

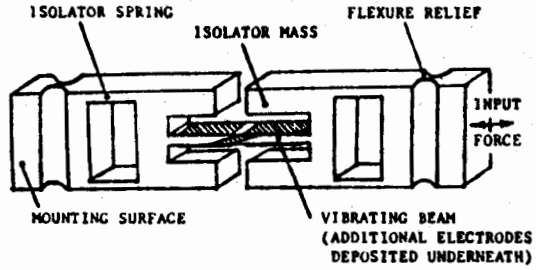

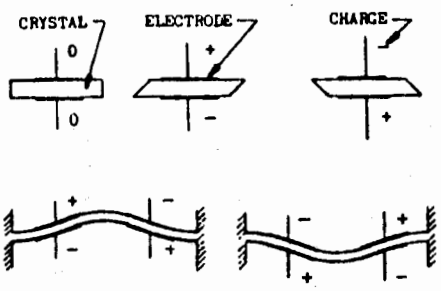

Figure 2
Single Beam Quartz Resonator

Figure 3 shows a double ended tuning fork (DETF) resonator force sensor which is basically two tuning forks joined at the middle.

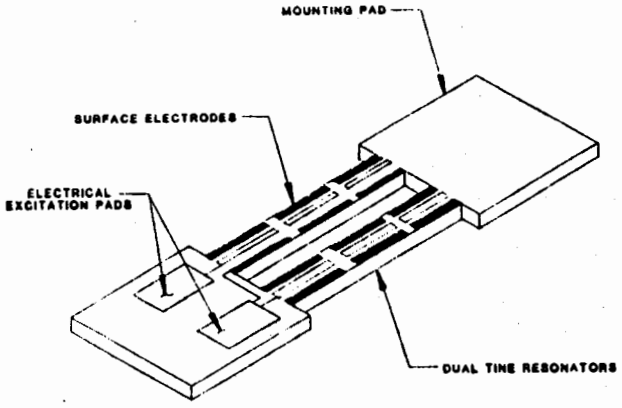

Figure 3
Double Ended Tuning Fork (DETF)

These DETF resonators can be manufactured by a photolithographic chemical milling process resulting in large quantity production with highly controlled and repeatable characteristics. The manufacturing process does impose restrictions on DETF size and load bearing capability. Therefore, the photolithographically produced DETF must be carefully mated with the pressure-to-force converting mechanism to achieve a broad range of pressure sensors.

Because the DETF consists of two identical beams oscillating in opposition, very little energy is transmitted to the mounting pad. This is similar to the musical tuning fork which has a high Q and a long lasting resonance because very little vibrational energy is lost through the handle. Nevertheless, extreme caution must be exercised in the mounting techniques to assure proper alignment, reduce mounting stresses, and prevent asymmetrical loading of the beams or adjacent mounting pad areas.

Both types of crystal resonators utilize the same principal of piezoelectric drive to achieve and maintain beam oscillations. Figure 1 of the single beam resonator shows schematically the placement of electrodes on the beam which are used with an oscillator circuit to maintain electrode excitation and mechanical vibration. The resonant frequency of the vibrating beam is determined by its dimensions, composition, and stress load. Under tension the frequency increases, as with a violin string. Under compression the frequency decreases.

Although the resonator will operate at normal ambient pressure, performance is significantly improved in a vacuum. The air loading and damping effects are removed under a vacuum allowing the resonator to operate at Q values of over 20,000. Vacuum operation further enhances resonator performance by preventing molecules from being absorbed or evaporated by the surface, thus improving the stability. For such small resonators, even one molecular layer of contaminant has an easily discernable effect.

Since the DETF resonator is manufactured by photolithographic means, the electrode pattern used to maintain oscillation is most easily produced on the plane surface of the crystal. Even though a different pattern of electrodes is used, the operating and performance requirements are similar to those for the single beam resonator.

QUARTZ TEMPERATURE RESONATOR

The quartz material used for fabrication of the pressure sensitive resonator has certain temperature characteristics related to changes in Young's Modulus, thermal expansion and piezoelectric constants that are reflected in changes in resonant frequency or sensitivity to

imposed loads. These changes in resonator performance with temperature are basically a class parameter of crystalline quartz. They are measurable, repeatable, and immutable. The best means of compensating for thermal effects of the quartz pressure resonator is with another quartz resonator that is only sensitive to temperature.

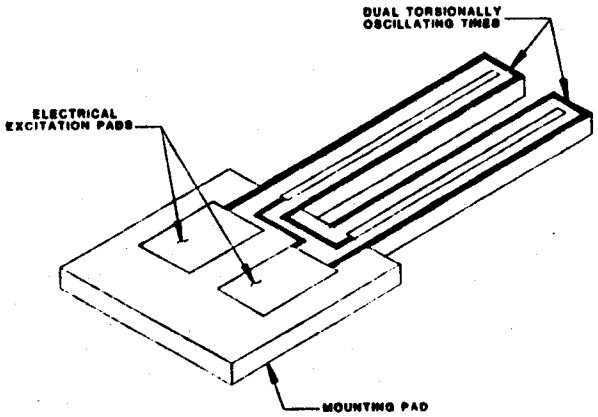

FIGURE 4
TEMPERATURE SENSITIVE QUARTZ RESONATOR

Figure 4 shows a diagram of a quartz crystal tuning fork that is designed to operate in a temperature sensitive mode of oscillation. This is an integral part of each pressure transducer so that it is most effective in compensating for thermal effects. A separate electrical oscillator is used to drive the temperature resonator. Thus, the two frequency outputs from the transducer represent applied pressure (with some temperature effect) and temperature (with no pressure effect). The two signals contain all of the information necessary to eliminate temperature errors resulting in a fully temperature compensated output for any combination of pressure or temperature.

OUTPUT SIGNAL

Each transducer produces two frequency outputs; one for pressure and one for temperature. The pressure resonator has a nominal frequency of about 38 KHz which undergoes a change of about 10% for application of full scale pressure.

The temperature signal has a nominal frequency of 172 KHz and changes about 50 ppm per degree C.

The relationship between pressure output signal and applied pressure can be expressed in terms of frequency or period. Because the transducer output frequency is lower than most counter timebases, it is most accurately measured by period counting, and the equation is commonly given in terms of output period rather than frequency. The characterization equation below can be derived from basic physical principles of fixed-fixed vibrating beams:

$$P = C(1 - T_0^2/Tau^2)[1 - D(1 - T_0^2/Tau^2)] \qquad \text{Eq. 1}$$

where C and D are calibration coefficients, T_0 is the output period of the pressure crystal at zero pressure, and Tau is the output period at applied pressure P. Note that the quantity $(1 - T_0^2/Tau^2)$ and the coefficient D are unitless. Therefore, the pressure units resulting from the equation are given in terms of the coefficient C. Once a valid set of coefficients is determined, then pressure units can be changed simply by multiplying the coefficient C by the appropriate conversion factor.

Temperature changes in the transducer introduce changes in the quartz pressure resonator and also in the pressure mechanism that can be compensated by adjusting the coefficients C, D, and T_0 accordingly. Normally this would be accomplished by changing the coefficients as a function of temperature. In fact, this technique is commonly used for transducers where temperature is measured by such means as thermistors or resistance elements. However, here the great advantage of the integral frequency output temperature resonator can be realized. Not only is the measured temperature more closely coupled to the sensing elements but the coefficients of the pressure resonator can be parameterized in terms of the frequency of the temperature resonator without having to solve for temperature as an intermediate step. This makes the algorithm simpler and has the additional benefit of eliminating the need for accurate temperature measurement during calibration. Only the frequency of the temperature resonator need be measured in order to obtain compensation. Of course, if the temperature signal output is to be used to determine actual transducer temperature, then its coefficients must be determined during calibration as well; however, it should be understood that temperature itself does not enter into the compensation except as the driving effect that changes <u>both</u> resonators simultaneously.

The output of the temperature crystal resonator is represented by the equations:

$$TEMP = Y_1U + Y_2U^2 + Y_3U^3 \quad (°C) \qquad \text{Eq. 2}$$

$$\text{where } U = U(t) - U_0 \qquad \text{Eq. 3}$$

where U(t) is the output period of the temperature crystal in microseconds at Temperature (t) and U_0

is the output period of the temperature crystal at zero degrees centigrade. The parameter U therefore has units of microseconds and the coefficient Y_1 has units of degrees centigrade per microsecond ($^{\circ}C/\mu sec$).

For purposes of defining the coefficients C, D, and T_0, only the parameter U is used. Temperature can be calculated using equation (2) if desired.

Parameterization of coefficients C, D, and T_0 is given by a general power series as follows:

$$C = C_1 + C_2U + C_3U^2 \qquad \text{Eq. 4}$$

$$D = D_1 + D_2U \qquad \text{Eq. 5}$$

$$T_0 = T_1 + T_2U + T_3U^2 + T_4U^3 \qquad \text{Eq. 6}$$

In order to obtain a reading of pressure, the two resonator output periods are measured and the equations 3, 4, 5, 6, and 1 are solved. Equation 2 need only be solved if one wants to know temperature, otherwise it is extraneous to the compensation algorithm. The output period measurement and calculation routine can be accomplished by a microprocessor at a rate in excess of 70 times per second with a resolution of 100 ppm or 0.01% of Full Scale.

CALIBRATION

In order to obtain the coefficients necessary (1 for temperature equation 3 and 9 for pressure equations 4, 5, and 6) it is necessary to measure the frequency (or period) of both quartz crystals on each transducer at a number of temperatures and pressures across the operating range.

Rather than computing C, D, and t_0 at a number of temperatures and then individually fitting the coefficients per equation 4, a more sophisticated way of determining the coefficients is to perform a full non-linear least squares fit which solves for all the parameters simultaneously. This latter approach yields slightly better fits for any given number of parameters and is less sensitive to small errors in the data.

Practically, it is desirable to stabilize the transducer at a given temperature and then apply pressure from a primary pressure source while measuring output of the two oscillators. This can easily be accomplished by a multiplexed data acquisition system which can handle up to a hundred transducers at one time. Here some of the advantages of the crystal temperature sensor become apparent. First, since both outputs are frequencies, they can both be interfaced through the same counting equipment without the necessity for analog to digital converters. Secondly, the temperature of the oven need not be known accurately for purposes of subsequent transducer temperature compensation.

Since the frequency of the temperature crystal is a sensitive and monotonic function of temperature, it will always return to the same frequency at that temperature (whatever it may be) Thus it is sufficient to relate the pressure coefficients to the temperature crystal output and not necessary to relate them to temperature. In this manner temperature can be eliminated from the fit routine and the calibration if desired. It is only necessary that the calibration oven be relatively constant during data taking. Of course, if one wants to use the temperature crystal output to measure temperature it can be done as shown in Equation 2; however, this is independent of thermal compensation and data fitting.

To obtain a statistically valid fit of the coefficients, a sufficient number of data points must be taken to assure redundancy. Since the third order of the parameter U is used, then at least four (and preferably more) sets of measurements must be made at independent values of U (or temperature). Similarly, at least three and preferably more sets of measurements should be made at independent values of tau (or pressure).

A reasonable calibration routine might call for 5 independent temperatures with 5 independent pressures at each temperature for a total of 25 data points. This gives sufficient and reasonable redundancy to check the goodness of fit for the 10 calibration coefficients.

OPERATION

The two outputs of the Digiquartz® pressure transducer can be measured by means of a gated high frequency clock or by a microprocessor or computer. Rapid update rates on the order of 70 times per second can be obtained while maintaining a resolution of 100 ppm. Or if desired, resolution as fine as 0.01 ppm can be obtained with measuring times on the order of one minute.

As an example, a transducer with 15 psi full scale capability has the coefficients:

U_0	5.785646	usec
Y_1	-3952.813	
Y_2	-9317.965	
Y_3	42720.22	
C_1	66.09318	psia
C_2	7.684055	
C_3	-49.86013	
D_1	0.0341230	
D_2	0.0	
T_1	26.78275	usec
T_2	-10.25156	
T_3	864.5186	
T_4	39104.41	

For some measurement of pressure, the output from the transducer is determined to be:

U(t) = 5.779755 usec
tau = 30.47256 usec

From equations 3, 4, 5, and 6 we obtain:

$$U = U(t) - U_0$$

$$= 5.779755 - 5.785646$$
$$= -.005891 \text{ usec}$$

$$C = C_1 + C_2U + C_3U^2$$
$$= 66.09318 + 7.68405(-0.005891) - 49.86013(-0.005891)^2$$
$$= 66.046182 \text{ psia}$$

$$D = D_1 + D_2U$$
$$= 0.034123 + 0.0(-0.00589)$$
$$= 0.034123$$

$$T_0 = T_1 + T_2U + T_3U^2 + T_4U^3$$
$$= 26.78275 - 10.25156(-0.005891) + 864.5186(-0.005891)^2 + 39104.41(-0.005891)^3$$
$$= 26.86515 \text{ usec psia}$$

The above coefficients (C, D, T_0) can then be used in equation 1:

$$P = C(1 - T_0^2/Tau^2)[1 - D(1-T_0^2/Tau^2)]$$
$$= 66.046183 \left(1 - \frac{26.86515^2}{30.47256^2}\right) \left[1 - 0.034123 \left(1 - \frac{26.86515^2}{30.47256^2}\right)\right]$$
$$= 14.6 \text{ psia}$$

If one also wants to know the temperature of the transducer then equation 2 can be used.

$$Temp = Y_1U + Y_2U^2 + Y_3U^3$$
$$= (-3952.813)(-0.005891) + (-9317.965)(-0.005891)^2 + (42720.22)(-0.005891)^3$$
$$= 22.95°C$$

This sequence of measurements and calculations can be accomplished at a high repetition rate providing excellent resolution and update speed for most high accuracy control.

APPLICATIONS

The "T" Series Digiquartz® pressure transducers are ideally suited for precision pressure measurement applications. They have been used on Air Data and Engine Control systems, energy exploration, oceanographic systems, pressure control systems, and as laboratory pressure transfer standards.

These transducers are available in a wide range of gage, differential, and absolute types with full scale pressure capability from 15 psia to 10,000 psia.

Below are models and specifications for typical transducers:

Performance:

Resolution	0.01 pp,
Repeatability	0.005% FS
Hysteresis	0.005% FS
Pressure Conformance	0.005% FS
Acceleration Sensitivity	0.0038%FS/g
Vibration Sensitivity	Negligible
Supply Voltage Sensitivity	Negligible

Characteristics (15 to 900 psi)

Nominal Pressure Frequency (zero to full scale)	40 kHz to 36 kHz
Nominal Temperature Range	172 kHz + 50 ppm/°C
Calibrated Temperature Range	-54°C to 107°C
Operational Vibration Spectrum	MIL-E-5400-111
Power Requirements	6 to 35 VDC, 0.002A
Signal Output	Square Wave, 4 V p-p
Size (with shock mount)	2.63 x 2.63 x 1.90 in (6.68 x 6.68 x 4.83 cm)
Weight (with shock mount)	15 oz (430 gm)
Overpressure	1.2 x full scale

Characteristics (2,000 to 10,000 psia)

Nominal Pressure Frequency (zero to full scale)	34 kHz to 38 kHz
Nominal Temperature Frequency	172 kHz + 50 ppm/°C
Calibrated Temperature Range	0 to 125°C
Power Requirements	6 to 35 VDC, 0.002A
Signal Outputs	Square wave, 4 v p-p
Size (with shock mount)	1.38 in dia x4.25 in. 3.51 cm dia. x 10.8 cm)
Weight (with shock mount)	7 oz (200 gm)
Overpressure	1.2 x full scale

CONCLUSION

The Paroscientific, Inc. "T" Series Digiquartz® pressure transducer is a unique high precision pressure sensor with inherently digital output for full temperature compensation. It interfaces easily with pressure measurement and telemetry or digital computer systems. It should prove valuable in such diverse fields as meteorology, air data systems, jet engine testing, environmental controls, flow metering, oceanography, digital process controls, and secondary pressure standard instrumentation.

Q: Lawrence A. Rempert: Are these commercially available and at what cost?

A: Donald W. Busse: Yes, they are commercially available. We have been making these devices about 16 years at Paroscientific, and we have done very little advertising. Everything is word-of-mouth. The original design was a vibrating beam, but recently we have come out with different models. The price on these devices is on the order of $2,400 to $3,500 each, depending on pressure range, the configuration of the transducer, whether it has full-thermal compensation, and whether it is operating with a microprocessor internally---but in that range, $2,500 to $3,500.

Q: Jim R. Miller (Redstone Arsenal, AL): Do you have a feel for the general temperature sensitivity of your device as a function of pressure, or is it a constant?

A: Donald W. Busse: The temperature sensitivity of this particular device, if you are operating with a microprocessor using the full thermal compensated model, is virtually nil. It will have a temperature error on the order of 0.01 percent of full scale within the range from -54 to 207°C. That means that whatever there is in there is compensated by the computer. You saw the equations for the calibration coefficients. They are in sometimes 3rd or 4th order terms. So, there are a lot of temperature characteristics going on within the quartz itself or within the mechanism, but once you measure that, and know what the coefficients are and compensate for them, then the thermal effects will be very small. Did I answer the question?

Q: Jim R. Miller: No, not exactly. The temperature sensitivity without any compensation, do you have a feel for that?

A: Donald W. Busse: Oh, without compensation. Yes. Without any temperature compensation, if you were to just take one set of coefficients and not let them vary with temperature, then the effect would be about 24 or 25 parts per million per °F on the average over, 50°F. The reason I say average is because the curve is basically quadratic, so it depends on where you are on the parabola. If you happen to get it right at the right place, it will be 0 temperature sensitivity; but, we very seldom operate right at the minimum of the curve. There are two basic temperature effects. One is on the tau zero term, the bias itself, and there is another term on the span or the temperature sensitivity. The second term for span is relatively small because it is related to the thermal expansion coefficient of the nickel in the bellows or the material in the Baurdon tube, and it is just the area expansion unit of temperature that's going on there. It's a pretty linear term and it's easy to compensate.

INTELLIGENT DIGITAL PRESSURE TRANSMITTERS FOR AEROSPACE APPLICATIONS

Donald W. Busse
Dr. Richard B. Wearn, Jr.
Paroscientific, Inc.

APRIL, 1987

INTRODUCTION

In earlier days of system engineering, many systems consisted of a grouping or collection of existent sensors and actuators to perform a specific task of sense - anticipate - react for some control function. With the advent of practical size computers, systems increased in size and complexity integrating more tasks, functions, and capability into one system, but most sensors changed very little except in size and accuracy. The smart part of the system remained in the computer and sensors were required to do little more than sense and report, usually in some time honored analog format that had to be converted eventually to a digital format for use by the computer.

More recently, the advent of the microchip has contributed to a profusion of "intelligent" devices and applications from automobile engine ignition fuel control systems and talking toys to sophisticated smart terminals and peripherals for large network computer systems. Smart equipment and hardware for integrated systems is becoming more the standard rather than the exception. The time has come for intelligence in peripheral system sensors of all types, particularly in aerospace systems which frequently require the ultimate in accuracy, speed, and applicability.

BACKGROUND

The Paroscientific, Inc. Digiquartz® Intelligent Transmitter consists of a Digiquartz® pressure transducer and a digital interface board in an integral package. Commands and data requests are sent via an RS232 channel and the transmitter returns data via the same two-way bus. Digital outputs are provided directly in engineering units with typical accuracy of 0.01% over a wide temperature range. Output pressure is fully thermally compensated using a quartz crystal temperature signal. All transmitters are preprogrammed with calibration coefficients for full plug-in interchangeability. The Intelligent Transmitter can be operated either as a stand-alone standard output pressure sensor with display or as a fully integrated addressable computer controlled system component.

The pressure sensor device for the Inteiligent Transmitter is the Paroscientific, Inc. Digiquartz® pressure transducer. These transducers use crystalline quartz as the key sensing elements for both pressure and temperature because of its inherent stability and precision characteristics. The pressure sensing element is a quartz beam which changes frequency under an axial load. Applied pressure is converted to a measurable force by means of a miniature electroformed bellows. This force is transmitted to the quartz crystal resonator by means of a pivotal lever arm as shown in Figure 1. The transferred force acts on the quartz beam inducing a controlled, repeatable, and stable change in the resonator's natural frequency which is measured as the transducer output. The load dependent frequency characteristic of the quartz crystal beam can be characterized by a simple mathematical model to yield highly precise measurements of pressure and pressure related parameters. The output is a square wave frequency which can be readily interfaced with air data systems.

The quartz crystal resonator operates in an ultra-high vacuum in order to eliminate mass loading and damping effects and to ensure the excellent stability characteristics. The bellows arrangement isolates the quartz element from the pressure media, eliminates density and humidity effects. In the absolute pressure transducers, the vacuum in which the resonator operates also serves as the reference vacuum. With an absolute pressure P applied to the bellows, and with the high reference vacuum internal to the housing, the bellows exerts a force proportional to the product of the absolute pressure times the bellows effective area.

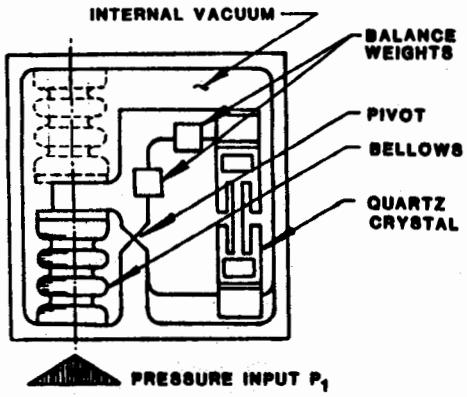

Figure 1: Absolute Pressure Transducer

Differential pressure measurements can be obtained by providing a second bellows on the opposite side of the pivotal lever arm as shown by the dashed lines in Figure 1.

Each pressure transducer also contains a second quartz crystal which is designed specifically for its temperature/frequency characteristics. This second quartz crystal is mounted in close thermal proximity to the pressure sensing crystal. The oscillating frequency of this temperature crystal varies in a known and measurable manner with respect to temperature. Thus, the outputs of the two crystals provide information on both pressure and temperature. Since both of the crystals are made out of crystalline quartz, the characteristics of one (the temperature crystal) can be used to compensate for the inherent temperature characteristics of the other (the pressure crystal), achieving optimum thermal compensation.

THE INTELLIGENT TRANSMITTER

The Digiquartz® Intelligent Transmitter consists of a standard Digiquartz® pressure transducer in any pressure range from 15 psia to 10,000 psia and a digital interface board in an integral package. The digital board has a microprocessor-controlled counter and RS232 port. The microprocessor operating program is stored in permanent memory (EPROM) and user controllable parameters are stored in user writable memory (EEPROM). The user interacts with the transmitter via the two-way RS232 interface. These transmitters output fully temperature corrected pressure information on a two way addressable RS-232 bus that can be interfaced to a computer or a stand-alone readout display.

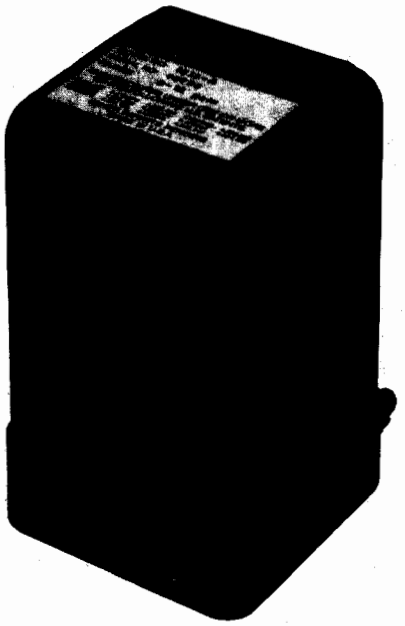

Figure 2
Intelligent Transmitter

The digital interface board contains a precision clock, counter, microprocessor for computation, logic circuitry for input-output control and EPROM and EEPROM memory for storing the operating program and calibration coefficients. Figure 3 shows a block diagram of the interface board circuitry and processing method.

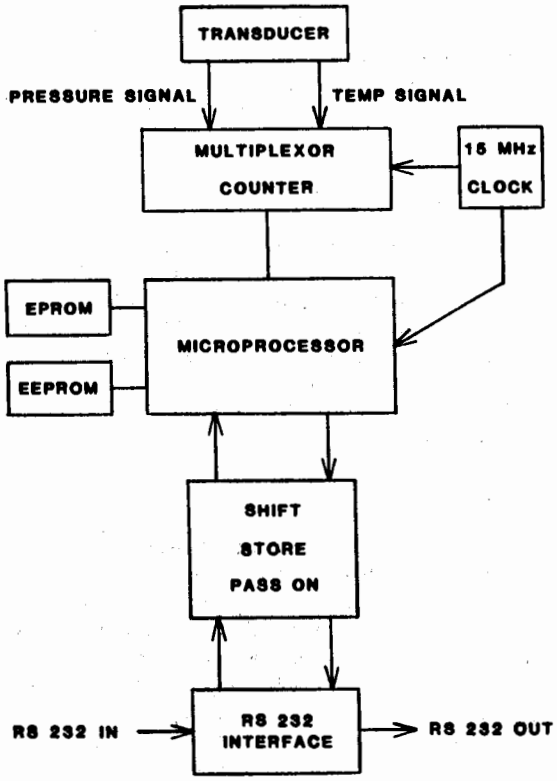

Figure 3
Digital Interface Board

Each Digiquartz pressure transducer provides two continuous frequency output signals, one corresponding to the pressure and the other to sensor internal temperature. The digital board measures the period of these two signals and calculates fully corrected pressure and temperature using the equations in Appendix A. The microprocessor monitors incoming commands from the computer. When a sampling command is received, the microprocessor selects the appropriate frequency signal source and makes a period measurement using a 15 MHz timebase counter. The counter integration time is user selectable. Some commands require measurements of both temperature and pressure signals. In that case, the temperature period is measured first, followed by the pressure period. When the period measurement is completed, the microprocessor makes the appropriate calculations and loads the data onto the RS232 bus.

The RS232 interface allows complete remote configuration and control of all operating parameters of the Intelligent Transmitter, including resolution, sample rate, integration time, and baud rate. Resolution is programmable from 0.05 to 100 parts per million depending on system requirements. Baud rate is user selectable from 300 to 19,200. Pressure data is available in eight different selectable standard engineering units. Up to 15 data readings per second can be obtained with normal sampling commands. More than 100 samples per second can be obtained with special burst sampling commands.

Transmitters are available in full scale absolute pressure ranges from 15 psia to 15,000 psia; full scale gauge pressure ranges from 15 to 200 psig and full scale differential ranges of 6, 12, and 20 psid.

The Intelligent Transmitters can be operated as a single standard output device or as an addressable chain of up to 98 transmitters on one RS232 port. Each transmitter can be addressed individually or globally. High baud rates allow multiple transmitter operation on one RS232 port without data backup or scrambling. Power supply requirements are 5 to 25 volts dc with current drain from 10 to 24 milliamperes depending upon the chosen sample rates.

OPERATION

The Digiquartz® Intelligent Transmitter can operate on any standard RS232 bus such as a PC port. Up to 98 individual Intelligent transmitters can be chained off one computer 2 way port to form a system of mixed pressure measurement functions and ranges as might be required by a fully integrated Aerospace system which could monitor or control airspeed, altitude, fuel pressure, engine pressure ratio, hydraulic pressure, etc.

Each Intelligent Transmitter can be addressed individually or collectively for separate or simultaneous pressure measurements. Since each transmitter is individually addressable it's operation can be controlled separately to change pressure units, resolution, or offset as required by the system computer.

Simultaneous pressure measurements can be made by a group of transmitters for later individual or sequential readout. This is frequently useful for strobing pressure measurements on a system such as a wind tunnel during rapidly changing or fluctuating conditions.

If a single stand-alone pressure measurement is required for, say, data recording or visual observation, the transmitter can be preprogrammed to output pressure information at a given resolution in chosen engineering units and then operated as an independent sensor feeding information to a printer, processor, or just a visual display such as the Model 710 Display shown in Figure 4.

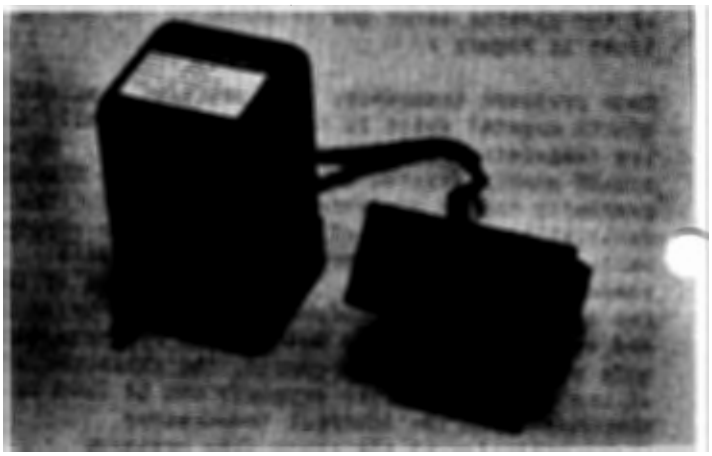

Figure 4
Intelligent Transmitter with
Model 710 Visual Display

The Intelligent Transmitter with the Model 710 Visual Display is completely portable with a small battery pack.

The Model 710 is a six digit LCD display in a standard DIN size panel mount enclosure. It displays pressure data from a Series 1000 Intelligent Transmitter. The display operates either as a stand-alone device with a transmitter or with a computer on line. For stand-alone operation, the display shows pressure whenever power is applied to the transmitter.

When a computer is on-line, the Model 710 can also be used to display other data calculated in the computer (filtered data values, time, temperature, error messages, etc.).

COMMAND FORMAT

All commands have the form *ddsscc____ <cr><lf>
Data framing is 8 data bits, no parity, with one stop bit

1. Each command starts with an asterisk.
2. The next 2 digits are the destination for the command (00-99)
   The controller (IBM PC, etc.) is address "00" and the transmitters are "01" through "98" with "99" for "global".
   A transmitter responds only to its own address or "99".
3. The next 2 digits are the source of the message (00-98).
4. The next 2 characters specify the type of message, and may be followed by more characters in some messages. Characters may be be upper case or lower case. Reply messages may substitute data for the "cc" characters.
5. Each message line is terminated by a carriage return <cr> and a <lf>.
6. Undefined commands are absorbed.
7. Commands arriving before a previous command is completed cancel the previous command.

A typical message from the PC to transmitter #1 asking for pressure:

*0100P3 <cr> <lf>

A typical reply from the transmitter to the PC:

*000114.573 <cr> <lf>

COMMAND LIST

P1	Sample and send one pressure sensor period
P2	Continuously sample and send pressure periods
P3	Sample and send one pressure
P4	Continuously sample and send pressure
P5	Sample and hold one pressure
P6	Sample and hold one pressure
P7	Burst sample pressure read temperature once; then continuously send pressure compensated using original temperature
Q1	Sample and send one temperature period
Q2	Continuously sample and send temperature periods
Q3	Sample and send one temperature
Q4	Continuously sample and send temperature
Q5	Sample and hole one temperature
Q6	Sample and hold one temperature period
DB	Dump buffer. Sends values being stored
VR	Read software version
BR	Enter baud rate. Must be global "99" command
ID	Auto-number transmitters in a loop.
EW	Enable EEPROM write for one command

NOTE: All remaining commands either read the present values of operating parameters or store new values in EEPROM. These commands cannot be global. Any command to change values in EEPROM must be immediately preceded by an EW command.

PR	Read/enter pressure resolution
TR	Read/enter temperature resolution
UN	Read/enter choice of pressure units
UF	Read/enter user definable units conversion factor

NOTE: REMAINING COMMANDS READ OR CHANGE CALIBRATION COEFFICIENTS. BE CAREFUL! Calibration Commands should never be sent as global commands

SN	Read/enter transmitter serial number
PA	Read/enter pressure adder
PM	Read/enter pressure multiplier
TC	Read/enter timebase correction factor
C1	Read/enter C1 pressure coefficients
C2	Read/enter C2 pressure coefficient
C3	Read/enter C3 pressure coefficient
D1	Read/enter D1 pressure coefficient
D2	Read/enter D2 pressure coefficient
T1	Read/enter T1 pressure coefficient
T2	Read/enter T2 pressure coefficient
T3	Read/enter T3 pressure coefficient
T4	Read/enter T4 pressure coefficient
T5	Read/enter T5 pressure coefficient
U0	Read/enter U0 temperature coefficient
Y1	Read/enter Y1 temperature coefficient
Y2	Read/enter Y2 temperature coefficient
Y3	Read/enter Y3 temperature coefficient

CHARACTERISTICS AND PERFORMANCE

Because the Digiquartz® pressure transducer uses a quartz resonator to provide high constraint to the pressure generator element (bellows or Bourdon tube) there is very little mechanical motion under load (100 microinches or less). This results in superior repeatability and minimal hysteresis. The crystals themselves produce the kind of stability characteristic of any quality quartz resonator. In addition, the lack of extraneous noise on the output signals because of the exceptionally high Q offers unparalleled resolution. The use of a frequency output quartz temperature sensor for temperature compensation yields an achievable accuracy of 0.01% Full Scale over the entire operating temperature range.

Thus the Intelligent Transmitter is capable of primary standard performance even under difficult system or field conditions. The standard digital output in a number of selectable engineering units on a high speed addressable data bus allows plug-in compatibility with most computer based systems. The transmitters are field interchangeable without recalibration or reprogramming.

Tables 1 2, and 3 list the performance, characteristics, and model ranges of the Intelligent Transmitters.

TABLE 1
PERFORMANCE

Repeatability	0.005% FS
Hysteresis	0.005% FS
Pressure Conformance	0.005% FS
Acceleration Sensitivity	0.0038% FS/g
Resolution (adjustable)	0.05 to 100 ppm FS
Baud Rate	300 to 19,200
Sample Speed	Up to 100 s/second

TABLE 2
CHARACTERISTICS

Size:	3.12 x 3.12 x 5.00 inches
Weight:	29 oz
Power Requirements:	5 to 25 vdc
Operating Temperature Range:	-54 to +100°C
Pressure Units:	User selectable. Choice of psi, mbar, bar, MPa, inches of Hg, torr, meters of water, or user definable
RS232 Bus:	Baud rates: user selectable from 300 to 19200 baud
Input Levels:	Any RS232 compatible level
Output Levels:	±5 vdc nominal
Data Framing:	8 data bits, no parity, one stop bit
Handshaking:	Not supported. Transducer is always ready to receive

TABLE 3
MODEL RANGES

MODEL	RANGE
1015A	0 to 15 psia (0.10 MPa)
1023A	0 to 23 psia (0.16 MPa)
1030A	0 to 30 psia (0.21 MPa)
1045A	0 to 45 psia (0.31 MPa)
1100A	0 to 100 psia (0.69 MPa)
1200A	0 to 200 psia (1.38 MPa)
1300A	0 to 1300 psia (2.07 MPa)
1400A	0 to 400 psia (2.76 MPa)
1900A	0 to 900 psia (6.21 MPa)
1015G	0 to 15 psig (0.10 MPa)
1030G	0 to 30 psig (0.21 MPa)
1100G	0 to 100 psig (0.69 MPa)
1200G	0 to 200 psig (1.38 MPa)
1006D	0 to 6 psid (0.04 MPa)
1012D	0 to 12 psid (0.08 MPa)
1020D	0 to 20 psid (0.14 MPa)
1002K	0 to 2000 psia (13.8 MPa)
1003K	0 to 3000 psia (20.7 MPa)
1006K	0 to 6000 psia (41.4 MPa)
1010K	0 to 10,000 psia (69.0 MPa)

APPLICATIONS

The Digiquartz® Intelligent Transmitters present a powerful solution to many pressure instrumentation needs. They combine the precise performance of the Paroscientific transducers with the speed, versatility, and convenience of a dedicated internal microprocessor. The RS-232 interface allows complete remote configuration and control of all operating parameters, including resolution, sample rate, integration time, and baud rate. The Intelligent Transmitter provides unparalleled accuracy across a wide temperature range in a package that ensures operation under adverse conditions of vibration and shock.

As a stand alone sensor or as a string of system sensors the transmitters offer versatility in operation and diversity in measurement, whether absolute or gauge, high or low pressure. The transmitters lend themselves well to system applications for both monitoring or control allowing various pressure ranges to be interfaced on one system port. An aircraft system might require two pressure ranges for static and dynamic pressure and additional ranges for fuel pressure, engine pressure ratio, etc. All could be accomodated on one data link. Calibration and Metrology laboratories or test facilities will find the transmitter useful, not only as a transfer standard but as an intelligent monitor of other equipment. For instance the unprecedented resolution of the transmitter enables it to make measurements of better than 1 ppm on primary pressure standards allowing personnel to study weight wobble or settling times during actual operation.

The engineers and scientists who are concerned with the ultimate in speed, precision, and adaptability will undoubtedly conceive of new and intriguing uses for these pressure transducers and transmitters. The versatility and broad applicability of these sensors should provide plug-in solutions to a wide variety of pressure measurement problems.

APPENDIX A: CALCULATION OF PRESSURE AND TEMPERATURE FROM PERIOD MEASUREMENTS

The transmitter calculates temperature and pressure from period measurements of two frequency signals. The equations used in the calculations are given below:

$$\text{temperature} = Y_1U + Y_2U^2 + Y_3U^3 \qquad \text{Deg C}$$

$$P = C(1 - T_0^2/Tau^2)[1 - D(1 - T_0^2/Tau^2)] \qquad \text{psi}$$

where Tau = pressure period in microseconds

U = (temp period) - U_0 microseconds

$C = C_1 + C_2U + C_3U^2$

$D = D_1 + D_2U$

$T_0 = T_1 + T_2U + T_3U^2 + T_4U^3 + T_5U^4$

These equations express temperature and pressure in terms of the transducer calibration coefficients:

Temperature coefficients:

U_0 Y_1 Y_2 Y_3

Pressure coefficients:

C_1 C_2 C_3 D_1 D_2 T_1 T_2 T_3 T_4 T_5

These coefficients are stored in EEPROM and can be obtained from the transmitter via the RS232 bus.

Q: Gordon E. Mills (Paine Corporation): How much internal heating do you get from converting your RS-232? Do you put, basically, 12 volts down the line and then convert it?

A: Donald W. Busse: We don't, at present, take the power off the RS-232 link. You can if you want to because RS-232 is always either +5 or -5 and you can draw some of the power. What we have chosen to do is to have a separate power input. You can power this with any DC source and you can have a power line on the link, if you want. Thus you can have a separate power source and just link the power through all of the transducers.

Q: Gordon E. Mills: How long a cable can you drive?

A: Donald W. Busse: That depends on the baud rate. With very low baud rates down around 300, we should be able to drive hundreds of feet of cable. With some of the new modems, at 300 baud rate, I'm told you can drive 12 miles with it. And, at the high baud rates you probably would be limited to a couple of hundred feet.

Q: Roger P. Noyes: I'm asking this question on behalf of myself, Peter Stein, and Richard Hasbrouck. If you have a differential pressure transducer listed and there is an error sometimes caused by common mode, reference pressure or line pressure, is that ever included in your accuracy statement, or do you have that separately?

A: Donald W. Busse: No, it is not. That is a separate error. In fact, I have a little Murphyism on that. There are two types of differential pressure transducers that we use. One gage, a bellows type, has one port open to atmospheric pressure. You can't put a lot of pressure on it because it can't sustain a lot of absolute pressure. The common mode error on that thing can be as high as 0.1 percent per atmosphere. Since most of these gages are operating in atmosphere, and atmospheric changes are usually small compared to a 0.10 of an atmosphere so the error is going to be 0.10 of that, or something like 0.01 percent for the absolute gages operating in an atmospheric environment.

We have another type which is a true differential that can operate at common mode pressure up to 900 psi. That device will have common mode error down closer to 0.02 percent per atmosphere. There you have to take into account the absolute pressure.

In fact, we are considering having a special device for some applications where you want to know both absolute and differential pressure. We can model the common mode error on the differential gage. All we have to do is measure the linear effect. If we are also measuring absolute pressure, we can then put that term into the model for the differential in the intelligent transmitter, and we can then automatically compensate for common mode.

Q: Gordon E. Mills: With your 36-46 KHz range, how long (how many seconds) do you have to accumulate the count to get your 0.01 percent?

A: Donald W. Busse: With the 15 MHz clock, if you accumulate the count for about 200 milliseconds, about 5 times per second, you would be getting around a part per million.

Q: Gordon E. Mills: Your basic transducer is working at roughly 40 KHz, and you have a 4 KHz change for the full 0 to full scale. As a result, you're not getting 4,000 in 1 second. Are you only getting 4,000 counts?

A: Donald W. Busse: What we are doing is measuring periods rather than frequency. What we do is count the output. Say, for example, it's operating at 40 KHz. We count the clock for 10,000 counts exactly. Ten thousand counts at 40 KHz takes about 0.25 of a second. For 0.25 of a second with a 15 MHz clock, we are going to see a little bit more than 3 million counts. You can get a resolution on the period of a little bit better than a part in 3 or 4 million, but only a 0.1 of 1 percent of that, the 4 KHz change, is due to pressure. We have to downgrade to about a part in 3 or 400,000 or probably a couple parts per million resolution at 4 or 5 times per second. If you chose to count for a longer period, you can get resolution virtually as fine as you want it. We have demonstrated resolution of a part in 100 million.

Q: Joe R. Costanza (Kaman Sciences Corp.): If I understand your connection scheme for all your transducers being connected together on one line, then if one transducer goes out, does that shut down the communication?

A: Donald W. Busse: Yes, it's like the old Christmas tree lights. If one quits working, then they are all dead because you have to have that one to transmit the information. I would like to make just one additional statement here. I do have two working models with a laptop computer, if anybody would like to see one work.

AIRCRAFT GROUND SPEED MEASUREMENTS USING LANDING GEAR VIDEO

by David Banaszak
Electronics Engineer
Aeronautical Systems Division
Air Force Wright Aeronautical Laboratories
AFWAL/FIBG, Wright Patterson AFB,OH 45433

Abstract

Recently AFWAL/FIBG installed video instrumentation to view and record landing gear motion on a C-141B and C-5A aircraft during taxi tests at Royal Air Force Base RAF Wethersfield, England to support a Rapid Runway Repair (RRR) project. The instrumentation included a video camera, a portable video cassette recorder (VCR) and a video monitor for each of three landing gears. This provided personnel on the aircraft the required real time observation of gear motion during aircraft taxi runs over runway repairs at speeds up to 80 Knots. In addition to discussing a system for visual observation of the landing gear, this paper proposes using video data to measure physical parameters such as ground speed by interfacing the video to a microcomputer. One can then automate the video observation, video display and computation of physical parameters from the video data. This paper briefly describes the video instrumentation used on the RRR test. For a typical low speed test run, it details the manual procedures used to compute ground speed by viewing the VCR tapes after completion of the testing. The paper then proposes a way to automate near real time ground speed measurements. In addition, advantages and disadvantages of using the video technique versus other ground speed measurement techniques are discussed.

Introduction

This paper describes two methods to measure ground speed of aircraft and other moving vehicles from video information. The first uses known distances between two points and the second uses known tire size. After discussing theory and trial runs with a truck, the paper shows how to measure ground speed from video tapes made during Rapid Runway Repair(RRR) aircraft taxi tests. The RRR video was designed to observe landing gear motion and repair degradation during aircraft taxi; however, for this paper the video tapes were used to compute aircraft ground speed during travel over the repairs.

The purposes of the RRR tests were to validate pre cast slab(PCS) and fiberglass mat(FGM) repairs, collect data on the performance of the two repair types under sustained airlift trafficking, and provide additional aircraft taxi data. AFESC/RDCR at Tyndall Air Force Base, Florida sponsored the RRR tests(Project AFES8502). The Aeronautical Systems Division's(ASD) Structures and Dynamics Division (AFWAL/FIB) of the Flight Dynamics Laboratory (AFWAL/FI) at Wright-Patterson Air Force Base , Ohio provided the instrumentation to ensure limit loads were not exceeded while taxing a C-141B and a C-5A over the two repair types at RAF Wethersfield, United Kingdom(UK) during October 1985. In addition to loads instrumentation, video instrumentation described in this paper was on the aircraft. This study of using video measurements is part of an In-House effort to investigate new instrumentation, facilities and techniques to measure static and dynamics loads data on Air Force Weapons Systems(Project 24010402).

Making Ground Speed Measurements

Assuming an object moves along the x-axis, the average velocity is defined as the ratio of the displacement to the time interval. This is often written in the form

$$\bar{v} = (x_2 - x_1)/(t_2 - t_1) = \Delta x/\Delta t \qquad (1)$$

also the instantaneous velocity is define as

$$v = \lim_{\Delta t \to 0} \Delta x/\Delta t = dx/dt \qquad (2)$$

where x_1 and x_2 are distances at times t_1 and t_2 and $\Delta x = x_2 - x_1, \Delta t = t_2 - t_1$.

Reference (1) explains velocity computations in detail. Knowing x_1, x_2, t_1, and t_2, one can compute average velocity. A person watching a moving vehicle could derive average velocity if his mind was quick enough to retain the visual image, keep track of time and distance and preform the calculations. A video cassette recorder(VCR) tape is capable of storing and

recreating the time history motion of an object! The Δt can be determine by using the video frame rate of 30 frames per second or using time superimposed on the video signal. Δx measurements can be computed from video using two methods: method 1) using known reference spacings and method 2)using the measured tire circumference. Examples using these two methods follow. Theory of VCRs and video can be studied in References (2) thru (5).

Truck Test Using Reference Spacings

Before using the video tapes on an aircraft, sample test runs using a pick up truck were made to check the methods. For method 1, two cones were set 100 feet apart on an abandoned aircraft taxi way. A portable camera and VCR were used to pan truck motion as it travelled pass the cones. The camera timer was superimposed on the video. The driver tried to hold the truck speed steady between the cones by using the truck speedometer. The log of video records made are shown in Table 1.

In the laboratory, records 2 and 3 were played back. Video frames were made with a video printer for the the 1st and 2nd cones as shown in Figure 1. Using d=100 feet and the VCR time, Table 2 was tabulated. For record 3, where the driver said he was right on 12 mph, the values computed from the 2 video frames and timer was 12.18 mph. On record 2, where the driver was not as steady, an average speed of 13.37 mph was computed.

Truck Test Using Tire Circumference

The truck tire had a measured circumference of 6.42 feet. By using the tape on the tires as shown in the truck figures and measuring angle changes $(\Delta\theta)$ and time changes (Δt) of the tape, the speed of the vehicle was derived using the following:

$$\bar{v} = |(\Delta\theta/360)c/\Delta t| \qquad (3)$$

where θ =tire rotation angle in degrees, c = tire circumference in feet and$\Delta\theta = \theta_2 - \theta_1$, where θ_2,θ_1 = angle at time t_2 and t_1 respectively.

Playback of video frames of truck records 2 and 3 are shown in Figures 2 and 3. The x marks were inserted manually to help determine tire rotation angle (θ) for each frame. The angles were measured with a protractor and ruler using standard positive angle convention. The computed speeds were as shown in Table 3. Two time measurement techniques were used: 1)the camera times and 2) using the fact that the VCR frame advance button was pushed exactly 30 times between stopped frames. Average velocity based on these two time measurements are shown in the table. This techniques would also be applicable to an aircraft if high light contrast source markers were on an appropriate part of the tire. In future one piece of tape will be marked to aid in angle identification and increase the folding frequency at which aliasing starts. If the tire rotates fast enough, optical aliasing can make the tire appear to move backwards. Reference (6) discusses optical aliasing in detail.

Description of Video on RRR Test

For a full description of the complete RRR test instrumentation see Reference (7). Figures 4 and 5, show cross sections of the two repairs. The FGM repair was anchored every 18 inches. The PCS repair consisted of 7 slabs by 7 slabs for a total coverage of 14 meters by 14 meters. Figure 6 shows the C-5A taxing over the precast slab repair. During an event the aircraft taxied over the PCS and FGM repairs. During back taxi(BT) events, the aircraft travelled over the repairs in the reverse direction.

The video equipment used on the RRR test aircraft were as follows: three color video monitors, three portable VHS VCRs with AC to DC power adapters, three CPD video cameras and power supplies. A Static Frequency Converter was used to convert aircraft power to 115 VAC, 60 Hertz power. Except for VCRs, identical equipment were on both aircraft. The cameras and monitors were used to observe the gear during each test run. The total RRR instrumentation are shown in the block diagram in Figure 7. The video system was mounted in a 19 inch rack as shown in Figure 8 and secured with aircraft cargo straps to a pallet as shown in Figure 9.

All video components were in the rack, except for the three cameras located on the aircraft exterior as shown for the C-141 in Figure 10. The cameras provided an optimum view of the gear motion, tire rotation and repair movement during each test run. A typical camera mount is shown on the C-141B in Figure 11. The cameras were mounted each morning and removed each evening. Two cameras viewed the main landing gears and the third viewed the nose landing gear. On the C-5A, the cameras pointed at the forward left main and aft right main landing gear. An operator started the VCRs prior to repair encounter and stopped them at the end of the test run. IRIG-B time code was recorded on the VCR's audio tracks as shown in the block diagram in Figure 12. Personnel on the aircraft viewed the real time video data during each test run.

On the C-141B one portable VCR was used to record events mostly on the right main landing gear while taxing over the repairs. The VCR was switched to the nose or left main gear as required. All three gear were viewed on the video monitors by on board test personnel. Table 4 summarizes C-141B video records.

TABLE 1 Video Tape Records of Truck Run

Record	JVC Tape Counter	Desired Speed	Tape Speed	Comments on Tape
1	0-6	12 mph	ELP	Tape said was 14 mph
2	6-26	12 mph	ELP	
3	26-100	12 mph	SP	Right on
4	100-160	unknown	SP	
5	160-212	25 mph	SP	
6	212-250	Accel. Run	SP	

a) Record 2, 1st Cone, d=0 feet, t=35.7 seconds

c) Record 3, 1st Cone, d=0 feet, t=27.2 seconds

b) Record 2, 2nd Cone, d=100 feet, t=40.8 seconds

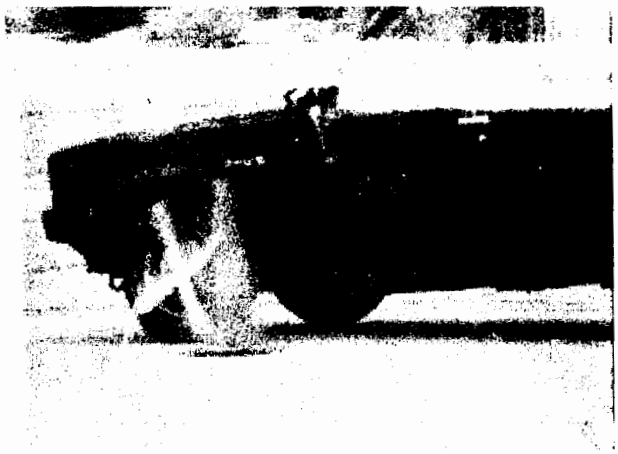

d) Record 3, 2nd Cone, d=100 feet, t=32.8 seconds

Figure 1. Truck Travelling Past Parking Cones.

TABLE 2 Truck Test Results Using Known Distance Theory

	Truck Record 2	Truck Record 3
Cone 2 time(seconds)	40.8	32.8
Cone 1 time(seconds)	35.7	27.2
Δt(seconds)	5.1	5.6
Δx(feet)	100	100
$\bar{v}$(miles per hour)= $\bar{v}_{mph}$	13.37	12.18
Driver's Comments	14 mph try again	12 mph right on

Where $\bar{v}_{mph} = (\Delta x/\Delta t)$ (feet/second) x .682 (mph/feet/second).

a) Frame 1, t=36.4 seconds, θ = 27 degrees

d) Frame 4, t=36.8 seconds, θ = 141 degrees

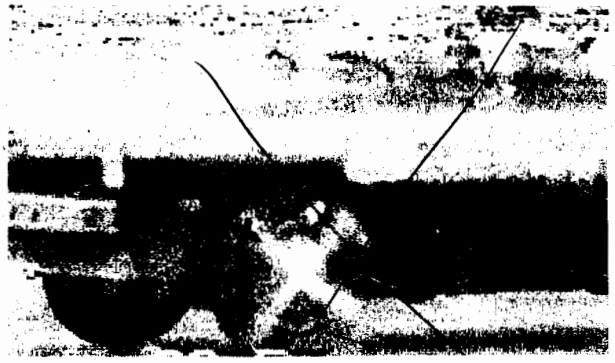

b) Frame 2, t=36.5 seconds, θ = 141 degrees

e) Frame 5, t=36.9 seconds, θ = 301 degrees

c) Frame 3, t=36.6 seconds, θ = 283 degrees

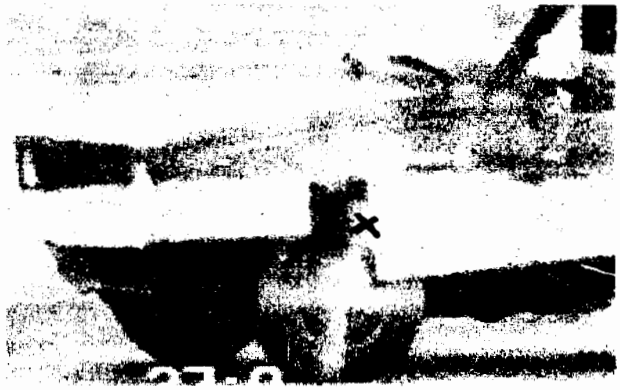

f) Frame 6, t=37.0 seconds, θ = 89 degrees

Figure 2. Truck Record 2 Video Frames.

a) Frame 1, θ = 45 degrees

c) Frame 1+60, θ = 331 degrees

b) Frame 1+30, θ = 9 degrees

d) Frame 1+90, θ = 281 degrees

Figure 3. Truck Record 3 Video Frames.

TABLE 3 Truck Test Results Using Tire Size Theory

Record-Frame	θ(degs.)(1)	$\Delta\theta$(degs.)	t(secs)	Δt(seconds)	$\bar{v}_{mph}$(2)	$\bar{v}_{mph}$(3)
2-1	27	—	36.4			
2-2	141	114	36.5	.1	13.91	
2-3	283	142	36.6	.1	17.32	
2-4	141	218	36.8	.2	13.30	
2-5	301	160	36.9	.1	19.52	
2-6	69	128	37.0	.1	15.62	
3-1	45	—	28.2			
3-2	9	324	28.5	.3	13.18	11.83
3-3	331	322	28.8	.3	13.09	11.75
3.4	289	318	29.1	.3	12.93	11.60

(1) Angle θ measured with a protractor and positive angle is counter clockwise.

(2) Average v= $\bar{v}_{mph} = [c(\Delta\theta/360)/\Delta t] \times .682[mph/fps] = (\Delta\theta/\Delta t) \times .0122$. (i.e. using time)

(3) Average v= $\bar{v}_{mph} = [c(\Delta\theta/360)/\Delta f] \times .682[mph/fps] = (\Delta\theta/\Delta t) \times .0365$. Since there were 30 pushes(f=30) of frame advance button each .3 seconds. That is, $\Delta t = \Delta f/3$. (i.e. record 3 using frame count)

(4) Tape said 14 mph on Record 2.

(5) Where c=6'5"= 6.42'= measured tire circumference.

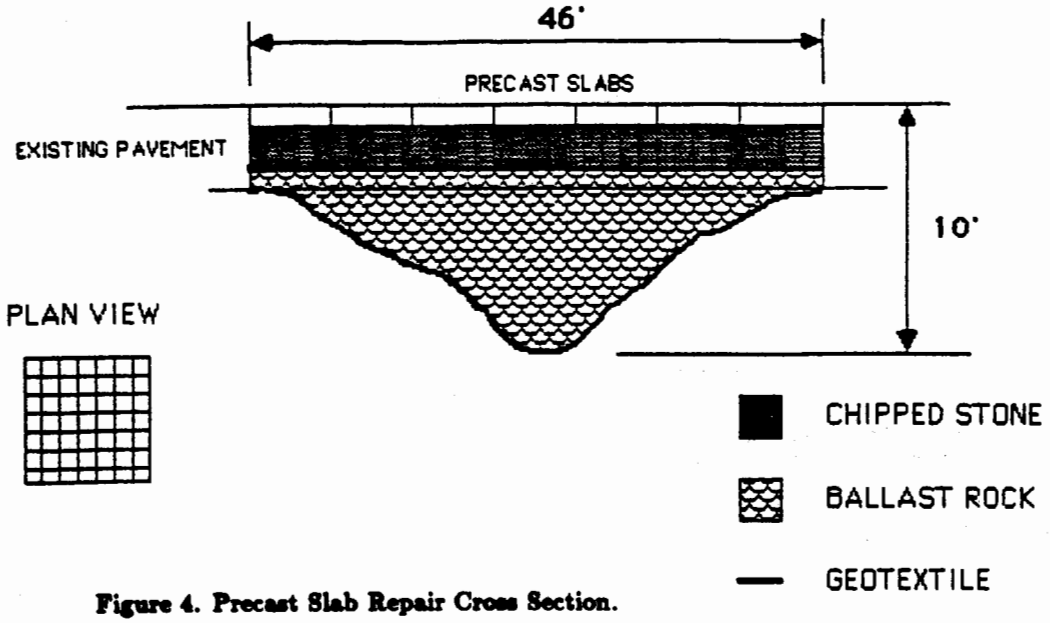

Figure 4. Precast Slab Repair Cross Section.

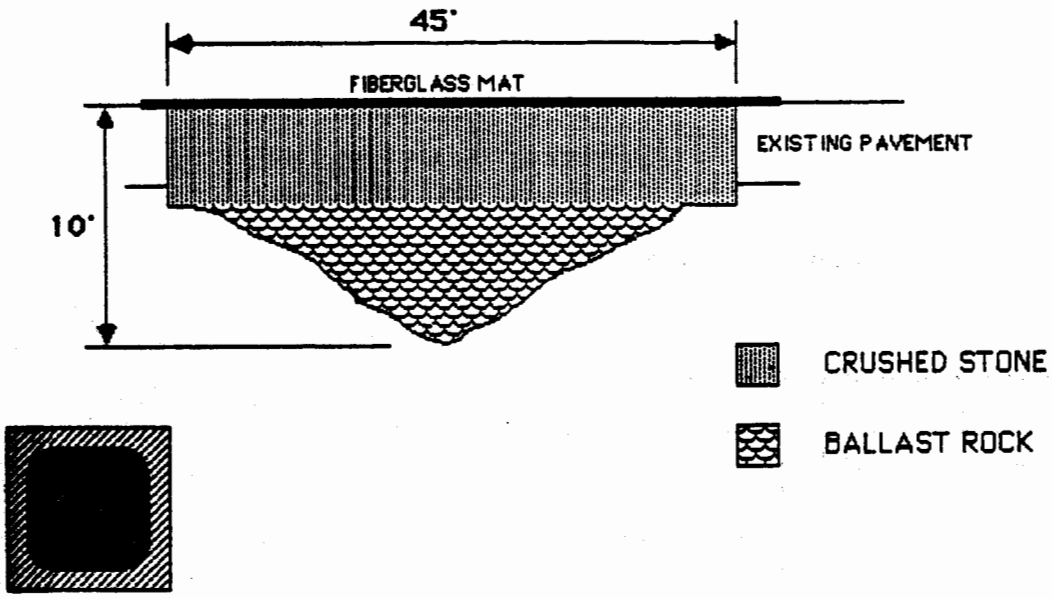

Figure 5. Fiberglass Mat Repair Cross Section.

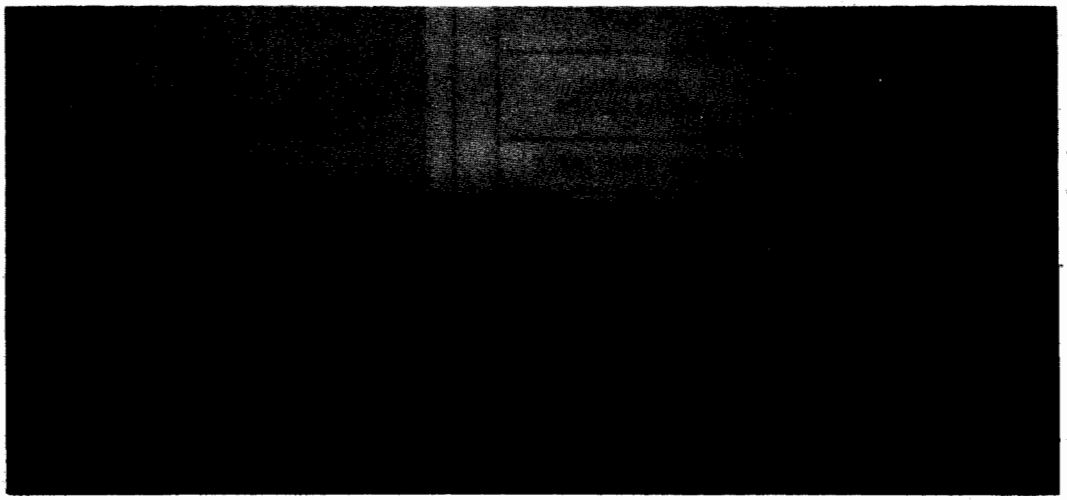

Figure 6. C-5A on Pre Cast Slab at RAF Wethersfield.

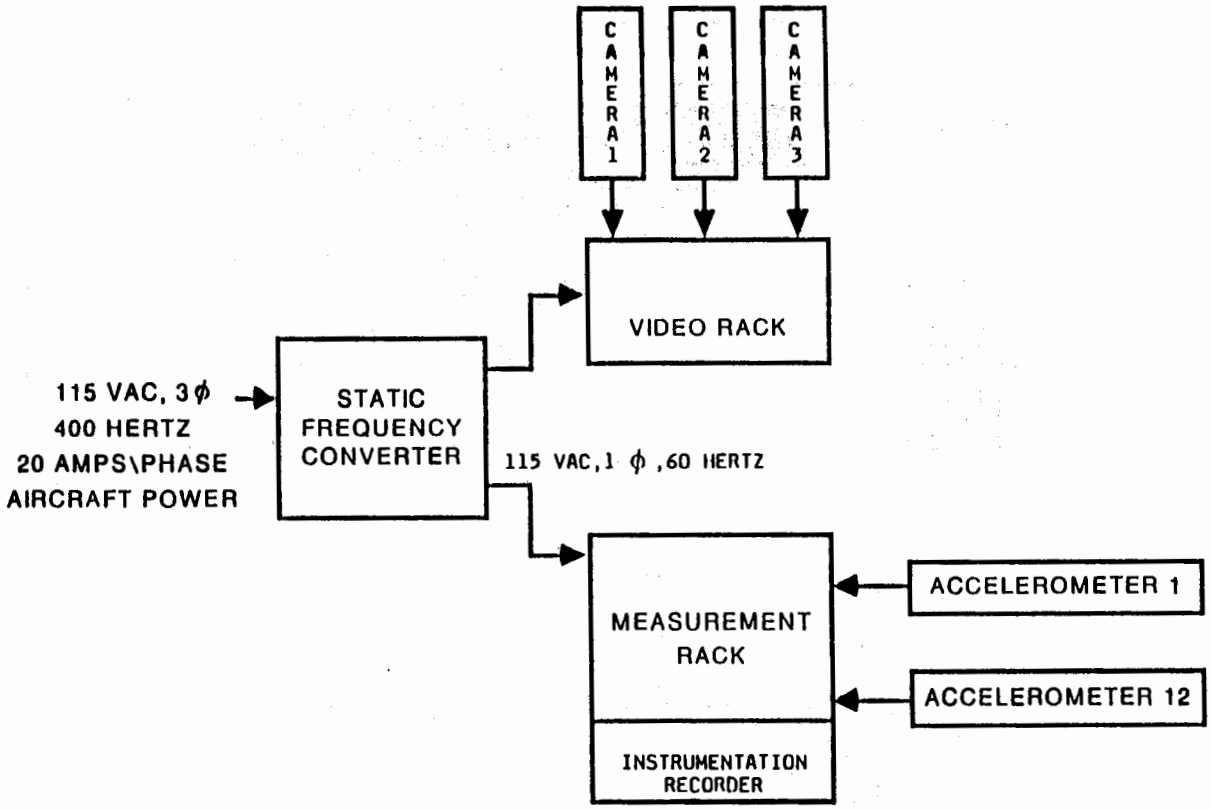

Figure 7. Block Diagram for Rapid Runway Repair Instrumentation.

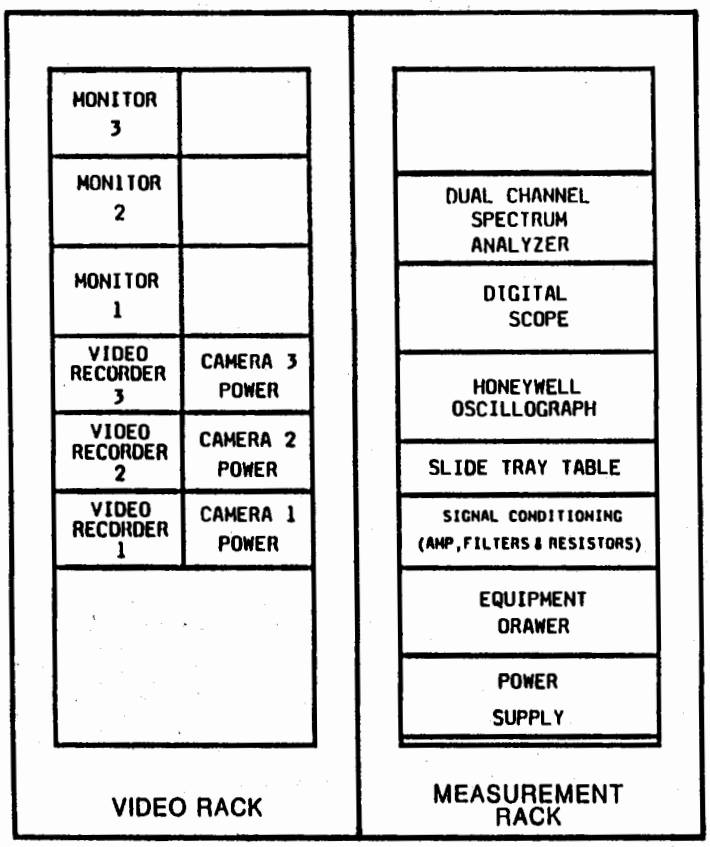

Figure 8. Equipment Layout for Project Rapid Runway Repair.

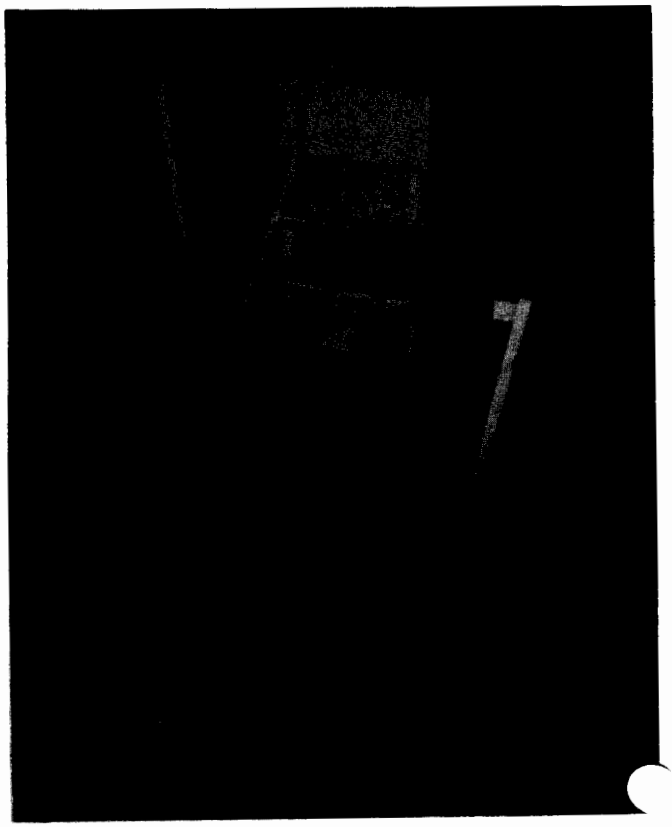

Figure 9. Equipment on 463L Pallet in C-5A.

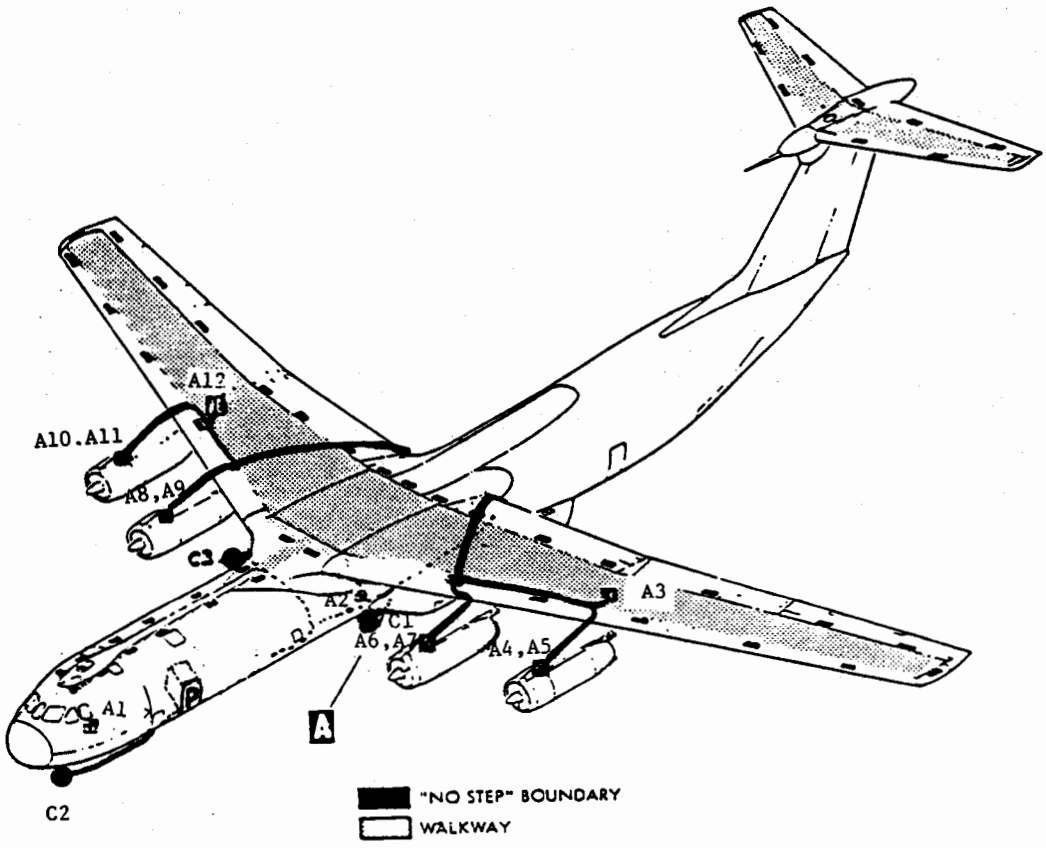

C-141B AIRCRAFT

SYMBOLS:

P Pallet with Honeywell 101 Recorder, Measurement Rack, Video Rack,and Power Converter
● C1 Camera 1 Looking at Left Gear
● C2 Camera 2 Looking at Nose Gear
● C3 Camera 3 Looking at Right Gear
Accelerometer (1 axis) A1,A3,A12
Accelerometer (2 axes) A4,A5 A6,A7 A8,A9 and A10,A11

NOTES:

FS 497	Service Outlet on Left Side of Aircraft 115VAC,400 Hertz,3 phase, 20 amps/phase
FS 428-500	Equipment on Type 463L pallet
FS 930	C.G. Accelerometer
FS 1020	Main Wheel Well Inspection Windows
FS 1045	Cyrogenic Plug Locations

Figure 10. C-141 Instrumentation Locations.

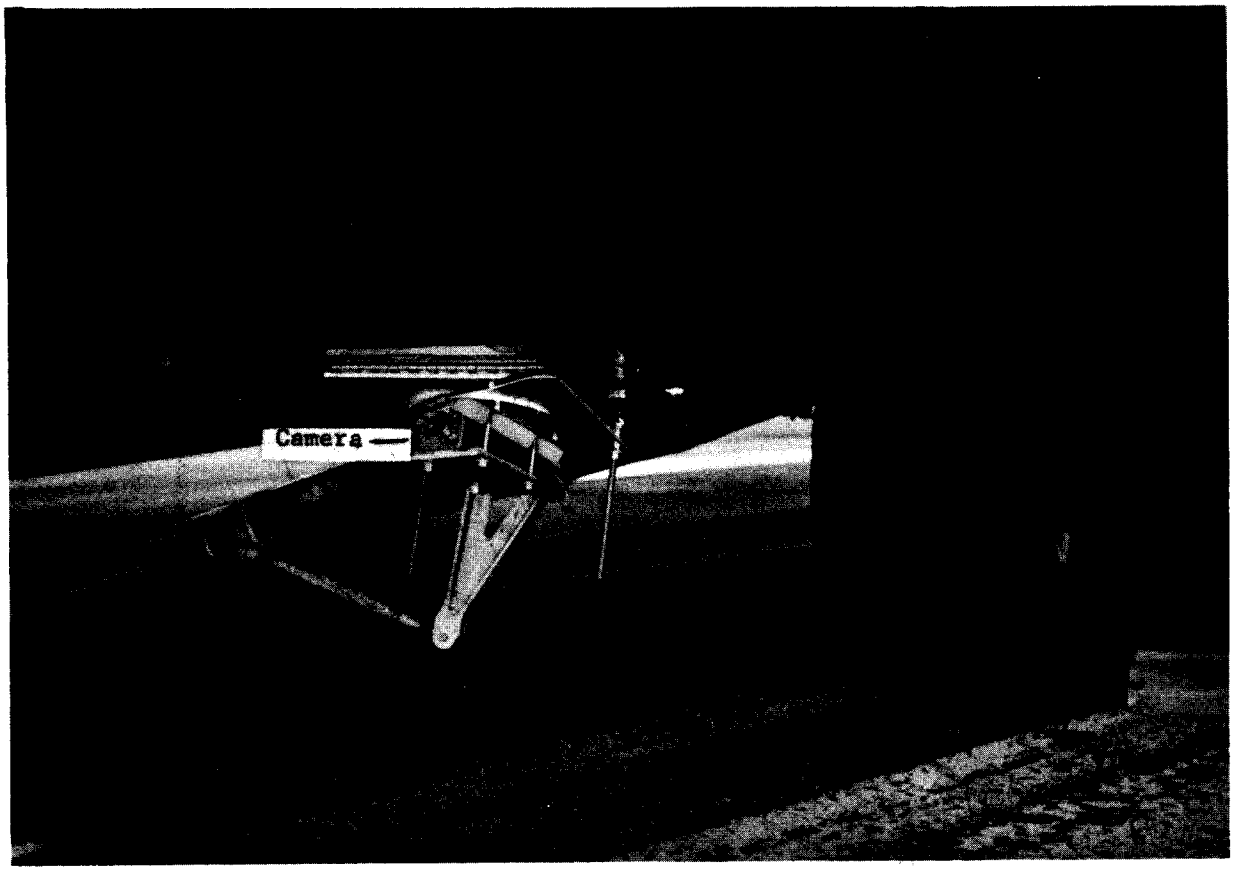

Figure 11. Left Camera Mounted on C-141.

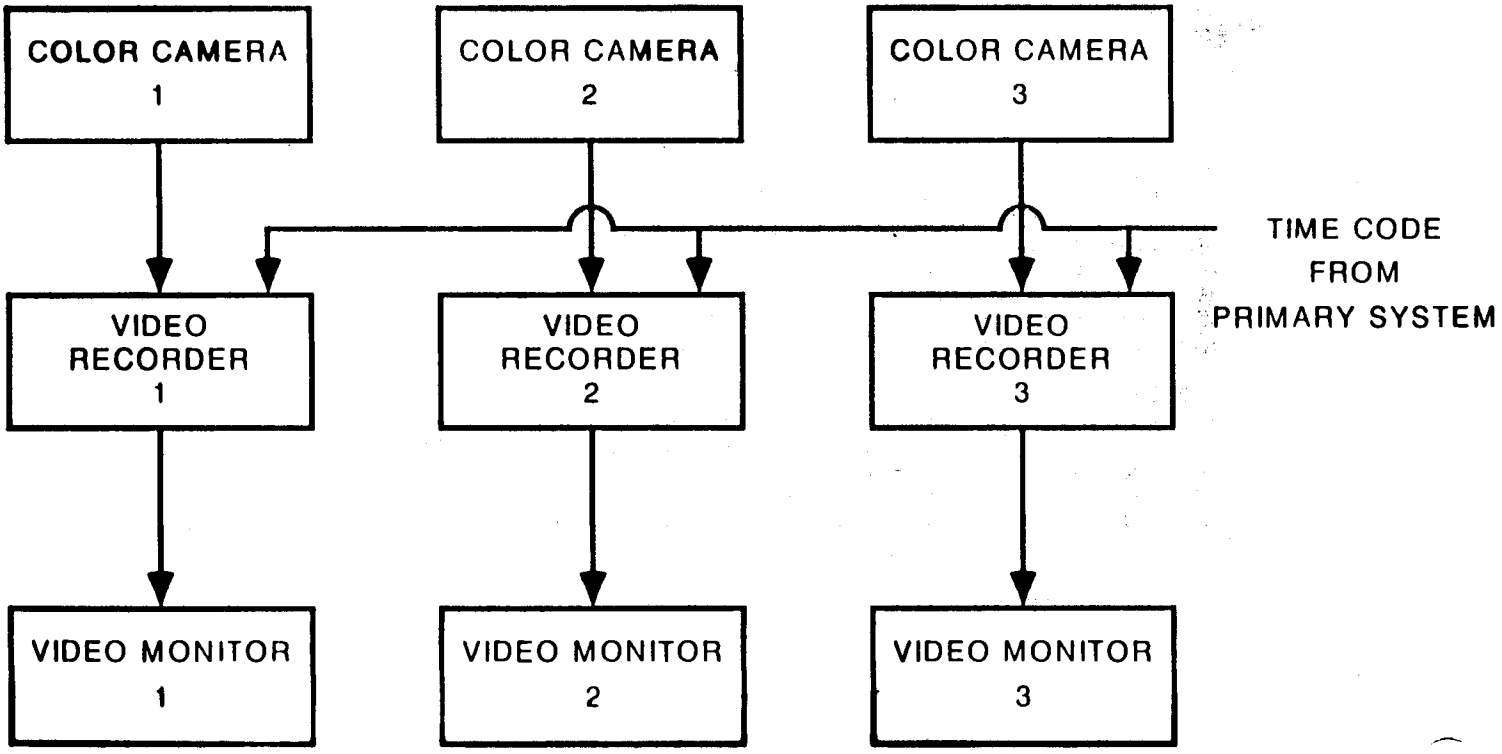

Figure 12. Video System Block Diagram.

For the C-5A, three VCRs were used and video data were recorded for test event for all three gear.

Ground Speed by Viewing C-141 RRR Video

Using the known reference spacing of 2 meters square, 7 x 7 array of pre cast slabs, it is possible to measure fairly high aircraft ground speed using 30 video frames (60 fields) per second sample rates. If the aircraft traveled over one slab in a 60th of a second, the speed is

$$\bar{v} = \frac{2meters}{(1/60)seconds} = 120m/s \approx 232Knots \qquad (4)$$

After the tapes were brought back from the RRR tests, the following procedures were used to check out a typical 5 Knot back taxi run (event 27A in Table 4) of the C-141 aircraft. The tapes were dubbed with video time inserted into the picture to help measure time. Next, voice was dubbed on audio track 2 with event descriptions as shown in Tables 4. The IRIG-B time code was left intact on track 1 of the stereo VCRs. These preparations made tapes suitable for post processing to determine aircraft taxi speed and to compare the results with pilot's comments on the log sheet.

For the C-141 test event 27A, the speed of travel over the and precast slab repairs were derived at an engineer's desk as follows:

1. The video tape was played back and the VCR pause button pressed when the aircraft tire touched a slab seam division line.

2. A hardcopy of the video frame was made as shown in Figure 13.

3. Steps 1 and 2 were repeated for the 8 seam lines of the 7 slabs.

4. The video frame timer was used to determine the time to transverse the slab.

5. The time and know distance of 2 meters for each slab were typed into a microcomputer spreadsheet as shown in the table in Figure 14.

6. The micro's spreadsheet was used to compute Vknots in the table and plot the bar chart of Vknots versus time as shown in Figure 14.

7. The table could then be uploaded to a central computer for inclusion into a report.

For the fiberglass mat on event 27A the above procedures, were repeated, except now there was two know reference lines, the beginning and the end of the repair which was a known distance of 13.716 meters. Video frames over the fiberglass mat and resultant computations are also shown in the table of Figure 14.

The computed velocities were between 2 and 4 knots for event 27A, which was less than the 5 knot target. This is not surprising, since is is very difficult to taxi a large aircraft at a constant low speed. Further studies of faster speed records should be made in the future.

Proposed Video Ground Speed Measurement

A block diagram of a potential system to automate the above process is shown in the block diagram of Figure 15. A desired goal is to display video and velocity time histories simultaneously while at the test site. This could be accomplished by showing the digitized video and time history in two windows of a multitasking microcomputer. As can be seen from the block diagram, the system would required high video digitizing rates and a large amount of memory.

For the RRR test special markers on the aircraft tires would have been preferred since seam lines do not have high optical contrast. That is , Method 2 would be more general for any aircraft test and more conducive to automation. Also, for Method 2 just tire size needs to be measured, and the time increment delta t can be as small as the frame or field rate allows.

The basic proposed system in Figure 15 requires a frame or field digitizer interfaced to a computer. Counting of frames and fields would be used to determined Δts and fast software algorithms are needed to compute angles ($\Delta\theta$) and present the resulting time history in different windows on the computer CRT. For faster speeds and frequencies, the ability to separate the two video fields per frame would also be helpful.

More elaborate video processing systems include the Sun video digitizing system, Kodak's SP-2000 high speed video system, or DEC's MicroVax II with plug in frame grabber cards. The desired proposed system should be smaller that the above cited systems.

Advantages and Disadvantages of Video Data

Video offers capabilities that are not normally available on tests such as RRR. Real time observation and recording of landing gear motion during the test was a real help in making on-site decisions about proceeding to the next test event. Video provided a real time display of what happened to the gear during each test run. Video can be an inexpensive and quick way to view motion of a gear which is normally measured with a displacement transducer. The camera is a noncontacting transducer that does not interfere with gear motion. Other noncontacting displacement measurement of low frequency data on tests such as Large Space Structure experiments is very feasible.

TABLE 4 VIDEO TAPE RECORDS ON C-141B(TN 67-954)

Recorder:RCA Portable Tape Speed:EP Video Track:Camera Audio Track:Time code

Date	JVC Counter	Event Description
10/6	0000-0427	Aircraft inside hangar and equipment inside
	0477-0642	C-141 leaving hangar and inside aircraft
	0688-0692	Still of Right Main Gear
10/7	0696-0705	Still of Right Main Gear-Practice
	0705-0707	Gap before LIGHTWEIGHT RUNS
	0707-0719	(7) 60 Knot Acceleration
	0724-0764	(7A) 5 Knot Back Taxi
	0767-0778	(8) 60 Knot Braking
	0784-0826	(8A) 5 Knot Back Taxi
	0827-0844	(9) 80 Knot Acceleration
	0844-0896	(9A) 5 Knot Back Taxi
	0896-0915	(10) 80 Knot Deceleration(no braking)
10/8	0915-1023	Gap Before HEAVYWEIGHT RUNS
	1023-1083	(27A) 5 Knot Back Taxi
	1083-1105	(28) 10 Knot Taxi
	1105-1143	(28A) 5 Knot Back Taxi
	1143-1157	(29) 20 Knot Taxi
	1157-1159	Still of Right Main Gear
	1159-1190	(29A) 5 Knot Back Taxi
	1190-1204	(30) 40 Knot Braking(just before mat)
	1203-1253	People checking brake and tire temperatures
	1253-1279	(30A) 5 Knot Back Taxi
	1279-1299	(31) 40 Knot Acceleration
	1299-1322	(31A) 5 Knot Back Taxi
	1322-1334	(32) 40 Knot Braking
	1334-1366	(32A) 5 Knot Back Taxi-Left Main Gear
	1368-1384	(33) 60 Knot Acceleration-Left Main Gear
	1384-1414	(33A) 5 Knot Back Taxi-Left Main Gear
	1414-1423	Still of Nose Gear
	1423-1439	(34) 60 Knot Braking-Nose Gear
	1439-1452	Turning around-Nose Gear
	1452-1502	(37A) Taxi Turn
10/9	1507-1553	(34A) 5 Knot Back Taxi
	1553-1567	(35) 80 Knot acceleration
	1567-1610	(35A) 5 Knot Back Taxi-Left Main Gear
	1610-1628	(36) 80 Knot Deceleration-Left Main Gear
	1628-1662	(36A) 5 Knot Back Taxi-Left Main Gear
	1662-1695	(39A) 5 Knot Back Taxi
	1695-1707	(47) 60 Knot Braking
	1707-1760	Taxi Turn over Pre Cast Slabs
	1760-1804	Taxi Turn over fiberglass

NOTE: All records are of right main gear unless otherwise described.
Audio dubbed Right channel for all test events on 11/13/85
Time Code recorded on site on Left and Right channels for all events.

a) Seam 1, Slab 0, t=43.45 seconds

b) Seam 2, Slab 1, t=44.60 seconds

c) Seam 3, Slab 2, t=46.37 seconds

d) Seam 4, Slab 3, t=47.47 seconds

e) Seam 5, Slab 4, t=48.99 seconds

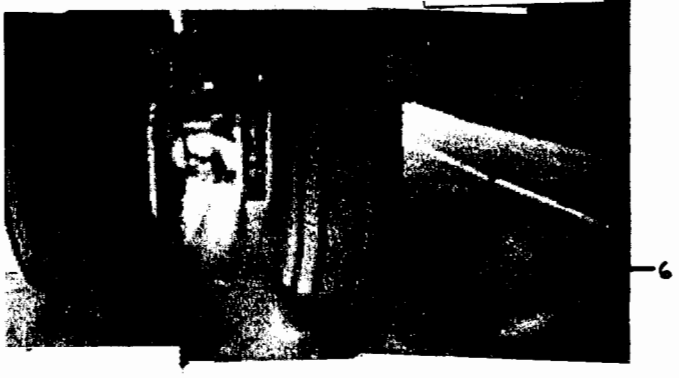

f) Seam 6, Slab 5, t=50.37 seconds

g) Seam 7, Slab 6, t=51.81 seconds

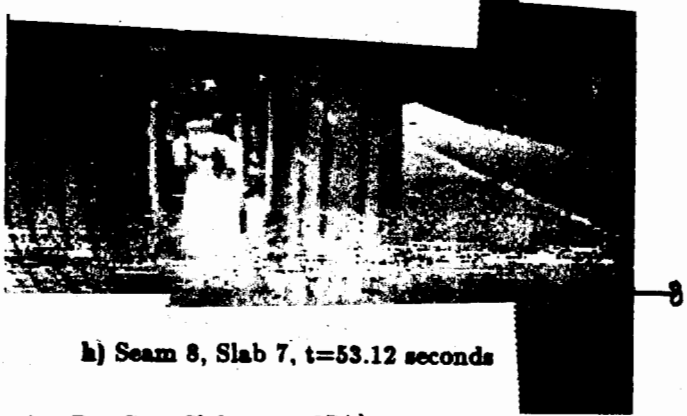

h) Seam 8, Slab 7, t=53.12 seconds

Figure 13. C-141 Video Frames Crossing Pre Cast Slab(event 27A).

EVENT# 27A

Fibreglass#	D(meters)	delta d	t(seconds)	delta t	v=d/t(m/sec)	v(knots)
0	0	0	5.24			0.00
1	13.716	13.716	17.80	12.56	1.09	2.12

SLAB#	d(meters)	delta d	t(seconds)	delta t	v=d/t(m/sec)	v(knots)
0	0	0	43.45	0.00	0.00	0.00
1	2	2	44.60	1.15	1.74	3.38
2	4	2	46.37	1.77	1.13	2.20
3	6	2	47.47	1.10	1.82	3.53
4	8	2	48.99	1.52	1.32	2.56
5	10	2	50.37	1.38	1.45	2.82
6	12	2	51.81	1.44	1.39	2.70
7	14	2	53.12	1.31	1.53	2.97

KNOTS VERSUS SLAB NUMBER FROM VIDEO

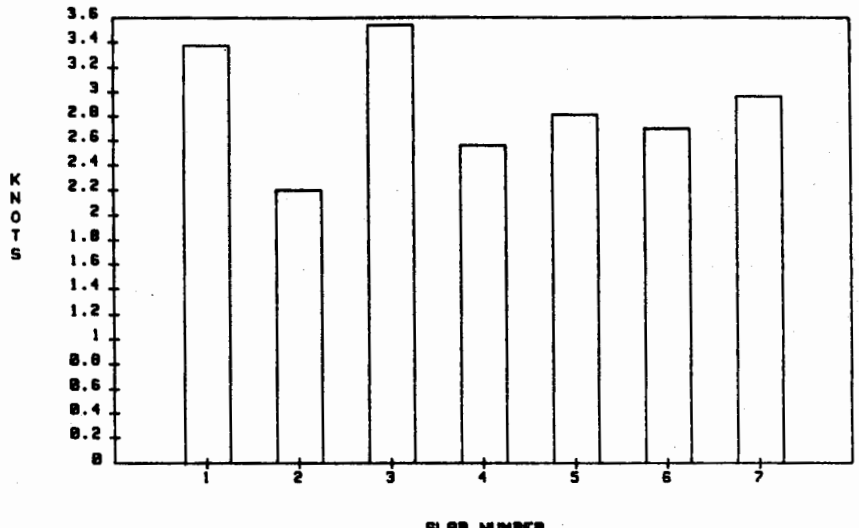

Figure 14. Knots versus Slab Number Table and Plots.

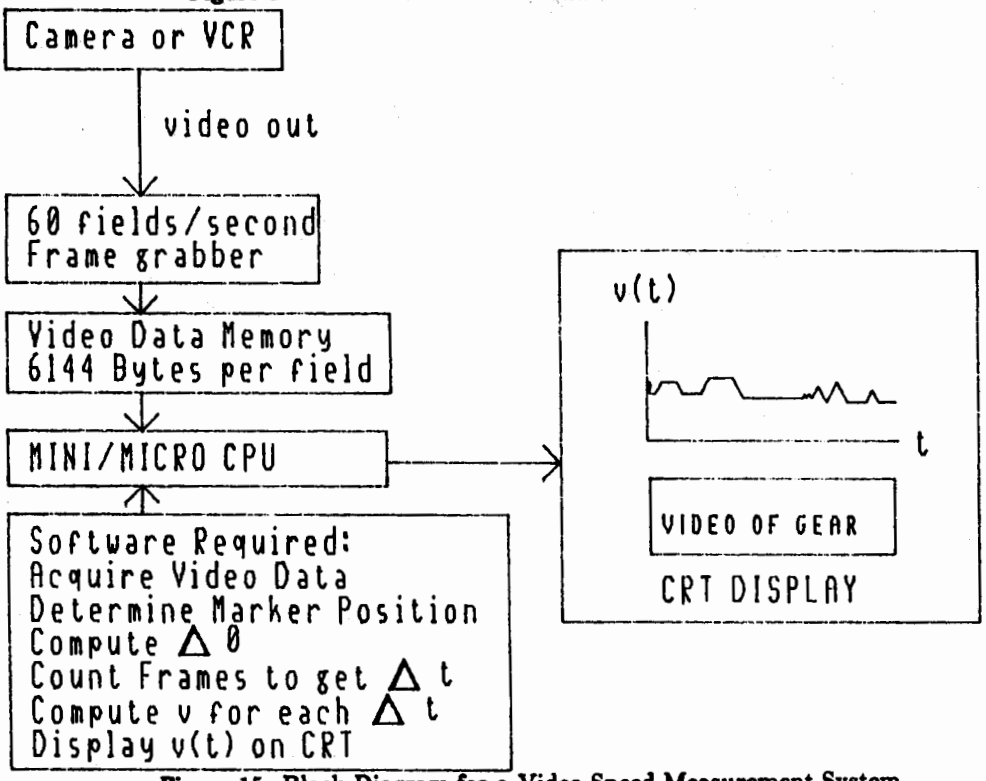

Figure 15. Block Diagram for a Video Speed Measurement System

Video provided documentation in areas that are unreachable with conventional still cameras during aircraft motion. The camera was located remotely from the aircraft gear and operator. An inexpensive, commercially available VCR was used. Also, an advantage is that one can quickly obtain hardcopy prints of video frames as done in this paper. A higher resolution video copier enhances the quality of the hardcopy video prints.

Disadvantages of this particular video system was lack of moisture proof cameras in event of rain. Also the camera lens is vulnerable to being hit by flying debris unless some type of protective lens cover is used. Lighting in the area of the camera was important, especially under the belly of an aircraft. Since commercial video looks at 30 frames(60 fields) per second, optical aliasing must be considered. Currently it might be a difficult and expensive to interface video to a computer, especially considering memory required, video frame digitizing rate required and proper design of software. This disadvantage should disappear as video and computer technologies advance.

Summary and Conclusions

For the RRR test, comparison of video computed speed compared favorably with logged speeds. Further studies should be done to compare video to conventional transducer techniques, preferably using a prototype automated system.

In the past, image processing was solely in the domain of high cost tests such as the space program. On the RRR tests, the video cameras worked well in a location where humans or transducers could not perform. The real time video on the aircraft was an excellent engineering tool to evaluate gear motion during the test events. With proper camera placement and gear marking, actual gear displacements could also be measured using video.

The video data quality was good. Future tests should include video timers. The concept of deriving ground speed from video has been demonstrated and a proposal has been made to automate the process. A goal is real time velocity time histories using a computer and video. Video data may become a requirement for future structural tests as the interface between video and computers becomes more refined. For test requiring low frequency displacement measurement of structures, video can be eventually used to replace conventional contacting displacement transducers and accelerometers.

Acknowledgment

Mr. Earl Rogers of AFWAL/FIB did the mechanical and electrical design of the RRR instrumentation. Discussions with Gerald Plzak, Gene Madux, John Riechers and Anthony Gerardi of AFWAL/FIB and Tom Smith of Tech Photo(4950TESTW/RMPI) provided the author with valuable technical insight in merging the technologies required for this paper.

References

(1) Sears,F.W. and Zemansky,M.W., **University Physics Third Edition**, Addison-Wesley Publishing Company, Reading,MA,1964.

(2) Terman,Frederick E.,"Chapter 25 Television", **Electronic and Radio Engineering Fourth Edition**, pp977-1014, Mc-Graw Hill, New York,1955.

(3) Costello, Marjorie and Heiss, Michael, **1986 Buyer's Guide to Home Video**, HP Books,Inc., Tucson,AZ, 1985.

(4) Bishop,John M., **Home Video Production**, McGraw-Hill,New York,NY,1986.

(5) Cannon, Don L. and Luecke, Gerald, "Chapter 7 Radio and Television Systems", **Understanding Communication Systems**, Texas Instruments Learning Center, Dallas,TX, 1980.

(6) Enochson, Loren, "Accurate Digital Signal Processing Mandates Antialiasing Filters", *Personal Engineering and Instrumentation News*, pp39-42, Aug 1986.

(7) Banaszak, David and Rogers, Earl, AFWAL-TM-85-258-FIBG, **Rapid Runway Repair Test Description**, Dec 1985, AFWAL/FIBG, WPAFB, OH 45433.

Q. Gordon E. Mills: How expensive is that video printer?

A: David L. Banaszak (U.S. Air Force): This is the better one and it's about $1,200. Mitsubishi and Tektronics make them. It's still got a way to go, but it's getting there and this is one that has 16 levels of gray. I like it because you can take it off a VCR. There are a lot of black and white ones with a higher resolution. You have to make that tradeoff. As you get more levels of gray, you take memory or you take more pixels; each way you take memory.

A TEMPERATURE CONTROLLED PRESSURE TRANSDUCER FOR MEASURING ENGINE INLET PRESSURE

Edward N. Kachman, Jr.
McDonnell Aircraft Co.
Senior Engineer
Flight Test Data Systems
Electro-Mechanical Design

John Hayer
Kulite Semiconductor Products
Vice President - Marketing

ABSTRACT

A typical instrumentation application in each fighter aircraft full scale development program is the measurement of pressures at the engine inlet. These measurements serve two purposes. One is to determine inlet duct recovery, and the other to measure pressure distortions produced by the inlet duct. This demands low measuring errors over a typical frequency range of 0 - 200 Hz. The temperature environment is the range of total temperature experienced by the aircraft. The frequency response requires that a transducer be installed in the duct at the engine inlet. The transducers must be small to minimize interference with airflow. The wide temperature extremes to which the transducers are subjected cause an unacceptable zero shift. Past practice was to use remotely located transducers in a temperature controlled box to measure low frequency pressure. The higher frequency component was measured by a transducer in the duct. A small temperature controlled transducer has been developed to measure the full range of frequency and pressure. The design goal is for error not to exceed 0.05 psia or 0.5% of reading, whichever is greater, for a 50 psia transducer subjected to an environment of −65°F to +400°F.

The design of the heated probe began with a study of past MCAIR inlet surveys and the establishment of the following guidelines:

- The width of the cantilever rake used in the F-18 was 0.40 inches. It is assumed that dynamic considerations of this supporting structure will be the same on future development aircraft.
- The inlet transducer face must be dished to accept air at various angles-of-attack.
- Accuracy Requirements: Static - 0.05 psia or 0.5% of reading, whichever is greater.
  Dynamic - Flat thru 200 Hz
- The temperature control band is to be as narrow as possible.
- Operation of the heater and controller from unregulated aircraft 28 VDC.

Fig. 1 describes the configuration of the probe used in earlier flight test inlet surveys.

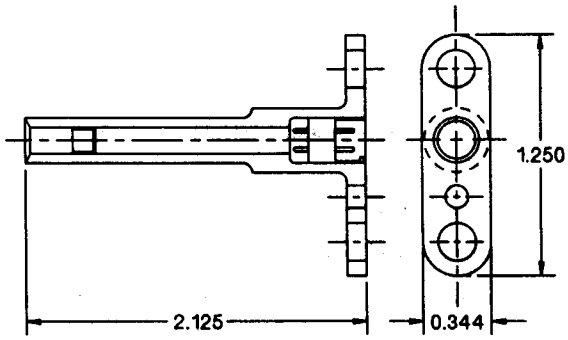

Fig. 1 Dynamic Rake Probe Previously Used for Inlet Surveys

Kulite semiconductor products was contacted and agreed to work with MCAIR on the project. A review of the specifications led to the recommendation of a XCE-093 high temperature pressure sensor. It was then decided to insert the sensor into a 0.125 inch diameter tube. The tube would float inside the housing between two isolators. A feasibility thermal analysis was performed.

Regardless of the velocity of a fluid past the probe, the lowest temperature the outside surface of the probe can attain is that of the fluid. If the transducer case is maintained at −65° and the heated tube at +400°, the areas of the surfaces can be approximated and heat loss calculated for conduction and radiation as shown in Fig. 2.

A prototype probe was designed and constructed. The configuration of this unit is shown in Fig. 3. The heater core on the first unit started with an aluminum rod. A 60° × 0.005 deep double helical groove was cut on the outside of the rod. The rod was then anodized, cut to length, and drilled from both ends, 0.093 × 0.60 deep from one end, and 0.063 thru from the other. Bare resistance wire and bi-filar wound in the groove. Isolators were machined from teflon rod and installed on the ends of the tube.

Kulite was sent the information on the heater for comment. Their recommendation was to replace the anodized aluminum heater tube with "Kovar", a cobalt-nickel-iron alloy which has a thermal coefficient of expansion matched to silicon semiconductor material.

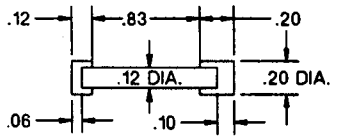

Sizing

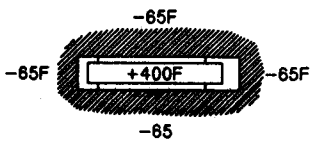

Boundary Conditions

Conduction thru the Isolators

$$\frac{1.5\ \text{Btu/in.}}{\text{hr ft}^2\ ^\circ\text{F}} \times \frac{1.3\times10^{-3}\ \text{ft}^2}{0.07\ \text{in.}} \times 480^\circ\text{F} \times \frac{0.2931\ \text{W/hr}}{\text{Btu}} = 3.79\ \text{W}$$

Conduction thru Air

$$\frac{0.0225\ \text{Btu/ft}}{\text{hr ft}^2\ ^\circ\text{F}} \times \frac{1.7\times10^{-3}\ \text{ft}^2}{1.6\times10^{-3}\ \text{ft}} \times 480^\circ\text{F} \times \frac{0.2931\ \text{W/hr}}{\text{Btu}} = 3.12\ \text{W}$$

Radiation
Assuming Ideal Conditions

$$\frac{0.1713\times10^{-8}\ \text{Btu}}{\text{hr ft}^2\ ^\circ\text{R}^4} \times 1.7\times10^{-3}\ \text{ft}^2 \times 7.164\times10^{8\,^\circ\text{R}^4} \times \frac{0.2931\ \text{W/hr}}{\text{Btu}} = 0.62\ \text{W}$$

The Sum
3.79 W + 3.12 W + 0.62 W = 7.53 W

GP71-0319-2

Fig. 2 Initial Analysis

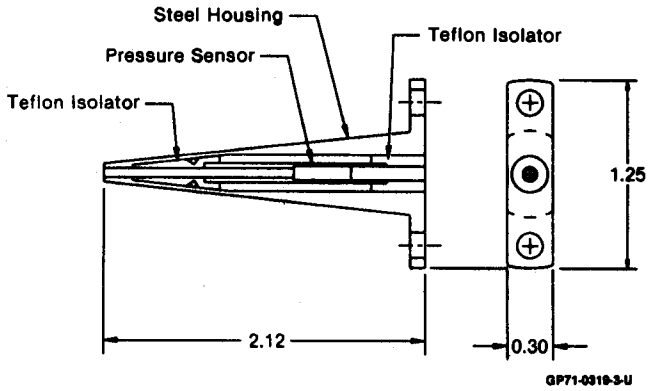

GP71-0319-3-U

Fig. 3 Prototype Probe Assembly

To achieve the same rates of heat transfer as the original unit, metal to metal contact between the heating element and the tube was required. A 0.125 diameter × 8.0 inch long Kovar rod was grit blasted, and 1 mill of ion vapor deposited aluminum was applied. The aluminum was then densified by shot-blasting. The process was repeated to insure a thick, uniform coating. The tube was anodized, cut to length and drilled. The heater core was now electrically non-conductive but retained essentially the same thermal characteristics as the anodized aluminum unit.

The tube was bi-filar wound with resistance wire. Terminations were made to the lead wires by silver brazing 28 AWG stranded copper wire into a brass tube with the resistance wire. The isolators were installed on the ends of the tube. The resistance wire and terminations were then coated with Sauereisen electrical resistor cement. The cement was oven cured. The assembly was installed into the housing. A thermocouple replaced the pressure transducer.

After a 1/2 hour cold soak at −65°F, a power supply was used to slowly energize the heater. Stabilization of the thermocouple at 400°F was achieved using 7.2 watts. The power supply was shut down and the unit was allowed to return to −65°F. When 7.2 watts was applied, a temperature of 400°F was achieved in 137 seconds. Steady state power readings were taken as the chamber temperature was varied from −65 to +400°F, while the thermocouple was maintained at 400°F. Readings are recorded in Fig. 4.

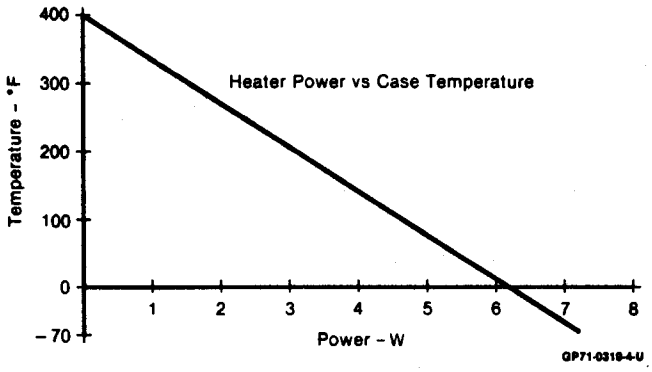

GP71-0319-4-U

Fig. 4 Prototype Probe Performance

The unit was brought to Kulite for transducer installation. The transducer assembly was installed into the heater tube using high temperature epoxy. RTV was used to backfill the cavity for wire strain relief and pressure tightness.

A Doric DC7000 digital temperature controller was used for the next phase of the evaluation. This setup is described in Fig. 5. Temperature sensing of the bridge was accomplished by measuring the voltage between the span compensation resistor and the bridge. The output at this point was approximately 2.1 mV per °F. The actual resistance change at the bridge was 10% per 100°F. Pressure calibrations were run at 11 points between −66 and 396°F. 20 pressure points were taken at each temperature. The results of this test are

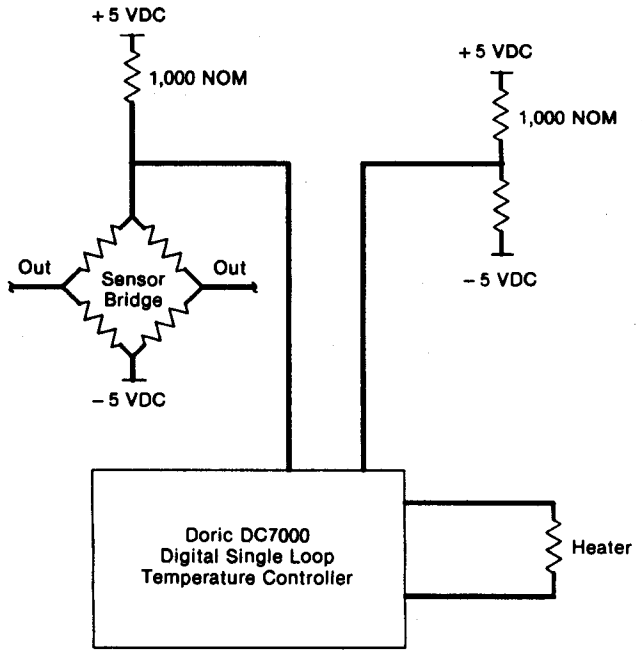

GP71-0319-5-U

Fig. 5 Prototype Controller

displayed in Figs. 6 thru 9. The degraded performance above 200°F was attributed to a 50 PPM resistor used for span compensation. This resistor was set in RTV, 0.25 inches back from the sensor. There is a 400 degree gradient between the sensor and the outer surface of the housing. This gradient and the temperature coefficient of this resistor would affect the control set point.

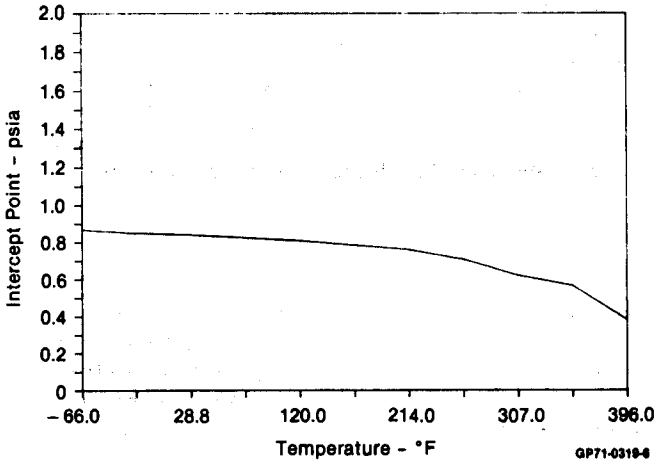

Fig. 6 Zero Shift

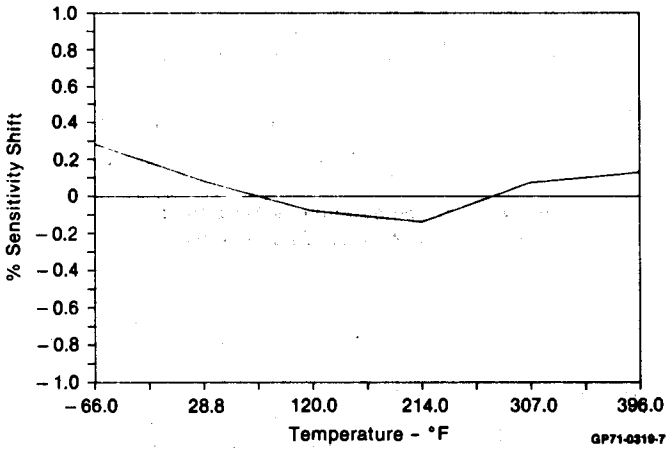

Fig. 7 Sensitivity Shift

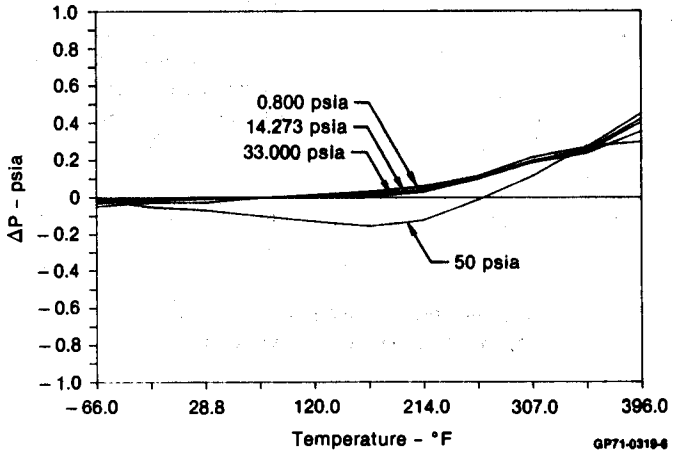

Fig. 8 Absolute Pressure Variation

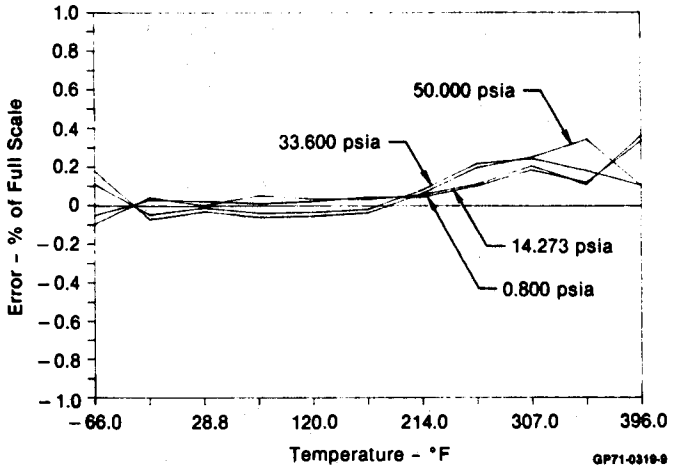

Fig. 9 Sensor Error

A frequency response test was run and compared to the predictions of a flight test dynamic pressure transmission line computer model. The results are displayed in Fig. 10. A linearity test was run between 140 and 160 dB at 1,000 Hz. The results of this test are displayed in Fig. 11.

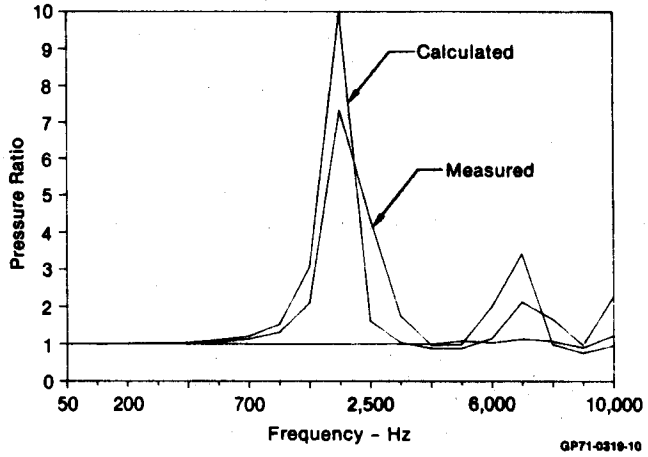

Fig. 10 Frequency Response

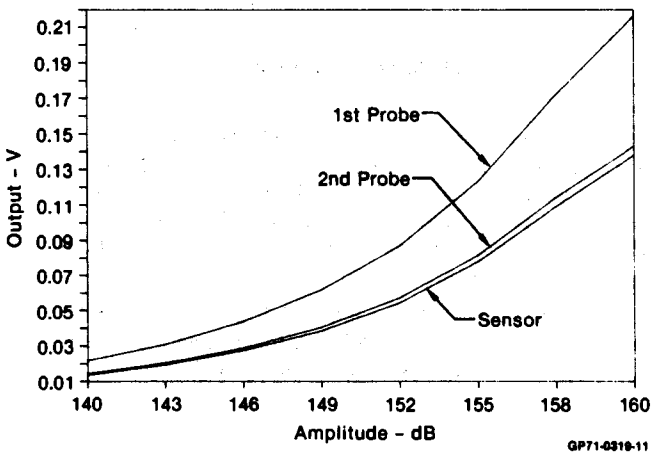

Fig. 11 Frequency Response
Linearity at 1 KHz

It was discovered after testing that the 18 0.006 diameter holes in the anti-impingment screen were drilled equally spaced on a 0.062 diameter circle. The tube leading to the transducer had a 0.062 diameter internal diameter. The holes were 50% blocked.

The results of various evaluations indicated the need for a redesign with emphasis directed at the following problems:

1. Manufacturing Difficulties
2. Temperature Control
3. Frequency Response
4. Incorporation of an Electrical Connector.

The redesigned probe is shown in Fig. 12. The body of the housing was enlarged at the face so that the sensor could be brought closer. (0.50 inches to sensor face vs 1.25) to improve frequency response. A chamfer was added for broader angle-of-attack pressure acceptance. The unit then lengthened to achieve a 1/5 length to width ratio. The 6 degree internal taper was replaced with a drill point. A pocket was added in the mounting face to accept a 9 pin high temperature plastic micro-D connector. The forward and aft teflon isolators were reduced in length to what was considered to be minimum mechanical, thermal and producibility requirements. This brought the transducer tube forward. The heater tube length was reduced by 40%, effectively reducing the thermal time constant of the system as well as improving the frequency response. The internal diameter of the tube leading to the sensor was increased from 0.062 to 0.072. The hand wound resistance wire heating element was replaced with an etched foil device. A temperature control thermistor was placed next to the diaphragm, and another on the face of the screen. This should provide a more accurate representation of the temperature than the previous unit. Also provided was the ability to actively monitor temperature during evaluation.

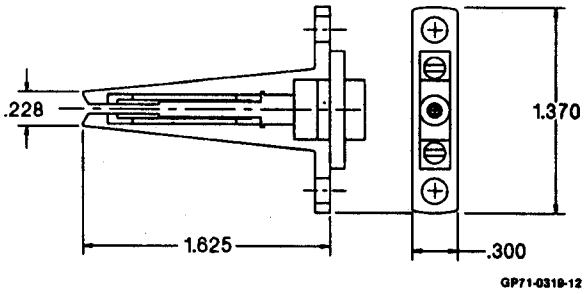

Fig. 12 Redesigned Probe

A finite element analysis was run on MCAIR's Heatran Thermal Analysis Program. Static and dynamic analysis were run. The computer verified the simplified static model, and provided a dynamic model to estimate transient conditions which would be encountered during various flight conditions. The results are displayed in Figs. 13 - 17.

Four units were built. Three contained 50 psia sensors and were designed to operate at 400°F. A fourth unit contained a 30 psia sensor and was designed to operate at 170°F.

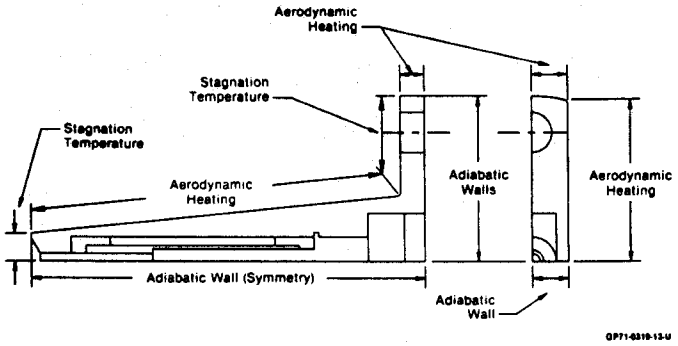

Fig. 13 Boundary Conditions Imposed on the Model

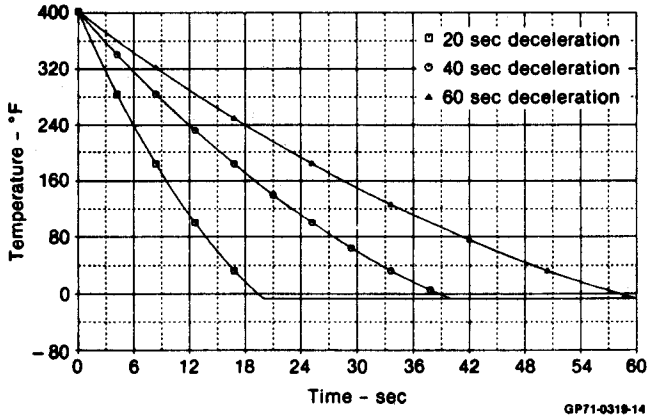

Fig. 14 Total Temperature vs Time for a Mach 2.46 to Mach 0.9 Deceleration

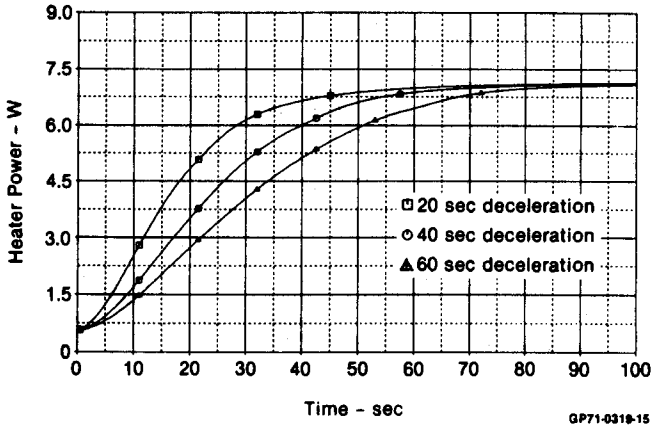

Fig. 15 Heater Power vs Time for a Mach 2.46 to Mach 0.9 Deceleration

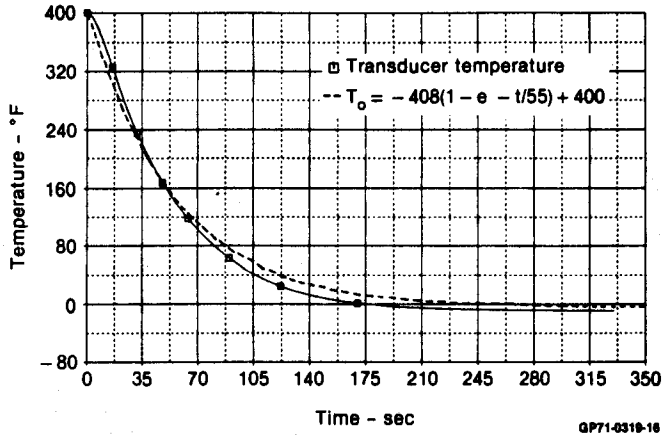

Fig. 16 Transducer Temperature vs Time for a 408 Degree Fahrenheit Temperature Drop

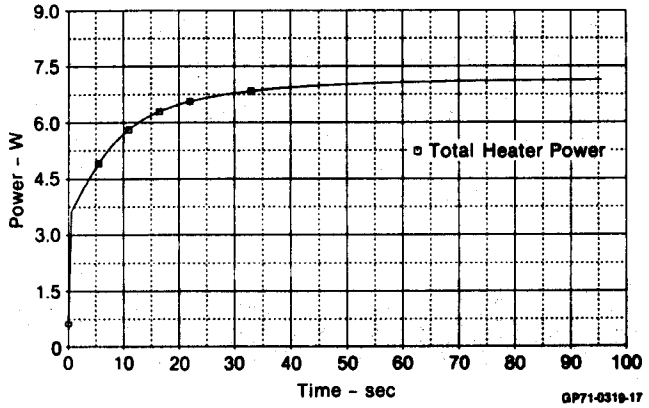

Fig. 17 Required Heater Power vs Time for a 408 Degree Fahrenheit Temperature Drop

The Doric controller could not respond to transients. A new controller, shown in Fig. 18, would be required for a wind tunnel evaluation. An error signal is obtained from a thermistor bridge. This signal is amplified and "lead" compensated to stabilize the control loop. The error signal is then sensed by a comparitor which drives a power transistor which controls the heater. The controller operates in a pulsed mode rather than a true proportional mode to minimize power dissipation in the controller.

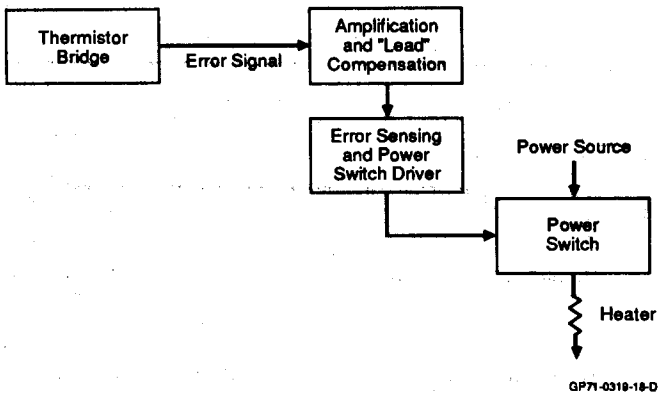

Fig. 18 Temperature Controller Block Diagram

Problems in the application of the new design started with the flexible heater. High temperature strain gauge techniques were used to attach the heater to the core. When the heater approached 400°, the adhesive softened and the heater sprung from the core. Fiberglass yarn was tied around the heater and wetted with adhesive. This prevented the heater from unwinding, and also provided a strain relief for the lead terminations. The diameter of the housing cavity had to be increased to allow this now secure heater assembly to fully enter the housing.

The controller used a 200K nominal thermistor. The control resistance was 1K nominal. An open in the thermistor wiring when the unit is in a high temperature ambient environment can char the sensor in about 5 seconds. The first unit tested failed because of this mechanism. The low temperature unit overheated, less severly, but enough to sever the thermistor wires, rendering it inoperable. A third unit burned up when the controller never switched off. A fourth unit made it thru all testing unaffected. The evaluation of this unit is described in Figs. 19 - 22. The zero shift was reduced to about 0.10 psi over the test temperature range. A 5-1 improvement over the first unit, but not quite good enough. Resistance readings of the bridge indicated a temperature variance of 5° from the set point over the test range.

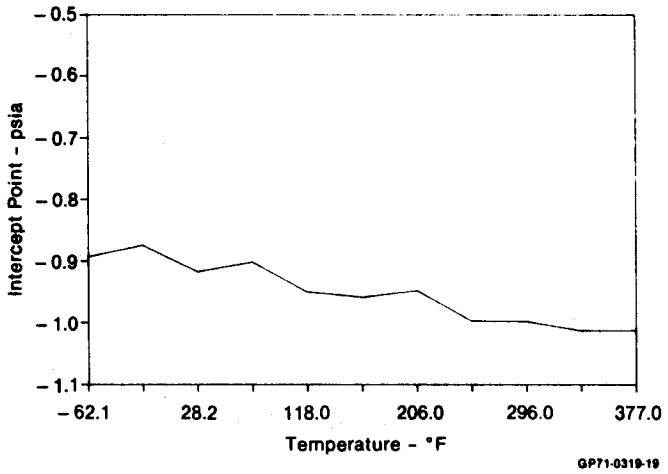

Fig. 19 Zero Shift

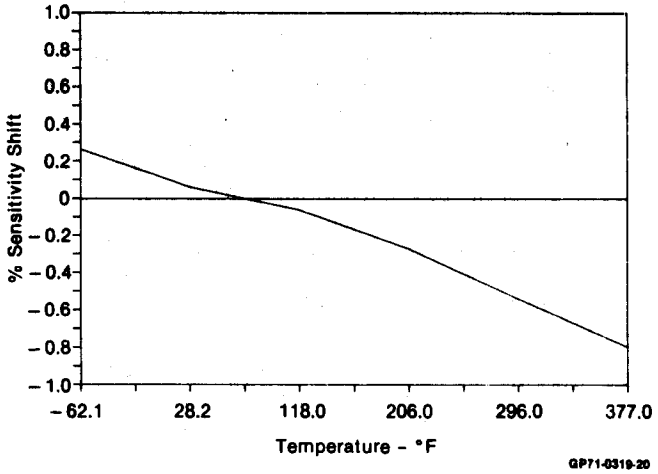

Fig. 20 Sensitivity Shift

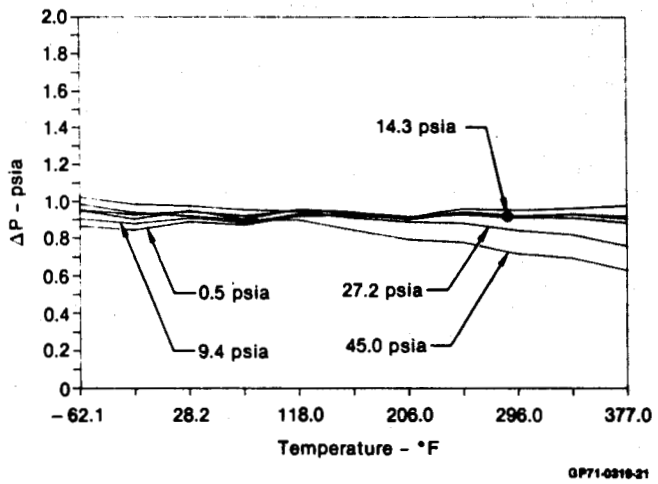

Fig. 21 Absolute Pressure Variation

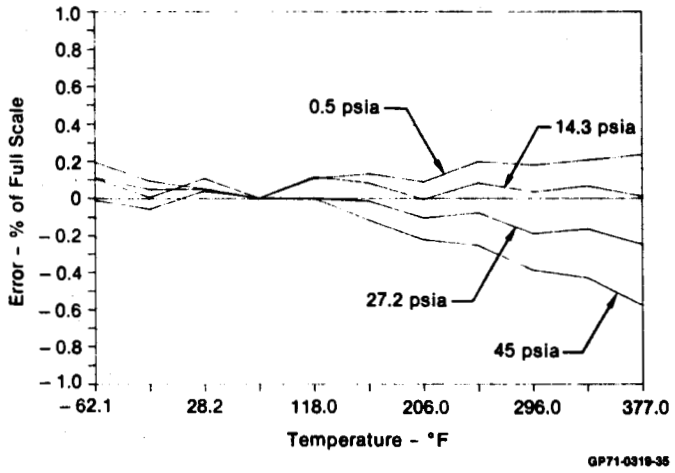

Fig. 22 Sensor Error

The scatter of the data points led to an evaluation of the test procedures and equipment used. It was discovered that an appreciable time constant was present in these units. Readings taken going up in pressure were lower than those taken while coming down. The automated calibration system at MCAIR takes pressure readings from the test article about 2 seconds after stabilization. The transducer would respond to 99.9 percent within a second or so, then 60 to 180 seconds would be required for the unit to return within 0.005 psia. The units were returned to Kulite for evaluation. It was discovered that protective coatings on the diagram were the culprit. The coatings were removed, and a return to an atmospheric value within 0.005 psia within 12 seconds of 35 psia step change resulted.

Frequency response tests were run. Results were acceptable from a frequency response view. Actual test results were significantly different from computer predictions. See Figs. 11 and 23.

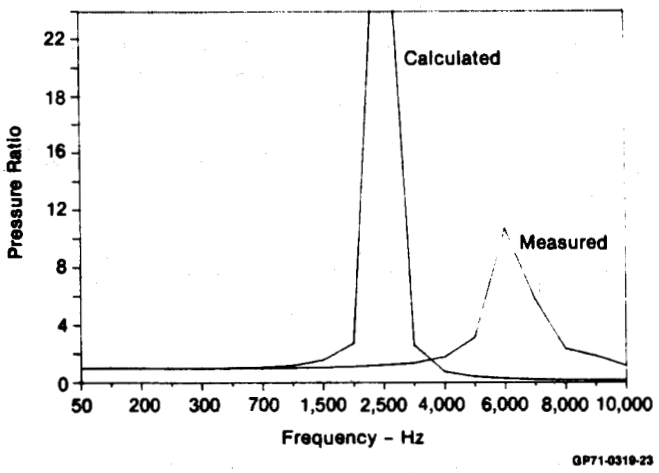

Fig. 23 Frequency Response

A wind tunnel test was run. Fig. 24 shows the startup of the first test. The duty cycle of the heater goes from about 20% before the test to about 50% at Mach 0.45 and 30 psia. Fig. 25 shows the thermistor output over this same period. Fig. 26 shows the heater duty cycle at Mach 0.85 and 40 psia. A spectrum analyzer was placed on the output during wind tunnel testing. A peak of around +30 dB was seen at about 5.0 KHz.

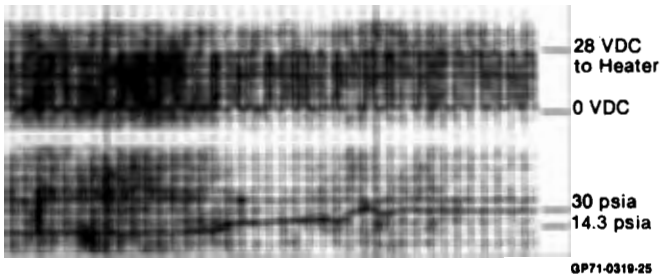

Fig. 24 Heater Power vs Tunnel Pressure on Startup
Mach 0.5

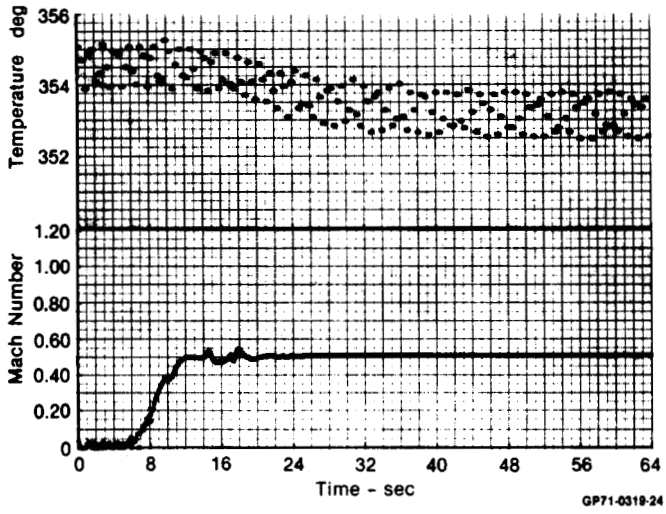

Fig. 25 Mach No. and Probe Temperature vs Test Time

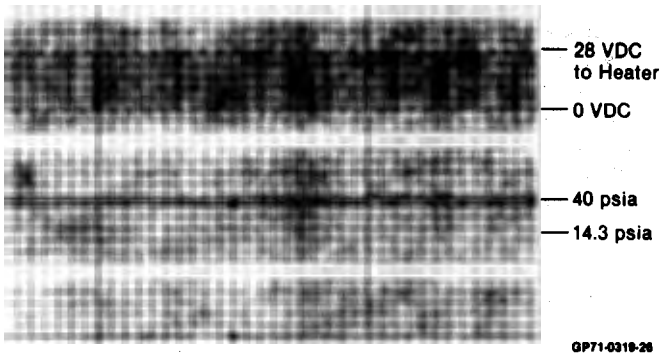

Fig. 26 Heater Power vs Tunnel Pressure
Mach 0.85

The evidence of hysteresis levels and the general problem of inaccuracies at low pressures led to the investigation of using a differential transducer. This design is shown schematically in Fig. 27. The following guidelines were established for the implementation of this design:

- The reference pickup diameter must maintain the reference chamber within 1.5 psia of duct pressure during aircraft accelerations and decelerations. Response to engine surges is not required.
- The cross section of the reference chamber must be adequate to maintain equal pressure to all the transducers.
- The frequency response of the differential and reference transducers is to be greater than the frequency components in the reference chamber.

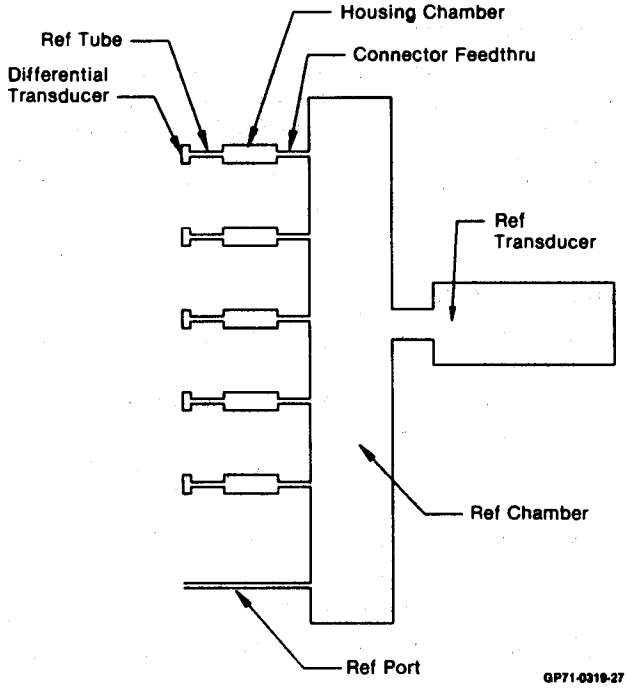

Fig. 27 Differential Inlet Pressure System

The differential system was modeled using low-pass filter characteristics. This model is shown in Fig. 28. It was decided that the above conditions could be met. No testing or other confirmation of this model is available.

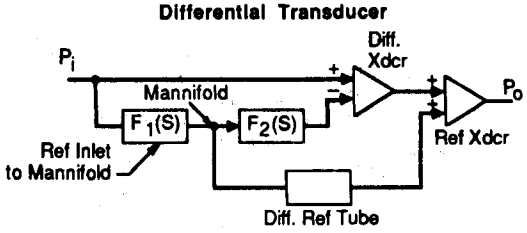

$$P_o = P_i - P_iF_1(s)F_2(s) + P_iF_1(s)$$
$$P_o = P_i[1 - F_1(s)F_2(s) + F_1(s)]$$
$$P_o/P_i = 1 - F_1(s)F_2(s) + F_1(s)$$

Assume Low Pass Characteristics for $F_1(s)$ and $F_2(s)$

$$F_1(w) = 1/1 + j\ w/w_1 \quad F_2(w) = 1/1 + j\ w/w_2$$
$$P_o/P_i = 1 + F_1(w)[1 - F_2(w)]$$
$$= 1 + \frac{1}{1 + j\ w/w_1}\{1 - \frac{1}{1 + j\ w/w_2}\}$$
$$= 1 + \frac{1}{1 + j\ w/w_1}[\frac{j\ w/w_2}{1 + j\ w/w_2}]$$
$$= 1 + \frac{j\ w/w_2}{(1 + j\ w/w_1)(1 + j\ w/w_2)}$$
$$= \frac{(1 + j\ w/w_1)(1 + j\ w/w_2) + j\ w/w_2}{(1 + j\ w/w_1)(1 + j\ w/w_2)}$$
$$= \frac{1 + j\ w/w_2 + j\ w/w_1 - w^2/w_1w_2 + j\ w/w_2}{1 + j\ w/w_2 + j\ w/w_1 - w^2/w_1w_2}$$
$$= \frac{(1 - w^2/w_1w_2) + j(w/w_1 + 2w/w_2)}{(1 - w^2/w_1w_2) + j(w/w_1 + w/w_2)}$$
$$= \frac{(1 - w^2/w_1w_2) + jw(w_2 + 2w_1)/w_1w_2}{1 - w^2/w_1w_2 + jw(w_1 + w_2)/w_1w_2}$$

Let $w_2 = Kw_1$

$$= \frac{(1 - w^2/Kw_1^2) + jw(K + 2)/Kw_1}{(1 - w^2/Kw_1^2) + jw(K + 1)/Kw_1}$$
$$= \frac{[(K - w^2/w_1^2) + j\ w/w_1(K + 2)]}{[(K - w^2/w_1^2) + j\ w/w_1(K + 1)]}$$

Let $w/w_1 = R$

$$= \frac{(K - R^2) + jR(K + 2)}{(K - R^2) + jR(K + 1)}$$

Taking Magnitude

$$M = \{\frac{(K - R^2)^2 + (R(K + 2))^2}{(K - R^2)^2 + (R(K + 1))^2}\}^{1/2}$$

GP71-0319-28

Fig. 28 Low Pass Filter Model

The next generation of the inlet probe is now in work. Heaters will use resistance wire coated with polimide insulation, wrapped around the core, and coated with high temperature epoxy. Connectors with pressure reference ports have been received. The controller was modified. This is shown in Fig. 29. The controller now provides a constant voltage to the bridge. The error signal used to control the heater is developed by sensing the current supplied to the bridge. The first prototype transducer was used for a controller evaluation. The results are displayed in Figs. 30 and 31. The accuracy requirements can now be met on any given day. Day to day repeatability errors, however, exceeded the specifications. An evaluation was run on a daily basis. The heater was left on for 8 hours. Calibrations were run in the morning and in the afternoon. A repeatability of about 0.025 psia was realized after 8 days. Indications are that a cyclic temperature burn-in may reduce this error. In use day-to-day zero shifts can be tolerated by initialization of data to pressure values obtained from ambient readings taken from a ground based pressure measurement system.

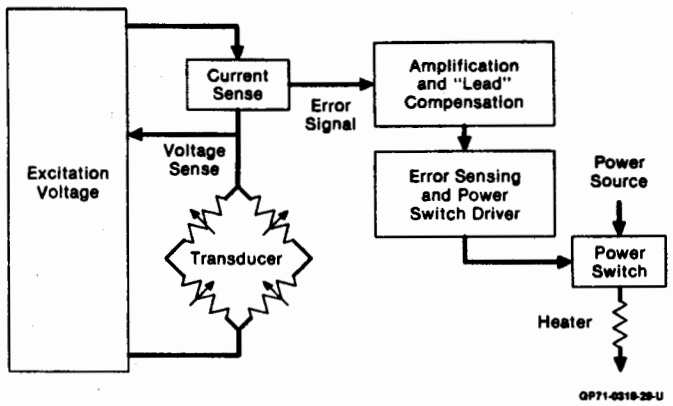

Fig. 29 Improved Temperature Controller Block Diagram

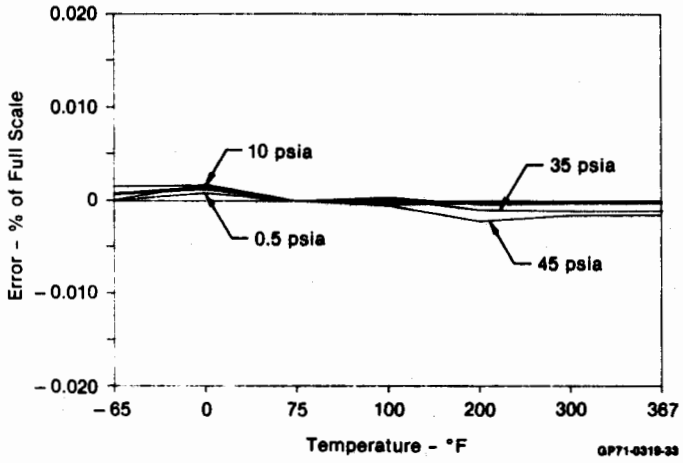

Fig. 30 Transducer Error

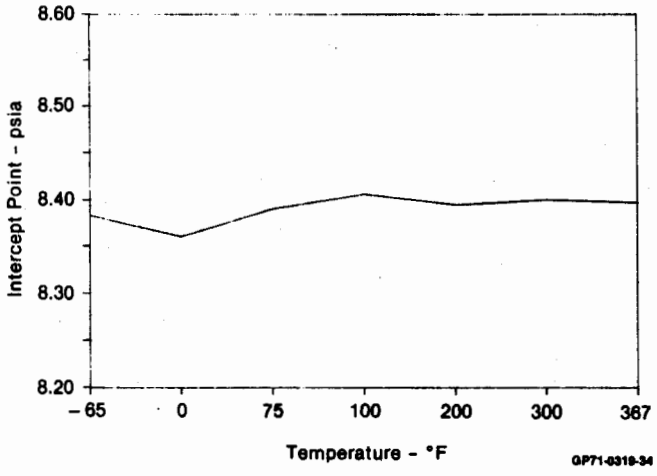

Fig. 31 Zero Shift

Controller cycling stopped around 360°F. This is an indication that temperature control was lost. The set point was determined by measuring bridge resistance with the unit in a chamber at 400°F. No power was applied to the bridge during this calibration. Self-heating of the bridge was determined to be responsible. Set points of follow-on units will be 50°F above the desired ambient temperature.

CONCLUSIONS:

It is possible to install a miniature pressure sensor in a housing and provide temperature control in as hostile an environment as the inlet duct of a high performance aircraft. Greatly improved performance of the pressure transducer is the result. This can be accomplished without compromising any features of probes now used for dynamic pressure measurement.

The time constant and hysteresis levels present in this type of silicon transducer increase as diaphragm deflection increases. As attempts are made to recover pressures of 50 psia in 0.01 increments and beyond, these errors become significant. The greatest accuracies would be realized if a differential duct rake could be produced with the same confidence levels as an absolute unit. Improved computer modeling and dynamic testing will be required for the development of such a device.

Kulite is confident that transducers can be provided to meet the needs of this device if a definitive test procedure can be established to assure that transducers selected will perform as required.

ACKNOWLEDGMENTS

The authors gratefully acknowledge the leadership of Robert Eagleton, the technical skill of Robert Grant, the steady hands of Scott Goodman, Bret Boman and Larry Haas for the thermal analysis, Ken Stark for the countless calibration runs, and James Clark and the MCAIR wind tunnel group for their contributions to this effort.

BIBLIOGRAPHY

(1) MCAIR 72-043, System for Evaluation of Inlet Dynamic Distortion.

(2) Air 1419, Inlet Total Pressure Distortion Guidelines for Gas Turbine Engines.

(3) AIAA-81-1393, F/A-18A Inlet/Engine Compatibility Flight Test Results.

(4) Marks Mechanical Engineers Handbook, Ed. 6.

(5) On the Dynamics of Pneumatic Transmission Lines Transactions of the ASME, May 1957.

Q: Charles R. Belensky (Grumman): Did you use the same technique for the severe scaled-down wind tunnel?

A: Edward Kachman: That was run in the wind tunnel. The probe was run in the wind tunnel. If you mean the scaled down version of the same thing using the same temperature control techniques; no we haven't. If you could get a heater small enough, it wouldn't be a problem.

Q: Charles R. Belensky: That's why I am curious because we have the same problems when we do wind tunnel studies except we are using the same type of rake and kulite pressure transducers. You have the same temperature problems, so I'm interested in your technique. Could it possibly be used on a small scale?

A: Edward Kachman: The hole in the housing is 0.2 of an inch in diameter and that contains the heater, the probe and everything else quite well. You need at least 0.005 on a wall I imagine.

A: Charles R. Belensky: That's right.

COMMENT: Edward Kachman: So you need about 205.

Q: Harvey Weiss (Grumman): I assume, just from the photo, that the Stathams were closely coupled to the actual ports on the rake giving them, I'm guessing, a flat response to perhaps 7-10 Hz. That may or may not be the case, but that's a guess on my part. And given the fact that the temperature response, as illustrated, was something like 10-20^{0} per second (I believe that was the number): couldn't a reasonable high-pass filter essentially cutting off the DC response at 3 or 4 Hz do enough to get rid of the apparent 0 shift because of the temperature just leaving a little bit of a hole in the merged data? The question: Is it really worth the trouble to make the kulite data so accurate? How much does it weigh into the overall distortion or the end product of what you are trying to come up with, the distortion coefficient, in the recovery, averaging over some 48 pressure transducers? Do you feel that it is worthwhile to proceed to try to get such a high accuracy in this kind of environment using this type of stuff?

A: Edward Kachman: It has been seen to be worthwhile just to get rid of the plumbing to the Stathams. It really isn't that difficult to do.

Q: Harvey Weiss: So, the aim then is to really have a single transducer system. In other words, to have a system that, essentially, we can get down to roughly DC by accounting for the ...in other words, get rid of the Stathams. Is that the aim?

A: Edward Kachman: Well, we have nothing personal against Statham.

COMMENT: Harvey Weiss: I mean the low frequency transducer end of it. That's the point, I assume.

A: Edward Kachman: One of the points of what we are doing is cost. For a flight test program, if you have to buy 96 transducers instead of 48 plus all the plumbing and wiring, you can eliminate that by just running wires and comming up with the same accuracy that you had before, you will do much better.

Q: Harvey Weiss: One more question. How are you measuring this frequency response pneumatically? It sounded like you were talking about 2500 Hz. What technique were you using to get 2500 Hz worth of pressure?

A: Edward Kachman: That was done between 140 and 160 dB and we have an acoustic driver in a tuned chamber.

Q: Harvey Weiss: Okay, so its very, very low level we're talking about?

A: Edward Kachman: Yes.

Q: Gordon E. Mills: What is the total pressure at that ram inlet?

A: Edward Kachman: The total pressure can vary from 1 or 2 to 50 psi, so this covers the full range of pressure.

BALLISTICS PRESSURE TRANSDUCERS AND THEIR APPLICATION

John M. Kubler and Urs Roesli
Kistler Instrument Corporation
Amherst NY 14120

For more than 20 years, piezoelectric transducers have been used to measure internal ballistics pressure. Although copper crusher cylinders are still used, today's refined measuring technique allows not only the indication of peak pressure, but also the measurement of the complete pressure curve, which is increasingly used for the acceptance testing of ammunition.

Pressure transducers designed for ballistics measurements are capable of withstanding the rough environment typical of ammunition testing such as:

- High pressures which translate to high stresses for the transducer
- Extreme high temperature during the firing
- Corrosion and erosion through aggressive powder gases

Depending upon the ammunition used and the installation, the specific load to which the transducer is exposed may vary greatly. Kistler has developed special transducers capable of sustaining these high requirements.

Following are a few of the problems and their solutions. Additional technical details can be found in our Data Sheets and in the Technical Note 55.201.

THE PRESSURE TRANSDUCERS AND THEIR ENVIRONMENTS

REDUCED MOUNTING SENSITIVITY WITH THE ANTI-STRAIN DESIGN

The pressure not only acts upon the diaphragm, but also on the surrounding areas of the transducer. These pressure induced stresses can cause deformation of the mounting bore which in turn can change the mounting preload.

A transducer which produces an output due to the mounting preload is said to be mounting sensitive. During actual firings, the signal is superimposed on the actual pressure signal and causes inaccuracies.

The tightening forces alone can produce a strain equivalent to 150 bar (3% of FS). Depending upon the mounting configuration, the stresses induced into the sealing area may be even higher. Tests have shown errors of up to 7 percent are possible.

After many years of development, shoulder and front sealing type transducers are now available which exhibit very low mounting sensitivity. This patented, antistrain design which effectively isolates the sensing element from the mounting thread and the sealing area, reduces the torque and mounting stress induced output to less than 35 bar or approximately 0.7 percent of full scale.

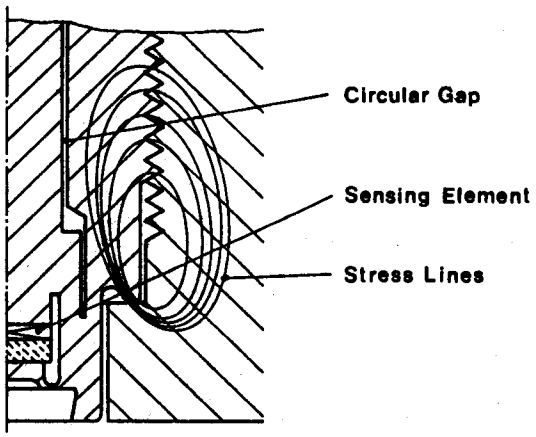

Figure 1: Transducer with shoulder seal (recessed sealing surface and anti-strain design)

Figure 1 shows how the sensing element is isolated through a circular gap from the mounting strains. Changes in stresses due to the deformation of the surrounding areas are not transmitted to the element.

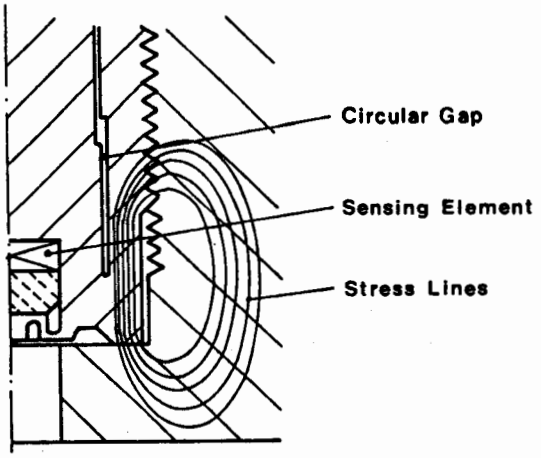

Figure 2: Transducer with front seal and anti-strain design

Similar to the shoulder sealing transducer, the front sealing sensing element is also de-coupled from the housing so that the mounting stresses have no effect.

SEALING

There are several methods used to seal high pressure transducers. The conventional, still widely used flat steel or copper washers, Figure 3, require accurately machined mounting bores and high tightening torques of up to 35Nm (25 lbf ft). The sealing force must be high and the outer diameter of the seal ring must be contained inside the mounting bore to assure a reliable seal.

The patented Kistler seal is a small metal ring which is placed in the specially formed transducer sealing area and works in principal similar to an O-ring, see Figure 4. It offers several advantages:

- The seal ring is made out of a soft, corrosion resistant Cr-Ni alloy
- The seal is self-sealing with the gas pressure, acting similar to an O-ring
- The sealing is assured with a relatively low tightening torque of 10Nm (7.5 lbf ft)
- There are no special requirements for the hardness of the sealing surface
- The seal is easily replaced.

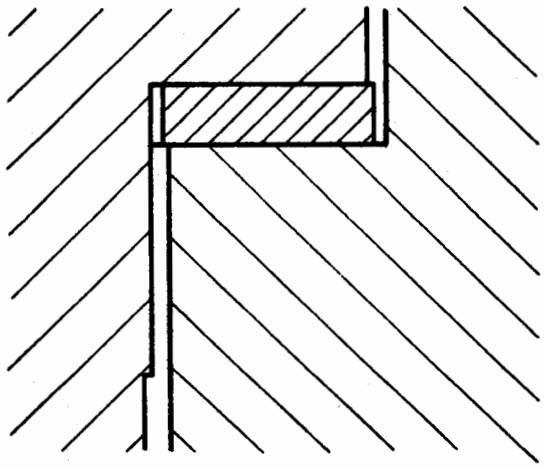

Figure 3: Conventional flat washer seal

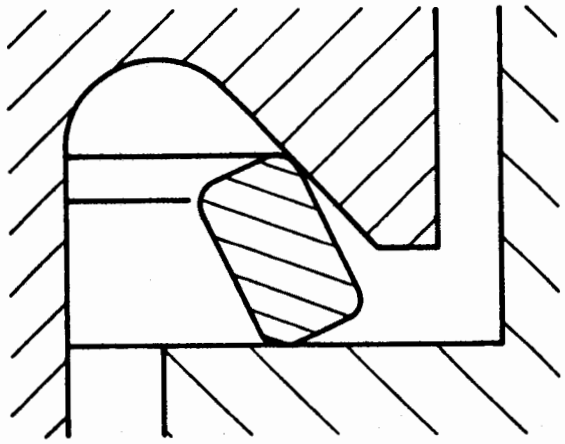

Figure 4: Seal ring prior to the deformation

During the tightening of the transducer, the seal ring is deformed and the upper and the lower sealing edges are formed to the counter surfaces, see Figure 5.

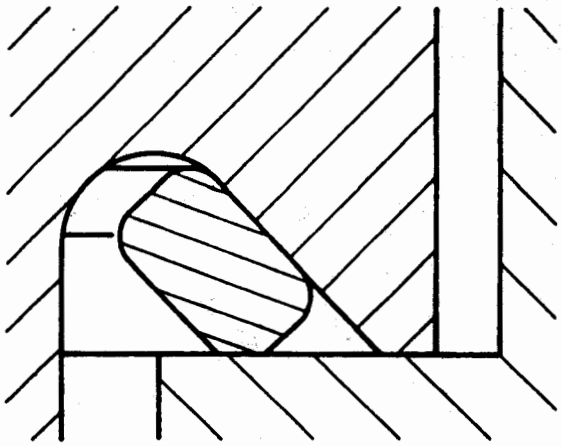

Figure 5: Seal ring after tightening of the transducer

Because of the defined contact area between the transducer and the sealing surface, the relatively low tightening torque of 10Nm, (7.5 lbf ft) the sealing surface does not sustain any damage.

PREVENTION OF THE QUARTZ CRYSTAL TWINNING

When the conventional quartz crystals in pressure transducers are subjected to high mechanical stresses, the so called twinning of the Dauphiné, see Reference 1), type can occur. A twinned quartz crystal usually will have a reduced sensitivity or in extreme cases it can even have a reversed charge polarity. The susceptibility for twinning increases with higher temperatures and higher pressures.

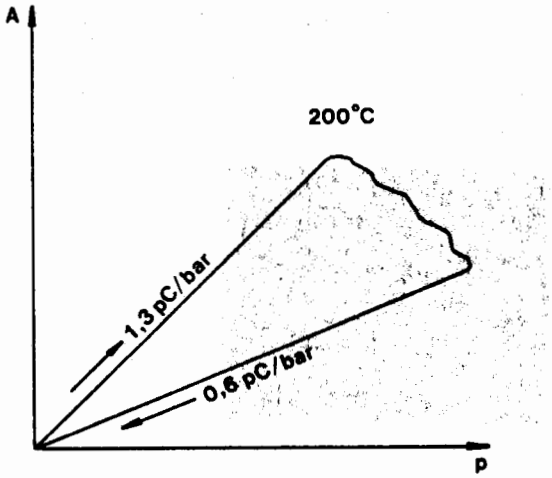

Figure 6 shows the effect of twinning during a load cycle at a temperature of 200°C. The reduction in sensitivity is not completely reversible.

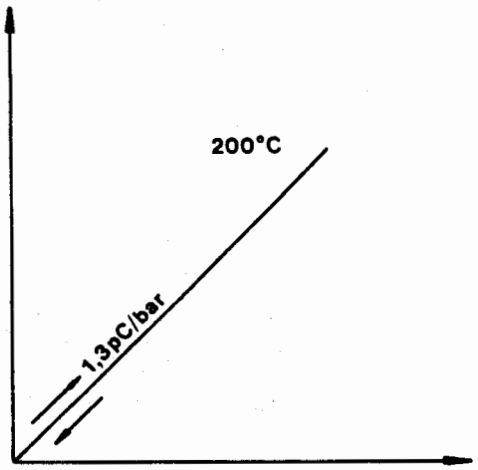

Figure 7:

Kistler is the only manufacturer of ballistics pressure transducers with crystal research and manufacturing facilities capable of manufacturing the quartz from the raw material to the finished element. Through patented, special quartz cuts, the problem of twinning has been practically eliminated, see Reference 2). Transducer elements with these specially cut and treated quartz cyrstals can sustain the combined extremes of temperature and pressure.

THERMAL PROTECTION

The brief thermal shocks occuring during the burning of the gun powder heats the diaphragm of the transducer. As a result, the diaphragm is distorted, generating a force to the element which is then interpreted as an error (thermal shock, flame error).

The thin sheet metal diaphragms used on the model 6201, 6203 and 6211 have a small flame error, but at the cost of life and stability. On the other hand, the machined diaphragm of the new transducers model 6205, 6207, 6213, 6215 and 6217 are more durable and have a better stability. Through the patented design, the flame error is much smaller than comparable conventionally designed machined diaphragms.

Many Kistler ballistics pressure transducers can be fitted with a special thermal protector. They practically eliminate the already small error, see Figure 8, and at the same time protect the diaphragm against erosion.

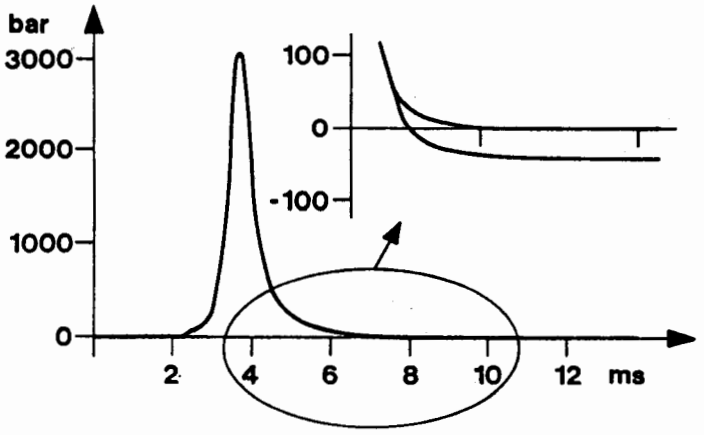

Figure 8:

THE EFFECT OF A LONG PRESSURE PASSAGE

Some installations require that the diaphragm of the pressure transducer is recessed from the pressure cavity. If the passage is long, it will have the effect of a low pass filter. Low frequencies are measured without error. The higher frequencies (in the range of the passage resonance) are amplified resulting in signal amplitudes several times higher than the actual pressure. Frequencies above the passage resonance are highly attenuated or are not even indicated. A step like pressure increase results in a damped resonance.

Figure 9 shows the effect of the passage resonance to the measuring results when subjected to a short pressure pulse in a hydraulic system. If the passage is too long, a short pressure pulse cannot be accurately measured even when using a transducer which has a very high resonance frequency.

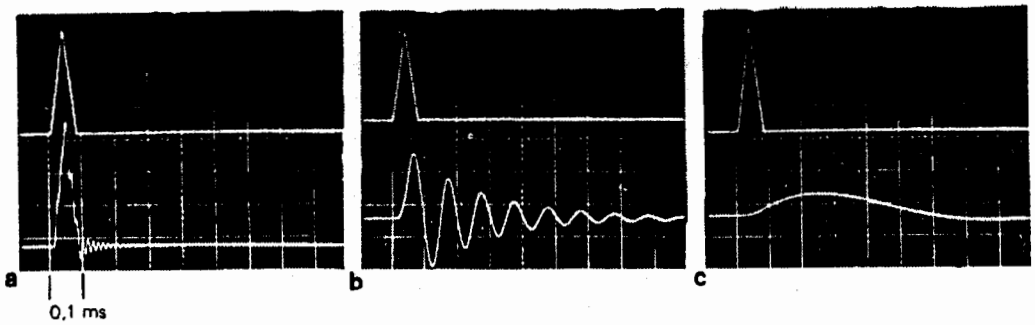

Figure 9: The effects of a long pressure passage

Pressure pulses in a hydraulic system (water) with a pulse width of 80 µs and various passage length:

a) passage length 3.5mm; res. freq. 100kHz
b) passage length 35mm; res. freq. 10kHz
c) passage length 350mm: res. freq. 1kHz

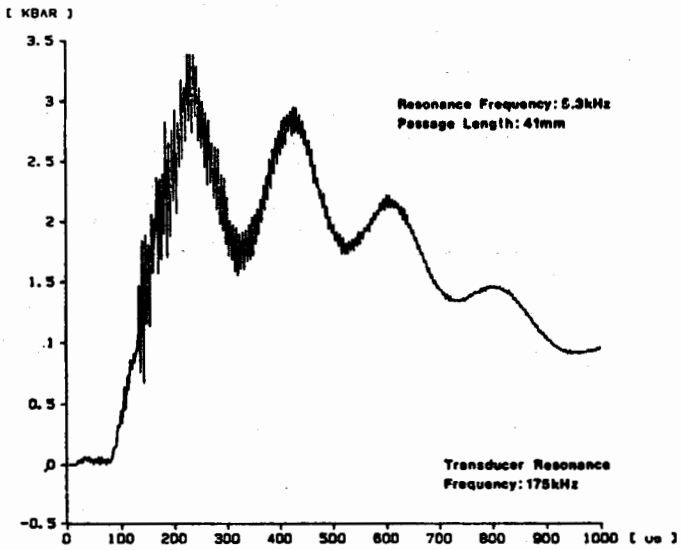

Figure 10: Pipe oscillation of a 35mm long gas passage, measured with a 6211 pressure transducer

The Kistler transducer program covers the complete ballisitcs applications:

SHOULDER SEALING TRANSDUCERS

With their recessed sealing surface, shoulder sealing transducers can be installed with the diaphragm flush to the test chamber. This eliminates the pressure passage which can resonate during fast pressure pulse measurements. The transducers model 6201B, 6203 and 6211 have been in use worldwide for over 15 years; the 6203 is approved by the NATO for the ammunition acceptance testing.

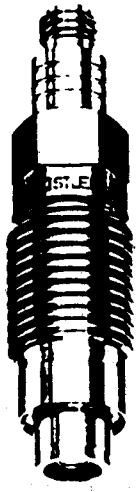

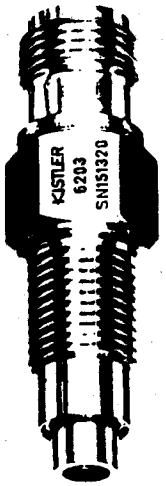

Figure 11: Shoulder sealing transducers

6201/03 Measuring Range 0 to 5000 bar, over range 5500 bar;
6211 Measuring Range 0 to 7500 bar, over range 8000 bar;
207C/607C (not shown) Measuring Range 0 to 5000 bar, over range 6000 bar

Shoulder sealing transducer characteristics for model 6201, 6203, 6211 and 207C/607C:

- For general ballistics pressure measurement from 1000 bar 7500 bar
- Over 10,000 units in use worldwide for 15 years
- Approved by the NATO (model 6203)
- Preformed sheet metal diaphragm with small thermal error (except 207C/607C)
- Easily replaceable thermal protector for further reduction of the thermal error, increase in life expectancy and protection against erosion (especially with aggressive powder)
- Relatively insensitive to contaminations and grease effects

The new transducers models 6205, 6206 and 6207 have a machined diaphragm with thermal shock compensation. Therefore, these transducers can be used without additional thermal protection. They are dimensionally interchangeable with the other shoulder sealing transducers.

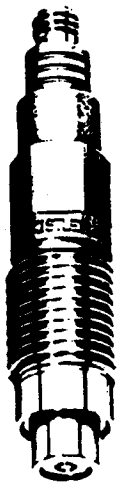

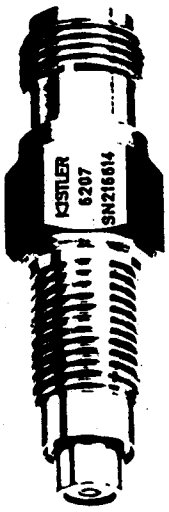

Figure 12: Shoulder sealing transducers 6205/6206/6207

Measuring range	0 to 5000 bar
Over range	6000 bar

Shoulder sealing transducer characteristics of the new model 6205, 6206 and 6207:

- For general ballistics pressure measurement from 50 to 5000 bar
- High sensitivity stability
- Very high resonance frequency
- Durable machined diaphragm with small thermal error
- Easily replaceable thermal protector for further reduction of the thermal error and protection against erosion (especially with aggressive powder)
- Small mounting sensitivity, insensitive to various installation conditions due to the anti-strain design

The transducers exhibit an excellent linearity and are also suitable for exact measurements in low pressure applications such as shot gun shells, pistol and revolver ammunitions. The anti-strain design eliminates the error due to varying tightening torques and conditions of installations. They have a very high resonance frequency and are therefore suitable for fast pressure pulse measurements.

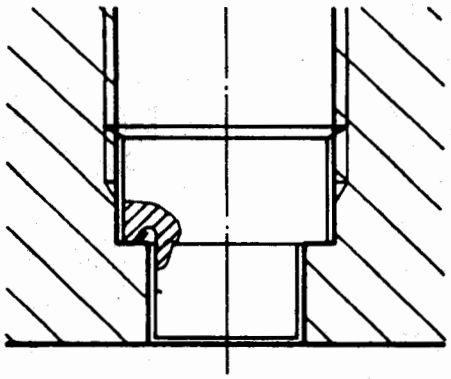

Figure 13: Flush mounted, shoulder sealing transducer with the anti-strain design

FRONT SEALING TRANSDUCERS

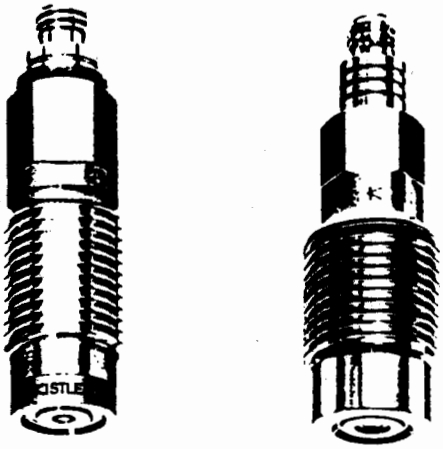

Figure 14: Front sealing transducers

6213 Measuring Range to 10000 bar, over range 11000 bar;
6215/6217 Measuring range 0 to 5000 bar, over range 6000;
217C/617C (not shown) Measuring range 0 to 5200 bar, over range 6000 bar

The front sealing transducers are especially suited for internal ballistic pressure measurements which require a pressure passage (e.g. cartridge mouth). Since there is no gap between the element and the mounting bore typical for shoulder sealing units, they are less sensitive to contamination or to the buildup of a grease layer.

For this same reason, front sealing transducers are especially well suited for closed bomb testing, where the use of grease to reduce short and long term thermal error is important.

Their excellent linearity makes them also equally well suited for low pressure measurements.

The front sealing transducers model 6213, 6215 and 6217 have the anti-strain element, and are therefore insensitive to changes in mounting torque and condition of installations. Thanks to the special diaphragm design with thermal shock compensation, they require no thermal protection and can be used for longer test periods without removal for cleaning.

Front sealing transducers characteristics model 6213, 6215/6217 and 217C/617C:

- For general pressure measurement in ballistics for pressures from 50 to 10,000 bar
- Usable for smaller caliber because of the small passage volume
- Especially suited for closed bomb testing due to the insensitivity to contamination and effect of grease
- High sensitivity stability
- Durable, machined diaphragm with small thermal error
- An additional thermal protector can be used for further reduction fo the flame error and protection against contamination and erosion (especially with aggresssive powders)
- Low mounting sensitivity and insensitive to various mounting configurations thanks to the anti-strain design
- Insensitive to contamination and grease shields

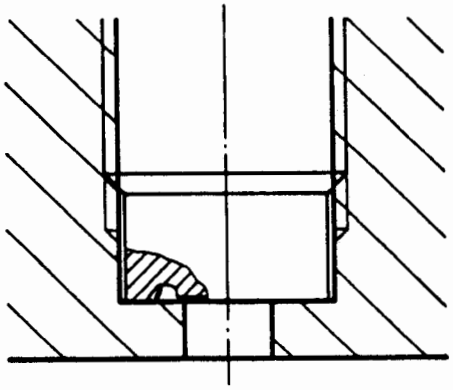

Figure 15: Front sealing anti-strain transducer, installed in mounting bore with passage

Optimal protection of the transducer against the hot gases can be accomplished, when using the thermal protector with the internal shield. See Figure 16, transducer model 6215 with thermal protection.

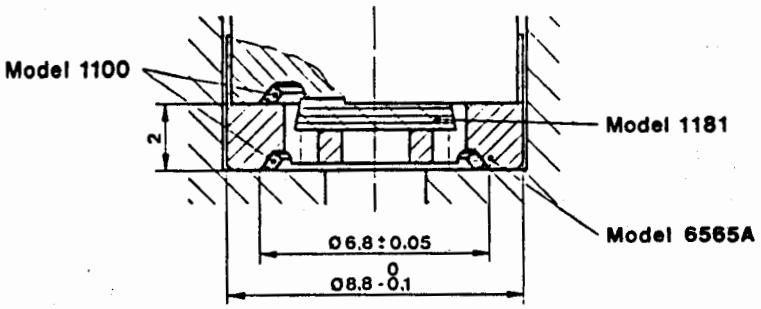

Figure 16: Front sealing transducer with heat protection shield

CONFORMAL PRESSURE TRANSDUCERS

A quartz transducer is in principal, a force transducer. The pressure is converted into a force through the effective surface area of the diaphragm. Because in ballistics measurements, the diaphragm is typically very highly stressed during the peak pressures, a diaphragm type transducer has a restricted life.

The conformal transducer has no diaphragm, its life expectancy is therefore practically unlimited. The force sensitive front section B is machined to conform to the shape of the cartridge A which acts as the diaphragm. The pressure inside the cartridge forces the case against the transducer. The protecting sleeve C isolates the sensing area of the transducer from the bore and mounting stresses (Figure 17).

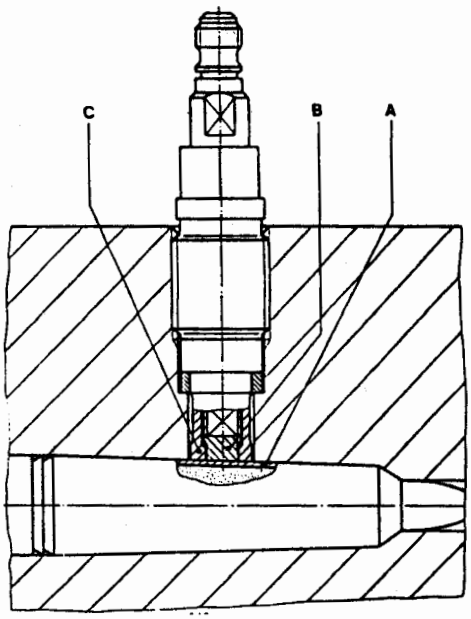

Figure 17: Conformal transducer installed flush with the cartridge. The cartridge wall is acting as the diaphragm.

Unlike the conventional ballistic transducers, which measure the smallest gas pressure increase during the initial combustion phase, the conformal transducer senses the pressure only after the cartridge has been slightly deformed and is firmly contacting the front of the transducer. As tests have revealed, the pressure required for this deformation varies only slightly for a given cartridge size of the same material. Accordingly, the deformation pressure for a given cartridge case may be added to the peak pressure to obtain the peak pressure occuring inside the case.

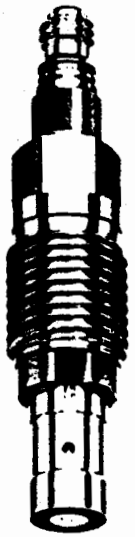

Figure 18: Conformal Transducer 6231A

Measuring range	0 to 5000 bar
Over range	6000 bar

Conformal transducer characteristics model 6231A:

- A transducer without diaphragm for measuring the cartridge pressure without drilling the case
- Practically unlimited life expectancy since the cartridge case acts as a "throw away" diaphragm
- Especially suited for peak pressure measurement during acceptance testing of ammunition
- Can be used with steel, plastic and cardboard cartridge materials
- The patented protecting sleeve design allows for uncritical installation eliminating mounting sensitivities

SUMMARY

Over the years, the ballistics pressure measurement has become more accurate and sophisticated. Continuing research and development of new transducers along with extensive field testing has improved the performance and accuracy. Currently available ballistics pressure transducers are offered in a wide variety of configurations to satisfy most of the applications and requirements.

REFERENCES

1) Cady, W. G.; Piezoelectricity, (An Introduction to the Theory and Applications of Electromechanical Phenomena on Crystals); New York, Dover, 1964

2) Tichy, J., Gautschi, G.; Piezoelektrische Messtechnik, Berlin, Heidelberg, New York, 1980

Q: Friedrich Ruckenbauer (AVL List): What type of ballistic transducer uses the polystable cut element?

A: John Kubler: The 6205, 6206, 6207... there is a whole series. I can give you model numbers. New releases will have polystable elements built in.

OPEN QUESTION AND ANSWER PERIOD FOR ALL PAPERS IN SESSIONS 1 AND 2

COMMENT: Peter Stein: The strain relief mounting technique should be considered almost any time you put a pressure transducer into a pipe wall, because there have been some horrible stories about forces from vibration getting into pressure transducers. That design looks neat.

Q: Peter Stein: For Donald Busse of Paroscientific...In your first paper you emphasized that this particular vibrating quartz transducer was meant primarily for laboratory work. Your second paper says it is for measurements under severe environmental conditions, which prompts a question. You've evacuated the inside of the transducer so the only heat transfer mechanism is by induction; convection is out. If there are temperature gradients, the process fluid, which you want to measure the pressure, is always hotter or colder than the transducer itself. Is it possible that the little tine which sticks out to measure temperature, doesn't quite measure the same temperature as the vibrating element which is in an enclosed thermal conduction path? Is the tine just a little cooling fin sticking out?

A: Donald W. Busse: The small temperature sensor element you are talking about is, in most cases, within that closure itself. It is mounted to the pressure sensor crystals that are mounted on the same surface. They should measure the same temperature and are probably within an 1/8 inch of each other. It is true that it is evacuated inside so the only thing the primary temperature heat is through conductivity. But you do get substantial radiant effects from the transducer itself. To get good temperature compensation using the crystal, we don't want to have a very large gradient with the transducer, and we could have a relatively large gradient if we had good thermal conductivity of the transducer itself. One of the slides from the first paper did show that the transducer was surrounded by a substance that isolates it from mechanical shock and vibration. It also provides very good thermal isolation; the time constant is about 30 minutes. So even if you immerse this thing in an entirely new thermal environment, the thermal rates cannot be very high because we've cut down on the conductivity of the basic transducer itself. The differences between what we measure as temperature and what the pressure sensor sees is very small because the sensor is very close to the pressure sensor.

Q: Roger Noyes: I'd just like to comment on Peter and Don's discussion here. We've had some experience with the Paroscientific transducer. We have had them installed and it is compatible with the rest of our thermal electronics. We have found in our condition that when we drive very long lines there is some heat effect because of the line drive within the transducer. And it does give us an error. The error is not large, and once we discovered what it was, we reasonably took it out. Basically, the answer to that problem is to calibrate under the conditions you are going to use the transducer.

COMMENT: Patrick L. Walter: I just had a comment that I was going to make on the first paper of this morning which I believe was given by Mr Gierer. Anyhow, it was on the self-monitoring and reporting transducer and specifically talked about piezoelectrics. The first

approach is to assess how much you reduce the reliability of the transducer by giving it the capability to check itself because you've added a complication to prove something is reliable. That's just a philosophical thought, and I don't suppose you can give an answer to that. On piezoelectric specifically, and I suspect a lot of the people here know it but a few may not. One way to check it is to break into the ground side of the coax cable if you have a piezoelectric with a high impedance output. Break into the ground side with a series resister and then AC couple into that a signal from a power supply that is itself isolated. You want the power supply isolated because typically the piezoelectric case is grounded. Insert a voltage into that ground side and go through the capacitor; the crystal itself looks like a capacitor. Of course, you have to do this during a period of inactivity. Now you've generated an AC charge that you can feed into your charge amplifier. You have continuity through the cable and it shows that you have, in fact, the connector hooked to the accelerometer and that you do have a capacitive element in there. It doesn't show anything more than that. The accelerometer could be loose and rattling around and you can still get an answer. Steve mentioned in his lithium niobate development that he looked at two crystals one driving the other. Of course his application was quite unique in that he's looking at nanosecond type resolution. But I know that about 20 years ago NASA was funding a dual transducer element where essentially you had one crystal driving a second one to verify the integrity of the accelerometer itself. Now about that same time 20 years ago, there was a lot of work going on just in getting the amount of mounted resonant frequencies of transducers by coupling two transducers together and putting a voltage into one and using it to electrically stimulate the other. There's some work there that has been done and for whatever reason I think that's been largely abandoned. But I think there are some avenues that you can try to do self checks on piezoelectric accelerometers.

Q: Ronald Tussing: When you pointed out all the characteristics of the PVF2 you mentioned it was acoustically similar to the water, the impedance. I have the impression that you were pushing the current mode for that material; however, you corrected me saying you weren't pushing either one and that the voltage mode or the high input impedance mode would not have any of the problems they say the quartz or tourmaline or some other gauge would have.

COMMENT: Friedrich Ruckenbauer: Some words about the philosophy of self-testing transducers. I have researched the properties of some of these transducers for self test because piezoelectrics, especially quartz transducers, have very high resonance. Sometimes you can test these by impulse excitation, the pattern depending on the size. Another way you can do it is with a continuous excitation by a sinusoidal signal of the resonance frequency, like a normal resonator. I will present a system for testing pressure transducers in this way in my paper on Thursday.

Q: Thomas Naughton (Dresser Industries): I have a question for Mr Busse. When I looked at the specifications and heard about the temperature as high as 107°C with accuracies of 0.01 percent, I wondered about the absolute versions and the altimeters. What is the stability

in the reference side if you were to stay at elevated temperatures for a long time? The pictures seem to point out a great deal of metal inside. Would there be some out-gassing or possibly something from other mounting mechanisms?

A: Donald W. Busse: We have done quite a bit of study on the stability aspect of these transducers. It becomes more important for the lower pressure transducers such as the altimeters and the 15psi transducers. When you get to higher pressure transducers its not as important, but you do get vacuum deterioration in the device if you don't do anything about it. There is out-gassing from the elements but that isn't the primary source of vacuum deterioration for us because when the transducers are fabricated we do bake them at a very high temperature for an extended period of time, like 350^{o}F for one to two weeks. As a result, they are fairly well out-gassed. The primary source of gases that tend to deteriorate the internal vacuum (which is your reference) generally come from very minute leaks in the transducers. In the case of early model transducers where we were sealing leaks with epoxies, we could measure the leak rate of the transducer on the helium mass spectrometer. We have very very small leak rates and yet after some time, we would notice vacuum deterioration. This was caused by a problem known to manufacturers of microelectronics devices. When they seal their caps on lids with epoxy, they find they get water migration. It wasn't a leak actually, it was a chemical sort of hand-over-hand of the water through the salient. Since then we have addressed the problem by going to electron beam welding techniques. Now we have hermetic seals and then as a further precaution, we introduced an active getter within the transducer so that in the case of secondary leaks and out-gassing, the getter will tend to clean up the environment and maintain a good hard vacuum.

SESSION 3

CALIBRATION TECHNIQUES

PROBLEMS WITH FREQUENCY CREATION IN NONLINEAR MEASUREMENT SYSTEMS

Patrick L. Walter
Supervisor
Rocket Range Systems Division
Sandia National Laboratories
Albuquerque, NM

ABSTRACT

Nonlinearities in measuring systems are shown to severely distort dynamic signals. Constraints in measurement system bandwidth in linear components physically located after nonlinear components can disguise the fact that signal distortion has occurred. This article provides examples of both nonlinear measuring components and resultant distorted signals as well as explains why signal distortion occurs. Guidance for measurement system design to preclude data distortion caused by measurement system nonlinearities is provided.

INTRODUCTION

Any measurement system intended to record dynamic data should be designed to be linear. Even when a nonlinear process is encountered in a measurement system, such as the modulation associated with various recording techniques, the overall system should still be designed to provide a linear input-output relationship. The components of a measuring system include such devices as transducers, signal conditioning amplifiers, analog filters, etc. Typically, these all possess a linear input-output relationship.

An understanding of linear systems has to begin with mathematics. The systems we are interested in are continuous time (t) systems, i.e., those whose output signals can be measured at any value of time. We are interested in time-invariant systems; systems whose characteristics do not change with time. If an input $i_1(t)$ to a single-input single-output system produces an output $o_1(t)$, and an input $i_2(t)$ produces an output $o_2(t)$, then concurrent inputs $a(\text{times})i_1(t)$ and $b(\text{times})i_2(t)$ must result in an output $a(\text{times})o_1(t)+b(\text{times})o_2(t)$ for the system to be linear. Linear systems are those which satisfy this principle of superposition. All linear systems have associated with them a unique frequency response function $H(j\omega)$. For measurement systems, this frequency response function is characterized by its log amplitude and phase versus log frequency responses as Bode plots. Nonlinear systems are systems which are not linear. They do not possess a unique frequency response function.

The following section provides a practical example of the preceding mathematical concepts through the description of a nonlinear measuring system component. The remainder of this work expands the limited quantity of literature(1)(2) available as a technical resource to experimentalists acquiring dynamic measurements.

NONLINEAR FILTER EXAMPLE

Filters are one of numerous components found in measurement systems. Low-pass filters are those which pass frequencies from at or near 0 Hz to some high frequency limit, usually specified by the frequency where 3 dB amplitude attenuation occurs. Curve A in Figure 1-A (measured with a rms meter) shows the amplitude frequency response of a low-pass filter with a -3 dB frequency of approximately 1200 Hz. Figure 1-B shows the phase lag versus frequency response for this filter. Both these curves were generated with a sinusoidally varying input voltage applied to the filter. This input resulted in a low frequency output equal to 60 percent of the filter's linear amplitude range. Curve B of Figure 1-A shows the amplitude frequency response of this same filter generated with a sinusoidally varying input voltage which resulted in a low frequency output of 20 percent of the filter's linear amplitude range. Note that when normalized the two curves are different (superposition is not satisfied). The difference between these curves is electrically caused by slew induced distortion.(3)(4)(5)

The filter characterized in Figure 1 is constructed around two identical operational amplifiers. Exceeding the small signal bandwidth of these amplifiers results in signal amplitude attenuation; exceeding the power bandwidth results in signal distortion due to system nonlinearities. This distortion (slew induced) is related to the slowness of the amplifiers' feedback loops. The distortion is level sensitive in terms of amplitude and frequency.

AMPLITUDE FREQUENCY RESPONSE

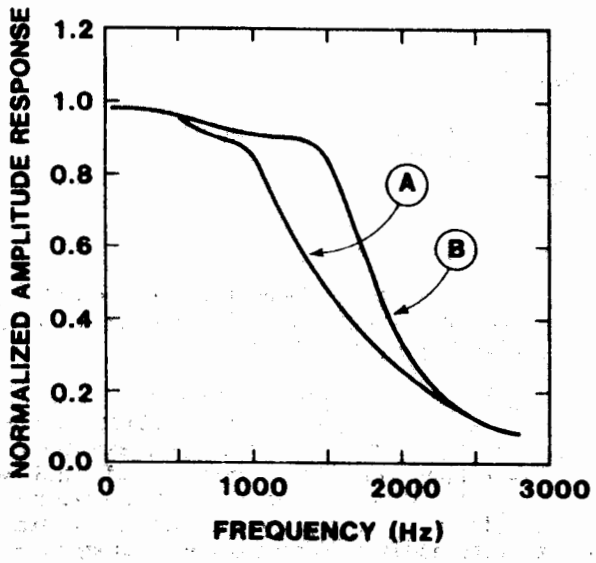

Figure 1-A

PHASE FREQUENCY RESPONSE

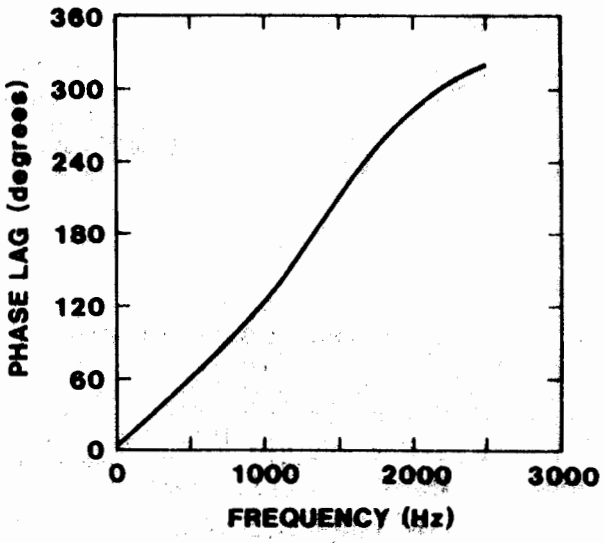

Figure 1-B

LINEARITY

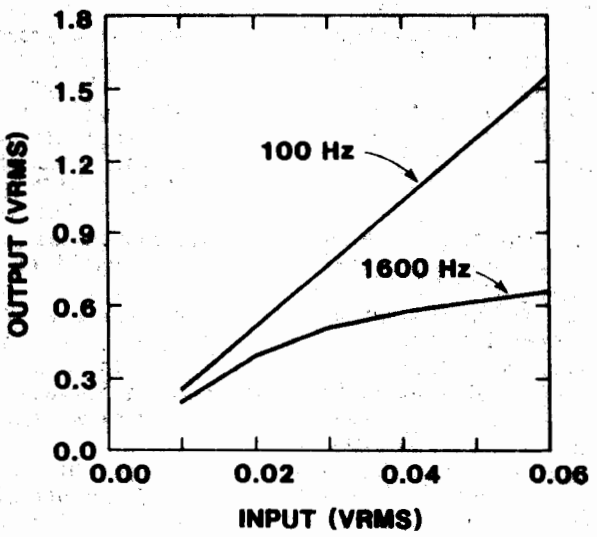

Figure 1-C

Figure 1. Nonlinear Filter Characterization

The signal slope (SS) of a sine wave of peak amplitude V at a frequency f is:

$$SS=2\pi Vf. \quad (1)$$

In Figure 1-A, at the higher input signal level and the higher frequencies the maximum output-voltage or slew rate of change of the amplifiers in the filter is being exceeded. This results in the nonunique amplitude frequency response characteristic of a nonlinear system.

Figure 1-C provides further characterization of the nonlinearities associated with this particular filter. At 100 Hz the two curves of Figure 1-A superpose indicating the filter to be linear at this frequency. The test data presented in Figure 1-C confirm this observation. At higher frequencies, however, the two curves of Figure 1-A differ. The test data in Figure 1-C taken at 1600 Hz provide confirmation of inadequate filter design.

FREQUENCY CREATION IN NONLINEAR SYSTEMS

This section illustrates the frequency creation process associated with nonlinear systems. Figure 2-A shows a decaying sinusoidal signal analytically described by the following expression:

$$3e^{-60\pi t}\sin(1999\pi t). \quad (2)$$

Signals such as this are common in the response of electrical oscillator circuits and structural mechanical systems to transient excitations. Figure 2-B describes three output (o) versus input (i) relationships; the first is linear and the second two are nonlinear. The relationships are:

$$o=i,$$
$$o=i \text{ for } -1\leq i\leq 1 \text{ and } o=\text{sgn}(i)^{*}\text{for } |i|>1, \text{and} \quad (3)$$
$$o=\tanh(i).$$

The signal of Figure 2-A is then individually passed through each of the systems described in Figure 2-B. In Figure 2-C, the system output looks just like the input when passed through the linear system. The Fourier amplitude spectrum of the signal in Figure 2-C is shown in Figure 2-D. Note the spectral content is centered at a single frequency. Figure 2-E describes the output signal which results from passing the input signal through the nonlinear system described by sgn(i) for $|i|>1$. Its amplitude spectrum is described in Figure 2-F. Note that additional spectral content is generated with peaks occurring at more than one frequency. Figure 2-G shows the result of passing the same input signal through the nonlinear system described by tanh(i). Again, as shown in Figure 2-H, additional spectral content and peaks are generated. Figures 2-F and 2-H could be erroneously interpreted to indicate the presence of multiple resonant frequencies in an electrical or structural system where only one exists.

*recall sgn(i)=+1 for i>+1 and -1 for i<-1

Figure 3-A presents test data recorded from a strain gage attached to a structural system. These have a duration of approximately 0.5 seconds. Figure 3-B presents the Fourier amplitude spectrum of these data; signal content extends to 1000 Hz. Figure 3-C shows the result of truncating the signal in Figure 3-A. Such a truncation could physically occur by overdriving an instrumentation amplifier, a tape recorder, or some subsequent piece of signal conditioning associated with the data channel. The amplitude spectrum of the data in Figure 3-C is computed, its value is subtracted from that in Figure 3-B, and the absolute magnitude of the difference between these two spectrums is plotted as in Figure 3-D. The significance of the plot in Figure 3-D is to illustrate that the nonlinear truncation operation on the data resulted in the generation of erroneous spectral content at all frequencies across the data band analyzed from 10 Hz to 1000 Hz.

A significant problem can occur if the frequency bandwidth of the measurement system becomes limited by a subsequent system component after the one responsible for the truncation.(6) The resultant filtering of the data will obscure the fact that data truncation has occurred by both rounding truncated signal peaks as well as reducing their amplitude. Recorded data can be accepted as valid while containing erroneous signal spectral content.

Figure 4 illustrates exactly such a problem. Figure 4-A shows an unfiltered (1 MHz bandwidth) acceleration-time record from a structural test. The recording accelerometer is specified linear to 10,000 gs peak-to-peak and the signal conditioning amplifier ranged linear to 20,000 gs peak-to-peak. The data indicate the accelerometer has been overranged and the amplifier driven into saturation with resultant data truncation (note "clipping" at +14,000 gs) over the first 1.0 millisecond of time. Clearly, one might expect problems when attempting to correlate these data to results of structural analysis. Figure 4-B results from passing the data in Figure 4-A through a simple low-pass RC filter with a -3dB frequency of 10 KHz. Such filtering could occur due to the capacitance associated with a long cable attached to the accelerometer's output leads. This filtering has eliminated all evidence of the nonlinear process which occurred. If only the data in Figure 4-B were available to base a decision on, erroneous test data would be accepted as valid.

To prevent this problem from occurring, transducers with a wide dynamic range should be used to prevent them from overranging. In addition, the frequency response of any measuring system which records dynamic data should be constrained at the transducer's output to the maximum capabilities of the overall system. This constraint minimizes the opportunity for the

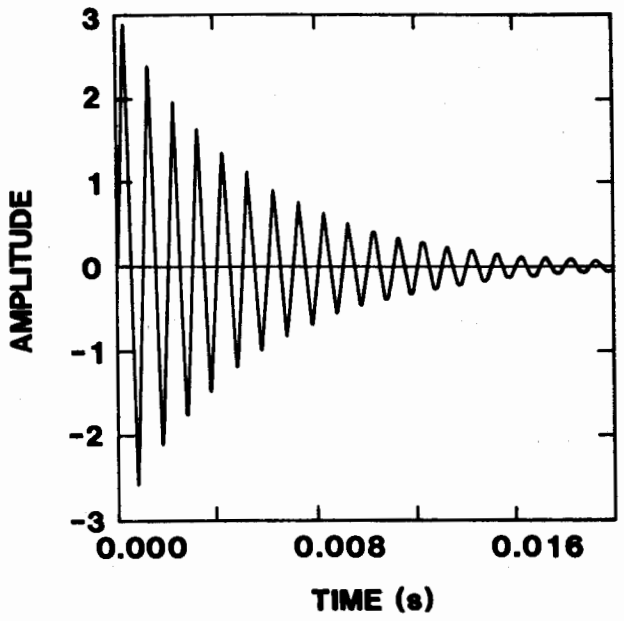

Figure 2-A

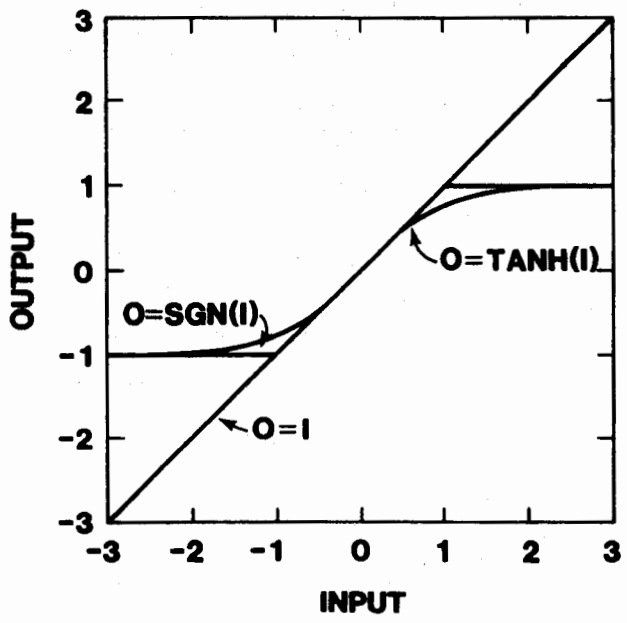

Figure 2-B

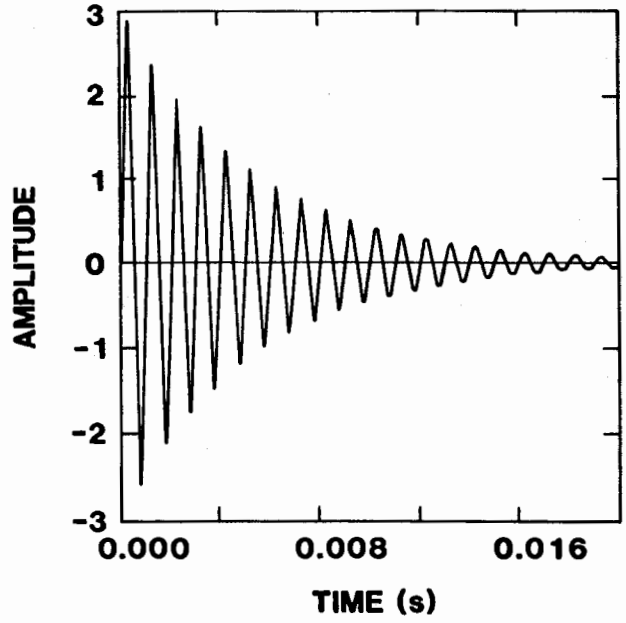

Figure 2-C

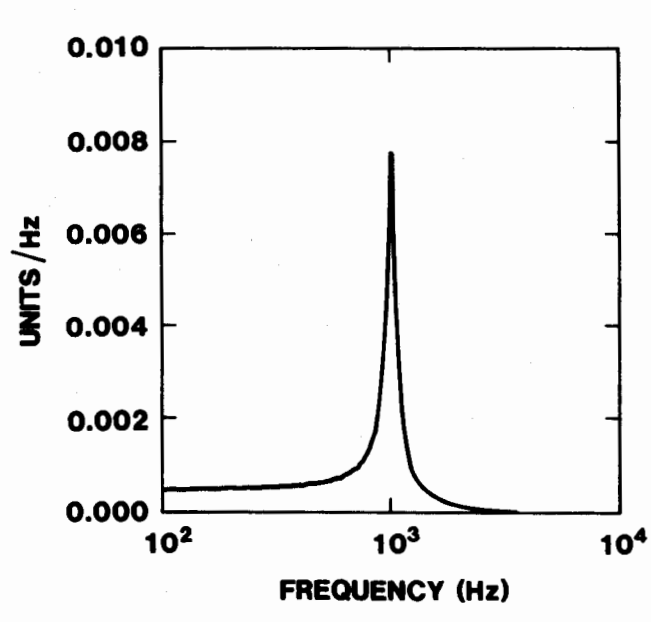

Figure 2-D

Figure 2. Frequency Creation Through Nonlinear Operations on a Decaying Sinusoid

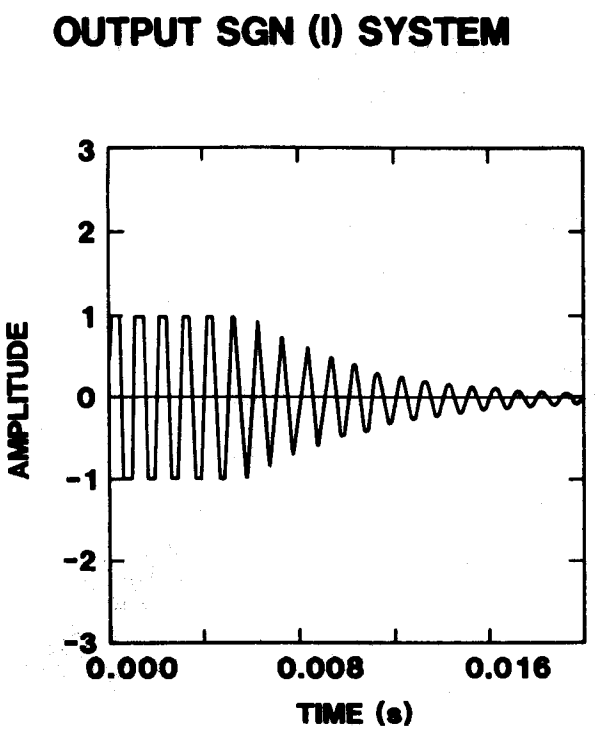

Figure 2-E

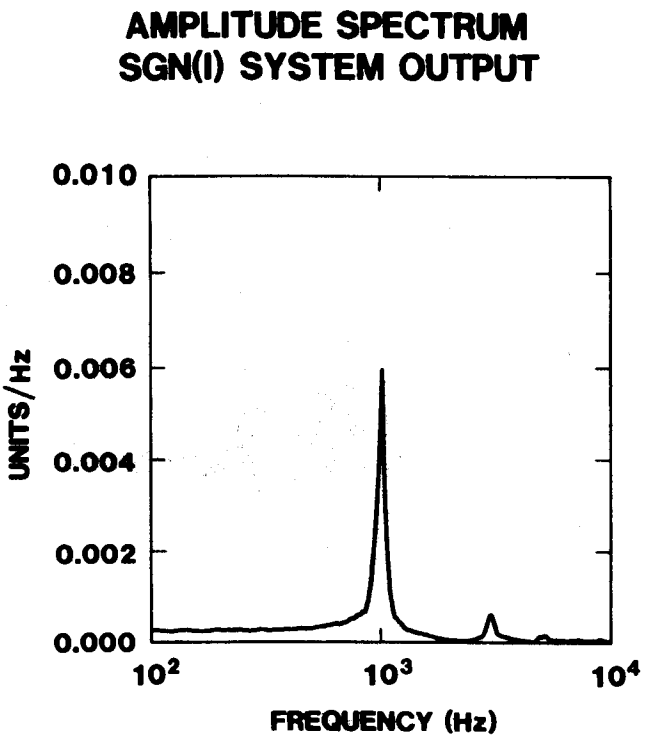

Figure 2-F

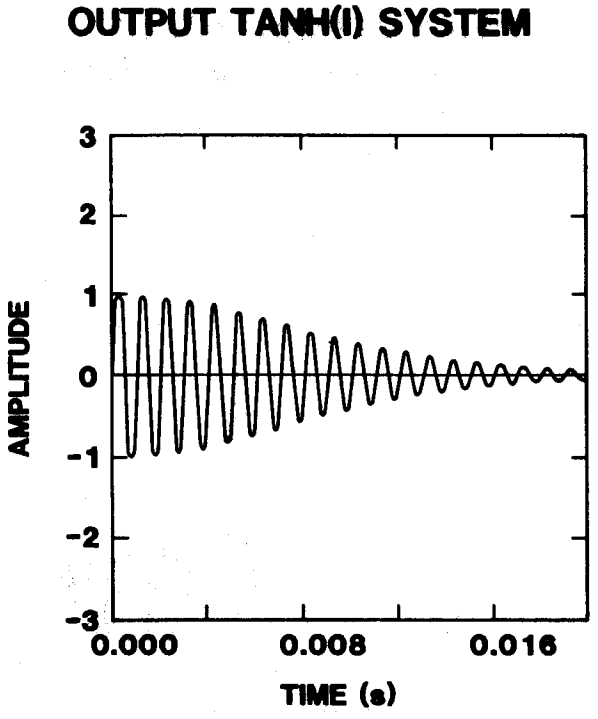

Figure 2-G

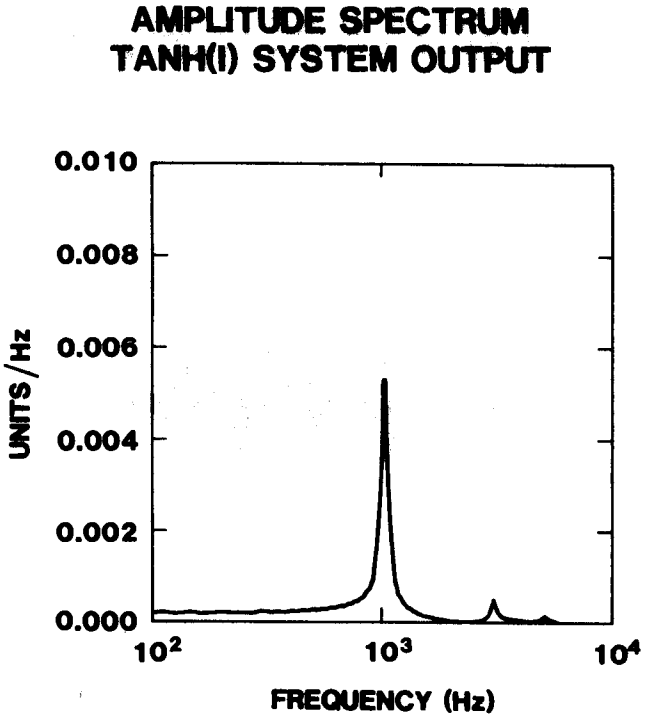

Figure 2-H

Figure 2. Frequency Creation Through Nonlinear Operations on a Decaying Sinusoid

STRAIN GAGE DATA

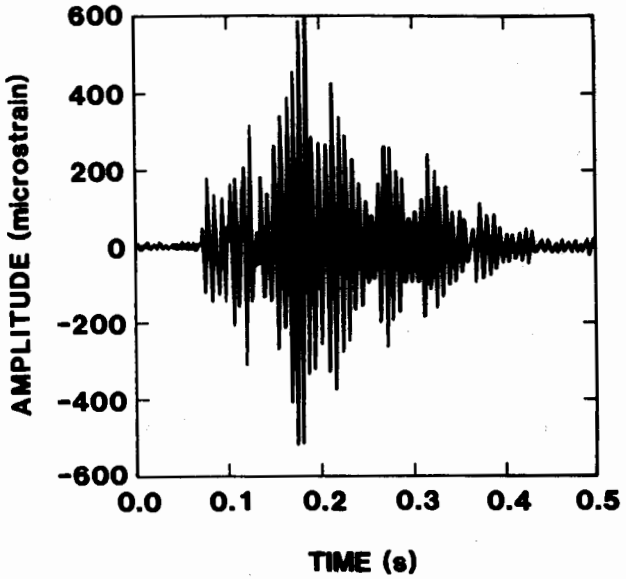

Figure 3-A

AMPLITUDE SPECTRUM
OF STRAIN GAGE DATA

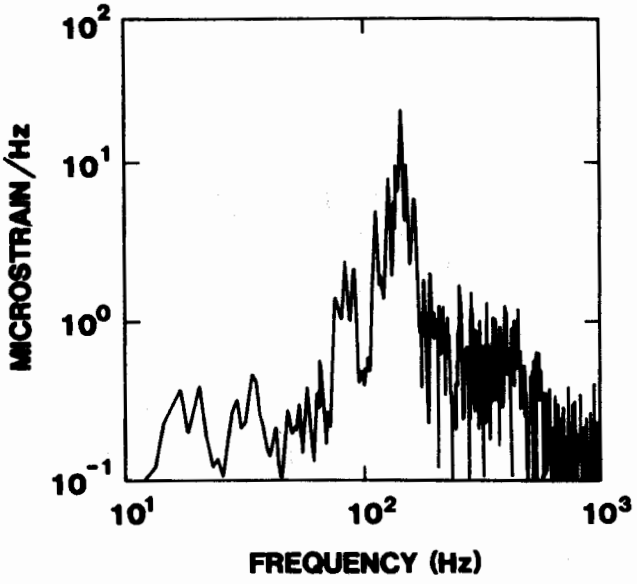

Figure 3-B

TRUNCATED STRAIN GAGE DATA

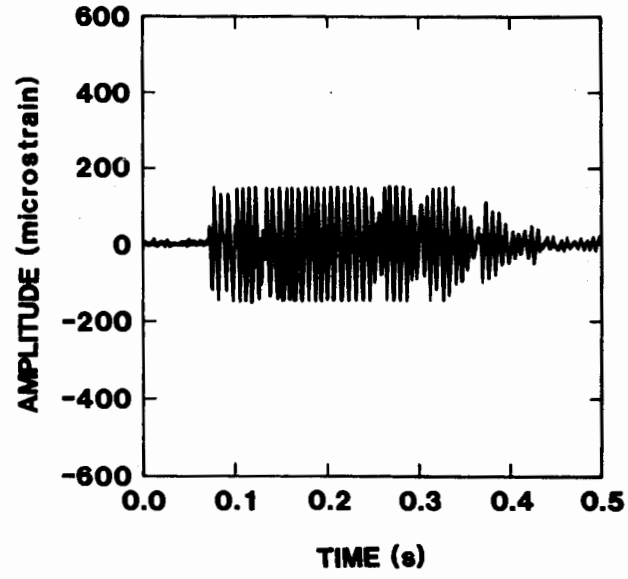

Figure 3-C

ABSOLUTE MAGNITUDE
OF DIFFERENCE SPECTRUM

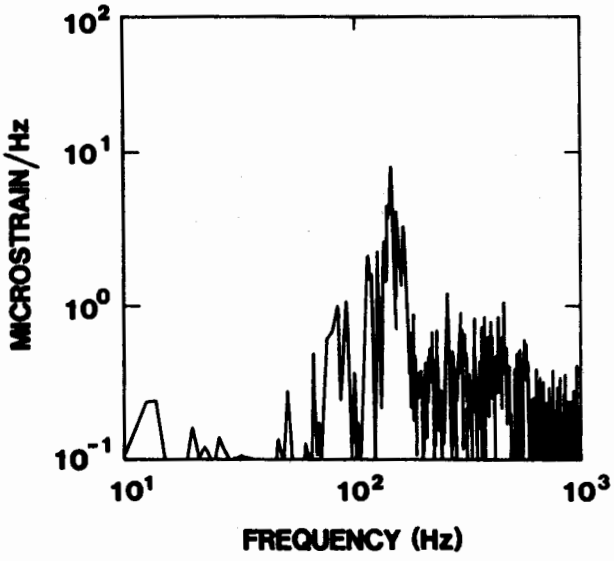

Figure 3-D

Figure 3. Frequency Creation Through Truncation of Recorded Strain Data

UNFILTERED ACCELERATION DATA

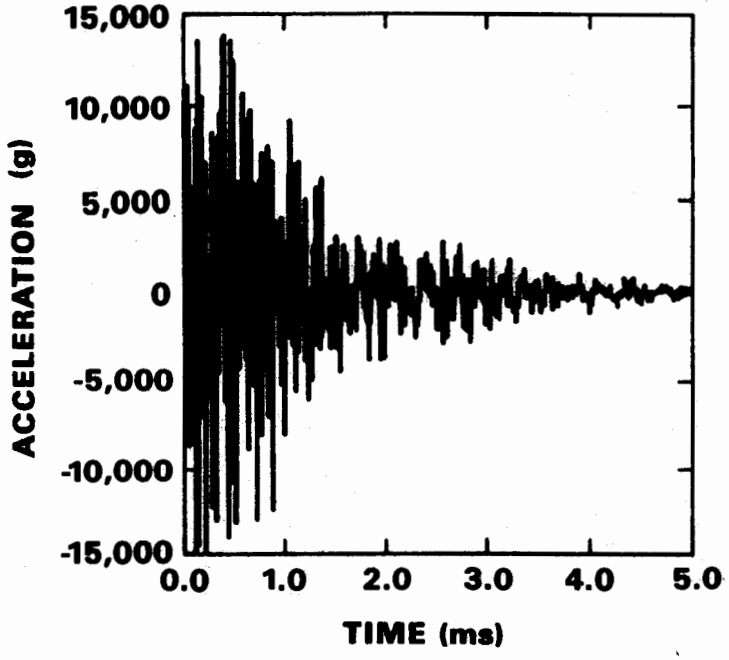

Figure 4-A

10Kz RC FILTERED ACCELERATION DATA

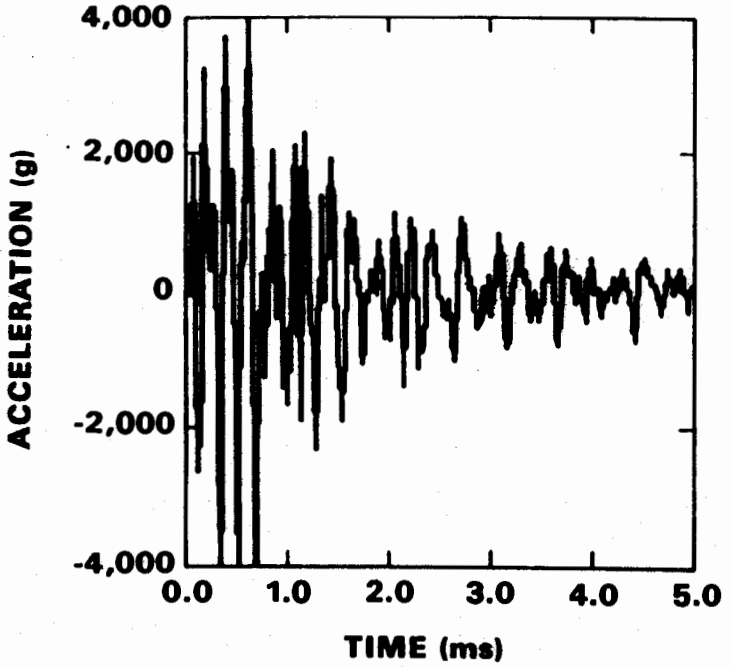

Figure 4-B

Figure 4. 10 KHz RC Filtered Acceleration Data

measurement system to be overdriven by prohibiting input frequencies in excess of those which can appear in its output. Any overranging which does occur within a system's bandwidth will then clearly be observable allowing the resultant output signal to be discarded.

HOW NONLINEAR SYSTEMS CREATE FREQUENCIES

The concept of how nonlinear systems create frequencies is simple to describe. If a nonlinear system's input-output relationship is smooth and well behaved, it can be approximated over a finite interval by a polynomial relationship as:

$$o=(c0)+(c1)i+(c2)i^2+(c3)i^3+... \qquad (4)$$

For a linear system, only coefficients c0 and c1 are non zero. For nonlinear systems, coefficients above c1 also become involved.

Transient signals contain a continuous frequency spectrum. The effect of system nonlinearities can be demonstrated, however, by considering an input signal to be comprised of only two frequencies:

$$i(t)=\sin((\omega 1)t)+\sin((\omega 2)t). \qquad (5)$$

If only coefficients c0 and c1 exist, the system response to this input signal occurs at the same frequencies as the input. The c0 coefficient generates an additional dc component. If the coefficient c2 exists, trigonometric identities show frequencies to be created at $2(\omega 1)$, $2(\omega 2)$, $\omega 1-\omega 2$, and $\omega 1+\omega 2$. Similarly, if the coefficient c3 exists, frequencies are created at $\omega 1$, $3(\omega 1)$, $\omega 2$, $3(\omega 2)$, $2(\omega 2)-\omega 1$, $2(\omega 2)+\omega 1$, $2(\omega 1)-\omega 2$, and $2(\omega 1)+\omega 2$. Note that frequencies are created at, above, and below the system input frequencies.

A mathematically more sophisticated explanation of how nonlinear systems create frequencies would point out that multiplication in the time domain (e.g., nonlinear terms such as i^2) is equivalent to convolution in the frequency domain. Specifically, if i(t) is the input signal and $I(j\omega)$ its Fourier transform, then $i^2(t)$ transforms as:(7)

$$i^2(t) \leftrightarrow \frac{1}{2\pi}\int_{-\infty}^{\infty} I(jx)I(j(\omega-x))dx. \qquad (6)$$

The convolution process, in this case attributable to the nonlinear term $i^2(t)$, would "smear" the continuous spectral content of any transient input signal i(t).

The fact that nonlinear processes create frequencies points out the need for additional caution in designing measurement systems to record dynamic signals. Earlier, it was pointed out that a significant problem can occur if data are truncated and then have their bandwidth limited by subsequent measurement system components. To preclude truncation from occurring, data channels are sometimes designed with devices such as log amplifiers to accomplish data compression. After data transmission occurs, linearization is attempted by antilog amplifiers to recover the original input signal. For example, this technique could be used when recording the output of resonant systems (electrical or mechanical) whose response to unknown transients can vary over wide amplitude ranges. The data compression device (e.g., log amplifier) generates frequencies not present in the input signal. If these frequencies are not all uniformly passed with a linear phase shift in the transmission process,(8) the inverse to the compression operation will not restore the original input signal.

CONCLUSION

Measurement systems intended to record dynamic data must be designed to operate within their respective linear ranges. Nonlinear systems create frequencies at, above, and below the spectral content of their individual input signals. Overdriving measurement system components introduces nonlinearities through signal truncation. Subsequent to this truncation, any limiting of the bandwidth of these signals by other measurement system components can result in erroneous data being accepted as valid. Constraining the frequency response of a measuring system at its front end to the maximum frequency capabilities of the overall system is recommended to allow any signal overranging which does occur to be clearly identified. Signal compression is not a reliable solution to problems associated with system components being overdriven. If frequencies generated through signal compression are lost or attenuated in subsequent transmission, the inverse of the compression operation will be unsuccessful in restoring the input signal.

REFERENCES

(1) Stein, P. K., "Dynamic Measurements on and With Non-Linear Systems: Problems and Approaches", Proceedings First International Modal Analysis Conference, Orlando, FL, hosted by Union College, Schenectady, NY, Nov. 1982, pp. 358-389.

(2) Wright, C.P., "Dynamic Data Invalidity due to Measurement System Non-Linearity", Western Regional Strain Gage Committee Proceedings, Society for Experimental Mechanics, Phoenix, AZ, Feb. 12-13, 1985.

(3) Thomsen, C. and Moller, H., "Swept Measurements of Harmonic Difference Frequency and Intermodulation Distortion", Bruel & Kjaer Application Notes, Naerum, Denmark, (undated).

(4) Jung, W. G., Stephens, M. L., and Todd, C. C., "An Overview of SID and TIM, Part I", Audio, Vol. 63, June 1979, pp. 59-72.

(5) Jung, W. G., Stephens, M. L., and Todd, C. C., "An Overview of SID and TIM, Part II", Audio, Vol. 63, July 1979, pp. 38-47.

(6) Walter, P. L. and Nelson, H. D., "Limitations and Corrections in Measuring Structural Dynamics", Experimental Mechanics, Vol. 19, No. 9, Sept. 1979, pp. 309-316.

(7) Chirlian, P. M., Signals, Systems, and the Computer, Intext Education Publishers, NY, Ch. 2, 1973, p. 79.

(8) Walter, P. L., "Effect of Measurement System Phase Response on Shock Spectrum Computation", The Shock and Vibration Bulletin, Part I, May 1983, pp. 133-142.

Q: James Rieger (Naval Weapons Center): I guess I'm a Communications Engineer because one of the things I like to do and recommend is the use of compression based on a logarithmic compression of the envelope of the signal. Now I realize, that if the signal attacks faster than the thing reacts, I will generate clipping right at the beginning, but most of the rest is removable. It does not increase the bandwidth as a result of doing those things which do not involve clipping and its recoverable. I cite as an example the sound tracks from most of the satellite born radio and TV signals, and also the systems called Beta Hi-Fi and VHS Hi-Fi which employ compression to make the dynamic range work and sound like an horrendous signal-to-noise ratio. The problem with most accelerometers is that you ask the person, who wants you to telemeter their accelerometer channel, what kind of levels do you expect? They say, if we knew what levels to expect we wouldn't be putting on an accelerometer, would we? You set the thing so it doesn't clip and you wind up seeing on the playback the 400 cycle "stuff." They reply with you seem to have a lot of 400 cycle vibration which is really noise. Tell me where you get the idea that compression necessarily distorts?

A: Patrick A. Walter: As you are well aware, compression is a standard item that is used in conjunction with this communication per se. I was talking about any time you do data compression you've have a nonlinear system. Just by definition, you do create frequencies by going through the nonlinear operation. And the comment I was talking about is the extension of that thought process to where someone takes the accelerometer. Someone might come to you or one of your cohorts at China Lake, and say this accelerometer is irrelevant. It's just one example of what we're talking about right now. Someone comes to you with an accelerometer saying they don't know what the amplitude level is that they are going to record. To accommodate them, instead of conditioning it to a standard linear amplifier, you choose to condition it to a log amplifier. And that's where the problem starts. But you're going to take that log amplifier and put it through an FM channel which I went through. Your FM channel can handle 40 kHz of data. Let's say your input signal has 4 kHz frequency content in it, and in that case the 4 kHz in the signal is compatible with the bandwidth that you can extract from your VCO. As soon as you put it through that nonlinear amplifier, instead of a linear amplifier you've greatly extended its bandwidth. You have more than 4 kHz frequency intelligence now that's going to modulate your VCO. You've passed the 4 kHz down to the ground and then through your nonlinear operation which is the inverse to the log amplifier, but you don't have all your data intelligence in the bandwidth. So specifically, I was talking about incorporating the nonlinear element into the signal conditioning amplifier.

Q: R. Maglic: I want to ask you a question, but first I want to make a comment. The comment is that I don't believe that polynomial explains nonlinearity. It is only a mathematical way of saying that the diode can modulate and demodulate. The real physical cause of nonlinearity has to be searched for in the physical phenomena and not in mathematical formulas. And in this case, for instance, it may be

that the filter is producing the nonlinearity, the clipping, or it may be other parts and that is where the interesting part of the study is. I also wonder how difficult is symmetrical clipping because if you have nonsymmetrical clipping, you have what is called second harmonic generation not just third harmonic like you should. You talked about dynamical nonlinearity which is the frequency domain. The question I wanted to ask you is there an amplitude nonlinearity also?

A: Patrick Walter: Let me see if I can answer that question. The first comment was about the polynomial and that's exactly right. That polynomial doesn't represent the diode clipping whatsoever. The thing the polynomial represents is that it has some nonlinear elements in it and it is just illustrative of how nonlinearities can result in some extraneous frequencies. It is there by virtue of explaining the mechanism by which some of these frequencies come into play, and it would take a much more mathematical form to describe these examples that I showed you here. The question was about the amplitudes we talked about in the frequency domain. Does that extend to amplitude nonlinearity, and are the two really synonymous? If you have a nonlinear system, it has to show up both in the frequency domain and the amplitude domain. And that's what the filter example illustrated. When you were at low frequencies where you weren't having problems with amplifier slew rates, those two amplitude frequency responses lay on top of one another, so you did have a unique frequency response function or a unique transfer function. Then subsequently when I showed you that input-output relationship that was run at 100 Hz, you had a straight line relationship. The amplitude domain and the frequency domain were complementary. And then if you went out from that same filter to 1600 Hz, where the frequency response function was nonunique, those two amplitude frequency responses deviated when you went back and tried to repeat that same amplitude linearity check at 1600 Hz. The curve bent if you recall and does whenever you have a nonunique frequency response function. If you do a linearity check by going up and down in amplitude over the range, you will find, in fact, that you have some kind of hook in your curve--you don't have a straight line relationship.

Q: Bill Anderson: Pat, you said that one of the goals should be to limit the response at the sensor. For an instrumentation engineer, many times that's a difficult thing to do and what I would like are some examples of how you would recommend limiting that response at the sensor?

A: Patrick Walter: Basically, I think that in instrumentation systems what you want to do is realize that any instrumentation system is, as you well know, just a filter. Sometimes your instrumentation system response might be limited by the tape machine, but then you can think of the tape machine as just a filter. And so if you realize you're going to filter somewhere in the system, the thing is to constrain yourself with some filtering at the front end of the system. It's just active filtering that allows that to happen.

AN APPLICATION OF PARAMETER ESTIMATION THEORY IN LOW FREQUENCY ACCELEROMETER CALIBRATION

B. F. Payne
M. R. Serbyn
National Bureu of Standards
Gaithersburg, MD 20899

Low frequency accelerometers, velocity transducers, and seismometers are used extensively to investigate vibrations on mechanical structures. The measurement of low frequency (1-100 Hz), low amplitude (<10 mV) signals from these transducers has been a problem for conventional data acquisition systems. This paper describes a system for low-frequency transducer measurements which first digitizes the voltage signal utilizing a commercial high speed digitizer. Software routines developed at NBS for a desktop computer then estimate the rms amplitude, dc offset, and any distortion components in the transducer signal.

Using a software based system with a high-speed sampling voltmeter provided great flexibility in developing a system for this particular application. Compared with previous systems for low-frequency vibration measurements at the National Bureau of Standards, the present approach is also more accurate.

INTRODUCTION

This paper describes a useful extension to a system for calibrating accelerometers in the frequency range 1 Hz to 200 Hz. The system is documented in a recent publication of the ISA [1]. The present paper is a supplement to the ISA paper in that it uses the same experimental setup, except for the data acquisition system and the signal processing software. The emphasis of this paper is on the new data acquisition hardware and software. The system uses a high-speed dc digital voltmeter for measurements of low-frequency ac transducer signals. Because of its high sampling rate and IEEE interface capability, this voltmeter is ideal for a computer-controlled low-frequency voltage measurement system.

DESCRIPTION OF THE CALIBRATION SYSTEM

The calibration system uses a fringe-counting interferometer for displacement measurement. The interferometer shown in fig 1 consists of the laser light source, two beam splitters mounted directly on the head of the laser and a 1/2 inch retro-reflector mounted on the shaker table. The interferometer measures the displacement of the shaker table with reference to the beam-splitters mounted on the laser. The light emerging from the interferometer produces interference fringes on the photo-detector. The laser has a wavelength, λ, of 632.8 nm and the detector is a silicon photo-diode with a signal amplifier (gain of 20) having a bandwidth of approximately 1 kHz to 3 MHz. The counter measures the number of fringes corresponding to the shaker displacement amplitude [2]. The acceleration is given by eq (1), where f is the vibration frequency, n is the number of fringes/cycle , d is the displacement amplitude in meters, and g is the standard acceleration of free fall, 9.80665 m/s^2.

$$a = (2\pi f)^2 d/g = \lambda n \pi^2 f^2 / 2g \qquad (1)$$

The sensitivity of the accelerometer is calculated by:

$$S = E/a \qquad (2)$$

where E is the amplitude of the voltage output from the accelerometer. The present paper describes the procedure used to measure E.

LOW-SIGNAL-LEVEL MEASUREMENTS

One difficulty in obtaining accurate readings of accelerometer signals encountered in low-frequency measurements has been the low voltages produced. A typical accelerometer sensitivity is nominally 10 mV/g. For a 2-Hz signal and a displace-

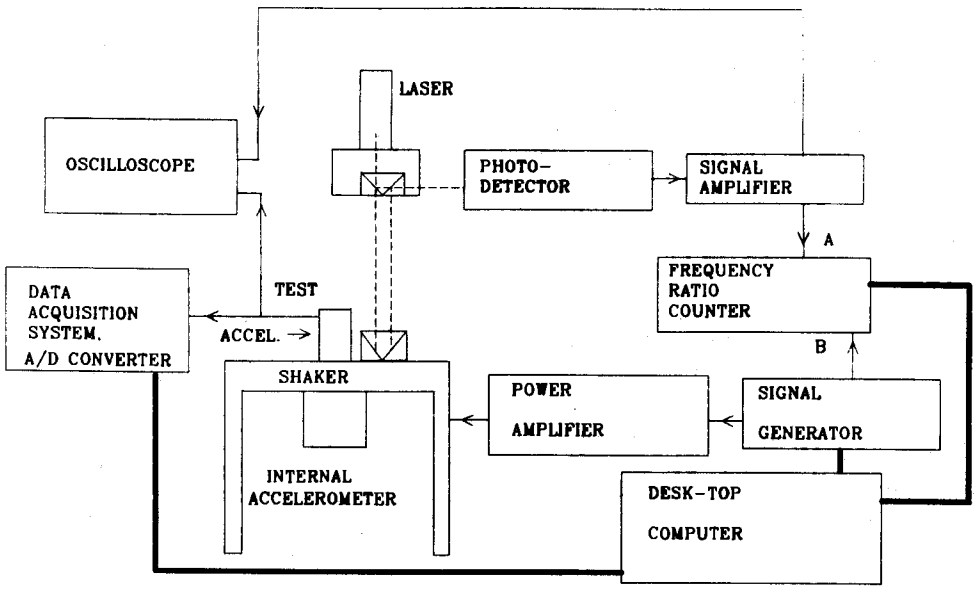

FIGURE 1. FRINGE-COUNTING INTERFEROMETER CALIBRATION SYSTEM

ment of one inch, a signal of approximately 2 mV is produced. This low voltage is difficult to measure for most commercial ac digital voltmeters. But it is often desirable to make measurements at much lower voltages since most low-frequency accelerometers can respond to micro-meter displacements. Table 1 gives voltages corresponding to several displacements, at 2 Hz for an accelerometer of 10 mV/g nominal sensitivity.

In the following section outlining the parameter estimation procedure, it is shown how accurate measurements can be obtained at the displacement levels given in the above table, even for accelerometers with low sensitivity.

TABLE 1

Displacement and Corresponding Acceleration and Voltage at 2 Hz for a 10 mV/g Accelerometer

Displacement double amplitude mm	Displacement double amplitude inch(approx.)	Acceleration amplitude g	Voltage amplitude mV
25	1	0.2	2.0
10	0.39	0.08	0.8
5	0.20	0.04	0.4
2	0.08	0.016	0.16

PARAMETER ESTIMATION ALGORITHM

The algorithm developed for processing the noisy low-frequency signals in the present application is a special case of a more general parameter estimation problem. Only an outline of the special-case theory will be given here; the ramifications of the bigger problem will be discussed in a later paper. It is planned also at that time to compare the results obtained by several approaches, including synchronous detection, Fourier analysis, and maximum likelihood detection.

For this application the task is to estimate the amplitude $\sqrt{(A_1^2+B_1^2)}$ of a sinusoidal signal from data $x(t)$ which may contain noise $\eta(t)$ and a dc offset A.

$$x(t)= A+ A_1\cos\omega t +B_1\sin\omega t + \eta(t) \qquad (3)$$

The angular frequency ω is presumed to be known and the noise is assumed to have a Gaussian distribution with mean $\eta(t) = 0$ and a constant variance

$$\overline{\eta^2(t)} = \sigma^2 \ . \qquad (4)$$

Following [3], we define

$$\varphi_1(k\Delta t)=\cos\omega k\Delta t - \frac{\sin[(N+1/2)\ \omega\Delta t]}{(2N+1)\ \sin(\omega\Delta t/2)} \qquad (5)$$

and $$\varphi_2(k\Delta t) = \sin\omega k\Delta t \qquad (6)$$

where Δt is the sampling period, and k is an integer.

For 2N+1 samples taken uniformly over a time interval [-L,L],

$$x_k = x(k\Delta t)= A_0 + A_1\ \varphi_1(k\Delta t) + B_1\ \varphi_2(k\Delta t) + \eta(k\Delta t) \qquad (7)$$

where k= -N, ... , -2,-1,0,1,2, ... N,

$$\Delta t=L/N \qquad (8)$$

and

$$A_0 = A + A_1 \frac{\sin[(N+1/2)\ \omega\Delta t]}{(2N+1)\ \sin(\omega\Delta t/2)} \ . \qquad (9)$$

Applying the method of maximum likelihood [4] to the sampled function x_k, the following formulas for the estimates A_0^*, A_1^*, and B_1^* can be derived:

$$A_0^* = \frac{1}{2N+1} \sum_{k=-N}^{N} x_k \qquad (10)$$

$$A_1^* = \frac{\sum_{k=-N}^{N} x_k\ \varphi_1(k)}{\sum_{k=-N}^{N} \varphi_1^2(k)} \qquad (11)$$

$$B_1^* = \frac{\sum_{k=-N}^{N} x_k\ \varphi_2(k)}{\sum_{k=-N}^{N} \varphi_2^2(k)} \qquad (12)$$

where $\varphi_1(k)$ and $\varphi_2(k)$ are calculated from (5) and (6). The estimated dc offset is calculated from eq (9), using the estimated values of A_0 and A_1:

$$A^* = A_0^* - A_1^* \frac{\sin[(N+1/2)\ \omega_1 L/N]}{(2N+1)\ \sin(\omega_1 L/2N)} \ . \qquad (13)$$

Using the estimates given by eqs. (11), (12), and (13) the defining eq (7), may be rewritten as

$$x(kL/N)=A^*+E^*\cos(\omega t+\arctan(-B^*_1/A^*_1)) +\eta(kL/N) \qquad (14).$$

where the amplitude of the ac voltage is

$$E^* = \sqrt{[(A_1^*)^2+(B_1^*)^2]} \ . \qquad (15)$$

Using eq (14), the signal waveform can be reconstructed from the estimated parameters and the residue can be be tested for randomness.

The noise can be calculated from eq(4) and eq(7):

$$\sigma^* = \left(\frac{1}{2N+1} \sum_{k=-N}^{N} [\ x_k - A_0^* - A_1^*\varphi_1(k) - B_1^*\varphi_2(k)\ ]^2\right)^{1/2} \ . \qquad (16)$$

Without any additional measurements we can compute confidence limits for the estimated parameter values. In the present application, a number of useful simplifications are possible because of the following conditions: (1) the number of samples is very large, (2N+1) >>1, and (2) the length of the record covers two cycles of the sinewave, that is, $L=2\pi/\omega$. The most important consequences of these conditions are that the t-distribution is closely approximated by the Gaussian distribution; the variances of A_1^* and B_1^* are approximately equal, and all results are identical with those obtained on the basis of a least-squares fit [5].

Thus, the confidence interval for A^* becomes

$$[A^* \pm t_\alpha \sigma^* / \sqrt{(2N)}]. \quad (17)$$

where t_α is the value of

$$t = \frac{A^* - A}{\sigma^* / \sqrt{(2N)}},$$

corresponding to the confidence coefficient $(1-\alpha)$.

Similarly, according to reference [6] the approximate confidence interval for the function E^* can be computed as follows:

$$E^* \pm t_\alpha \left[\left(\frac{\partial \sqrt{(A_1^2+B_1^2)}}{\partial A_1} \right)^2 s^2(A_1) + \left(\frac{\partial \sqrt{(A_1^2+B_1^2)}}{\partial A_2} \right)^2 s^2(B_1^*) \right]^{1/2} \quad (18)$$

where $s^2(A_1^*)$ and $s^2(B_1^*)$ are the variances of A_1^* and B_1^* respectively. Since for integral number of cycles and N large, $s(A_1^*) \approx s(B_1^*) \simeq \sigma^* / \sqrt{(2N)}$ [3], this expression reduces to

$$E^* \pm t_\alpha \sigma^* / \sqrt{(2N)} . \quad (19)$$

Remembering that A_1 and B_1 represent peak values and σ^*, a rms value, a "relative" confidence interval can be stated in the following simple, but meaningful, form:

$$1 \pm \frac{t_\alpha}{\sqrt{(N)}} / \frac{\text{Signal}_{RMS}}{\text{Noise}_{RMS}} . \quad (20)$$

Figure 2 shows a family of confidence limits computed from this expression.

APPLYING THE ALGORITHM TO ACCELEROMETER CALIBRATIONS

This measurement technique was applied to accelerometer calibration at low frequencies (1-200 Hz) by the use of a high-speed voltmeter which can sample as fast as 100,000 voltage samples/second and ranges automatically down to 40 mV full scale with a resolution of 10 μV. The output from the accelerometer under test is connected to the sampling voltmeter. This voltmeter under computer control can be programmed to select the sampling rate and number of samples. The captured data samples are transferred to a desk-top computer for analysis. The voltage of the test accelerometer is calculated by eq (15) given above. Also the dc-offset voltage and the noise are calculated by equations (13) and (16) respectively.

The ability of the parameter estimation algorithm to extract small sinusoidal signals from noisy transducer signals provides a means of measuring much lower acceleration levels than previous measurement systems.

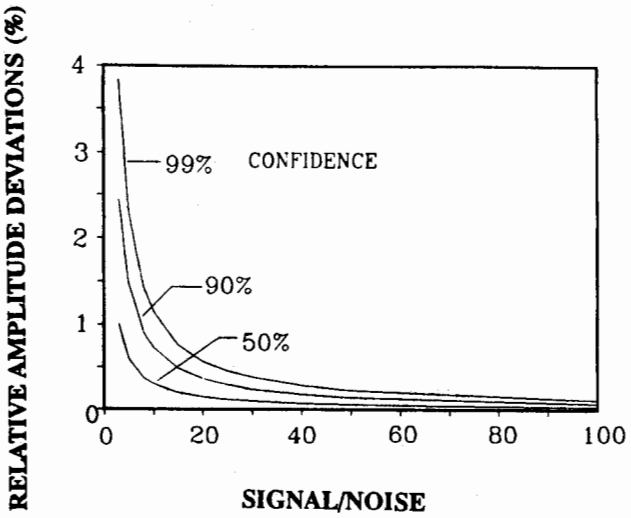

FIGURE 2. CURVES FOR CALCULATING CONFIDENCE LIMITS

ESTIMATING ERRORS

In order to check the functional relationships shown in figure 2, a computer program was written in Pascal to simulate typical data and to calculate the expected errors. The program generated a sinusoidal waveform with random noise, dc-offset, and phase shift according to eq (14). The algorithm was then used to calculate the sinusoidal voltage component, the dc-offset, and the signal to noise ratio.

The example shown in figure 3 is a computer generated 1 volt, 2-Hz sinusoidal signal with added random noise. The voltage corresponding to the sinusoidal 2 Hz component was computed from eq. 15 and the noise from eq. 16. A sample run consisted of 1001 digitized data points (two cycles) for a 2-Hz, 1-volt signal, using

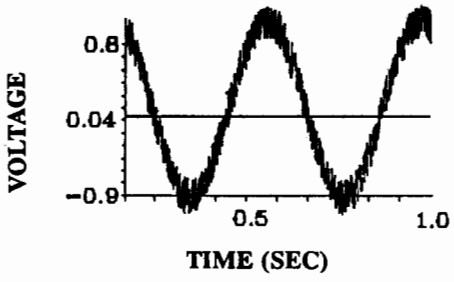

FIGURE 3. COMPUTER GENERATED SIGNAL WITH NOISE AND OFFSET

a phase of 25 deg and a dc-offset of 10 percent. Five hundred such sample runs were taken and their estimated voltages were compared to the original 1 Volt. The number of voltages outside 5%,4%, 3%, 2%, 1%, 0.5%, 0.35, 0.2%, and 0.1% was recorded in each case. By introducing differing amounts of random noise into the simulated signal, a set of estimated voltage-amplitude deviations was computed for a wide range of S/N ratios. Figure 4 shows a family of errors-versus-confidence curves for 3 values of S/N ratios computed from eq (20). The results of the simulated tests just described are also shown in figure 4. For example, for a S/N = 3, the number of sample runs whose estimated voltage lies outside a 3% band was 20 out of 500 runs. This is plotted as a 3% relative amplitude deviation at a 96% confidence level.

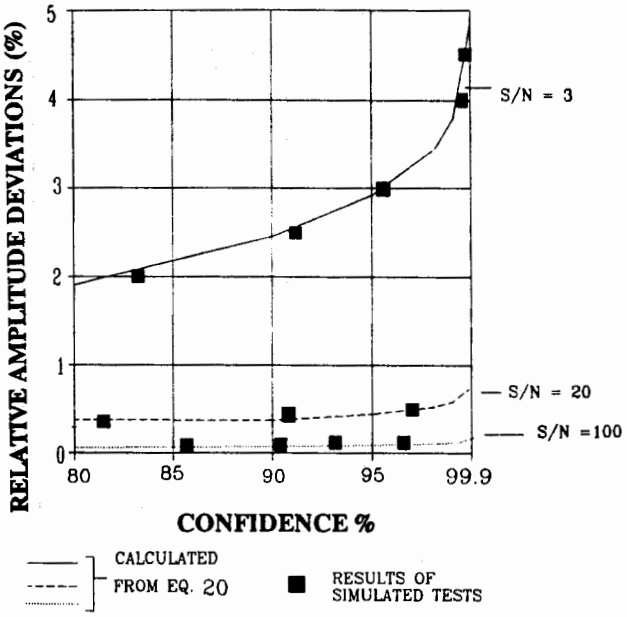

FIGURE 4. CONFIDENCE LIMITS FOR SOME TYPICAL S/N RATIOS

Table 2 shows data for an accelerometer with a nominal sensitivity of 500 mV/g, calibrated at 10 Hz over a wide acceleration range. The sensitivities shown are the average of 25 runs (of 1001 samples each).

TABLE 2

Calibration Data for a 500 mV/g Accelerometer at 10 Hz

Peak Acceleration (g)	Measured Sensitivity (V/g)	Fringes/ cycle (approx.)	Peak(mV) Voltage (approx)	Sig/ Noise (approx)	Voltage Error (%) Expected
0.96	0.5254	30,000	504	190	<0.1
0.48	0.5255	15,000	252	480	<0.1
0.10	0.5256	3280	52	335	<0.1
0.06	0.5258	1820	30	300	<0.1
0.004	0.5243	120	2	20	0.3
0.0006	0.5103	18	0.3	3	1.5

The expected voltage error in table 2 was estimated from figure 2. Not only the error in estimating the voltage signal, but also the low fringe count contribute to the uncertainty of the sensitivity measurement in the lowest acceleration shown in table 2. The frequency counter is set to count over approximately a 10-s interval to minimize the errors due to a small fringe count. The lowest acceleration shown in table 2 (0.0006 g) would not be considered a valid calibration and is shown only to illustrate the errors involved in measurements at this extreme.

In order to test the advantages of averaging, twenty five simulated sample runs (of 1001 digitized data points) were taken and the average voltage and S/N ratio were computed for the 25 runs. Ten such sets of 25 runs each were computed and the errors shown in figure 5 were calculated from the maximum spread in the voltages of the ten runs. By introducing

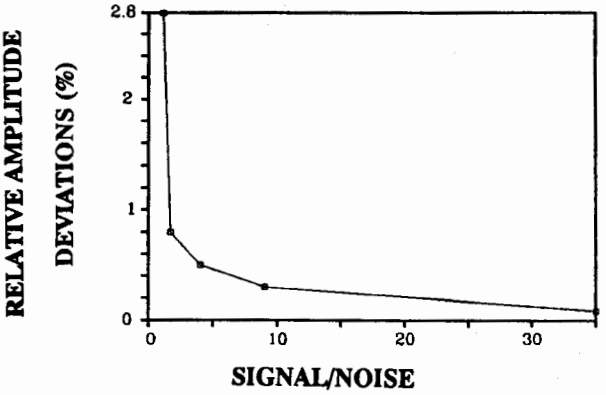

FIGURE 5. EXPECTED DEVIATIONS USING SIGNAL AVERAGING

Table 3
Effect of Averaging on Expected Error

Accelerometer Sensitivity	Acceleration g/1000	Voltage mV	S/N	Expected Voltage Error	
				No Averaging	With Averaging
500 mV/g	4	2	20	0.3	0.2
	0.6	0.3	3	1.6	0.6
10 mV/g	30	0.3	5	1.5	0.5
	80	0.8	6	1.2	0.4

differing amounts of random noise a set of errors was calculated for a wide range of S/N ratios. Examples were also computed using different phases and offsets. Varying the phase and offset did not change the general results shown in figure 5. Other examples using smaller voltage amplitudes down to less than 0.5 mV were computed to test the calculations for round-off errors. The results for smaller voltages are similar to the data in figure 5.

Table 3 shows data for the the accelerometer of Table 2 and also an accelerometer of 10 mV/g using averaging of 25 sets of data.

SUMMARY

A low-frequency calibration system for accelerometers has been developed which uses a fringe-counting interferometer and a high-speed digital acquisition system for accurate low-frequency, low-voltage measurements. The low-voltage measurements are possible due to the use of a parameter estimation algorithm which calculates the sinusoidal voltage output of a transducer in the presence of noise and dc-offset voltage. Confidence limits have been calculated for measurements in the presence of constant offsets and random Gaussian noise. Some examples of the type of measurements possible using the parameter estimation are the following (for an accelerometer of 500 mV/g sensitivity). Accelerations of 0.004 g were measured with a 90% confidence limit, with a voltage error estimate of 0.3% (S/N=20). By signal averaging of 25 sets of data, the error estimate can be reduced to 0.2%. Similarly, for a 10 mV/g accelerometer, an acceleration of 0.08 g was measured at a 90% confidence limit with 1.2% estimated error (S/N=6), which reduces to 0.4% after signal averaging.

ACKNOWLEDGEMENTS

This work was supported in part by the Aerospace Guidance and Metrology Center, Newark Air Force Station, Ohio. Dr. Steven E. Fick of NBS designed the photodetector signal amplifier and made improvements in the photodetector circuit to improve the high frequency response. Mr. W. Bach of Hewlett Packard Co. assisted in computer software support for this system. Mr. D.R. Flynn of NBS offered valuable suggestions in critiquing this paper. These contributions are greatly appreciated.

REFERENCES

1. B.F. Payne, "An Automated Fringe Counting Laser Interferometer for Low Frequency Vibration Measurements", ISA International Instrumentation Symposium, May 1986, Proceedings pp. 1-7.

2. R. Koyanagi, "Development of a Low-Frequency-Vibration Calibration System", Experimental Mechanics, Vol.15,No. 11, pp. 443-448, Nov. 1975.

3. M. G. Serebrennikov and A.A. Pervozvanskii, Extraction of Hidden Periodicities, 'Nauka' Publishers, Moscow, 1965 (in Russian), p.99.

4. H. Cramer, Mathematical Methods of Statistics, Princeton University Press, 1946, p. 498.

5. J.V. Beck and K.J. Arnold, Parameter Estimation in Engineering and Science, John Wiley & Sons, 1977, p.134.

6. J. R. Green and D. Margerison, "Statistical Treatment of Experimental Data", Elsevier Sci. Publ. Co. 1978, pp. 111,87.

Q: Roger Noyes: You talked about your voltage error. My first question is how good is your input?

A: B. F. Payne: In what sense?

Q: Roger Noyes: How well do you know the errors in your input acceleration, your interferometer system?

A: B. F. Payne: Okay! That's a different subject and that was discussed in the earlier paper. We know our acceleration to be within 1/2 percent which includes cross-axis motion, harmonic distortion, and interferometer alignment on the order of 0.5 percent. This paper is focusing primarily on how well we can measure our voltages, which has been one of our problems.

Q: Roger Noyes: My next question is: Obviously you are the bureau so you have to calibrate what people send you, but are the people who are sending these in using a similar system to look at their voltage outputs?

A: B. F. Payne: Not to my knowledge. There's every conceivable kind of measurement system being used, depending upon the company. There are a good many companies and laboratories who use the fringe counting method. Its becoming sort of an international standard method for low frequency measurements. And there are some laboratories who have this, some do not. I don't know of anyone who is using the parameter estimation theory at this time.

Q: Torben Licht: You were talking about measuring these very low levels with accelerometers. Have you any idea of how stable the outputs you are going to measure are from the accelerometer? In my opinion, the main problems at these low frequencies are not to measure the voltage but to have something stable out of the accelerometer system at all.

A: B. F. Payne: That's true. As I've said, we get all types of accelerometers; we can't pick and choose the ones we do. This particular one is very stable. We checked it over many months under different conditions and it is very stable. However, there are others which are not so stable. They change from day to day, so that's why we're reluctant to say that we can do 10 percent calibrations when there are so many different kinds. And you are quite right in your point.

Q: Torben Licht: Very often, even cable problems can be very severe. One other question: Have you considered measuring the actual X_t from the laser signal itself, which can be done but it's not easy?

A: B. F. Payne: Yes, that is one of the things we would like to do and I know you've done, that is, your company has done quite a bit of work in that. And we're looking forward to investigating that.

Q: R. Maglic: I'm just curious to know if you know what type of noise you have in the accelerometer?

A: B. F. Payne: I knew someone would ask that.

Q: R. Maglic: I mean the frequency. Is it 1/f noise? My second question is: Where would that noise come from? Do you have any idea of the origin?

A: B. F. Payne: Yes, we have done some investigation as to the type of noise. And most of the time the accelerometers exhibit a random noise with sort of a Gaussian distribution. We've tested the mean, the noise mean, and found it to be very close to zero, which is one test for randomness. We think that the main source of the noise comes in the signal conditioner. Most of the time it is broadband noise and it varies with the signal conditioner. There are some very low signal conditioners and there are some where the noise comes quite a bit higher.

Q: Bob Temes (Bourns Instruments, Inc.): I noticed in your table that in your equations for your signal-to-noise ratio, expressed in milli gs, is pretty constant in the lower level. It's about 0.2 of a milli g. I noticed that the noise becomes less than that as you go up in the high level inputs. Are you testing this on a seismic bed? Are you taking about the type of milli gs that are comparable to seismic disturbances during the test?

A: B. F. Payne: Well, I'm not really sure. I'm not really in that field. We do have this on a big isolation table; a type of granite suspended with air springs, so we do not get as much ground disturbance.

Q: Bob Temes: Is it natural to expect that the noise level would not decrease with an increase in input g level? Is it considered constant, in other words?

A: B. F. Payne: Frequently it does not stay constant, it will increase. In other words, if you go higher in g level the noise will be amplified. However, you usually get a benefit by going to a higher g level in your signal to noise as is shown here. Now as you go up from 0.5 to 1 g, it decreases. That's because of our shaker performance. It's not quite as good as at 1 g.

Q: Harvey Weiss: I can't see the numbers but can you give me a general idea of the kind of deviation from, a linear extrapolation of the data, we are getting? In other words, if the user would simply get down to areas that he's usually accustomed to in normal operation, like 2 Hz, he's probably going to just linearly extrapolate down to dc. How much can he be off, given the theory and the experimental work, and some of the calibrations that you people have performed?

A: B. F. Payne: Well its hard to make a general statement because it varies with the type of accelerometer. There are some that are as flat as can be down to dc, and there are others that have the low frequency rolloff. It depends and it is also complicated by the signal conditioner. It depends on how the signal conditioner is

built, the filters in it and that kind of thing. There are some that you can draw a straight line through and there are quite a few that we get that you can't do that to. You have to calibrate it at the frequency that you want it.

Q: R. Maglic: I'm going to mention one experience that we at Honeywell had with the sensor which we call SD3000. We had exactly the same problem, and what we did was to make an acoustic analog for the pressure sensor. We presented all the channels, all the diagrams and everything electrically. And it corresponds to the inductances and capacitances and the capacitance would be proportional, lets say to the diaphragm compressibility to how much that can bend. That way, we were able to find exactly what was causing these oscillations, what was causing the upshot and what was causing the negative; so there is nothing magic about that. I'm very glad to hear that you were able to solve the problem by changing the input orifice. But the thing that is really important is to collect every little mechanical opening, nonopening or channel length that contributes to those things; it is called electrical engineering transient analysis.

CALIBRATION ANOMALIES OF A MINIATURE DYNAMIC PRESSURE SENSOR

Martha Pierce Willis
Rockwell International/Rocketdyne Division
Canoga Park, California

ABSTRACT

During the calibration of a miniature, dynamic pressure sensor at ambient and cryogenic temperatures, several output anomalies were encountered. An abnormal negative excursion of the output signal was observed when a positive step pressure was applied, with a superimposed high frequency oscillation. Torque sensitivity, acceleration, line pressure, application rate, and temperature tests were performed to determine the cause of this unexpected behavior. The high frequency oscillation was believed to have been caused by mechanical strain induced on the sensor through the calibration hardware during operation. This output was eliminated by changing the sensor restraining mechanism. The sensor's negative deflection, when a positive pulse pressure was applied, was found to be caused by temperature transients. The thermal transient error was eliminated by placing a thermal barrier on the sensor diaphragm. The sensors were calibrated in this manner. A second miniature sensor similar in its operation and performance characteristics, but made by another manufacturer, was tested. It was concluded that the observed calibration characteristics are inherent in the sensor design.

INTRODUCTION

The Santa Susana Field Laboratory is a rocket engine and laser test facility. The instrumentation laboratory at this facility calibrates and services pressure, temperature, force, flow, vibration, and position sensors. A request was made of this laboratory to evaluate and calibrate a miniature dynamic pressure sensor. The sensor's intended use was to measure flow stability in an ambient and a cryogenic medium. During the evaluation and subsequent calibration, output anomalies were encountered. To determine if the calibration anomalies encountered with this sensor were design or manufacturer related, a second sensor made by another manufacturer was tested. Both sensors had similar operating characteristics and design. This paper discusses the tests performed on these sensors and the output anomalies encountered. Appendix 1 lists general specification information for those sensors tested.

TEST SETUP

Calibration and evaluation of dynamic pressure sensors consists of the following: visual inspection, proof pressure and leak tests, sensititivy versus line pressure tests, and sensor sensitivity to pressure tests. Tests are performed over the intended operating temperature range.

Sensors are proof pressure and leak tested to verify structural and seal integrity under load conditions. These tests are performed on a static pressure console using gaseous nitrogen as the pressurant. Sensors are pressure cycled several times at their maximum working pressure and at 1-1/2 times that value. Those sensors employed in cryogenic service are usually temperature cycled between pressure cycles.

Sensitivity versus line pressure tests are performed on a high line pressure pulse calibration system. This system provides a positive step pressure pulse of up to 20 psi at line pressures up to 4000 psi. These tests are generally performed on new or repaired sensors and can be performed at ambient and cryogenic temperatures. Outputs are recorded on a digital transient recorder (Fig. 1).

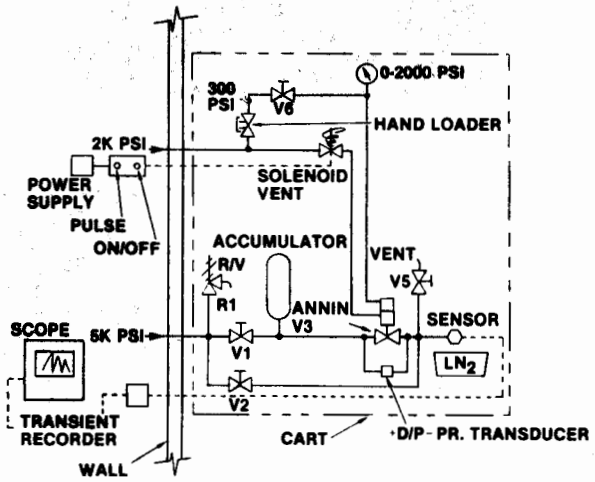

Fig. 1. High Line Pressure Pulse Calibration System

Sensor sensitivity is determined on an ambient line pressure pulse calibration system. The pressurant is gaseous helium. Positive step pressures up to 100 psi may be applied to the sensor. This test may also be performed at cryogenic temperatures. The outputs are recorded on a digital transient recorder (Fig. 2).

SENSOR CALIBRATION

The miniature pressure sensor tested had a 100 psi dynamic range and was going to be used at up to 5000 psi static pressures. Each sensor was visually examined, then proof tested at 7500 psi, and leak tested at 5000 psi. During these operations, no unusual sensor behavior was noted.

On the ambient line pressure pulse system, the units were subjected to step pressures of 10, 50, and 100 psi. These were done at ambient and -320 degrees Fahrenheit. Four sensors were tested and their outputs resembled those of Fig. 3. Each sensor tested showed a varying degree of the same characteristics--an abnormal negative output excursion when a positive pulse pressure was applied, and a high frequency oscillation superimposed on the pulse trace.

To verify calibration system integrity, a second dynamic sensor with similar operating characteristics, but not of the miniature design was simultaneously pressure pulsed along with the miniature unit. Figure 4 shows the relative dimensions of the two sensors. The sensors were subjected to a 100-psi pulse of gaseous helium at ambient temperature. The test results are shown in Fig. 5. The miniature unit again responded unexpectedly while the second sensor responded in a manner indicative of normal calibration system operation.

The miniature sensor was tested for sensitivity versus line pressure. Sensors were subjected to positive pressure steps of 20 psi at a 1000 psi line pressure. Figure 6 is representative of the outputs seen. They show the output of a single sensor tested twice under the same conditions. The

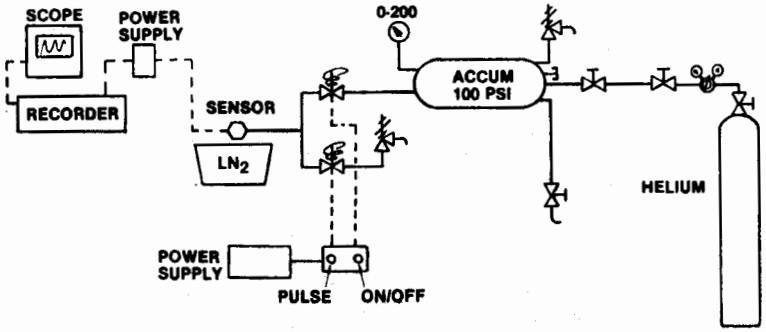

Fig. 2. Ambient Line Pressure Pulse Calibration System

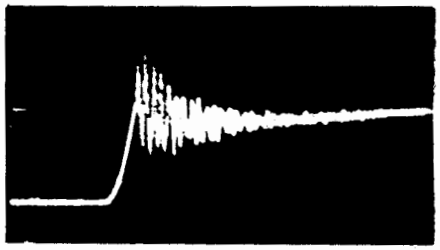

(A) 10 psi Pulse, 4 msec/Division, 20 mV/Division

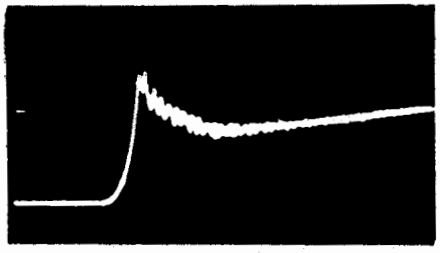

(B) 50 psi Pulse, 4 msec/Division, 80 mV/Division

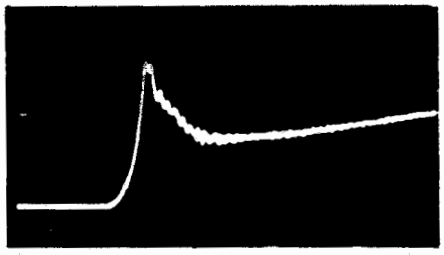

(C) 100 psi Pulse, 4 msec/Division, 133 mV/Division

Fig. 3. Miniature Sensor Subjected to Step Pressures at Ambient Line Pressure and Temperature

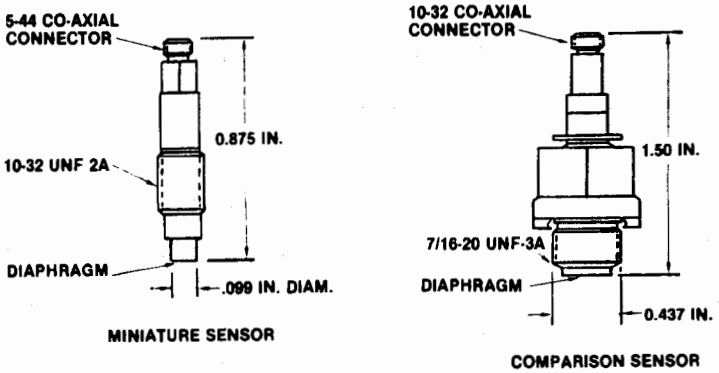

Fig. 4. Miniature and Comparison Sensors

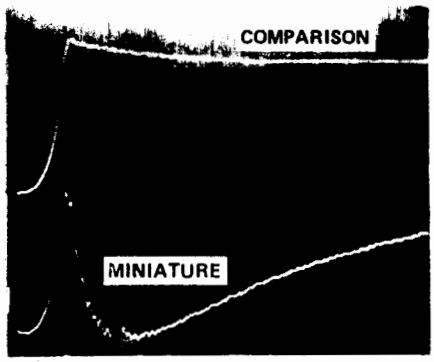

Fig. 5. Sensor Traces at 100 psi Pressure and Ambient Temperature

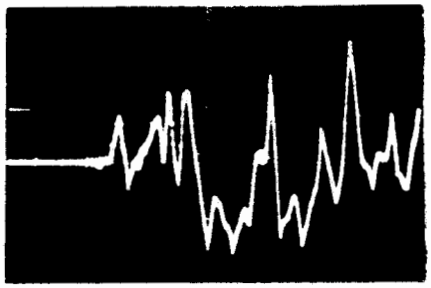

(A) Miniature Unit - Test No. 1
1000 psi Line Pressure, 20 psi Step Pulse,
10 msec/Division, 500 mV/Division

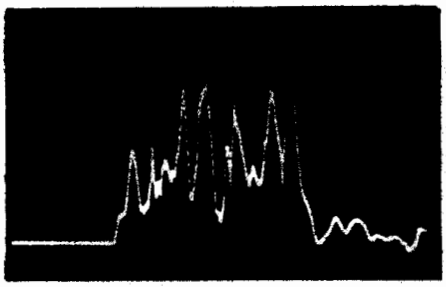

(B) Miniature Unit - Test No. 2
1000 psi Line Pressure, 20 psi Step Pulse
10 msec/Division 500 mV/Division

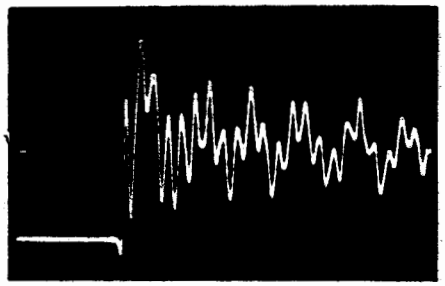

(C) Comparison Sensor - Nonminiature Unit
1000 psi Line Pressure, 20 psi Step Pulse, 10 msec/Division, 80 mV/Division

Fig. 6. Miniature and Comparison Sensor Output on High Line Pressure Calibration System

output varied in frequency between 175 and 325 Hz and were nonrepeatable. Results were similar for all other units of this type tested. To verify system operation, the comparison sensor mentioned in the previous paragraph was then tested. The output of this sensor is shown in Fig. 6(C). The output seen repeated with each pressure pulse. Frequencies seen on the output of the comparison sensor are approximately 250 and 80 Hz. These values correspond to the calculated values of tube resonance for the primary tube lengths in the high line pressure calibration system. Using the equation for a closed pipe $F = c/4L$ and the primary tube lengths of 12 and 42 inches, the values calculated were 275 and 78.5 Hz, respectively. The frequencies measured on the miniature sensor output histories fall into the range of the calculated frequencies for tube resonance, however, because of the nonrepeatable nature of this output, it was suspected that the sensor was responding to something other than pressure.

Several tests were conducted to determine the source of these uncharacteristic behaviors. Tests were performed to determine sensor sensitivity to torque, acceleration, line pressure, application rate, and temperature.

RESULTS

The installation torque and acceleration sensitivity tests showed that the sensor responded as the

manufacturer's specification implied. These parameters were not considered related to the behavior seen during the calibration process.

The sensor was placed on both the ambient line pressure and the high line pressure pulse calibration systems. Without pressure on the system, it was mechanically operated. The sensor was found to produce the same signal as was seen superimposed on the pressure trace. Figure 7(A) is a typical example of the sensors' response to the mechanical operation of the ambient line pressure calibration system. Figure 7(B) is the response of the sensor to the mechanical operation of the high line pressure calibration system. This output resembles that of Fig. 6(A) and (B), confirming that the output was not due to pressure alone.

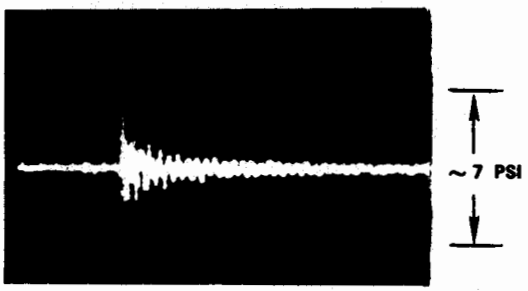

(A) Ambient Line Pressure, 14.5 mV/Division

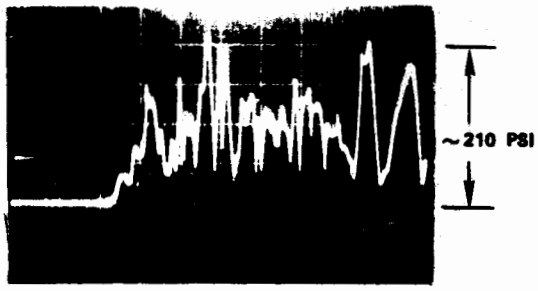

(B) High Line Pressure 500 mV/Division

Fig. 7. Miniature Sensor Output on Both Calibration Systems with Mechanical Operation Only (No Pressure Applied)

The original calibration adaptor for the sensor was made from an AN 806, 1/4-inch plug. It was coupled to the calibration console by means of a 3.5-inch section of 1/4-inch stainless steel tubing. Figure 8(A) shows this adaptor. To verify that the signal seen was not due to chattering of the sensor diaphragm against the side wall of the adaptor, the adaptor was modified by opening up the through hole. This had no affect on eliminating the oscillating signal superimposed on the pressure trace.

Vendor literature for the miniature sensor states that cable motion can induce strain on the sensor body, and that this strain can produce signals that will add to the sensor output giving erroneous data. This had been taken into account prior to calibration and cables had been secured. It was then believed that the output seen was caused by mechanical strain induced on the sensor through the calibration hardware during operation. the calibration adaptor was modified by shortening and stiffening the coupling to the calibration system. The oscillating output was eliminated. Figure 8(B) is the modified adaptor.

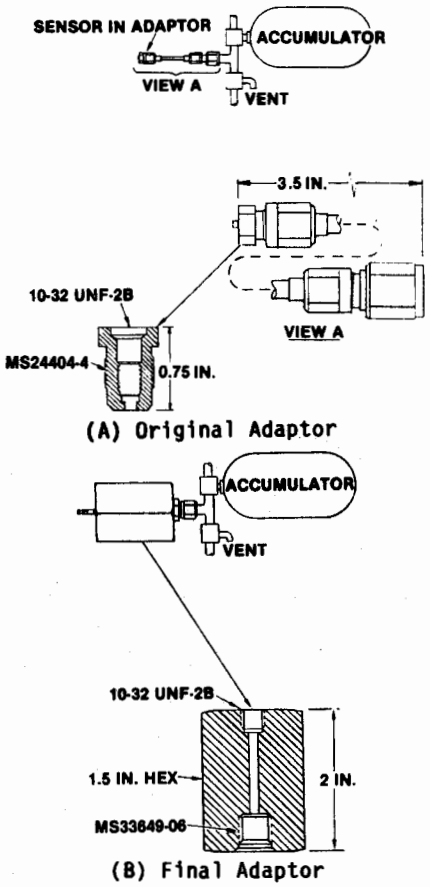

Fig. 8. Calibration Adaptors Used During Testing

Application rate tests were performed to determine the effect this had on the negative excursion of the output when positive pressure was applied. It was found that the negative output excursion could be eliminated. It was believed that the slower application rate was decreasing thermal shock to the unit and temperature tests were conducted.

As stated in the reference article, most sensors of this type are temperature compensated, however, this compensation is only effective when the diaphragm, sensor shell, crystal and compensating elements are thermally stabilized. A thermal shock immediately stress the sensor diaphragm, which is coupled to the quartz element. This gives an erroneous signal until the sensor comes to equilibrium. The sensitivity of a particular sensor to a thermal transient depends on its materials, construction, and arrangement of its quartz elements.

Using a 0.010-inch diameter thermcouple mounted in the sensor calibration adaptor, the temperature differential of the gas during calibration was measured. This was done with a 100 psi pulse (where the negative excursion was the greatest). The temperature differential was found to be approximately 50°F. Based on the calculated final temperature of 107°F (PV = nRT) and an initial temperature of approximately 68°F, the calculated temperature differential is 39°F. This verifies the measured differential as reasonable. A thermal barrier was then placed on the sensor diaphragm during calibration and the negative output was eliminated. The results are shown in Fig. 9. Of the sensors tested, the thermal transient error decreased the sensor's calculated sensitivity at 100 psi, ambient temperature, and line pressure by an average of 23 percent.

FURTHER TESTING

A second miniature sensor made by another manufacturer was tested in a similar manner. The purpose was to determine if the calibration anomalies encountered with the first miniature unit were design or manufacturer related. Both of these sensors were quartz type, voltage mode, low impedance, dynamic pressure sensors with similar ranges and operating characteristics. Figure 10 shows the relative size of the alternate miniature sensor to the original sensor.

The results of the tests resembled those seen with the first unit. The sensor was sensitive to thermal transients generated by the calibration compressed gases. It was also sensitive to the

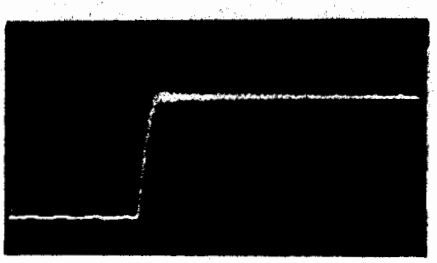

(A) 10 psi Pulse, 4 msec/Division, 23 mV/Division

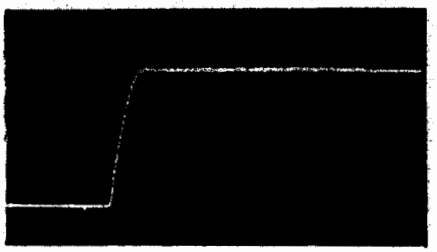

(B) 50 psi Pulse, 4 msec/Division 100 mV/Division

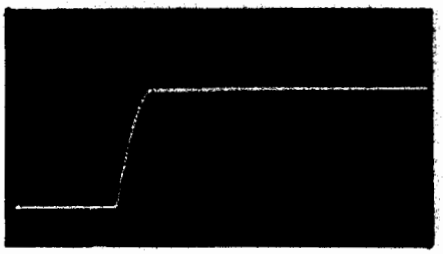

(C) 100 psi Pulse, 4 msec/Division, 235 mV/Division

Fig. 9. Miniature Sensor with Thermal Barrier Subjected to Step Pressures (Line Pressure and Temperature are Ambient)

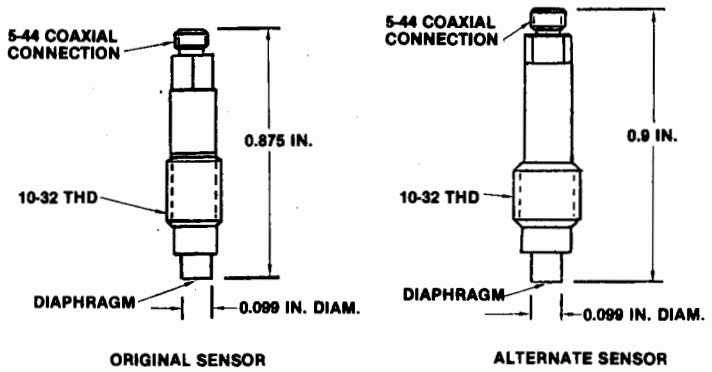

Fig. 10. Miniature and Alternate Sensors

mechanical strain induced by the mechanical operation of the calibration system. Figure 11 shows the sensor output when pulsed with 100 psi at ambient temperature and line pressure with and without a thermal barrier. Figure 11(C) is the sensor response to the mechanical operation of the calibration system.

CONCLUSION

The anomalies seen during the calibration of a miniature quartz sensor were inherent in the design. The application of a thermal barrier to the sensor diaphragm enabled this type of sensor to be calibrated using the calibration systems available. Care should be taken when using this type of sensor to ensure that the sensor will perform satisfactorily in the intended use environment.

BIBLIOGRAPHY

U. Dubendorfer and P. Wolfer, "State of the Art of Pressure Measurements in Combustion Engines," Proceedings of the Instrument Society of American Conference, 8 May 1984.

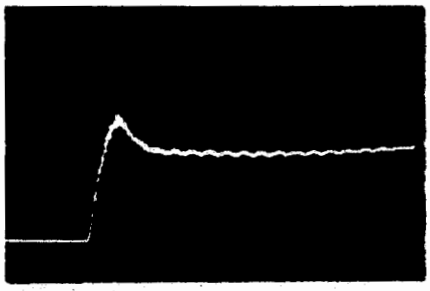

(A) Ambient Temperature, No Thermal Barrier, 100 psi Pulse, 4 msec/ Division, 0.727 volt/Division

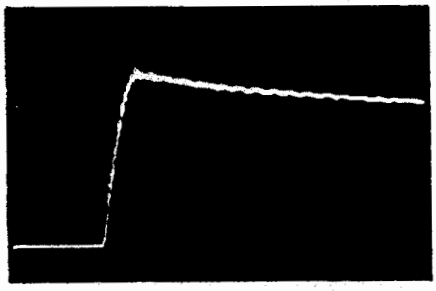

(B) Ambient Temperature, Thermal Barrier 100 psi Pulse, 4 msec/Division 0.727 volt/Division

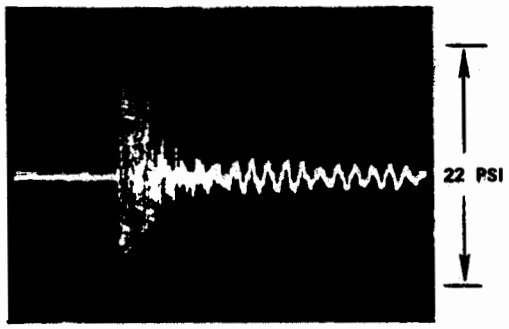

(C) Ambient Temperature, No Pressure Applied, 4 msec/Divison, 0.1 volt/Division

Fig. 11. Alternate Sensor Response to Calibration Testing

Appendix 1 - Sensor Specification Information

SPECIFICATION PARAMETERS	SUBJECT MINIATURE SENSOR	COMPARISON NONMINIATURE SENSOR	ALTERNATE MINIATURE SENSOR
DYNAMIC RANGE, psi	100	500	100
STATIC RANGE, psi	8000	7500	250
NOMINAL SENSITIVITY, mV/psi	8	10	20
RISE TIME, μsec	1.0	2.0	2.0
DISCHARGE TIME (CONSTANT), sec	1.0	1.0	1.0
ACCELERATION SENSITIVITY (psi/g)	0.05	0.002	0.003
TEMPERATURE RANGE, °F	−100/+250	−423/+212	−100/+250

COMMENT: Jim Lally: Just a couple of comments. Measurements of this type in combination with the thermal shock without a thermal ablative are virtually impossible. This is I think, a good example of the necessity, when you get into a specialized application, of very close cooperation in working with application engineers to discuss the special nature of the measurement. I noted a couple of things in the cryogenic tests were done at -320°F, whereas most of the sensors which were specified were listed as -100°F. So they were somewhat testing out of specifications. I know in our sensors in the cryogenic area have a special cryogenic circuit. These are used by Rocketdyne, incidentally, and others but we have a special cryogenic circuit for the basic reason that standard microelectric circuits under cryogenic temperatures can themselves produce a very high frequency noise. They can fail very quickly. They may operate or they may not, but they can produce a very high frequency noise. Another source of the possibility of high frequency noise I noted from an application by the National Bureau of Standards Laboratory in Boulder, Colorado. They were taking some measurements in a cryogenic fluid where they were plunging the sensor into the fluid and getting a high frequency noise. In that particular situation, they determined there was actually a boiling effect occurring at the diaphragm of the transducer, and in this case the sensor was actually measuring pressure changes that were occurring at its interface with the cryogenic fluid.

COMMENT: Martha Willis (Rockwell International): I'd like to comment on that. First of all, I figured that someone would notice on the general specification that some of the sensors were rated at -100°F. The miniature sensor that I tested was not procured by our laboratory. It was procured by our program people who sometimes have a tendency to look in a catalog and select what they want. And they had worked out with the manufacturer that the sensor was going to perform fine under those cryogenic circumstances; we were simply acting as the calibration lab. The other thing I wanted to let you know is that we are very familiar with the product. I'm one of the people at Rockedyne that uses your sensors, and the comparison sensor that we tested is a modification of your 102 sensor. The unit we were using for a comparison does have your cryogenic circuit in it, and it always performed very well.

Q: Peter Stein: From the description of your test setup, it appear that you can calibrate differential pressure transducers at high-line pressure. Can you superimpose that little pulse on top of a high common line pressure on the differential transducer?

A: Martha Willis: You mean record the output of the differential transducer?

Q: Peter Stein: Well to have a differential pressure transducer to have both sides of it, say at 5000 psi, and then to superimpose on one side of the pressure pulse. Is that possible with your setup?

A: Martha Willis: I'm not quite sure what you're asking. Yes, that is what we do. We have a differential pressure transducer in that system. We come up to line pressure, stabilize it, and then increase the pressure on one side of the system.

COMMENT: Peter Stein: That kind of information is very much needed by of us.

Q: Melton Hatch (EG&G Energy Measurements, Inc.): What was the ablative material that you referred to?

A: Martha Willis: It's one that is recommended in much of PCB literature. It's black electrical tape. We find that the problem with black electrical tape, though, is when you do the cryogenic calibration you have to watch because the masting on the tape starts to pull away from the diaphragm, so you have to keep replacing the tape. Also, we haven't found it has been really effective in environments where the sensor is seeing a really high temperature variation. A material that we have used quite often is called Flexfram. I believe they use it to paint battleships, but it has worked really well for us.

SOFTWARE DESIGN FOR COMPENSATED DEAD-WEIGHT TESTING*

Paul A. Klevgard
Metrology Engineer
Sandia National Laboratory
Livermore, California

ABSTRACT

A dead-weight tester is a precision instrument which generates a known pressure in a fluid by balancing a weighted, movable piston upon that fluid. Many calibration laboratories are faced with the task of writing their own computer programs to do all of the calculations involved in dead-weight testing. Such programs must perform all of the standard compensations: temperature correction for piston area, local gravity correction for the weights, air buoyancy weight correction if the tester is used in the gage pressure mode, and residual bell jar pressure correction when the tester is used in the absolute pressure mode. A choice of units--psi, MPa, KPa--for the pressure output is also desirable. All of these corrections are discussed and the relevant formulas and sources are cited.

In addition, it is possible to design the software so that all of the compensations are accomplished before the calculations begin that select the weights to be added to generate a specific pressure. The result is that integer pressure values rather than decimal fraction pressure values are generated: a very useful feature when calibrating instruments with analog displays (dials). An automated pressure controller for the dead-weight tester's bell jar is also discussed.

INTRODUCTION

The use of a programmable calculator or computer to carry out the calculations involved with dead-weight pressure testing is now commonplace in metrology laboratories. Such programs invariably compute the weights to be used for generating a specific pressure, and they may also carry out the corrections which apply to this pressure.

Nevertheless, there exists a diversity of approaches both in terms of the structure and the function of such computer programs for dead-weight testing.

Here at Sandia National Laboratories, Livermore, a program has evolved which combines the features of several different approaches. This software was designed with three specific requirements in mind. First, it had to be completely generalized, both in terms of units (pounds per square inch, mega-pascals, or kilopascals), and in terms of pressure mode (gauge or absolute). Second, it had to incorporate all the various corrections which are a part of accurate dead-weight testing and make these corrections before the actual assignment of the weights for a specific test. And third, it had to permit the operator to generate integer pressure values as an aid in calibrating instruments with analog displays (dials).

CONTROL OF CONDITIONS

There are four corrections which apply to dead-weight test calculations. The weights must be corrected for local gravity, and--if the testing is for gauge pressure--for air buoyancy. In addition, the piston area must be corrected for temperature. And finally, when the test is run in the absolute pressure mode, the residual bell jar pressure upon the piston must be calculated. The two weight corrections may be expected to remain constant throughout a test interval. The other two corrections will be nearly invariant providing the experimenter observes some precautions during testing.

The temperature of a piston tends to rise during a test as it accumulates heat from friction and from the radiant energy thrown off by the energized drive motor. The experimenter is well advised not to run this motor and rotate the piston except when actually ready to generate a controlled pressure.

For tests in the absolute mode the residual bell jar pressure should be maintained at the level of 100 microns of mercury. This assures an adequate amount of gas lubrication for the piston and provides a known correction value for residual gas pressure upon the piston. Unfortunately, maintaining a 100 micron pressure level is not always easy; an undersized vacuum pump takes too long to get to this level, and an oversized pump will soon pull the bell jar atmosphere down below this level. For this reason, many experimenters use the 100 micron level merely as a target; they record the actual bell jar pressure at the moment of stable piston float and apply an after-the-fact correction to determine the actual pressure their loaded piston generated.

*This work supported by the U.S. Department of Energy under Contract DE-AC04-76DP00789.

At Sandia Livermore we decided to control the bell jar pressure using a Granville-Phillips series 275 vacuum gauge connected to their series 216 automatic pressure controller. A vacuum pump continuously pulls on the bell jar while the pressure controller leaks sufficient dry nitrogen into the jar to maintain a 100 micron Hg pressure level. The unit's pressure sensor is a heat loss Convectron gauge which utilizes conduction cooling at lower pressures and convection cooling at higher pressures. The sensor is mounted on top of the bell jar while the servo-controlled leak valve is rack mounted and connected to the bell jar by a two-foot length of vacuum hose (see Appendix A).

The system has proven very successful and allows the experimenter to devote his full attention to other aspects of the test. A comparison of manual versus automatic control is shown in Figure 1. The solid line shows pressure variations over three minutes for the automatic control system. The broken line shows variations over a similar interval when an operator manually adjusted the valve to the vacuum pump while simultaneously watching the piston float position and recording the reading of the gauge under test. The ordinate units are the analog output in millivolts of the Granville-Phillips pressure display. One hundred millivolts corresponds to a pressure change of approximately 20 millitorr.

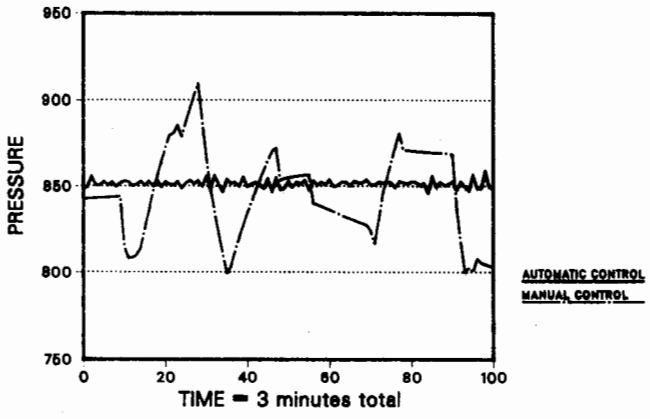

Figure 1. Pressure Level in Dead-weight Tester Bell Jar.

DESIGNING THE SOFTWARE

The program was written in BASIC for the IBM-PC. Earlier versions ran on two Hewlett Packard computers, the 9845 and the 9825. The dead-weight tester used was a Ruska model 2465 capable of both absolute and gauge pressure testing. The program may be easily adapted to other dead-weight testers and to other computers.

The flowchart of Figure 2 depicts the overall structure of the program. Until point B the program is either inputting information or making corrections to the weights or piston. At point B the program enters a loop which is not exited until all of the specified pressure values have had their appropriate weight sequences computed and printed out.

The beginning lines of the program, labeled "INITIALIZE" in Figure 2, accomplish some of the necessary housekeeping duties including dimensioning arrays and specifying integer variables. The next section of the program, namely "ENTER TEST INFORMATION" in Figure 2, accepts all of the information relevant to the instrument or gauge being calibrated. In addition, it records what pressure units are being used and whether the test is conducted in the gauge or absolute mode. All of this information is assumed to remain unchanged throughout any retests.

The next program section accepts input information that is likely to change during a retest. The temperature requested refers to the temperature of the dead-weight gauge's piston which should be checked periodically during the course of a test. By extension, this temperature is also assumed to characterize the ambient air in the buoyancy/atmospheric-weight calculations. The number of tests is also requested here after which subroutine "Assign" (called in line 530) reads the mass values of the instrument's machined weights into array W. Subroutine "Enter" (called in line 550) then allows the operator to enter the specific pressure values desired for the number of tests requested. Since the weight values in array W are in terms of pound-mass in vacuum, if the pressure values requested are in metric units, subroutine "Convert" changes them to pounds per square inch for the purpose of calculations within the program.

At this point in the program (line 580), array W contains the uncorrected pound-mass values for the two pistons and their machined weights. Of course, a one pound mass (in vacuum) exerts a one pound force only in those localities where the effects of gravity are equal to the reference standard value of gravity. The experimenter may obtain his or her local gravity acceleration value in milligals ($1/1000\ cm/sec^2$) from the National Geophysical Data Center in Boulder, Colorado (303-497-6120). The correction factor is then expressed as this value divided by the standard gravity value (980665 milligals). This conversion of mass to force is accomplished in lines 590-660 of the program. An air buoyancy correction factor (F) is applied at the same time.

For this buoyancy correction, the force exerted by a machined weight (or piston) is reduced by the pound-force (weight) of the air it displaces. For tests in the absolute mode, the machined weights are in a bell jar containing such a rare atmosphere (100 microns Hg) that buoyancy effects are negligible. But for tests in the gauge mode, air buoyancy becomes significant, and this correction factor is determined in the subroutine "Gauge". This subroutine requires two additional input quantities assigned to their respective variables: atmospheric pressure in millimeters of mercury (variable PRES) and relative humidity as a percent (variable HUM). With T as the Celsius temperature of the air and V as the vapor pressure of water at these conditions, the density of air in milligrams per cubic centimeter is:

$$Pv = \text{Density}_{(air)} = 0.464554 \times \frac{(\ PRES - .0037803 \times V \times HUM\ )}{(\ T + 273.16\ )}$$

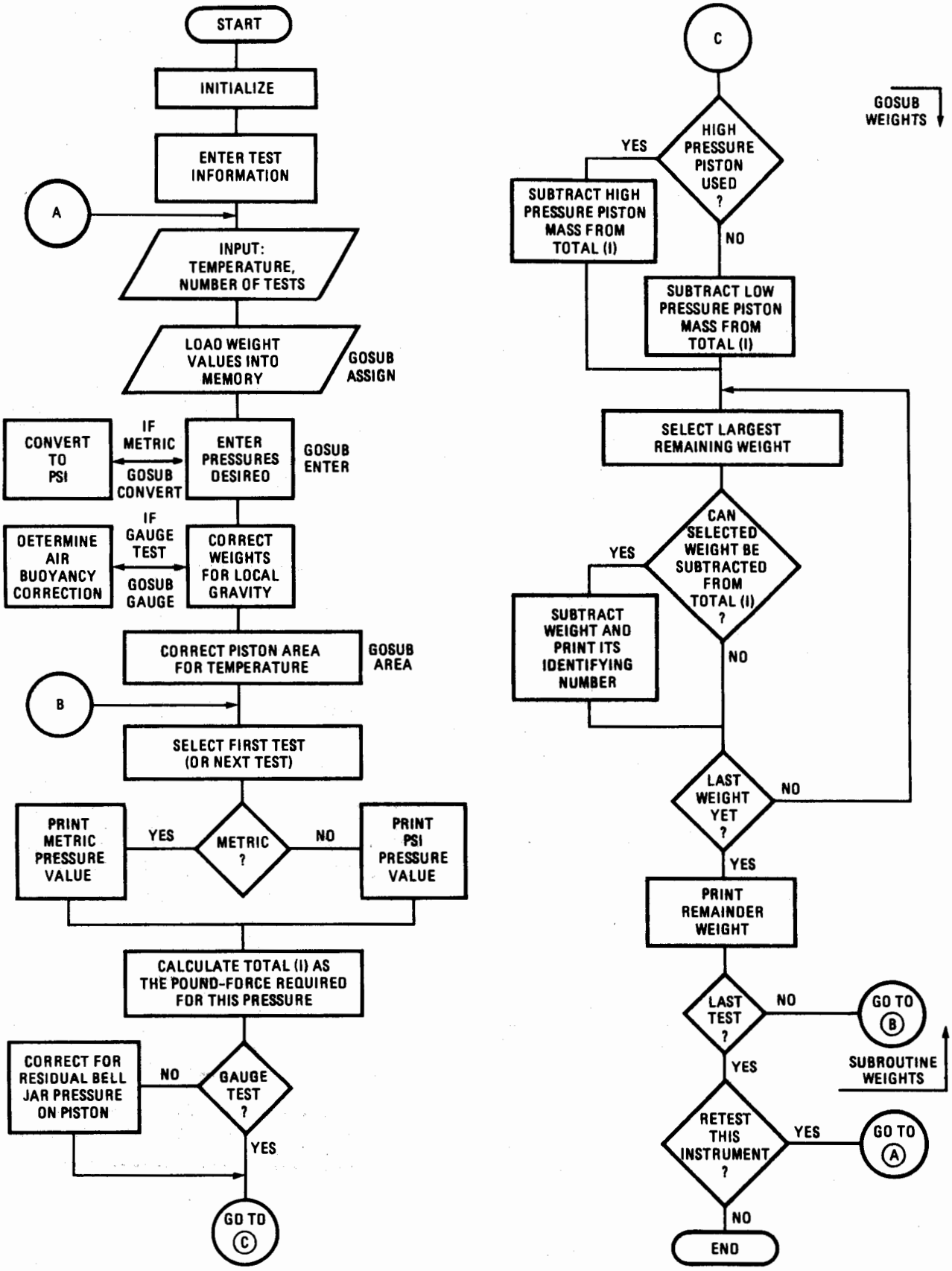

Figure 2. Flowchart of Overall Program Structure

Between 20 and 30 degrees C the vapor pressure of water V may be approximated by the formula

$$V = 1.435 \times T - 11.72.$$

Air density Pv may then be expressed as:

$$Pv = \frac{[.464554 \times PRES - HUM \times (.00252 \times T - .020582)]mg}{(T + 273.16)\ cc} \quad (1)$$

The ratio of this density divided by the density of the machined weights constitutes the buoyancy defect and this defect subtracted from 1 becomes the multiplier (F) which converts mass in vacuum to equivalent mass in atmosphere.

By the time that line 670 of the main program has executed, corrected pound-force values are stored in array W. The next module of the program corrects the measured area of the piston for the effects of thermal expansion or contraction. These calculations, accomplished in subroutine "Area", depend upon piston expansion coefficients furnished by the manufacturer. Upon return from this subroutine, the program is at point "B" of the flowchart which marks the beginning of the output loop.

The counter for this loop is the variable I. Each time through the loop the desired pressure is recalled from memory as the P(I) value of array P. This P(I) value is printed out along with the appropriate units which have been chosen, metric or psi. The pound-force needed to generate the P(I) pressure value is computed as P(I) times the corrected piston area and the result is stored in array TOTAL as TOTAL(I). If this is an absolute test, then pound-force TOTAL(I) must be diminished by the pound-force which the bell jar's residual pressure (100 micron Hg = 0.001934 psi) applies to the piston, namely 0.001934 x piston area. Subroutine "Weights" is then called to divide up the TOTAL(I) pound-force into a specific sequence of numbered machined weights plus a leftover.

Subroutine "Weights" first subtracts the pound-force of either the high or low pressure piston from Total(I). The remaining Total(I) is then tested against the pound-force value of each of the remaining fifteen machined weights taken in descending order. Only if Total(I) is larger than a particular machined weight is the weight number printed out and the corresponding pound-force subtracted from Total(I). Weight number 6, which doesn't exist, is assigned a very large, arbitrary value so it can not be chosen. When all fifteen machined weights have been tested against a diminishing Total(I), the remainder of Total(I) is converted to grams and printed out as a "remaining weight". This remaining weight, selected from a metric weight set, is placed atop the machined weights during a test to achieve the exact pound-force required upon the piston.

At the completion of subroutine "Weights", program execution returns to point "B" of the flowchart to begin evaluation of the next desired pressure value. This continues until each pressure value has its corresponding set of machined weights (plus leftover) printed out. The program then comes to rest at the last decision diamond of the flowchart and, depending upon the input, either ends or returns to point "A" for a retest of the instrument.

REFERENCES

(1) Pontius, Paul E., "Mass and Mass Values," NBS Monograph 133 (1974), p25.

APPENDIX A

DEAD-WEIGHT TESTER PRESSURE CONTROL SCHEMATIC.

The dead-weight tester bell jar is continuously evacuated by the vacuum pump. The pressure signal from the Series 275 transducer goes to the readout which sends the value to the Series 216 controller. The controller compares this value to the setpoint and adjusts the controlled-leak servo system accordingly.

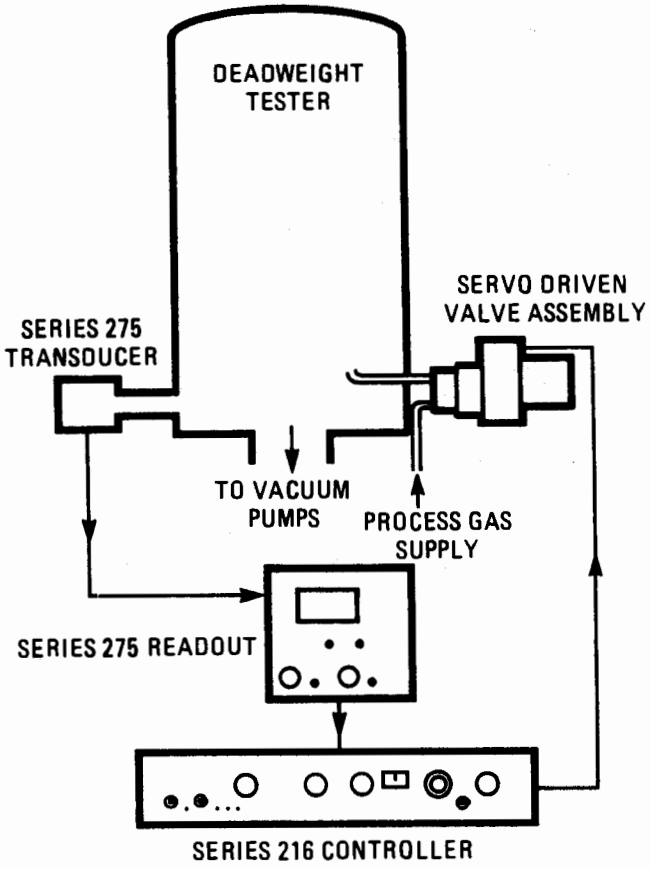

Figure A-1. Vacuum Control System.

GRANVILLE-PHILLIPS SERIES 275
VACUUM GAUGE AND CONVECTION GAUGE TUBE

CONVECTRON GAUGE TUBE: All welded, stainless steel contruction that provides an effective RF barrier for the sensor. No solder flux is used; the sensor is gold plated tungsten wire and the assembly is bakeable to 150° C. The temperature compensated heat loss sensor utilizes conduction cooling to sense pressure at lower pressures. At higher pressures, it utilizes convection cooling in which gas molecules are circulated through the gauge tube by gravitational force. Gauge tube axis must be horizontal for accurate pressure measurements above 1 Torr. A bridge circuit is an integral part of the gauge tube. Accuracy at 760 Torr of nitrogen is about 1%; repeatability is within 1/10 millitorr at 1 millitorr. The unit is computer calibrated at the factory. The sensor plus readout is much less expensive than a capacitance manometer.

DIGITAL READOUT AND CONTROLLER: Aside from displaying the current pressure and scale (mTorr or Torr), this unit contains the electronic feedback loop which keeps the Convectron gauge tube sensor at a constant temperature. Two setpoint on/off switches are provided. The unit contains a 16K read-only-memory (ROM) which is furnished programmed to the correct pressure calibration curve of nitrogen.

GRANVILLE-PHILLIPS SERIES 216 AUTOMATIC
PRESSURE/FLOW CONTROLLER AND SERVO DRIVEN VALVE

AUTOMATIC PRESSURE/FLOW CONTROLLER: A transducer (i.e., Series 275 vacuum gauge and Convectron gauge tube) senses the pressure in the chamber and supplies a corresponding voltage to the Series 216 controller. The controller conditions this input voltage and compares it with the reference voltage dialed in on the front panel. The difference

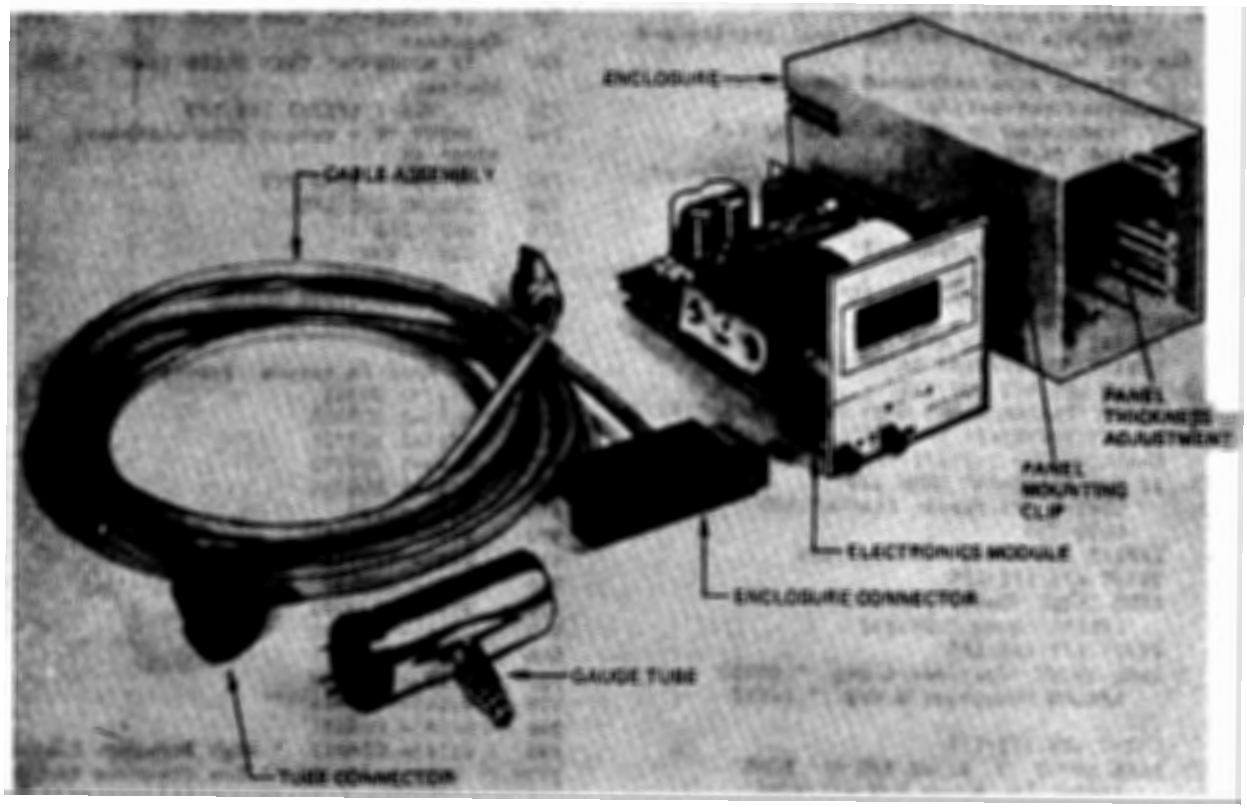

Figure A-2. Digital Readout Convectron Vacuum Guage - Series 275.

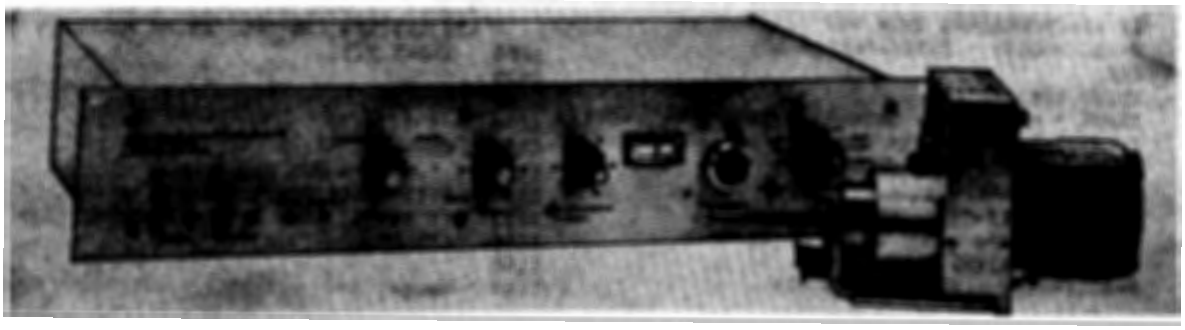

Figure A-3. Automatic Pressure/Flow Controller Series 216.

between the input and the reference voltages is the error signal which is used to control the servo motor drive circuity. When operating at optimum conditions, the controller will control to an accuracy greater than 0.5% of the transducer full scale input signal.

SERVO DRIVEN VALVE: An all metal, bakeable valve capable of controlling pressures from vacuum up to 115 psia. The random drift per day is less than 0.1% full scale of the input signal.

APPENDIX B

DEAD-WEIGHT TEST COMPENSATION PROGRAM - IBM-PC

```
10   OPTION BASE 1 : LF$=CHR$(10)        '   IBM-PC
     "DWT.BAS"
20   '
30      ' RUSKA GAS DEADWEIGHT TESTER
40      ' True Pressure Determination
50      ' Weights corrected for local gravity and
     for air buoyancy.
60      ' Piston area corrected for thermal
     expansion/contraction).
70      ' Translated to MS-DOS BASIC by P.A.
     Klevgard, 03/87.
80      ' SANDIA NATIONAL LABORATORY - LIVERMORE,
CA.
90    '
100    DIM W(20),P(15),TOTAL(15)  : CLS
110    DEFINT I,J,N
120    LPRINT LF$;CHR$(27)+"&l1L"  'HP THINKJET
     PERFORMATION SKIP
130    LPRINT "   RUSKA AIR"
140    LPRINT "DEADWEIGHT TEST";LF$
150    PRINT LF$;LF$;LF$;LF$
160    INPUT "Piston Used? H-Hi Press; L-Lo";PIST$
170    IF ASC(PIST$)<91 THEN 190
180    N=ASC(PIST$) : PIST$=CHR$(N-32)
190    IF NOT PIST$="H" THEN 220
200       LPRINT "Hi Press. Piston";LF$
210       GOTO 230
220    LPRINT "Lo Press. Piston";LF$
230    PRINT LF$;LF$;LF$
240    LINE INPUT "Date:";DATE1$
250       LPRINT "Date:";DATE1$
260    PRINT LF$;LF$;LF$
270    LINE INPUT "Customer & Org.:";CUST$
280       LPRINT "Customer & Org.:";CUST$
290    CLS
300    PRINT LF$;LF$;LF$
310    LINE INPUT "S, R, or S/N #:";NUM$
320       LPRINT "S, R, or S/N #:";NUM$
330    PRINT LF$;LF$;LF$
340    INPUT "Celsius Temp.:";T
350       LPRINT "Celsius Temp.:";T
360    PRINT LF$;LF$;LF$
370    INPUT "G-Gauge; A-Absolute";MODE$
380    IF ASC(MODE$)<91 THEN 400
390    N=ASC(MODE$) : MODE$=CHR$(N-32)
400    CLS
410    PRINT LF$;LF$;LF$
420    INPUT " MPa or KPa Units?  Y-Yes; N-No";MET$
430    IF ASC(MET$)<91 THEN 450
440    N=ASC(MET$) : MET$=CHR$(N-32)
450    PRINT LF$;LF$;LF$
460    IF NOT (MET$="Y") THEN 510
470       INPUT "MPa = M;  KPa = K";E$
480    IF ASC(MET$)<91 THEN 500
490    N=ASC(MET$) : MET$=CHR$(N-32)
500    CLS : PRINT LF$;LF$;LF$
510    INPUT "Number of Tests:";N
520       LPRINT "Number of Tests:";N;LF$
530    GOSUB 820  ' To:  Assign
540    FOR I=1 TO N
550    GOSUB 1030   ' To:  Enter
560    IF MET$="Y" THEN GOSUB 1100  ' To:   Convert
570    NEXT I
580     '
590     ' Air buoyancy correction for gauge test
600    F=1  ' No correction for absolute test
610    IF MODE$="G" THEN GOSUB 1160 ' To: Gauge
620     ' Gravity correction = .9992005 for
     Livermore, Calif.
630     ' Weight Correction Follows:
640    FOR I=1 TO 17 '
650    W(I)=W(I)*.9992005*F  '
660    NEXT I '
670     '
680    ' Piston area correction for temperature
     only.
690    GOSUB 1270   ' To:  AREA
700     '
710    IF MODE$="G" THEN GOSUB 1910   ' To:
     Gagetest
720    IF MODE$="A" THEN GOSUB 1640   ' To:
     Abstest
730       CLS : LPRINT LF$;LF$
740    INPUT "R = retest this customer;   ENTER =
     STOP";S$
750    IF S$="" THEN 780
760    LPRINT LF$;LF$
770    GOTO 340
780    CLS : END
790     '
800     ' SUBROUTINES FOLLOW
810     '
820 ' Assign:  '
830     ' Mass in vacuum; Report of 9/1/81.
840    W(1)=1.30081
850    W(2)=1.300775
860    W(3)=1.300751
870    W(4)=1.300791
880    W(5)=1.300755
890    W(6)=9E+10
900    W(7)=.520288
910    W(8)=.520283
920    W(9)=.260139
930    W(10)=.130085
940    W(11)=.052031
950    W(12)=.052027
960    W(13)=.026015
970    W(14)=.013016
980    W(15)=.006493
990    W(16)=.026013  ' High Pressure Piston Mass:
1000    W(17)=.104055  ' Low Pressure Piston Mass:
1010    RETURN
1020     '
1030 ' Enter:
1040    CLS : PRINT LF$;LF$;LF$;LF$
1050    PRINT USING "& ##&&&&&&&&&";"TEST
     NUMBER";I;CHR$(13);LF$;LF$;LF$
     LF$;LF$;LF$;LF$;LF$;"ENTER PRESSURE  VALUE"
1060    INPUT P(I)
1070    '
1080    RETURN
1090     '
1100 ' Convert: '
1110     ' MPa to PSI conversion
1120    P(I)=P(I)*1000/6.8948
1130    IF E$="K" THEN P(I)=P(I)/1000
1140    RETURN
1150     '
1160 ' Gauge: '
```

```
1170   CLS : PRINT LF$;LF$;LF$;LF$
1180   INPUT "Relative Humidity in percent?";HUM
1190   LPRINT USING "& ##.#&";"Rel.Hum.-";HUM;"%"
1200   PRINT LF$;LF$;LF$
1210   INPUT "Atmos.Pressure in mm Hg?";PRES
1220   LPRINT USING "&###.##&";"Atm.mmHg=";PRES;LF$
1230   PV3=(.464554*PRES-HUM*(.00252*T-
     .020582))/(1000*(T+273.16))
1240   F=1-PV3/7.8
1250   RETURN
1260    '
1270 ' AREA: '
1280  'Piston area= AREA sq.in.; Coefficient of
     thermal expansion = COEF
1290    '  Note: COEF is in units of sq.in./sq.in.
1300   IF NOT PIST$="H" THEN 1340
1310   AREA=.0130135  ' This line for high
     pressure piston
1320   COEF=.0000091
1330   GOTO 1360
1340   AREA=.520646  ' This line for low pressure
     piston
1350   COEF=.00002
1360   A=AREA*(1+COEF*(T-23))
1370   RETURN
1380    '
1390 ' Weights: '
1400   IF NOT PIST$="L" THEN 1430
1410      TOTAL(I)=TOTAL(I)-W(17)
1420      GOTO 1480
1430   IF NOT PIST$="H" THEN 1460
1440      TOTAL(I)=TOTAL(I)-W(16)
1450      GOTO 1480
1460   CLS : PRINT  LF$;LF$;LF$;"Error in piston
     choice;hit CTRL/BREAK"
1470      STOP
1480   IMAGE$="   Wt._#####"
1490   FOR J=1 TO 15
1500   IF NOT (TOTAL(I)>W(J)) THEN 1530
1510      TOTAL(I)=TOTAL(I)-W(J)
1520      LPRINT USING IMAGE$;J
1530   NEXT J
1540      GOSUB 1600  ' To:  Grams
1550   IMAGE$="& ###.### &&"
1560   LPRINT USING IMAGE$;"Remaining
     Wt.=";TOTAL(I);"grams";LF$
1570      LPRINT LF$
1580   RETURN
1590    '
1600 ' Grams: '
1610   TOTAL(I)=TOTAL(I)*453.592
1620   RETURN
1630    '
1640 ' Abstest: '
1650    ' With bell jar at 100 microns, psi on
     piston = .001934
1660   FOR I=1 TO N '
1670   TOTAL(I)=A*(P(I)-.001934)  '
1680   IF MET$="N" THEN GOSUB 1740  ' To: Psia
1690   IF MET$="Y" THEN GOSUB 1800  ' To: Mpabs
1700   GOSUB 1390   ' To:  Weights
1710   NEXT I
1720   RETURN
1730    '
1740 ' Psia: '
1750   LPRINT "PSIA Pressure-"
1760   IMAGE$="   ###.##"
1770      LPRINT USING IMAGE$;P(I)
1780   RETURN
1790    '
1800 ' Mpabs: '
1810   IF E$="M" THEN GOTO 1860
1820   LPRINT "KPa Absolute-"
1830   IMAGE$="   ######.###"
1840      LPRINT USING IMAGE$;P(I)*6.8948
1850   RETURN
1860   LPRINT "MPa Absolute-"
1870   IMAGE$="   #.###"
1880      LPRINT USING IMAGE$;P(I)*.0068948
1890   RETURN
1900    '
1910 ' Gagetest: '
1920   ' For gauge test, atmospheric pressure plus
1930   ' zero weights equals zero gauge pressure.
1940   FOR I=1 TO N
1950   TOTAL(I)=A*P(I)
1960   IF MET$="N" THEN GOSUB 2020  ' To: Psig
1970   IF MET$="Y" THEN GOSUB 2080  ' To: Mgage
1980   GOSUB 1390  ' To:  Weights
1990   NEXT I
2000   RETURN
2010    '
2020 ' Psig: '
2030   LPRINT "PSIG Pressure-"
2040   IMAGE$="   ###.##"
2050      LPRINT USING IMAGE$;P(I)
2060   RETURN
2070    '
2080 ' Mgage: '
2090   IF E$="M" THEN GOTO 2140
2100   LPRINT "KPa Gauge Press-"
2110   IMAGE$="   ######.###"
2120      LPRINT USING IMAGE$;P(I)*6.8948
2130   RETURN
2140   LPRINT "MPa Gauge Press-"
2150   IMAGE$="   ##.###"
2160      LPRINT USING IMAGE$;P(I)*.0068948
2170   RETURN
```

COMMENT: Donald Busse: I would like to share some of the problems that we've experienced on some of our dead-weight testers. One that I hadn't seen in the literature before is an error dead-weight tester. We found an electrostatic effect on the suspended weights that are electrically isolated during suspension. We think the effect probably comes about because of the automatic drive mechanism which uses a rubber o-ring as a drive wheel. We might be depositing a static charge on the weights, and we've observed errors that are equivalent to about 150 microns back pressure in the bell jar. And this usually gives sort of an additional weight to the system. Another effect that we like to compensate for, although it is not a very large effect, is in a liquid system. Using a liquid system always does compensate for height but we sometimes forget to compensate for height even in an error system when we are calibrating dry. And again, a height change from the piston to the calibrated transducer of one foot, is equivalent to back pressure of about 25 microns. Both of those things we ran across ourselves, and I don't know if you've had similar experiences.

COMMENT: Paul Klevgard (Sandia National Laboratory, Livermore, CA): Yes, I for one would be interested in any other comments on electrostatic. I had not heard that before.

COMMENT: Roger Noyes: I just have a comment. We've worked a little bit with Paul over the years and exchanged some things. And I have a very similar program, not as fancy; however, it is written in Pascal too, if that would be of help to anyone.

COMMENT: Vern Bean (National Bureau of Standards): I know something about an electrostatic problem. This occurs very often in the Bell & Howell, CEC 50 psi piston gage. When the rotating weight hanger comes down, it rubs on those two or four plastic buttons on top of the cylinder. An electrostatic charge is generated on the tops of those plastic buttons which gives you electrostatic forces as much as 25 parts per million of one atmosphere. The obvious way to correct that is to remove the buttons, don't let the weight hang or rub on the buttons, or coat the buttons with aluminum or some conducting layer so the charge leaks away. There is another paper by Chris Suntan of New Zealand who also talks about electrostatic effects on piston gauges. He runs a fine stainless steel wire over his weight hanger just prior to measurement.

Q: Paul Klevgard: Was this a problem for the Ruscoe Denway testers too or mostly the CEC?

A: Vern Bean: We have never seen it in a Ruscoe, only in the CECs. We have coated our stops to avoid that problem. This problem was reported at the ISC meeting in San Diego, two years ago by Welsh Gildner and myself.

Q: Daniel Cook (Proportion-Air, Inc.): Could you tell me whose servo valve you used on that bell jar problem?

A: Paul Klevgard: That I believe was a Grandville Phillips servo as well. It is a complete system.

Q: Daniel Cook: Do you know more specifically how well that was regulated? You showed it in an overhead display there, but I didn't get a good feel for what percentage of regulation that was.

A: Paul Klevgard: I don't have the exact figures, but I would say it was probably within ±2 or 3 microns from the set point.

VERIFYING THE LOW FREQUENCY PERFORMANCE OF PIEZOELECTRIC ACCELEROMETERS

Ernst Schonthal
Product Manager
Bruel & Kjaer Instruments, Inc.
Marlborough, MA 01752 U.S.A.

Abstract

Piezoelectric accelerometers are not capable of a true DC response. The actual low frequency limit is determined by the preamplifier to which the accelerometer is connected and governed by the following parameters:

- The noise floor of the preamplifier (charge amplifiers)
- The input impedance of the preamplifier (voltage amplifier)
- The environment acting on the accelerometer.

When verifying the low frequency performance of a piezoelectric accelerometer it is therefore important to include the associated preamplifier in the procedure.

Introduction

To illustrate the low frequency performance of a piezoelectric accelerometer, a simple RC network can be used where the following equations define the relationship between V, I, Q and C.

V = Voltage I = Current
Q = Charge C = Capacitance of ideal capacitor

$$V = \frac{Q}{C}$$

$$I = \frac{dQ}{dt}$$

$$I = C\frac{dV}{dt}$$

When an ideal capacitor is charged to a voltage V_o, the voltage appearing across the capacitor will be stored. (The leakage resistance is infinite.) However, a real capacitor has a certain leakage resistance. The stored charge will leak away and the voltage drops exponentially at a rate determined by the time constant τ of the system. See Figure 1.

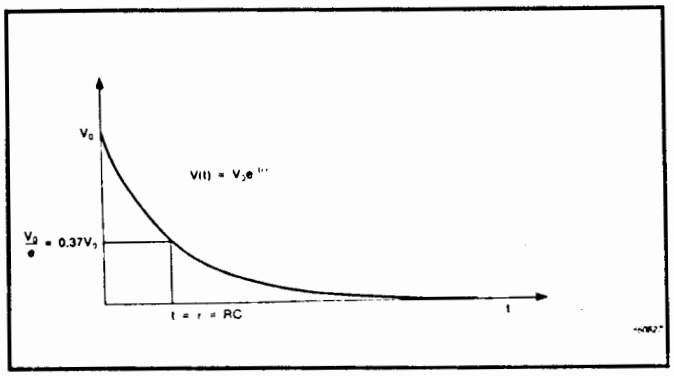

Figure 1. The exponential decay of the voltage across a capacitor, demonstrating the time constant τ

For measurement on sinusoidal signals the time constant τ will affect the low frequency performance of the system.

Figure 2 shows the equivalent circuit of an accelerometer loaded by the equivalent capacitance and resistance of the cable and preamplifier.

Using the definitions given above, the circuit equation can be simply written as:

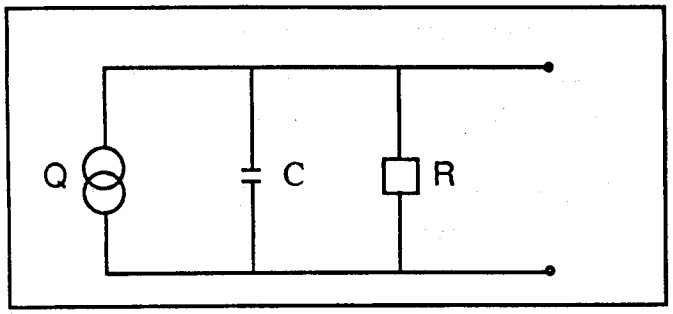

Figure 2. Equivalent circuit of an accelerometer loaded by the equivalent capacitance and resistance of the cable and preamplifier

$$I = \frac{dQ}{dt}$$

$$= \frac{V}{R} + C\frac{dV}{dt}$$

If the currents and voltages are assumed to be harmonic functions, the following can be derived:

$$V = \frac{Q}{\left(1 + \frac{1}{j\omega RC}\right)C}$$

$$= \frac{Q}{\left(1 + \frac{1}{j\omega\tau}\right)C}$$

$$= \frac{Q(1 + j1/\omega\tau)}{(1 + 1/\omega^2\tau^2)C}$$

Initial conditions and DC values are omitted.

The complex expression shows that the output has a magnitude |V| and a phase angle ϕ relative to the input given by:

$$\tan\phi = 1/\omega\tau$$

$$|V| = \frac{Q\sqrt{1 + 1/\omega\tau^2}}{(1 + (1/\omega\tau)^2C}$$

When $\omega\tau = 1$, $\tan\phi = 1$, $\phi = 45^\circ$

$$V = \frac{Q}{\sqrt{2}C}$$

The frequency where $\omega\tau = 1$ ($2\pi fRC = 1$) is

$$f_L = \frac{1}{2\pi RC}$$

$$= \frac{1}{2\pi\tau}$$

This is referred to as the lower limiting frequency (LLF) and is characterized by a 3 dB drop in the output signal level accompanied by a 45° phase shift.

Accelerometer with Charge Amplifier

One of the many advantages of using a charge amplifier with the piezoelectric accelerometer is a very well defined lower limiting frequency. Change in the resistive input load will not affect the lower limiting frequency of the charge amplifier.

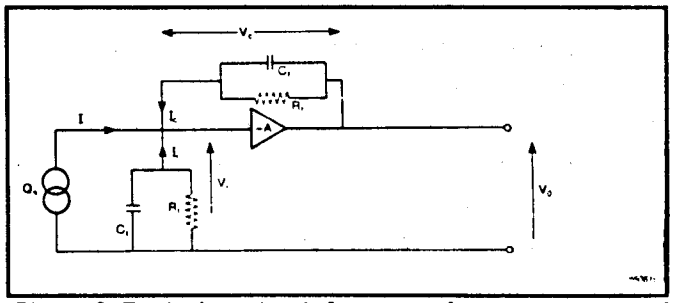

Figure 3. Equivalent circuit for an accelerometer connected to a charge amplifier

Figure 3 shows the equivalent circuit for an accelerometer connected to a charge amplifier. If A and R_f are very large, the output voltage V_o from the charge amplifier is

$$V_o = -\frac{Q_a}{C_f}$$

Since Q_a is proportional to the acceleration of the accelerometer, the overall sensitivity of the accelerometer/preamplifier combination can be controlled by varying C_f. Making R finite, the above expression can be written to include its effect:

$$V_o = -\frac{Q_a}{C_f\left(1 + \frac{1}{j\omega R_f C_f}\right)}$$

Hence, by varying the time constant of the feedback loop in the charge amplifier, the low frequency response of the charge amplifier is controlled.

The sensitivity and lower limiting frequency are not changed significantly by changes in the capacitive and/or resistive loading of the charge amplifier input. However, if the resistive load at the input drops to below 10 MΩ, the noise from the charge amplifier will start to increase with the most significant changes at the lower frequencies.

Contamination in the connectors of the accelerometer and charge amplifier could cause the resistive load at the charge amplifier input to drop, thus increasing the noise from the charge amplifier and reducing the low frequency performance of the system.

Accelerometer with Voltage Amplifier

Compared to the charge amplifier, the voltage amplifier has some operational disadvantages. The overall sensitivity varies with the capacitive load at the input, and changes in the resistive load at the input will alter the lower limiting frequency.

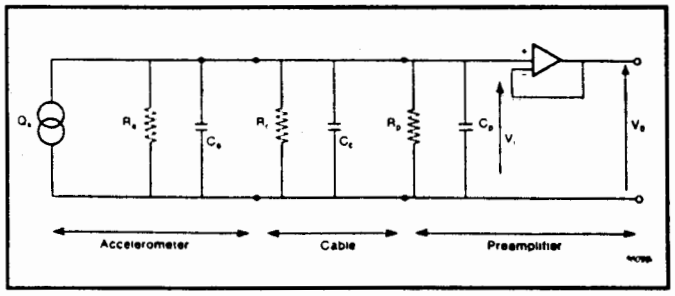

Figure 4. Equivalent circuit of a voltage amplifier using a piezoelectric accelerometer as a voltage source

Figure 4 shows the equivalent circuit of a voltage amplifier with a piezoelectric accelerometer acting as a voltage source. The output V_a from the accelerometer with no cable connected is

$$V_a = \frac{Q_a}{C_a}$$

R_a is a very high parallel resistance and can be ignored. The voltage at the input of the amplifier V_i can be written

$$V_i = \frac{Q_a}{C_a + C_c + C_p}$$

and it can be seen that an increase in the cable capacitance (a longer cable, for example) will reduce the input voltage to the voltage amplifier.

From the discussion above, the lower limiting frequency is expressed as

$$f_L = \frac{1}{2\pi R_t C_t}$$

where

$$C_t = C_a + C_c + C_p$$

and

$$1/R_t = 1/R_a + 1/R_c + 1/R_p$$

To ensure that the voltage amplifier can provide a useful performance down to a frequency of 1 Hz, the RC product must be very large. This is accomplished by designing the voltage preamplifier with a very high input impedance.

From the above, it is seen that increasing C_t by adding, for example, a longer cable between the accelerometer and the preamplifier, the overall sensitivity will be reduced but the RC product will increase. On the other hand, a reduction of R_t due to contamination or temperature will reduce the RC product, resulting in an increase of the lower limiting frequency.

Verifying the Low Frequency Performance of a Piezoelectric Accelerometer with a Charge Amplifier

Unless the low frequency performance must be documented with a chart showing sensitivity vs. frequency, the low frequency performance of an accelerometer and charge amplifier combination can be verified by measuring the leakage resistance of the accelerometer with the cable attached and by measuring the noise floor of the charge amplifier.

The leakage resistance of a piezoelectric accelerometer is normally on the order of 100,000 MΩ at room temperature, and decreases as temperature increases. Under normal circumstances, and within

the normal temperature rating, the leakage resistance will not drop to a level that affects the performance of the charge amplifier. Figure 5 shows an experimentally derived relationship between the narrow band preamplifer noise and the input resistance. The noise is expressed as $V/\sqrt{BW}$.

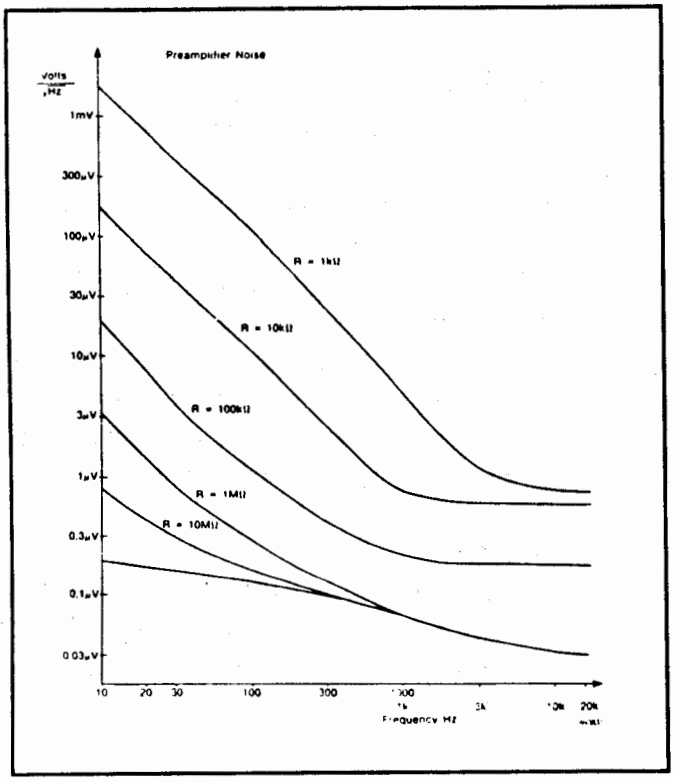

Figure 5. The relationship between input resistance and noise for a charge amplifier

The noise floor of the charge amplifier is measured with a capacitive input load equivalent to the combined capacitance of the accelerometer and the cable used. In practice an input adaptor with a built-in capacitor is often used. The noise floor is normally stated in equivalent pC referred to the input over a given frequency range. The noise can also be stated as unit/$\sqrt{Hz}$.

Verifying the Low Frequency Performance of a Piezoelectric Accelerometer with a Voltage Amplifier

If a self-generating piezoelectric accelerometer is used, the same procedure used for the charge amplifier can be applied. The leakage resistance of the accelerometer is measured. If the accelerometer is used at or close to the maximum temperature rating, its leakage resistance should be measured at the operating temperature.If the input impedance of the voltage preamplifier is known, it is a simple matter to calculate the lower limiting frequency.

The noise floor of the amplifier is measured with an equivalent capacitive input load.

For a piezoelectric accelerometer having integral electronics (impedance converter) it is necessary to make a dynamic measurement in order to verify the low frequency performance.

Contamination inside the accelerometer housing, caused for example by moisture due to condensation during rapid temperature changes, could cause the leakage resistance to decrease, raising the lower limiting frequency.

The associated power supply should be included in the measurement since the coupling capacitor in conjunction with the input impedance of the following instrument forms a high-pass filter governing the lower limiting frequency. This high pass filter will also introduce a phase shift, which will affect the measurement.

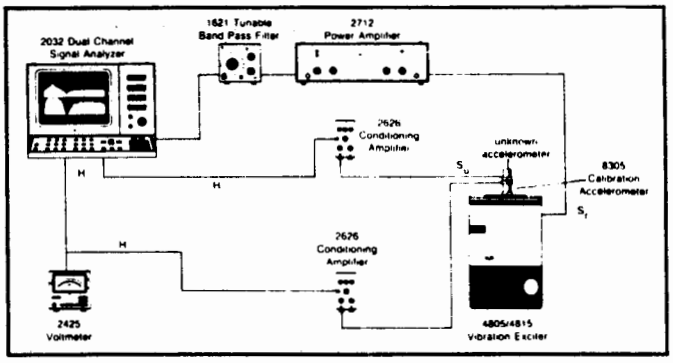

Figure 6. Instrument setup for measuring the low frequency performance of an accelerometer

Figure 6 shows an instrument setup for a low frequency performance measurement of a piezoelectric accelerometer with an associated preamplifier.

A random excitation signal in the frequency range 5 Hz to 100 Hz is used. With the maximum displacement limited to 0.5 inch by the vibration exciter, the acceleration signals produced are very small. Triboelectric cable noise, base bending, and strain applied to the accelerometer connector will affect the measurement result. The operator must pay close attention in order to minimize these effects.

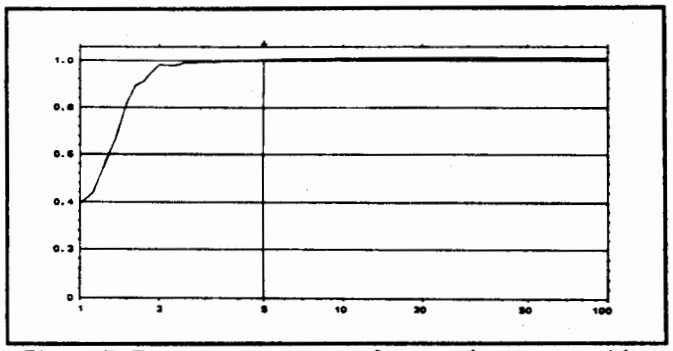

Figure 7. Frequency response of an accelerometer with a charge amplifier

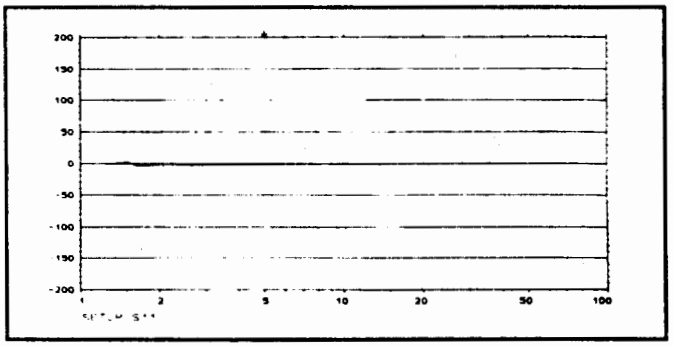

Figure 8. Phase response of an accelerometer with a charge amplifier

Figure 7 shows the resulting frequency response of an accelerometer with an associated charge amplifier.

The relative phase between the unknown accelerometer and the standard reference accelerometer is also available and is shown in Figure 8.

Conclusion

Many factors can influence the measurement of acceleration at low frequencies. A verification of the low frequency performance of the accelerometer and preamplifier combination can greatly improve the confidence of a given measurement and should be part of the measurement procedure. One may argue that the cost involved in the low frequency performance measurement is rather high, but compared to the money invested on a decision based on faulty measurements, the investment is minimal.

References

1. Serridge, Mark, B.Sc.; Bruel & Kjaer Denmark
2. Licht, Torben R., M.Sc.; Bruel & Kjaer, Denmark
3. "Piezoelectric Accelerometer and Vibration Preamplifier Handbook", Oct. 1986

CHARACTERIZATION OF ACCELEROMETER MOUNTINGS IN SHOCK ENVIRONMENTS

V. I. Bateman
Modal and Structural Mechanics Division

O. M. Solomon, Jr.
Telemetry Technology Development Division

Sandia National Laboratories
Albuquerque, NM 87185

ABSTRACT

This report describes the shock test characterization of four accelerometer mounting techniques which are: adiprene and wax, polysulfide rubber and wax, restrained adiprene, and hard mount. The mountings have all been used in field tests, and the shock testing provides some simulation of the field test environments. The characteristics of these mountings are analyzed in the time-domain and in the frequency-domain and are compared to the response of a reference accelerometer at two different shock levels, approximately 2 kg and 7 kg. While soft mounting techniques can be used to guarantee accelerometer survival in severe mechanical environments, this report documents the tested mounting materials to be highly nonlinear. These nonlinearities result in significant data distortion at frequencies above a few hundred hertz.

INTRODUCTION

High shock levels break accelerometers. To measure acceleration in severe environments, it is often necessary to isolate the accelerometer from part of the shock wave. Accelerometers are frequently soft-mounted to accomplish this goal. However, the soft-mounted accelerometer must not be isolated from the physical phenomenon that is to be measured (that is, the desired low frequency portion of the shock wave). In previous work, soft-mount techniques have successfully measured the intended physical phenomenon. Reference [1] describes an experiment in which an accelerometer is appropriately soft-mounted to an aluminum ring. A soft-mount technique has also been used to measure low frequency accelerations [2]. The soft-mount techniques presented in this report are different than those in the referenced work.

The purpose of this report is to demonstrate the time-domain and the frequency-domain characteristics of several different types of accelerometer mountings in high shock environments which are typical of field test conditions. The four different types of accelerometer mountings are: adiprene (DuPont L-100) and wax (Polyethelene Glycol and Vinyl Pyrrolidine), polysulfide rubber (TRA-CON PSR 503/20) and wax, restrained adiprene, and hard mount. All of these mounting techniques have been used for field test in the past. Their characteristics can influence the test data substantially, so it is hoped that the data provided here will allow an intelligent selection of future accelerometer mountings.

This work originated with a desire to determine the response of the accelerometer mountings used for scale model impact tests performed at the Naval Surface Weapons Center. In previous tests, there had been problems with accelerometer response. The tests were impacts of test vehicles into various media so that the resulting acceleration environment contained both large amplitudes and high frequencies. The accelerometers, which were originally specified and which were hard mounted in the scale model, showed a zero-shift; that is, they did not return to zero output after the test environment was removed. Consequently, a different type of accelerometer, an Endevco 2263, was chosen for the scale model tests. The 2263 is a tri-axial, piezoresistive accelerometer which required special mounting techniques in order to survive the impact environments. Two different range 2263's were used: 7.5 kg and 20 kg. The 7.5 kg 2263 (2263-7.5k) was mounted in polysulfide rubber (PSR) and wax; the 20 kg 2263 (2263-20k) was mounted in molded adiprene and wax.

In addition to the two mounting techniques used for the scale model tests, two other mounting techiques were investigated: restrained adiprene and hard mount. The restrained adiprene technique consists of encapsulating the accelerometer in molded adiprene and then placing the encapsulated accelerometer in a metal cannister. A nut closes the top of the cannister and is hand-tightened to restrain the adiprene. The restrained adiprene technique has been used in earth penetrators so that the accelerometer would survive the earth impact and penetration. The Endevco 2263-20k was mounted with the restrained adiprene technique and is evaluated in this report. The hard mount is simply the mounting of an accelerometer directly onto a smooth metal surface (32 finish or better). For example, the Endevco 7270 is attached with two screws. The hard mount technique has been used more often in recent years because improvements in technology allow the accelerometers to survive and to operate in more severe mechanical environments.

All four of the above mounting techniques were tested in the shock lab with a special fixture designed specifically for the mounting characterization. The response of the accelerometers is compared to the response of a Kistler 805A accelerometer mounted on the shock table on which the test fixture was located. Comparisons of the Kistler 805A output to the output from each accelerometer mounted with the techniques under study are made both in the time-domain and in the frequency-domain.

ACCELEROMETER CALIBRATION

There were four accelerometers used for this study. Each of the accelerometers was calibrated in the Sandia's Transducer Calibration Laboratory. A Kistler 805A calibration is shown in Figure 1. The 805A has a range of 100 kg and a resonant frequency of 60 kHz; it's frequency response is typically flat to 10-12 kHz. The 805A is a piezoelectric accelerometer which was developed for shock testing and is used as a secondary standard for calibration as well as the reference accelerometer in the Shock Lab. The calibration shown in Figure 1 is for an 805A (S/N 5043) used as a reference in this study and shows typical 805A characteristics.

The calibration for the 805A was performed on the Ball Drop Calibrator. This calibrator was developed by the Transducer Calibration Laboratory and is used for high-g accelerometer calibration (10-12 kg maximum). Typical pulse widths achieved for the calibrator are 200-300 microseconds so that the maximum input frequency excitation is generally 3-5 kHz for any particular g-level drop. The reference accelerometer is the Endevco 2270 which is a piezoelectric accelerometer with a range of 15 kg. Calibration consists of a series of drops at different shock levels. The data from both the reference and test accelerometers are filtered at 10 kHz with a 6-pole Butterworth filter. The sensitivity is defined as the slope of a least-squares, straight-line fit to a plot of measured peak output in volts as a function of peak g-level. If the transducer has sufficient output at the lower acceleration levels available on the vibration shaker, its sensitivity is also measured from a steady-state sinusoidal input. Calibration standards require the sensitivity measured with the Ball Drop Calibrator to be within 8% of the sensitivity measured on the Unholtz-Dickie shaker described below.

Figures 2 and 3 show calibrations for the two different versions of the Endevco 2262 triaxial, piezoelectric accelerometer; both were performed at 50 g's on the Unholtz-Dickie shaker. The Unholtz-Dickie shaker has a 300 pound-force exciter with a three-quarter-inch, maximum, peak-to-peak, displacement over a frequency range of 2 Hz to 10 kHz. The sensitivity of the accelerometer being calibrated is calculated with the acceleration sensed by the reference accelerometer, an Endevco 2270, at specific frequencies in the 2-10 kHz range. Figure 2 shows the calibration for the Endevco 2263-7.5k coated with PSR. The 2263-7.5k has a range of 7.5 kg and a resonant frequency of 70 kHz. As can be seen from Figure 2, the PSR adds a resonance with a sensitivity gain of 3.41 to the frequency response at about 3kHz. Figure 3 shows the calibration for the Endevco 2263-20k encapsulated in molded adiprene. The 2263-20k has a range of 20 kg and a resonant frequency of 100 kHz. Figure 3 shows that a resonance at about 3 kHz with a sensitivity gain of 5.23 has been added by the molded adiprene. The purpose of these two calibrations was to ensure that the accelerometers were functional before they were used for shock tests. It was not possible to remove the adiprene and the PSR from the two 2263's for the calibrations, so the calibrations were performed with these two soft-mount materials. Thus, the resonances found in the calibration do not characterize

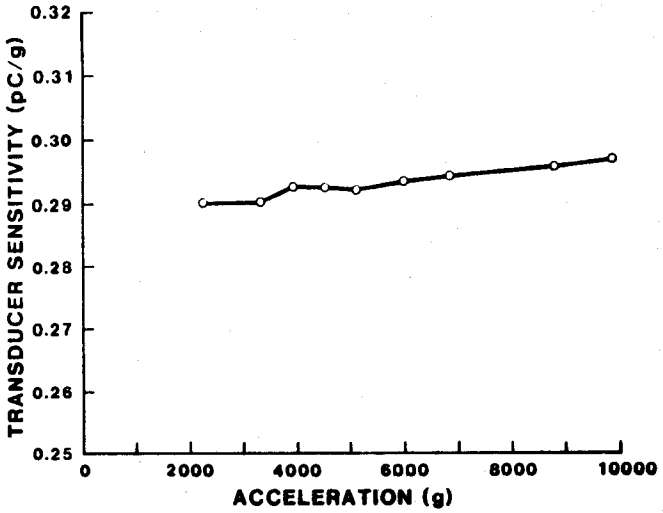

Figure 1. Ball Drop Calibration of Kistler 805A (S/N 5043) Reference Accelerometer (1/29/86).

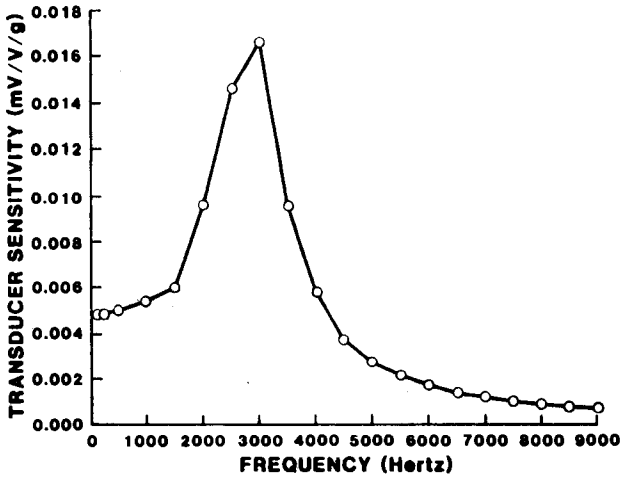

Figure 2. Unholtz-Dickie Shaker 50 g Calibration for the X-Axis of the Endevco 2263-7.5k Accelerometer (S/N AB-21) Coated with Polysulfide Rubber (3/6/86).

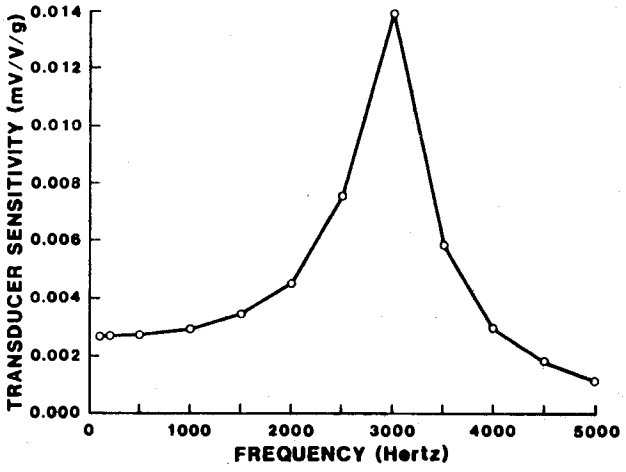

Figure 3. Unholtz-Dickie Shaker 50 g Calibration for the X-Axis of the Endevco 2263-20k Accelerometer (S/N AA-08) Encapsulated in Molded Adiprene (2/3/86).

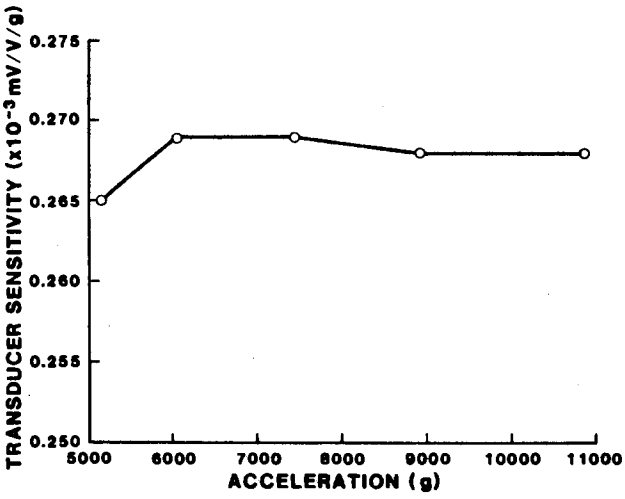

Figure 4. Ball Drop Calibration of Endevco 7270 (S/N AAD 91F) Accelerometer (4/8/86).

either the accelerometer response alone or the response of the complete soft-mount technique used in field test. However, since the amplifications occur at low frequency and low acceleration, the resonances are significant and indicate a potential for data distortion.

Figure 4 is the the calibration for the Endevco 7270 which was performed on the Ball Drop Facility. The 7270 has a range of 70 kg and a resonant frequency of about 800 kHz. The calibration shows that the sensitivity of the 7270 is constant to within + or - 0.5% of fullscale over the calibration range of 11 kg.

ACCELEROMETER MOUNTINGS SHOCK TESTS

The characterization of the accelerometer mountings was accomplished with shock table testing in the Shock Lab. Originally, the scale model was to be used for the shock table testing. However, the initial measurement of the response of the accelerometers in the scale model to drops on the shock table showed considerable structural response. The structural response resulted from the scale model itself and the fixture which restrained it on the shock table as shown in Figure 5. In order to minimize structural response effects, two fixtures were designed to test the accelerometer mountings on the shock tables; these fixtures are shown in Figures 6 and 7. Both fixtures are made of Type 304 Stainless Steel (QQ-S-763) which is the same material as that used for the scale model nose. The 28.6 mm thick flanges on the fixtures simulate the scale model nose thickness; the large flange diameter is required for the hole pattern on the shock table. The depth of the hole for the fixture in Figure 6 allows the accelerometers to be potted with the same depth of wax as that in the Sea Lance scale models. Likewise, the fixture shown in Figure 7 simulates the geometry of a typical earth penetrator cavity for restrained adiprene.

The shock table test procedure will be described for one accelerometer mounting; the procedure was essentially the same for all mountings tested. The fixture was mounted on the shock table with four, 9.5 mm (3/8 in.) bolts. The Kistler 805A reference accelerometer was mounted on the table as close to the fixture as possible. A one-point electrical calibration of the instrumentation system at 1 kHz was performed for the maximum anticipated g-level which was 10 kg for all of the accelerometer mountings tested. This sensitivity was used to convert the data stored on the Nicolet digital oscilloscope to physical units (g's).

To ensure that all accelerometers were operating properly, the initial shock test was at a level of about 1 kg with a pulse width of 5 msec. This low-level, long-duration shock was properly sensed by all accelerometers regardless of mounting. Since the response to this initial shock was the same for the accelerometer in the mounting under test and the reference accelerometer (Kistler 805A), all portions of the test configuration were considered to be operating correctly. As part of this test, the zero levels before and after the shock were checked to ensure that they were the same.

Subsequently, five shocks of near identical waveform with a pulse width of 0.5 msec were measured at each of two levels: 2 kg and 7 kg (approximately). The two responses from the accelerometer in the mounting under test and from the reference accelerometer were stored on a floppy disk in the Nicolet oscilloscope for data reduction.

DATA ANALYSIS

The data on the Nicolet floppy disks were converted to ASCII format in order to perform the analysis on an IBM-PC. The data were converted to physical units, g's, with the sensitivity calculated from the shock lab instrumentation system calibration at 1 kHz. For each shock level and for each accelerometer or accelerometer mounting response, the five shock tests were averaged.

The time-domain linearity analysis procedure is outlined in Figure 8. The basis for the procedure is that, if r(t) is the response of a linear system to the excitation a(t), then c*r(t) is the linear system's response to the excitation c*a(t). To use the procedure, the system under analysis must be excited by two signals that have the same shape (that is, a(t) and c*a(t) differ only by a scaling factor). The system H is linear provided that the two accelerometer mounting responses, normalized as shown in Figure 8 by the corresponding peak values of the table accelerations, a(t) and c*a(t), are equal. If the system is nonlinear, then amplification (or attenuation) of the peak pulse value, as well as distortion of the pulse shape occurs. In this test configuration, the two table accelerations are operated on by a

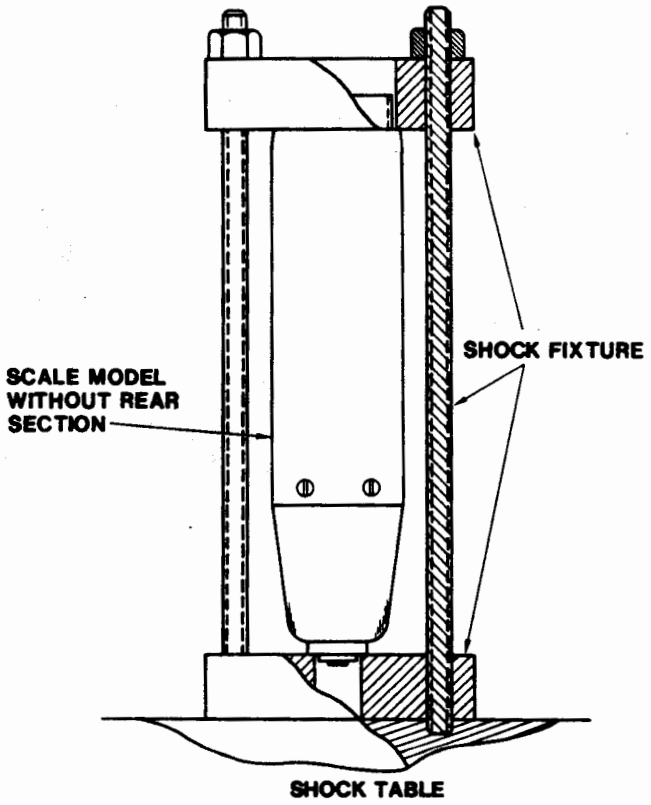

Figure 5. Configuration for Shock Tests of Scale Model.

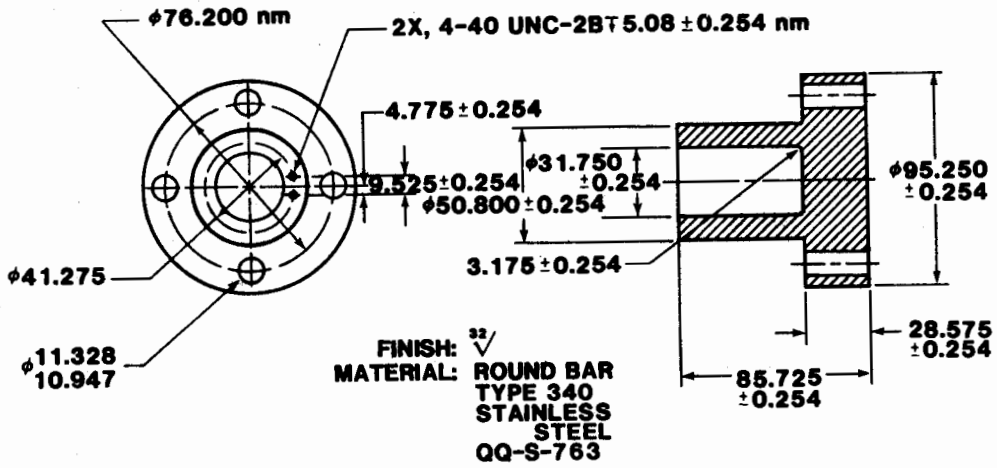

Figure 6. Fixture for Shock Tests of Accelerometers Mounted in Wax and Hard Mount.

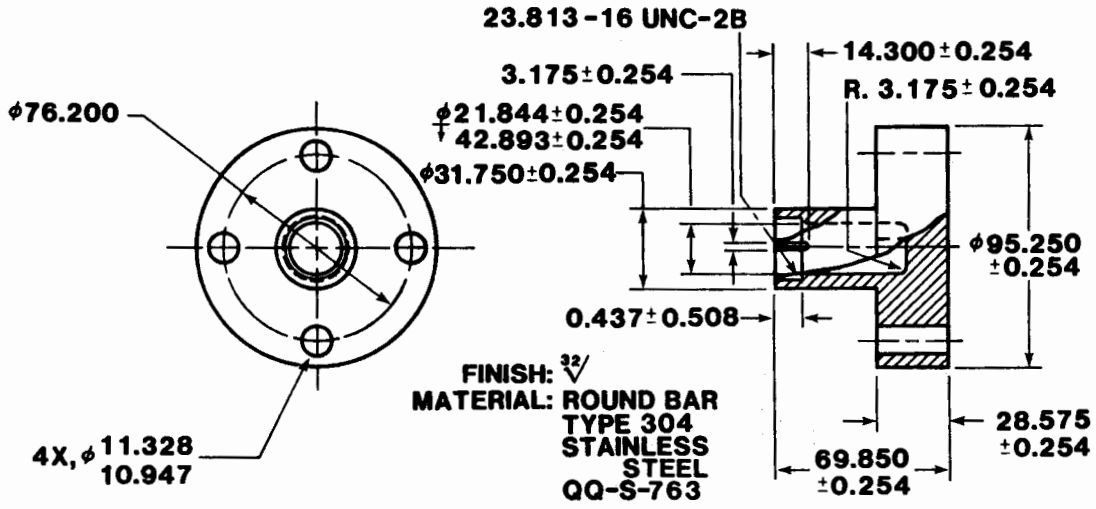

Figure 7. Fixture for Shock Tests of Restrained Adiprene Accelerometer Mounting.

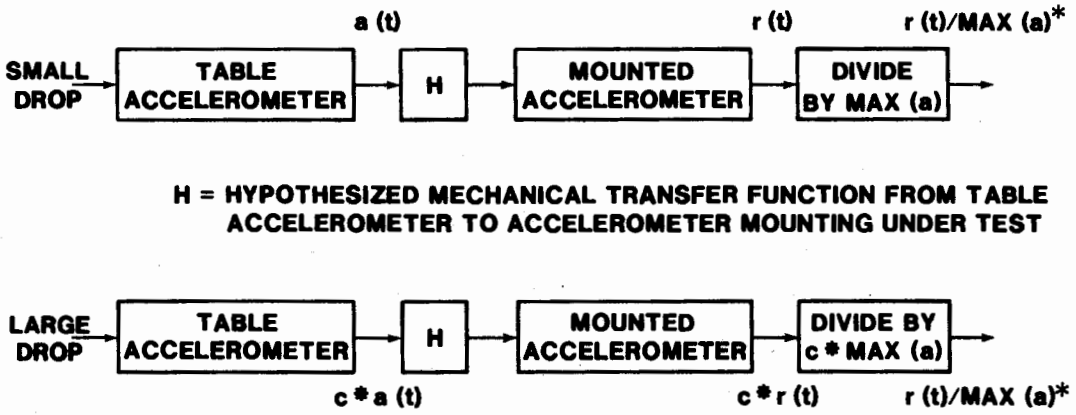

Figure 8. Time-Domain Linearity Test Block Diagram and Procedure for Normalization of Accelerometer Mountings Time Response with Kistler 805A Accelerometer Reference Response.

linear transfer function which represents the mechanical structural response between the reference accelerometer on the table and the accelerometer mounting under test. As a consequence, the measured accelerometer responses differ by the same constant scaling factor, c, as the table accelerations. A mounting, which has a linear response, should have identical time responses for the two shock levels after normalization. The responses were normalized by the average peak value in g's for the 805A reference accelerometer as shown in Figure 8. The peak values varied somewhat for each accelerometer mounting test and are shown in Table 1.

Additionally, the averaged, time-domain responses for the reference accelerometer and the accelerometer mountings were transformed into the frequency-domain; a frequency-domain linearity analysis was then conducted on the data as shown in Figure 9. The two block diagram paths are for the two shock levels and show how a frequency response function is calculated between the reference accelerometer and the accelerometer mounting. The frequency response function, defined here as the mounted accelerometer's Fourier transform divided by the reference accelerometer's Fourier transform, should have the same value at each frequency for the two shock levels if the accelerometer mounting is linear. If the magnitude of both the frequency responses of the transducer is unity, then the calibration of the transducer is accomplished by applying a simple scale factor to each measurement. When the shape of the magnitude of the frequency responses of the transducer is the same but not unity for all frequencies, the calibration of the transducer is frequency dependent (for example, 1 g/V at 1 Hz but .1 g/V at 1000 Hz). If the frequency response function is not linear over the range of input shock levels, then the interpretation of the accelerometer mounting response becomes impossible in many cases because, in field test, the input shock level is generally unknown.

RESULTS

The results of the data analysis are time-domain and frequency-domain plots of normalized accelerometer response. Since the data for each level and each accelerometer or accelerometer mounting was averaged, all data discussed in this section represents the average of five shocks at the same level. In all subsequent figures, both levels of shock tests, 2 kg and 7 kg, are shown. The lower level, about 2 kg, is represented by a solid line; the higher shock level, about 7 kg, is represented by a broken line. Figures 10-13 are time-domain data which have been processed according to the procedure shown in Figure 8. Figure 14 is frequency-domain data which have been processed according to the procedure shown in Figure 9.

Figure 10 is the normalized 805A reference accelerometer time-responses for all four accelerometer mountings tests which have been filtered at 10 kHz. Because of the normalization, all the peak values are 1.0. The pulse shapes show exceptional repeatability between the two levels for each mounting test and indicate that input shock to the different mountings was well-defined and had essentially the same frequency content. This is further verified by Figure 11 which is the same data as that in Figure 10 filtered at 1 kHz. Figure 11 shows that the pulses have consistent shape at the two levels for a particular mounting and for the different accelerometer mountings tested.

Figures 12 and 13 are the time-responses of the four accelerometer mountings to two shock levels. The responses have been filtered at 10 kHz for Figure 12 and at 1 kHz for Figure 13. Since the plots have been normalized with the amplitude of the 805A response, they show amplification relative to the 805A. The most significant amplification in Figure 12, about a factor of 2.5, occurs for the PSR and wax and for the adiprene and wax mountings at the lower shock level of about 2 kg. The amplification decreases for these two mountings to about 1.5 at the high shock level of about 7 kg. The restrained adiprene mounting in Figure 12 shows an amplification of about 1.5 at the higher shock level and a slight attenuation at the lower shock level. However, the restrained adiprene has a significant amount of higher frequency content in its response. The hard mounted 7270 has an average peak value of 1.0 for the two shock levels, so it has essentially the same pulse response as the 805A.

In Figure 13, the time-responses of the four accelerometer mountings have been filtered to 1 kHz. First, it is important to note that the hard mounted 7270 response is not detectably different from the 805A shown in Figure 11. This indicates that the fixture used for these tests does not influence the accelerometer response in the time-domain and that the hard mounted 7270 duplicates the reference 805A response for these test conditions. The

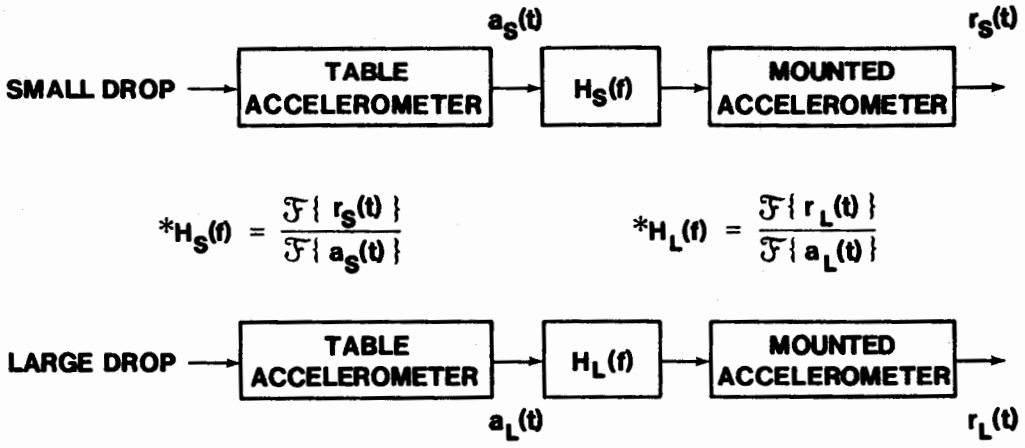

Figure 9. Frequency-Domain Linearity Test Block Diagram and Procedure for Transfer Function Calculation with Kistler 805A Accelerometer Reference Spectrum.

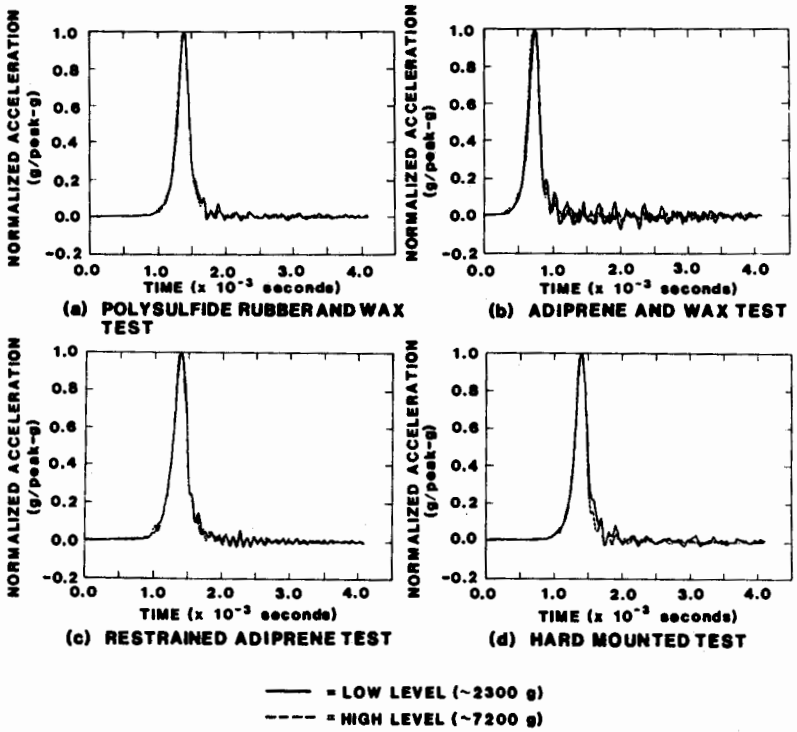

Figure 10. Normalized Time Histories of Kistler 805A Reference Accelerometer for Four Accelerometer Mountings Shock Tests and for a Filter Cutoff Frequency of 10 kHz.

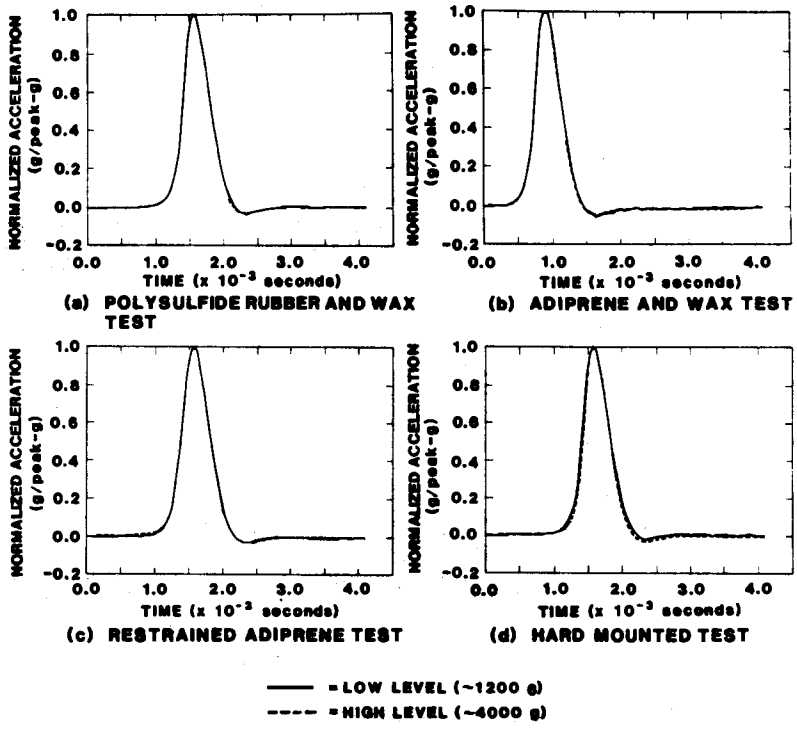

Figure 11. Normalized Time Histories of Kistler 805A Reference Accelerometer for Four Accelerometer Mountings Shock Tests and for a Filter Cutoff Frequency of 1 kHz.

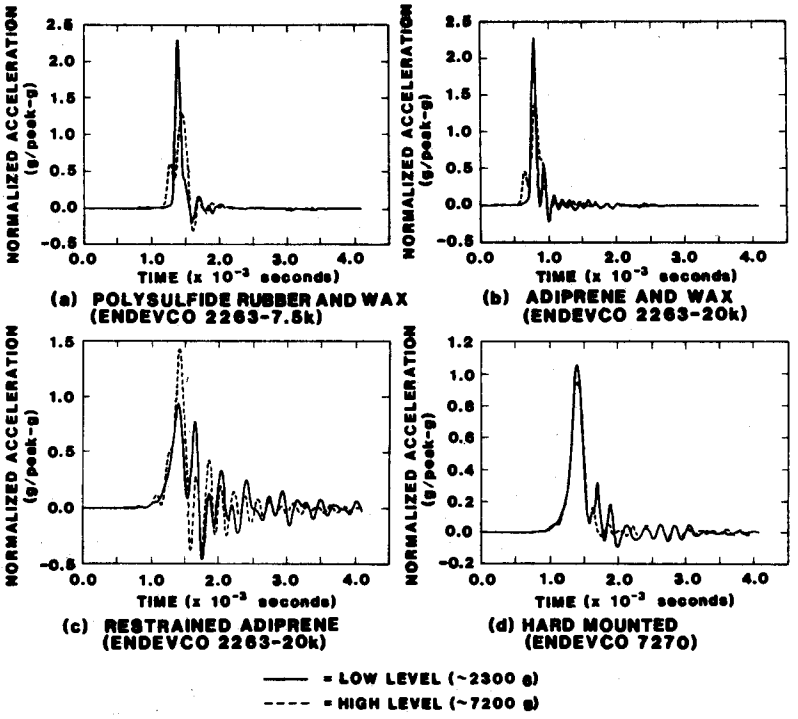

Figure 12. Normalized Time Histories for Four Accelerometer Mountings and for a Filter Cutoff Frequency of 10 kHz.

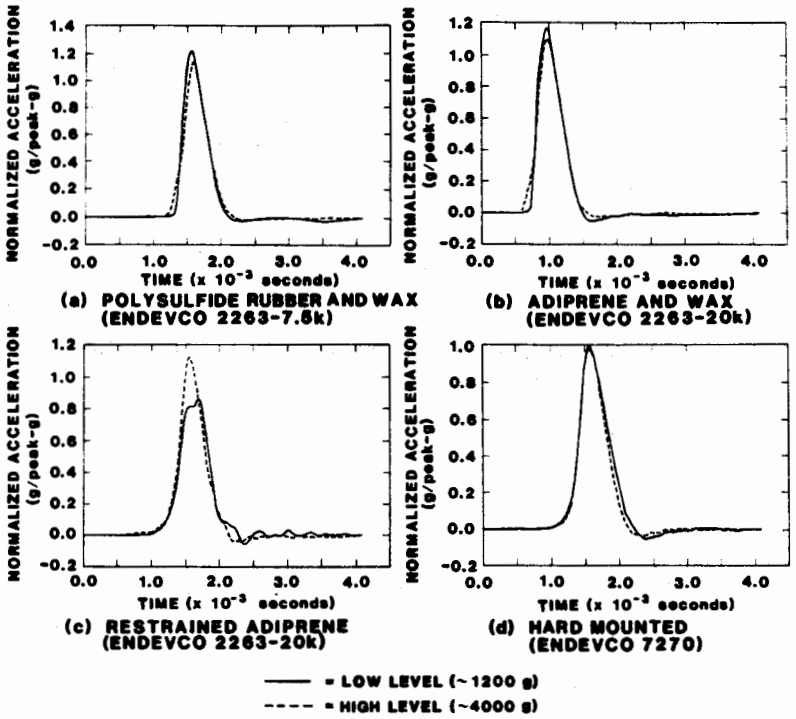

Figure 13. Normalized Time Histories for Four Accelerometer Mountings and for a Filter Cutoff Frequency of 1 kHz.

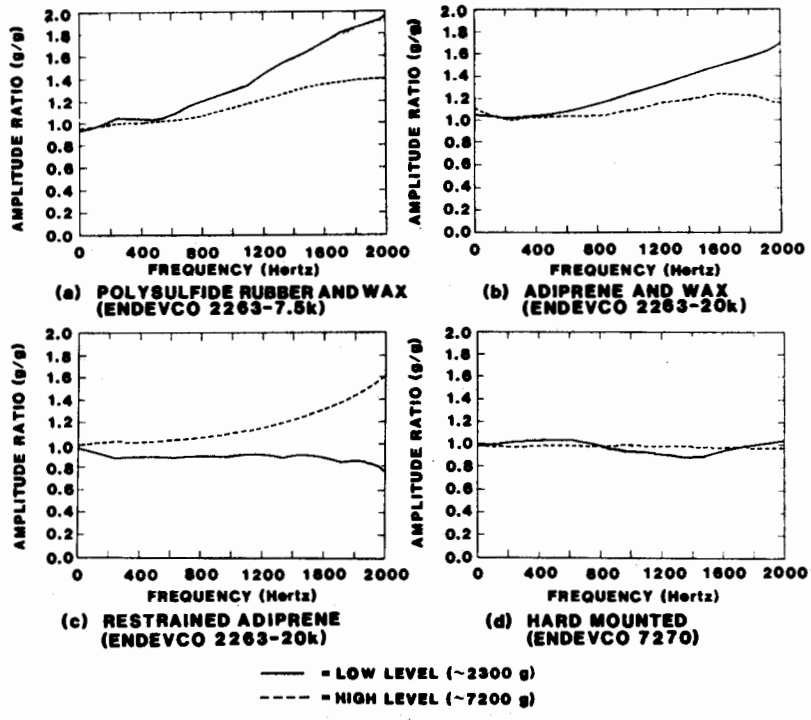

Figure 14. Transfer Functions (Mounted Accelerometer Spectrum/Reference Kistler 805A Spectrum) for Four Accelerometer Mountings.

amplification for the other mountings is about 1.2 for all mountings and levels except for the restrained adiprene which shows an attenuation of about 0.8 for the lower shock level as well as a distortion of the peak shape.

The magnitude of the frequency response function for each accelerometer mounting is shown in Figure 14; the frequency response function is defined as the mounted acclerometer's Fourier spectrum divided by the 805A reference acclerometer's Fourier spectrum at one of the two shock levels, 2 kg or 7 kg. The frequency response functions are shown to 2 kHz because the individual responses indicate a consistent attenutation of about 30% by 2 kHz, so the input and response measurements do not have significant energy content for the frequencies above 2 kHz. The magnitude of the frequency response function for the hard-mounted 7270 is about 1.0 for all frequencies and both shock levels which again indicates that there are no significant structural response frequency components from the fixture in the 7270 response. The wax and adiprene mount shows divergence in the frequency response function between the two levels above about 400 Hz.

CONCLUSIONS

The results of the characterization of the four accelerometer mountings indicate that the accelerometer response is valid over a limited frequency range for the shock levels tested. Table 2 gives approximate frequency ranges and expected peak amplifications for the four accelerometer mountings. Clearly, the hard mount has the best characteristics of the four accelerometer mountings tested because it reproduces the input shock peak and has a linear transfer function for the two shock levels tested.

The PSR and wax mount, and the adiprene and wax mount have approximately the same characteristics; they both amplify the input shock peak and show linear transfer function behavior to frequencies greater than 1 kHz. Data measured with accelerometers in these two mountings could be improved with scaling by the average amplification factor as long as it was not used for frequencies greater than 1.2 kHz as shown in Table 2.

The restrained adiprene mounting has the worst characteristics. Because it amplifies for one level input and attenuates for the other level input, it would be impossible to scale the accelerometer response measured in field test unless the field shock level was known from another measurement. The restrained adiprene mount also has the most limited linear frequency range.

All four of the mountings that were tested are linear in a low frequency range extending from 0 Hz to approximately 600 Hz. Consequently, all mountings can be double integrated to give accurate velocity and position provided that the accelerations are first filtered at less than 600 Hz. One should not conclude from our study that all measurements made with soft-mounted accelerometers are useless because all soft-mounting techniques were not considered. However, a soft-mount is a significant modification to the acceleration measurement system, and its overall impact on the measurement system must be evaluated before the acceleration data can be used properly. The three soft-mountings studied here are definitely not adequate for determining structural response above 1 kHz.

REFERENCES

1. D. K. Overmier and M. J. Forrestal, "Experiment for Evaluation of Acceleration Measurement Capability," AIAA JOURNAL, Vol. 13, No. 9, pp. 1234-1236, September 1975.

2. D. K. Overmier and P. L. Walter, "A Shock-Isolated Package for an Earth Penetrator Instrumentation System: Design Analysis and Test Results," SAND80-1197, Albuquerque, New Mexico: Sandia National Laboratories, 1980.

Table 1: Peak Acceleration Values Measured by the Kistler 805A Reference Accelerometer and Utilized in the Normalization of Accelerometer Mountings Time-Domain Responses.

Mounting	Low Level		High Level	
Filter Cutoff	1 kHz	10 kHz	1 kHz	10 kHz
PSR and Wax	1367 g	2574 g	3935 g	6995 g
Adiprene and Wax	1044 g	2083 g	3833 g	7068 g
Restrained Adiprene	1398 g	2388 g	4595 g	7626 g
Hard Mount	1302 g	2369 g	4123 g	7637 g

Table 2: Time-Domain Peak Amplification and Linear Frequency Range for Four Accelerometer Mountings.

MOUNTING	TIME-DOMAIN PEAK AMPLIFICATION*		LINEAR FREQUENCY RANGE**
	Low Level	High Level	
Polysulfide rubber and Wax	1.15	1.20	0 - 1.1 kHz
Adiprene and Wax	1.15	1.10	0 - 1.2 kHz
Restrained Adiprene	0.85	1.15	0 - 0.6 kHz
Hard Mount	1.00	1.00	0 - 2.0 kHz

* Data is filtered at 1 kHz.

** Data is unfiltered. Linear frequency range is defined as frequencies where the magnitudes of the low and high level transfer functions differ by less than 0.15.

Q: Torben Licht: What was your criteria for selecting these rubber materials?

A: Vesta Batemen (Sandia National Laboratories): They had been used in field tests.

COMMENT: Torben Licht: If you don't want too much amplification at the resonant frequency of your system, one candidate could be a butadiene rubber which gives a much higher damping.

COMMENT: Vesta Batemen: As I said, the motivation for the work was the desire to analyze the accelerometer data that had already been taken at field tests, so I analyzed the mountings that had been used. Let me explain furthur. It is only in the past year that we've been getting good field test data with accelerometers that are hard mounted so they don't break. So we had to use some kind of technique to get any data at all. These techniques were adapted because they allowed the accelerometers to survive.

Q: Torben Licht: What about temperature ranges?

A: Vesta Batemen: Typically in a penetration event, there is not a significant temperature excursion. The penetration into water or earth is just not long enough for conduction to occur, so temperature is not a significant variable in accelerometer responses.

Q: R. Maglic: Are results reproducible?

A: Vesta Batemen: Well the results that were presented here are reproducible in the sense that the responses to the shocks were consistent. But one of the problems with these soft-mounting techniques is that they are not in themselves reproducible. The PSR was just painted on by hand. Another variable in the mounting technique is that the Endevco 2263 is a Triax and they is hold it. Since they didn't have a reference, they would put it in the wax where it would solidify. Soft mounting is very difficult to reproduce in itself.

Q: Alex Karolys (Endevco): Did you actually come out with the transfer functions? Did you model the equations for the transfer functions using the Fourier transform?

A: Vesta Batemen: Do you mean did I try to fit a model to the transfer functions? No, I was essentially looking for linearity in the response. I was not trying to model the soft-mounting technique.

Q: Ray Reed: Vesta, I think you answered this question indirectly but someone surely will ask it. The Endevco 7270 seems to perform better than any of these. It survived the test that you performed. Why was it not used directly instead of with the soft mounts?

A: Vesta Batemen: I don't think it was available at the time.

COMMENT: Ray Reed: Yes, I believe that's true. The point to be made is that the 7270 is a new accelerometer which has much better survival characteristics under the shock loadings. The other accelerometers were stopgap methods that had to be used to perform certain tests when no other techniques were available.

COMMENT: Peter Stein: You say that the mounting techniques were nonlinear above about 1 kHz. Now, in a nonlinear system if this accelerometer is exposed to the structural resonances to which it is attached, then you'll create difference frequencies between the various structural modes which may appear in the bandwidths below 1 kHz. You'll never really know it if you filtered it.

COMMENT: Vesta Batemen: Yes, that's true. That is why I went to the simple fixtures instead of using the scale model itself to do the test. You're right, additional nonlinearities could be introduced by the test structure itself.

A MICROPROCESSOR BASED DIGITAL PRESSURE TRANSDUCER

Gordon E. Mills

Product Development Supervisor

Paine Corporation

Seattle, Washington

ABSTRACT

A bridge type pressure transducer and a temperature sensor monitored by a local microcomputer chip gives better transducer accuracy than using a remote data converter. Continuous, real-time (local) signal averaging is possible and can preserve system accuracy in the presence of process noise. The transducer's local microcomputer also improves system performance and reliability.

INTRODUCTION

This paper contains insights gained from the soon to be completed design of a "smart" microprocessor based pressure transducer. Because of the small size of this unit, low component count and low power dissipation are crucial. Some key characteristics of this planned product are:

1 single supply, low voltage, low power, ratiometric, voltage to frequency converter technology

2 user programmable data averaging period

3 small, fully hermetic package

4 multiple transducers may be connected to the system controller with one five wire cable

5 immunity against a single transducer failure shutting down entire system

6 interface module to RS-232 or other standards

7 short (two byte) serial asynchronous data query for speed

A discussion of converting physical stimuli into electrical signals that are useful in a control or monitoring system environment can be broken down into three areas:

1 the physical interface, or sensor,

2 the sensor signal converter, and

3 the network and overall control system used for control or monitoring.

First, the sensors presently used in this design are a Wheatstone bridge type piezoresistive pressure sensor and a platinum RTD temperature sensor. These devices have been in use for decades, and modern semiconductor amplifiers have greatly improved the design and performance of the associated signal conditioning equipment.

Some relative advantages of this pressure sensor technology can include; accuracies of better than one percent over a wide temperature range, moderate cost, temperature compensatible output, good long term repeatability, fast (millisecond) response times, direct analog output signal, ruggedness, small size, wide range of pressure media compatibility with or without an isolation diaphragm, hermetic sealing available to keep media and environment away from transducer elements, a wide range of pressures can be designed for, and several hundred volts of electrical isolation from the pressure media.

Some relative disadvantages of this same technology can include; small direct analog output is in the millivolt range and is susceptible to small leakage currents on long cable runs, production techniques for temperature and gain compensation tend to be labor and time intensive, sensor zero and span nonlinearities can be difficult to compensate and require difficult sensor designs, very low frequency low pass analog filters are not practical, and changes in the excitation voltage show up as a proportional variation in the output signal.

Figure 1 shows room temperature and 350 degree Fahrenheit hysteresis curves for a typical bridge transducer that has been compensated using temperature sensitive resistors. Figure 2 shows data for an uncompensated sensor built with very similar geometry but using titanium instead of 15-5 PH. As can be seen from this data, a signal converter with the ability to interpolate from a characterized transducer curve and a characterized temperature curve can result in a device with better than 0.1% accuracy.

Now for the sensor signal converter. A present generation microcomputer (Motorola MC68HC11) is used to control the conversion process, enhance the result, and communicate this sensor information to the system. The local microcomputer presently handles these sensors, but additional transducer inputs and outputs such as pulse trains (rpm), limit switch, 0.25% (8 bit) accuracy analog inputs, and a 12 bit digital to analog (D/A) converter to drive a voltage or current output are possible.

A primary benefit of being able to use a local microcontroller to combine pressure and temperature information to get accurate data is the ability to use a less critical sensor design to reliably support a data acquisition network with an overall accuracy of a few tenths of a percent. While the network controller could potentially perform similar data enhancements, the probability of an error due to an uncertain transducer characteristic would be high. Also, the long signal path from the transducer to a remote analog to digital (A/D) converter is susceptible to sources of error such as uncertainty of independent reference voltages in the separated sensor and converter, leakage currents, and radio frequency fields. In particular, multiplexed data converters which may only see the pressure signal a small fraction of the time are especially prone to aliasing errors if the signal is noisy or changing.

A block diagram of the present transducer design is shown in figure 3. Voltage to frequency converters are used to obtain the pressure and temperature signals. The 125 KHZ (max), hardware controlled, pressure signal converter can give 12 bit accuracy at 20 conversions per second, and provide accumulated averages with no missing counts. The platinum RTD converter uses software controlled feedback to produce +/- 0.5 degree fahrenheit data in less than 5 seconds. Both converters are ratiometric for voltage and clock frequency, so that neither the 5 volt regulator output or the microcontroller oscillator frequency are critical.

A commonly used data converter is the integrating dual slope A/D device, readily available in integrated form. The low leakage and low dissipation factor requirement for this A/D's integrating capacitor tends to make this component relatively large, expensive, and of low reliability and limited temperature range if it uses plastic. Figure 4 shows a dual slope signal conversion timing diagram. Since the input signal is only integrated during a fraction (usually less than half) of the conversion cycle, sensitivity to higher frequency aliasing signals is worsened. If accurate, longer period averages are to be accumulated by the microcontroller, then an anti-aliasing filter needs to be put in front of the converter. This filter compromises performance at high sampling rates and represents additional analog circuit complexity.

Since the voltage to frequency type of converter is continually integrating the input signal and accumulating a total count with no missing pulses, high frequency aliasing effects are relatively reduced in the V/F's long term average. It is possible to have the micro controller monitor for a ratio between two different averaging periods to determine whether there is an ongoing problem with signal or noise aliasing using the averaging period selected.

In any real control situation, the ability to eliminate signal aliasing effects and withstand various sources of noise while maintaining accurate signal information with a known phase relationship is critical. A succinct discussion of the requirements of a real time control system is given in a report written by T. G. Sharpe and G. E. Forquer of Collins Avionics Division of Rockwell. This report is appendix 3 (page 80) of ARINC specification 429.

In a digital communication network implementation, fewer interconnecting wires are needed than would be required to bring out data from the analog pressure transducer (and the RTD for temperature information), especially if the control system uses more than a single sensor. Figure 5 shows a hierarchical digital communications network.

As continually smaller transducers are designed, low power dissipation becomes an important requirement. An elevated internal transducer temperature reduces the external ambient operating temperature range and can also produce undesirable side effects such as high leakage currents in semiconductors, thermocouple voltages from dissimilar metals, etc.

In a hermetic transducer housing that is about 1 inch in diameter and a few inches long, the thermal impedance, to the external ambient, of a component mounted on a circular hybrid wafer inside the housing can be in the range of 18 to 35 degrees centigrade per watt. The present transducer design consumes less than a third of a watt at 5 volts. However, one design parameter that is difficult to control is the power requirements of the serial communications driver.

A temperature compensated 15-5 PH tube type transducer has good wide temperature range stability and hysteresis.

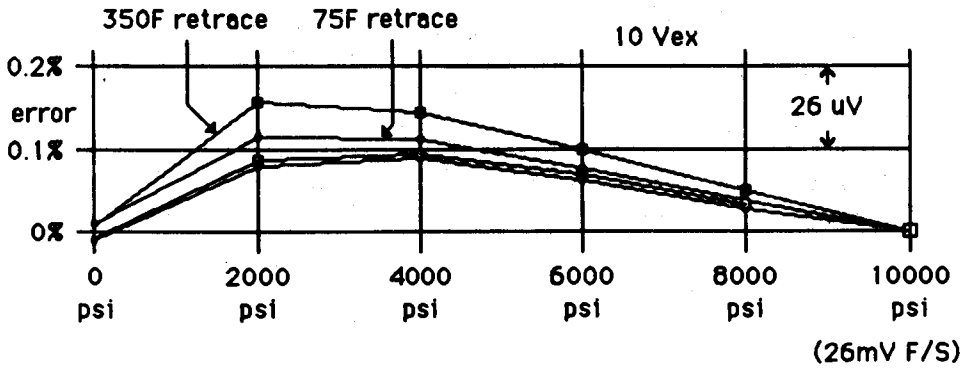

FIGURE 1

A titanium tube type transducer has small normalized error and hysteresis

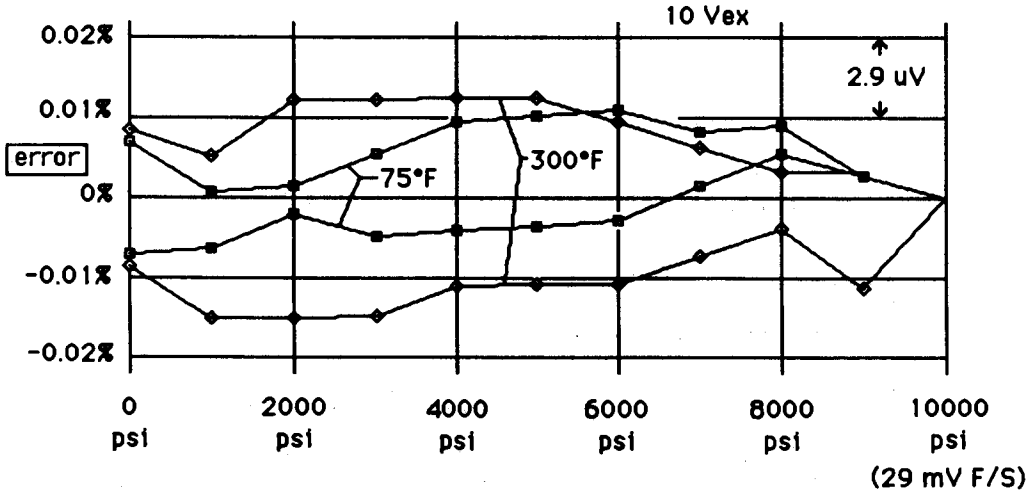

FIGURE 2

Low part count transducer system eases miniaturization

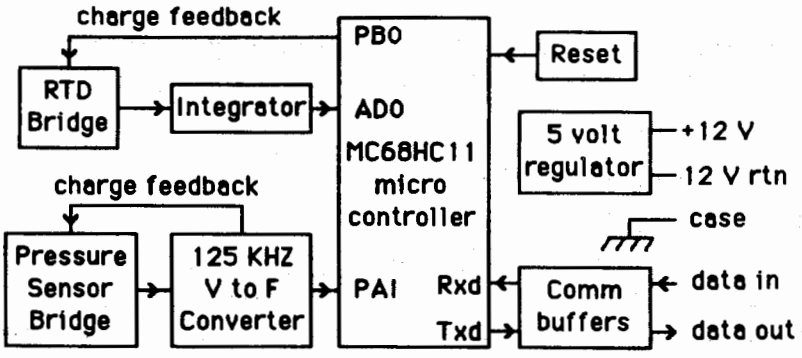

FIGURE 3

A dual-slope A to D converter sees the input for only part of a conversion cycle.

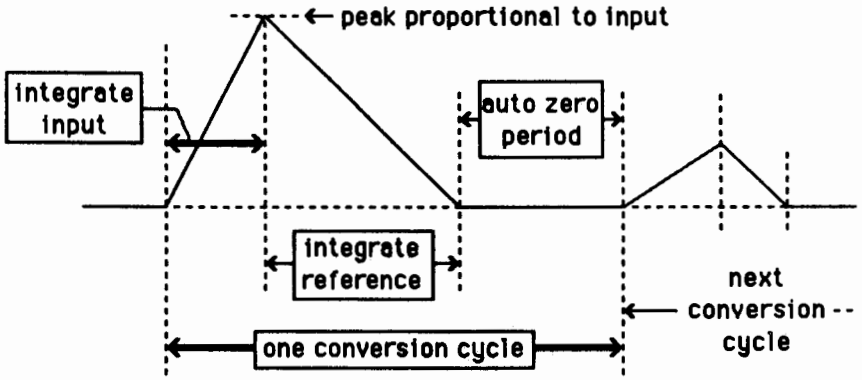

FIGURE 4

Multiple transducers can be easily interconnected in the network.

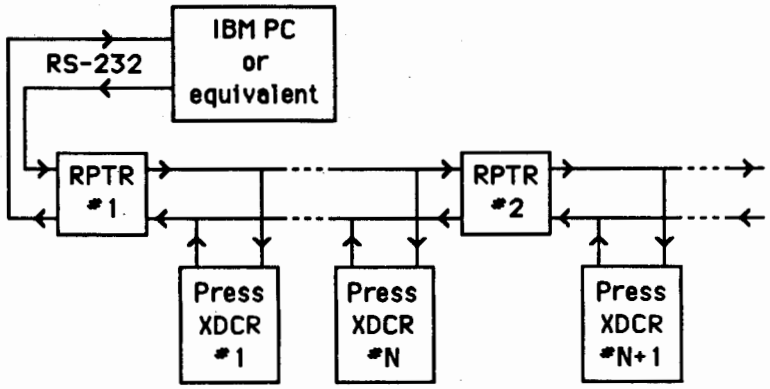

FIGURE 5

Figure 6 shows a list of several possible communication standards. Due to complexity or high power dissipation, most, if not all, of these standards are undesirable. For example, consider the relatively common RS-232 standard, even though it is not a party line data link in the standard definition. Assume a cable capacitance of 50 pF per foot, a communications line length of 100 feet, a baud rate of 9600, and a voltage swing of 20 volts. Then if bits in the data stream are alternating highs (+10 volts) and lows (-10 volts), the average current is I = (baud rate) * 1/2 * C * V^2 = 9.6 mA. If the output voltages, +10V and -10V, are derived from the regulated 5 volt supply, then the actual current required from the 5 volt supply is 18.2 mA (assuming a lossless voltage converter), just to drive the cable capacitance. One or more RS-232 type inputs, at 3K to 7K ohms each, monitoring the driven line would require an additional few milliamperes per receiver. The actual quiescent power requirements of the RS-232 type driver can be in the range of 0.5 to 20 mA.

Thus, a single channel RS-232 driver in a system type environment can cause the 5 volt regulator, operating with a nominal input of 12 volts, to dissipate a few tenths of a watt or more. A party line standard, such as RS-485, has a quiescent device current requirement on the order of 60 mA, and is intended to drive low impedance (75 ohm) cables and terminations, requiring 50 to 100 mA additional current.

Data skew is an additional consideration. In the case of RS-232, the line driver must be able to source or sink no more than 12 mA and no less than 6 mA. So consider the case of the the 100 foot long, 5,000 pF cable above. Since:

I = C * (delta voltage) / (delta time), then

(delta time) = C * (delta voltage) / I, so

(delta time) = (5000 pF) * (10 volts) / (6 mA)
= 8.3 uSec skew

The differential driver skew due to a possible 6 mA source and sink driver imbalance would be 4 uSec, which is 4% of one bit time frame at 9600 baud. Differential skews of less than 20% are desirable.

Thus, a simple, but presently non standard, communications adapter is desirable to provide two benefits to the network. These benefits are; 1) continued normal operation, even though one of the transducers in the control loop has had a communications failure, and 2) a low power dissipation in the transducer housing. The repeaters (RPTR) shown in figure 5 utilize a two level active current source to communicate with the transducers. In the event of a communications failure (possibly due to a transducer's shorted current sink driver, or a hung up microcomputer, etc.,) the repeater's active current source and the good drivers' sink capability would be increased by a factor of about three. The current sink capability of the known good transducers is also increased and held high to overcome the "drag" of the failed unit. Power dissipation has been moved from the transducer to the current source interface. A normal current source value of 6 mA and a driver current sink capability of 12 mA would provide a balanced differential skew and be able to work with line lengths up to a few hundred feet at 9600 baud. Longer distances would be managed by using relatively high current drivers in the communications adapter and repeaters. An optical modem link would also be useful to complete a network.

A two byte, asynchronous command and response protocol is used for the primary data transfer technique. Figure 7 is present to help visualize a fixed portion of the communications response time lag. Twelve bit information with an overall accuracy of about 0.25% is being transferred, so two 8 bit bytes is a minimum. A proposed makeup of the control and data words is shown in figures 8 and 9. For non time critical queries about an internal status, serial number, calibration information, etc., one or more of the eight command codes can be used to initiate a multibyte, including longitudinal checksum, data transfer.

From a system standpoint, overall data confidence is improved by the presence of the microcontroller. It can be used to act only upon (parity) verified commands, keep track of transducer history such as serial number, original transducer specifications such as offset and span, any historical overpressure events, self testing of some analog circuitry, and self testing of control program check sums.

CONCLUSION:

Overall, it appears reasonable to construct a high performance, system oriented digital transducer to operate on a low supply voltage at low power. Such low power allows for transient protection elements which make a robust device in the "real" world. Data acquisition system reliability and accuracy are improved due to the performance verification capability of the "smart" transducer.

RS-232	ARINC-429	HPIL
RS-422	4-20 mA	SP-50
RS-423	MA BELL	IEEE P1118

FIGURE 6 **Assorted communication standards**

The serial data from the slave is delayed from the command.

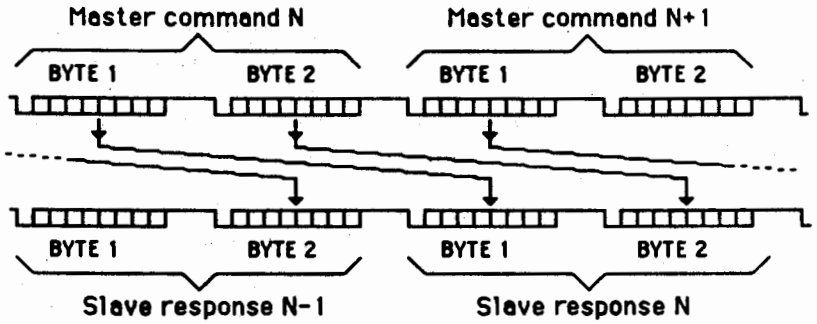

FIGURE 7 **Serial data command and response timing relationship**

The full MASTER control word is two serial bytes of information.

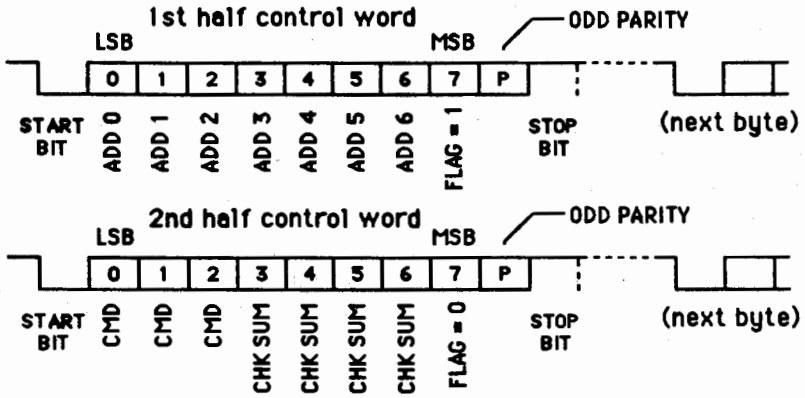

FIGURE 8

The full slave response word is two serial bytes of information.

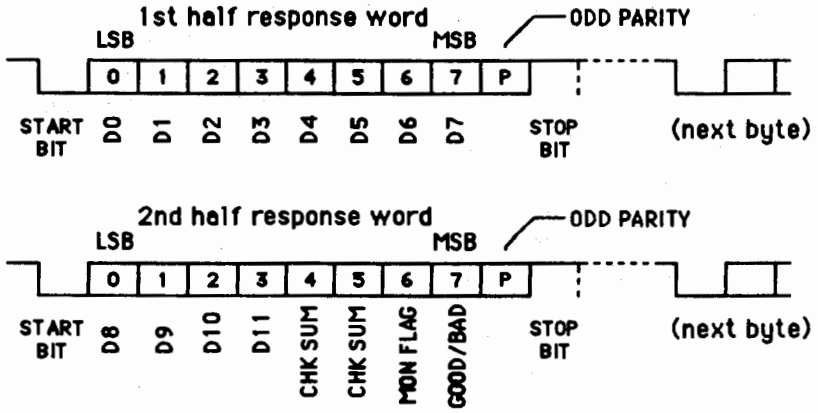

FIGURE 9

SESSION 4

MANUFACTURER PRESENTATIONS

DYNAMIC CONFORMITY AND DYNAMIC PEAK PRESSURE ACCURACY TWO NEW FEATURES OF PRESSURE TRANSDUCERS

by Gerhard RESCH,
Chief Engineer
Development of Sensors and High Pressure Techniques
AVL List Ges.m.b.H., Graz, Austria

When measuring the gas pressure history in guns by means of piezoelectric pressure transducers, the dynamic requirements to be met are very high for these measuring gauges in order to obtain the accuracy specified. Nowadays, the accuracy requirements lie within 2 % from the peak pressure, some users already demanding 1 % with twin measurements. For the gas pressure difference measurement on large caliber barrels particularly high demands are made on the measuring accuracy. With this measurement, which is more and more introduced for modern high efficiency weapons due to safety reasons, the pressure difference between breech pressure and chamber pressure near the projectile base has to be measured. As the difference is formed, minor measuring errors lead to considerable errors and uncertainties at the safety evaluation of the ammunition.

In order to obtain this high measuring accuracy, special measuring and calibration techniques are necessary allowing to quantatively determine the dynamic measuring properties of transducers. For many years it has been sufficient to describe the dynamic measuring properties by indicating the natural frequency of the pressure transducer. The article "acceleration sensitivity and resonance characteristics of piezoelectric pressure transducers" by Friedrich Ruckenbauer and Klaus C. Harms deals in detail with the fact that only indicating the natural frequency is rather insufficient.

This article, however, discusses another time range, i.e. the range where gas pressure measurements in guns are made. Fig. 1 shows the different time ranges. The time axis is presented in logarithmic scale and shows the ranges, "natural frequency", "measuring range and dynamic calibration", as well as the "static calibration" range.

It can be clearly seen that these 3 ranges are separated from each other by approx. the factor 1000. Here, we will discuss the time window between 1 and 10 milliseconds.

Dynamic calibration of pressure transducers

Based on the established principle for obtaining high measuring accuracy, requiring that the measuring device is to be calibrated under the same conditions which will prevail during application, a dynamic pressure calibration device is necessary in our case with a time window from 1 to 10 ms and an amplitude range, which covers the pressure scale of modern gun weapons i.e. from a few hundred MPa to approx. 800 MPa.

Sufficient attempts were made by different institutes in order to solve the problem of dynamic pressure calibration by means of a hydraulic pressure chamber. The hydraulic pressure pulses are generated by converting the kinetic energy of an impact mass or pendulum into hydraulic energy by means of a piston. Some results are known where pressure pulses in the millisecond range and with a few hundred MPa peak pressure could be realized. However, with all these methods one can not determine the height of the pressure amplitudes due to physical relations, which e.g. can easily be done with the pressure balance through the piston surface and the acting force on it, but only by measurement with the reference pressure transducer.

Since 1980, AVL has been dealing with the dynamic pressure calibration (1) and has been able to make considerable progress with the absolute calibration based on intense research work in cooperation with the Technical University of Graz, (2). The essential innovation is a calculation model, which allows to describe the hydraulic pressure pulses mathematically. For the first time it is possible to calibrate dynamic hydraulic pressure calibrators in absolute pressure units.

Theoretical basis for the calculation of hydraulic pressure pulses

As already mentioned the pressure pulse is generated in a hydraulic pressure chamber. This pressure chamber is housed in a high pressure measuring head of steel. The pressure chamber is filled with a hydraulic liquid and is closed towards outside by a precisely fitted piston.

An impact mass transmits its kinetic energy via this piston to the liquid in the chamber and the piston moves into the pressure chamber. During this action the liquid is compressed and the pressure of the liquid is increased. After transfer of the total kinetic energy to the liquid, the maximum pressure is reached and the motion of the piston and the impact mass is reversed. In first approximation this pressure system can be described by a spring-dashpot system, see fig. 2.

For this very simple model the following equation of motion applies if:

- there is a linear relation between pressure and compressibility
- there is no piston friction
- the pressure chamber is ideally stiff.

$$m\ddot{x} + cx = 0$$

By solving this equation the pressure-time profile can be calculated for these ideal conditions.

$$p\ (t) = Va\sqrt{\frac{m}{V \cdot K}}\ \sin\left(\frac{A}{\sqrt{m \cdot V \cdot K}} \cdot t\right)$$

Thus, the maximum pressure is

$$Pmax = va\sqrt{\frac{m}{V \cdot K}}$$

and the duration of the pressure pulse is

$$T = \sqrt{m \ .\ V \ .\ K}\ \frac{\pi}{A}$$

where

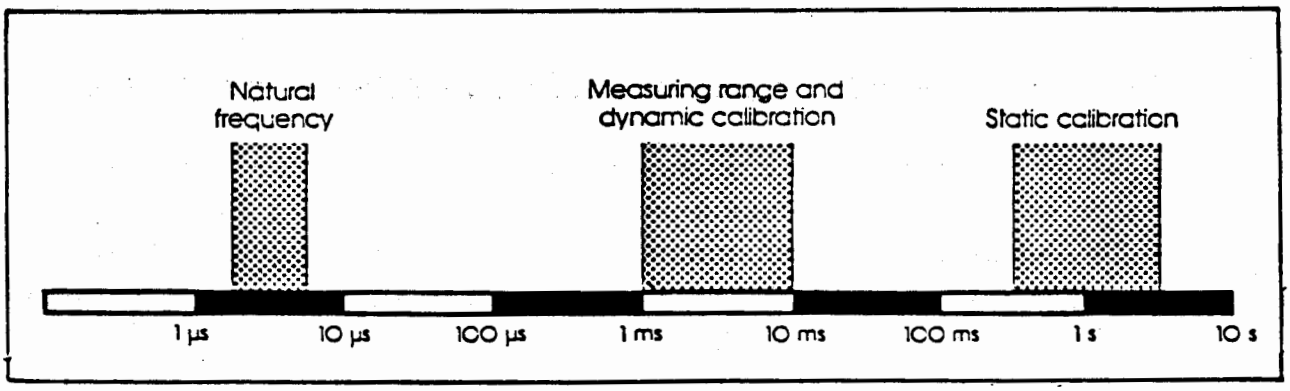

Fig. 1: time windows for piezo electrical gauges

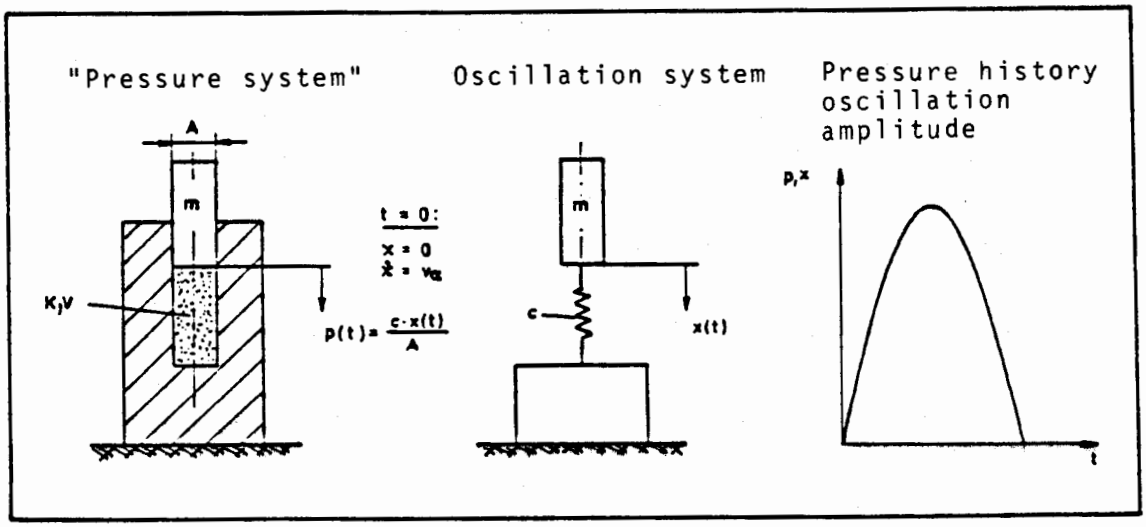

Fig. 2: ideal-model for a dynamic pressure calibrator

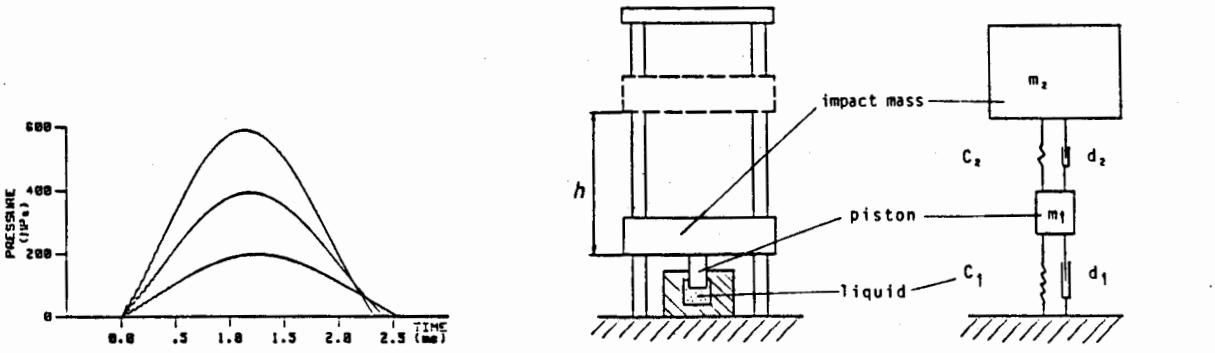

Fig. 3: 2-mass oscillating system

K = liquid compressibility
V = liquid volume
m = mass (piston + impact mass)
va = initial velocity of m

In practice, this simplified calculation can only be applied for an approximate pressure calculation. This is mainly due to the fact that the liquid compressibility strongly depends on the pressure.

The left side of fig. 3 shows essential characteristics of the real pressure pulse measured by a piezoelectric pressure transducer in the measuring chamber. The curve analysis leads to the following results:

- with increasing amplitude the total duration b of the pressure pulse is reduced; i.e. the elastic force is non-linear (progressive)
- the ratio between rise time a and total duration b is below 0.5 i.e. the oscillations are damped
- at the beginning of the curve the fundamental oscillation of the pressure pulse shows superimposed oscillations with higher frequencies, which, however, die out soon. It can be proven that these oscillations are longitudinal oscillations of the piston.

The mathematical description of the pressure curve shown in fig. 3 leads to a dual spring-dashpot system. Only very difficult calculations can provide a solution, and the non-linear spring-dashpot model make these calculations even more demanding.

Further development of this calculation method made it possible to use a simplified mathematical model for computing the maximum pressure and the duration of the pressure pulse, which provides the same results for these two quantities as the more complicated two-mass model mentioned above.

This model (see fig.4) presents a spring-dashpot system with non-linear spring and non-linear damping characteristics. If this spring-dashpot system is deflected with the velocity $\dot{x}(o) = va$ from the static equilibrium at the time $t = o$, one will receive, depending on the quantity va, an amplitude shape $x(t)$ as a function of time as

shown on the left side of the figure.

The differential equation therefore is

$$m\ddot{x} + d(\dot{x}) \cdot \dot{x} + c(x) \cdot x = o$$

The spring-dashpot system is described by the system characteristics $c(x)$ and $d(\dot{x})$, i.e. with given initial conditions one can determine the amplitude shape $x(t)$ as a function of time and thus also the shape of the pressure curve $p(t)$.

For calibrating the Dynamic Pressure Calibrator one proceeds in reverse order as, for the time being, the two system characteristics $c(x)$ and $d(\dot{x})$ are still unknown. These two system characteristics can be determined as follows:
one carries out tests at different heights of fall and records the individual velocity of the impact mass at the time when it hits the piston. Furthermore, one only records the shape of the pressure pulse as a function of time in the pressure chamber, e.g. by a piezoelectric pressure transducer, which will give a family of pressure curves according to fig. 4 on the left side. It is important that for the calculation of the system characteristics only the pulse shape is considered. From this pulse two time intervals - beginning to maximum of pulse and pulse duration - are derived.

From the so determined characteristic times a and b, which depend on the individual impact velocity or heights of fall, one will receive after detailed calculations $c(x)$ and $d(\dot{x})$. Further parameters needed are : masses of piston and impact mass, and piston area. The liquid volume or any other properties of the liquid are not required. As shown above, the Dynamic Pressure Calibrator can be calibrated by using this mathematical model and we are left with the simple conclusion that a certain shape of the pressure curve and thus also a certain maximum pressure correspond to a certain impact velocity of the impact mass.

As the impact velocity in return directly depends on the height of fall, one finally arrives at the relation between height of fall and maximum

pressure which is very important for the application when used as pressure calibrator. That means that one clearly knows the necessary height of fall for a certain calibration pressure required. With a static pressure balance, the calibration pressure directly depends on the quantity of the masses acting on the piston, with the AVL Dynamic Pressure Calibrator, it directly depends on the height of fall. Each AVL Pressure Calibrator is calibrated in our factory according to the way described above. After calibration the relation between height of fall and pressure generated is "burned" into this system, so that then an exactly known pressure can be generated by only knowing the height of fall and without using the mathematical model.

Functional description of the AVL B 620 Dynamic Pressure Calibrator (DPC)

The Dynamic Pressure Calibrator (see fig. 5) is easy to handle and guarantees high reliability. The maximum pressure required can be set by means of a switch on the control panel and the supporting arm for the impact mass automatically moves to the corresponding height of fall. The calibration procedure is activated by a button releasing the impact mass, which falls downwards in the precision guide rods without almost any friction and hits the piston. The velocity loss compared to free fall with friction and air resistance is approx. 0.2 %. A velocity measuring system records the impact velocity for control purposes.
After the pressure pulse generation the impact mass is immediately stopped by the safety catch when moving upwards. Then the impact mass is pneumatically lifted to the supporting arm. After that the calibrator is ready for the next calibration procedure with same or different heights of fall. The calibration procedure can also be controlled by a computer allowing fully-automatic operation.

Fig. 6 shows the measuring head, which can house up to four pressure transducers.

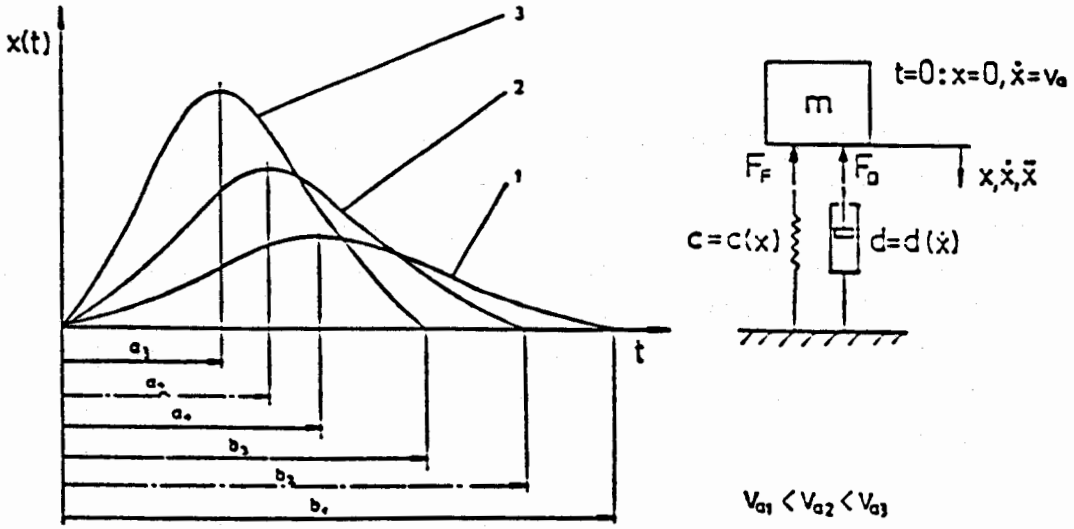

Fig. 4: AVL mathematical model for dynamic pressure calibrators

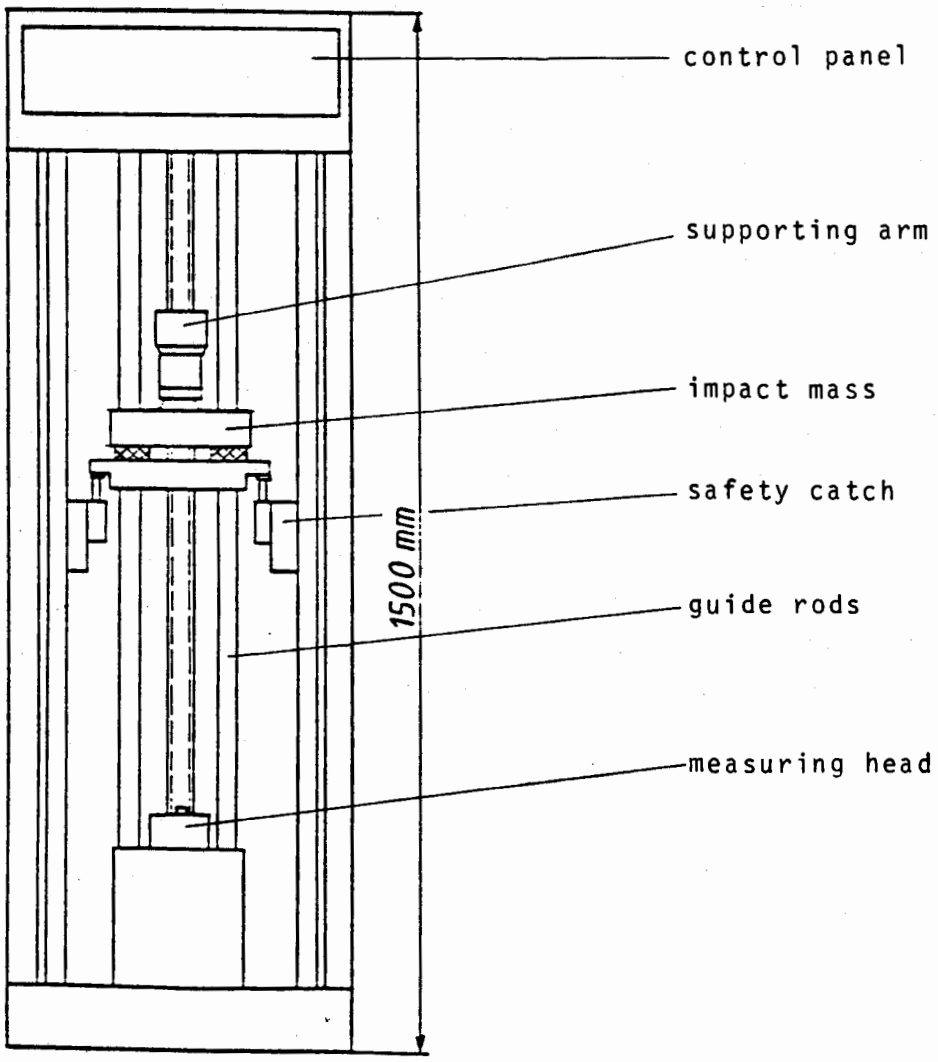

Fig. 5: Dynamic Pressure Calibrator B620
range 100 ... 800 MPa
pulse deration 2.5 ms

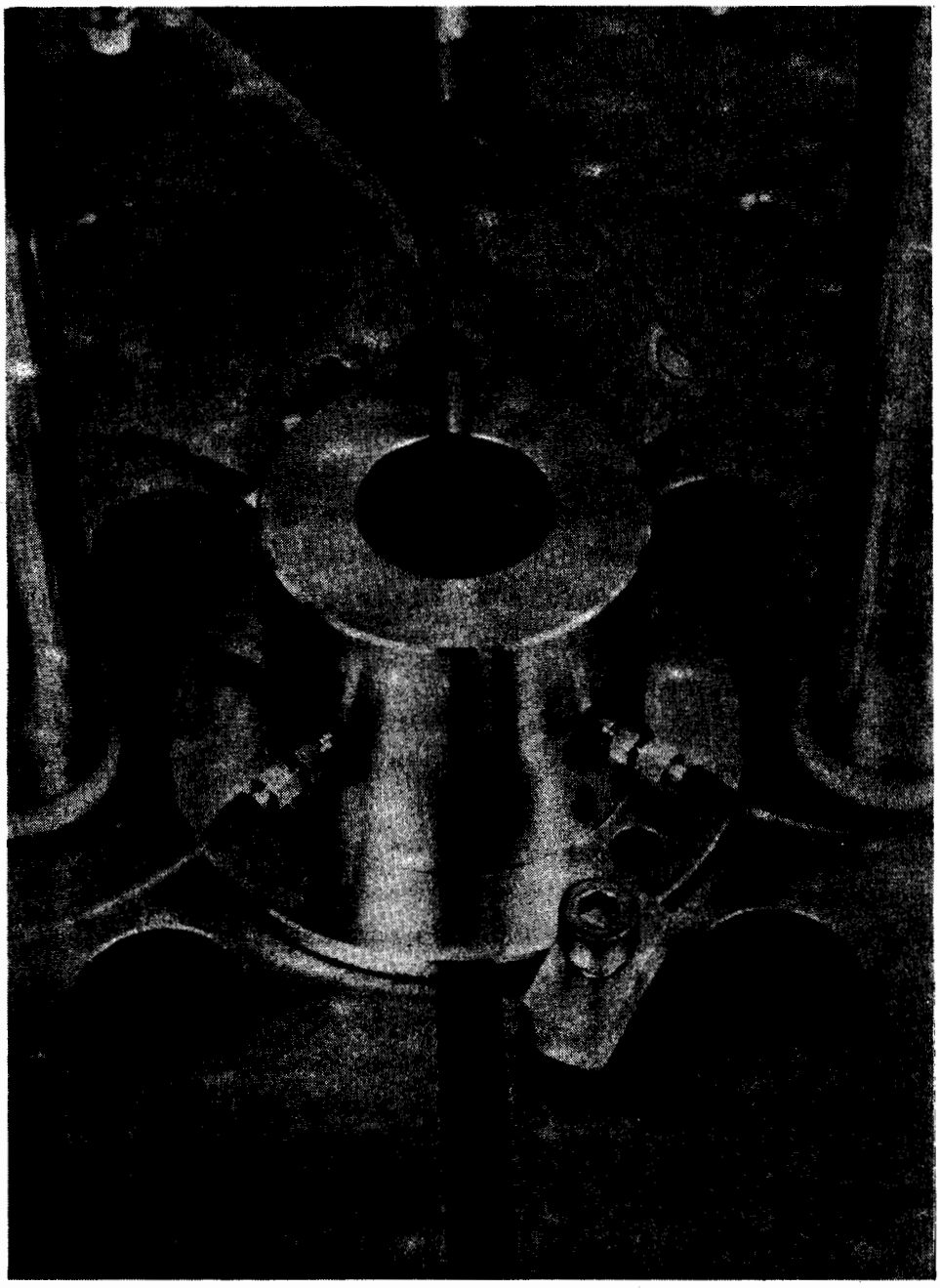

Fig. 6:. B 620 Measuring Head

Specifications of the B 620 Dynamic Pressure Calibrator

The maximum pressure can be set in steps of 1 MPa within the range of 100 MPa to 800 MPa. The pulse duration is approx. 2.5 msec. The accuracy of the maximum pressure set is 2 % within the range of 100 to 200 MPa and 1% within the range of 200 to 800 MPa. The percentage indications refer to the current pressure set and not to the final value of 800 MPa. Please note the particular high reproducibility of 0.5%, which in most cases is even higher i.e. 0.1 to 0.2 %.

We are aware of the fact that currently it is still difficult to prove the accuracy indication for the pressure values as, apart from the method developed by AVL for the calibration of a dynamic pressure calibrator, no other calibration method is known, and even Bureaus of Standards probably cannot prove and confirm the accuracy. However, we will try to obtain an official calibration approval for our method together with authorities responsible for calibration.

Till then one can rely on the plausibility of the measuring results obtained. In connection with this the following experience has been gained.
Piezoelectric pressure transducers of different types and manufacturers were statically calibrated. Most of the transducers showed a very good compliance with each other when calibrated on the Dynamic Pressure Calibrator.
The deviations of the maximum pressures measured were below 0.5%. This leads to the conclusion that these pressure values also have a very high plausibility in absolute terms i.e. accuracy. Otherwise, all these transducers must have the same systematic error, even though they are of quite different design. Therefore, the latter is rather unlikely.
On the other hand the maximum pressures measured with above transducers comply within 1 % with the pressures set on the B 620. For this reason, the accuracy indications for the B 620 DPC have a very high probability of correctness in absolute pressure units.

Dynamic conformity and dynamic peak pressure accuracy

The introduction of dynamic pressure calibration in absolute pressure values leads to new evaluation criteria for the dynamic measuring properties of pressure transducers. Features derived therefrom are: dynamic conformity and dynamic peak pressure accuracy. For explanation of these terms see fig. 7.
If a pressure history is measured simultaneously with various pressure transducers, the dynamic conformity will describe the quality regarding the conformity of the pressure curves recorded. The dynamic peak pressure accuracy describes the quality of the conformity between the static and dynamic sensitivities of a pressure transducer i.e. if a pressure pulse with e.g. 500 MPa is generated on the B 620 DPC and the static sensitivity at 500 MPa is used for the pressure transducer, 500 MPa will also be indicated on the DPC in ideal circumstances. Both features can be easily determined on the B 620 DPC.

Fig. 8 shows some typical examples for dynamic diagnostics of ballistic pressure transducers.

Future prospects

For many applications, the dynamic pressure calibrations may become an excellent alternative to the static calibration.

The reasons therefore are:

- Normally the results of static and dynamic calibrations comply with transducers showing no abnormities
- With the B 620 DPC an absolute calibration (comparable with a pressure balance) is possible (even without a mathematical model) and the obtainable accuracy of B 620 with 1 % of the maximum pressure is sufficient
- Insufficient dynamic measuring properties can be determined
- Qualitative evaluation of the pressure transducer over the total pressure-time profile is possible, e.g. difference pressure curve with reference pressure transducer

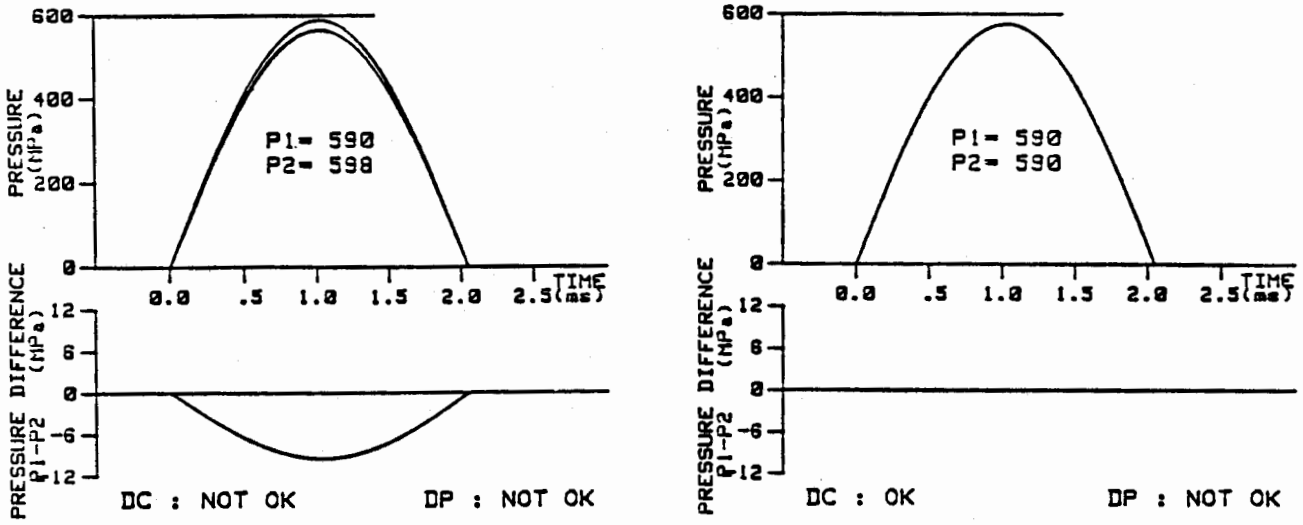

DC : DYNAMIC CONFORMITY

DP : DYNAMIC PEAK PRESSURE ACCURACY

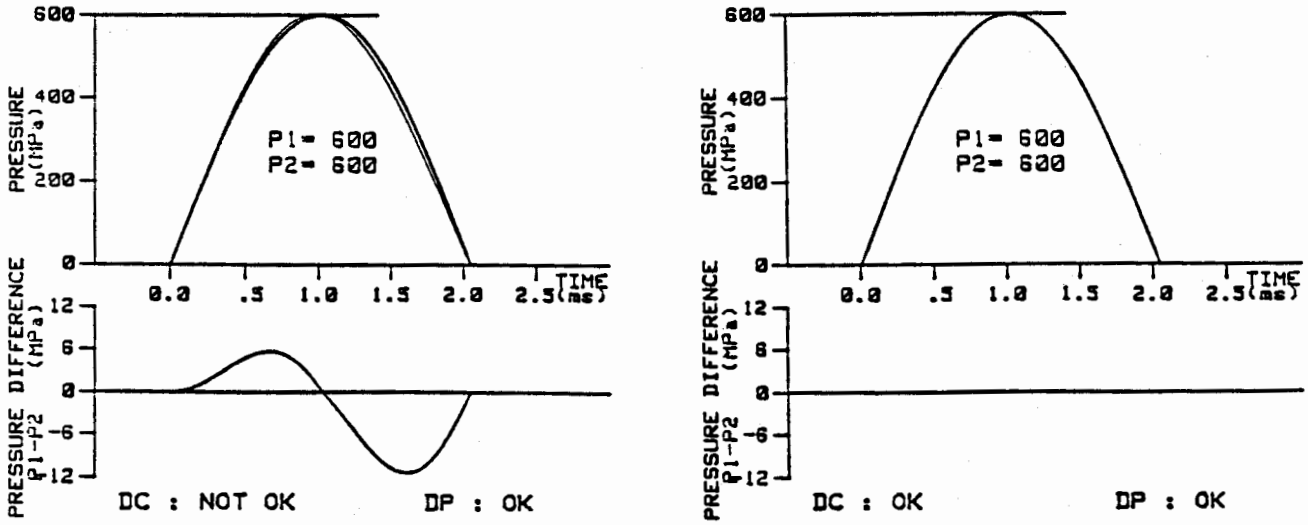

Fig. 7: definition of dynamic conformity and dynamic peak pressure accuracy

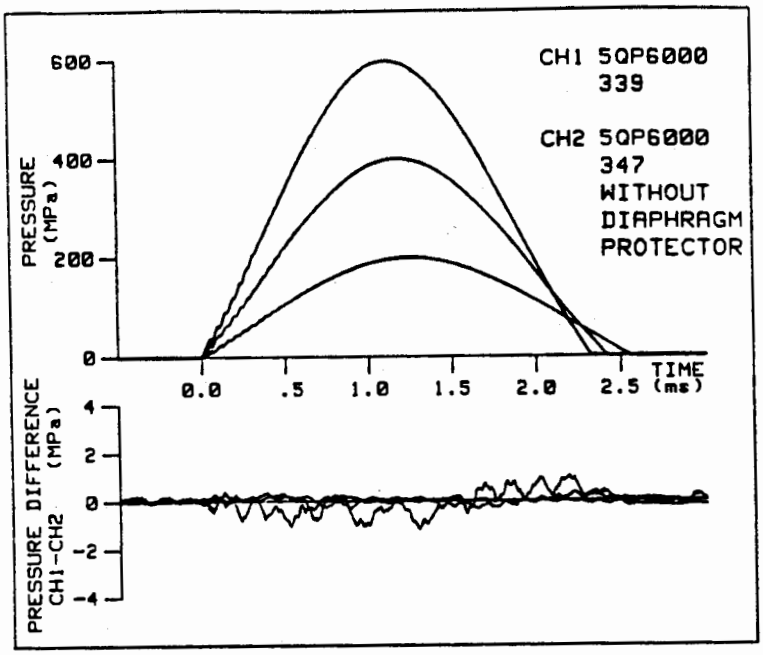

Two AVL 5QP6ooo transducers, both without Z3302 diaphragm

Result:

DC: o.k.
DP: o.k.

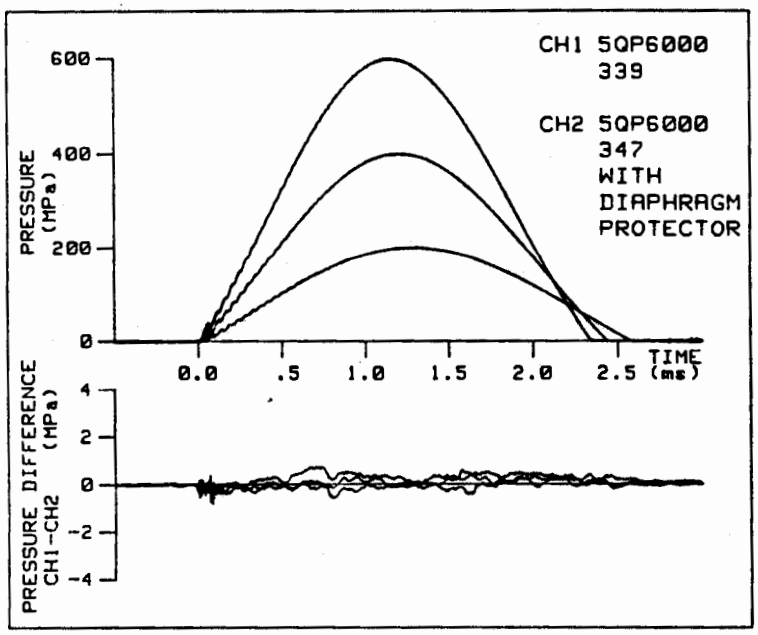

Same set-up as above transducer (CH 2) with diaphragm protector

Result:

DC: o.k.
DP: o.k.

Not influenced by diaphragm protector

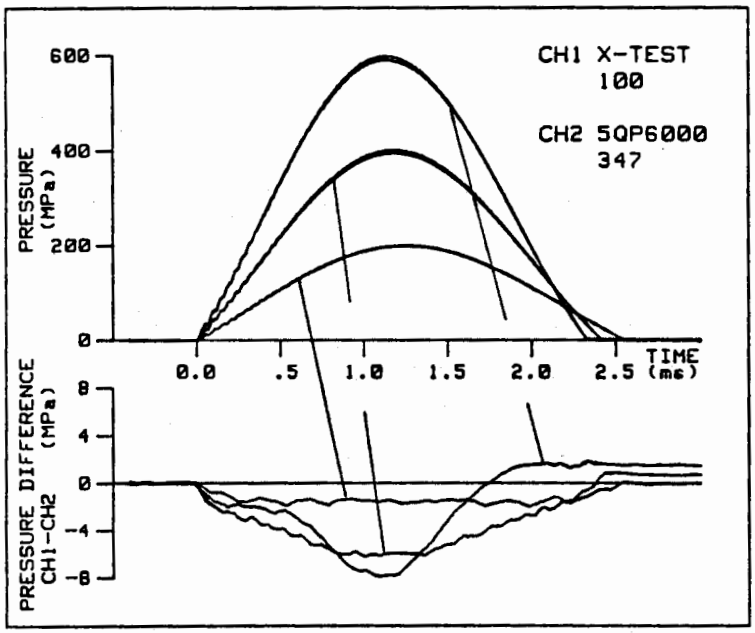

Dynamic diagnostic by means of dynamic calibration

Result:

DC: not o.k.
DP: not o.k.

Fig. 8:

Dynamic Diagnostics of Ballistic Pressure Transducers

- The wear of the pressure transducer is considerably lower than during static calibration due to the short pulse duration of B 620, which eliminates the danger of "calibration till death"
- The actual calibration procedure can be carried out very quickly
- Compared with a pressure balance far less devices are required for a pressure range up to 800 MPa, which presents a decisive advantage in costs for B 620.

By means of the calibration developed by AVL and using a mathematical model it is assured that various Dynamic Pressure Calibrators of the B 620 type provide results, which are identical between each other. It is to be hoped that the Bureaus of Standards will soon be able to find a method in order to confirm the accuracy of B 620.

Remarks

Parts of the article on the theory of the dynamic pressure calibrator derive from the dissertation by Dr. Walter Schwelberger, which was carried out at AVL, Graz, together with the Institut für Verbrennungskraftmaschinen und Thermodynamik (Institute for Combustion Engines and Thermodynamics) headed by Prof. Rudolf Pischinger of the Technical University in Graz, Austria, between 1984 - 1985.

The author thanks Mr. Franz Lammer for the thorough realization of the tests and Mrs. Ulrike Wutti for the translation.

Bibliographical references:

(1) G. Resch, W. Klöckl :
Dynamic Calibration of Pressure Transducers for Interior Ballistic Measurements
6th International Symposium on Ballistics, Orlando, Florida, 1981

(2) W. Schwelberger :
Der kalte Druckstoß (The Cold Pressure Pulse)
Ein Verfahren zur dynamischen Prüfung von Hochdruckaufnehmern
(A method for dynamic testing of high pressure transducers)
Dissertation at the Technical University in Graz, 1985

Q: J. R. Miller (Redstone Arsenal): Did I understand you to say you calibrated your calibrator with a transducer?

A: Gerhard Resch: No, we calibrate our system with a mathematical model, once in the factory. The system characteristics that are nonlinear, spring and damping characteristics, are used in calculating when given pressure. This matrix is stored in equilibrium after the calibrator calibrates itself.

Q: J. R. Miller: Do you have any copies of your paper here today?

A: Gerhard Resch: Yes.

Q: Edward Hartman (Caterpillar, Inc.): What is the maximum peak pressure that you can generate with the calibrator? And what is the commercially available price?

A: Gerhard Resch: The answer to the first question is 800 MPa. For the pressure pulse generating unit without any data reducing system, the price is in the range of $65,000-$70,000 United States dollars at the current exchange rate.

Q: Torben Licht: How do you get around to the classical problems of falling mass machines, including the problems of sliding mass along the rod and the deterioration of impact surfaces with severe impact? One of the big items you have to get around is using shop machines to make acceleration calibrations. As far as I know, no one has really gotten around that.

A: Friedrich Ruckenbauer: Through a long development process, we find that we have no friction in the guiding system for the falling mass. The velocity loss when the guiding system is used when compared to freefall is only about 0.2 percent. To measure the air resistance and friction of the guiding system, we use special air bearings that are very constant and a velocity measurement system. Also, we use it with special software for control purposes only as a calibrator after the initial calibration. The computer results show that the friction is too high. The reproducibility of results using this calibrator is specified as 0.5 percent. In normal cases when you have one pressure point, the reproducibility is only 0.1 to 0.2 percent.

Q: Bill Leisher (Sandia National Laboratories, Albuquerque, NM): We used a system very similar to this one for about 15 years. I understand that when it started they also tried to make the mathematical model calibrate the system as you have done here. Some of the problems encountered were the sealing of the pistons and the distortion of the pistons, which goes up to 100 K psi. And under those conditions the piston does give significant distortion so this area is no longer the static area which is measured. I would like to know how you overcame those problems?

A: Friedrich Ruckenbauer: When we started with our calculation model, we used a system that needed the parameters of both the liquid and the measuring head. We had not been successful because all these elastics are at the high pressure which resulted in deformations. Our current mathematical model uses a measuring head as a black box. The system, spring and damping characteristics are the sum of the liquid only in addition to the elastic distortions of the measuring head and the distortions of the piston area. In that way, you have the overall characteristics, which at the moment, is our best solution.

Q: Gordon Mills: How do you deal with the variable amount of air trapped in the compressible liquid?

A: Friedrich Ruckenbauer: Here on the top is a small device used in mounting the transducers. They have a special feeling system to get the air bubbles out. A most important point is that the pressure chamber always has the same amount and quality of liquid without air bubbles. This influences the results strongly.

Q: Peter Stein: A two-part question. All of your data show the comparison between two transducers. Do we assume that one of them serves as a reference standard, or are there just two transducers that the customer supplies to evaluate against each other?

A: Friedrich Ruckenbauer: Yes, there are two transducers. You can define one transducer as a reference transducer, but you know the peak pressure from the calibrator. You can see if your reference transducer is working correctly under peak pressure.

Q: Peter Stein: And my second question. There will be a fair amount of acceleration and stress on the body of the mount that must reflect in some output from the transducer unless you've taken some special precautions because there are good accelerometers and strain gauges on all these pressure transducers.

A: Friedrich Ruckenbauer: We have a large big counter mass on the base plate in some tests. By mounting a transducer which was not connected in pressure, the noise is very low because the impact of the falling mass is large, but it is absorped by the fluid. Because the power acceleration of 2.5 milliseconds is a good damping, the impact does not cause distortion. That is our experience with high pressure transducers, but if it were a high sensitive, low pressure transducer, I don't know if it would help.

ACCELERATION SENSITIVITY AND RESONANCE CHARACTERISTICS OF PIEZOELECTRIC PRESSURE TRANSDUCERS

by Friedrich Ruckenbauer and Klaus C. Harms
Senior Project Engineers
Physics Research & Development Department
AVL List Ges.m.b.H., Graz, Austria

1. Introduction

Piezoelectric sensors are especially suitable for dynamic measurements, in particular, piezoelectric pressure transducers. Based on the high stiffness and the low masses these transducers show very high resonace frequencies and low acceleration sensitivities. Up to now these influences have been neglected. However, due to increased accuracy demands even minor deviations from the measuring signal have to be considered. (See fig. 1). With measurements outside the catridge case high pressure peakes occur, which excite high frequency resonances in the transducer.

2. Computation models

The simplest model for simulating the pressure transducer is a spring-dashpot model. If there are more resonances an expansion to a multiple spring-dashpot model is usually made (see fig. 2). When accelerometers or certain pressure transducer types are used, this model will provide a good resonance frequency behavior under the following conditions:

- harmonic oscillations
- low coupling between the individual resonance modes
- mass concentration on the front side of the transducer in particular, with accelerometers
- no sensitivity change due to load (linear model)

If above requirements are not met a spring-dashpot model cannot be used. Then an acoustic wave guide model has to be used. The following system conditions have to be fulfilled:

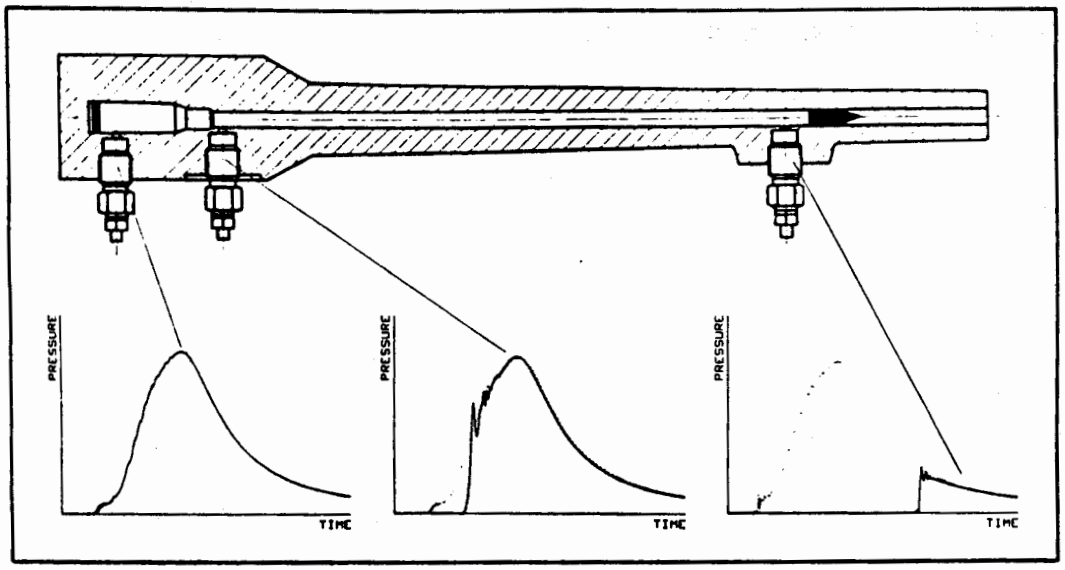

Figure 1: Pressure measuring points on guns

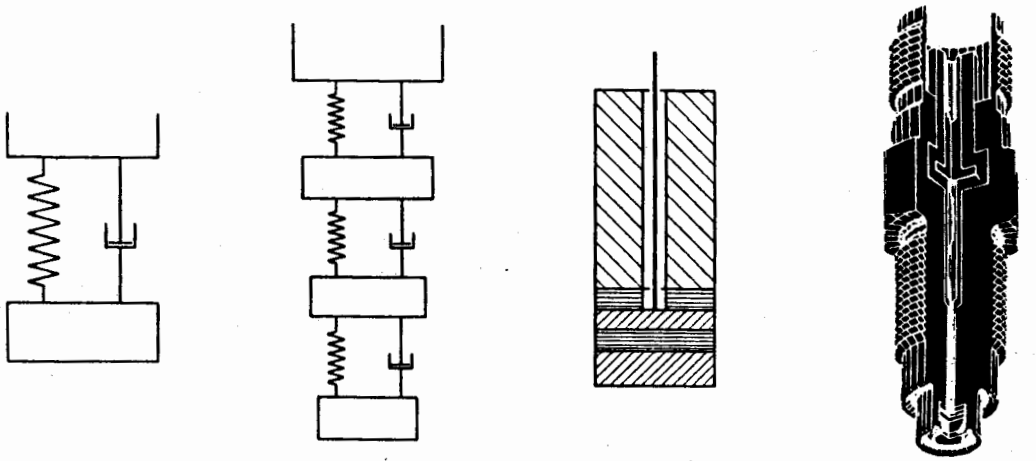

Spring-dash-pot model

Multiple spring-dashpot model

Acoustic wave guide model

CAD model

Figure 2: Piezoelectric transducer models

- low mass load (in front of the transducer due to diaphragm)
- almost equal diameters of transducer elements
- acoustic material data have to be available

This simplified acoustic wave model provides better results than the spring-dashpot model. However, at the actual transducer various parameters are unknown such as the acoustic coupling between thread and adapter, the impedance steps due to changes in diameters, the impedance steps caused by the surface roughness of the individual components, and the acoustic coupling above the transducer sealing zone etc.

3. Measurement of resonance characteristics

In order to obtain information on resonance behavior of the pressure transducer an accurate measurement is necessary. Ideally, this information can be obtained from one measurement, however, there are some issues which cannot be solved at the same time. The ideal measurement system does not influence the measuring units. In case of resonance frequency measurements each mechanical arrangement is acoustically coupled and results in additional acoustic resonances.
In order to eliminate these influences we have developed a purely electrical measuring system, the PIEZO-SCAN.

3.1 Piezo-Scan measurement technique

An electrical excitation stimulates the pressure transducer to acoustic oscillations. These oscillations cause mechanical strain, which can be measured by means of the charge signal. This idea seems to be successful, however, there are some differenes between the pressure measurement and the data obtained by the Piezo-Scan resonance characteristics. The main difference between the Piezo-Scan method and the pressure stimulation of the transducer lies in the fact that, in case of the Piezo-Scan, the excitation comes from the quartz crystal and in case of the pressure stimulation, the excitation is caused by the diaphragms.

This shows that the individual resonance modes provide different coupling coefficients.

3.2 Piezo-Scan features

- Very high frequency resolution and accuracy
- Quality factor measurement is possible
- No influence of mechanical adapters
- Measurement of acoustic coupling through the adapter
- All possible modes which can influence the signal can be detected (longitudinal and transversal modes)
- All influences on the resonance behavior can be detected (e.g. influences caused by heat, coupling medium, high pressure, sensitivity changes of quartz elements, mechanincal deformation of transducers).

3.3 Measurement results with the Piezo Scan

Fig. 3) Picture of the Piezo-Scan
Fig. 4) Simplified diagram of measurement circuit
Fig. 5) Resonance characteristics of free transducer
Fig. 6) Resonance characteristics of free and clamped transducer
Fig. 7) Coupling of long and short resonance rods at the transducer with front sealing for comparisons in the range of 200 to 300 kHz
Fig. 8) Coupling of long and short resonance rods at the transducer, which has been fixed at the hexagonal end.
Fig. 9) Coupling of short resonance rod at a transducer with front sealing over the full range.
Fig. 10) Comparison of resonance spectrum and Fourier analysis of a shot.

3.4 Theoretical aspects of resonance behavior

Fig. 11 shows the variation between the amplitude ratio A/Ao and the phase versus the frequency ratio in case of different damping factors.
The resonance superimposition also occurs far beyond the resonance frequency.

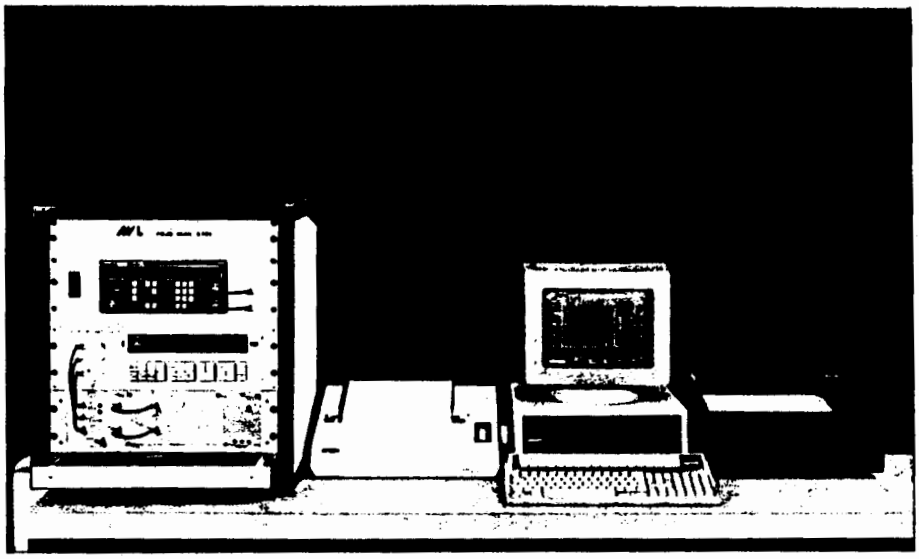

Fig. 3: Piezo-Scan

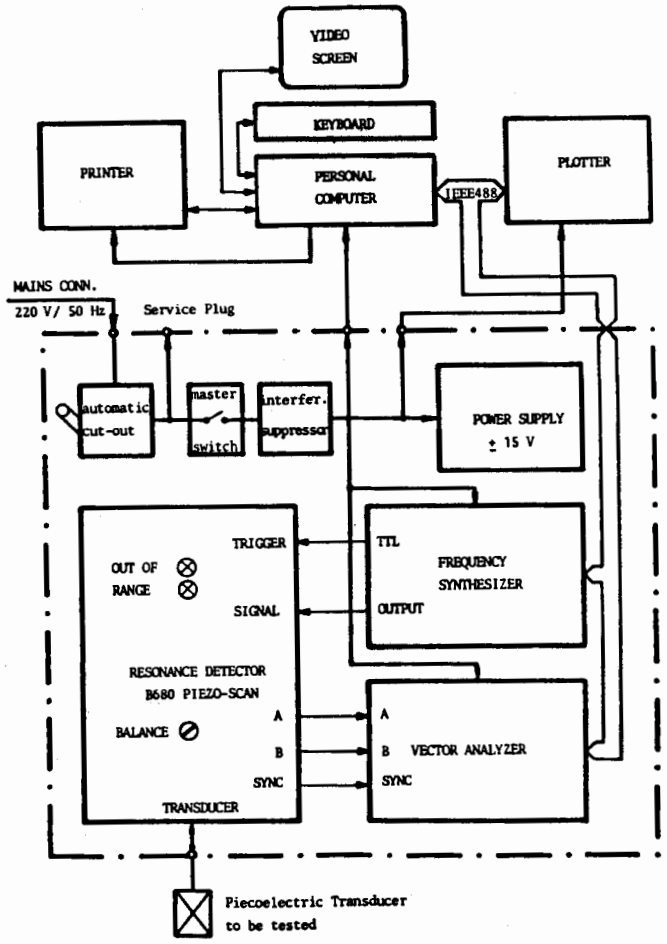

Fig. 4: Simplified diagram of measurement circuit

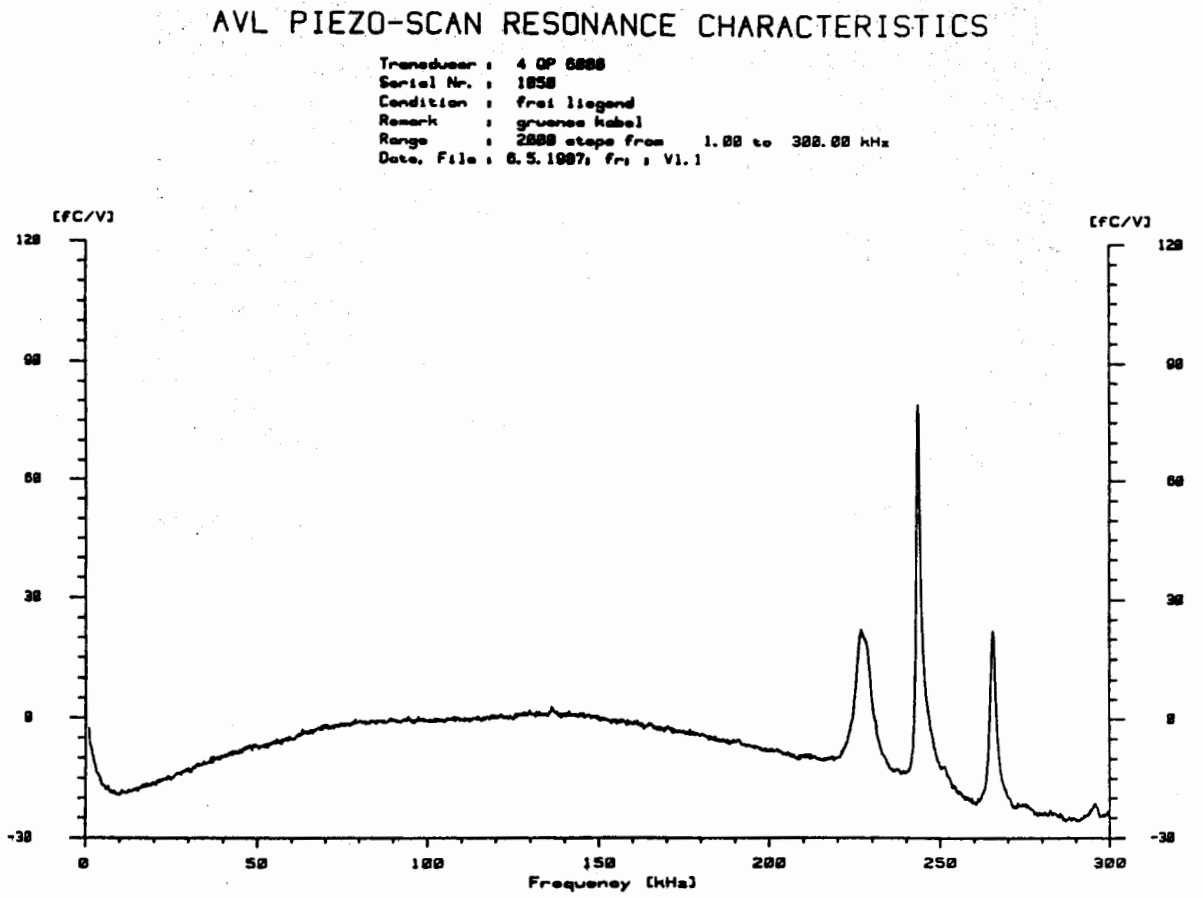

Fig.5: Resonance characteristics of free transducer

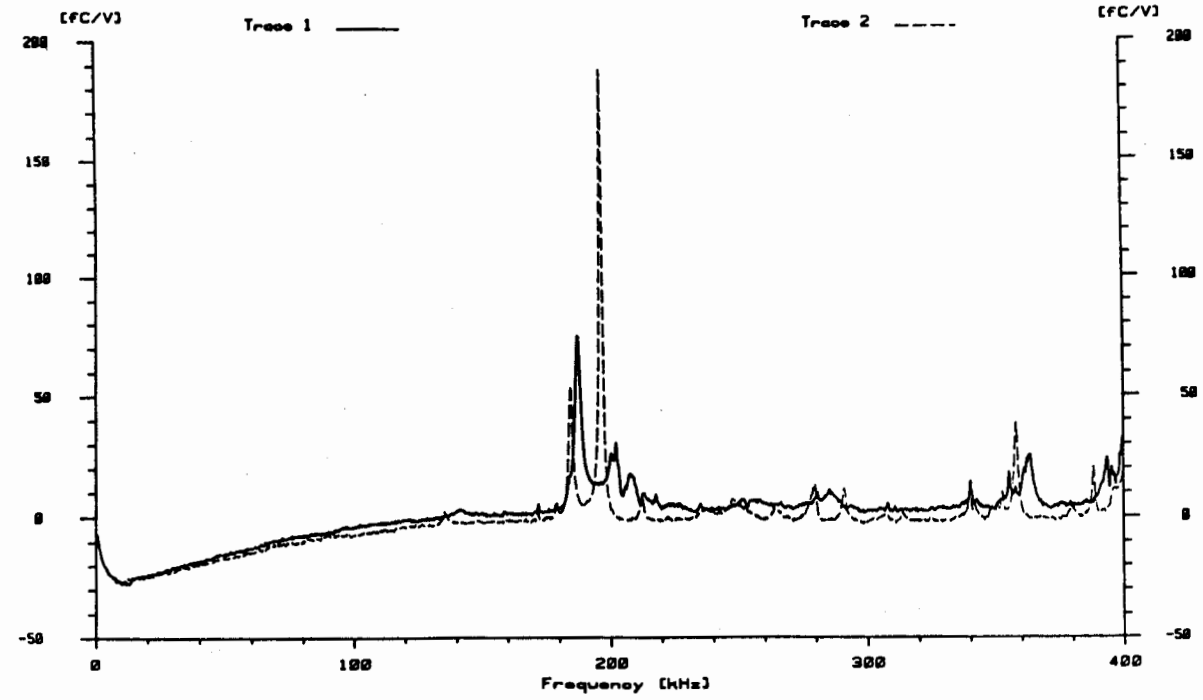

Fig. 6: Resonance characteristics of free and clamped transducers

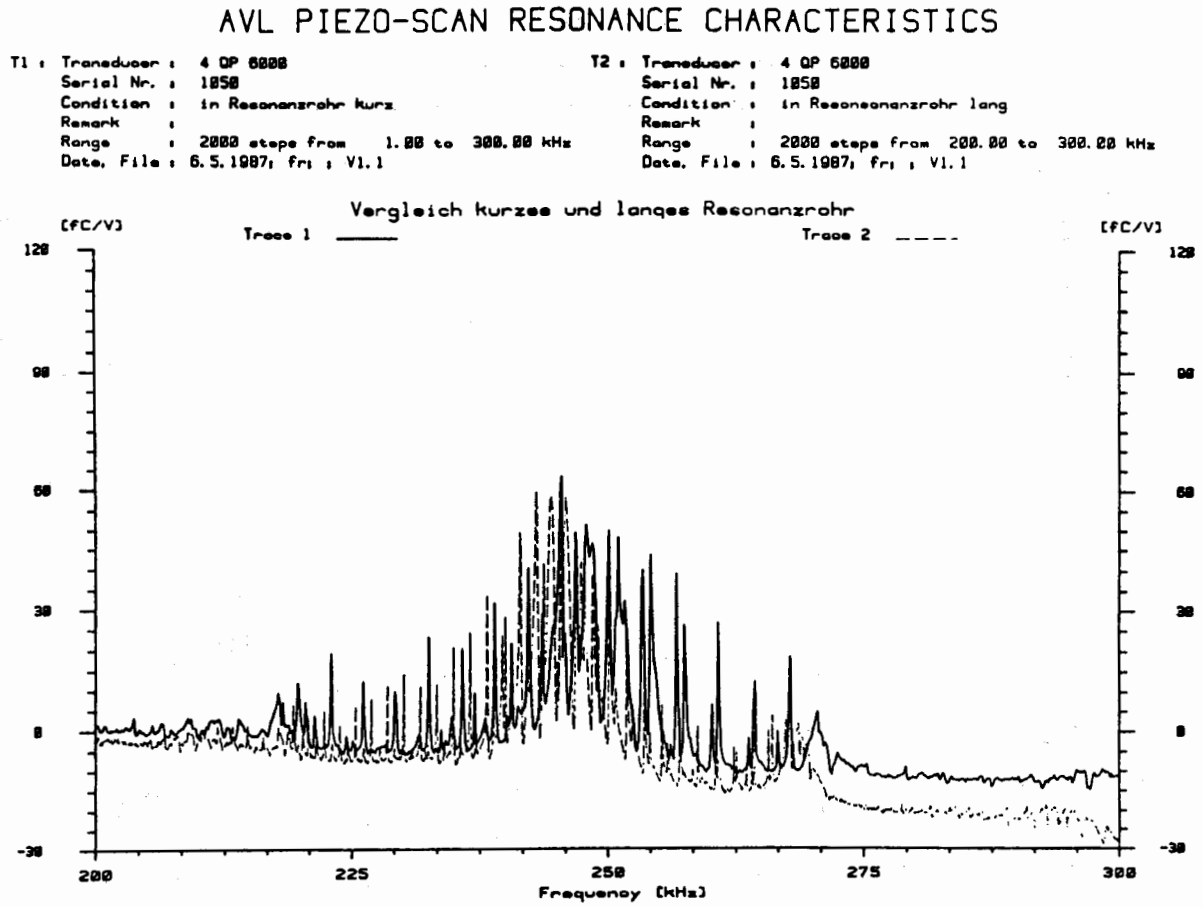

Fig. 7: Coupling of long and short resonance rods at the transducer with front sealing

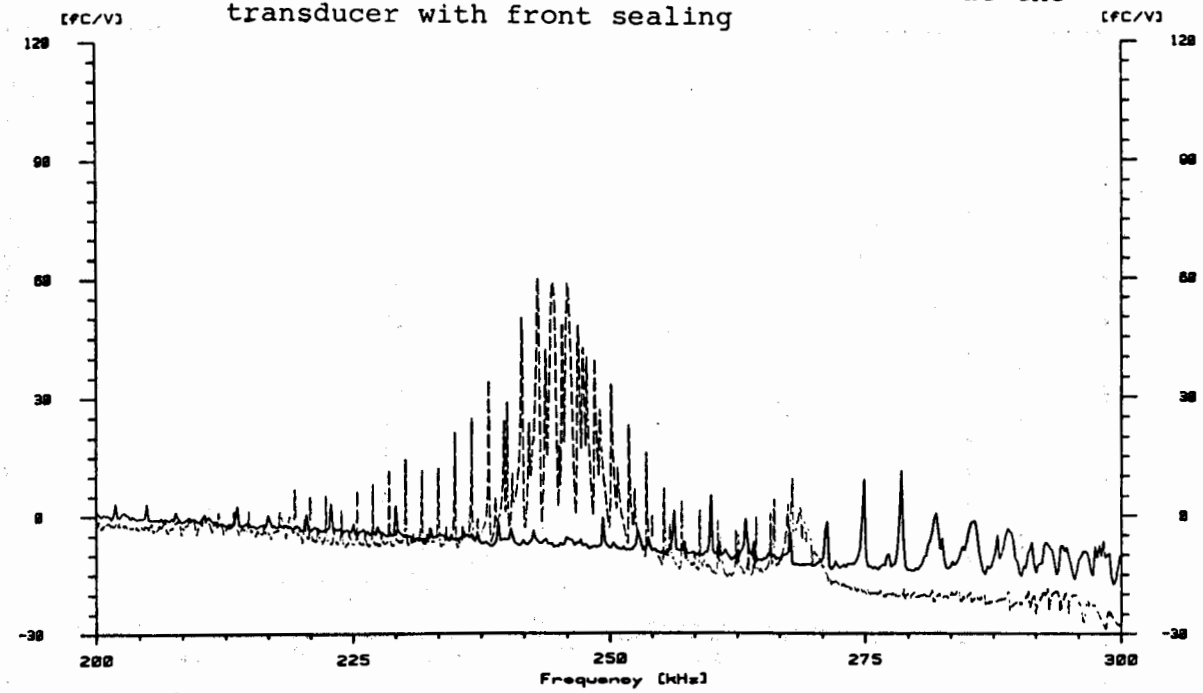

Fig. 8: Coupling of long and short resonance rods at the transducers, which has been fixed at the hexagonal end

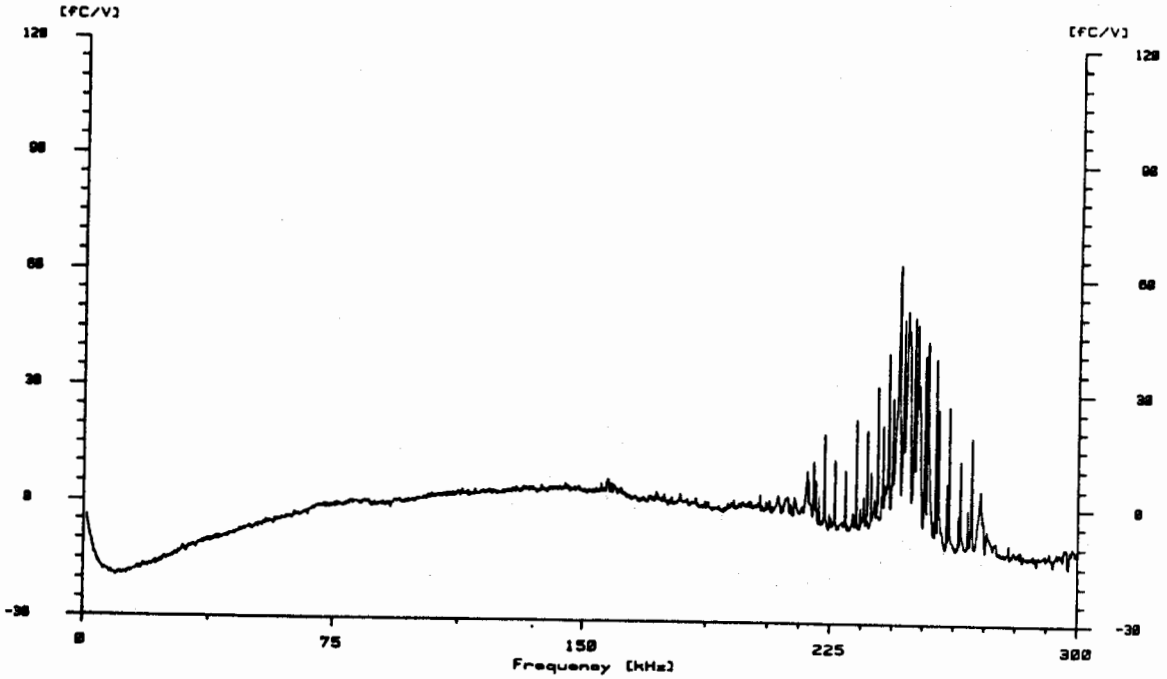

Fig. 9: Coupling of short resonance rod at a transducer with front sealing

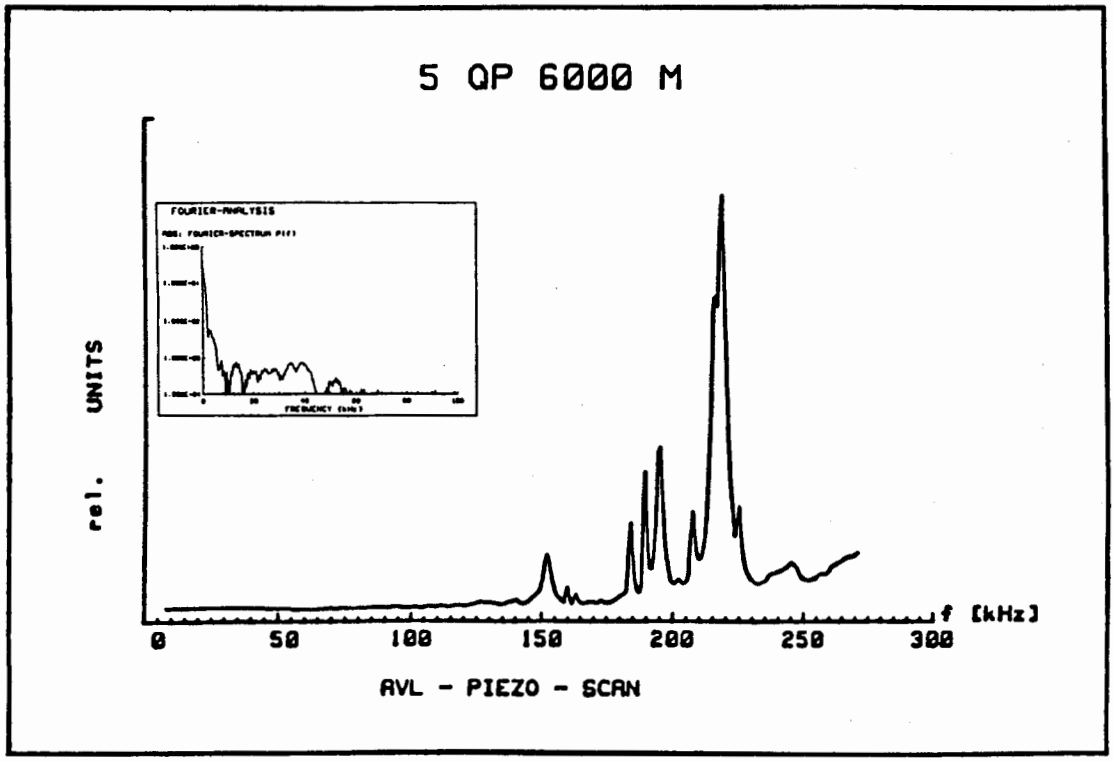

Fig. 10: Comparison of resonance spectrum and Fourier analysis of a shot

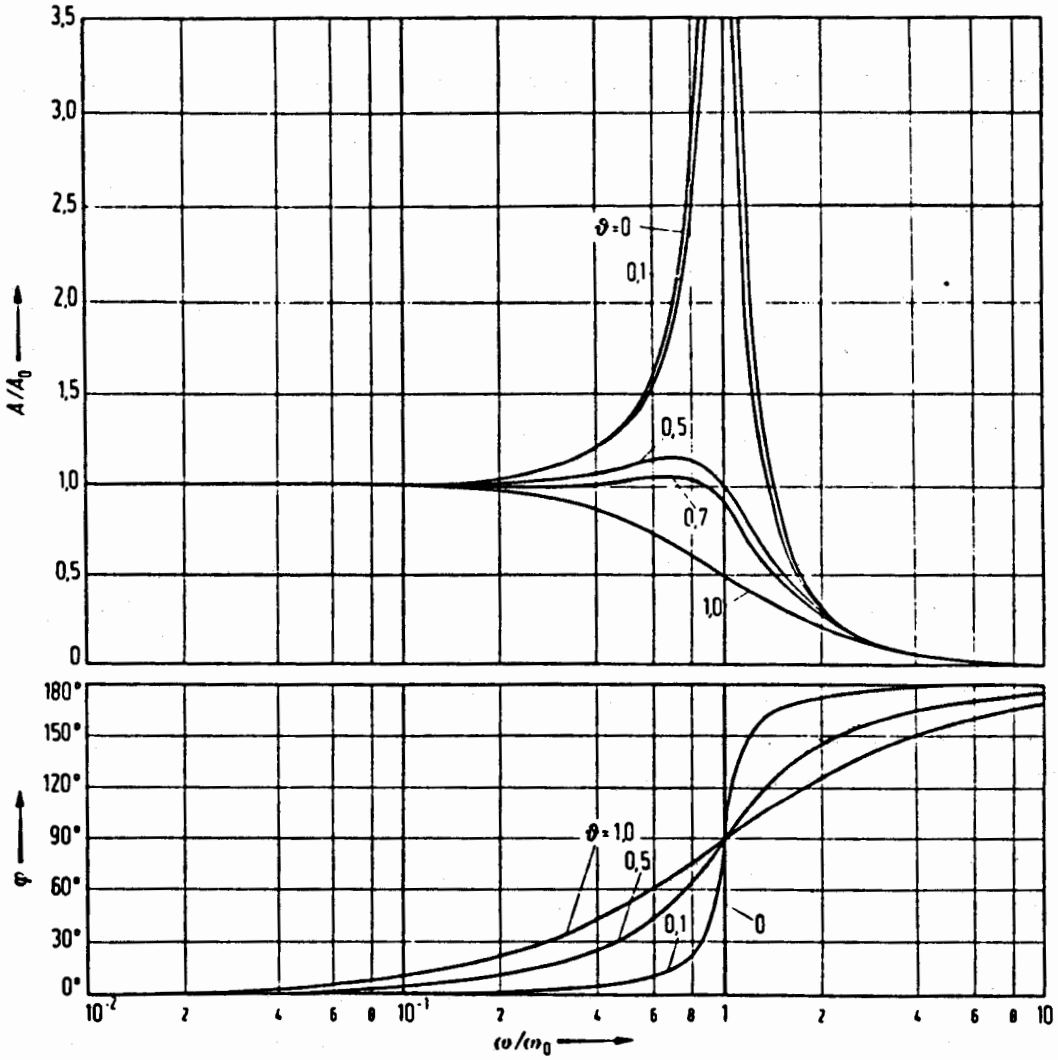

Fig. 11: Variation between the amplitude ratio A/Ao and the phase versus the frequency ratio in case of different damping factors

As general rule you will obtain 1% of the resonance superimposition at 10 % of the resonance frequency.

Conclusions

The following facts have to be considered when choosing the transducer type and at the installation of the transducer:

- Depending on the actual accuracy of measurement, the pressure transducer must have a high main resonance frequency.

- The deviation of main frequencies caused by pressure and heat are not important if the main resonance frequencies are high enough.

- No low resonances, in particular, no resonances caused by installation of the transducer should occur in the dominant Fourier spectrum of the signal.

- In order to obtain well reproducible installation conditions the resonance spectrum should be measured.

- The influence of grease and other pressure transmission media on the resonances can be determined and an appropiate damping factor set.

- The Piezo-Scan resonance spectrum provides and excellent control system for the variation of transducer specifications.

4. Measurement of acceleration sensitivity

The acceleration sensitivity is defined as the signal of the transducer activated by the acceleration of the system. If piezoelectric transducers are used, the unit is pC/(m/s2). In practice the unit MPa/g is more helpful as it provides a direct comparision to the signal to distortion ratio. The typical figure for the acceleration sensitivity with ballistic pressure transducers is 0.0001 MPa/g, i.e. the signal deviation of 1 MPa requires an acceleration of 10,000 g.

4.1 Possible accelerations during a shot

The main acceleration is obtained by the acceleration of the barrel recoil, however, additional bending oscillations and acoustic waves in the barrel have to be considered. Extremely high acceleration levels occur with transducers mounted in projectiles. Depending on the type of installation the longitudinal or transversal acceleration sensitivity has to be taken into account.

4.2 Measurement systems

As shown above the acceleration sensitivity of the piezoelectric transducer is very low. Therefore, a high sensitive system for detecting such low signal levels is necessary. The resolution of the system has to be lower than 0.001 pC/g in order to measure the acceleration signal with usual shaker systems. We have fulfilled this requirement by using a low noise frequency response analyzer.

Fig. 12 shows the acceleration test stand and fig. 13 presents a simplified circuit diagram.

The B 671 Acceleration Test Stand is a computer-controlled automatic test equipment consisting of a personal computer, a frequency synthesizer and a frequency response analyzer. The output signal of the frequency synthesizer is controlled by the computer via an IEEE 488 bus and amplified by a power amplifier. It excites the vibration of the shaker. A high precision accelerometer is used as reference measurement system for the acceleration generated by the shaker. The tested transducer is mounted back to back to the reference accelerometer. Both charge-signals are converted to voltage signals by low noise charge amplifiers. These signals are analyzed by the frequency response analyzer. An oscilloscope is used for monitoring the signals. The data is transferred to the personal computer in order to obtain the measuring diagram. Printer and plotter are additional means used for data output.
In addition to the normal menu-controlled measurement an automatic calibration for charge amplifiers is carried out and a computer-controlled set-up of the acceleration level is possible.

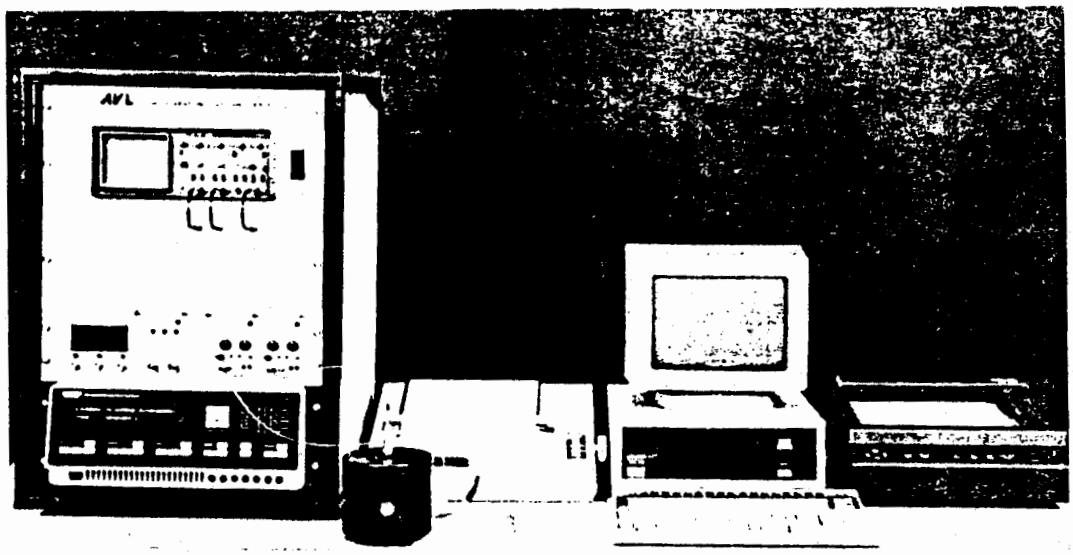

Fig. 12 : Acceleration Test Stand

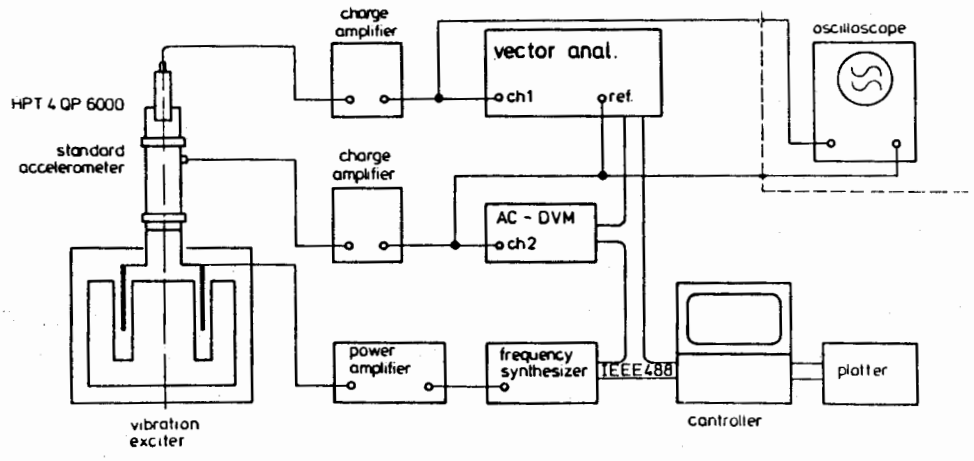

Fig. 13 : Simplified circuit diagram

Fig. 14 shows a measuring plot of a water-cooled pressure transducer with acceleration compensation. Within this frequency range hardly any resonances occur.

Fig. 15 presents printer outputs of the same transducer type, once with, and once without cooling water. The software allows an output in the individual language chosen from the program. The measurement system is highly sensitive, e.g. even a small water drop can be determined due to its surface oscillations.

Fig. 16 shows a transversal sensitivity curve of an accelerometer (Bruel and Kjaer). The bottom figure gives a comparison with transducers with front sealing transducers at different frequencies. The different sensitivity distributions provide more complicated behavior models of the transversal acceleration sensitivity of this transducer.

Bibliographical references:

1. G. Resch:
Applied Piezoelectric Pressure Measurement Technique in Interior Ballistics
3rd International AVL Symposium on Ballistics, Graz, 1982

2. G. Resch:
Progress in Gas Pressure Measurements of Guns
Proceedings of US Army Test & Evaluation Command, Aberdeen, April 8, 1986

3. J. Tichy, G. Gautschi:
Piezoelektrische Meßtechnik (Piezoelectric Measuring Techniques)
Springer Verlag (published by Springer), Berlin, 1980

4. Bruel & Kjaer:
Piezoelectric Accelerometers: Theory and Application Notes,
Danmark 1979

MESSUNG DER BESCHLEUNIGUNGSEMPFINDLICHKEIT

Messobjekt:
Seriennummer : 1148
Type : 12 QP 300cvk
Kommentar :

Messergebnisse: (Mittelwerte zwischen 0.06 kHz und 0.18 kHz)

Beschleunigungsempfindlichkeit : 218.46 fC/g
Beschleunigung : 2.70 g
Phasenlage : -63.82 grd

Konfiguration:
Ref.-Accelerometer : 1.260585 pC/g
Shaker-Type : B&K 4809
Ladungsverst.(ref) : 100 pC/V
Ladungsverst.(mess): 10 pC/V
Messpunkte-Anzahl : 100

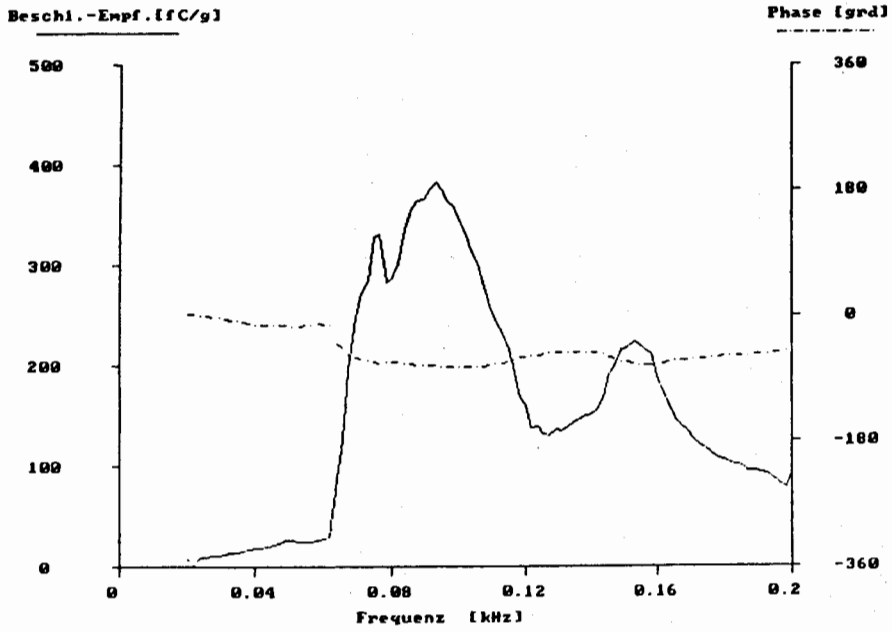

MESSUNG DER BESCHLEUNIGUNGSEMPFINDLICHKEIT

Messobjekt:
Seriennummer : 1148
Type : 12 QP 300cvk
Kommentar : Messung ohne Kuehlwasser
Geber ausgeblasen

Messergebnisse: (Mittelwerte zwischen 0.06 kHz und 0.18 kHz)

Beschleunigungsempfindlichkeit : 5.35 fC/g
Beschleunigung : 4.74 g
Phasenlage : 2.76 grd

Konfiguration:
Ref.-Accelerometer : 1.260585 pC/g
Shaker-Type : B&K 4809
Ladungsverst.(ref) : 100 pC/V
Ladungsverst.(mess): 1 pC/V
Messpunkte-Anzahl : 100

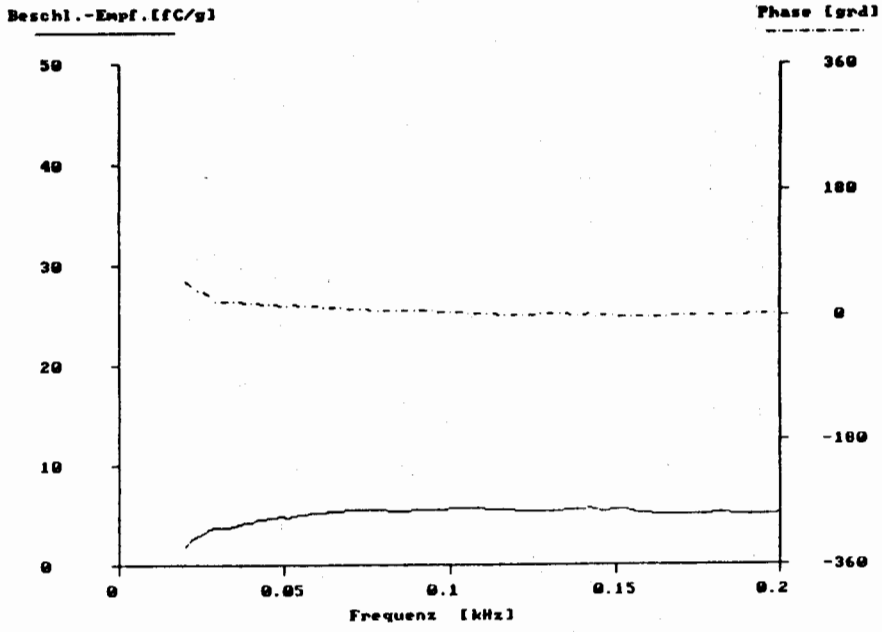

Fig. 15: Printer output of a water-cooled transducer, once with and once without cooling water

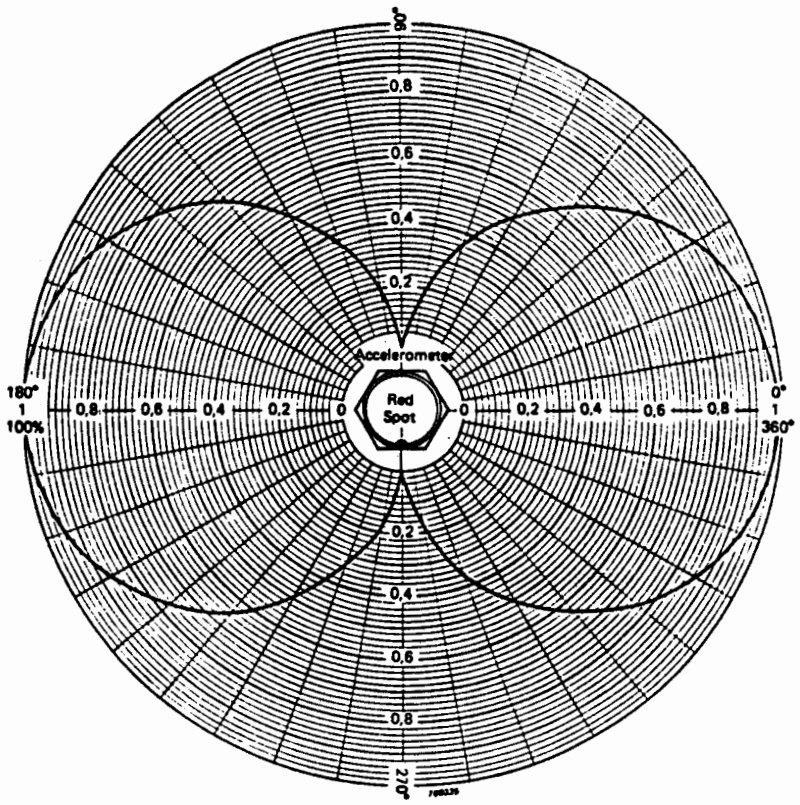

Chart for determining accelerometer transverse sensitivity in any direction when the maximum transverse sensitivity is known

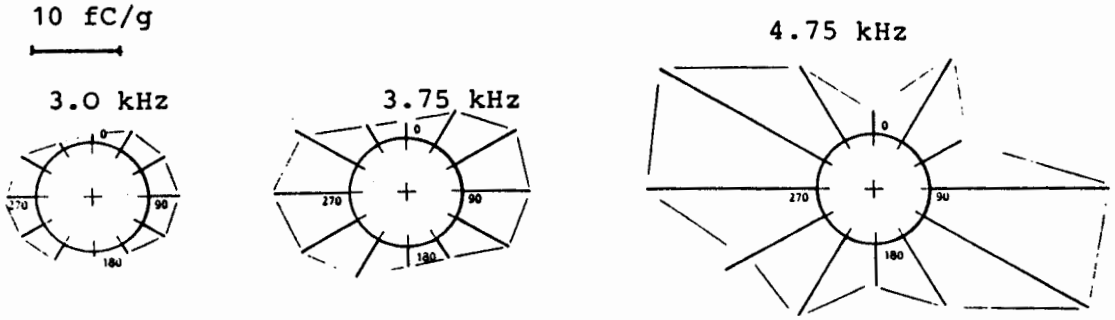

Fig. 16: Transversal acceleration sensitivity of piezo-electric transducers :

a) accelerometer according to Bruel & Kjaer

b) transducer with front sealing

INTERCHANGEABILITY: an IMPROVED WEIGHING TECHNIQUE

David First, President DJ Instruments, Inc.

SUMMARY

Accurate and reliable weight/mass measurements with load cells require reliable procedures as well as accurate/reliable measurement instrumentation. This paper describes a procedure, utilizing currently available instrumentation, which simplifies recertification logistics, improves utilization of existing hardware, eliminates disastrous effects on program schedule of instrument failure, while maintaining or improving overall weighing accuracy.

Today's "typical" weighing system consists of two parts, a digital display instrument and load cells. Once certified as a system, these parts are "married" forever. If one part of the system fails, or is damaged, the complete system must be returned for recertification. Obviously no weighing can take place while the system is being recertified.

The weighing system discussed in this paper adds a third component to the above described system (a Standardizer) and modifies the instrument specifications so that the instrument calibration is independent of load cell and cable characteristics. (Interchangeability) In an Interchangeable system the load cell and Standardizer are independently certified and then the instrument is certified by the Standardizer. Thus the load cell and instrument are no longer married.

The Gage and Standards Center, Naval Weapons Station, Seal Beach, Pomona Annex has been using the Interchangeablity concept for about 18 years. The recertification cycles which they use for the various weighing system components are shown and, recertification data taken on two load cells over a five year period are included in Appendix 1. Appendix 11 shows typical resolution, accuracy, Interchangeability etc. specifications that are obtainable with present day instrumentation.

WHAT IS INTERCHANGEABILITY?

Interchangeability, with regards to weighing systems, is the ability of the instrumentataion to work with any commercially available load cell with out change of accuracy and without requiring end to end calibration. Thus a simple definition of "Interchangeability" is: "Interchangeablilty is the opposite of end-to-end calibration." Most of the specifications for interchangeable instrumentation are the same as standard instrumentation, that is, resolution, linearity, stability, etc. must all be suitable for the level of accuracy required. The additional requirements for interchangeability are: instrument accuracy, linearity, stability, etc. must not be affected by load cell characteristics or cable length and, a removable Standarizer is required.

Nominal bridge resistance of a load cell may be 350 ohms, but the actual input/output resistance may vary due to the addition of balance and calibration resistors. The calibration factor of many types of weighing instruments interacts with these load cell parameters, thus changing load cells changes the instrument calibration factor. However calibration accuracy of an "Interchangeable" instrument is not sensitive to these variations so it can be used with any load cell without loss of calibration accuracy. Actually, for general usage, the instrument should be able to handle 120 to 700 ohm bridges without loss of accuracy.

A six wire, remote sense load cell connection is used to eliminate the effects of cable length, so that instrument calibration will not change if ten feet or a thousand feet of cable are used between the load cell and instrument.

The Standardizer (load cell simulator) is used to set instrument calibration. It should have several output levels over the range of interest so that linearity and repeatability can also be verified. It should also have a means for checking Interchangeablility, that is, a variable signal lead and excitation resisitance. (The DJ-101ST Standardizer varies signal lead resistance from 240 ohms to 1240 ohms, and excitation input resistance from 240 ohms to 65 ohms). The accuracy of the instrument must remain within acceptable limits when subjected to input/output resistance changes of this magnitude.

If the instrument meets these requirements it can be used "interchangeably". Then, any load cell which has a millivolt per volt calibration can be used interchangeably with it.

HOW IT WORKS

An interchangeable system consists of load cell/cable, instrument and Standardizer. In an Interchangeable system the instrument is merely a comparitor/interpolator between the load cell and the Standardizer. Calibration and proper functioning of the instrument is established by the Standardizer. Then the instrument, after calibration, relates and interpolates the output of the load cell to the calibration established by the Standardizer.

The instrument can be calibrated to read directly in engineering units or to read "100%" full scale. In this latter case, 100% represents nominal full scale load cell output (say for example 2mv/v). With the 100% calibration, the instrument can then be used with any load cell capacity, (this makes Interchangeable instrumentaion ideal for multiple cell testing machine calibration kits). Since most accurate weighing requires data correction to account for gravity, buoyancy, etc. translation

from percent to weight poses little additional effort.

COST SAVINGS

Interchangeablity provides significant long term cost savings through simplified recertification procedures, less program interruption and down time, greater use of existing equipment, and less "back-up" equipment required.

Load cells and Standardizers are recertified, not the instrument, so the instrument stays "in the field" and can be in use 100% of the time. By having one more Standardizer than there are instruments, the "extra" Standardizer can be certified and then substituted for each of the Standardizers in the field, permitting periodic recertification of all Standardizers without loss of field operating time. Similarly, an extra load cell of each capacity in use can be certified and then substituted, one at a time, for each load cell in the field, permitting field equipment to be continuously recertified without interupting field weighing operations. In case of damage or failure, a damaged load cell can be replaced by a certified load cell or the instrument can be repaired/replaced without requiring that the entire system be returned for recertification (which would be the case with end-to-end calibration). It is easily shown that the long range cost savings through Interchangeability far outweigh the initial additional cost of the Standardizer.

INTERCHANGEABILITY IS NOT NOVEL

After all, when you buy a digital voltmeter, you don't have it end-to-end calibrated with the voltage measurement you are going to make. The voltmeter accuracy is presumed independent of the measurement to be made.

In the early days of the load cell (and until fairly recently) the load cell accuracy was better than the readout instrumentation. With a strain gage bridge the instrument has to read an extremely low level signal, to measure this voltage on a ratio basis (six wire), and to contend with a high common mode voltage on the signal leads.

In the early days of strain gage instrumentation, various approaches were taken to solve this problem, involving both AC and DC excitation, but none had the perfect answer. Thus, on high accuracy weighing systems, the user was "trained" to use end-to-end calibration. What we are proposing here is to "untrain" the user.

We did start manufacturing Interchangeable instrumentation in the early 'sixties and its advantages were recognized and put to use at a few facilities. (see appendix 1). But, unfortunatly,

the instrument was large and heavy and, besides, end-to-end was "the only way to go" at many facilities.

In the past 5/10 years, instrumentation technology has caught up to and passed the load cell so Interchaneablilty is now quite practical. However end-to-end calilbration is firmly entrenched in the recertification proceedure, and will take a while to change. Needless to say, Interchangeable instruments can be end-to-end calibrated, so if you are required to use end-to-end calibration today it still makes sense to buy Interchangeable instrumentation and thus prepare for the future.

CONCLUSION

Using Interchangeable instrumentation, which is currently available, eliminates the constraints of end-to-end calibration thus permitting greater flexibility in the use of existing hardware and results in less "down time" due to recertification and repairs.

As you up-date your present weighing instruments it will pay in the long run to replace them with Interchangeable instruments, even if end-to-end recertification is presently required, thus preparing for future programs which will permit Interchangeability.

AUTHOR BIOGRAPHY

BS Degree in Electronic Engineering from Case Institute of Technology. Starting job at Raytheon, instrumentation experience at BLH, co-founder of Bytrex, Inc. (later named Schaevitz-Bytrex, later still Tyco-Bytrex). Co-founder and currently President of DJ Instruments, Inc.

APPENDIX 1

The Gage and Standards Center, Naval Weapons Station, Seal Beach, Pomona Annex has, as one of its tasks, to furnish equipment for accurate mass (weight) measurements on large programs. This includes weight measurement of components manufactured at various geographic locations, then a combined weighing of these components assembled. Needless to say, it is mandatory that the measured weight of the assembled components equal the total of the weighings of the individual components.

In anticipation of the logistics problem of maintaining numerous widely scattered "certified" weighing stations, Navy Pomona started using interchangeable instrumentation in the mid 'sixties. The typical "field" weigh station, in this program, utilizes four load cells with one instrument(the instrument has interchangeablity as well as accuracy) and one Standardizer. Additional instrumentation and load cells were added as the programs expanded.

INTERCHANGEABLITY provided four advantages in this program: a) simplified recertification, b) flexibility, c) simplified maintenance/repair and, d) less backup equipment required.

Simplified Recertification

Fig. Append 1 outlines the recertification cycles for the various weighing system components. A DJ-100 series Megadigit indicator is associated with each dead weight tester and each of these indicators is certified by its DJ-101ST Standardizer. Output data from the instrument, corresponding to weight applied to the load cell, is recorded in millivolts per volt.

It is seen that the load cells are recertified every six months (or every 12 months, depending on the program) and the Standardizer is recertified every year. Most important, note that the instrument is not returned at all for recertification. It is scheduled for general maintenance every five years.

Flexibility

All load cells are interchangeable, so weighing capacity at any location can be changed by sending out a new set of load cells. Also, load cells can be interchanged among several programs.

Simplified Maintenance and Repair

Since all load cells and instruments are interchangeable, any load cell or instrument can be replaced without dismounting the remaining load cells.

Less Backup

Since each load cell is interchangeable with all others, and since instruments can be field repaired without recertification, it is not necessary to "back up" each critical field weighing station with a complete instrument/load cell system.

REPEATABILITY

Repeatability, in particular repeatability over a long period of time, is the cornerstone of accurate weight measurement. It represents the ability of a weighing system to be calibrated and then maintain that calibration over a long period of time.

Pages 8&9 show fifteen sets of data taken on each of two 0.3k load cells, over a period of 5.5 years. Note that the instrument reads in percent so 100% equals 0.3k.

Also shown is a summary of: a) AVERAGE reading for each weight, b) MAXIMUM deviation and the STANDARD deviation from the average also, c) the STANDARD deviation, as a percentage of applied load. Since Standardizers are recertified every year, this data would include four or five changes and recertifications of the Standardizers (and perhaps one or two repairs of the instrument).

Note that this data includes non repeatability of the load cell incurred during more than five years of field use, as well as the effects of handling, shipping etc.

Information shown is an "in house" summary of data taken on the load cell. It is used to monitor long term performance of the load cell and is not the certified data sent out with the load cell.

FIGURE APPEND 1

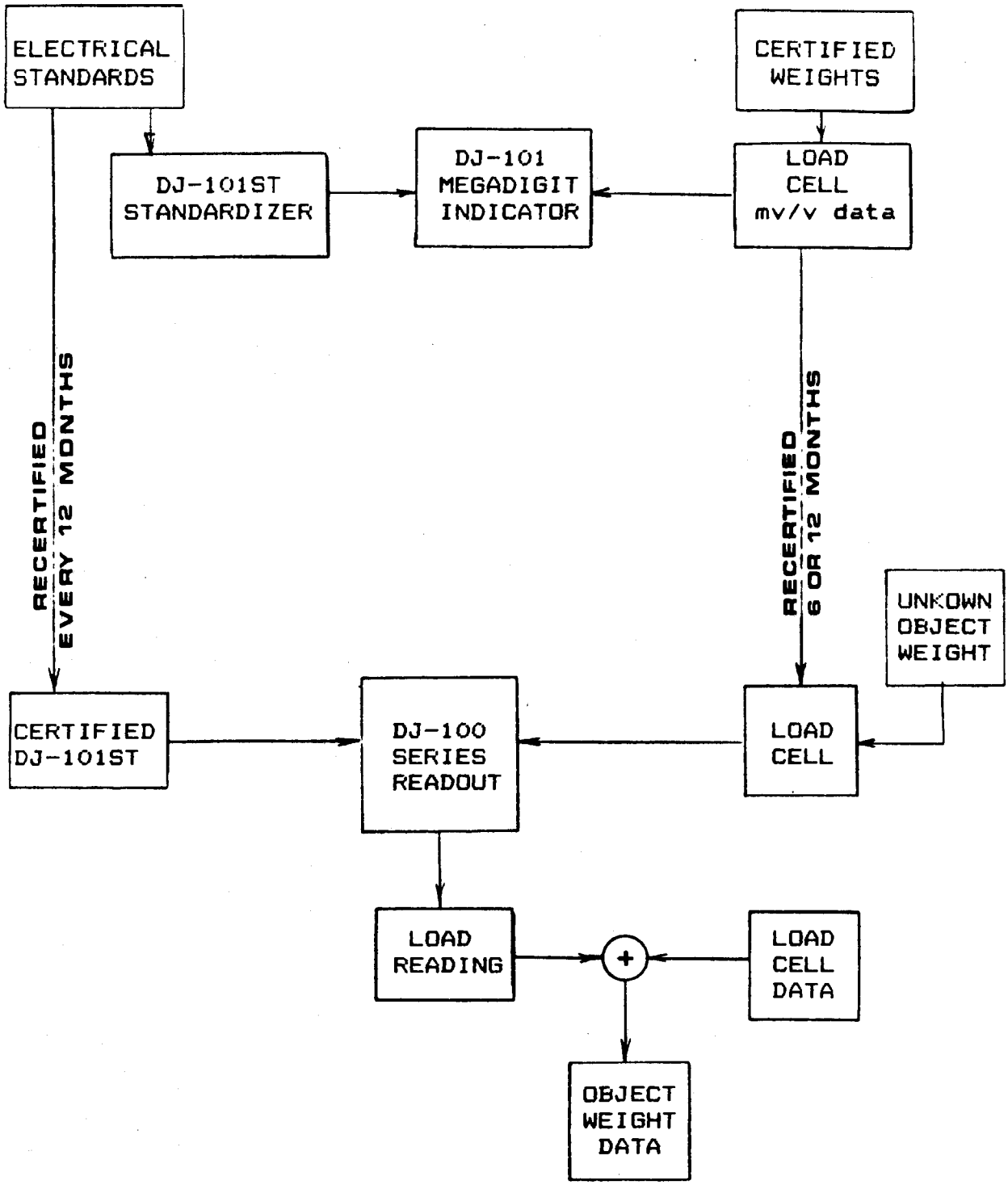

TENSION .3K Load Cell S/N 41174 Bottom

Values Given are a Three Run Average of the
DJ Model 100A Indicator Readings (%)

Date

Applied Force	40	60	80	100	140	160	180	200	240	280	300
04-77	13.338		26.673	33.340	46.675	53.341	60.008	66.674	80.005	93.333	100.000
09-77	13.336		26.670	33.336	46.672	53.342	60.006	66.671	80.007	93.333	99.998
02-78	13.334		26.667	33.334	46.669	53.336	60.002	66.669	79.994	93.334	99.997
04-78	13.334		26.672	33.340	46.678	53.343	60.011	66.677	80.009	93.340	99.998
09-78	13.338	20.004	26.665	33.335	46.673	53.339	60.005	66.674	80.002		100.003
12-78	13.334	19.999	26.667	33.333	46.666	53.339	60.007	66.672	79.994		99.997
05-79	13.339	20.005	26.671	33.340	46.674	53.339	60.005	66.670	80.000		99.997
11-79	13.335	20.004	26.673	33.338	46.670	53.337	60.003	66.674	80.002		99.994
01-80	13.336	20.005	26.671	33.338	46.672	53.340	60.005	66.670	80.004		100.003
04-80	13.334	20.001	26.670	33.336	46.673	53.340	60.007	66.675	80.008		100.005
12-80	13.335	20.000	26.667	33.334	46.668	53.338	60.002	66.679	79.996	93.333	99.992
2-80	13.336	20.000	26.669	33.336	46.671	53.340	60.005	66.669	79.999	93.330	99.994
8-81	13.333	20.003	26.669	33.338	46.677	53.342	60.008	66.672	80.008	93.334	100.000
12-81	13.334	20.001	26.667	33.334	46.670	53.335	60.002	66.666	79.999	93.334	99.998
11-82	13.330	19.998	26.665	33.331	46.662	53.339	60.004	66.672	79.993	93.333	99.991
Average Reading	13.335	20.002	26.669	33.336	46.671	53.339	60.005	66.672	80.001	93.334	99.998
Maximum Deviation from Average	.005%	.004%	.004%	.005%	.007%	.005	.006	.007	.008	.006	.007
Standard Deviation from Average (%)	.002%	.003%	.003	.003	.004	.002	.003	.003	.006	.003	.004
Standard Deviation % of Applied Load	.018%	.013%	.010%	.008	.009	.004	.004	.004%	.007	.003	.004

TENSION .3K Load Cell S/N 41181 Top

Values Given are a Three Run Average of the
DJ Model 100A Indicator Reading (%)

Date *This Data Point Not Used

Applied Force	40	60	80	100	140	160	180	200	240	280	300
04-77	13.317		26.633	33.293	46.613	53.275	59.936	66.598	79.922	93.247	99.909
09-77	13.317		26.629	33.294	46.611	53.276	59.934	66.598	79.919	93.243	99.907
02-78	13.313		26.632	33.291	46.612	53.272	59.935	66.595	79.913	93.237	99.899
04-78	13.313		26.633	33.295	46.618	53.275	59.937	66.598	77.923	93.244	99.906
09-78	13.317	19.971	26.629	33.286	46.608	53.272	59.929	66.592	79.915		99.905
12-78	13.314	19.972	26.631	33.288	46.606	53.268	59.930	66.591	79.924		99.894
05-79	13.319	19.975	26.632	33.295	46.615	53.276	59.936	66.587	79.916		99.904
11-79	13.312	19.974	26.633	33.290	46.608	53.279	59.928	66.591	79.913		99.903
01-80	13.312	19.970	26.632	33.286	46.604	53.265	59.924	66.584	79.907		99.894
04-80	13.313	19.970	26.630	33.288	46.610	53.270	59.932	66.593	79.917		99.904
12-80	13.316	19.964	26.624	33.283	46.608	53.273	59.934	*66.987	79.920	93.242	99.902
2-80	13.313	19.966	26.628	33.288	46.605	53.267	59.930	66.585	79.908	93.230	99.890
8-81	13.314	19.972	26.638	33.292	46.614	53.272	59.932	66.591	79.915	93.235	99.897
12-81	13.315	19.973	26.630	33.289	46.610	53.268	59.931	66.591	79.914	93.234	99.891
11-82	13.317	19.968	26.623	33.281	46.607	53.265	59.933	66.587	79.908	93.237	99.899
Average Reading	13.315	19.970	26.630	33.289	46.610	53.272	59.932	66.591	79.916	93.239	99.900
Maximum Deviation from Average	.004%	.006%	.007%	.008%	.008%	.007	.006	.007	.008	.009	.01
Standard Deviation from Average (%)	.002%	.003%	.004	.0042	.004	.004	.004	.005	.005	.006	.006
Standard Deviation % of Applied Load	.016%	.017%	.014%	.013%	.008%	.008	.006	.007	.007	.006	.006

APPEND 11
SPECIFICATIONS

	UNITS	DJ-101	DJ-102	DJ-110	DJ-320/13
Span Adjustable	mv/v	1-15	1-15	1-15	1-6
Resolution	% full scale	.0001	.0005	.0005	.002
Linearity	% full scale	±.0015	±.0015	± 0015	±.004
Total Range	% full scale	−2%/+121%	−2%/+121%	−2%/+121%	−5%/+110%
Zero Adjust Range	% full scale	±5%	±5%	±5%	±5%
Tempco Zero	micro-volts/°F	±.05	±.05	±.05	±.2
Tempco Span	% reading/°F	±.0005	±.0005	±.0005	±.001
Interchangeable	See note 1	Yes	Yes	Yes	Yes
Transducer Bridge	ohms	80-1000	80-1000	80-1000	80-700
Bridge Assymetry (common mode)	% max	40	40	40	15
Polarity Reversing Switch		Yes	Yes	Yes	Yes
Excitation (Transducer)	VDC	5-10	6-10	6-10	10
Remote Sensing (6-wire)		Yes	Yes	Yes	Yes
Standardizer		Optional	Optional	STZ-2	NA
Number of load cell channels		4	4	1	1
Input Connectors		5	5	1	1
Display Digits		7	7	7	6
Count By (min increment)		1	1,2,3,4,5,6,7	1,2,3,4,5,6,7	1,2,3,4,5,6,7
Programmable Decimal Point		No	Yes	Yes	Yes
Size: W & D & H	inches	21×22×18½	21×22×18½	19×21×7	8×11½×3
Weight	pounds	75	75	50	10
Power		← 115 VAC ±10%, 60 Hz →			
OPTIONS					
DJ-101-ST	Standardizer	Yes	Yes	NA	NA
BCD Output	Parallel	Yes	Yes	Yes	Yes
RS232C/20ma TTY		Yes	Yes	Yes	Yes
Remote Channel Select		Yes	Yes	NA	NA
Hold (freeze) Display		Yes	Yes	Yes	Yes
Suitcase Type Case	Metal	NA	NA	NA	Yes

Additional detailed information is available on each type of instrument.

REPEATABILITY

DJ-101:	±(.0005% of reading + .001% full scale + 0.05 microvolt)
DJ-102, DJ-110:	±(.001% of reading + .001% full scale + .05 microvolt)
DJ-320/13:	±(.002% of reading + .002% full scale + .2 microvolt)

ACCURACY

DJ-101:	±(.001% of reading + .002% full scale + 0.05 microvolt)
DJ-102, DJ-110:	±(.002% of reading + .002% full scale + 0.05 microvolt)
DJ-320/13:	±(.003% of reading + .003% full scale + .2 microvolt)

NOTE 1: The maximum added calibration uncertainty, due to changing any indicator with any combination of load cells and/or interconnecting cable, does not exceed ±0.005% of reading from 100% full scale down to 10% full scale. This applies to any transducer specified and for any full scale calibration between 1 mv/v and 15 mv/v. Uncertainty within ±0.01% on DJ-320/13.

NOTE 2: Accuracy statement does not include error of calibration standard.

Specifications subject to change without notice.
Terms and conditions of our standard one-year limited warranty apply.

D • J INSTRUMENTS INC.

18 REPUBLIC ROAD, N. BILLERICA, MA 01862 tel. (617) 667-5301

COMMENT: Roger Noyes to David First: One of the things you didn't mention is that you can program your readouts in engineering units. We have found that is very helpful to keep the technicians from doing conversions.

Q: Patrick Walters: Do you have a standard isolator circuit and what frequency do you run your carrier? Do you use a simple RC filter in the demodulator? What kind of demodulation filter do your use?

A: We have several different frequencies depending on the system. Most of our industrial devices run at a 0.5 or 1 MHz. The high temperature devices run as displacement transducers at 25 or 50 kHz Since the entire sensor is encased in inconel, we have to penetrate the inconel window to look at the particular target. In order to do so, we drop the frequency of the oscillator or the carrier in those two particular systems. On the output of the demodulator, we do use a simple RC filter there, go into a differential amplifier, and then linearize the output through a log-amp converter, which is kind of unique in the industry. Not many companies use the log amps to linearize the output from transducers. Then we have further filtering on down the line of the dc section. I might add that these systems have zero offset controls so that you can put zero volts out of the system at any displacement up to about 50 percent. You can also set the output in engineering units in either metric or English.

Q: R. Maglic: How accurate is your pressure sensor?

A: Our pressure transducers have a button on the back of the diaphragm and this button rather than the diaphragm itself allows the eddy currents to stay inside the transducer itself and not leak out through the diaphragm. We only use about .0075 full diaphragm deflection for full-scale pressure. We are looking at less than 0.001 of an inch deflection with a 1/2-inch diameter, so we don't get a great deal of bow. And you are right; there are more accurate pressure transducers on the market but none that go to 1200^{o}F.

APPLICATION OF A PRECISION MEASUREMENT TECHNOLOGY

An Instructional Seminar

SEMINAR OVERVIEW

PURPOSE

This seminar is designed to familiarize you with who we are and our technology, and to help find solutions to position measurement problems.

Kaman Measuring Systems Seminar Workbook SWB 865

WHO WE ARE

Kaman Corporation, headquartered in Bloomfield, Connecticut, is a half-billion dollar a year firm with over 40 years experience as a leader in aerospace, industrial, and consumer products. The three subsidiaries are: Diversified Technologies, Industrial Distribution, and Music.

DIVERSIFIED TECHNOLOGIES

- **KAMAN INSTRUMENTATION** specializes in high technology products for research, industry, and government. We manufacture RF transmission and delay lines, neutron generators for oil well logging, **and precision displacement measuring systems for industrial and laboratory applications**.

- **KAMAN SCIENCES** is involved in matters of deterrence, nuclear weapons effects, and enhancement of command, control, communication and intelligence systems. They also provide engineering and technical analysis services to the Space Command and software for the radio and TV broadcast industry. An ancillary product line provides ceramic coating for bearing surfaces and sharpening systems.

- **KAMAN AEROSPACE** manufactures the US Navy SH-2F LAMPS (Light Airborne Multi-purpose System) MK1 Helicopter. They are also a major subcontractor, providing components for the Air Force's B1 and C5B, the Boeing 767, the Navy's F-14 and A6, the Space Shuttle, and the H-60 and H-53 helicopters.

- **KAMATICS** manufactures high-performance self lubricating bearings and KAflex® couplings: high technology mechanical drive couplings that accept misalignment and require no maintenance.

- **AIR KAMAN** provides aviation services for the Jackson Port Authority in Florida and also provides manufacturing space for Kaman Aerospace's control surface assemblies for the C5B.

INDUSTRIAL DISTRIBUTION

- **KAMAN BEARING AND SUPPLY** companies include 149 service centers in the United States and Canada that constitute the largest bearing distribution network in America. They stock and distribute bearings, power transmission equipment, hydraulics, industrial rubber products, and fluid power components.

MUSIC

- The Kaman music divisions include manufacturing and distribution. The **OVATION** acoustic and acoustic electric guitars and **KAMAN MUSICAL STRINGS** are the focus of the manufacturing segment. Ovation guitars are used by major artists worldwide. Kaman music companies distribute traditional instruments as well as synthetic/electric sound generation products. In addition to the Ovation line, they distribute the products of many other manufacturers including Seiko, Clarion, Takemine, Applause, and Sony.

ABOUT KAMAN INSTRUMENTATION AND OUR MEASURING SYSTEMS

Kaman Instrumentation has been a pioneer in noncontacting displacement measuring systems for over 25 years. Our patented inductive bridge systems provide high resolution, accuracy, and repeatability with a low noise floor. Unlike many other measurement technologies, ours is virtually unaffected by environmental contaminants such as oil, dirt, humidity, radiation, stray RF and magnetic fields. Kaman Measuring Systems provide efficient, cost-effective solutions to measurement problems in a broad variety of manufacturing and laboratory applications. Our systems have earned a reputation for excellence in aerospace, auto assembly and testing, computer peripherals, steel fabrication, biomedical research labs, food processing plants, power generation facilities, and many, many other industries. The majority of our sales are to prior customers, a testimony to the reliability and effectiveness of Kaman Measuring Systems.

WHERE WE ARE

Headquartered in a 60,000 square foot research and manufacturing facility in Colorado Springs, Colorado, we have sales representatives across America and worldwide. In addition to the domestic representatives listed on the following map, there are sales offices in Japan, Australia, Korea, South Africa, Belgium, Luxumbourg, Netherlands, England, Finland, France, Italy, Spain, and Sweden. Contact us in Colorado Springs at (303) 599-1825 for additional information.

TYPICAL APPLICATIONS

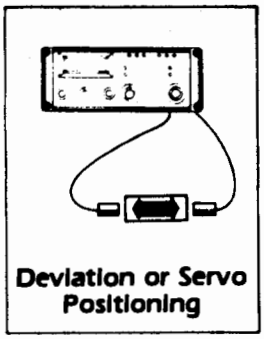
Deviation or Servo Positioning

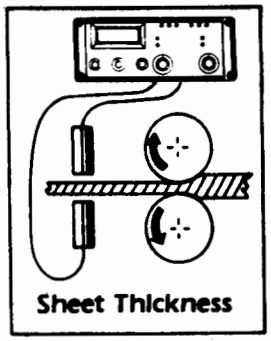
Sheet Thickness

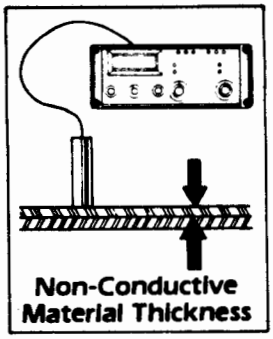
Non-Conductive Material Thickness

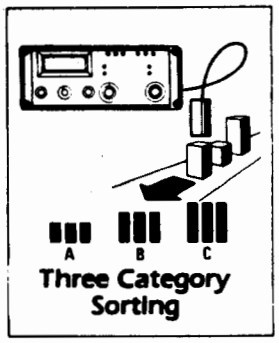

Three Category Sorting

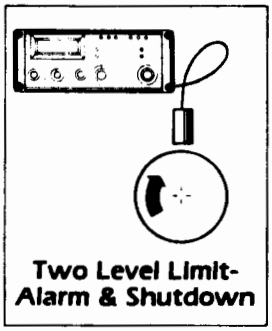
Two Level Limit-Alarm & Shutdown

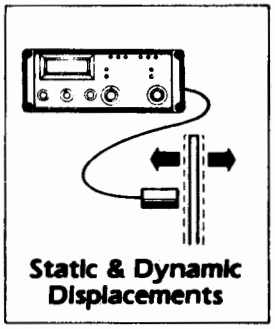
Static & Dynamic Displacements

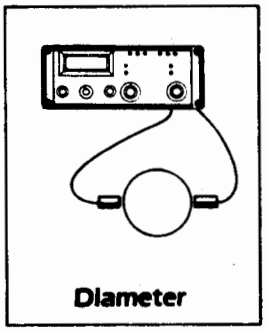
Diameter

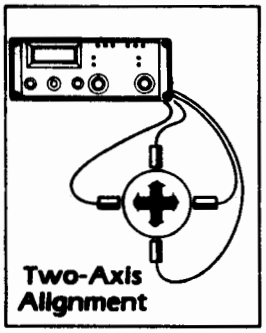
Two-Axis Alignment

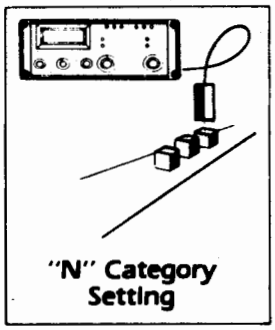
"N" Category Setting

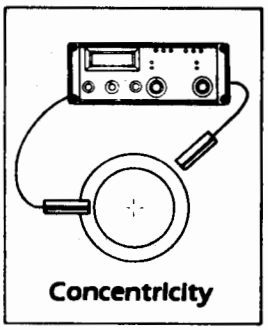
Concentricity


Orbit Tracing

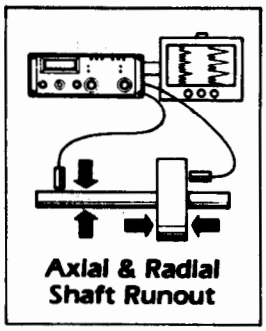
Axial & Radial Shaft Runout

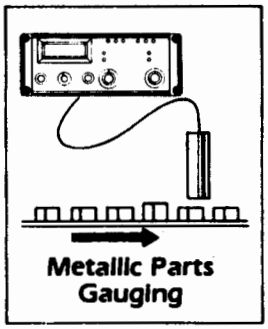
Metallic Parts Gauging

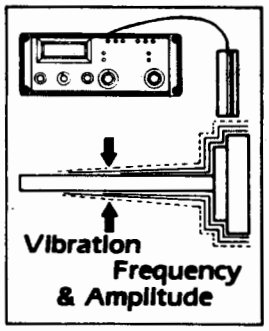
Vibration Frequency & Amplitude

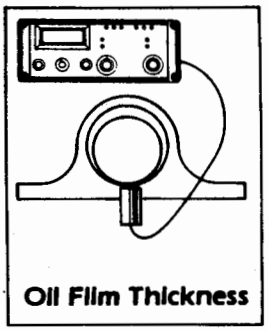
Oil Film Thickness

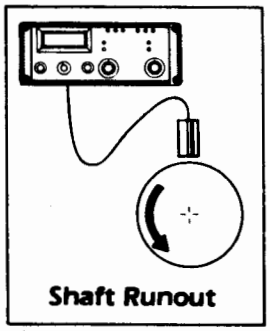
Shaft Runout

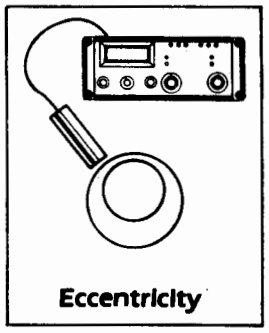
Eccentricity

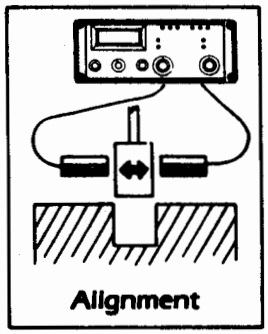
Alignment

GLOSSARY OF RELEVANT TERMS

ACCURACY

The ratio of error to full scale output, expressed as within ±x percent of Full Scale Output (FSO).

A/D CONVERTER

A device that converts an Analog signal to Digital.

ANALOG OUTPUT

Output voltage of a system that is a continuous function of the target position relative to the sensor.

DIMENSIONAL STANDARD

A standard of measurement or precision reference against which you correlate the output of the system, i.e., a micrometer fixture, feeler gages, precision ceramic spacers, etc.

DRIFT

Undesirable change in system output over a period of time while the sensor/target position is constant. It may be unidirectional or cyclical and is caused by such things as aging of the electrical components or by environmental changes impacting the system.

EFFECTIVE RESOLUTION

An application dependent value determined by multiplying the Equivalent RMS Input Noise specification (below) by the square root of the measurement bandwidth.

ELECTRICAL RUNOUT

An error voltage introduced to the output as a result of variations in the permeability of ferro magnetic targets.

EQUIVALENT RMS INPUT NOISE

A figure of merit used to quantify the Noise contributed by a system component. It incorporates into a single value, factors influencing a noise specification such as signal-to-noise ratio, noise floor, and System Bandwidth. Given a measurement system's sensitivity and the level of "white noise," Equivalent RMS Input Noise can be expressed using actual measurement units.

ERROR

The algebraic difference between the indicated value and the true value of the measurand (below). Usually expressed as a percent of the Full Scale Output.

FREQUENCY RESPONSE

The change with frequency of the output measurand amplitude ratio (and the phase difference between output and measurand) for a sinusoidally varying measurand applied to a transducer within a stated range of measurand.

FULL SCALE OUTPUT (FSO)

The voltage output measured at full scale displacement or the maximum displacement for which a system is calibrated. The algebraic difference between the end points.

GAIN

The function of increasing or decreasing Sensitivity (below). Changing gain will increase or decrease the slope of the output curve.

HYSTERESIS

The difference in system output at any given displacement when that displacement is approached first from one direction and then the opposite direction. When activating switch points, this refers to a designed lag effect between switch point pull in and drop out.

LINEARITY

The maximum deviation of any point of a calibrated system's output curve from a best fit straight line. Expressed in actual units, e.g., microinches.

MEASURAND

A physical quantity, property, or condition that is measured. Buzzword for the thing you're measuring.

MEASUREMENT BANDWIDTH

The difference between the upper and lower Frequency Response limits of a system. Our standard system bandwidth is Zero to 30,000Hz.

MEASURING RANGE

The full range of target motion over which the various specifications such as resolution, linearity, and sensitivity can be met. Expressed as the upper and lower limits of a sensor's measuring capability.

NOISE

Any unwanted electrical disturbance or spurious signal that modifies transmitting, display, or recording of desired data.

NULL GAP

The point at which the target is equidistant from each sensor of a differential pair. System output at null is 0Vdc. The actual gap is measured from the sensor face to the corresponding target face and includes a required offset.

OFFSET

The minimum distance between the sensor face and the target. This is usually specified in mils and dependent upon sensor type. Offset is necessary to both prevent the target from striking the sensor face and to optimize performance.

OUTPUT

The electrical quantity produced by the sensor and modified by the system as a function of target position relative to the sensor.

REPEATABILITY

The ability of a system to consistantly reproduce output readings when applying the same Dimensional Standard to it repeatedly, under the same conditions, and in the same direction.

RESOLUTION (Dynamic)

An application dependant value determined by multiplying the equivalent RMS Input Noise specification by the square root of the Measurement Bandwidth.

RESOLUTION (Static)

The smallest discernable change in target position relative to a reference.

SCALE FACTOR

See Sensitivity, below. Usually expressed as millivolts per mil (XmV/mil) or millivolts per millimeter (XmV/mm). Also called Gage Factor.

SENSITIVITY

The ratio of change in system output in Volts to a change in relative position of the target. Simply put, volts out per unit of displacement.

STABILITY

The ability of the system to retain its performance throughout its specified operating and storage life.

SYNCHRONIZATION

In this context it refers to a process where two or more systems are slaved to a master system. This is done to prevent beat note interference or cross talk between rnultiple sensors in close proximity and driven by different oscillators.

THERMAL SENSITIVITY SHIFT

A change in the slope of the calibration curve (sensitivity) that is a function of temperature only.

TRANSDUCER

A device which provides a useable output in response to a specified measurand.

VARIABLE IMPEDANCE TRANSDUCER

A device that applies a stimulus (the field produced in a coil by a single frequency AC current) to a conductive target, measures the total opposition to that field by the target, and converts it into an electrical signal proportional to the position of the target relative to the coil (sensor).

ZERO SHIFT

Movement of the output curve up or down across the x-axis (see figure, page 33) without changing the slope (gain) or linearity of the curve. Accomplished using the zero control.

NONCONTACTING MEASUREMENT DEVICES

There are a number of noncontacting measurement devices on the market, each with advantages and disadvantages. Here is a brief overview.

DEVICE	ADVANTAGES	DISADVANTAGES
Air gaging	it works	costly (requires a clean air supply system, pressure transducer, and electronics), very limited range, user sensitive, environmentally sensitive
Capacitance stray and grounded	stray capacitance is relatively target insensitive	costly, difficult to linearize, environmentally sensitive (need a constant dialectric and clean surface)
Infrared or photonic, and fiber optics	reasonable cost, small spot size, will work with most target materials	environmentally sensitive (requires a clean reflective target), limited range, poor linearity
Laser	greater range, excellent resolution and linearity	very expensive, difficult to set up and use, environmentally sensitive
X-Ray and Beta backscatter	effective density measuring device, handles a wide pass line variation, effective with most materials	expensive and hazardous to use, limited to thickness only
Ultrasonic	long measuring ranges (in feet), good linearity	limited applications and frequency response, poor resolution
Hall effect	inexpensive	needs a magnet for a target, poor linearity, temperature sensitive
Eddy current (Colpitts)	inexpensive, unaffected by nonconductive intervening material, easy to use, prefers highly resistive targets, long term stability	requires conductive target, limited range, poor linearity over full range, temperature sensitive, no zero offset, cannot synchronize, limited sensor cable length, high output impedance, poor frequency response, high noise floor
Inductive bridge	inexpensive, excellent linearity, easy to calibrate, temperature stable, unaffected by intervening nonconductive material, good frequency response, very high resolution, easy to use, long term stability, low impedance low noise floor, can be synchronized, zero offset capability	requires a conductive target

SYSTEM OVERVIEW

Kaman Measuring Systems use the principle of impedance variation caused by eddy currents induced in a conductive target by a sensor coil. The sensor coil is one leg of a balanced bridge network activated by a high frequency generated by a crystal controlled oscillator. Excitation of the sensor coil generates an electromagnetic field that couples with the target. The strength of the electromagnetic coupling between the sensor and target depends upon the gap between them. Signal conditioning electronics sense impedance variation as the gap changes and translate it into a usable displacement signal. This technology is capable of submicroinch resolution. Information on the following pages further details how this is done.

NONCONTACT MEASUREMENTS

As illustrated at right, the basic function of these systems is to accurately monitor a target's position relative to a reference plane. Out of this simple principle is born a surprising variety of measurement applications.

SYSTEM COMPONENTS

The major components of a complete system are the **sensor, a cable** connecting it to the **signal conditioning electronics**, and some **output analysis device** that uses the signal to either convey information to the user, to record it, or use it to control equipment.

NONCONTACT MEASUREMENTS

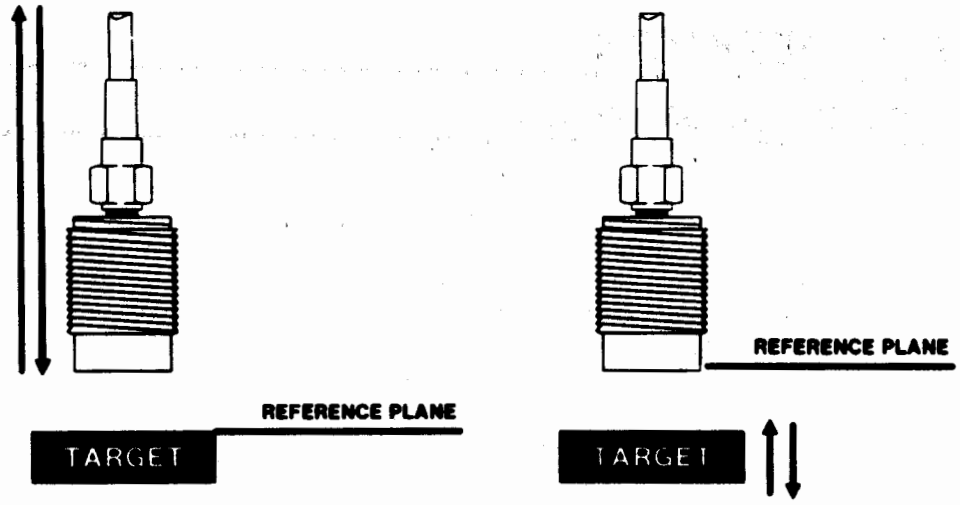

THE PRIMARY FUNCTION OF NONCONTACT DISPLACEMENT MEASURING SYSTEMS IS TO MONITOR THE POSITION OF A TARGET RELATIVE TO SOME REFERENCE PLANE

SYSTEM OVERVIEW

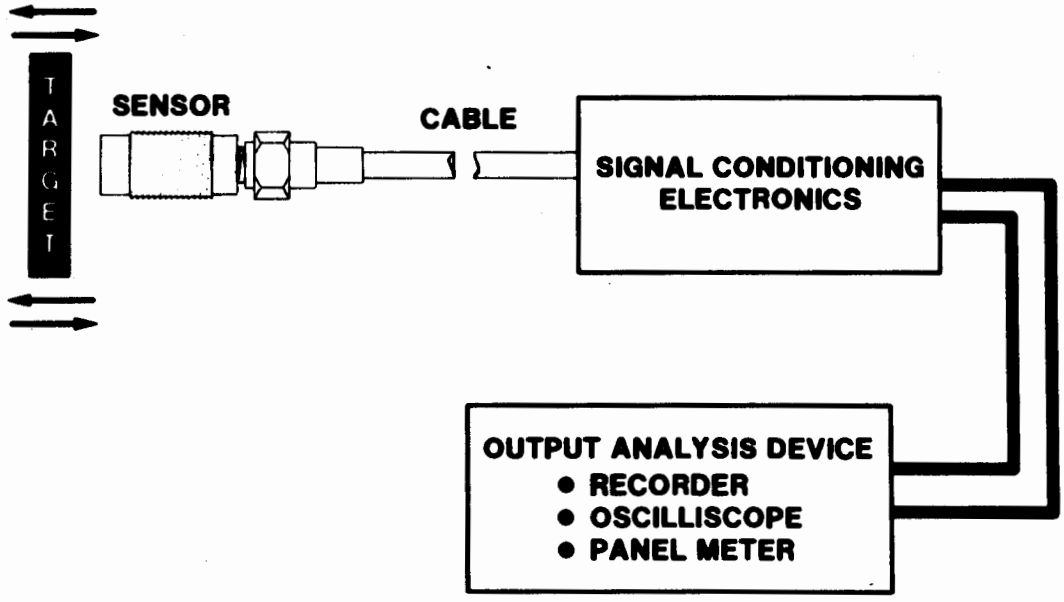

SYSTEM OPERATION

COLPITTS OSCILLATOR SYSTEM:

A Colpitts oscillator system such as the KD-2400 is a two transistor circuit that uses an oscillating coil in the face of a sensor to measure the proximity of a conductive surface. When in range of the sensor coil, the target "pulls" the oscillator which changes both the frequency and amplitude of the oscillation. As the target moves away from the face of the sensor there is an increase in the amplitude signal (opposite, bottom). There is also a frequency change but this is small compared to the amplitude change, so we don't use it.

The block diagram at right shows the major components of a KD-2400 Colpitts system. The target positions 1, 2, and 3 relate directly to the bottom illustrations. The left one shows how signal amplitude increases as the target moves away from the sensor coil.

This system is not highly linear over its entire range as shown (somewhat exaggerated) in the figure at lower right. However, it is quite linear in the middle of its range. So, if you were doing vibration measurements, for example, and set the gap for the measurement at the middle of the sensor's range, you would be using the most linear segment.

The gain control adjusts the slope of the output curve. Increasing gain provides a higher ratio of output voltage per unit of displacement and vice versa. With the KD-2400, voltage output is also dependent upon voltage input and the system can accept up to 24Vdc.

The KS-1000 proximity switches are similar in appearance and design. Instead of going to an emitter follower, the signal is sent to an adjustable voltage comparator which switches at a user selected voltage load determined by target proximity. This provides high precision: 10 microinch repeatability at a constant temperature.

These units can be temperature sensitive and the electronics are compensated using a thermister. They also like highly resistive targets: magnetic tape, bronze, carbon, tire belts, and discontiguous targets.

SYSTEM OPERATION
COLPITTS OSCILLATOR SYSTEMS

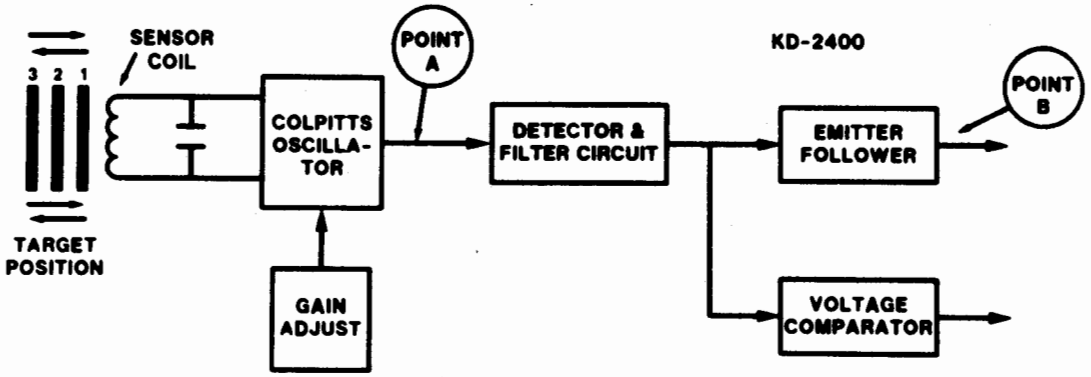

SYSTEM OPERATION
SIGNAL LEVELS VS TARGET DISPLACEMENT

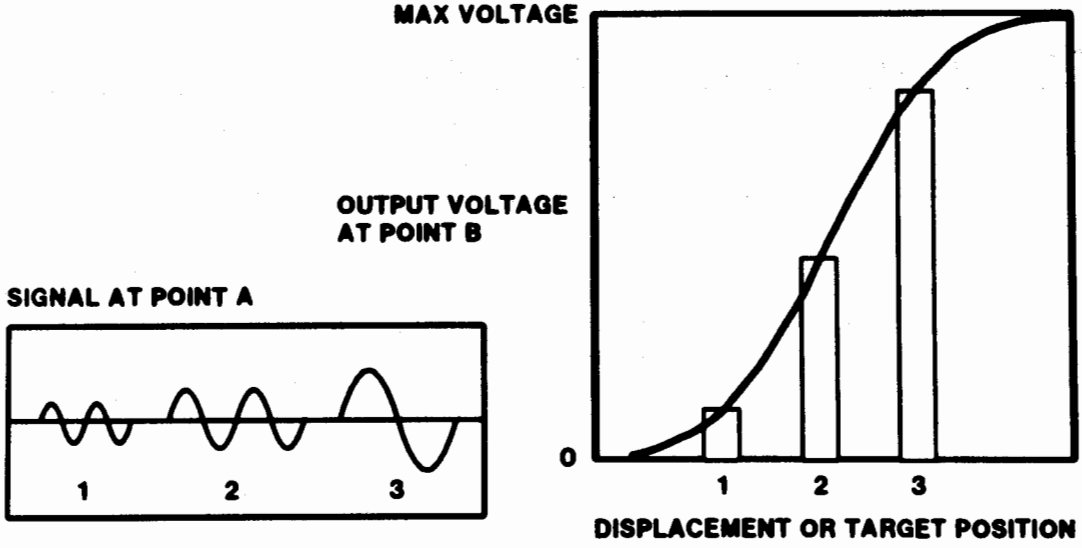

SYSTEM OPERATION

INDUCTIVE BRIDGE MEASURING SYSTEMS

The majority of our systems use an inductive bridge as illustrated in the block diagram at right. Here a crystal controlled oscillator drives a wheatstone bridge. We can tune the bridge to be near resonance so that slight changes in inductance in the sensor coil (caused by changes in the electromagnetic coupling between the sensor and the target) provide big shifts in the output of the bridge.

Sensor cable capacitance is a part of the capacitance used to resonate the bridge. Therefore, if a sensor cable longer than 30 to 40 feet is used with a 1MHz oscillator, the circuit could go over resonance. By going to a 500KHz oscillator you can use longer sensor cables since it now takes approximately four times more capacitance to resonate the bridge.

Like snowflakes, no two oscillators are identical, nor do they oscillate at precisely identical frequencies. As a result, sensors driven by different oscillators and mounted less than three sensor diameters apart may experience beat note interference. Slaving several systems to a master system/oscillator eliminates this problem.

The block diagram shows a sensor with two coils, one is active and one a reference coil. Both function as legs of the bridge. The reference coil enhances temperature compensation but makes for a large sensor. We make numerous low profile and small single coil sensors. In these, temperature compensation is effectively accomplished using phasing techniques.

SIGNAL LEVEL vs. TARGET DISPLACEMENT

The signal from the bridge is tied to a phase sensitive synchronous demodulator which also receives a reference signal from the oscillator. As impedance changes with changes in the proximity of the target, there is a change in the phase and amplitude of its input signal. The demodulator output is a logrithmic curve, **A**, in the lower figure. This shows that as the target moves further away from the sensor, there is a corresponding decrease in output voltage per unit of displacement. To convert this to a useful output, the signal goes to the log amp converter which linearizes the curve, **B**, providing 0.5% or better linearity. From here the signal goes to an output amplifier which has a gain adjust, allowing the user to modify the slope of the curve, **C**. Also, the Zero adjust can be used to zero offset the output (page 33).

SYSTEM OPERATION

INDUCTIVE BRIDGE MEASURING SYSTEMS

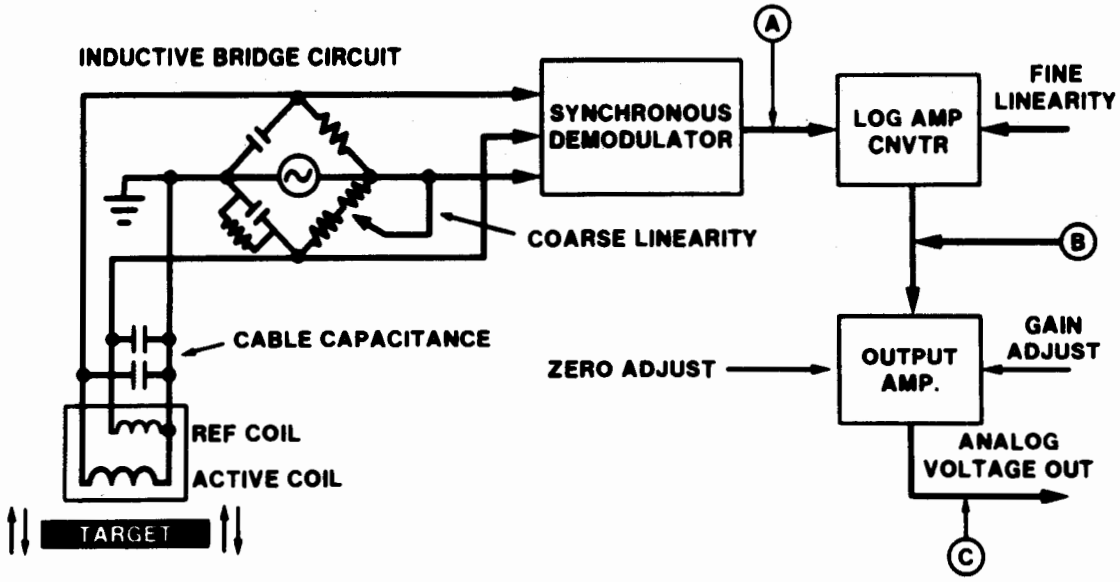

SYSTEM OPERATION

SIGNAL LEVELS VS TARGET DISPLACEMENT

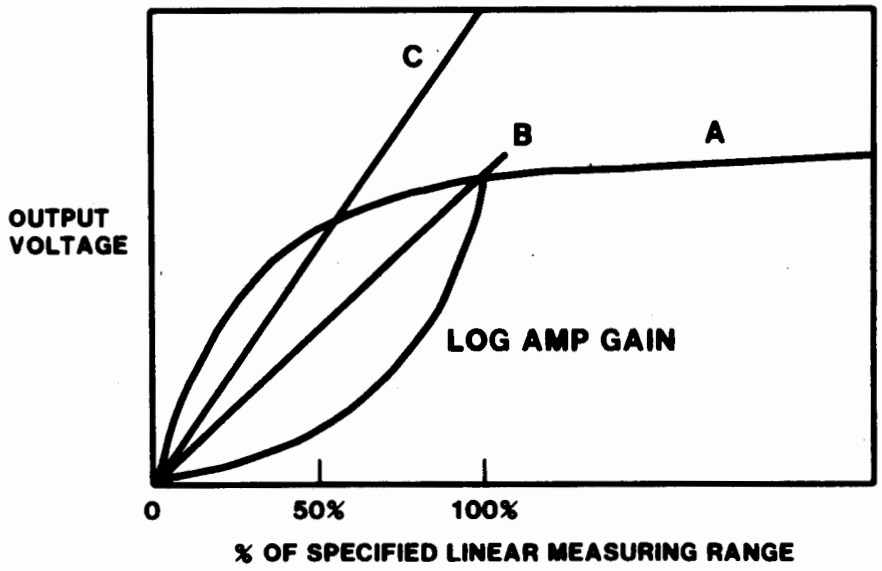

These two figures show the output curves for a system calibrated beyond normal range (overranged) and one calibrated over a shorter than specified range. In an overranged system you get a very high log amp gain which makes the system less stable. It gets less linear, more temperature sensitive, and sensitive to other things as well. For example, cable movements that cause small changes in capacitance would be negligible in an underranged or normally calibrated system. But in an overranged system, because of the high log amp gain, cable movement could show up as output voltage changes causing as much as a 10 mil shift.

Conversly, calibrating over a smaller range requires a lower log amp gain, moves the calibration points closer together, and results in a more linear and stable output.

SYSTEM OPERATION
SIGNAL LEVELS VS TARGET DISPLACEMENT

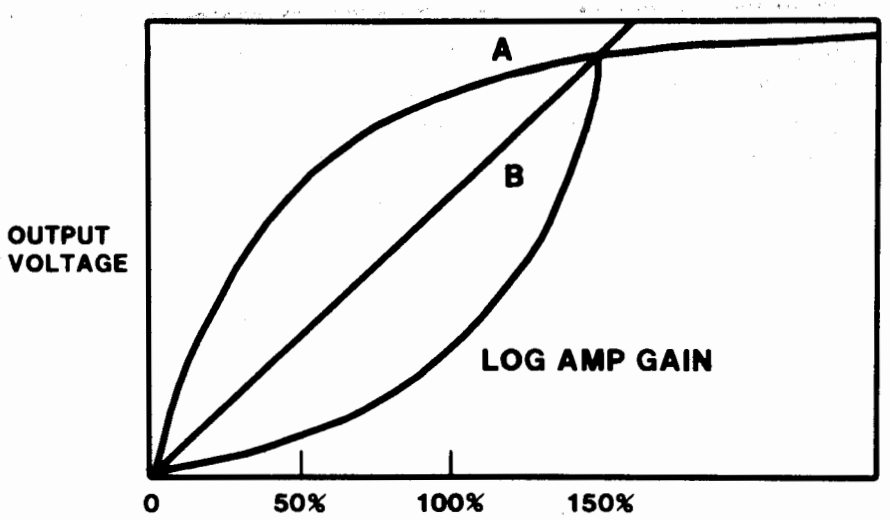

% OF SPECIFIED LINEAR MEASURING RANGE
(TYPICAL FOR OVER-RANGED INDUCTIVE BRIDGE TYPE SYSTEMS)

SYSTEM OPERATION
SIGNAL LEVELS VS TARGET DISPLACEMENT

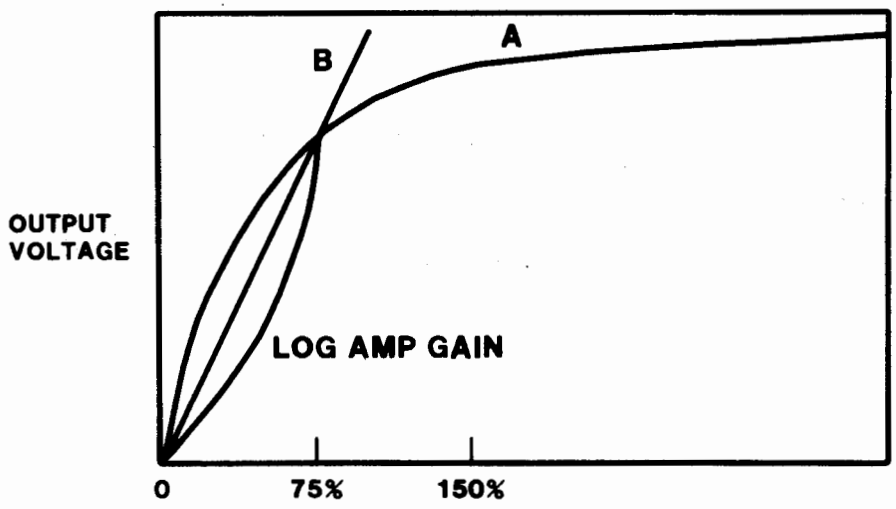

% OF SPECIFIED LINEAR MEASURING RANGE
(TYPICAL FOR UNDER-RANGED INDUCTIVE BRIDGE TYPE SYSTEMS)

SYSTEM OPERATION

THE SUBMICROINCH MEASURING SYSTEM

The KD-2810 Submicroinch Measuring System is capable of resolution to better than 0.1 microinch over a 1 mil measuring range. If you compare the electronics portion of the block diagram at right to the previous one for a standard bridge system, there is only one significant difference: the absence of a log amp converter.

In this system we use a sensor capable of a 40 mil measuring range but calibrate it over a 1 mil range near the beginning of the curve. Because the 1 mil segment (left figure) is so small, as the expanded curve in the right figure shows, the "curve" is extremely linear. Calibrated at 1Vdc output per mil, the Submicroinch system provides very high resolution. The trade-off is the limited measuring range.

SYSTEM OPERATION

SUB-MICROINCH MEASURING SYSTEM

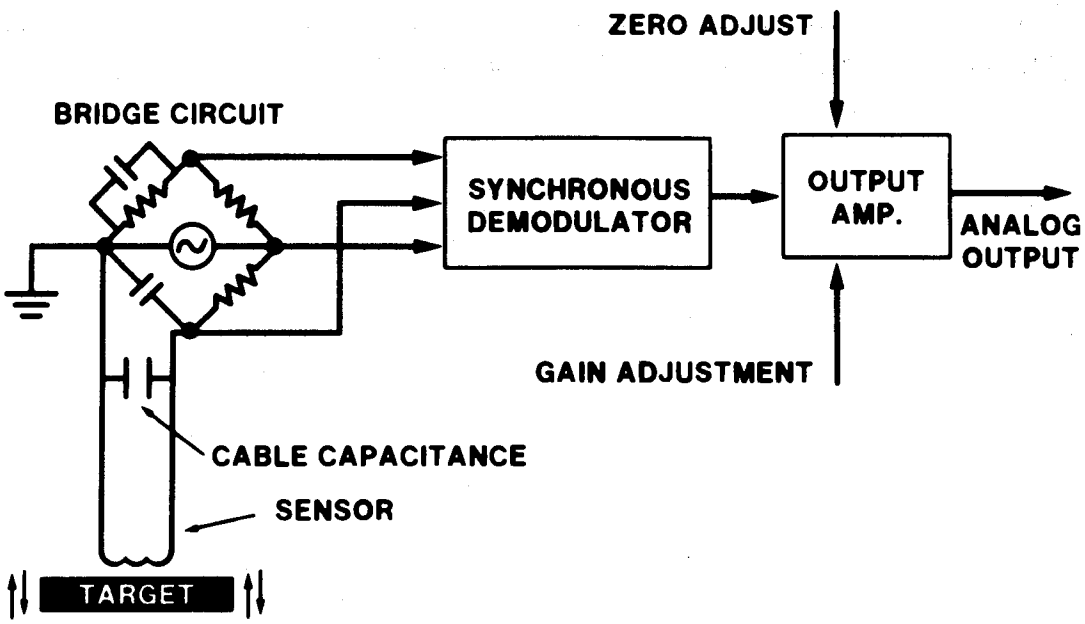

SYSTEM OPERATION

OUTPUT SENSITIVITY

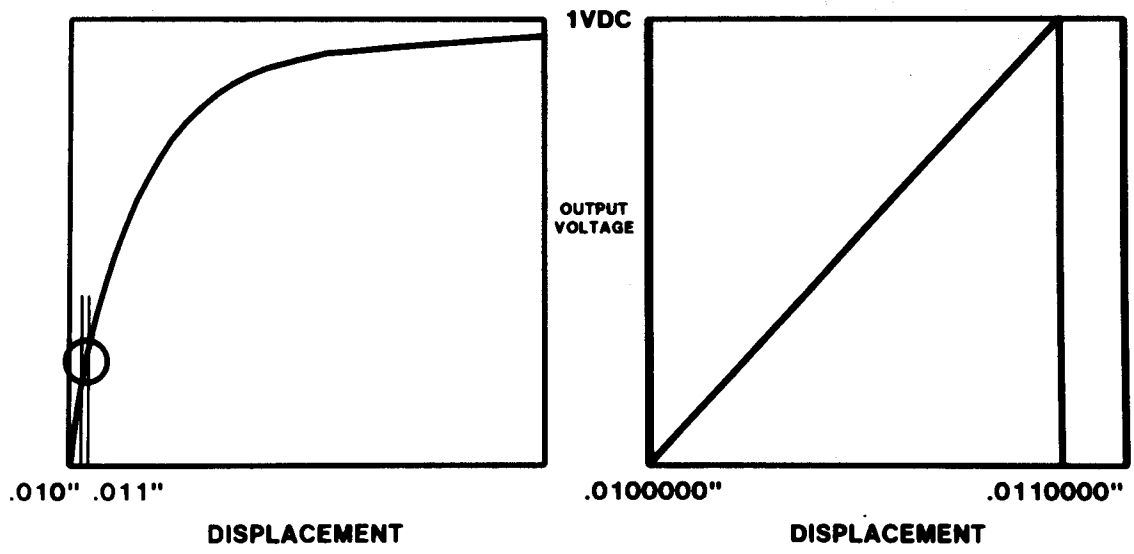

SYSTEM OPERATION

KD-5100 DIFFERENTIAL MEASURING SYSTEM (previously called the Differential Impedance Transducer)

The KD-5100 significantly advances inductive measurement technology. This system provides exceptional resolution, repeatability, and nulling accuracy for detecting the aligned (centered) position of a conductive target relative to a pair of noncontacting sensors.

In differential measurement applications, two precisely matched sensors are positioned on opposite sides (or ends) of a target. The sensor to target relationship is such that as the target moves away from one sensor it moves toward the other an equal amount.

As the block diagram shows, the coils of a pair of sensors are on opposite legs of an instrumentation bridge circuit. The bridge is balanced and the differential output is zero when the sensors are equidistant from the target at the null gap or centered position.

As the target moves away from one sensor and toward the other, the coupling between each sensor and its target is no longer equal, resulting in an impedance imbalance between the sensors. This imbalance is detected at the bridge. The bridge output is demodulated and presented as a linear analog signal directly proportional to the target's position. The output is bipolar, providing not only magnitude but direction of misalignment. Only A−B, or differential output is available. Individual outputs from each sensor are not accessible.

In this design, intervening summation amplifiers and the additional noise and drift they add to a system are eliminated. As a result, the differential system achieves extremely high resolution: 2.5Å or better.

Using electronically matched sensors on opposing legs of the same bridge essentially cancels temperature effects common to the sensors and cables of a differential pair. This is also true for the mechanical aspects of the sensor/target system. Assuming the thermal characteristics of each sensor and target track perfectly with each other, dimensional changes due to temperature are self cancelling.

SYSTEM OPERATION
DIFFERENTIAL IMPEDANCE TRANSDUCER

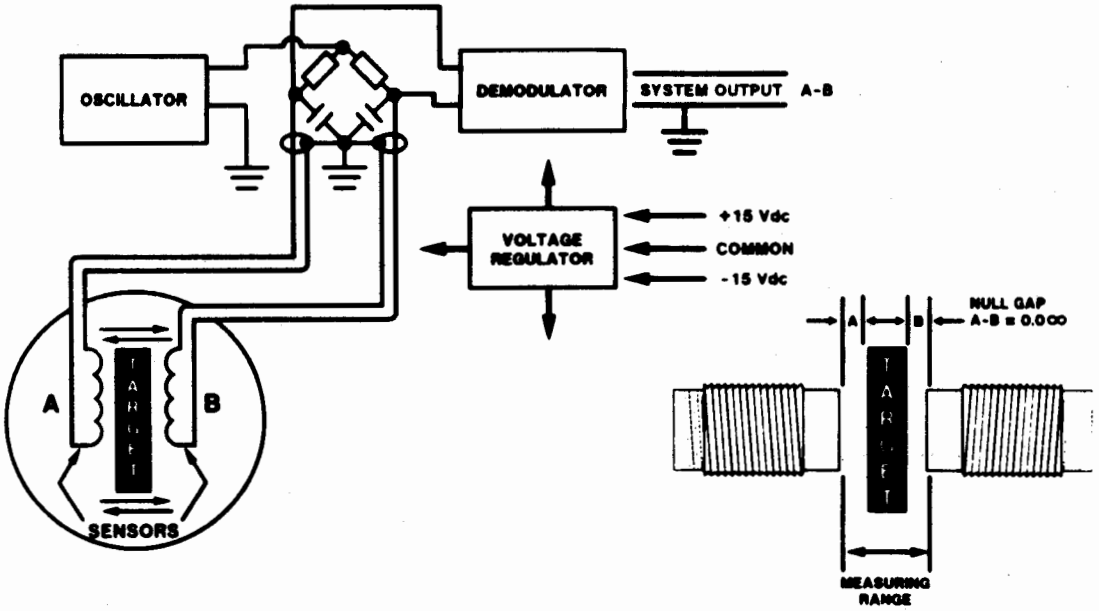

SYSTEM OPERATION
DIT SYSTEM OUTPUT

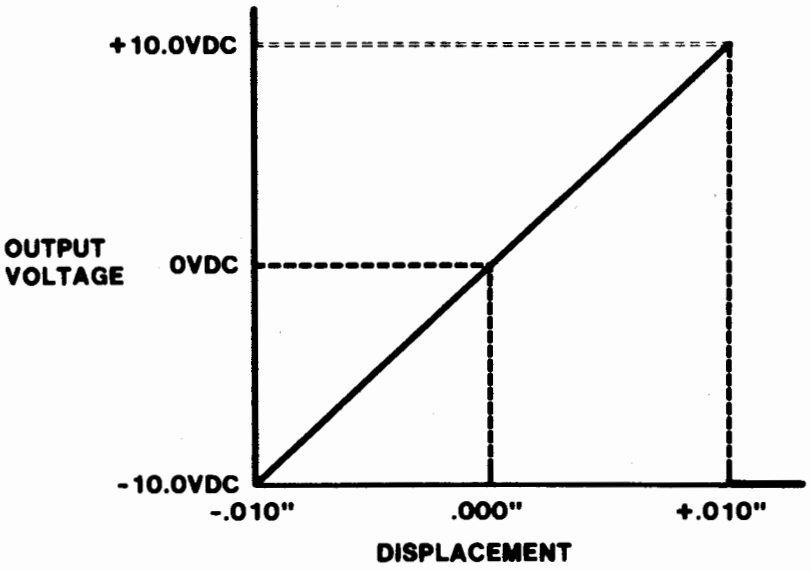

APPLICATION CONSIDERATIONS

KEY QUESTIONS

To begin seeking solutions to a measurement problem there are a number of key questions to ask yourself. The answers will help to determine if our systems will solve your measurement problem and, if so, which system and sensor combination is best. As you read these you can note your special questions on the opposite page.

- **What is my measuring range?** A sensor's range is a function of its diameter. The bigger the diameter, the greater the range. This fact has trade-off implications. You may need more range but not have mounting space for a larger diameter sensor. And the larger sensors are not capable of the higher resolution of the smaller ones. The smaller sensors and their variety of configurations make it easy to get into some pretty out-of-the-way places. They also have greater accuracy than the larger diameter sensors, but have correspondingly less range.

- **What is my target material?** Magnetic or nonmagnetic? This influences system selection, carrier frequency, and sensor selection. What is the type of material, its size, its shape, its thickness? Highly conductive targets like aluminum and copper are best though any conductive target will work. Smaller sized and odd shaped targets are acceptable but may impose limitations. Minimum target thickness is determined by the material and carrier frequency. The field does penetrate below the surface. There is less penetration in highly conductive materials and at a higher carrier frequency. Minimum thickness for gold or aluminum is 18 mils at 500KHz, 90 mils for inconel. These values are reduced 67% at 1MHz. For thinner materials the field will "shine through" the material but you can still get useful information.

- **How much space do I have for sensor mounting?** This may influence sensor selection and impact your **measurement objectives**.

- **What are my measurement objectives?**
  What kind of resolution do I need? The smaller sensors are capable of better resolution, and the KD-2810 microinch system and particularly the KD-5100 Differential Measuring System are capable of the best resolution. If your minimum requirement is for 10 mil accuracy, there is no need to have a system capable of submicroinch measurements.
  What are my repeatability, linearity, and frequency response requirements? These are all stated system parameters (specifications) that you take into account for system/sensor selection.

- **What are my environmental conditions?** Temperature fluctuations could impact system performance. We can compensate for this in most instances. Will the sensor or electronics be under pressure or exposed to environmental contaminants: water, dirt, oil, stray RF or magnetic fields? Inductive measurements are virtually unaffected by these contaminants but the sensor and/or electronics aren't and may have to be protected—remote mounting, NEMA enclosures, waterproofing, etc.
  Fixture stability is of paramount importance. Unstable fixturing will invalidate most measurements. At submicroinch resolution the world becomes "rubber" making stable fixturing all the more important. The accuracy of a measurement is a function of two things—our system and your fixturing.

APPLICATION CONSIDERATIONS

SENSORS

Sensor Size vs. Measuring Range
Shielded vs. Unshielded

SYSTEM PERFORMANCE

Mounting Considerations
Target Material

The figure at right illustrates the correlation between sensor diameter and measuring range.

This figure points out the effect shielding has on field size. In an unshielded sensor the field is approximately 2.5 to 3 times the diameter of the sensor. With a shielded sensor there is eddy current loss as the field interacts with the shielding, reducing its size to 1.5 to 2 times sensor diameter. Shielded sensors also become sensitive to cross axis motion. With an unshielded sensor you will get more measuring range from the same size coil.

APPLICATION CONSIDERATION
SENSORS
SENSOR SIZE VS MEASURING RANGE

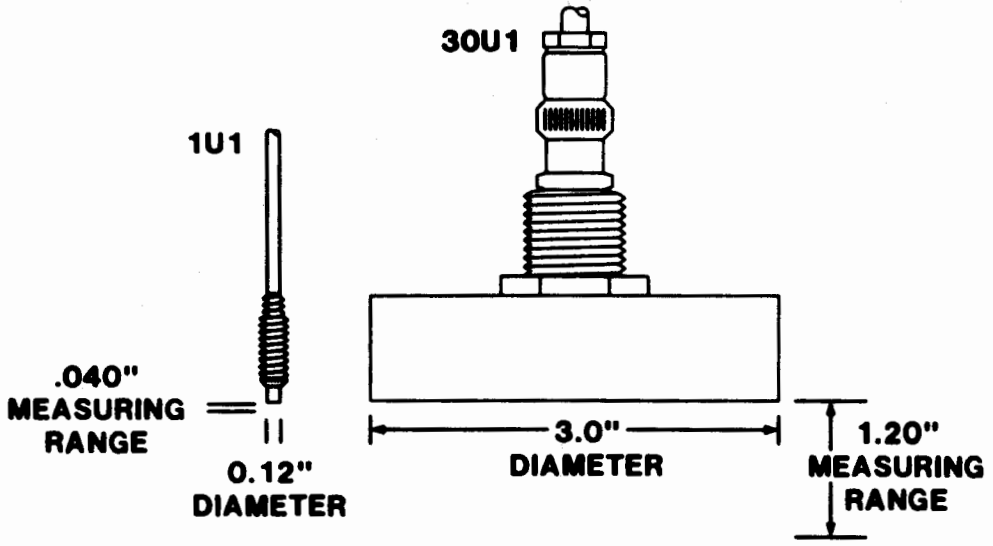

APPLICATION CONSIDERATIONS
SENSORS
FIELD SIZE VS TARGET SIZE
(RULES OF THUMB)

2.5 TO 3 TIMES THE DIAMETER OF AN UN-SHIELDED SENSOR

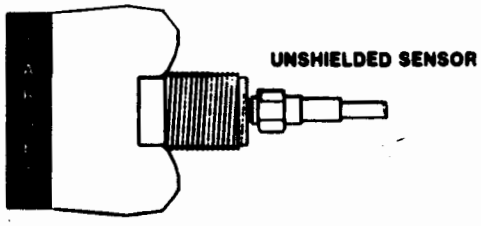

1.5 TO 2 TIMES THE DIAMETER OF A SHIELDED SENSOR

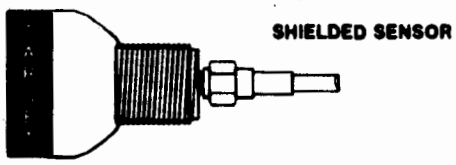

☐ EDDY CURRENT FIELD DISTRIBUTION PATTERN

APPLICATION CONSIDERATIONS

SENSORS

The two figures at right illustrate one way target shape affects system output. The "W" curve shows how output voltage changes as a small diameter rod passes beneath the face of the sensor. This example assumes that the rod's movement is only in the horizontal plane and that its vertical distance remains constant. The field of a coil is strongest at its outer edge (an exception to this is in pancake coils). Therefore, when the rod is at positions 1 and 3 (far right) there is the greatest coupling with the rod, the greatest eddy current loss, and therefore the lowest voltage output. In position 2, there is less coupling and a corresponding increase in voltage output.

Ideally a target should be flat and as large as a sensor's field but, as long as a target is accurately positioned, our systems obtain useful information from smaller and different shaped targets.

MOUNTING CONSIDERATIONS

STANDARD PERFORMANCE

This illustration and those on the next page provide sensor mounting considerations and show how **conductive material** in the mounting fixture impacts system performance.

Here we see parameters for sensor mounting that, when met, prevent interaction between the sensor's field and the fixture.

Larger sensors should be mounted on a nonconductive standoff.

When recessed in conductive material, an unshielded sensor should have an area cleared out around it 3 times its diameter and 1.5 to 2 times its diameter back from the face. Shielded sensors require a smaller area removed and are best for flush mounting in a conductive fixture.

APPLICATION CONSIDERATIONS
SENSORS
ANALOG VOLTAGE ROD POSITION

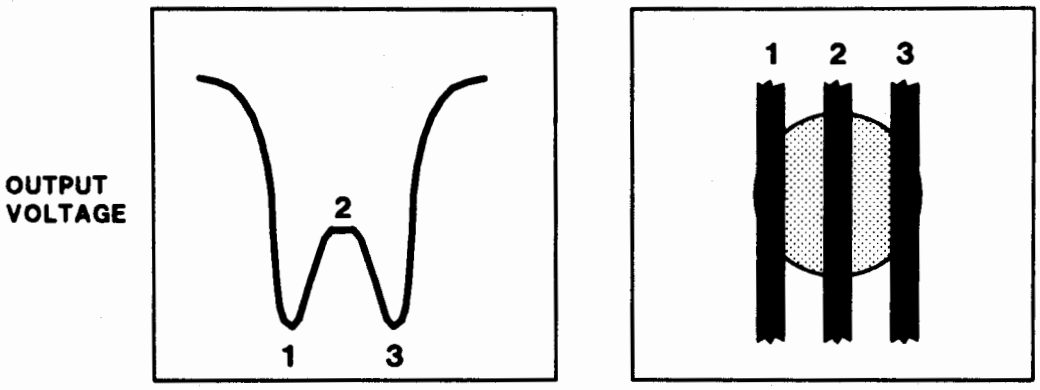

TARGET POSITION

TARGETS SMALLER THAN THE RECOMMENDED SIZE WILL BE POSITION SENSITIVE IN THE HORIZONTAL PLANE

APPLICATION CONSIDERATIONS
SENSORS
MOUNTING CONSIDERATIONS

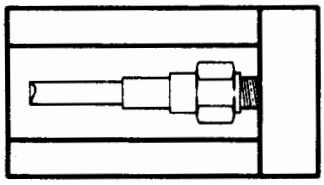

NONCONDUCTIVE STANDOFF

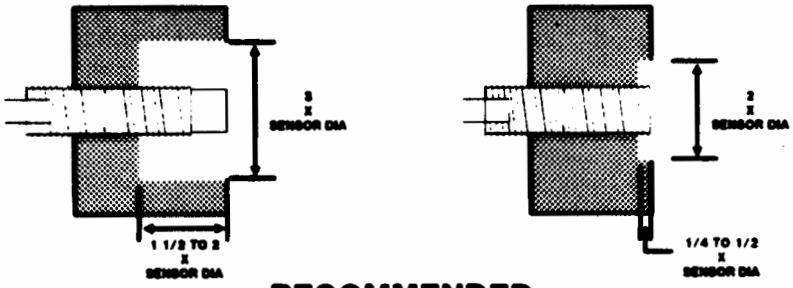

RECOMMENDED
NO INTERACTION

MOUNTING CONSIDERATIONS

REDUCED PERFORMANCE

Here we see sensor mounting in a conductive fixture that is acceptable but yields reduced system performance. In this instance it is best to calibrate the system with the sensor mounted in the application fixture or in a test fixture that accurately duplicates application mounting conditions. In this way you can compensate for most of the sensor interaction with the fixture during calibration.

NO PERFORMANCE

The bottom right illustration shows what you should **never do**: mount a large sensor right up against a conductive plate or embed an unshielded sensor in conductive material. The back and side loading is so great, calibration is impossible.

SUMMARY

For **REDUCED** performance:

- Use less than a full sized target
- Overrange the system
- Mount the sensors in close proximity to conductive objects—other than the target
- Use extra long sensor cables
- Use maximum gain settings

For **STANDARD** performance, it is best to:

- Use a full sized target.
- Mount the sensor away from conductive objects—other than the target
- Select a system with a linear range required by the application.

For **IMPROVED** performance:

- Use a full sized target.
- Use a nonmagnetic target material when the option exists.
- Provide a stable environment.
- Keep conductive objects away from the sensor.
- Use a sensor with a greater range than that required by the application.

APPLICATION CONSIDERATIONS
SENSORS
MOUNTING CONSIDERATIONS

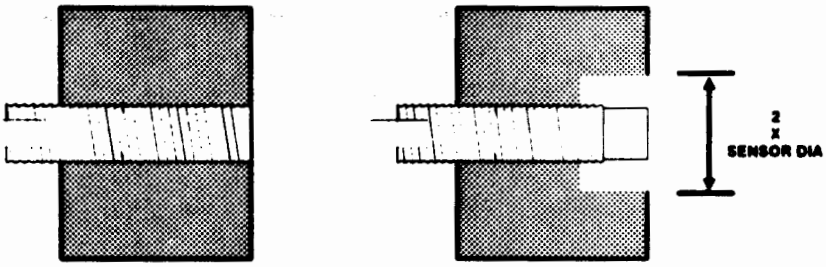

EFFECTIVE RANGE REDUCED
CALIBRATE IN PLACE
OR
USE SIMULATED MOUNT

APPLICATION CONSIDERATIONS
SENSORS

MOUNTING CONSIDERATIONS

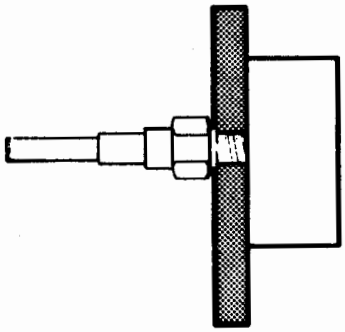

CONDUCTIVE PLATE

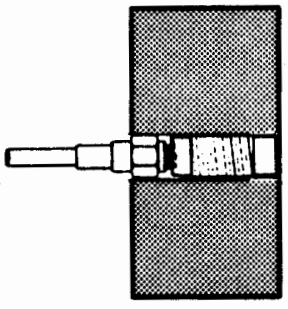

MAXIMUM INTERACTION
SIDE & BACK LOADING
NEVER RECOMMENDED

APPLICATION CONSIDERATIONS

Sensors

The figure below shows system performance vs. measuring range throughout and beyond a sensor's specified range.

This graph shows what happens to such relative factors as stability, linearity, noise floor, and resolution as the target gets further away from the sensor. As long as you stay within a sensor's specified measuring range, the change in these factors is held to a very workable .1%. In the first half of the range it is quite improved. On the other hand, overranging the sensor significantly degrades performance though you can still get usable information.

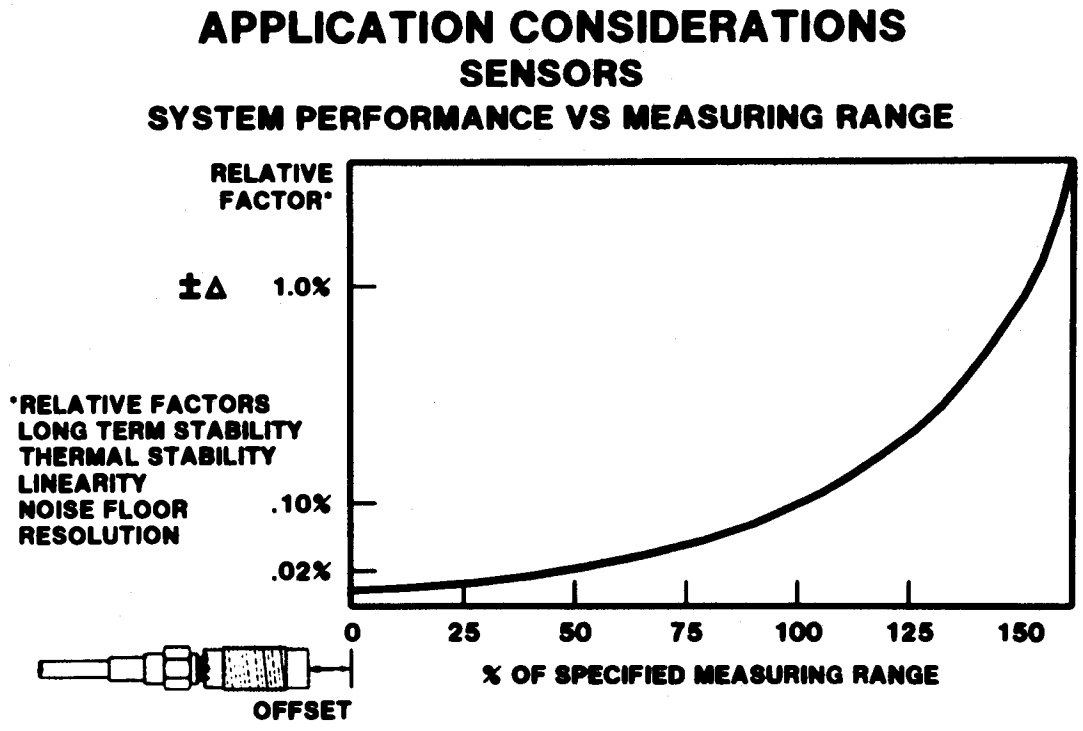

APPLICATION CONSIDERATIONS

Analog Output of Kaman Measuring Systems
Impedance: 5 ohms (typical)
Current: 15 to 35mA (typical [system dependent])

Kaman Measuring systems provide more than just displacement data:

ADDITIONAL FUNCTIONS

DIMENSIONING—The Summation Function Card: This provides one of three kinds of information:

1. Differential alignment or centering, (A−B)
2. Outside diameter (OD) or thickness, C−(A+B)
3. Inside diameter (ID), C+(A+B)

The A−B function is for sensing the alignment or centering of a target between the sensors of two measuring channels. When the target is centered the output is zero. Deviation right or left of center yields a + or − voltage output directly translatable to engineering or metric units.

In the C−(A+B) function, "C" represents the separation distance between the sensors. It is a constant algebraically summed with (A+B), "A" is the distance from one sensor to the target and "B" the distance from the other sensor to the target. You can do either absolute OD (sometimes limited by system voltage capability coupled with scale factor) or a deviation measurement from a nominal OD. The C+(A+B) function is for inside diameter measurements and, as in the C−(A+B) function, you can do either absolute ID (though this is often limited by the maximum distance of the inside diameter vis-a-vis sensor size) or, preferably, a deviation measurement from some nominal ID which is typically not limited by the ID distance.

LIMIT DETECTION—Using the Dual Channel Limit Detector Function Card: This function card contains four separate voltage comparators arranged in pairs. One pair monitors the output from one measuring channel and the other pair may monitor another channel. One or both pair can monitor the output of one or two other function cards. Both pair of comparators can also monitor one channel to do three category sorting.

When paired, comparators function as a "window comparator." This window (Go) is the range between preset high and low limit switch points.

Two output device options are available. The 4N33 optical isolated output has a system isolated ground to prevent ground loops and is suitable for controller or microprocessor input. The second is an open collector output suitable for tripping relays or for connection to test, recording, or other control devices, particularly those requiring a higher source current.

PEAK DETECTION—Using the Peak Detector Function Card: This function card provides an output voltage proportional to the maximum and/or minimum amplitude of an analog input voltage from one measuring channel. It can also accept input voltage from other function cards. The card uses two monolithic peak detection integrated circuits. One detects the positive peak voltage and the other the "negative" peak. This negative peak can be either the lowest positive input voltage or a negative voltage. Working together they perform the peak to peak function. These detectors capture very narrow pulses and then "hold" the voltage in capacitors that have a droop rate of .1mV/ms.

The Peak Detector card performs the following functions:

1. Plus Peak: In this setting the card outputs a signal equal to the most positive input signal.
2. Negative Peak: In this setting the card outputs a signal equal to the least positive or most negative input signal.
3. Peak to Peak or Total Indicated Runout (TIR): In this setting the card outputs a signal equal to the difference between the maximum and minimum input signals.
4. Peak Hold: This setting is a "not update" mode. Once given a hold signal the card ignores new peaks.
5. Reset: A reset signal of +5 to +15Vdc discharges the hold capacitor to its starting charge position.

This card is for use in **dynamic** applications. It is most commonly used in the peak to peak mode. Sample applications are: the detection of total indicated runout of a rotating shaft, the axial runout of a computer disk, or the peak to peak amplitude of an ultrasonic welding horn. The card has two limit detector circuits with open collector outputs that are usable for alarm and shutdown of equipment or for inputing to test, recording, or other control devices.

All of these functions are available via plug in function cards for the KD-4000 Family of electronics.

CALIBRATION CONTROLS

Most systems have user adjustable calibration controls either accessible externally or, as in some systems in the KD-4000 Family, on the PC cards and accessible beneath an easily removable panel.

The photo below shows the calibration controls on a KD-4000 Family RF card.

The following discussion of Calibration Procedures explains the use and illustrates the effect these controls have on system output curves.

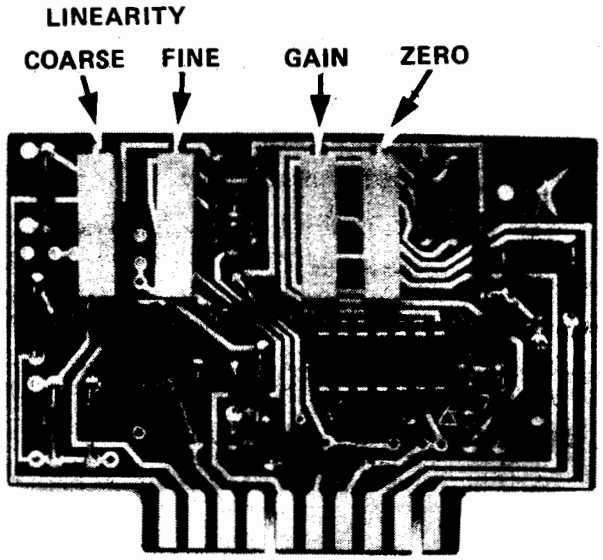

KD-4000 Family RF Card Calibration Controls

CALIBRATION PROCEDURES

Define the Measurement Span
Calibration Procedures
    Use of Zero and Gain Controls
Define Resolution/Sensitivity
    Full Span Calibration
    High Linearity Band Calibration
Define Dimensional Standard
Define Target
Define the Measurement Span

Each sensor has a specified measurement span and standard operation requires that you calibrate the sensor over this span. Best linearity exists at mid-span. It is **not** necessary to calibrate the sensor over the full specified span. In fact it is often advantageous to calibrate over a reduced span.

The figure below shows various optional calibrations.

If you calibrate between the 25% and 75% points, this shorter calibration span, or one within this area no smaller than 25% of the overall span, provides improved linearity.

If you calibrate the sensor over a span that is less than 25% of the specified span or calibrate in a span that is beyond the specified max range, in effect overranging the sensor, there will be decreased linearity and degraded overall performance.

CALIBRATION PROCEDURES
DEFINE THE MEASUREMENT SPAN

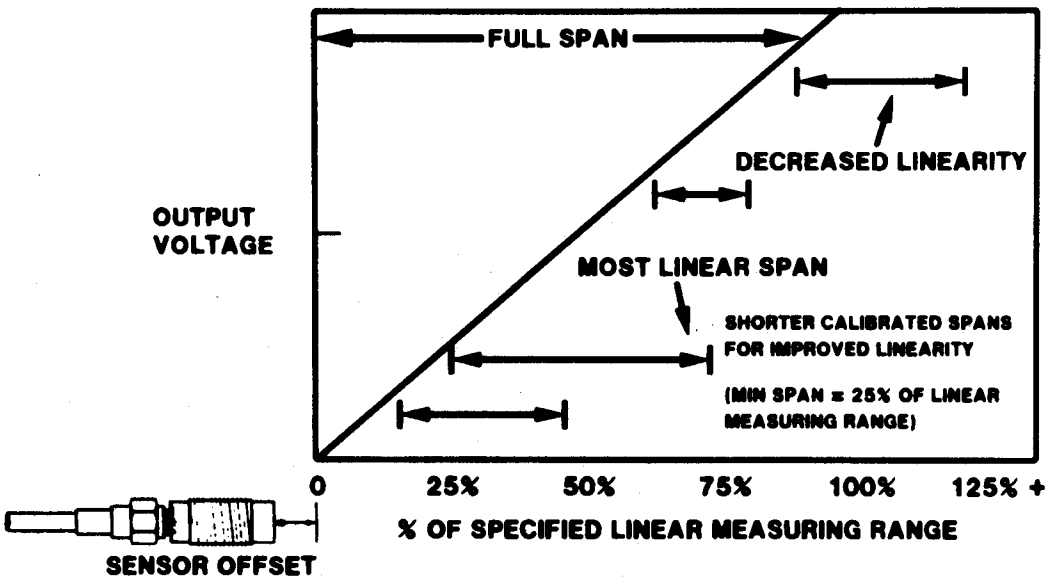

CALIBRATION PROCEDURES

Zero Offset and Gain Controls

These facilitate the use of oscilloscopes, oscillographs, chart recorders, data loggers, A to D converters, panel meters, and more.

ZERO OFFSET CONTROL: The Zero control (in addition to adjusting the zero point during the calibration process) adjusts the point at which a channel's output crosses the x-axis. This bit of abstract definition is illustrated to the right.

Adjusting the zero control after calibration is complete shifts the curve up or down. You can shift up to 60% of the output below the x-axis without altering output linearity. This has the advantage of placing the zero volt output signal anywhere along the measuring range up to the 60% point. This provides a simple way to read a plus and minus deviation from some predetermined point/distance from the sensor. If you are measuring a target at the mid point of a sensor's span, by shifting the curve down to 50% of FSO, subsequent readings will be + or − deviations from this point. This is preferable for some applications and useful for input to a signal conditioning device requiring a bipolar signal such as an A to D converter.

GAIN CONTROL: Sensitivity, scale factor, or gage factor all refer to the same thing—volts out per unit of target displacement. The Gain control is for adjusting and/or changing system sensitivity. If you want to calibrate your system at 100mV/mil this means that for each mil of displacement change, there will be a tenth of a volt shift in system output, or 1 volt for every 10 mils.

In the KD-4000 Family, by selecting the right gain and/or shifting the decimal placement on the digital display, you can read the output directly in engineering or metric units.

Increased sensitivity (gain) will not improve resolution per se. Increased sensitivity may improve the ability to resolve a position change, **depending on the equipment used to monitor analog output**. If the sensitivity is set at 1mV/mil and you have a digital display with 1mV readout capability, then best resolution is 1 mil. However, if the sensitivity is 100mV/mil then you can resolve 10 microinches on the same digital display.

Effective (dynamic) resolution is more directly affected by a system's signal to noise ratio and the monitoring device used. Increased sensitivity will not improve dynamic resolution. When you increase the gain, you increase the noise floor as well.

The bottom figure shows changes in the slope of the curve with changes in gain only. There are practical limits to how high you can adjust the gain. Eventually you reach a point where very small target movement yields high voltage shifts, reaching saturation rapidly and causing instability. If you set the gain too low, the signal gets down into the noise floor. Yet between these extremes there is a great deal of latitude.

After calibration, adjusting the gain control only may yield a slight but easily corrected shift in the zero intercept and in linearity.

CALIBRATION PROCEDURES
ZERO OFFSET CONTROL

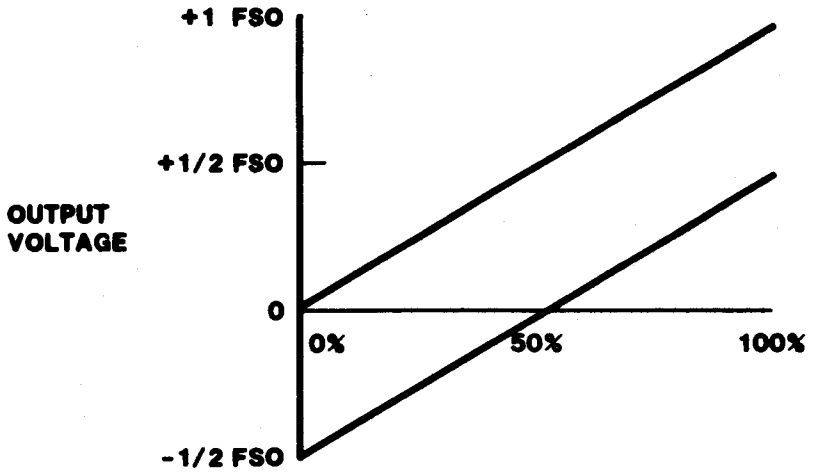

% OF SPECIFIED MEASURING RANGE

UP TO 60% OF THE CURVE CAN BE SHIFTED BELOW THE "X" AXIS (WITH NEGLIGIBLE IMPACT ON SYSTEM LINEARITY)

CALIBRATION PROCEDURES

DEFINE SENSITIVITY (OR GAIN MV/MIL) NEEDED FOR MEASUREMENT (SENSITIVITY = VOLTS OUT PER UNIT OF DISPLACEMENT)

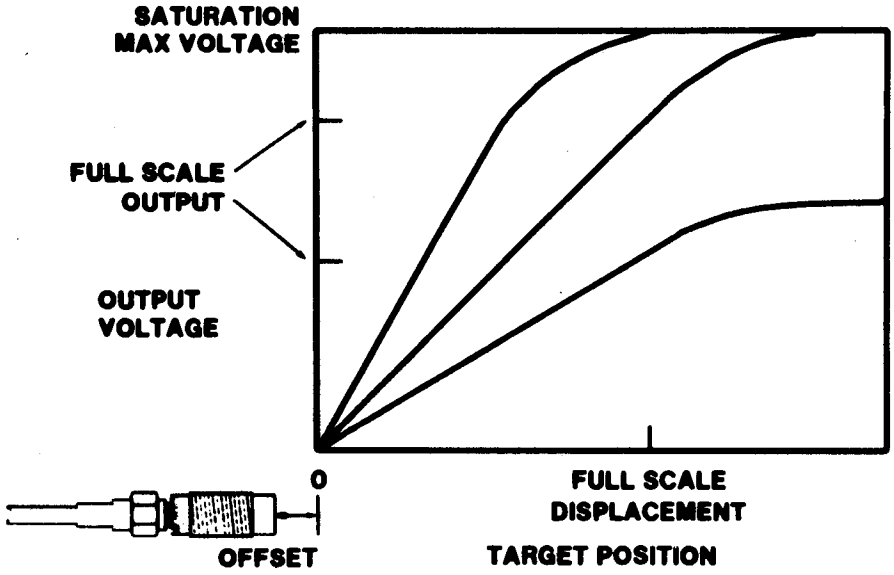

CALIBRATION PROCEDURES

Full Span Calibration: The top figure shows a typical linearity curve for a full span calibration. The Calibration Procedures are as follows:

- Using a Dimensional Standard (page 36), position the target at maximum range for that sensor. This assumes a standard calibration.
  - *Adjust the coarse **linearity** control so the output voltage equals your desired Full Scale Output (FSO). For example, if full displacement is 80mils and you are using a scale factor/sensitivity of 100mV/mil, then your output voltage at full scale will be 8 volts.
- Move the target in to the zero point (There will always be an offset, usually 20% of full span. This is required to optimize performance and to keep the target from striking the sensor face).
  - *Adjust the **Zero** control for zero volts output.
  - Move the target to 50% range.
    - *Adjust the **Gain** control for 50% of the FSO—4 volts in the above example.

Repeat these adjustments in sequence several times to complete the calibration. There are techniques to modify and/or hasten this process in the instruction manuals.

This results in a calibrated curve that deviates from an ideal curve by no more than .5% of FSO. A typical curve, shown at top right, is "S" shaped with the greatest linearity at mid span and the greatest nonlinearity at the 25% and 75% points.

High Linearity Band Calibration:

As stated earlier, you don't have to calibrate over the full span. The figure at right shows the advantages of doing a High Linearity Band calibration. By moving the Zero and Linearity calibration points closer together, to the 25% and 75% points in this example, and calibrating over the reduced span, you significantly improve the linearity of the output. **Linearity on the order of .2% to .1% or better is not unusual.**

CALIBRATION PROCEDURES
FULL SPAN CALIBRATION

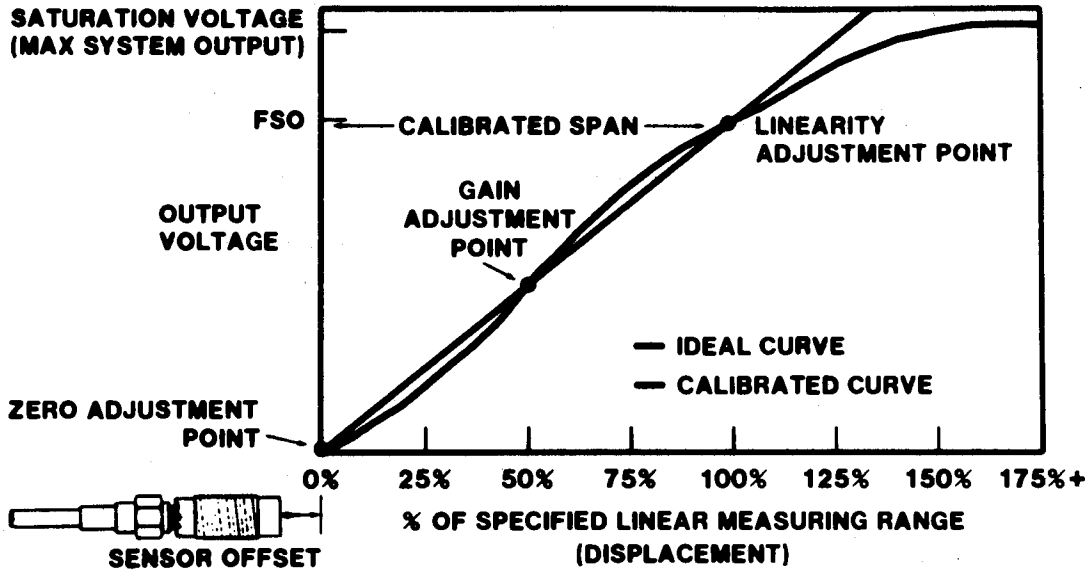

CALIBRATION PROCEDURES
HIGH LINEARITY BAND

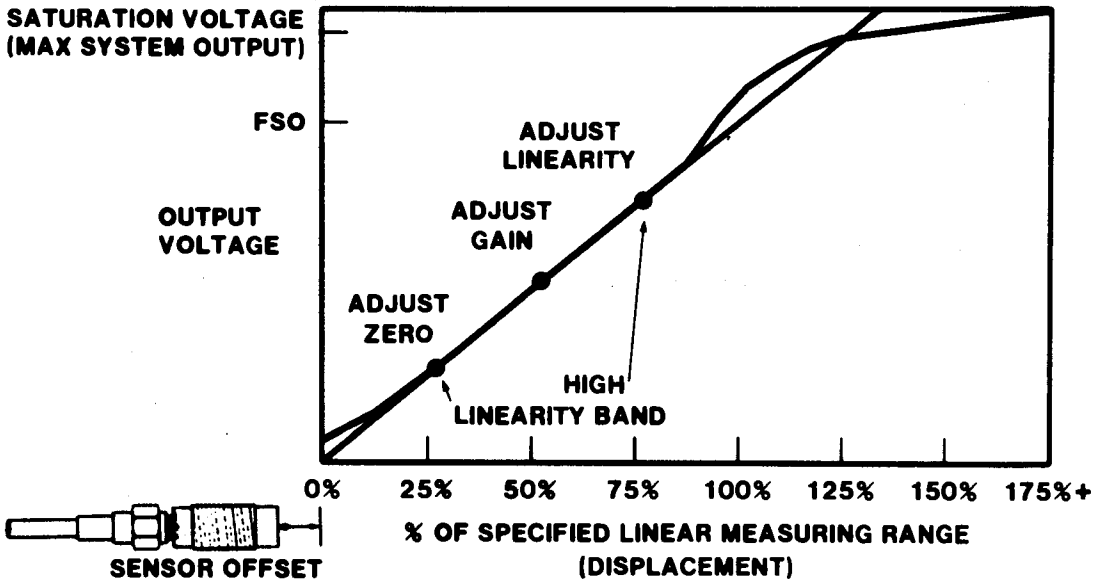

CALIBRATION PROCEDURES

DEFINE YOUR DIMENSIONAL STANDARD

The reason for calibration is to verify that system output relates to some known physical displacement—a reference standard with a known degree of accuracy.

For most purposes a micrometer calibration fixture is preferred. For larger sensors we recommend available ceramic calibration spacers manufactured to precise tolerances.

For the KD-5100 Differential Measuring System, we use a computer controlled laser interferometer as a dimensional standard because of the high resolution capability of these systems.

THE TARGET: When calibrating, use the actual target or a sample that is the same material and shape as the application target.

The figure below shows that the shape of the target can affect a sensor's effective measuring range. In this instance, the highly curved target reduces the effective range 50%.

CALIBRATION PROCEDURES
TARGET SHAPE

HIGHLY CURVED SURFACE **VS** **FLAT SURFACE**

THE EFFECTIVE MEASURING RANGE IS REDUCED

APPLICATIONS – TYPICAL SOLUTIONS

Applications categories include: Displacement, Vibration, Alignment, Dimensioning, and Sorting.

APPLICATIONS:

Though we list five separate measuring categories, in reality these are all variants of one theme: displacement. We define displacement as a measurement of distance between a sensor and a conductive object, usually with repeated measurements of that object or ones like it. We also call this a position measurement. We distinguish between this and measurements that use raw displacement data to tell more about the target than just its distance from the sensor:

- Vibration: peak amplitude or frequency
- Alignment: x, y, and z axes
- Dimensioning: Internal Diameter (ID), Outside Diameter (OD), or thickness
- Sorting: multiple category sorting, parts gaging

Most of these more involved measurements require the use of a function card or specially designed systems: the KD-2714 Dual Axis Alignment System or a dual axis KD-5100 Differential Measuring System.

How you use the measurement information is application dependent. You may simply want to read the measurement output on an analog or digital meter or input it to an oscilloscope, chart recorder, alarm and shutdown circuits, an industrial process controller, a computer, or some other analysis or control device.

OPEN AND CLOSED LOOPS

When you just read, record, or analyze the measurement information in some way we refer to this as an open loop application. But, when the output is fed back to a mechanisim that acts to control some aspect of the process dependent upon target position, this is a closed loop.

Closing the loop is accomplished by sending the output from a Kaman Measurement System to a process or control device that compares the output to some reference or standard to derive an error signal. Using this error signal, the controller initiates a command sequence resulting in some type of action (Figure 1). This "action" can be anything from triggering an air burst to kick out a defective part; holding an object in a fixed position (vibration damping); indexing to a new part in an automated machining process; repositioning the target the sensor(s) is (are) monitoring in a closed loop servo positioning application; or, assuming no error is detected, taking no action at all and continuing the process.

The above discussion of open and closed loops defines the extent of any commonality. The variety of techniques and actual applications is almost limitless.

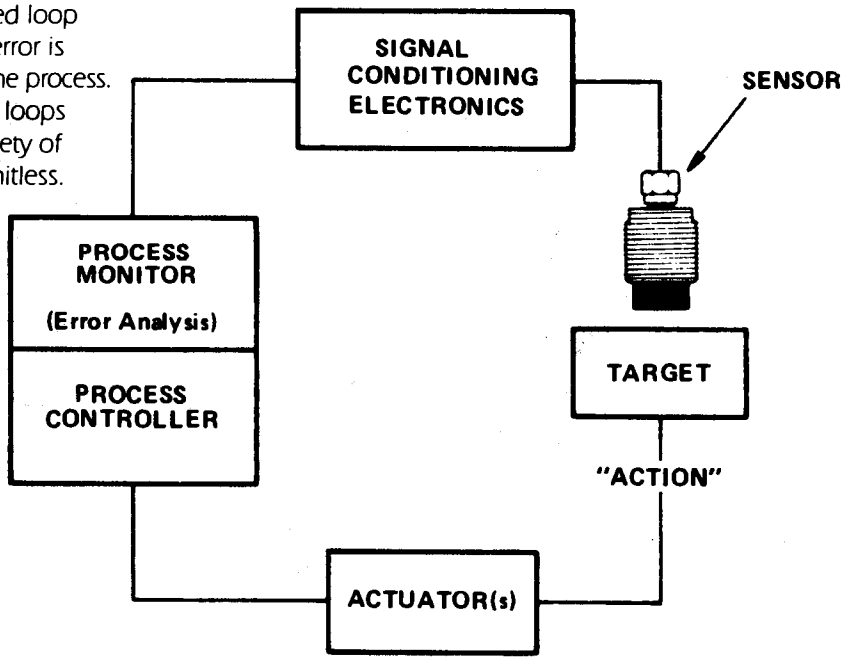

Figure 1
Closed Loop

APPLICATION EXAMPLES

What follows are examples of the five measurement categories: displacement, vibration, alignment, dimensioning, and sorting. We provide both open and closed loop examples to show practical applications of our technology and to promote ideas for solving measurement problems for your particular application.

This workbook's Application Considerations section brought up "Key Questions" you should ask to help arrive at a sensor and system selection. Each of the following examples includes a brief description of how the systems chosen provided answers to some of those questions.

A. DISPLACEMENT

There are a variety of ways to obtain and use simple displacement information. The following three examples include a web thickness measurement to show that, with appropriate fixturing, you are not limited to measuring only conductive targets.

1. Robot Repeatability Testing: The changeover to robotics in so many areas of manufacturing brings with it the problem of both qualifying the repeatability of those robots and of monitoring their performance over time. A major US automobile manufacturer specifies Kaman Measuring Systems for its Robot Assessment Program. Using adjustable test stands with sensor holders having three sensors each, they test robot repeatability and accuracy in three axes (x, y, and z) at two measurement points in the robot's arc of movement (Figure 2).

Figure 2

Robot Repeatability Testing

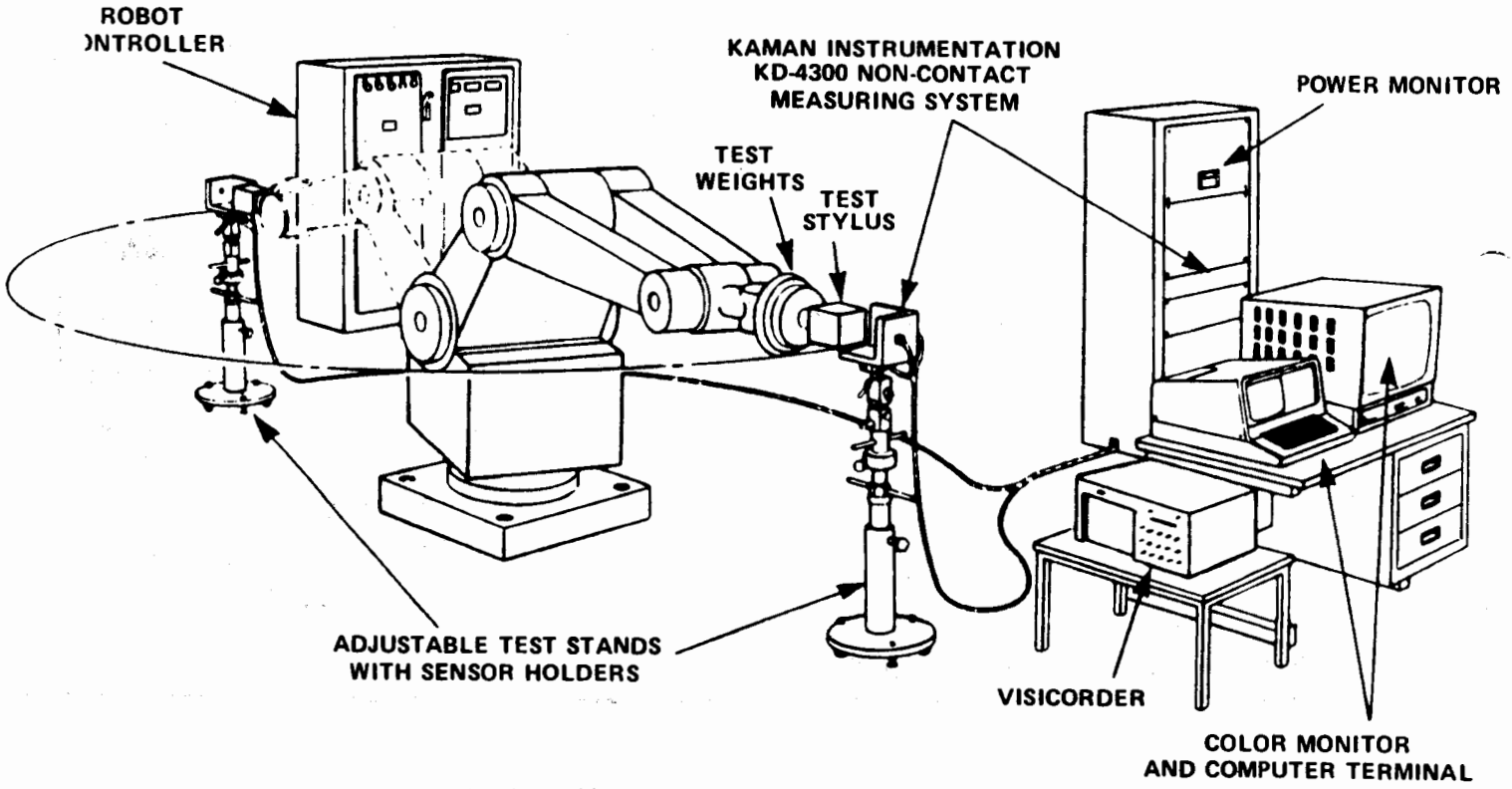

For each sensor this is a simple position measurement. Our unit monitors how repeatably the robot positions its target relative to its programmed coordinates. The sensor fixture (detail, Figure 3) is made of a nonconductive material, in this instance, delrin. The sensors must have repeatability equal to or better than the value of the increment specified for the robot. For example, if you want to measure repeatability to within .005" then the sensor chosen should be capable of that, or preferably, five times better (.001").

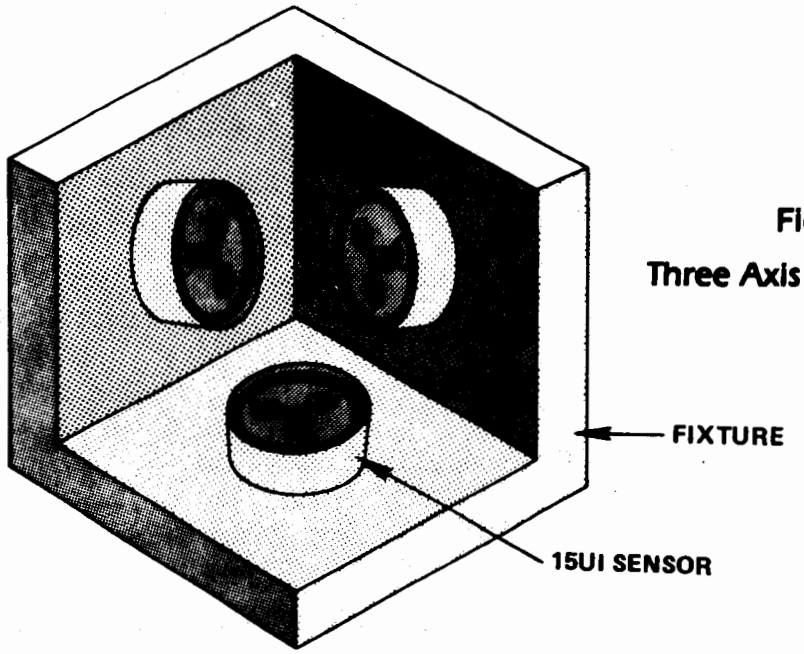

Figure 3
Three Axis Sensor Fixture

The key questions asked in system selection were: How many measuring channels are required? What is the measuring range, the required resolution? The need to test three axes, x, y, and z, at two places in the robot's arc of movement called for six measuring channels. We prescribed an aluminum target so target material was not a factor influencing system selection. Solution: the eight channel KD-4300. Two requirements dictated sensor selection. First, the need for resolution to .001" and second, the user initially did not have total faith in the repeatability of the robots to be tested. He therefore wanted a sensor with adequate standoff to prevent sensor damage. The 15U1 sensor with a .6" measuring range met both requirements. In a similar application, a different user specified the 3U sensor, not needing the greater measuring range, wanting instead this sensor's higher resolution.

Another benefit of using the KD-4300 is that, although the sensors are mounted within an inch of each other, beat note interference is not a factor because one oscillator drives all measuring channels in this system. And if it is necessary to test the robot arm's movement at another point in its arc, or if it is mounted on an x-y table, there are two more measuring channels available in the KD-4300 to measure these other positions.

Depending on robot type and the application, the possibilities are almost unlimited. You could use substitute targets with sensors built in or the sensors could be mounted on the robot's end effector. The next logical step is to use the sensor's readings as inputs to the robot controller to achieve real-time control, constantly adjusting its process, thereby closing the loop.

2. Valve Control: This application is for monitoring valve actuator position for purposes of flow valve control throughout a refinery. The output shafts of pneumatic actuators, piggybacked onto the flow valves, control valve position and subsequent flow rate. The control input/signal to change process flow rate comes to the actuator as an air pressure change. This signal pressure causes the piston and output shaft in the actuator to move, repositioning the flow valve. Our sensor, built into the actuator, measures the position of a 304 stainless steel rod threaded into the other side of the actuator's piston (Figures 4a and 4b). Our measuring system thus provides feedback for the servo control loop for accurate valve positioning and error detection.

The solutions to some measurement problems sometimes call for more than an off-the-shelf item. The pneumatic actuator in this application is already widely used and required a measuring system that could either be attached to or built into it as well as one that could withstand the extremes of outdoor use. Our applications engineer came up with a creative adaptation of one of our more basic and inexpensive systems, potting the electronics (soon to be introduced in microchip form) in a modular unit that bolts directly to the top of the actuator valve. The sensor coil was wound around a hollow nonconductive tube through which the 304 stainless rod moves (Figure 4b). A stainless steel target rod was chosen because of the corrosive environment. The electronics chosen prefer stainless or ferro-magnetic targets. Though this is an unorthodox application of standard components (excluding the coil), it does show how our applications engineers can work with you to come up with effective solutions to almost any measurement problem.

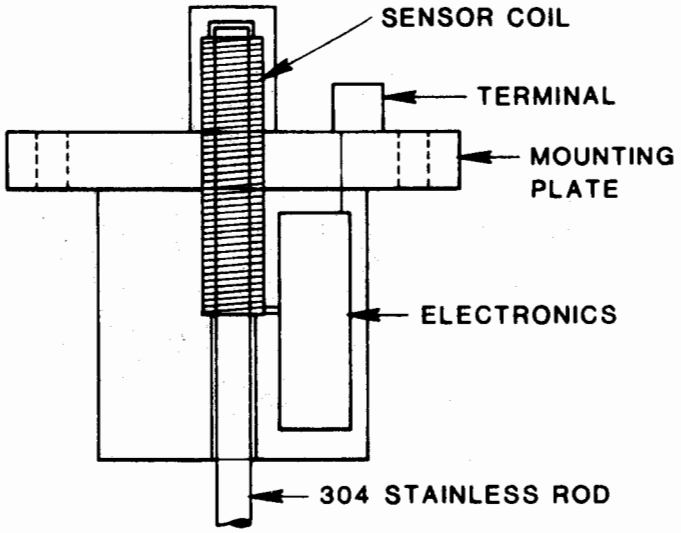

Figure 4a
Actuator Position Sensing Electronics

The plunger's travel in and out of the coil corresponds to the degree of valve opening. This travel influences the amount of electromagnetic coupling between the coil and the plunger. This is the same effect achieved as a target moves toward or away from a standard sensor. A computer relates the displacement information to the degree of valve opening. It uses this information to compute any error between controller input and valve position and then regulates air flow to the actuator valve. The measurement output from all actuator valves is routed to a computer control center that monitors and regulates the entire refining process.

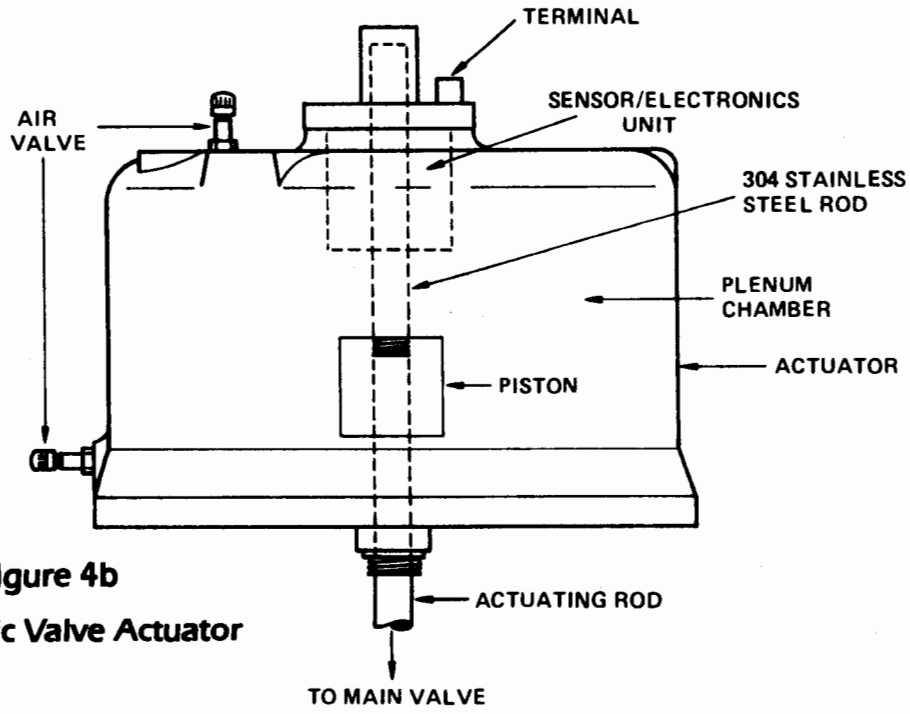

Figure 4b
Pneumatic Valve Actuator

3. Web Thickness Measurements: A unique feature of our technology is that it senses through most nonconductive media with little or no effect on output. A benefit is that only one channel of electronics can provide thickness information for nonconductive webs when measured against a conductive backing.

Using this technique you can effectively measure the thickness of rubber, cloth, and plastic sheets, plywood or other sheet wood products, wire (yes, it's conductive but fixturing is the trick), wire insulation, paint thickness (an application for the Space Shuttle fuel cell), and more.

One application using this technique is the manufacture of printer's felt. This is a continuous wide cloth belt upon which wood pulp is spread in manufacturing newsprint and other papers. The web is made of cotton and wood fiber batting that is needled, soaked, rolled, and dried to final thickness. An operator adjusts roller spacing to control the thickness of the belt in the drying/rolling process.

Testing a sample after manufacture and discovering it out of tolerance was costly, and stopping the process to take measurements, impractical. Therefore the manufacturer was confronted with the problem of continually measuring the thickness of the felt web belt as it was being dried. We recommended a sensor mounted in a sliding shoe sensing through the felt to a metal backing plate (Figures 5a and 5b).

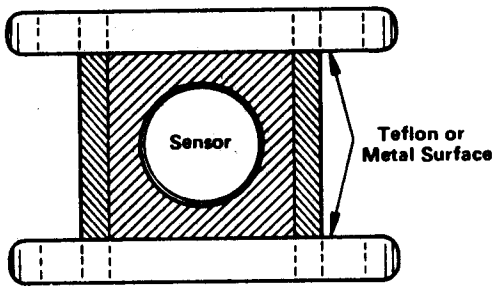

BOTTOM VIEW

Figure 5a

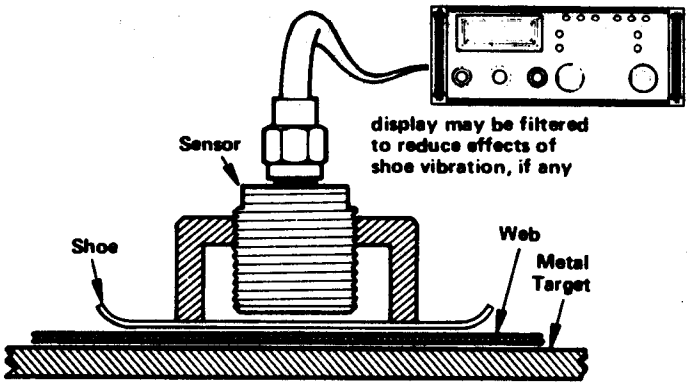

SIDE VIEW

Figure 5b

Sliding Shoe for Nonconductive Web Thickness Measurement

The relatively wet and dirty manufacturing environment dictated a NEMA enclosed system. Additionally, the sliding shoe vibrated randomly as it passed over the felt so the ability to filter system output was another requirement. Both are features of the KD-4000 Family. The thickness of the web, up to .250", dictated target range, a key question for sensor selection. Though aluminum is our preferred target material, this would corrode in the wet environment and also leave black marks on the felt. So 304 stainless, a good target for our systems, was chosen for the metal backing plate. The resulting system was a single channel, NEMA enclosed KD-4100 with internal power supply and a window kit so the filtered display could be read directly by the operator. A 6U sensor fit the bill for measuring range.

We calibrated system output to read directly in engineering units so the operator could monitor actual thickness of the printer's felt and make adjustments to the rollers as necessary. This was highly cost effective in reduction of wasted product and time.

a. Other Ideas: The shoe can be a sliding device with a teflon coated, steel, or other surface dictated by the stiction or abrasive qualities of the web material. Another technique is to mount the sensor in a fixture that rides over the web on a roller (Figure 6). If there is no need to filter the output or, if a NEMA enclosure is not necessary, both the KD-2300 and KD-2310 Series work perfectly well in this kind of application.

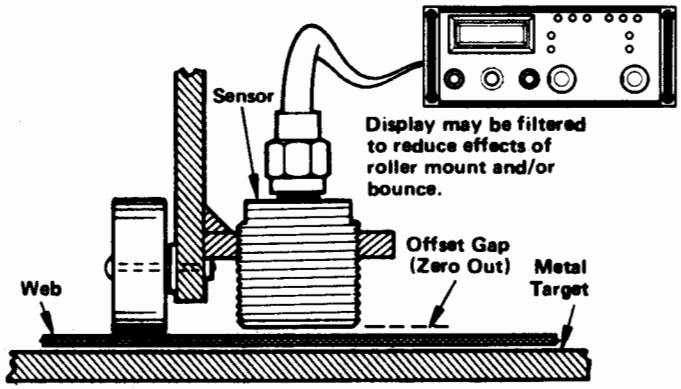

Alternate Fixture

Other displacement applications:

servo positioning
oil film thickness
artificial heart servo control feedback
computer read/write head flying height
robotic welding servo control feedback
paper pulp refiner control feedback
plastic film and paper thickness
foil pack capacity for pharmaceutical products
dynamic and static structural loading measurenents (bridges, dams airframes)
thin membrane structural profiling (antenna, nose cone)
freight train weighing
railroad track straightness
rail corrugation
turbine blade tip growth
deep hole core sample deflection
turbine blade straightness
fuel injector valve lift measurements
print head solenoid movement
material testing (stretch and compression)
paper roll splicing sequence measurement

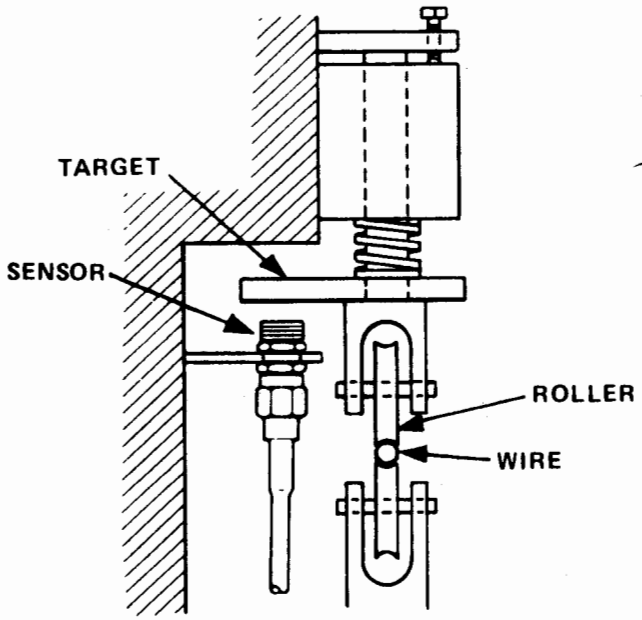

Figure 7

Wire Diameter Measurement

Figure 7 illustrates yet another way to measure thickness using the output of one measuring channel. Here a wire (rod, sheet, etc.) passes through two rollers, one fixed and the other spring loaded. A target is mounted on the spring loaded fixture with the sensor looking at it. Target movement is directly proportional to changes in wire thickness or diameter.

B. VIBRATION:

1. Ultrasonic welding is used for welding plastic sheets and fine metal parts. For an ultrasonic welder to function properly, its feed horn must vibrate at a very precise amplitude. Our systems are used to calibrate the welders for this amplitude.

Depending on manufacturer and application, feed horns vibrate at 10, 20, or 40KHz and are powered by an electromagnetic driver. The manufacturers, as well as their service facilities and some end users, calibrate the driver using a KD-2300-.5SU or -1SU system monitoring the amplitude of vibrations at the end of the feed horn.

A key question asked to determine system selection involved frequency response. The KD-2300 has excellent frequency response, 50KHz at the 3dB point. A second requirement was a sensor that had a small spot size and provided very good resolution over a small measuring range. Usually, feed horns for welding plastic vibrate 2 to 3 mils. For these we recommend the .5SU sensor which has dynamic resolution of 25 to 30 microinches over a 20 mil measuring range. For larger feed horns vibrating 5 to 7 mils we recommend the -1SU with a 50 mil measuring range and 50 microinch dynamic resolution. These sensors are fixtured to measure at mid span providing sufficient latitude for error in placement of the target without affecting the quality of the measurement. The feed horns are made of either aluminum or titanium, both excellent targets for the KD-2300. Only one channel of electronics is necessary for this application, further pointing to the KD-2300 as the solution.

The users input the signals from the KD-2300 to an RMS reading voltmeter or oscilloscope to monitor the amplitude of vibrations while adjusting the driver.

2. Shaft Vibration: Bearing wear in circulation pumps used in reactors and numerous other applications can give rise to excessive vibration and ultimately, pump failure. Safety requirements dictate constant vibration monitoring for these pumps. This wear shows up as axial and radial pump shaft runout.

This application requires two measuring channels to monitor runout. The Peak Detector card measures total indicated runout (TIR) and is a feature of the KD-4000 family so we recommended a KD-4200 system with a Peak Detector card for each channel. For an application where excursions of 1.5 to 2 mils are considered out of limits, we recommended the 3U sensor with dynamic resolution down to 50 microinches. The pump shafts were made of 316 stainless steel, a good nonmagnetic target. If the pump shafts were magnetic steel we would have recommended a dual coil 1U2, 2U2 or 6U2 sensor made for magnetic targets.The sensors were threaded into adaptors screwed into the pump housing. One sensor monitored shaft end play/axial runout and the other, side play/radial runout (Figure 8).

The Peak Detector function card's voltage output translates to actual shaft runout in mils. A feature of these cards is inclusion of two adjustable setpoints. With these you adjust for whatever voltage level or trip value you want for the card's open collector outputs. The trip value chosen can correspond directly to an unacceptable degree of shaft runout in mils. In this application, the open collector outputs were wired to alarm and shutdown circuits, providing a warning when vibration reached an unacceptable threshold and equipment shutdown if it exceeded the threshold.

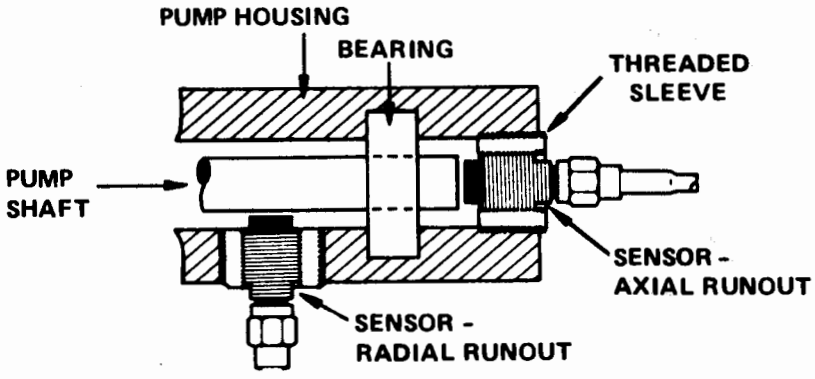

Figure 8

Axial and Radial Shaft Runout

Other vibration applications:

orbit tracing
dental drill vibration
vibration monitoring: gas centrifuge enrichment of nuclear fuels
silicon wafer slicing blade monitoring
mirror alignment applications
computer hard disk runout
helicopter transmission runout
pump rotor clearance
sonic head vibration
loud speaker deflection
gas turbine shaft runout
saw blade measurent (vibration and noise)

In a pump application, if the sensors are exposed to water you must protect them to prevent the water from shorting out the sensor coil.

If the application involves fluids at elevated temperatures (above 220°F [104°C]) we recommend the use of the KD-1925 high temperature sensor compatible with the KD-4000 family electronics. This sensor's operating temperature range is 0°F to 900°F (25°C to 482°C) with an operating pressure range to 5000 psi. This sensor has a welded inconel case and normally requires no special environmental protection.

1. Image Stabilization: The following application uses two axes of alignment information from the KD-5100 Differential Measuring System for image stabilization and/or positioning in an electro-optical assembly. The assembly configuration can include either a vibration isolation mirror, a fast steering mirror, a dither mirror, or any other closed loop mirror positioner.

Each of these are aerospace applications. The combination of high and low frequency vibration found in aerospace vehicles makes some form of vibration damping essential for any optical system.

The "key questions" for system selection in these applications address the need for very high resolution and dual axis measurements. Additionally, aerospace applications require Mil Spec construction. The KD-5100 differential system with subnanometer resolution and two axes of measurment was designed for such applications. It uses a hybrid built to MIL-M-38510E, Appendix G, in a system designed to Standard General Requirements for Electrical Equipment MIL-STD-454. The KD-5100's output is bipolar, providing both magnitude and direction of misalignment for both axes — needed information for fast steering mirrors and vibration isolation mirror assemblies. Copper or aluminum tabs are mounted as targets along the x and y axes on the back of the mirror (Figure 1). In some cases the actual beryllium copper or aluminum mirror assembly acts as a target material for the inductive sensors.

The same image reflected by the stabilization/ steering mirror in an electro-optical system also enters a receptor such as a charged couple detector (CCD). The CCD feeds its information to an image processor that analyzes the image to separate useful motion (target tracking) from high speed motion induced by vibration.

The image processor has a two dimensional array in x and y coordinates and can distinguish the direction and magnitude of motion (+ or −) for each coordinate. These coordinates correspond to the mirror's x and y axes, monitored by the KD-5100. Its sensors detect mirror position to generate an error signal. The signals from the KD-5100 and image processor go to a summation network. The summed voltages then go to the control unit, a microcomputer that compares the image processor command signal to the error signal from the KD-5100. The control unit generates a correcting input for a driver that activates voice coils or PZT actuators to position the mirror.

Figure 2 is a block diagram of this system. The summation network, control unit, driver, voice coils, and KD-5100 make up the closed servo positioning loop. The external reference signal comes from the image processor. The loop shown inside the dotted line repeats for the y axis.

In monitoring the alignment of the mirror's x and y axes, the KD-5100 derives error inputs for the mirror, thereby using alignment information to solve a vibration damping and/or positioning problem.

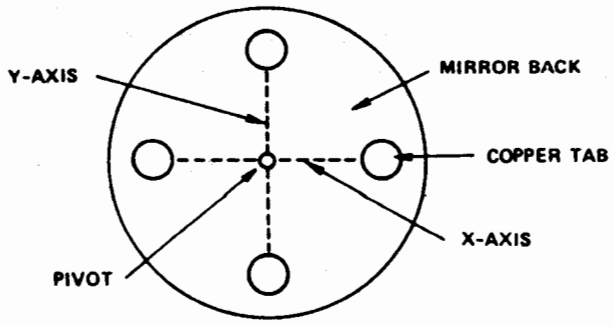

Figure 9a
Mirror Back with Copper Tabs

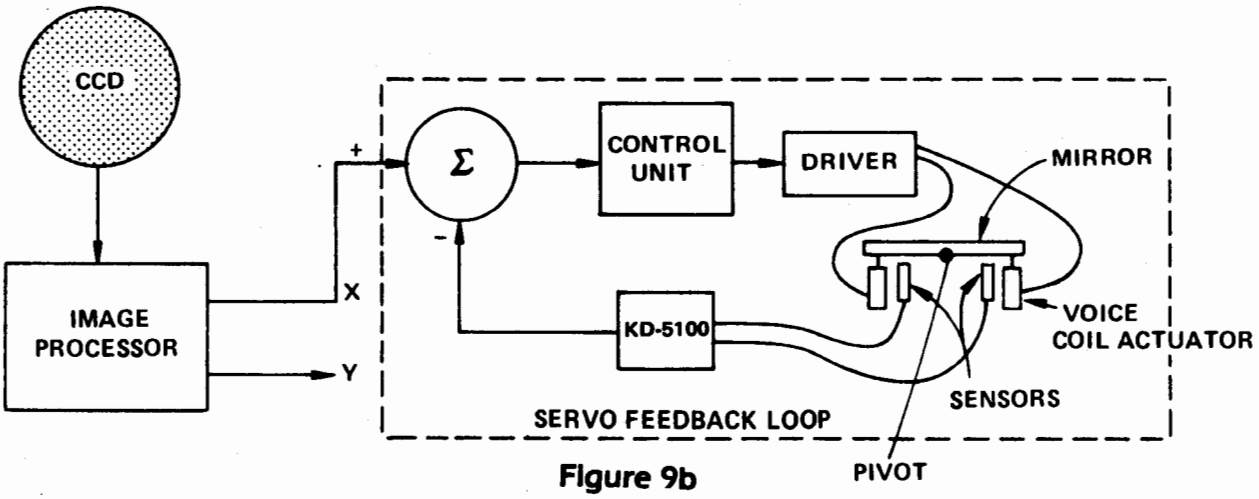

Figure 9b

Block Diagram: Mirror Alignment System

2. Can Manufacture: The two piece container industry has an ongoing need to make sure the punch and redraw dies that form the cans out of blanks are properly aligned. Mild misalignment results in cans with unequal wall thickness. Greater misalignment tears the blank. Gross misalignment destroys the punch and die pack, a costly malfunction.

Operators previously checked alignment using feeler gages. This allowed room for operator error, had to be done often, and of course could not match the .0002" accuracy of our KD-2714 Alignment System. The benefits of accurate alignment are fewer wasted pieces, reduced wear and resultant equipment costs, and, most significantly, a ten to twentyfold increase in the number of cycles (cans) between alignments.

One user of the KD-2714 Alignment System reported approximately 100,000 cycles between required alignments using the old feeler gage method. With the KD-2714 they now get well over one million cycles and have approached two million, a remarkable increase in productivity.

The KD-2714 is a differential alignment system using a sensor ring designed to fit into a die pack (Figure 10). The punch is inserted between opposing sensors mounted on x and y axes in the ring. The punches are made of carbide or M-2 steel, both good targets for this system. The operator adjusts the punch until the output from both axes/measuring channels equal zero. Some manufacturers use two rings, one at the front of the die pack and one at the rear to provide angular alignment information as well.

Other alignment applications:

fast steering mirrors
seam tracking
sounding rocket image trackers
robotic tactile sensing
mask alignment
parts positioning or sheet metal edge detection
narrow gap welding seam tracking
shaft alignment
tensile testing

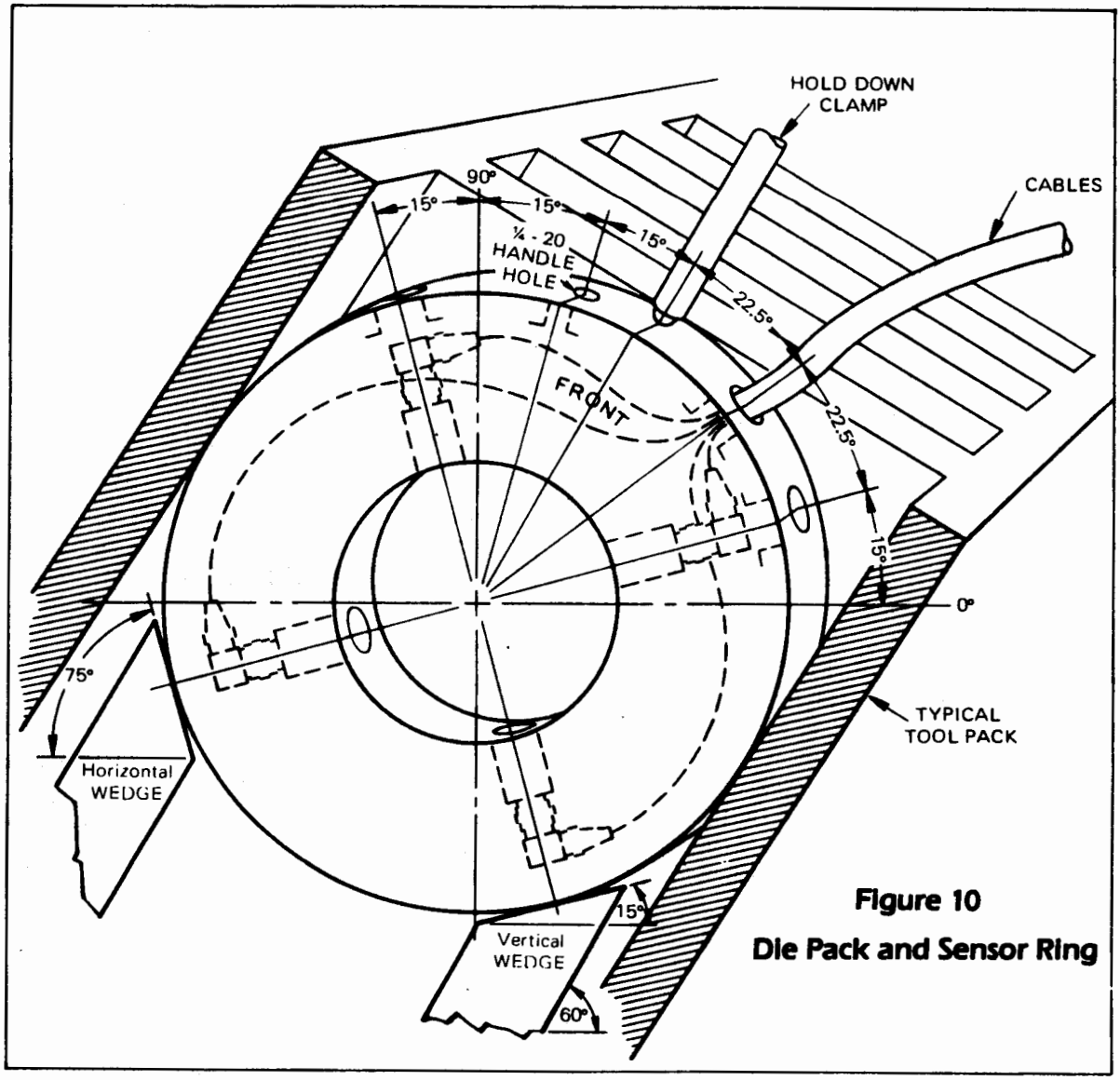

Figure 10
Die Pack and Sensor Ring

D. DIMENSIONING

We provide two dimensioning examples here. The first is an open loop application for measuring the internal diameter (ID) of reactor heat exchanger and control rod tubes. The second is a closed loop example of thickness measurements for the manufacture of computer hard disk substrates. These measurements are expressed algebraically as C+(A+B) for ID and C−(A+B) for thickness (or OD) measurements: where C = the total distance between sensor faces, A = the distance from sensor A to the target, and B = the distance fron sensor B to the target (Figures 11a, 11b, and 11c).

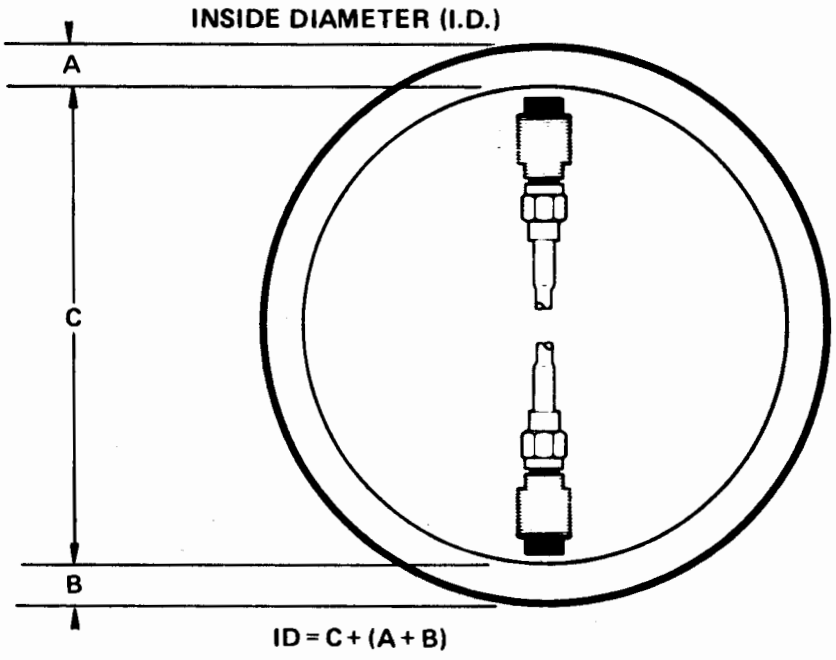

Figure 11a

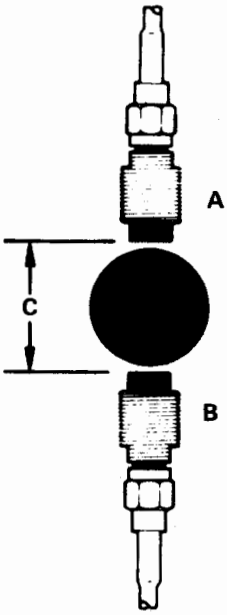

Figure 11b

Dimensioning: ID, OD, and Thickness

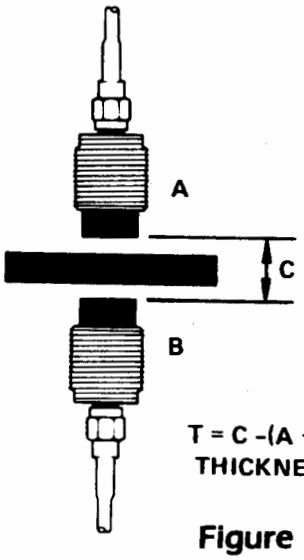

Figure 11c

1. Tube ID: We provide two examples. Both are for tubes used in nuclear reactors. One example is for control rod tube manufacture and the other for in situ inspection of heat exchanger tubes in the radioactive environment of a reactor core that has been on line a number of years.

In this instance the question "What function do I need to perform this measurement?" dictates system selection. ID measurements require a Summation function card, an add-on feature of the KD-4000 Family. The measuring range and accuracy requirements were easily met by a number of sensors but the small ID of the tubes measured, .365" to .485" ID, made it necessary to develop

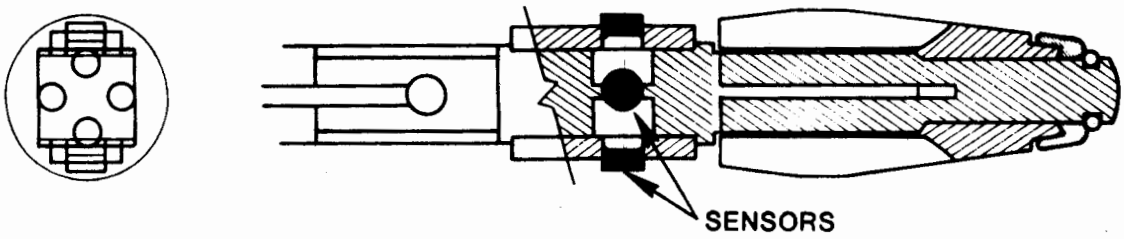

Figure 12
ID Measurement Probe Tip

a special probe (Figure 12). Each probe mounted four standard Model B sensor coils capable of 10 microinch resolution. Four sensors per probe called for a system with four channel capacity, the KD-4300. This system included two Summation function cards (one for each opposing sensor pair) to perform the C+(A+B) function for the two axes of measurement.

The control rod tubes are made of zircalloy, an excellent target material. The heat exchanger tubes are made of inconel, a good target similar to 304 stainless in its properties, so target material did not call for any special considerations in system or sensor selection.

The probe used in control rod tube manufacture was 36" long and inserted into the tubes to inspect the ID. Measurement information was fed into a microprocessor along with other parameters for final acceptance or rejection of each piece.

The second ID application called for a way to check for corrosion on the outside of the heat exchanger tubes in the steam generator of a nuclear reactor. Corrosion occurs where the tubes are held in place by the tube sheets. A consequence of the corrosion is denting on the inside of the tube. The radioactive environment dictates remote inspection. Inspection provides early warning of impending failure, a failure that would cause radioactive water to mix with secondary cooling water resulting in radioactive steam being released into the atmosphere.

The probe was the same configuration used in the previous example but only four inches long and slightly larger in diameter. The user attached it to a flexible plastic rod to push the sensor through the heat exchanger tubes to give the operator information on any changes in inside diameter. In addition to high resolution, our sensors were chosen because the environmental radiation has no effect on the measurement.

In this application the output from the Summation cards was fed into a data logger for later analysis.

2. Disk Grinding: A supplier of computer hard disk grinding machines for a major computer firm uses Kaman Measuring Systems for in-process measurements.

A fourteen stage disk grinder grinds the disks to their final thickness. Although the sensors are bathed in the coolant slurry, there is no loss of measurement accuracy.

A thickness application requires a Summation card to solve the C−(A+B) equation, calling for a KD-4000 Family system. The manufacturing environment further required a NEMA enclosure, a dual channel KD-4100, to protect the electronics. A sensor with adequate standoff was necessary to clear the substrates as they were loaded and unloaded from the station. This requirement, as well as the need to measure to within a ±.2 mil accuracy, was met by the 3U sensor. All substrates are made of aluminum, the preferred target material.

An industrial process controller monitors the summed output from the KD-4100. When the substrate is ground to the final thickness of .075", ±.0002", it stops the process and indexes to a new disk.

A KD-4200 system with 1U sensors having smaller spot size is used for inspection of the finished substrates prior to polishing to final thickness and plating.

Other dimensioning applications:

OD measurements
ID measurements
concentricity
steel belted rubber tire thickness
voice coil concentricity
oil well casing ID, OD, and straightness
thickness of copper clad PCB
pipe insulation thickness
disk thickness
turbine blade profile
coating thickness measurement
brick thickness
wire insulation thickness
turbine rotor stator bar insulation thickness
high voltage cable insulation thickness

E. SORTING

Most sorting applications are the closed loop variety. A measurement system monitors conductive parts and, based on presence or absence, size, shape, position, etc., it signals an automatic controller to reject or reroute pieces as required by the manufacturing process.

1. Four Category Sorting: This application required a noncontacting system to read four target parameters: presence and three positions (Figure 13). The targets were electrical contacts (magnetic steel, silver plated on one side) traveling through a nesting fixture on their way to be welded to a bimetalic leaf spring. The end products were electrical thermo protection contacts.

In this application, small target size called for a sensor with correspondingly small spot size, the 1U. It also required a voltage comparator to switch on the different voltages resulting from various target positions. The Dual Channel Limit Detector card, a feature of the KD-4000 Family, has the necessary comparators. A single channel KD-4100 was the solution.

The part sorting process is relatively simple. The system output varies according to the proximity and shape of the target (see Figure). When the part is absent there is no electromagnetic coupling and system output is very high or in saturation. When the part is correctly oriented there is more coupling and system output (for this application) is 5 volts. When upside down, the target presents greater area to the sensor with greater coupling and system output drops to 3.5 volts. When the target is on edge it passes even closer to the sensor and output drops to 1.5 volts.

Four Category Sorting

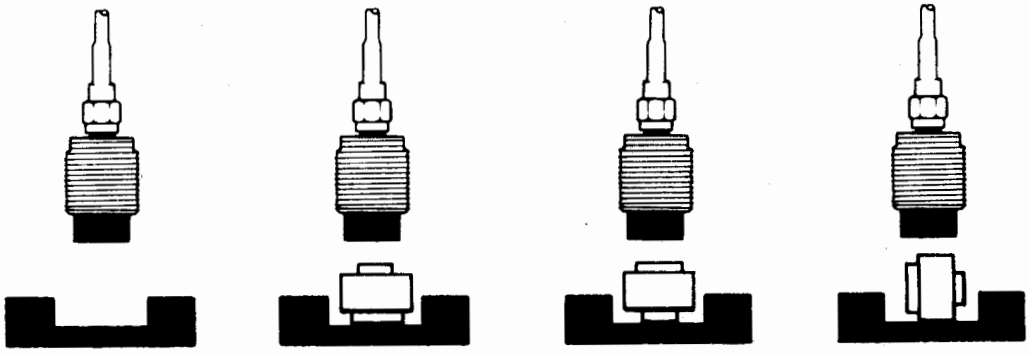

Saturation Voltage 7.5—10.0+ Vdc Not Present | **5.0Vdc Located Properly** | **3.5Vdc Upside Down** | **1.5Vdc On Edge**

Figure 13

The voltage comparators on the Limit Detector card were adjusted to switch on these voltages. Since this function card is made for a maximum of three category sorting, this four category application required the simple application of external logic in the form of OR gates. An Allen-Bradley controller received the displacement information and controlled the operation. If a part were correctly positioned it moved ahead to be welded; absent, and the table indexed to the next track; incorrect orientation triggered an air burst which kicked the part into a hopper for resorting.

2. A three category sorting application involved the manufacture of fuses having a glass envelope with metal end caps. This application required a KD-4100 system using 1U sensor and a Dual Channel Limit Detector Function card. Here the window comparator on the Limit Detector card provided Low, Go, and High indications. The fuses passed the sensor on end so it could detect one of the metal end caps and get displacement information (Figure 14). If the fuse was too long there was greater magnetic coupling with the target yielding low output voltage (Low) and it would reject. If it was the correct length it would pass on for packaging, (Go). If it was too short (High) it was rerouted for the addition of solder to one end to bring it into tolerance.

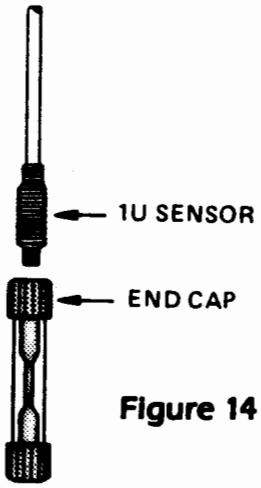

Figure 14

3. Go, No-Go Sorting: The need to simply detect the presence or absence of parts in this application called for the KS-1001 proximity switch. It is an adjustable noncontacting switch capable of 10 microinch repeatability. Parts decended from a hopper through a plastic tube on their way to an indexing machine. The sensor monitored through the tube to detect the presence or absence of a part. The adjustable switch point voltage was set to trip when no parts were passing through the sensor's field. When the hopper was empty or plugged, the voltage change tripped a relay, signaling the operator.

The KS-1003 and KS-1004 Proximity Switches have an adjustable switch point as well as analog output. The KS-1004 is optimized for dynamic applications.

Other sorting applications:

"N" category sorting
in cage ball bearing presence
metalic parts gaging
ceramic capacitor positioning
rivet head height
drill bit diameter sorting

KAMAN INSTRUMENTATION

...solving your position measurement problems

Introduction

Do you have a position measuring problem that demands precise, repeatable results? Whether you want resolution in mils or angstroms, we have a system that will meet your needs.

Kaman Instrumentation's displacement measuring systems are for precision noncontact position measurements of metal objects. They also do contact thickness measurements of nonconductive film or web materials.

The systems and sensor options described in this brochure offer the opportunity for solutions to a wide variety of applications problems. The number of applications for both laboratory and industrial environments is as broad as your imagination.

About Kaman Instrumentation

We are a wholly owned subsidiary of Kaman Corporation of Bloomfield, Connecticut, a half-billion dollar a year firm with 40 years' experience as a leader in aerospace, industrial, and consumer products. Operating under the aegis of the parent company, Kaman Instrumentation's Measurement Systems Group draws on over 25 years of experience with our inductive position measurement techniques.

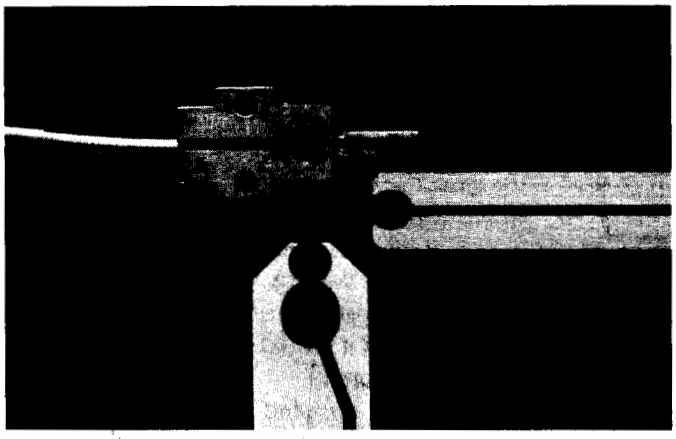

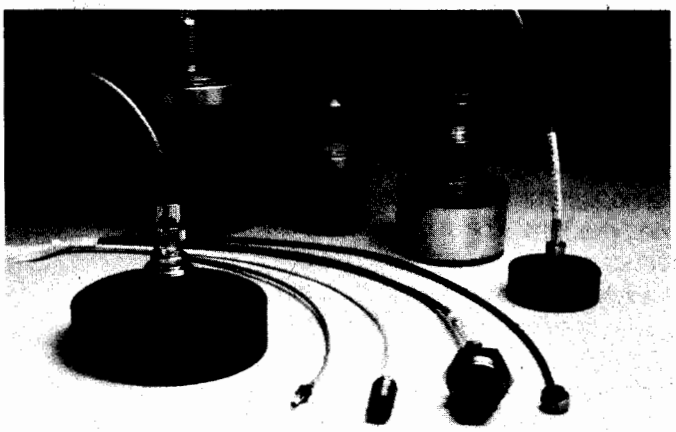

Sensor Options

Over 20 standard sensor options range in size from .080" to 3.0" in diameter with measuring ranges from .010" to 2.25". We can also work with you to build special sensor configurations to solve unique application problems.

KD-5100 Differential Measuring System

Tomorrow's technology today. This compact system provides unprecedented resolution to one nanometer.

The differential impedance transducer solves problems such as detecting mirror positioning, vibration sensing, and precise x-y stage alignment. This hybrid based unit has two channels with two sensors per channel for dual axis alignment. The output is bipolar, providing not only magnitude but direction of misalignment.

- Manufactured to MIL38510E, Appendix G
- Sensitivity up to 40V/mm
- Temperature effects at the sensor/target interface less than 1 microinch per °F
- Ideal for differential (A-B) applications for centering nonmagnetic targets

The KD-4000 Family of Displacement Measuring Systems

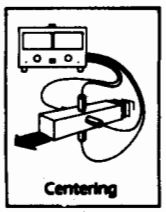

VERSATILE, COST EFFECTIVE SOLUTIONS TO A BROAD VARIETY OF MEASUREMENT PROBLEMS

The KD-4000 Family includes three series of measuring systems. Each of these uses a motherboard with plug-in PC cards making a system easy to service through "board swapping." This minimizes system down time so your production and process control equipment is back on line with a minimum amount of effort and lost time.

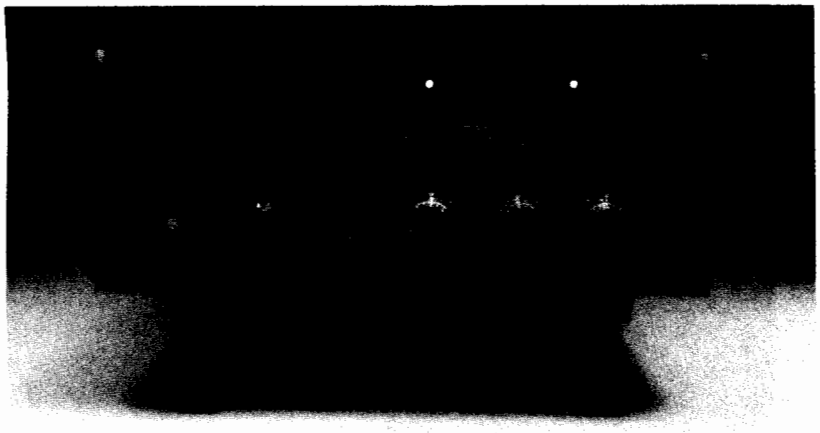

KD-4100 Series

The KD-4100 Series comes in either single or dual channel configurations protected in water and dustproof NEMA-4 enclosures. The larger enclosure is available with an optional built-in power supply, digital panel meter, and window kit.

KD-4200 Series

The KD-4200 Series comes in a "half rack," benchtop or rack mountable enclosure as either a single or dual channel system. KD-4200 systems have a built-in power supply and 3½-digit panel meter. Multiple front panel display options are available.

KD-2300 Family

The KD-2300 is equally effective with both magnetic and nonmagnetic targets. It features the smallest of any of our sensors (.080"/2mm diameter) among its sensor options.

All KD-2300 systems come complete with sensor, cable, and electronics.

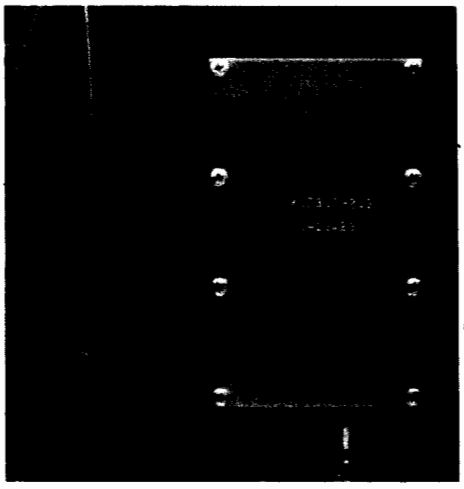

KD-2310

This system provides improved linearity and long-term stability over the KD-2300 as well as a family of sensors with different mechanical and performance profiles.

This system is designed for use against either magnetic or nonmagnetic materials.

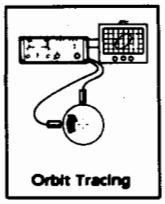

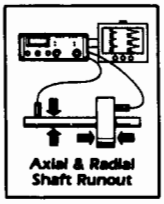

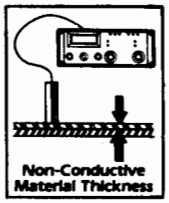

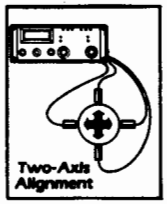

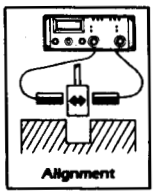

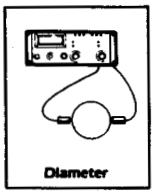

KD-4000 Family Features:

- Excellent long-term stability and repeatability
- High resolution and linearity
- Low output impedance
- High frequency response
- Multiple configuration options
- User adjustable calibration controls (zero, gain, and linearity)
- Simple interface with lab instruments and process control equipment
- Functional flexibility with add-on function cards

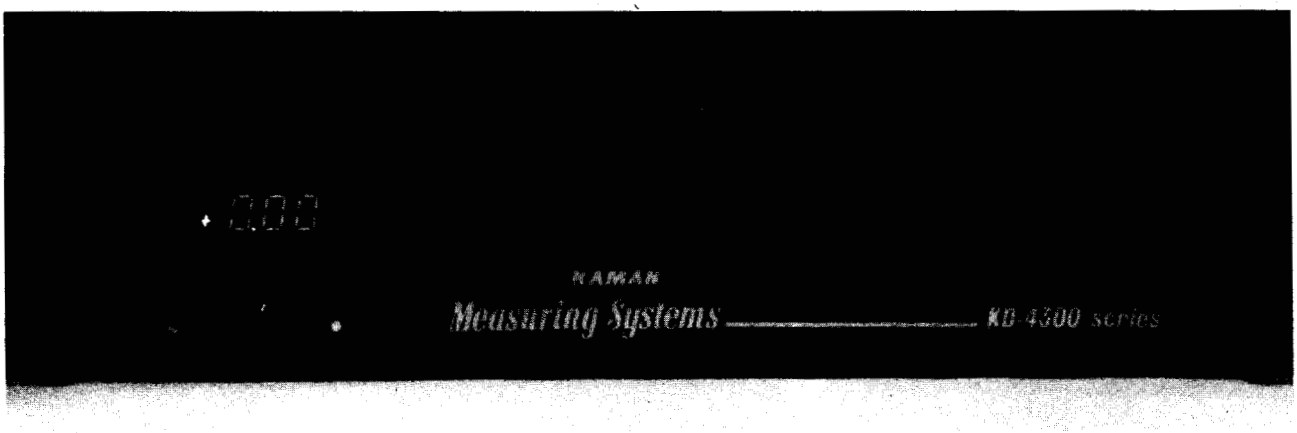

KD-4300 Series

The KD-4300 Series is an eight channel capacity unit in a 19" rack mount/bench top enclosure. This system has an internal power supply, 3½-digit panel meter, and room for up to eight function cards.

Application Information

The addition of one or more function cards to the basic system increases the utility of the KD-4000 Family. The following functions are available: summation for ID, OD, thickness, and centering; peak detector with comparators for alarm and shutdown indications; dual channel limit detector for high/low limits, automatic parts inspection and sorting; RMS to DC conversion; auto zero; and low pass filter.

KD-2300 and KD-2310 Series Features:

- Proven long-term stability and repeatability
- High resolution and linearity
- Low output impedance
- High frequency response
- Linear measuring ranges from 0 to .010 inches through 0 to 2.400 inches
- User-adjustable calibration controls (zero, gain, and linearity)
- Simple interface with lab instruments and process control equipment
- Multiple sensor options with broad temperature operating ranges

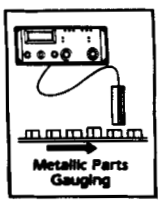

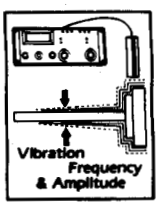

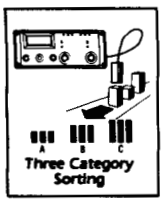

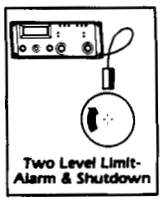

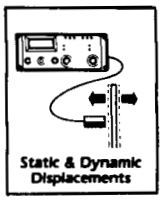

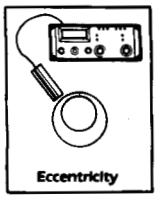

SESSION 5

ABSTRACTS OF MINIPAPER PRESENTATIONS

SENSOR SPECIFICATIONS

- Linearity - Typically 0.5% of Full Scale Output
- Resolution - 0.01% of Full Specified Measuring Range or Better with Filtering
- Sensitivities Are Factory Settings. They Are User Adjustable (Contact Us).

S = Shielded Sensor
U = Unshielded Sensor
B = Flat Configuration
2 = Dual Coil for KD-4000 Magnetic Applications
M = Magnetic

KD-4000 FAMILY AND KD-2310 SERIES

SENSOR OPTIONS		0.25S	1U	1U2	1S	2UB	2S	2U2	3U	4SB	4S	6U	6U2	15U	15U2	30U	30U2
KD-4000 FAMILY			●	●		●	●	●	●		●	●	●	●	●	●	●
TARGET MATERIALS	NON-MAGNETIC		●			●			●			●		●		●	
	MAGNETIC			●				●					●		●		●
KD-2310 SERIES		●	●		●	●	●		●	●	●	●		●		KD-2350	
TARGET MATERIALS	NON-MAGNETIC	●	●		●	●	●		●	●	●	●		●		●	
	MAGNETIC					●	●		●	●	●	●		●		●	
MEASURING RANGE	INCH	0.010	0.040	0.040	0.040	0.080	0.080	0.080	0.120	0.160	0.160	0.240	0.240	0.600	0.600	1.2	1.2
	mm	0.25	1	1	1	2	2	2	3	4	4	6	6	15	15	30	30
SENSITIVITY KD-4000 / KD-2310	mV/mil	100	100 / 10	100	25	100 / 10	10	100	10	10	10	10	10	10 / 1	10	1	1
	mV/mm	1000	1000	1000	1000	1000	1000	1000	1000	1000	1000	1000	1000	100	100	100	100
SENSOR DIAMETER	INCH	0.08	0.12	0.187	0.28	0.31	0.375	0.35	0.33	0.875	0.625	0.56	0.54	1.50	1.50	3.0	3.0
	mm	2.0	3.1	4.7	7.0	7.9	14.7	8.9	8.4	22.2	24.6	14.2	13.7	38.1	38.1	76.2	76.2
THREAD SIZE		10-32 UNF-2A		1/4-40 NS-2A	M7 x 1	N/A	15/32-32 NS-2A			N/A	3/4-20 UNEF-2A			MOUNTING HOLES		3/4-20 + MOUNTING HOLES	UNEF-2A

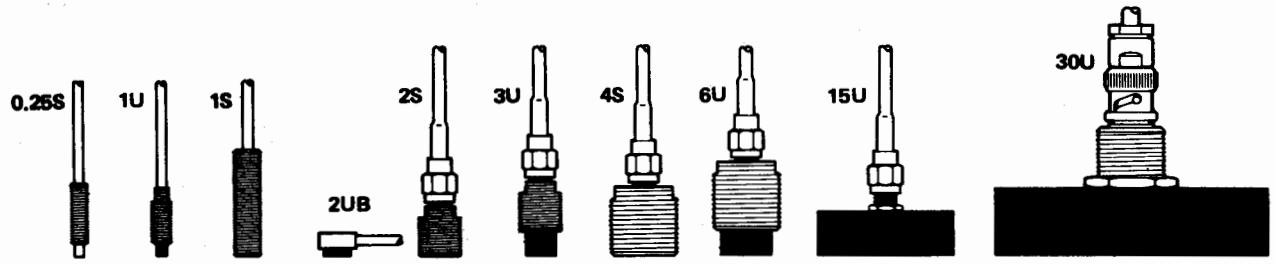

KD-2300 SERIES

SENSOR OPTIONS		0.5SU	0.5SUM	1S	1SM	1SU	1SUM	2S	6C	8C	10C	10CU	12CU
TARGET MATERIALS	NON-MAGNETIC	●		●		●		●	●	●	●	●	●
	MAGNETIC		●		●		●	●	●	●	●	●	●
MEASURING RANGE	INCH	0.020	0.020	0.040	0.040	0.050	0.050	0.100	0.250	0.500	0.750	1.00	2.00
	mm	0.5	0.5	1.0	1.0	1.25	1.25	2.5	6.4	12.7	19.1	25.4	50.8
SENSITIVITY	mV/mil	50	50	20	20	20	20	10	5	2	1	1	0.5
	mV/mm	1000	1000	1000	1000	1000	1000	1000	1000	100	100	100	100
SENSOR DIAMETER	INCH	0.08	0.08	0.25		0.19		0.38	0.76	1.25	2.00	1.40	2.90
	mm	2.0	2.0	6.4		4.8		9.6	19.3	31.8	50.8	35.6	73.7
THREAD SIZE		M3 x 0.5		1/4-40 NS-2A				15/32-32 UNS-2A	7/8-14 UNF-2A		7/8-14 UNF-2A		

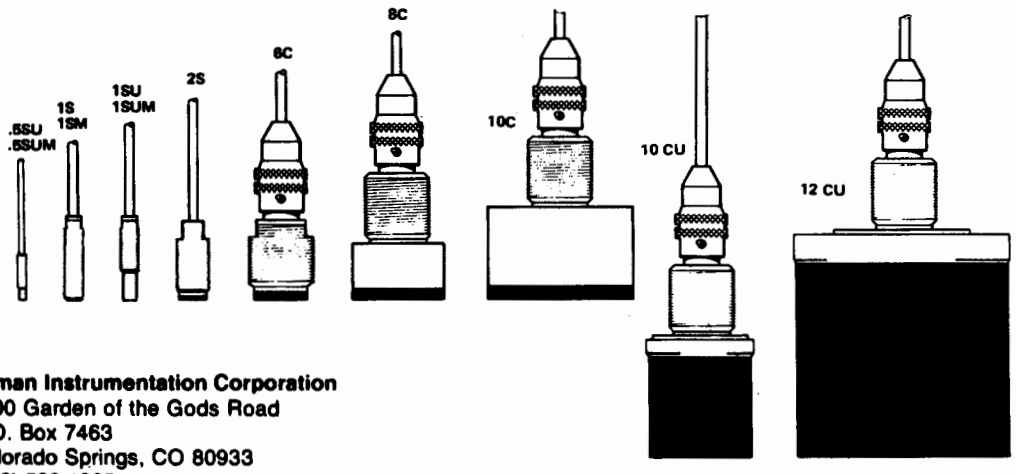

SPECIAL SENSOR CONFIGURATIONS:

The sensors shown on this page are standard sensors for the KD-2300 and KD-4000 Families of measuring systems. Other configurations are available including flat sensor probes from 1.75" to 8" long, designed for the computer hard disk industry.

And . . . we can work with you to custom design special sensor configurations to solve application problems where one of our 25 standard sensors won't fit. This usually involves mounting one or more of our many sensor coil configurations in a sensor body designed for your specific application. We have custom built sensors for nuclear reactor service, oil exploration, biomedical use, airborne night vision systems, valve control, laser mirror alignment, and more.

Call or write Kaman Instrumentation for more details. Ask for the catalog of our full product line, the "Measurement Solutions Handbook."

Kaman Instrumentation Corporation
1500 Garden of the Gods Road
P.O. Box 7463
Colorado Springs, CO 80933
(303) 599-1825

IMPROVED TECHNIQUES FOR MEASUREMENTS OF VELOCITIES WITH PIEZOELECTRIC TRANSDUCER PINS

Paul V. Whalen
AD/3246 Test Wing
Eglin AFB, FL

High frequency piezoelectric transducer pins have been used for some time by the Armament Division (AD) at Eglin AFB to measure the time-of-arrival (TOA) of explosive shock waves at selected positions on munitions so that detonation velocities could be calculated to support munitions development. However, because of the very high frequency data sampling requirements and the limited size of available digital memory, applications have been limited by a small data acquisition window. This problem has been alleviated at the AD by replacing several digital waveform recorders with a 14-track 2MHz analog tape recorder. Consequently, the data acquisition window is increased by many orders of magnitude (several hours long rather than 8.16 milliseconds with digital waveform recorders at the same sample rate) with only one order of magnitude loss in time resolution. Additionally, no post test period for non-volatile data storage is required, only one recorder is required for 14 data channels, and the problem of false triggering is eliminated.

Another problem has been that individual pin transducer outputs are uncalibrated and nondistinct. This means that the pins had to be arranged so that each of several pins on a single channel had a distinct time window when it was expected to trigger. Consequently, the number of pins which could be multiplexed into a single-channel digital data recorder has been severely limited by the difficulty of interpreting the data.

Several approached are being investigated at the AD to generate a unique output for each individual pin on a data channel. One approach simply allows each pin to be arbitrarily set to generate a positive or negative voltage deflection. Another approach generates a characteristic pulse width (time duration), while a third approach generates a characteristic pulse height (voltage level) for each individual pin. Individually, or in combination, these techniques will greatly increase one's data collection ability by allowing one to learn more information from the same pin transducer arrangement (i.e., what direction the shock wave was traveling).

AN INEXPENSIVE MILLITORR (GAGE) PRESSURE SOURCE

William B. Leisher
Sandia National Laboratories
Albuquerque, NM

This paper describes a fixture that can supply relatively stable pressures for pressure transducer calibrations in the millitorr to torr range (gage or differential) without requiring a temperature controlled room or chamber. Effects of room air currents are minimized by the use of an atmospheric stilling chamber. Stability, for a five minute period, is better than 4% at 1 millitorr and approximately 0.1% for pressures from 10 millitorr to 1 torr. The drifts are slow, permitting readjustment of the pressure before making readings. It is believed that the poorer stability at one millitorr is caused by fluctuations in the gas supply pressure. An MKS model 310CH, 0-1 torr differential head was used to monitor the test pressure.

The fixture is assembled from "Junk-Box" parts--a needle valve, a porus metal snubber or additional needle valve, a 15-in. length of 0.25-in OD by 0.19-in. ID smooth bore tubing, a 12-in. length of 0.125-in. OD by 0.062-in. ID smooth bore tubing, some 0.25-in ID plastic tubing, a few tubing fittings, and a cardboard box for a stilling chamber. Assembly, in order of flow direction, is as follows: gas source, needle valve, snubber, 0.19-in. ID tubing, metal tubing tee (run), 0.062-in. ID tubing, plastic tubing, and stilling chamber. The branch of the metal tubing tee supplies the test pressure to the test and reference transducers. The low-pressure or atmospheric ports of the test and reference transducers and the discharge of the 0.062-in. ID tube are connected to each other and to the interior of the stilling chamber with the plastic tubing.

Operation is simple, the needle valve controls a gas flow through the tubing. The snubber and 0.19-in. ID tubing are used to establish laminar flow before reaching the 0.062-in. ID tubing which serves as a restrictor to cause a pressure rise at its inlet. This pressure rise is the test pressure. Because of the laminar flow, the pressure rise, which is tapped from the branch of the tee fitting located between the two pieces of smooth bore tubing, is free of turbulence, and temperature change effects appear only as viscosity changes (the square root of the absolute temperature). The restrictor discharges into the plastic tubing connecting the low-pressure or atmospheric ports of the test and reference transducers to the stilling chamber. Gas flow is approximately 4 cubic centimeters per second at 1 torr and is essentially proportional to test pressure. The Reynolds number in the restrictor is about 160 at 1 torr.

DESIGN AND APPLICATIONS OF A HIGHLY STABLE MINIATURE PRESSURE TRANSDUCER

Ronald Poff
Endevco, Capistrano, CA

A miniature high stability absolute pressure transducer has been developed for aerospace oriented high reliability applications. The design incorporates a state of the art silicon microsensor which has the strain elements electrically isolated from the sensor structure by an oxide barrier. This

feature gives good insulation characteristics over a much wider temperature range than conventional sensors with diode isolation. The sensor is hermetically sealed into a metal fitting. All inorganic materials are used with no epoxies utilized in the structure of the transducer. The result is a very stable and repeatable transducer in a miniature size (six grams). The performance matches that of much larger units which have been available previously.

Several long term high reliability applications are discussed. The transducer is being used to measure barometric pressure within +9 millibar total error band. Testing with jet fuel, fluorocarbons and hydraulic fluids is reported. Mil-Std-810C testing for shock, vibration, low and high temperature, humidity, salt fog and dust is reported as is data on short and long term stability.

THE 155mm BALLISTIC RAIL GUN CHARACTERIZATION OF THE ACCELERATION/DECELERATION VECTOR

Dr. John R. Zimmerman and Michael J. Paduano
U.S. Army Armament Research, Development & Engineering Center
Dover, NJ

The development of artillery projectiles incorporating guidance, sensing and telemetry systems; or other sophisticated mechanical, optical or electronic devices created the need for a method to dynamically test the ability of those items to survive the high-g launch environment of a large gun and still function properly. The Ballistic Rail Gun permits soft recovery of a special carrier projectile containing the test specimen within 104 feet of muzzle exit after subjection to the actual launch environment of a 155mm howitzer. The carrier projectile is fitted with a special concave nose scoop which affects transfer of energy to a captive rail water deceleration system. Recovery and analysis of the components or system carried within the projectile can then be performed.

The crux of this paper is a discussion of the instrumentation techniques which have been employed to measure and characterize the projectile motion in-bore (acceleration) and in-rail (deceleration). These techniques have included lasers, magnetic based devices, radar and telemetry. Refinement of the ability to measure and characterize the projectile motion has been a continuing process. Initial work has been performed on the development of a memory transducer which can be placed in the carrier projectile, and interrogated after soft recovery. Status of the evolving transducer development, and problems encountered will be discussed.

MINIATURE SILICON TEMPERATURE SENSOR WITH HIGH OUTPUT VOLTAGE, HI-RELIABILITY AND FAST RESPONSE

Herbert Chelner
Micron Instruments, Inc.
Simi Valley, CA

Presented in this paper is the design configuration, test data, applications and some packaging options for a miniature silicon temperature sensor which is unusual in its simplicity and versatility of use.

Although the resistance change with temperature of this sensor is non-linear, an output voltage which is linear and proportional to temperature can be achieved with the use of a single resistor when operated within its design limits.

The sensor is .060 x .005 x .0005 inches and has .002 inch diameter gold lead exiting from either end. The small mass and size permits extremely fast response to thermal changes and permits flexibility of packaging.

Since the sensor is etched from a solid piece of silicon, a minimum of molecular slippages and/or dislocations is achieved. The gold lead wires and sintered gold pads present an attachment method which is highly reliable. The final product is relatively insensitive to contamination (no junctions that are susceptible to contamination) and of high stability and high reliability construction.

The gage factor of the sensor is low and bonding to high expansion metals, such a aluminum, results in a very minor slope change.

When connected into a bridge configuration using three resistors as complimentary legs of a bridge and excited with six volts, an output change of 2 volts between -65°F and +165°F is obtained. The sensor could be operated directly into a 8.0 volt Digital Panel Meter and read directly in °F. The output over this temperature is linear within 1°F.

HIGH SPEED DIGITAL DATA ACQUISITION SYSTEM

Richard D. Talmadge
Air Force Wright Aeronautical Laboratories
Wright-Patterson AFB, OH

The Structural Vibration Branch (FIBG) of the Air Force Wright Aeronautical Laboratories (AFWAL) has been involved in the use of automatic gain ranging amplifiers for more than 20 years. These amplifiers are used to interface most all of the transducers used by FIBG to the recording systems. With the use of an Automatic Gain Ranging Amplifier (AGRA) the wide dynamic range of the transducers can by matched to the somewhat limited range of the recording and/or data acquisition system.

This paper will briefly describe the history of the AGRA and the current efforts to provide a complete system using this device.

In 1967 this organization sponsored the development of an AGRA to solve the problem of recording transducer outputs which have large dynamic ranges. This amplifier has been used very successfully for the past 20 odd years in flight testing as well as ground applications. In 1982 FIBG started an R&D effort with Aydin Vector to take this technology and upgrade it to the state-of-the-art in so far as accuracy and packaging concepts. In 1986 two contracts were let to Aydin Vector to build multiplexers using the AGRA as the signal conditioning element. The first contract was to build a 12 channel multiplexer with restricted bandwidth for the B-52/ALCM captive carry program. The second contract was to provide a general purpose multiplexer that contained 16 AGRAs and would produce an initial output stream of 4 megabits/second and be expandable to a full 16 megabits/second in the future. The initial bit rate of 4 megabits will allow for 16 channels at a bandwidth of 5,000 Hz while the future goal will provide 20,000 Hz bandwidth.

SESSION 6

DATA ACQUISITION

MEASUREMENT OF DYNAMIC PRESSURE IN INERT AND REACTIVE SOLIDS BY PVF_2 AND MANGANIN GAUGES

P. A. Urtiew and L. M. Erickson
University of California
Lawrence Livermore National Laboratory
Livermore, CA 94550

ABSTRACT

Dynamic pressure measurements in solids subjected to excessive loading conditions have recently been enriched by the deployment of a small, new self-powered, polarization type gauge. The transducer, known as PVF_2 (polyvinylidene fluoride), is a thin polarized sheet of polymer plastic which contains its own source of energy and does not require any external power supply.

For high pressure work the manganin gauge is considered the transducer of choice. However, even this gauge is undergoing constant modifications and improvements for better resolution and accuracy. Of particular interest to us is the high resolution which can be attained in the measurement of rapid pressure variation with time in high explosive materials during the build-up phase as well as during the pressure release phase behind a fully developed detonation wave.

Performance of PVF_2 and manganin gauges is discussed in detail showing both the pros and cons of each type as pertinent to the in situ pressure measurements. Potential values of PVF_2 gauges are indicated and compared to those of the standard manganin gauges.

NOMENCLATURE

A = active area, square centimeters
C = capacitance, microfarads
I = current, amperes
Q = charge, microcoulombs/cm^2
R = resistance, ohms
t = time, microseconds
V = signal amplitude, volts
σ = pressure, gigapascals subscript
o = initial state
s = shocked state

INTRODUCTION

In solid systems, where materials are subjected to dynamic loading an accurate characterization of response is very essential. Theoretical models use equations of state which are formulated on the basis of experiments and experimentally derived parameters. More sophisticated system designs require more accurate equation of state parameters, which in turn put additional constraints on the accuracy of experiments.

One of the important physical parameters lending itself to a better characterization of materials is pressure. This is especially true when the flow behind the shock wave is not steady but is rather highly dependent on time due to new processes triggered by a propagating shock wave. High explosive (HE) materials represent an outstanding example of such a case where shock waves trigger chemical reactions and the flow becomes very unsteady. Having an accurate account of pressure variation with time one can integrate one-dimensional hydrodynamic equations to obtain the rate of chemical energy release and the rate at which a simple burning process transits into the violent detonation phenomenon.

Pressure measurements under dynamic loading conditions is not a simple matter and requires both the durability of the gauge to survive an extremely hostile environment developed in the region of interest as well as the resolution accuracy of the gauge in time. At the Lawrence Livermore Laboratory (LLNL) we have devoted a great deal of effort to improve manganin pressure gauges for accurate and reliable in situ measurements in both inert and reactive media and to study the detailed shape of the Taylor wave in a detonating HE.

Recently, a relatively new ferroelectric gauge has been developed and described by Bauer[1] at the French-German Institute at St. Louis. We are currently testing this type of gauge under steady and unsteady transient conditions. In contrast to the manganin gauge it offers great simplicity and ease of operation. It is self powered and does not require extensive calibration. If shows great promise for some specific applications.

It is the purpose of this paper to describe these two techniques for measuring pressure under dynamic loading conditions, compare them to theoretical expectations and to demonstrate their accuracy and response. An attempt will also be made to indicate areas of possible improvement as well as areas of possible pitfalls.

MANGANIN PRESSURE TRANSDUCER

Manganin was first used as a pressure transducer in a hydrostatic apparatus by Bridgeman[2]. Later, Fuller and Price[3] and Bernstein and Keough[4] used manganin wires as dynamic stress transducers in inert materials. Wackerle et al.[5], Kanel and Dremin[6] and Burrows et al.[7] applied the gauge to reactive materials to study shock initiation and Taylor wave profiles in various explosives. Weingart et al.[8] and Erickson et al.[9] devised a low-impedance gauge etched from foil and insulated with polytetrafluoroethylene (PTFE) for use in making in situ measurements in reacting and detonating high explosives.

Manganin is well suited for use as a pressure transducer because it has a reasonably high coefficient of resistance change with pressure. The coefficient is positive, and its response is nearly linear. Of even greater importance is the fact that is has a very low coefficient of resistance in response to changes in temperature and thus a minimal correction is needed for shock heating. These gauges, do however, exhibit a small amount of hysteresis, e.g., once subjected to a given shock pressure they undergoe a permanent change in resistance.[10]

Gauge Design and Fabrication

Our manganin gauges are fabricated at LLNL using annealed, shunt-grade manganin foil of 25.4 μm thickness. The foil is composed of 85.90% (wt%) copper, 9.5% manganese, 4% nickel, 0.5% iron, and 0.1% silica. The transducers are etched from the foils using standard techniques and the electrical leads are plated with 8 to 10 μm of copper to reduce the lead resistance. Since the gauges have a low resistance it is necessary to make a four-terminal resistance measurement.

We have developed two gauge configurations: a single-ended gauge in which all four leads emerge from one side, and a double-ended (H-shaped) gauge. These configurations are illustrated in Fig. 1. Both gauges follow the same calibration curve, as described by Vantine et al.[10] However, since the single ended version allows greater flexibility in gauge placement within a target assembly, it is now used almost exclusively. The active elements of the single-ended and H-shaped gauges are 0.7 x 2.0 x 0.025 mm and 1.5 x 3.0 x 0.025 mm respectively. Their nominal resistance is 65 mΩ .

Gauges are bonded into "gauge stations" consisting of one or more gauges sandwiched between layers of PTFE dielectric. The bonding agent is fluoroethylene propalene (FEP), and the bonding is achieved by placing the sandwich in an evacuated fixture and inserting it into a press preheated to the melt temperature of the FEP. Details of construction have been reported by Erickson et al.[9].

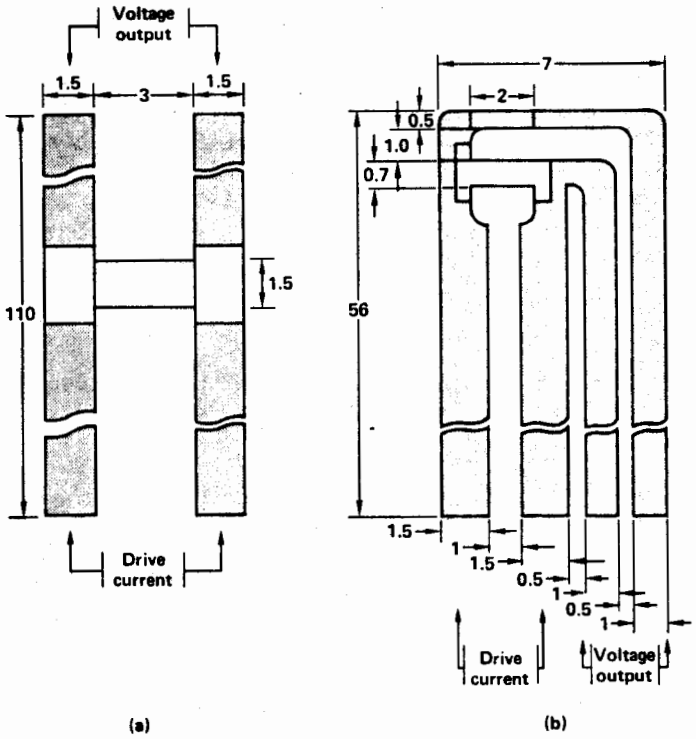

Fig. 1 Two manganin gauge configurations: (a) double ended and (b) single ended. Gauges were etched from a 25.4 μm-thick manganin foil. Shaded areas have 5 μmCu plating on each side to reduce lead resistance.

Experiment

During the experiment a 50-ampere pulse of current is supplied to the gauge prior to shock arrival, producing a resultant ambient voltage, V_o. The arrival of the shock wave produces an additional voltage ΔV. To enhance the accuracy of the measurement we use a modified bridge circuit to offset the ambient voltage as described by Vantine et al.[11]. The current in the gauge is also measured and the fractional resistance change is related to measured values of V_o, ΔV, I, and R_o as:

$$\frac{\Delta R}{R_o} = \frac{(V_o + \Delta V)}{IR_o} - 1 \qquad (1)$$

where R_o is the initial resistance of the gauge measured to ±0.01% accuracy, V_o is the ambient voltage, I is the current through the gauge, and ΔV is the change in voltage due to the pressure.

From the time resolved $\Delta R/R_o$ values one can evaluate the pressure profile using the calibration curves described in Ref. 10. The $\sigma - \Delta R/R_o$ fits are shown below.

$$\sigma(\text{GPa}) = .42 + 39.12\left(\frac{\Delta R}{R_o}\right) + 14.08\left(\frac{\Delta R}{R_o}\right)_s^2 - 7.59\left(\frac{\Delta R}{R_o}\right)_s^3$$

where:

$$\left(\frac{\Delta R}{R_o}\right)_s = \left(\frac{\Delta R}{R_o}\right) - 0.1\left(\frac{\Delta R}{R_o}\right)_{jump} + 0.04\left(\frac{\Delta R}{R_o}\right)_{jump}^2$$

represent the hysteresis corrected jump value of $\frac{\Delta R}{R_o}$ behind the shock front. A typical experiment with two manganin gauge stations imbedded in the LX-14 explosive is shown in Fig. 2. Also shown in this figure is the space time (x-t) plane of the propagating shock through the explosive and the corresponding pressure histories at the two gauge locations illustrating the predetonative build-up of pressure.

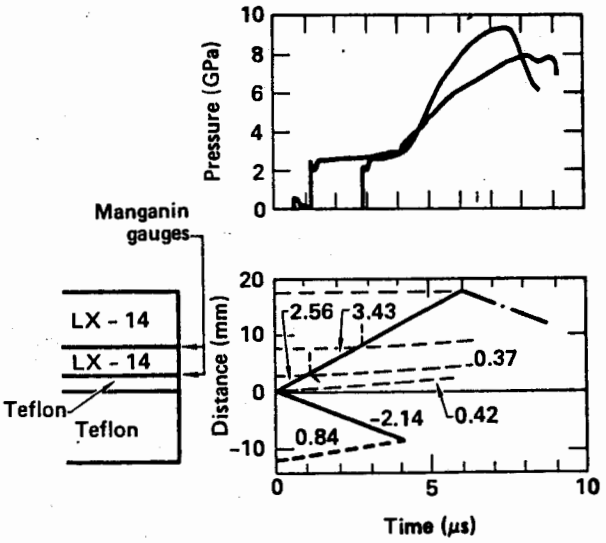

Fig. 2 A typical experimet with two manganin gauges illustrating the predetonation build-up in LX-14 explosive.

In inert materials the wave shapes are much simpler. Such is the case illustrated in Fig. 3. Here the manganin gauge is imbedded between the two stainless steel plates and a strong shock is produced by a symmetrical impact with another stainless steel flyer plate. The shock propagates through stainless steel and then reflects back from an aluminum plate as a rarefaction wave. The gauge experiences the first pressure pulse some 0.8 μs after the flyer plate impact and levels off at a pressure of 38 kb. This initial loading of the gauge is marked on Fig. 3 as point A. The two humps on the loading side of the record represent the local impedance mismatch between the teflon armor of the gauge and the surrounding target material-stainless steel. The reflected rarefaction wave reaches the gauge about 1 μs later (point B) slowly leveling off at about 18 GPa which is the pressure expected from stainless steel-aluminum interaction. The actual oscilloscope record is also illustrated in Fig. 3.

PVF_2 PRESSURE GAUGE

Another type of dynamic pressure measuring device is the PVF_2 (polyvinylidene fluoride) gauge which is in its early stages of development. Its primary advantages are in its simplicity of operation. In contrast to the just described manganin gauge it does not require an energy source, such as a constant current power supply. It has its own stored electric charge which is transformed into current upon subjecting the gauge to stress.

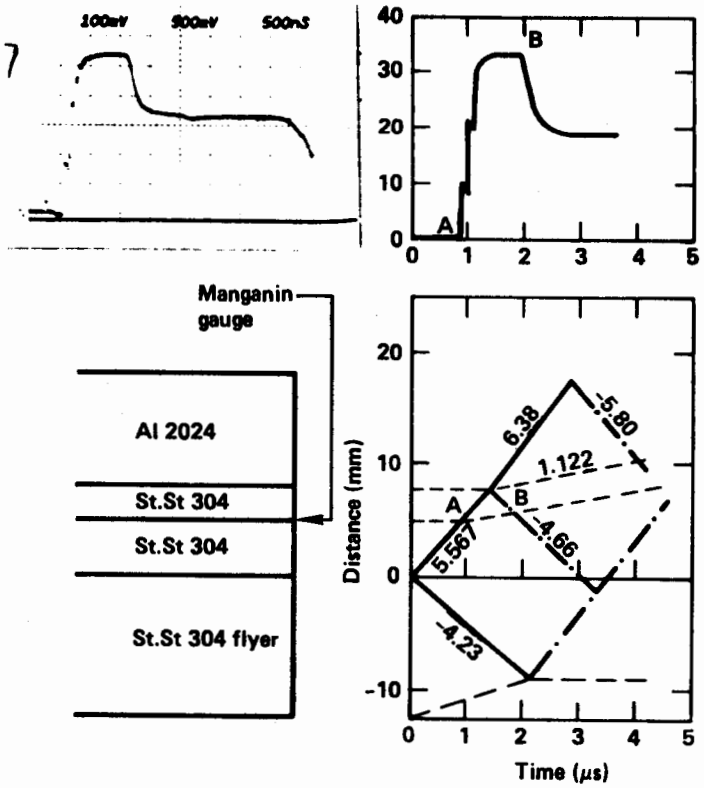

Fig. 3 Typical experiment illustrating performance of the manganin gauge in inert materials.

The polyvinylidene fluoride, also called PVF_2 or PVDF, is a semicrystalline polymer whose monomer is CH_2-CF_2. It is approximately 50%

crystalline and 50% amorphous. In 1969 Kawai[12] found that this material becomes strongly piezoelectric when it is first subjected to a mechanical stretching and subsequently to a slow cycling by a strong electrical field. An attempt to use this material as a pressure-measuring element was first described by Bauer[1] who has since then developed the gauge and fabricated it for experimental use.

At LLNL[13] we are testing these gauges for possible application in field tests where simplicity is considered a major advantage, and we have modified them slightly to suit our needs. Gauges made to our specification by Dynasen, Inc. are described below.

Description of the Gauge

The PVF_2 gauge consists of a thin polyvinylidene fluoride film sandwiched between two small squares of copper (or gold). Physical dimensions of the gauge are illustrated in Fig. 4. The thickness of the materials may vary. Thinner gauges are more sensitive but at the same time more difficult to handle and an optimum thickness is desired. Our gauges are 25 or 50 μm thick and the active area is 0.4 cm^2.

When dynamically loaded, the gauges experience a change in polarization roughly proportional to their linear compression. Such change in polarization results in a release of an electrical charge which is subsequently recorded as a V(t) signal through a resistive or a resistive-capacitive circuit. A resistive circuit records a current trace I(t) = E(t)/R which upon integration will yield the proper value of the charge

$$Q = \int_0^t \frac{V(t)}{R}\, dt \qquad (2)$$

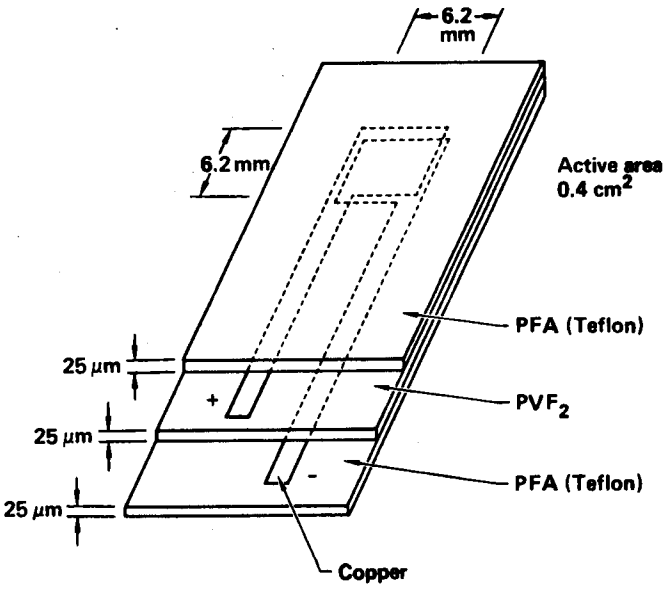

Fig. 4 The PVF_2 gauge.

The resistive-capacitive circuit performs the integration in the line and records the charge value directly as

$$Q = V(t)C\,\frac{R + R_o}{R_o} \qquad (3)$$

where R_o is the oscilloscope termination impedance of 50 Ω to match the cable impedance and C and R are the capacitance and resistance of the integrator circuit respectively. The two modes of data recording are illustrated in Fig. 5, which also demonstrates the relative accuracy required to time the recording of the event.

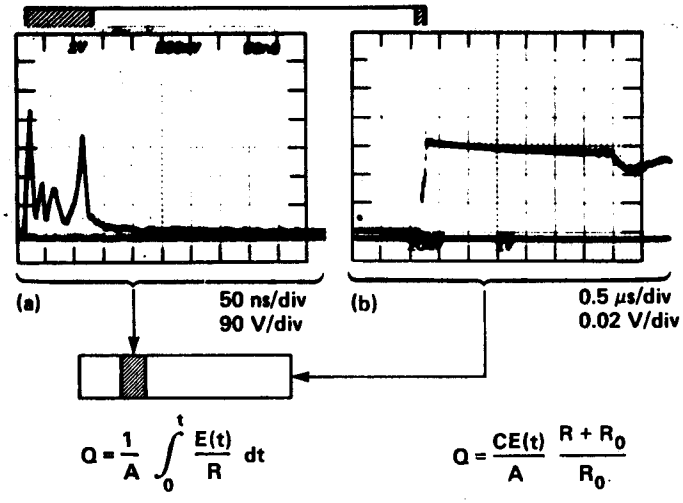

Fig. 5 Two modes of making measurement of the released charge Q. (a) current mode (resistive circuit) and (b) charge mode (resistive-capacitive circuit).

Results

In order to integrate the area under the current signal with any kind of reasonable accuracy the recording rate of that signal must be extremely fast resulting in a very small operating window. This is not too big a constraint in the laboratory where signal cables can be kept short and signal degradation kept to a minimum. However, in the field environment where recording equipment is far away from the occurring event, long cables may cause sufficient attenuation and degradation of the fast signals to make them unrealistic. In such an environment it is highly desirable to have an in line integrator (resistive-capacitive circuit) right next to the gauge.

Typical records for both types of recording modes are illustrated in Figs. 6 and 7. Both figures again represent composite pictures of the shot assembly, time-space diagram, pressure profile and the actual oscilloscope trace all drawn to the same time and space scales.

Figure 6 represents the pressure in a Teflon environment as it was reduced from the current signal using Eq. 2. Both current signal and

reduced pressure is shown in Fig. 6. Also shown is the record from a manganin gauge that was placed 5 mm in front of the PVF_2 gauge. Both records show fast rise and in this case the PVF_2 trace appearing much cleaner than that from the manganin gauge. However, in order to accurately resolve the area under the current trace we required a very fast scope and a very small recording window. The way to extend our recording times is to integrate the signal electronically by placing an integrator circuit immediately following the gauge. Pressure recorded in this manner is illustrated in Fig. 7. Here the gauge was placed in a ceramic high density aluminum oxide (AD998) environment with manganin gauge preceding the PVF_2 by 5 mm. Shown in this figure are records from both gauges. Correlation is good but the cross-talk between the two gauges is also evident. Release of electrical charge by the PVF_2 gauge introduces ringing noise onto the manganin gauge record.

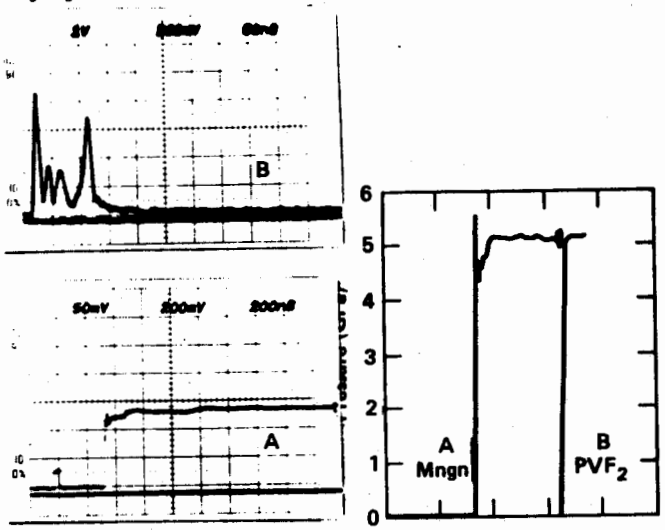

Fig. 6 Experiment with inert material (Teflon) demonstrating a comparison between manganin gauge and PVF_2 gauges in current mode.

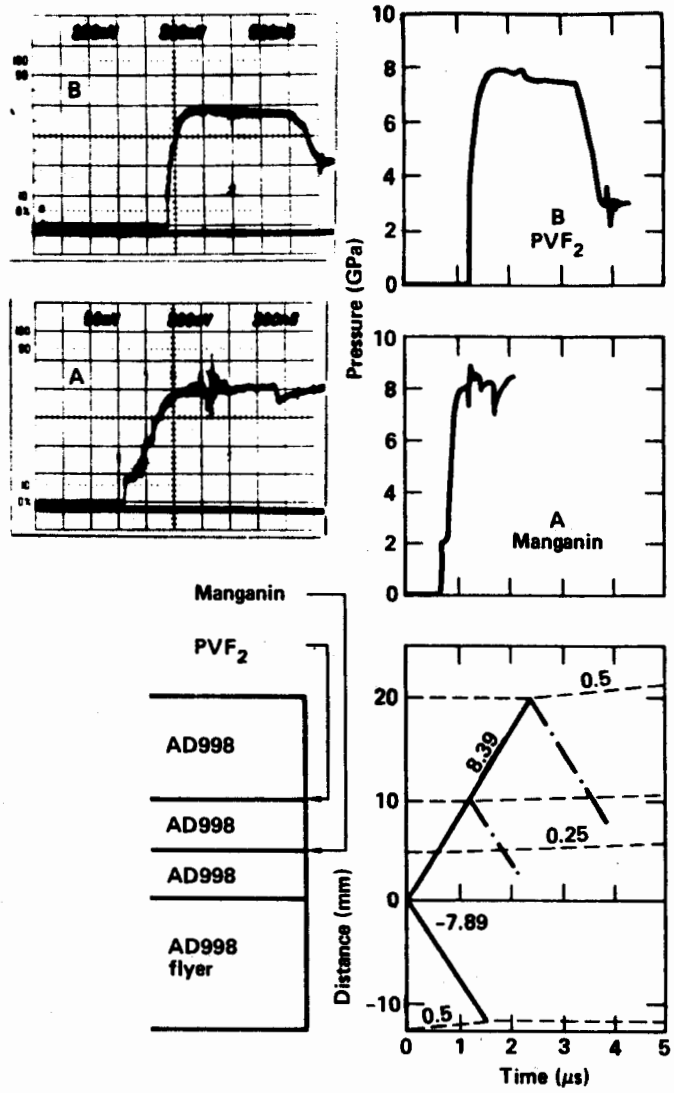

Fig. 7 An experiment with inert material (AD998) illustrating the comparison of manganin gauge with PVF_2 gauge in charge mode.

Calibration of the PVF_2 gauges was done on inert materials. Experiments were performed on our 101 mm gun capable of delivering a sabot of 1 kg at a velocity of up to 2.3 mm/μs . Depending on the material and the velocity of the sabot pressures can be easily achieved in the range of 0.3 to 40 GPa. The gauge performs well at pressures below 10 GPa. Above 10 GPa there are some ambiguities which lead us to believe that temperature effects may not be negligible.

These ambiguities are best illustrated on the calibration curves which are shown in Fig. 8. Included in this figure are calibration curves for the Dynasen 25 μm gauge and ISL-23 μm gauge. Also shown for comparison is the original calibration curve reported by Bauer[1] on his ISL gauge. Both gauges show one or two breaks in the lines. The behavior of the gauge in these intermediate areas has not yet been explored. At the present time one

can only speculate that at these pressures the response of the gauge is being affected by some presently unknown physical changes which have not yet been taken into account.

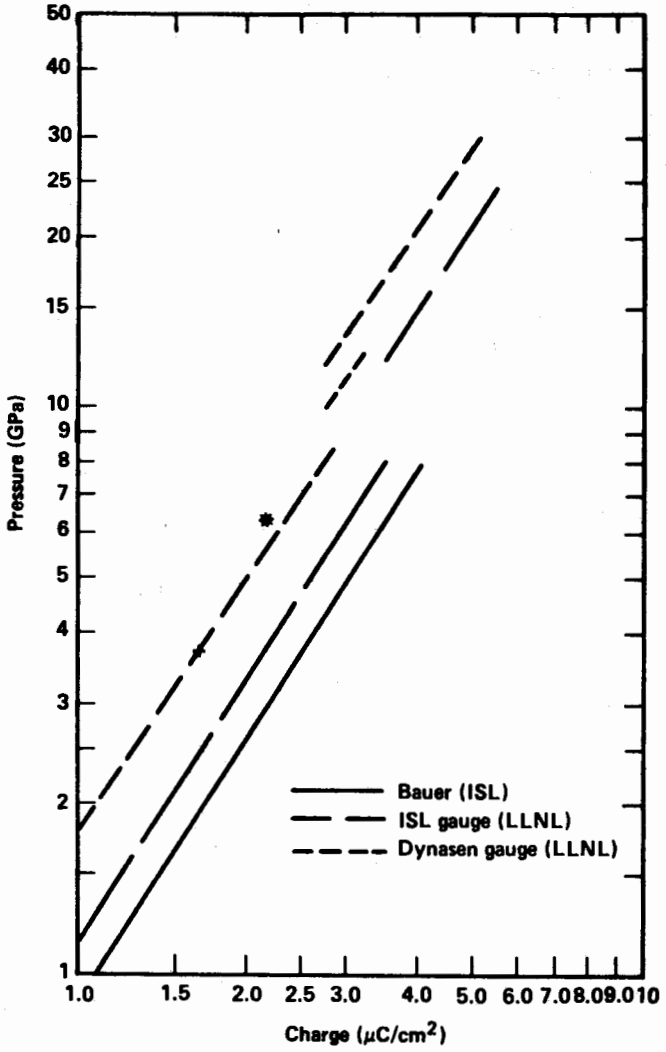

Fig. 8 Calibration curves of PVF_2 gauges from two different sources.

Such ambiguous response of the gauge can also be demonstrated on a single record where the gauge was subjected to two consecutive loadings of stress. This is shown in Fig. 9. Here the gauge was placed in a Teflon environment that was backed up by an aluminum plate. As the shock travels through teflon it loads the gauge to the expected level of 3.7 GPa and then upon reflection from aluminum it reshocks the gauge to an even higher pressure. Theoretical prediction of the reshocking pressure is indicated by a broken line and as one can see the experimental value based on the original calibratiojn line falls short of reaching that pressure. It appears that once shocked and held under a certain pressure and temperature the gauge material changes its internal characteristics and responds differently to a new load, i.e. it follows a different calibration curve. This is illustrated in Fig. 8 where the initial shock pressure is indicated by a cross and the predicted reshock pressure by a star.

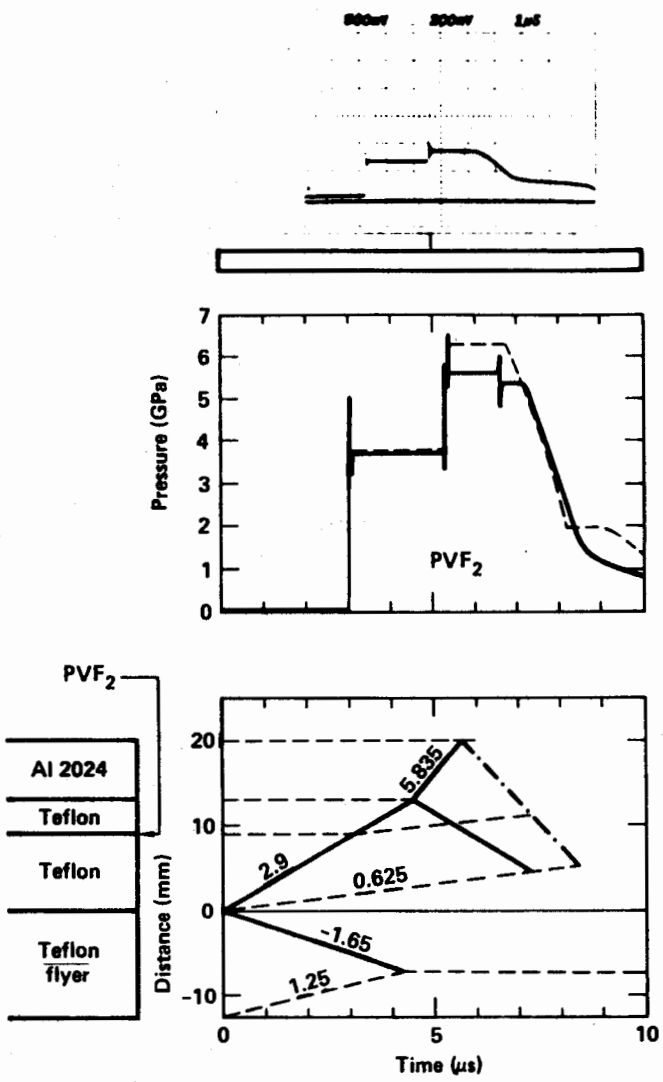

Fig. 9 An experiment with inert material (Teflon) illustrating peculiar behavior of the PVF_2 gauge upon reshocking.

SUMMARY AND CONCLUSION

Measuring pressure under severe dynamic loading presents a number of problems. It requires in situ gauges which would respond to pressure in a reliable manner and would survive such a severe environment. Two of such gauges have been described and their performance compared. While the manganin gauge has already acquired a stronghold in the laboratory as a reliable and accurate diagnostic tool for

measurements of high dynamic pressures the PVF_2 gauge is still in the development stage and needs further study to provide full understanding of its nature and to allow its useful application in a reliable fashion. Its simplicity and containment of its own energy source is a definite advantage over the manganin gauge in large field operations. However, its nonlinear and apparently non-unique (multiple calibration lines) response to pressure represents a serious disadvantage. Large amounts of electrical charge release from the PVF_2 gauges causes an electrical cross-talk between the gauges which may or may not be a detriment to the test. Such a cross-talk between the gauges can be useful in timing of the events taking place and getting accurate readings of the arrival times.

For field operations, where diagnostic equipment is remote from the experiment containing PVF_2 gauges, it is most desirable to have an electronic integrator perform the integration of the signal up front before it gets severely degraded by the long transmission lines. More work is needed to develop an integrator circuit which would be free of oscillations and yet provide reasonable amplitude and decay time.

The most important differences between the two gauges is their performance at pressures of 10 GPa and above. Fast response time of the PVF_2 gauge is very attractive, especially for measuring pressure in a non-steady regime such as in a detonation wave. However, these regimes usually occur at pressures 30 GPa and above while the ambiguities described here, presently limit the deployment of the PVF_2 gauges to the range of 10 GPa and below.

ACKNOWLEGEMENTS

The authors wish to thank Drs. E. Lee and B. Hayes for their continued interest and discussions on the subject and Mrs. Karen Spurlin for her invaluable assistance in preparation of this manuscript.

REFERENCES

1. Bauer, F. "Behavior of Piezoelectric PVF_2 Polymers Under Shock Wave Action," Proceedings of the 1st Symposium on Gauges and Piezoresistive Materials, A.D.E.R.A. - Bordeaux, France, 1981.

2. Bridgement, P. W., "Bakerian Lecture, Physics Above 20,000 kg/cm^2," Proceedings Royal Soc., London, A203, pp. 1-16, 1950.

3. Fuller, P. J. A., and Price, J. H., "Electrical Conductivity of Manganin and Iron at High Pressures," Nature, 103, pp 262- , 1962.

4. Bernstein, D. and Keough, D. D. "Piezoresistivity of Manganin," J. App. Phys., 35, pp. 1471-1474, 1964.

5. Wackerle, J., Johnson, J. O. and Halleck, P. M. "Shock Initiation of High Density PETN," Sixth Symposium (International) on Detonation, pp. 2-28, ONR ACR 221, Office of Naval Research, 1976.

6. Kanel, G. I. and Dremin, A. N. "Decomposition of Cast TNT in Shock Waves," Fizika Goreniya i Vzryva, 13, No. 1, pp. 85-92, 1977.

7. Burrows, K., Chivers, D. K., Gyton, R., Lambourn, B. D. and Wallace, A. A. "Determination of Detonation Pressure Using a Manganin Wire Technique," Sixth Symposium (International) on Detonation, pp. 625-636, ONR ACR221, Office of Naval Research, 1976.

8. Weingart, R. C., Barlett, R., Cochran, S., Erickson, L. M., Chan, J., Janzen, J., Lee, R., Logan, D. and Rosenberg, J. T. "Manganin Stress Gauges in Reacting High Explosive Environment," Proceedings of the Symposium on High Dynamic Pressures, pp. 451-461, Paris, France, 1978.

9. Erickson, L., Weingart, R., Barlett, R., Chan, J., Elliott, G., Janzen, J., Vantine, M., Lee, R., and Rosenberg, J. T. "Fabrication of Manganin Stress Gauges for Use in Detonating High Explosive," 10th Symposium on Explosives and Pyrotechnics, 21/1-7, San Francisco, CA., 1979.

10. Vantine, H. C., Erickson, L. M. and Janzen, J. A. "Histeresis-Corrected Calibration of Manganin under Shock Loading," J. Appl. Phys., 51(4), pp. 1957-1962, 1979.

11. Vantine, M., Chan, J., Erickson, L. M., Janzen, J., Lee, R. and Weingart, R. C. "Precision Stress Measurements in Severe Shock-Wave Environments With Low Impedance Manganin Gauges," Rev. Sci. Instr., 51, pp. 116-122, 1980.

12. Kawai, H. "The Piezoelectricity of Poly(Vinylidene Fluoride)," Japan J. Appl. Phys, 8, pp. 975-976, 1969.

13. Urtiew, R. A., Erickson, L. M., Hayes, B. and Parker, N. L. "Pressure and Particle Velocity Measurements in Solids Subjected to Dynamic Loading," Lawrence Livermore National Laboratory, UCRL-93213, 1985.

Q: Gordon Mills: How do you deposit conductors and what's the material? At the low range you discussed the nonlinearity. Is it 1 or 50 percent? How grossly nonlinear is it? And does the Pennwalt material operate in this mode or is that a different material basically?

A: Paul Urtiew (Lawrence Livermore National Lab.): In your first question on how to deposit the outgrowth, you are talking about the PVF_2 gauge of course. Dynasen has been plating the copper on the Teflon, and they sandwiched the PVF_2 in between. Bauer and Sandia, I understand, are sputtering the gold plating on their PVF_2 material. To answer the second question: Is the nonlinearity of the gauge the lower regime? I'm not an expert on the lower regime. We have not tried it, but the French have done a lower regime that is quite nonlinear. I can't tell you what the number is. And for the third question: Yes, Pennwalt has been involved in making the material from Dynasen because Dynasen gets its materiel from Pennwalt, whereas the French, and I believe Sandia, are getting it from a French company.

COMMENT: Ray Reed: I wanted to commend Paul for a good paper. I've enjoyed hearing it twice now. We heard another piece of this information in Cincinnati, Monday before we came here. I wanted to emphasize a couple of points that I think are important. Paul has indicated that the material is in it's infancy as far as being developed as a well-characterized shock stress gauge. I think it's a little bit premature to attribute any definite properties to the material. We know from our work at Sandia that there is a drastic difference in the behavior of different materials and materials polarized in different ways. You should not conclude from the results from one material that they apply to another material. In fact, Francois Bauer has published results on three different materials with which he has worked and he has gotten different calibrations for the three. The calibration is not characteristic of PVF_2; it is characteristic of a specific set of fabrication parameters. Another point, that I think should be made, for those of you who have need for stress measurement at very much higher levels. It is possible to use this material to 20 Giga Pascals or 200 kilobars and somewhere above that, but not as high as 300. On the other hand, it is also possible to use the material in an assembled gauge in such a way that the upper stress limit can be increased by roughly a factor of three. So it is certainly going to be possible to make some kind of measurements under special conditions up to about 600, possibly 700 killobars, but that has to be done by design. There are a number of other comments, but I guess in my years in the measurement business I have never seen our laboratories with quite as widespread interest in a material and as varied interest among different people as I have with this particular material Paul is describing.

A FULL-MOTION COMPRESSED DIGITAL TV LINK

Editors Note: This paper was presented by Mr. James Rieger, Naval Weapons Center; however, no copy of the paper was available for inclusion in the proceedings at press time.

Q: John Gierer: How much bandwidth do you need after you've encrypted it?

A: James Rieger: The encryption width a KG66 or a KGB68 is one to one, if you use the Mode B which is what everyone uses. If a 5 megabit rate goes in, that is what comes out. You will lose about 2 dB of signal noise.

Q: John Gierer: If I want a telemetry channel would it be done over existing telemetry or will the user be given some additional space in the telemetry band for video work?

A: James Rieger: Most of the video signals have been sent using the 1710 to 1830 MHz region. It wasn't exactly telemetry, but an analog signal. The analog signal, the TV signal, occupies from 20-25 MHz of bandwidth at the 98 percent point. What this will do is occupy less because the bandwidth will be almost equal to the bit rate; 5 megabits will occupy about 5 MHz of RF. We consider up to 20 at the highest rate to be transmittable. The 40 megabit rate would be used for a ground link for surveillance or for ground spring. It doesn't make things worse, it makes them better. In addition, the signal to noise for actually recovering this signal is a little less than it would be for the analog picture.

Q: John Gierer: Do you have a projected time frame for the availability for this equipment?

A: James Rieger: We should see the 40-cubic inch ones about August or September. We have a demo unit which is as big as a house. If you want to see it, come out to the Naval Weapons Center.

Q: John Gierer: When you say available, do you mean qualified units ready to use?

A: James Rieger: No, just the electrical system.

STRUCTCEL- A NEW INSTRUMENTATION SYSTEM

MICHAEL J. LALLY
RESEARCH ASSISTANT
MECHANICAL AND INDUSTRIAL ENGINEERING
UNIVERSITY OF CINCINNATI
CINCINNATI, OH 45221

DAVID L. BROWN
PROFESSOR
MECHANICAL AND INDUSTRIAL ENGINEERING
UNIVERSITY OF CINCINNATI
CINCINNATI, OH 45221

ABSTRACT-

Ensuring that military vehicles and weapons function normally in field operation, blast and other hazardous environments should involve experimental modal testing in the laboratory. For this experimental modal analysis, the STRUCTCEL™ is a new structured, systems concept. The multichannel measurement system offers low mass, low cost, high sensitivity, convenient plug-in installation and end to end calibration. These features combine to greatly simplify the measurement process while lowering the per channel cost of the system. Accordingly, all desired data points can be instrumented eliminating the need to "rove" accelerometers. Providing a consistent mass distribution, multichannel testing affords a more accurate modal model.

Incorporating many ergonomic, or human engineering aspects, the STRUCTCEL measurement system also addresses the problem of managing very large numbers of channels of data. Historically, test set up time for large multichannel systems has been longer than the actual test time. Utilizing snap-together mounting components, cut to length cables, insulation displacement connectors, patch panels, bus cables and a hand-held calibrator, the STRUCTCEL system eases the arduous task of cable routing, identification and calibration.

Complementing the STRUCTCEL system, the low cost DATA HARVESTER provides power, signal conditioning and filtering for multichannel applications while allowing for automatic control. The DATA HARVERSTER simplifies the task of book keeping and eliminates manual adjustments. Automating the measurement process saves time and helps to eliminate the human errors caused by fatigue during a large scale modal test.

INTRODUCTION-

Both economic and efficient, the STRUCTCEL measurement system has rapidly become a popular system for multichannel laboratory modal testing. Since its introduction at the 1986 International Modal Analysis Conference (IMAC), over a thousand STRUCTCEL channels have been utilized to test structures as varied as aircraft, automobiles, industrial robots and satellite dishes. Particularly in cases where modal modeling is conducted, multichannel testing helps satisfy the time invarience assumption.

The structured approach to testing features a low cost, low mass, high sensitivity, structrual sensing element which allows the user to instrument all desired data points. Acquiring data in sets, or more optimally in a single set, the STRUCTCEL measurement system provides a more consistent data base. Accordingly, the better data base affords the user a more accurate modal model. Implementing many ergonomic conveniences in the mounting, wiring, identifying and calibrating aspects, the structured approach to testing further simplifies the task of handling large numbers of channels of data.

Pioneered at the University of Cincinnati and designed jointly with PCB Piezotronics, the STRUCTCEL system continues to evolve as a cooperative effort with new advances in hardware, software and testing techniques. Formally introduced at the 1987 IMAC, a low cost, computer controlled, autoranging power supply now complements the STRUCTCEL measurement system. Dubbed the DATA HARVESTER, the 5.25x19x15 inch box simultaneously autoranges, records gains, sets anti-aliasing filters, powers and monitors overload conditions on 64 channels of data. Controlled by a powerful central processor, up to 1024 channels can be daisy chained to a single processing module. Communicating through a standard IEEE-488 or RS232 interface bus, the DATA HARVESTER outputs a low impedance signal properly conditoned for multiplexing and/or digitizing. A complete command set allows for easy programmabiltiy and automated testing.

THE SYSTEM CONCEPT-

Developed with practicality, simplicity and low cost in mind, the structured approach to testing functions to aid the experimentalist in obtaining a consistent, valid data base. Incorporating time saving features, the STRUCTCEL system and DATA HARVESTER minimize testing time thereby allowing more time for analysis and

design changes to be implemented before production begins. By instrumenting large numbers of data points (typically 64, 128, etc), the lightweight STRUCTCELs provide a more comprehensive data base while adding only a minimal, constant mass distribution. Accordingly, the resultant data base displays better spacial definition without the frequency shifts inherent to the method of "roving" accelerometers.

Modular mounting, wiring and calibration equipment allow for easy set-up, identification, calibration and management of large numbers of channels of data. Data channels are routed to patch pannels which consolidate the individual cables into multiconductor ribbon cables carrying signals to the DATA HARVESTER. Managing all channels in parallel, the DATA HARVESTER automatically sets maximum gain, then ranges down until the signals are just below a preset overload level. The conditioned, filtered data is now suitable to digitize and process.

Systematic test set-up and quick data acquisition combine to reduce errors, time and fatigue encountered when performing large scale modal tests.

COMPONENT FUNCTION, STRUCTURE AND BEHAVIOR-

The STRUCTCEL motion sensor functions to transfer low level, low frequency, vibratory motion into a convenient signal for analysis. The lightweight (2 gram), sensitive (≈200 mv/g) element utilizes a differential mass loaded diaphragm structure to obtain performance characteristics (over a 1-500 Hz range) similar to piezoelectric sensors, but at a much smaller price. Mechanical and differential coupling provide common mode rejection to help eliminate problems such as 60 cycle noise, while also exhibiting extremely low cross axis sensitivity (typicallly less than 1%). Packaged in a plastic transistor housing, the sensor plugs into a 3-pin mounting socket for easy connection. This modular concept prevails throughout the system design making set-up and operation quick and simple.

Complete with integral three conductor cable, mounting sockets attach to the test structure with a variety of adhesives. Depending on the desired frequency range and degree of permanence, hot glue, petro wax, duct putty and epoxy have been found suitable. Additionally, a triaxial adaptor block mounts at any measurement point to hold three STRUCTCELs with mounting sockets in an orthogonal orientation. To help eliminate errors due to misaligned sensors, an alignment tool utilizes bubble levels and reference pointers to help spacially orient the mounting pads and triaxial blocks.

After adhering mounting sockets, cables can be neatly routed and terminated in groups of 16 channels at patch panels off the structure. Wires should be routed off the structure as soon as possible and taped down while on the structure to help avoid potential nonlinearities due to cable vibration. Minimizing cable length helps reduce noise in the measurement system. An insulation displacement "gun" attaches a connector after the wires are cut to length and split apart. The connectors, which are available in single, triple and quadruple channel configurations, snap lock into a 16 channel patch panel. It is not neccessary to keep track of channel numbers at this point. Later, during calibration and installation, channel numbers and sensitivities can be automatically recorded or keyed in by the computer operator, along with the orientation of the point. Serving to adapt the single channel wires into a 37 conductor ribbon wire extension cable, the patch panel also has intelligence. When properly connected a LED indicates which bank of channels the extension cable connects to on the DATA HARVESTER (ie 1-16, 17-32, etc).

Designed for interfacing multiple STRUCTCEL sensors with a fourier analyzer or computer, the DATA HARVESTER eliminates tedious book keeping and manual adjustments. It simultaneously powers, conditions, filters and monitors overload conditions on all STRUCTCEL channels and outputs zero biased, properly amplified, bandlimited signals prepared for multiplexing, digitizing, processing and storing.

Modularly constructed, the DATA HARVESTER consists of four components. Housed in a 19 inch, rack mountable case, a mother board contains slots for connecting 16 signal conditioning cards, a processor module and a power module. Each plug-in card conditions four channels by supplying the STRUCTCEL signals with power and 8-50 dB gain (4 dB increments) range, as well as 8 pole, 48 dB/octave selectable filtering. Easy accessability to the cards allows for convenient serviceability and future addition of ICP cards. Visable through the smoked glass cover, two LED's per channel continuously monitor channel status. A red LED indicates an input fault such as a bad sensor, open connection or short circuit. A yellow LED alerts the operator of any overload conditions which may occur during testing.

Controlling the entire system, the processing module can manipulate channels in user defined groups or select individual channels. Its ability to address and operate all channels in parallel affords the speed necessary to manage large numbers of channels of sensors. A single processor module can control up to 1024 data channels making system expansion a very affordable option.

A dedicated, low cost power supply module supports the STRUCTCEL system. As an option, a general purpose version powers either STRUCTCEL or ICP sensors. The installation of this module allows the DATA HARVESTER to operate with any combination of STRUCTCEL and ICP cards intermixed.

All input and output connectors are located on the rear of the DATA HARVESTER. Four 37 pin D-type connectors (male) accept the multiconductor extension cables from the patch panels and four similar connectors (female) provide output access for a multiplexer or switcher and/or an analog to digital converter. Both IEE-488 and RS-232 interface options provide easy access for computer control. Virtually any desk top computer or main frame can be interfaced over the connection ports to provide automatic control of the

DATA HARVESTER. An inexpensive hand held controller which operates over the RS-232 port is also available.

By automating testing, human errors can be reduced and time can be saved while obtaining the best, quality data base possible. Ideally, a computer and software can implement automatic control allowing for operater interaction. Calibration procedures, including automatic sensitivity calculation and channel identification run interactively as each STRUCTCEL is installed. Prompting for user defined values, the program sets the desired filter cutoff and groups channels into user defined bunches. To further enhance the time savings, a cross point switch can be utilized to switch groups of channels at a time to be digitized. An 8 or 16 channel analog to digital converter is the last step before sending the filtered, conditioned data on to an analyzer.

The STRUCTCEL system has been specifically designed for large scale, multichannel use. Special attention has been given to the calibration and channel identification aspects of the system. Supplied with each system, a hand held calibrator outputs a constant 10 m/s^2 rms sinusoidal signal at 159 Hz. The calibrator employs an internal servo loop to supply the constant motion level to any accelerometer weighing up to 70 grams. A socket attachment with a jumper allows each STRUCTCEL to be placed on the calibrator with the output signal jumpered to the mounting socket attached to the test structure. This method supplies a quick and simple, single frequency, end to end calibration. Again utilizing software to automate, as each STRUCTCEL is calibrated, a computer could scan for the channel carrying the calibration signal and automatically record the rms voltage for the "one g" calibration. The terminal operator is responsible for keying in the serial number, point number and orientation.

Should the test organization require standard laboratory calibration, a simulator is available which outputs a selectable voltage at 100 Hz to provide channel identification. As each precalibrated STRUCTCEL is installed the channel must be identified and the precalibrated sensitivity must be recorded. In small channel installations, channel identification can be performed by disconnecting the STRUCTCEL and observing for the input fault LED on the DATA HARVESTER. Computer control could also identify the channel by scanning for the simulator signal. As each channel is identified and the STRUCTCEL installed, the terminal operator must key in the sensitivity, serial number, point number and orientation. After STRUCTCEL's have been installed and calibrated as well as point numbers, channel numbers and orientations matched, the set-up is ready for testing.

APPLICATIONS-

Any test structure requiring laboratory modal testing, especially those from which a modal model will be built, can benefit from using the STRUCTCEL modal array sensing system. As a typical example, a 60 channel test performed on an automobile frame will be examined. Constructed of spot-welded, stamped body parts, the "body-in-white" exhibits very light damping and complicated mode shapes. The structure's characteristics are historically problematic in respect to obtaining quality frequency responses.

Mass loading can become a problem with any structure that is lightly damped or has large, low mass components. The stamped side panels and roof of a unibody car frame typify this type of structure. To check for this potential problem, a single axis sensor is used to measure a frequency response function (FRF) of the component. Then the component is loaded with an amount of mass equivalent to the transducers that are used on it during the test and another FRF is measured. By comparing FRFs and looking for shifts in resonant frequency or changes in amplitudes, the effects of mass loading can be observed.

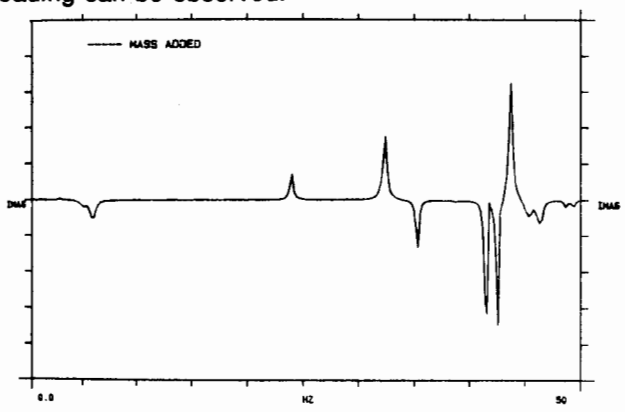

Fig 1. Mass loading effects using STRUCTEL system

As seen in figure 1, the light weight STRUCTCELs cause no mass loading effects on the car body (note dashed line matches solid line exactly). Had the structure been light enough to detect mass loading effects, instrumenting all data points still affords a distinct advantage. A constant mass distribution may cause some shift in the resonant frequencies, but the shift will be constant with respect to all measurements and then can be accounted for when modal modelling. "Roving" accelerometers causes inconsistant mass loading which cannot be accounted for when modeling. Additionally, variable frequency shifts are troublesome to parameter estimation programs.

To fully utilize the cababilities of the available test system, 60 single axis response measurements were taken in each of three sets. Installed in a triaxial block for convenience, the single axis STRUCTCELs were rotated and then mounted to measure a different orthogonal direction in each set. This set-up provided maximum spacial definition while adding only a minimal, constant mass distribution. The sensors required power from 4 PCB model 433A power supplies (15 channels each).

Mounted, wired and calibrated as previously described, the set-up was inexpensive, neat and time was held to a minimum. The calibration procedure was compiled by two people. One person removed the transducer from the mounting socket and placed it on

the calibrator mounting socked as the other visually scanned the power supply for the non-illuminated LED. Noting the channel number, the sensor was then jumpered back to the original mounting socket and calibrated with an oscilloscope and digital voltmeter. As a final step, the keyboard operator entered the sensitivity, point number and orientation of the channel. On the average it took 40 seconds to calibrate each channel.

The addition of the DATA HARVESTER could implement automated subroutines for even quicker calibration and identification. With larger savings in time, the actual testing time could be reduced by the autoranging ability and parallel control of all channels. The large percentage of test time occupied by the operator waiting to respond to a prompt or to reset for the next run could be virtually eliminated by computer controlling the test. As a result, the productivity of the test engineer is increased considerably.

To complete the test set-up, two shakers with load cells were implemented as references and the entire frame was mounted on air rides. The test time averaged 20 minutes per data set (1 hour total) with the STRUCTCEL system. A similar test conducted by "roving" two miniature (10 gram) triaxial piezoelectric accelerometers required 3.5 hours to acquire the same amount of data. Using the results of the latter test as representative of conventional testing, the two techniques are compared.

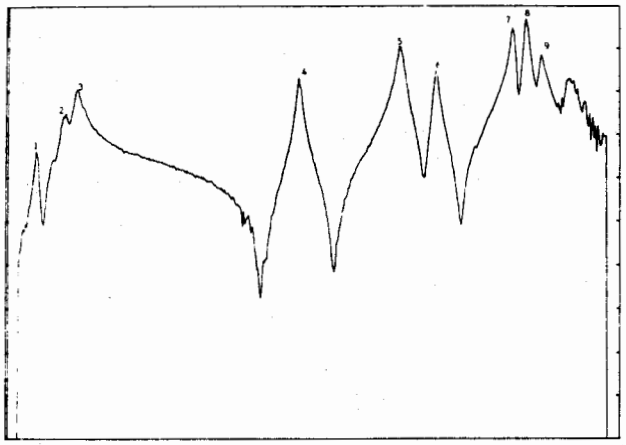

Fig 2. Driving point FRF using STRUCTCEL system

The driving point FRFs estimated for each test reveal a great deal. Figures 2 and 3 have been synthesized from the results of a Polyreference Time Domain parameter estimation program. The two tests were conducted on slightly different frequency ranges so mode numbers have been labelled for clarity.

The most apparent difference between the two plots is the smoothness of the STRUCTCEL response, even in problem areas such as antiresonances. At those frequencies, the lack of motion causes the signal to noise ratio to be extremely low. The cleaner response of the STRUCTCELs can be attributed to its better resolution. Responses of points located a large distance away from the forcing points are also aided by the better resolution.

Although not as apparent at first glance, the most serious difference between the two tests is that mode number 9 appears as two distinct modes, 9a and 9b, in the "roving" accelerometer test. This error is a function of the fact that in the data base of FRFs the resonant frequency of mode 9 appears at different frequencies, depending on the location of the two triaxial accelerometers. The parameter estimation algorithm calculated two separate modes in order to fit the variation in the the test data as accurately possible. Clearly, this miscalculation could cause major problems.

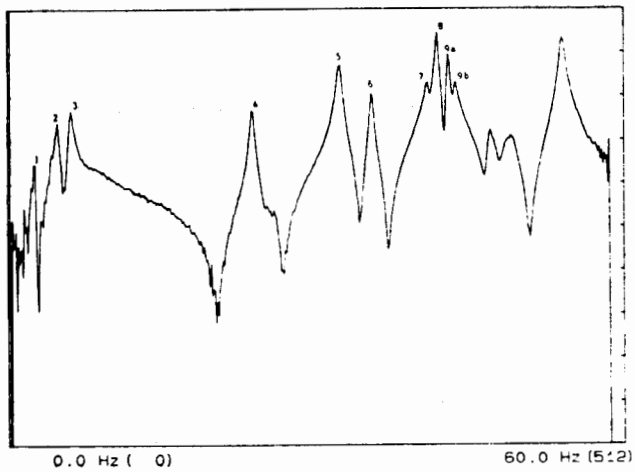

Fig 3. Driving point FRF using "roving" accelerometers

The most difficult portion of parameter estimation is selecting the number of degrees of freedom (ie. picking the number of actual modes) to use in the analysis. The Polyreference Time Domain algorithm attempts to aid the user in this choice by presenting an error chart. Visually selecting the point at which the slope changes, the error chart provides an estimate of the number of modes (both real and computational) in the band of analysis. The rank estimate provides an estimate of the actual number of modes. Figures 4 and 5 display the error charts and rank estimates for both tests.

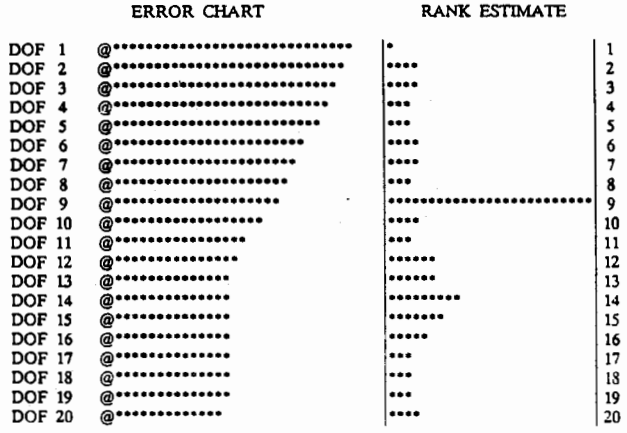

Fig 4. Modal parameter estimation error chart for STRUCTCEL system

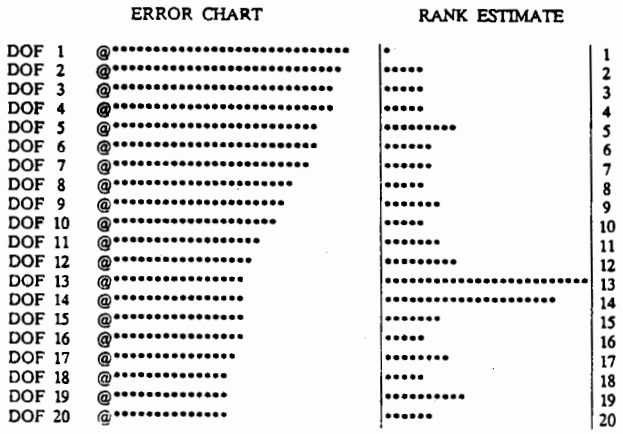

Fig 5. Modal parameter estimation error chart for "roving" accels.

For the STRUCTCEL data, the change in slope clearly occurs at the 13th DOF and likewise, the rank estimate displays 9 modes. Not nearly as definitive, the chart for the "roving" accelerometer test shows much more uncertainty in the point of slope change as well as its rank estimate. The major cause of these uncertainties is most likely, once again, the frequency shifts incurred by the variable mass loading of the "roving" triaxial acceleromters.

In the final generation, computational modes are deleted and the algorithm outputs a table of the resulting parameter estimates. The results are tabulated in figure 6. For each of the lower modes, the algorithm estimates the natural frequencies of the "roving" accelerometer test to be higher than those of the STRUCTCEL test. Mode 2, which is a rear panel (fore and aft) mode shows the largest increase in frequency. This mode is easily affected by the variable mass additions even though the additional mass is very small.

	LOW-COST ACCELEROMETERS		"ROVING" ACCELEROMETERS	
MODE	FREQ(Hz)	DAMP(%)	FREQ(Hz)	DAMP(%)
1	34.99	0.515	35.30	0.447
2	38.20	0.453	40.65	0.501
3	41.26	0.362	41.71	0.373
4	42.32	0.380	42.75	0.306
5	43.47	0.531	43.39	0.436
6	----	----	46.74	0.702

Fig 6. Frequency and damping estimates

It is important to note that in both cases the estimated modal parameters are a function of the test structure, fixturing and instrumentation (including mounting, sensors, cabling, etc). The multipoint STRUCTCEL test allows faster data aquisition and has a consistent mass distribution. This provides a more consistent data set for parameter estimation. The advantage is not that the data hasn't been affected, it is that the effects of the sensors are a constant and can be easily accounted for when correlating to finite element analyses or building a modal model. As shown, the same is not true for the traditional, "roving" accelerometer technique.

FUTURE CONSIDERATIONS-

With the continuing decrease in the per channel cost of measurement systems, multichannel testing is becoming the standard for obtaining experimental modal analysis data. The rapid increase in data channels (ie. measurement points) generates new possibilities in testing techniques. Ironically, the "latest" technique is merely a reimplementation of one of the earliest testing methods, sine testing.

During the early to middle sixties, sine testing was the technique used in performing modal analysis. The were two methods used:

1) Normal Mode Testing
   In normal mode testing, the modal eigenvectors are determined by applying a forcing vector which has been adjusted to excite a single vibration mode and directly measuring the output. Appropriating the force and positioning the exciter requires skilled operators.

2) Impedance Method
   In the middle sixties, with the advent of the swept sine testing equipment, the impedance method was developed. In this method, a set of frequency response functions are curve fit to determine the modal parameters.

The major disadvantage of both of these methods is that they were slow. The impedance method was slow for two reasons. Due to the expense of the data aquisition and data analysis systems, only a few channels of data could be processed at a time. The time consumed by the slow sweep was compounded by the fact that hundred and thousands of frequency response measurements are required in a typical modal test.

During the early seventies, the Fast Fourier Transform methods were developed. For single measurements they were orders of magnitude faster. They also allowed a wide range of different excitiation forces to be used (impact, random etc). As a result, the FFT methods significantly sped up the data acquisition cycle of modal testing.

In the late seventies, with the development of a series of advanced multi-input/multi-output parameter identification algorithms, it became evident that there is a significant increase in the consistency of the data base when acquiring the data from all response points simultaneously. This, in fact, was the primary driving force behind the development of the STRUCTCEL system.

With the FFT methods, as the number of data channels (input channels in particular) increase, the signal processing time increases exponentially. This has led to the current effort to re-establish the sine testing method. Sine testing is limited by the sweep time with the signal processing time being insignificant.

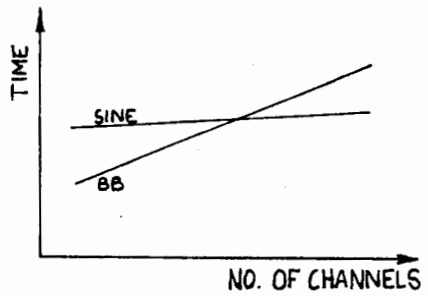

Fig 7. Sine testing vs. broadband testing comparison

As the number of channels increases, sine testing becomes more competetive with respect to total test time. As shown in figure 7, at higher numbers of channels sine testing is more effficient than broadband testing. The requirement on the computer system which performs the signal processing is also reduced. In fact, a simple desk top personal computer can perform the neccessary signal processing for the sine test. In contrast, a super-computer would be required to process the data for a six input, 750 output FFT test. In terms of cost, a sine testing system with 256 to 512 channels is approximately the same cost as a 16 to 64 channel FFT modal system.

CONCLUSION-

The STRUCTCEL system and DATA HARVESTER afford a great number of advantages to the experimentalist concerned with acquiring a quality, consistent modal data base. Providing high sensitivity, convenient installation, identification and calibration, the STRUCTCEL system, coupled with the DATA HARVESTER, is ideally suited for large scale multipoint laboratory modal testing (especially if considering modal modeling). Although limited to a controlled environment, performance comparisons show that for laboratory modal testing, the STRUCTCEL's characteristics provide data as good, if not better, than traditional transducers.

The advent of the DATA HARVESTER also opens new possibilities in multipoint testing techniques. Allowing hundreds of channels to be implemented affordably and processed quickly, sine testing with the DATA HARVESTER advances the experimentalist to the next generation of modal testing techniques.

ACKNOWLEDGMENT-

The authors wish to thank Jeff Poland for his extensive qualification testing of the STRUCTCEL system while researching his thesis. His work is the basis for the application section of this paper.

Thanks also to Bob, Rick and John Lally for their numerous inputs and reviews during the development of this paper.

REFERENCES-

(1) Lally, R. W., Poland, J. B., "A Low Cost Transducer System for Modal Analysis and Structural Testing", Sound and Vibration, January, 1986.

(2) Poland, J.B., "An Evaluation of a Low Cost Accelerometer Array System, Advantages and Disadvantages", Masters Thesis, University of Cincinnati, Mechanical Engineering Dept., 1986.

(3) Course Notes, "An Intensive Short Course on Modal Analysis - Basic Theory and Techniques", Structural Dynamics Research Laboratory, University of Cincinnati.

(4) "Operating Guide - STRUCTCEL Modal Array Sensing System", PCB Piezotroncs Inc., Depew, New York.

(5) Brown, D. L., "Keynote Speech - Modal Analysis - Past, Present and Future", Proceedings of the First International Modal Analysis Conference, 1982.

Q: Peter Stein: You've referred to the STRUCTCEL as a mass loaded differential diaphragm. From your other literature, I got the impression it uses some of that new polyvinylidene fluoride transducer. Are you empowered to tell us what is inside?

A: Michael Lally (University of Cincinnati): I am empowered to tell you that it is a mass-loaded piezo film. It is two diaphragms connected by a mass and that is the structure it uses to conduct sensing transaction.

Q: Patrick Walter: I have a question more relative to a test technique. You mentioned that you put a triax on there, and I understand the motivation was to get three axes at once so you would not have to worry about parameters changing with time. If you don't couple energy into all three directions in equivalent or comparable magnitudes, then you are concerned with fitting data where transverse sensitivity of the accelerometer becomes a factor. What are your general thoughts were along that line?

A: Michael Lally: Of course some of the modes, especially if you hit a mode of a structure, you're going to get a sensor that is giving basically noise. We are trying to instrument all our data points in all directions, so that we're not missing anything. Because these polyreference algorithms that have been developed, polyreference time and polyreference frequencies go through collecting and comparing all the measurements on the system. I'm not totally up to par on the mathematics of it, but I think there is a singular valued composition. The bad measurements are not going to hurt your data because you have other measurements which are the quality measurements. I can't give you a complete discussion on that, however, I would definitely refer you to Dr. Brown.

Q: Not audible.

A: Michael Lally: Right, you also have instrumenting on all points and a check between points; whereas before, you were taking only a few points. That's the big advantage of these polyreference algorithms; they provide a check on the parameters you are coming out with.

Q: Gordon Mills: When you get this large amount of data, is it compatible with any present or existing mechanical design tool such as a Hewlett-Packard CAD system? How do you process all this data in terms of redesigning?

A: Michael Lally: In the redesign, you come out with the modal models. We just got in the Hewlett-Packard big color work stations in Cincinnati and have the SDRC I-DEAS software. Right now we're in the process of integrating those together. The modal models I think are compatible with Systran software; I can't give you a total answer on that. At the present time, we are working on putting that together with CAD routines and that type.

Computerized Testing of High-Speed Data Acquisition Systems Underground

Joe R. Costanza
Software Systems Analyst
Measurement & Control Division
Kaman Sciences Corporation
Colorado Springs, Colorado
(303) 599-1746

ABSTRACT

During an underground nuclear test (UGT) fielding effort it is critical that all transducer channels are exhaustively tested for accuracy and reliability. As the number and complexity of the data acquisition systems increase the time available to troubleshoot each data channel decreases. The limited alcove space downhole prohibits a substantial increase in personnel to provide additional man-hours. Lastly, the operating parameters and characteristics of each transducer channel must be stored and verified if post test analysis is to be successful. A transportable system for testing a large network of transducer channels has been developed to address these problems.

INTRODUCTION

A typical UGT event may involve several hundred transducers, each with sample rates ranging from nanoseconds to milliseconds, sample sizes from 512 points to 32K points, sample precisions from 4 bits to 12 bits, and sample windows from tens of nanoseconds to several minutes. All of these various data acquisition systems must work perfectly the first time. There is no chance of re-doing the test and, should a failure occur, there is very little chance of examining the equipment to determine what went wrong. This coupled with a working environment that experiences large temperature fluctuations, power disturbances, and a dusty atmosphere make it obvious that a system is needed which quickly and frequently verifies the data collection electronics. The On-line Processor for Underground Systems, OPUS, was created for exactly these reasons.

The OPUS system has been built around a microcomputer platform with the Motorola 68000 processor at its heart. A complete system includes: a 16-color graphics display with a resolution of 640 x 500 pixels, a 20-Megabyte 5.25" hard disk drive and a 1-Megabyte 5.25" floppy disk drive, a custom digital interface board (DIB) for high-speed data collection, between 1 and 16 Digital Multiplexer Units (DMU) used in networking, a monochrome graphics printer, and a 400-watt uninterruptable Power Supply. The entire setup occupies the same space as a desktop computer.

OPUS is capable of loading and processing one thousand channels of data in approximately half an hour. Each channel can be graphically plotted for operator viewing or routed through signal processing software for automatic failure analysis. The system can acquire data at a rate of up to 9.8 Mbits per second (bps) for half second bursts, or gather decimated data for periods of several dozen hours. OPUS also contains an integrated database system for centralizing each channel's operating parameters. The networking structure, which connects OPUS to each of the transducer channels to be processed, supports up to 241 distinct data nodes. Each of these nodes may contain as many as 32 multiplexed transducer channels which yields a maximum capacity of 7712 channels for a single OPUS system.

DESIGN PHILOSOPHY

The system was designed to use as little custom hardware as possible. The hardware elements that have been engineered for OPUS, like the DMUs and the DIBs, were each designed to perform a single primitive task and contain no on-board intelligence. This philosophy was adopted primarily due to the nature of UGT work. The UGT community uses a wide range of transducer and data acquisition systems; a data processing board for every type of channel would be impractical and would limit OPUS's flexibility.

Figure 1.0 OPUS Configuration

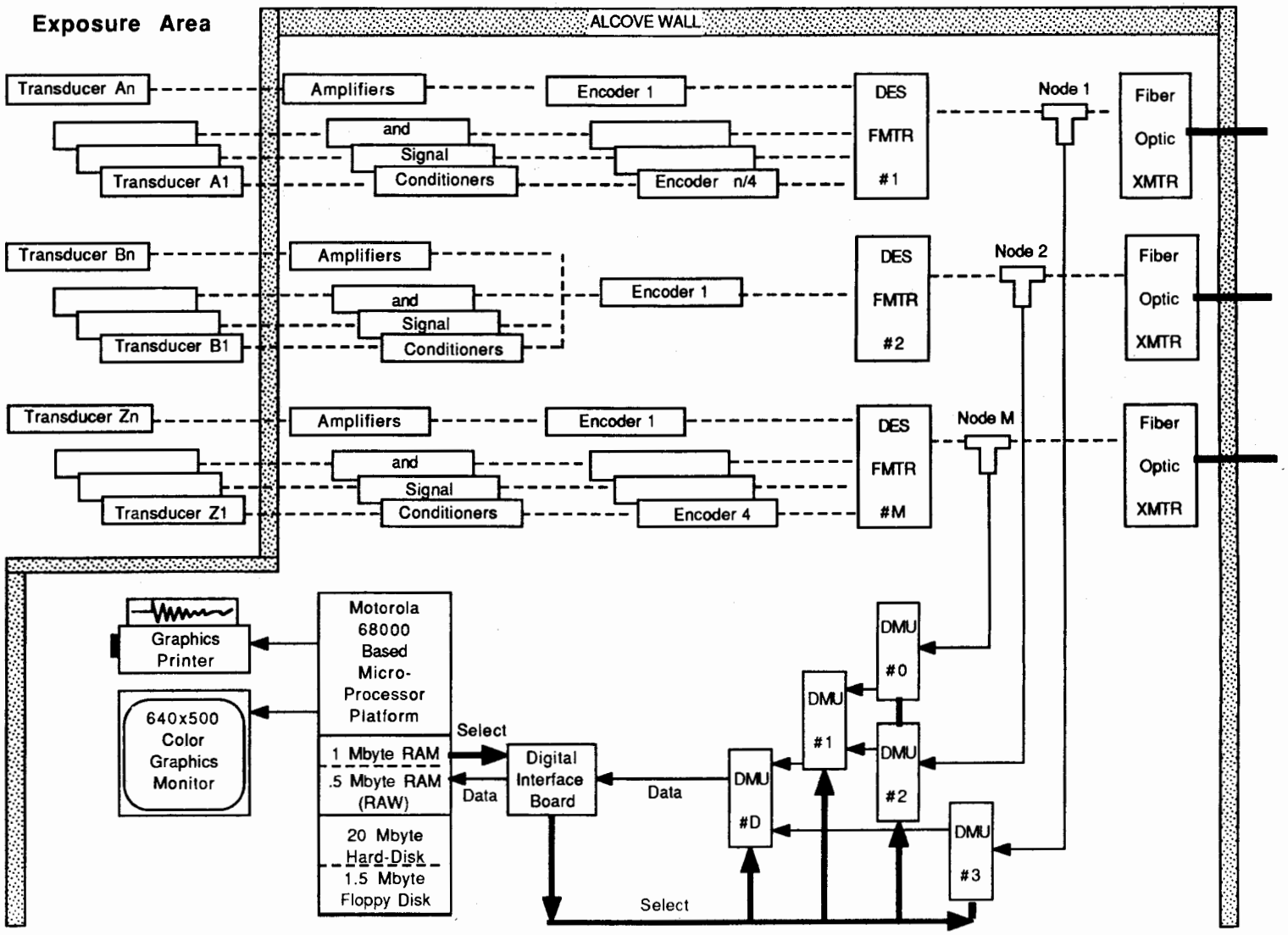

For this reasons OPUS was designed to collect and digest data in its lowest common denominator: the bit. A binary data stream, usually raw though sometimes preprocessed, is loaded into memory and a series of software routines are then applied. This method, while somewhat slower than a hardware or firmware solution, does not force the data to conform to a fixed format as is the case with most "black boxes." Although this places a larger burden upon software development, it gives OPUS the adaptability necessary to accommodate future data collection systems.

HARDWARE -- OVERVIEW

In a typical downhole configuration (Figure 1) the transducers are attached to signal conditioners, amplifiers, and A/D boards. Then these lines are usually, but not necessarily, connected to a Digital Encoding System (DES). The DES can perform two functions. First, it may store all the data in an on-board memory which can be recovered in the event of an up-hole recording system failure. Second, and more commonly, the DES multiplexes several transducer channels into a single output line. This second function is necessary for several reasons; it dramatically reduces the number of data cables that must be strung, and it makes more efficient use of the available bandwidth for each cable that is present.

Though DESs are usually present underground it should be noted that OPUS can operate without them and that they are not a part of the OPUS system itself. The only requirement for proper system operation is the inclusion of a synchronization pattern at some point within the data stream. This pattern is used by the Decoding software and is described later in the Decoding Overview section.

The point at which the data begins its journey up-hole via fiber-optic transmitter to the recording station (label "node" on Figure 1) is also the point at which the OPUS system taps into the bit stream. It is here that the experimenter's responsibility ends. If the data appears correct at point "node" but appears incorrect after processing up-hole then the fault must have occurred in either the transmission link, the above-ground recording system, or the above-ground processing software. This point of responsibility helps personnel both up-hole and down-hole isolate the source of the failure.

From each "node" the data enters the DMU network. At least one DMU is usually present in every OPUS configuration; a DES output line may be connected directly the DIB but this eliminates the networking capability. The OPUS microcomputer issues a series of commands to the network so that the desired "T" is routed to the OPUS DIB. The digital interface is the microcomputer's link to the outside world. It is through this board that network commands are issued and network data received. The data collected via the DIB is then placed in the microcomputer's main memory. An extraction routine then begins unpacking the bit stream into individual samples and demultiplexes (if necessary) these samples into their associated transducer channels.

THE DIGITAL MULTIPLEXER UNIT

The DMU is basically an addressable digital switch. Each unit contains 16 data inputs, one data output, a select input, four select outputs, and a DMU address DIP switch. The DMUs receive switching information packets from the OPUS digital interface board on the select input line and unconditionally retransmit this information on the four select output lines. Each switching packet is tagged with a unique target address and channel number. If the DMU address and the packet's target address match then the DMU connects its output line to the data input line specified by the packet's channel number. A DMU network is made by connecting select and data lines in a tree structure (see Figure 2).

Each of the 16 incoming data lines is optically isolated to avoid ground loops through the network. The signal levels for the data lines may range from 5.0 to 12.5 VDC (peak). The output data is simply a normalized copy of the incoming data. This "normalization" process involves rescaling the output voltage to +5.0 VDC and a rudimentary form of "squaring-up" the rising and falling edges of the signal. Both of these operations are required to accurately gather data at high-speeds; known voltage thresholds and rise times allow the digital interface board which is described later to operate at tighter tolerances.

THE DIGITAL INTERFACE BOARD

The digital interface is the link between the real environment and the computer's environment. Each unit has a select output, a data input, an external clock input, an extracted clock output, and

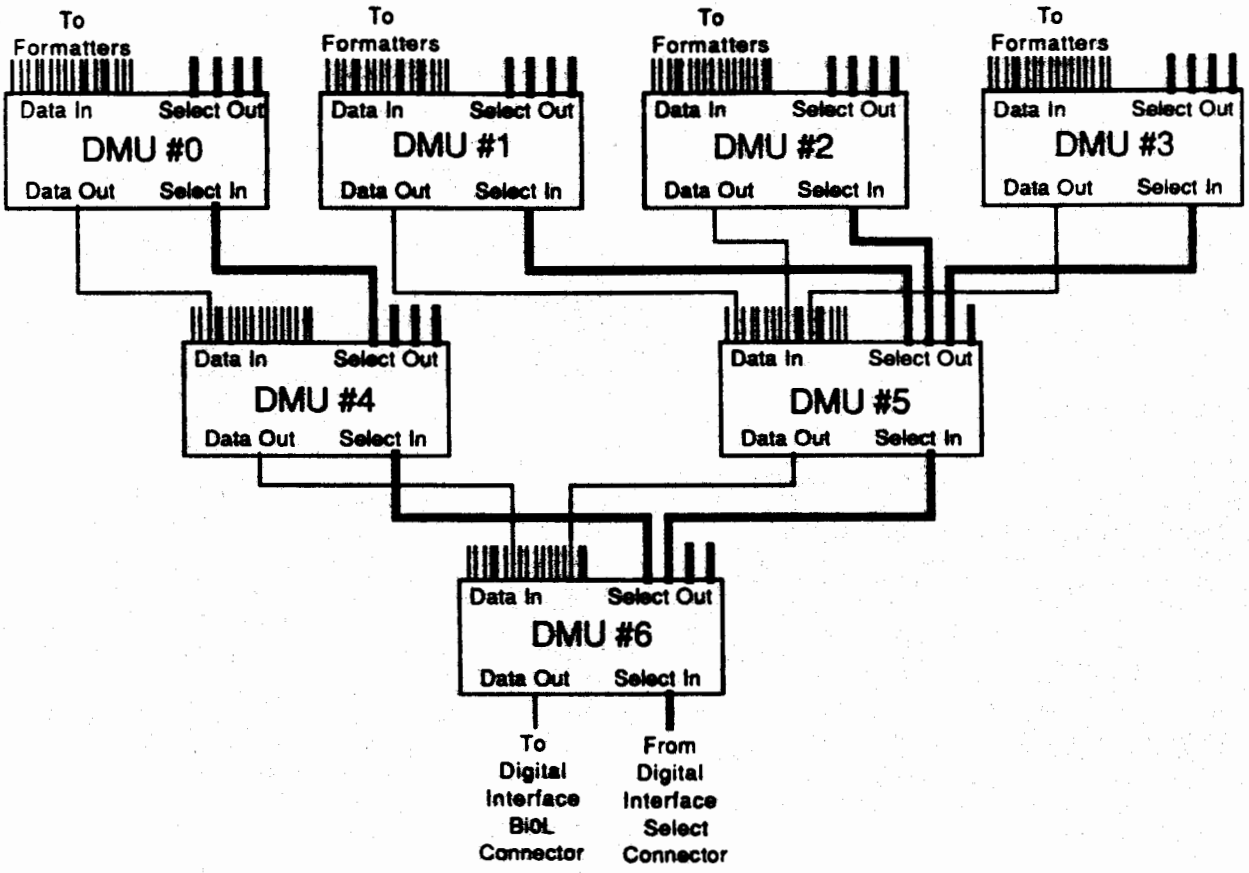

Figure 2.0 BiO-L Network

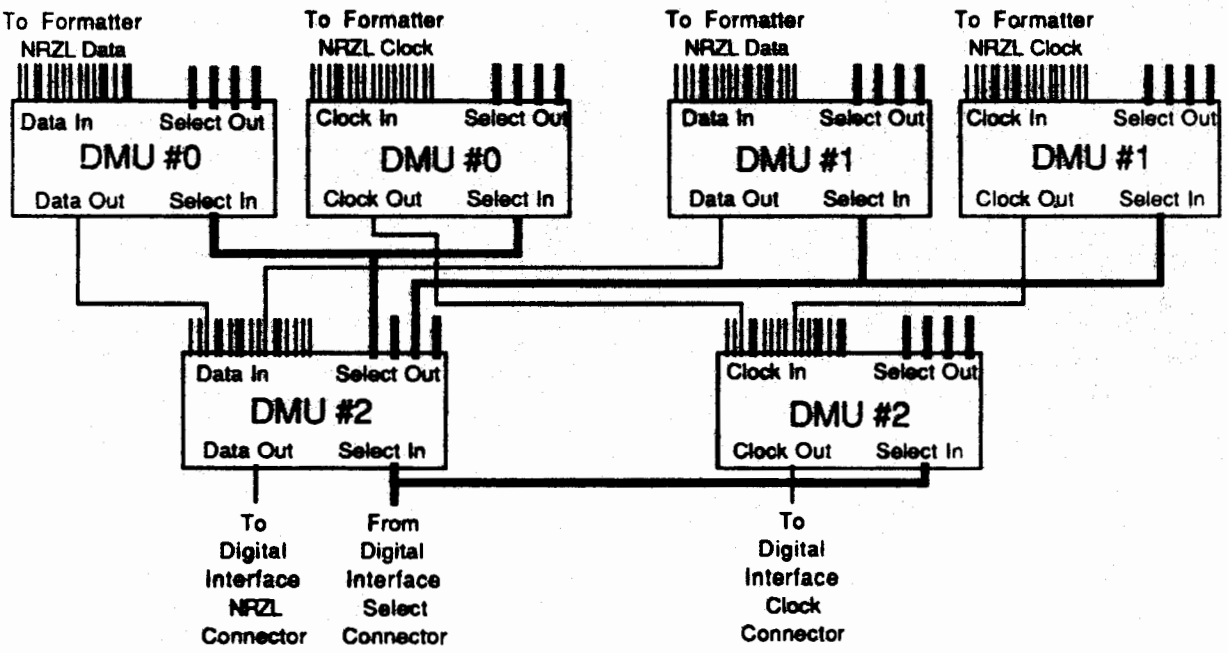

Figure 2.5 NRZ-L Network

several flag input lines. The input data line is optically isolated so that OPUS may be connected directly to the output of a DES unit. The digital interface ties to the microcomputer's data bus. This direct bus access allows the interface to behave just like any other location in the computer's memory and thus speeds data loading by eliminating the need for extensive software handshaking. As mentioned in the description of the DMUs, the DIB transmits its network commands to the multiplexers via the select output line. External events, such as triggers or status flags, are made available to OPUS on the flag input lines.

Information on the data input line enters the interface in the commonly used Bi-phase (or Manchester) format (Bi0-L). Since Bi0-L contains clocking information embedded in the input data the digital interface provides access to the extracted clock on the clock output line. By flipping a switch on the DIB back-panel the Non-Return-to-Zero data format (NRZ-L) may also be used. When using NRZ-L the companion clocking information must be supplied to the external clock input. Since NRZL requires the selection of both a clock and data line a specialized network must be constructed which uses pairs of DMUs. Each of the DMU pairs must have the same address and connection scheme. An example of an NRZ-L network is shown in Figure 2.5.

The incoming Bi0-L or NRZ-L bit stream is processed in the following manner. The interface collects from the incoming bit stream the next group of 16 bits. This 16-bit "word" is then then placed in a latch, a status line indicating "data available" is then set, and the interface begins collecting the next group of bits. The loading software now has access to the data word. Aside from this latch the DIB has no on-board memory in which to store incoming data; if the loading program does not collect the latched data before the next word is ready then the old data is simply overwritten by the new information. If the interface loses the input data signal from the DMU it will set a "no signal" status flag. This prevents the loading software from "locking up" the system while it waits for data to arrive.

SOFTWARE -- OVERVIEW

Since the OPUS system software performs the bulk of the data processing it will be discussed in somewhat finer detail. The software is organized into six different categories: Database, Network, Loading, Decoding, Analysis, and Plotting. With very few exceptions each module is an independent processing block with no overlapping functionality or interdependencies. The plotting package, for example, doesn't need to know at what bit rate the incoming data was loaded.

THE DATABASE -- TRANSDUCER PARAMETERS

The database software is a collection of modules which allow the user to add, delete, and modify almost any parameter associated with a given transducer in the OPUS network. The names, location, data rate, sample size, transducer type, gains, offsets, signal inversions, simulator types, calibration factors, etc., are all organized and maintained in a hierarchical linked-list database-record structure known as a tree (see Figure 3 for examples). Since the tree may grow or shrink at any time storage space for the database-records are dynamically allocated. Three different record types are used in the tree: Formatters, Encoders, and Channels.

Formatter records are assigned a unique integer number and are associated with a given node in the OPUS network. Since each node in the network may contain up to 32 channels the Formatter record contains the number of channels actually multiplexed, the output data rate, and the number of samples allowed for each transducer channel at this node.

At some point the analog information generated by each transducer must be passed through an A/D converter to be digitally sampled. This task is performed by what is known as an encoder board. The encoder board determines the rate at which the data is sampled so there is a corresponding database structure called an Encoder record. This record holds up to four different sample rates for each Encoder since some boards are capable of switching sample intervals several times during data acquisition.

Lastly, the Channel records specify the transducer names, the type of injected simulators used to exercise the channels, whether any of the channel's electronics invert the transducer data, and a calibration factor for conversion from digitizer counts to engineering units. The channel records also contain a group of reference parameters which the user may not modify directly; these are described in the Software Analysis section.

Each Formatter record may index up to eight encoder records. This simply means that from one to eight A/D boards may be available at each Formatter node. Each encoder board may support as many as 32 transducers at a time; therefore there are between one and 32 Channel records associated with each Encoder record. While this database structure has been tailored somewhat to the equipment used

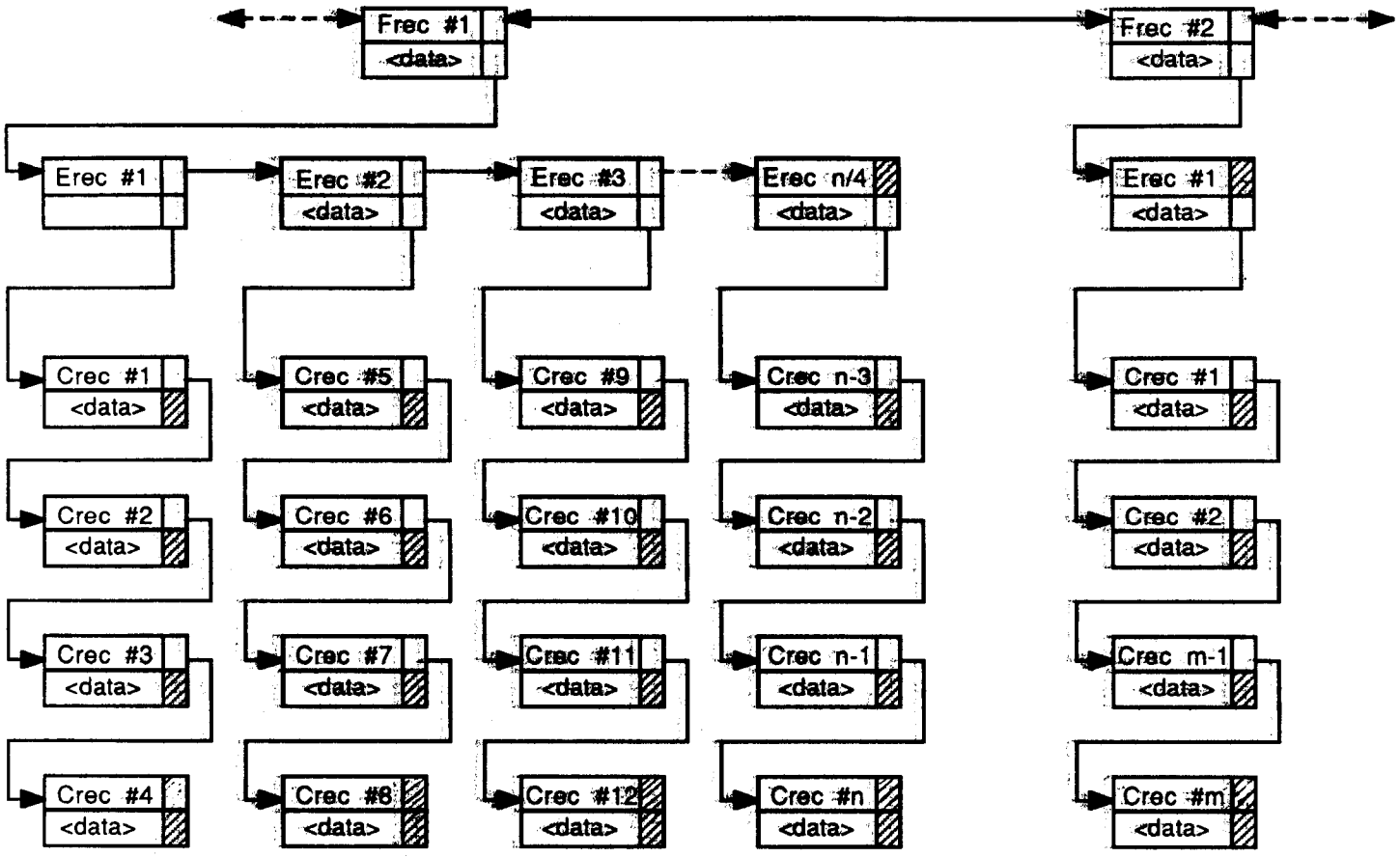

Figure 3.0 Database Structure

underground it should be apparent that this organization can be used to describe most any data collection system.

THE DATABASE -- NETWORK PARAMETERS

The database programs are also responsible for maintaining the DMU network itself -- establishing links between OPUS's DIB and the transducer channels. The OPUS network is keyed entirely upon formatter nodes. Up to 241 of these nodes may exist in a single OPUS network. To gain access to a single transducer channel involves gathering and processing the information for every channel multiplexed on that node. While this may seem inefficient at first it should be noted that examining channels sequentially by formatter rather than alphabetical channel order is the norm. In any event collection and processing of random data channels in the system is so fast and easy that it represents no real problem.

The OPUS Network tree is organized as a collection of 16 connection records. Each connection record represents a DMU in the network and therefore each record has 16 inputs and one output. The inputs indicate where the information routed through the DMU came from. The output indicates where the information will be going. The inputs may be either formatter numbers (leaves) or DMU numbers (branches). The output may be either a DMU number or the OPUS Digital Interface Board. Ultimately only one DMU, or one pair of DMUs (Figure 2.5), will connect to the DIB.

THE LOADER

The purpose of the loader is to gather external data from the DIB. A secondary goal is to isolate the rest of the system from the "mechanics" of the incoming data. These "mechanics" include DMU network switching, selection of data rates, and triggering or marking the data based upon external flags or events. A typical sequence of events leading up the Loading operation usually include the following: a specific channel or group of channels are selected for examination by the user, OPUS examines the database to determine which formatter node contains the channel(s), the program then scans the Network records for a path connecting OPUS to the formatter node, a series of network switching commands are issued via the DIB to all the DMUs in the system, the software then examines the Formatter record to collect any additional information regarding the upcoming load (ie, data rate, number of channels), and passes control to the Loading software.

The loading software operates in one of several collection modes: Normal, Compressed, and Polled. In each of these modes when a new data word is made available via the DIB it is stored in a sequential location in the microcomputer's main memory. This RAW data buffer is then the source for subsequent DECODE processing routines.

In Normal mode the loader ignores external events and/or status flags which may be supplied by the digital interface. This mode expects the hardware handshake between the DIB and the microcomputer's data bus to synchronize the incoming data. Once this assumption is made it allows the loading software to operate at its peak throughput: approximately 9.8 Mbits per second.

Compressed mode makes the same assumption to accomplish a different goal. In Compressed mode the data may be gathered at a data rate of up to 1.228 Mbits per second (8 times slower than that of Normal mode) but this restriction allows a much more sophisticated loading algorithm to preprocess the incoming information. This loading algorithm can, for example, keep track of exactly where and when the incoming bit stream should be decimated for long-term data loading.

The Polled data mode is typically used for very specialized data acquisition. In this mode the external data flags are routinely examined for information, then specific operations are performed based upon these flags. While it is the slowest collection mode it offers the most flexibility. And though the maximum data rate is dependent upon the complexity of the loading algorithm itself the Polled mode provides the means to perform almost any operation necessary to accurately collect the incoming information. Examples of the Polled loading mode are: Real-time analysis of the incoming bit-stream, time or event marking of data words, and the collection of data with very long sample intervals.

THE DECODER -- OVERVIEW

Once the raw bit-stream has been collected and stored in the system's memory the process of extracting the multiplexed transducer information begins. This operation performs two important tasks: it assures the integrity of the incoming information, and converts that information into a form more easily manipulated by other processing modules. The database provides the Decoder software with specifics concerning the bit precision of all the formatter's A/D boards and the number of channels multiplexed on that formatter.

This information, along with a quick description of the formatter frame layout, are all that are needed to begin parsing the bit-stream for the transducer data. Figure 4 shows the three types of fields present in every frame of formatter data. Again, as long as a SYNC field is present in the bit-stream an extraction algorithm can be developed to unpack the DATA.

Figure 4. DES Formatter Frame

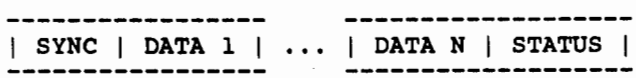

The SYNC field is simply a bit pattern of any length which cannot occur under normal conditions. Given a 12-bit A/D data word, and using an odd parity convention, a valid SYNC might be the 25 bit binary pattern of 1111111111111111111111111. Assuming that the even parity is maintained throughout the bit-stream no series of 12-bit data words (plus a parity bit) can be constructed to look like a SYNC word. The SYNC fields are typically much smaller, between 16 and 22 bits long, but they provide a fair measure of reliability.

The DATA field contains actual transducer information for each channel attached to the formatter along with some type of error checking mechanism. This field may contain up to 32 data words, each word associated with a different transducer channel, and all words ranging in length from one to 16 bits (excluding error checking bits). The error detection scheme is usually a one-bit parity check.

The STATUS fields are used to provide timing, mode, or additional error checking bits to the decoding program. This information is usually included in the data frame by the formatter but it can be added to the bit-stream by the Loading software based upon the external status flags on the DIB. The STATUS field may also contain a counter which supplies positioning information for the transducer data stored in the frame. For example a frame counter value of 24 would indicate that the items in the DATA field contains the 24th sample from every transducer attached to the formatter.

Given the above database and frame format information the decoding operation becomes relatively simple. Under ideal conditions the software need only:

1. Locate the SYNC word
2. Collect the next transducer DATA word
3. Verify that the parity bit matches the actual parity
4. Convert the data into a 16-bit 2's complement integer
5. Store the integer in a temporary buffer
6. Repeat Step #2 through #5 for all the channels
7. Fetch the STATUS word(s)
8. Verify the parity of the STATUS word(s)
9. Compare the STATUS mode against the expected mode
10. Construct the frame counter from the STATUS word(s)
11. Store all the transducer data words in separate channel buffers based upon the frame counter value
12. Repeat steps #1 through #11 for the total # of samples

DECODER ERROR DETECTION AND CORRECTION

The above steps will normally result in a valid, perfectly sequential collection of data points for each transducer channel connected to the formatter. Those instances in which these steps fail to generate usable data are "real world" faults such as signal line noise; this can cause data parity errors, SYNC errors, mode errors, and frame counter errors. A formatter which "drops bits" can also cause these failures. The accurate detection and correction of these types of failures are described below.

If a formatter begins to "drop bits" any type of error can occur in the bit-stream while decoding. Unfortunately, with the simple parity scheme for error detection there is a 50-50 chance that these faults will go unnoticed. This is where the SYNC word plays an important role. If the decoding program knows the number of bits between each SYNC word, and if the SYNC words do not appear in the bit stream at these regular intervals then this may indicate a SYNC-fault. Though SYNC-faults can also be caused by signal line noise

these random failures are not likely to manifest themselves as SYNC-faults on a regular basis. In OPUS, a counter keeps track of the total number of SYNC-faults. If this counter exceeds a specified threshold then the decoding program aborts with a SYNC-overflow condition. This can indicate one of two serious errors: either the formatter is malfunctioning or a formatter bit-stream has been loaded into memory with too few or too many channels multiplexed on it. This second condition could be caused by an improperly connected cable in the network, an invalid entry in the database, or a faulty DES unit. All of these conditions are serious and must be corrected if the post-test data reduction is to be meaningful.

As mentioned earlier, parity checking offer only a 50% chance of error detection per data word. However, if a burst of noise corrupts the incoming bit-stream then chances are good that at least one item in the formatter frame will appear invalid. In this event two choices are available:

1) The entire frame may be discarded.

2) Only the items in the frame which actually failed is discarded.

Which of these alternatives are used depends upon the nature of the bit-stream. If the transducer data is stored in a DES's encoder memory and then endlessly cycled out of the formatter then the entire frame may be thrown away and picked up on the next pass through the encoder's memory. If the information is cycled out of the formatter "real time" with no repetitions then only the faulty frame elements should be excised. In either of these instances a place holder indicating unreliable information must be substituted for all discarded data. These NULL data items fill the sample interval normally occupied by valid data and avoid "time compressing" the final image. A second benefit of these NULL data values is that the plotting package can perform special operations when NULL data items are encountered. OPUS, for example, does not display NULL data items on its plots but rather "blanks out" those portions of the graph.

ANALYSIS

To verify the operation of the amplifiers and filters attached to each transducer channel a simulator signal is usually applied at a point electrically equivalent to the output of the gage itself. This simulator is designed to exercise the equipment across its intended range and beyond. Several different simulator types including single-shot pulses and Calibration ID codes are used but only one, the "clipped sawtooth", will be discussed in this paper. Though the analysis algorithm may vary for each channel (depending upon the simulator type) the processing sequence remains the same.

The sawtooth simulator is shown in Figure 5. The simulator is injected into the post-transducer electronics at a voltage which exceeds the input limits of the A/D board. This is necessary for two reasons. First, it assures that the entire range of the A/D is exercised. Second, it verifies that the system can recover from a saturation condition which may be caused by the gamma response of the transducer. The resulting "clipped sawtooth" is the output expected by the analysis program.

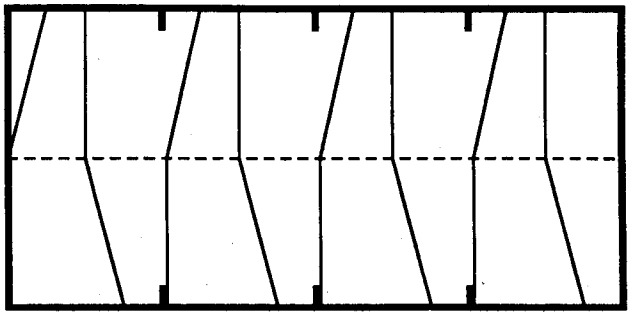

Figure 5.0 Clipped Sawtooth

Now that the simulator signal has been defined an algorithm must be developed to accurately describe and quantify the important characteristics of that signal. Failure conditions and thresholds are then assigned to the results of the analysis. This is all done prior to UGT fielding and is embedded in the OPUS program. Since encoders may have up to four different sample rates at different times in the sample period it becomes necessary to check for linearity between sample quadrants. In the case of the "clipped sawtooth" the analysis program should also check for saturation and center-line signal drift.

All of the above conditions may be tested by distilling the "clipped sawtooth" into two analysis parameters: positive and negative saturation widths (Psat and Nsat, respectively). The Psat and Nsat values represent the total time each peak was saturated. If both the Psat and Nsat values are greater than zero then the saturation requirement has been fulfilled. Linearity is checked by comparing the relative Psat and Nsat widths of one sample quadrant with all the other sample quadrants. Finally, a Psat and/or Nsat that have changed significantly from some "absolute reference" also indicates a drift condition.

Since the saturation level and center-line adjustment may vary from channel to channel the field operator must make a decision concerning the operational status of each channel. While OPUS allows fast and easy access to every channel in the network this type of manual verification on a channel by channel basis would become lengthy, tiresome, and keep trained personnel from other more important tasks. For this reason the OPUS system provides a reference storage feature. Once a channel has been properly adjusted the operator simply presses a button, that channel's data trace is passed through the analysis routine, and the resulting parameters are stored in the database as "absolute references." From that point on each time the same channel is loaded OPUS will automatically compare that channel to the references stored specifically for that channel.

If the operator wishes to perform an integrity check on all the channels for which an "absolute reference" has been stored then the Dry-Run feature may be invoked. This process begins with the program automatically finding the first formatter in the database. It then selects that formatter in the network, Loads the RAW bit-stream, and Decodes the information into individual transducer channels. Then, depending upon whether or not a reference has been stored for each individual channel, the analysis routines are applied to the data. The results are either stored in a summary table or plotted and sent to the hardcopy device. The next formatter in the database is then located and the process repeats. When all the formatters in the network have been examined the Dry-Run terminates and prints a status report.

PLOTTING

The graphics display is the final destination for almost all of the processed information. It is here that the operator examines the results of the Load, Decode, and Analysis operations. The plots all appear with linearized time scales; that is, differences in sample rates between quadrants will not result in a corresponding frequency-shift at each quadrant boundary. One, two, or four channels may be displayed on the screen at any one time. The single channel plots provide the finest detail and also allow the user to expand any segment of the image for closer examination. Four channel screen plots allow the user to quickly scan through all the available channels, or to compare results between channels.

During each of the OPUS operations a different set of status flags or messages is generated. The Load status is a short message lasting between 0.5 seconds and several hours which informs the operator whether or not the bit-stream signal is present. When the loader has filled the raw bit-stream buffer with data it passes control to the decoder. Another short message lasting between 6 and 12 seconds (depending upon the complexity of the extraction) appears to let the operator know that the decode operation is under way. When decoding has finished the plot package begins to generate the transducer channel images and the screen switches from text mode to graphics mode.

On every plot the decode status flags are displayed at the bottom of the frame which surrounds that channel's image. These flags indicate to the user any problems that were encountered during the decode phase of OPUS. There are two kinds of decoder faults: simple errors and overflow conditions. If no errors were encountered or a few simple errors were found and corrected by the decoding software then the frame surrounding each plot, including the channel name and decode flags, will be displayed in green. If any overflow condition was found during the decoding operations then the frame surrounding the plot, the channel name, and the decode flags will all be displayed in red.

If a channel does not have a stored reference then no waveform analysis is performed. In this case the data trace itself is displayed in yellow. If the stored reference closely matches the current data trace then the data trace is displayed in green. If the analysis operation indicates that any one parameter exceeds the allowed tolerance for that channel then the trace is displayed in red. In this way the operator's attention is drawn immediately to the faulty channel(s). A sample OPUS screen is shown in Figure 6.

With the ability to display four plots per screen, each with a sample size of up to 32K points, it becomes important to boost the performance of the graphics system for the volume of channels OPUS typically deals with. The principal speed improvement is realized by eliminating unnecessary graphics operations which overlap onto the same pixels on the raster display. This is done by determining the minimum and maximum data values associated with a single column on the graphics screen and then performing a single MOVE and DRAW for that column. This provides two enhancements to graphics throughput:

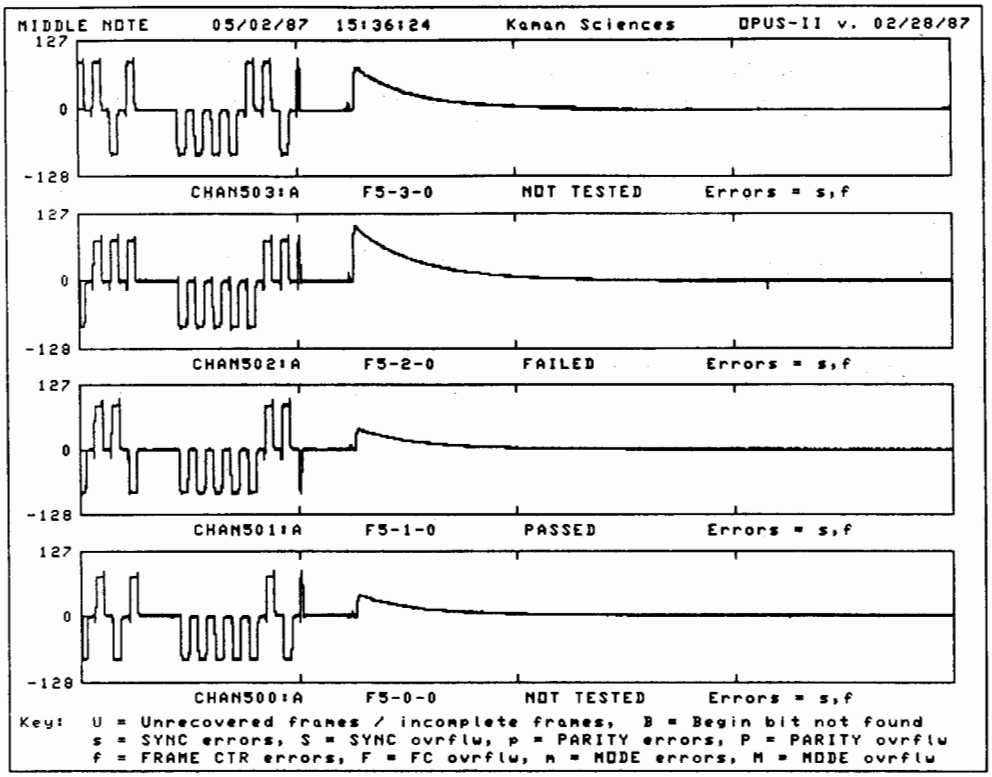

Figure 6.0 OPUS Screen Sample

1) An upper limit is set on the number of MOVE and DRAW commands issued to the graphics system that is totally independent of the number of data samples

2) Since only vertical lines are used during image generation an optimized DRAW algorithm may be developed based upon this assumption which is several times faster than a more generic DRAW utility. An additional performance factor is realized by eliminating as many floating point math operations as possible.

SUMMARY

Though the OPUS system by no means represents the only solution to computer aided testing of high-speed data acquisition systems, it has proven itself to be a fast, reliable, and versatile approach. Maintenance of both the hardware and software has been minimal and down-time caused by software failures occurs rarely. Constraints placed upon presentation size prohibit a detailed discussion of the algorithms used in the software, but each of the key design elements has been mentioned. OPUS has been used with great success on three UGT events and in that time several other useful functions have been incorporated into the software. Should the reader wish to discuss specifics concerning the material covered in this paper the author extends his welcome.

Q: Ray Reed: You talked about validation of your data acquisition, principally the instrumentation. Do you incorporate this technique for validating the instruments in any other way than calibration and continuity?

A: Joe Costanza: That is true.

Q: Ray Reed: Do you have any sensor validation features on this system?

A: Joe Costanza: No. Sensor validation is at a level where it is very difficult out in the field trying to install everything to actually stimulate the sensor itself and verify what it is doing. Most of the validation is on the acquisition system connected to the sensor to verify that signal conditioners and things like that aren't corrupting the information coming from the sensor itself.

A SEMI-HARDENED, NON-MULTIPLEX DATA ACQUISITION SYSTEM

FOR HOSTILE ENVIRONMENTS

by Gordon B. Dean
Director of Engineering
PACIFIC INSTRUMENTS
Concord, California

INTRODUCTION

For the purpose of creating a Data Acquisition System for on-board automobile crash test monitoring and recording, Pacific Instruments developed design concepts, testing techniques, and applications for a solid state transient portable compact system which can be used in many hostile environment conditions. The generalized, semihardened digital recorder takes advantage of the latest advances in technology, permitting big system features in this small, portable, high capacity system which can be operated in three ways: (1) directly from a computer,(2) with a hand held controller box connected to the system by cable,(3) fully automatically using a pre-programmed operating sequence.

A drawback to most hostile environment testing has been that large laboratory type testing equipment must be placed at a considerable distance from the event leading to problems caused by the electrical characteristics of the long cabling required. This compact and versatile miniaturized Data Acquisition package offers obvious advantages in lower cost, improved performance, and increased safety.

DESIGN AND CONSTRUCTION

Housed in an aluminum case measuring 10 x 10 x 18.5 inches, the Data Acquisition System contains the power supply, amplifiers, signal conditioners, control circuits, and digital memory circuits for 32 channels. The external input power source is 12VDC; computer control uses either the IEEE-488-1978 bus or RS-232. Computer programming is performed pretest, and debriefing is done post-test; during the actual hostile environment test, the operator may choose to keep the computer attached, or may operate the system with a hand held control box (Reference Figure 1).

While size, reliability and weight were prime design considerations, another important qualification of the Data Acquisition System is its ability to withstand 35G shocks and 10G vibrations ranging from 20Hz to 2000Hz. The system employs design concepts and components which had been thoroughly tested in hostile environments.

Thin wall aluminum housing forms a strong yet compact enclosure for the system; internal stringers similar to those in an airplane wing give it lightweight bracing. To limit card vibration against the guides and reduce shock to components, precision milled Delrin card guides form close fitting slots. To avoid board flex, which would pop ridged components off the printed circuit cards, cards are packaged into dual or triple card sandwiches using six to eight standoffs between the boards. This technique stiffens the assemblies.

Euro card connectors were selected for use with their dual spring contact design instead of card edge connectors because vibration can dislodge the flat spring contact of the female card edge connector. To eliminate the possibility of components vibrating out of the sockets, all components are soldered directly to the printed circuit cards without sockets. For added integrated circuit vibration tolerance, a drop of RTV rubber is placed under each IC prior to wave soldering. This both dampens the IC against vibration and prevents the IC from floating upward as it is wave soldered.

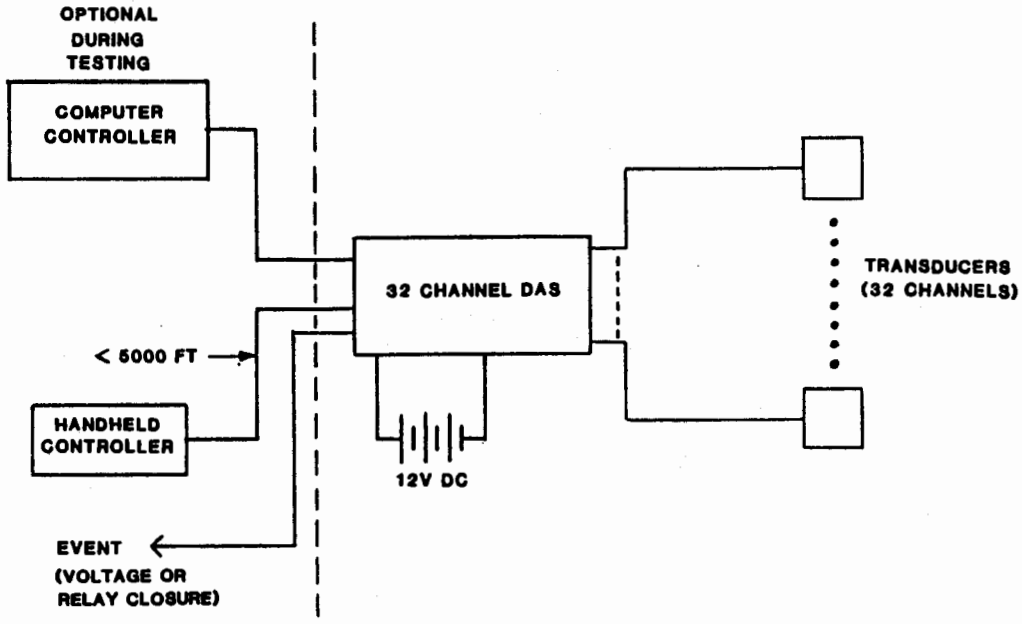

BLOCK DIAGRAM-DAS SYSTEM

FIGURE 1

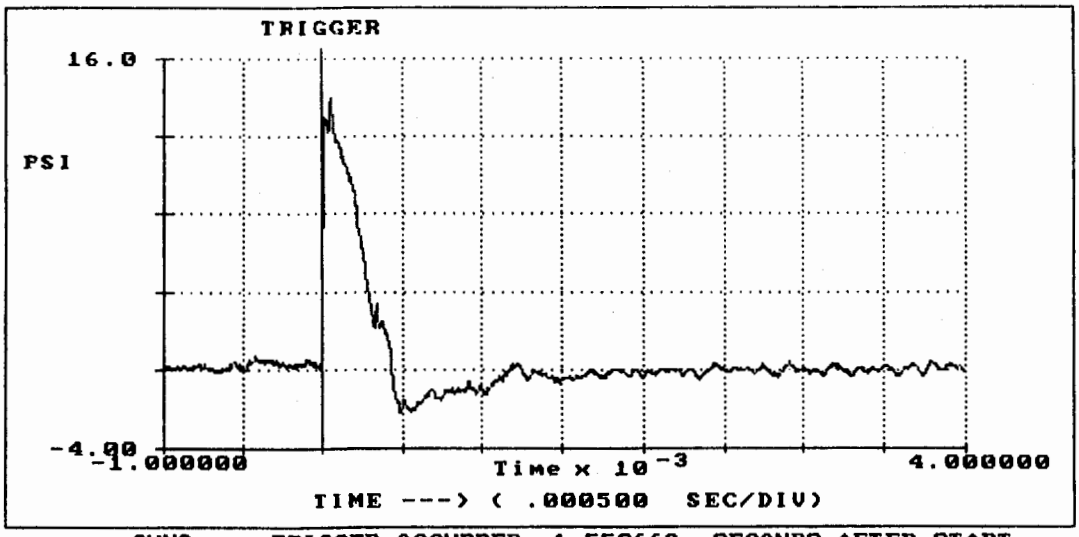

CRT PRESENTATION

FIGURE 2

FEATURES

To make the Data Acquisition System flexible and simple to operate, the following features are included:

A. Full programmability of gain, filter frequency, excitation voltage, discriminator trigger levels, and sampling rate. There are no manual adjustments.

B. A bridge auto-balance circuit

C. A built in resistance calibration circuit

D. Battery backed data and instruction retention.

E. Manual, semi-automatic and automatic operation

F. Twelve volt battery operation

G. Over-temperature indicator

TECHNOLOGY ADVANCES

The single most significant contribution to making possible the Data Acquisition System is the availability of larger semiconductor memories. The latest memories have provided the opportunity to dramatically increase length of recording while maintaining a high sampling rate. One year ago, a system using 16-bit words with a memory capacity of 256K samples of data would require 64 28-pin packages; today the 256K samples of data requires only 16 packages.

Reasonably priced hybrid analog to digital converters that operate with 12-bit words at 1MHz sampling rate have made possible high resolution digitizers. Just three years ago such converters cost six times today's price and required entire printed circuit cards.

Though not precisely a new technology, the microprocessor and associated development systems have made possible implanting the small sized Data Acquisition System with many important features.

OPERATION

Recognizing the importance of a simple and flexible operator interface, the system has three modes of operating. In its most sophisticated mode, the system is operated directly from a computer using high level commands. The operator has immediate access to the complete system setup, control of all programmable parameters, and debriefing of the recorded data. The operator can view data on the computer CRT in color plots of engineering units vs time, or one data set vs another data set (Reference Figure 2). Calculations converting the measured signals to engineering units are based on use of a third order polynomial of the form:

$$EU = Av^3 + Bv^2 + Cv + D$$

where:

EU is the engineering units value, v is the amplifier output in volts, and A,B,C,D are calculated coefficients.

The system controller generates the polynomial from inputs of (a) actual typed-in coefficients,(b) a set of typed in x-y data, or (c)data recorded automatically by use of the system's calibration feature. The advantage of the automatic calibration is that it self-corrects for system offsets, line losses, and other non-transducer produced errors.

In the semi-automatic mode, the operator commands the Data Acquisition with a hand held controller box connected to the system with a cable. He can manually reset, start, trigger, stop, calibrate, and test batteries. This is useful when the hostile environment forces the operator to stay as far away as 5000 feet while controlling the test recording process.

The fully automatic mode allows the operator to start a sequence of preprogrammed events by pushing a single button or providing a relay closure. A typical sequence is: RESET, PRECAL, START (begins taking data), WAIT FOR AN EXTERNAL TRIGGER, TAKE A PRESET AMOUNT OF DATA, STOP, DELAY TEN SECONDS, POST CALIBRATE, MEMORY WRITE PROTECT and POWER DOWN. The Data Acquisition System can be operated totally stand-alone without any control cabling attached by using the discriminator trigger circuit and the automatic mode of operation. Because an extended period of time may elapse between data collection and retrieval, the final steps included in the automatic test sequence place the memory in write protect mode and then depowers the system. The only way the system can be switched back on is by the operator physically moving a switch on the enclosure. Battery back-up is included to maintain data integrity.

DATA ACQUISITION

The Data Acquisition System can incorporate 200 or more individual channels, and can quickly present this data in readable terms. The inclusion of an on-board microprocessor makes several big system features practical. One feature is the system's ability to change the data sampling rate even during the process of taking data. By preprogramming, the sampling rates can be tailored to follow the expected actual data rates. This ability is the key to overcoming a major difficulty of solid state digital recording systems: the limited recording time available.

While other equipment, such as digital oscilloscopes, also collect and store digital data, the Data Acquisition System handles megabytes of data and must be able to present this data in readable terms. Figure 3 is a block diagram of a single channel of a Data Acquisition System. The front end is a high quality, differential input instrumentation amplifier combined with a signal conditioner. The amplifier incorporates a programmable 4 frequency anti-aliasing filter and ten programmable gain steps.

The heart of the amplifier is the Analog Devices hybrid programmable gain instrumentation amplifier, AD365. This device incorporates (a) Selectable gains of 1, 10, 100, and 500; (b) Gain error of +/-0.1%, 10ppm/deg.C; (c) Input offset 2uV/deg. C; (d) Bandwidth of 100KHz.

To enable hands off operation, an auto-balance circuit is included. This feature corrects for normal transducer unbalance. After the channel has achieved a balanced condition, the auto-balance clock is disabled to eliminate noise it might feed into the sensitive amplifier input.

The system provides a regulated excitation output since flexibility demands that the Data Acquisition System operate with a variety of transducers including bridge types. The excitation can be monitored in the channel's normal data collection path providing a reading of the exact value. A programmable calibration circuit parallels a bridge resistor with a known value calibration resistor, and the resultant offset is recorded along with the actual test data. Both the measured excitation voltage and the calibration data can be used for accurate data reduction.

The Filter's output is routed first to a sample and hold circuit and then to the analog to digital converter. The sample and hold circuit serves two purposes: It holds the analog input at a steady value while the analog to digital converter is reading the sample, and it allows precise time correlations between samples in a multichannel system.

The Analog Devices AD7572 is an example of the type analog to digital converter used. It features 135 milliwatts power dissipation, 12 bit resolution, 5 microseconds conversion times, and non-linearity of less than one LSB. The analog to digital converter is the largest power consumer in the system. In a small package system, power dissipation is particularly important, especially where the user's ability to provide 12VDC to the package for extended intervals may be limited. If heat build-up is allowed to occur in the package, it may impose unnecessary temperature coefficient errors. The small system design includes dual power modes: Standby and Normal power. In the Normal mode, all circuits are operative. This mode is for recording data. In the Standby mode, the analog to digital converters and the sample and hold circuits are depowered, reducing power input by 50 watts. If the temperature exceeds 50 degrees C, an over-temperature alarm goes off.

The system will trigger data recording in several ways: (a)through a voltage-sensitive trigger circuit which operates when an input signal exceeds a programmed voltage value; (b) by a preset time delay trigger circuit; (c) with a trigger provided via hardwire. Redundant triggers can be used. For example, in crash testing, the primary trigger is a switch contact activated when the auto bumper hits the barrier. The secondary signal is the discriminator trigger driven by an on-board accelerometer.

SHOCK AND VIBRATION TESTING

The Data Acquisition System was shock tested by placing it on an acceleration sled at the Chrysler facility in Chelsea, Michigan. Normally used to accelerate anthropomorphic test beds, the sled is accelerated by an air driven ram over a distance of about 150 feet. This test is identical to one of the system's applications. A total of 24 accelerations were applied in the six axis with no system failures; the acceleration applied was 35G

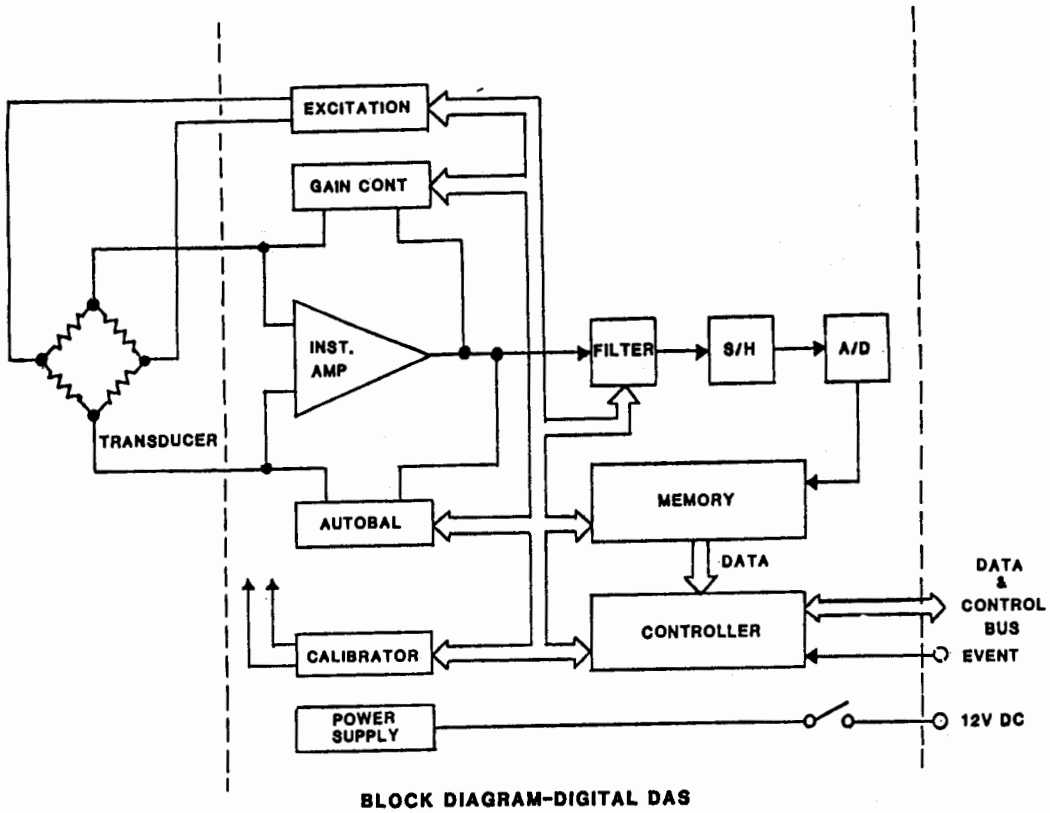

BLOCK DIAGRAM-DIGITAL DAS
FIGURE 3

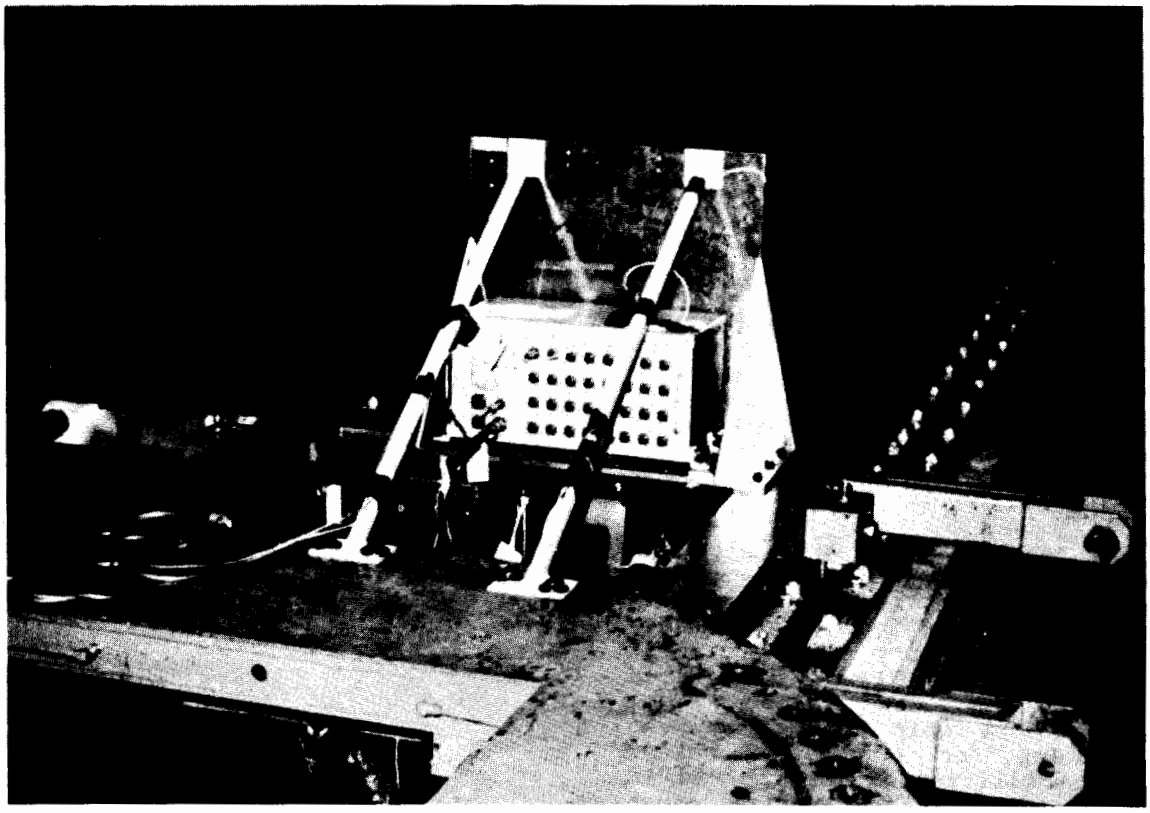

FIGURE 4: SHOCK TESTING

amplitude of 100 milliseconds duration (Reference Figure 4).

During the shocks, acceleration data was recorded by the unit under test. This method of testing proved that the system recorded the data continuously during the G applications. A sample of the data taken is shown in Figure 5. The dotted vertical line indicates the trigger event. Pre-trigger data is to the left of the trigger line.

For vibration testing we used a shaker table at the Chrysler facility in Detroit, using a mounting fixture to secure the Data Acquisition System to the vertical axis shaker head (Reference Figure 6). The tests pointed out two weak points without the system: A neoprene rubber card hold down pad abraded rapidly and the ridged welded electrical connection between a circuit card and a pair of card mounted AA size back-up batteries broke. The problem was not the mounting of the batteries but the extreme rigidity of the leads, which quickly work hardened.

PRODUCTION UNIT

Shown in Figure 7, the first production unit was changed from the prototype. More compact board spacing enabled the enclosure length to be reduced by 1.25 inches. Most screw type fasteners are replaced by rivets so they will not be loosened by vibration. The access methods to the connector panel were improved. Releasing 10 screws allows the front panel to pivot forward from the bottom edge giving good access to all connectors and indicators. The number of screws securing the top was reduced from 33 to 12. The majority of these engineering changes were devised from difficulties experienced in assembling the prototype system, and serve to improve the system's ease of maintenance.

CONCLUSIONS

The Data Acquisition System, with its rugged design, small size and special operating features, is fully functionable in hostile environments or anywhere that laboratory type equipment will not fit. It will work in limited access crawl ways and isolated compartments of a ship undergoing near miss testing, or to monitor blast effects on military equipment; and it is well suited to automotive crash testing facilities, where the 10 x 10 x 20 inch package can ride along on the crashing vehicle.

Within the small package, big system features such as the automatic operation mode, the quick presentation of engineering units data, redundant triggering operation make it useful in situations where accurate recording of data under hostile conditions is vital.

ACKNOWLEDGEMENT

The author wishes to acknowledge the support and guidance received from Mr. John Hueckel, President of Pacific Instruments.

SHOCK TEST RESULTS-ON BOARD SYSTEM MODEL 5600

MEMORY SIZE	=	64K SAMPLES	TRIGGER	=	RELAY CLOSURE
AMP GAIN	=	50	ACCEL SF	=	1.6 MV/G
G'S FS	=	+/- 62.5	FILTER	=	3 KHZ, 8 POLE
DATE	=	23 OCT. 1986	PROFILE	=	80 KHZ RATE
			INPUT	=	35G PEAK

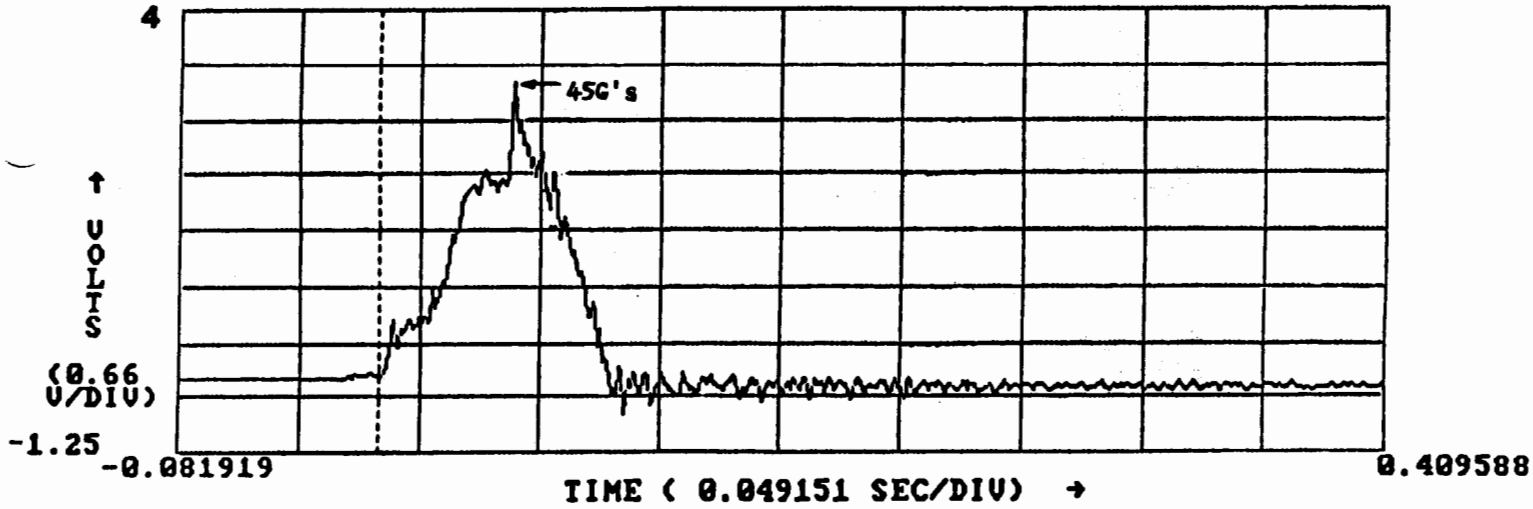

FIGURE 5: SHOCK DATA

FIGURE 6: DAS VIBRATION TESTING

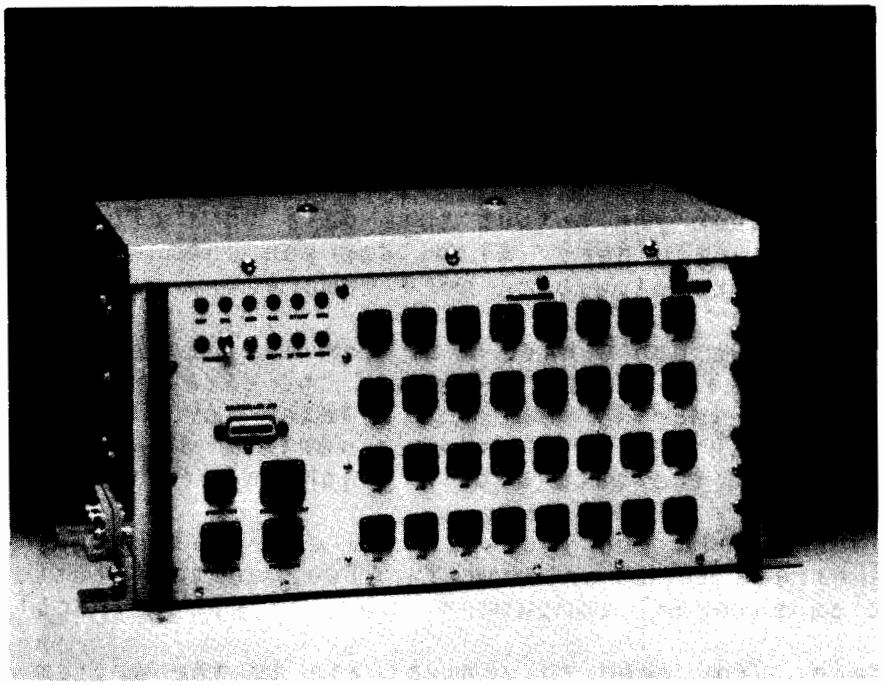

FIGURE 7: PRODUCTION DAS

A SEMI-HARDENED, NON-MULTIPLEX DATA ACQUISITION SYSTEM FOR HOSTILE ENVIRONMENTS

Q: Glen Roark (Kaman Sciences Corp.): How much bit resolution do you have on your digitizer?

A: Gordon Dean: Twelve bits.

Q: Ronald Tussing: Did you say the old system had 64K memory per channel or was that for all 32 channels?

A: Gordon Dean: Yes, the current system has 64K samples per channel, and the new one has 256K samples per channel.

Q: Bobby Reed: When you output this data to a plotter, can you drive it directly from a recorder? Also, can you communicate with the external memory, like piggyback more memory?

A: Gordon Dean: We don't have a driver as yet for a plotter. We do drive several printers that will print the data graphically with dot matrix printers, primarily the LA50 printer for the DEC system. And of course the IBM system will drive a variety of graphical printers. So yes we can print the data out in graphical form.

Q: Bobby Reed: Could you increase the external memory if you had a port to communicate to an external? Also, on the plotter, can you plot without an external computer? Does it plot directly?

A: Gordon Dean: You need to communicate to the system via RS232 or the IEEE bus. The external memory has a bit of a problem. We can increase the amount of memory on the system, and we have plans for doing so. But to be able to use an external memory where we would have to process the data to ship it out of the system could not be done at the speeds with which the system will run.

Q: Bobby Reed: Is the memory right now a physical space or an address?

A: Gordon Dean: It is a physical space: the CMOS RAM on each channel.

Q: Steven Chen (PCB Piezotronics): Do you provide real-time information on the system?

A: Gordon Dean: Yes, there is a feature called real-time monitoring where you can look at a single channel with the computer.

Q: Steven Chen: Do you provide the hour, date, minutes, and seconds? Suppose you have a shock that happened at 3 p.m. Do you record that time?

A: Gordon Dean: Yes, in a way. It's a little different than that. The answer to the question is yes because if you know the trigger time or if you know the start time when the system actually begins to record data, the system will record the start to trigger time with

respect to the start time given to it by the computer or relay closure.

Q: Steven Chen: Would you please tell me the power consumption in the active operation or as you mentioned the low-power operation?

A: Gordon Dean: The 32-channel system running at full power draws 8.1 amps at 12 volts.

Q: Steven Chen: That's the active mode?

A: Gordon Dean: That's the active mode. The low-power mode draws approximately 3.2 amps.

Q: Bill Cardwell (General Electric Company, Cincinnati): Are there environmental constraints on installing this? Can it take low temperature, high temperature and low-pressure environments in addition to being ruggedized for impact?

A: Gordon Dean: Pressure is 0 to 10,000 feet and the temperature range is the commercial temperature range. There is a sensor in it that will turn a light on its control panel when the internal temperature exceeds 50°C, but it is designed to operate in the commercial temperature range which is 0-70°C.

INTEGRATING THE LECROY 6880 WAVEFORM DIGITIZER INTO AN EXISTING INSTRUMENTATION SYSTEM

John R. Carrel
Electrical Engineer
Sandia Engineering/Software Department
EG&G Energy Measurements
Las Vegas, Nevada

ABSTRACT

The Digital Encoding System-7 (DES-7), designed by EG&G Energy Measurements for the Field Command Defense Nuclear Agency (FCDNA), is a high-speed digitizing system that utilizes LeCroy Model 6880 Waveform Digitizers. The system is housed in a CAMAC crate for use in the existing FCDNA data acquisition system. The data from the 6880 digitizers (digitizing at a rate over 1.35 gigasamples/second with an analog bandwidth of 250 MHz) requires a substantial amount of post processing to obtain recognizable data. The DES-7 system, composed of the existing FCDNA instrumentation system and a single-wide CAMAC module with a TMS32010 digital signal processor, provides the necessary functions to allow the collection of calibration data prior to the measured test for later use in the post processing effort.

INTRODUCTION

EG&G Energy Measurements was contracted by the Field Command Defense Nuclear Agency (FCDNA) to design and develop a system to be called the Digital Encoding System-7 (DES-7) that would incorporate the LeCroy 6880 digitizer into the existing FCDNA instrumentation system. Because of its high-speed data acquisition capabilities, the data from the 6880 digitizer requires a substantial amount of post processing before any data can be recognized. This need for post processing requires that any system utilizing the 6880 digitizer must have the ability to perform a certain amount of mathematical calculations in order to retrieve coherent data. A system needed to be developed that would utilize the speed and efficiency of the existing hardware and yet would allow for the post processing required by the 6880 digitizer.

To fulfill this need, EG&G Energy Measurements developed a new electronic module to augment the capabilities of the existing hardware. This module, the Auxiliary Formatter, provides the necessary functions to allow the collection of the calibration data prior to the actual data acquisition. The calibration data is transmitted to a remote location along with the measurement data, where post processing is performed on a VAX-11/750 computer. This module has the added capability to perform a minimum set of post processing, via a GPIB interface port inside the module, so that the local user can observe the data from the digitizers and can verify the crate system.

This paper will present EG&G Energy Measurement's DES-7 system, including a description in some detail of the LeCroy 6880 Waveform Digitizer and its application within the existing FCDNA data acquisition system.

THE 6880 WAVEFORM DIGITIZER

The 6880 Waveform Digitizer, developed and built by LeCroy Research Systems Corporation, is a Computer Automated Measurement And Control (CAMAC) module which consumes only three slots in a crate. Because of its small size, many digitizers can be housed in the same CAMAC crate, allowing for efficient use of the limited space in the instrumentation area. The 6880 digitizer samples data at a rate of 1.348 gigasamples per second. The analog input to the digitizer has a 250 MHz bandwidth with two external inputs that can be summed together. Each of these inputs has an input amplitude range of 500 mV. In addition to these inputs, an internally generated dc offset and reference clock can be internally added to the input signal.

When the 6880 digitizer is armed and triggered, it captures, digitizes, and stores 10,240 data points. This gives the 6880 the ability to digitize 7.5 microseconds of data with a resolution of 741 picoseconds per sample. Because of its large data record, the 6880 digitizer lends itself to use in digital signal processing operations such as filters and fast Fourier transforms. (Figure 1 shows the architecture of the 6880 digitizer.)

*This work was supported by the U.S. Department of Energy under Contract No. DE-AC08-83NV10282.

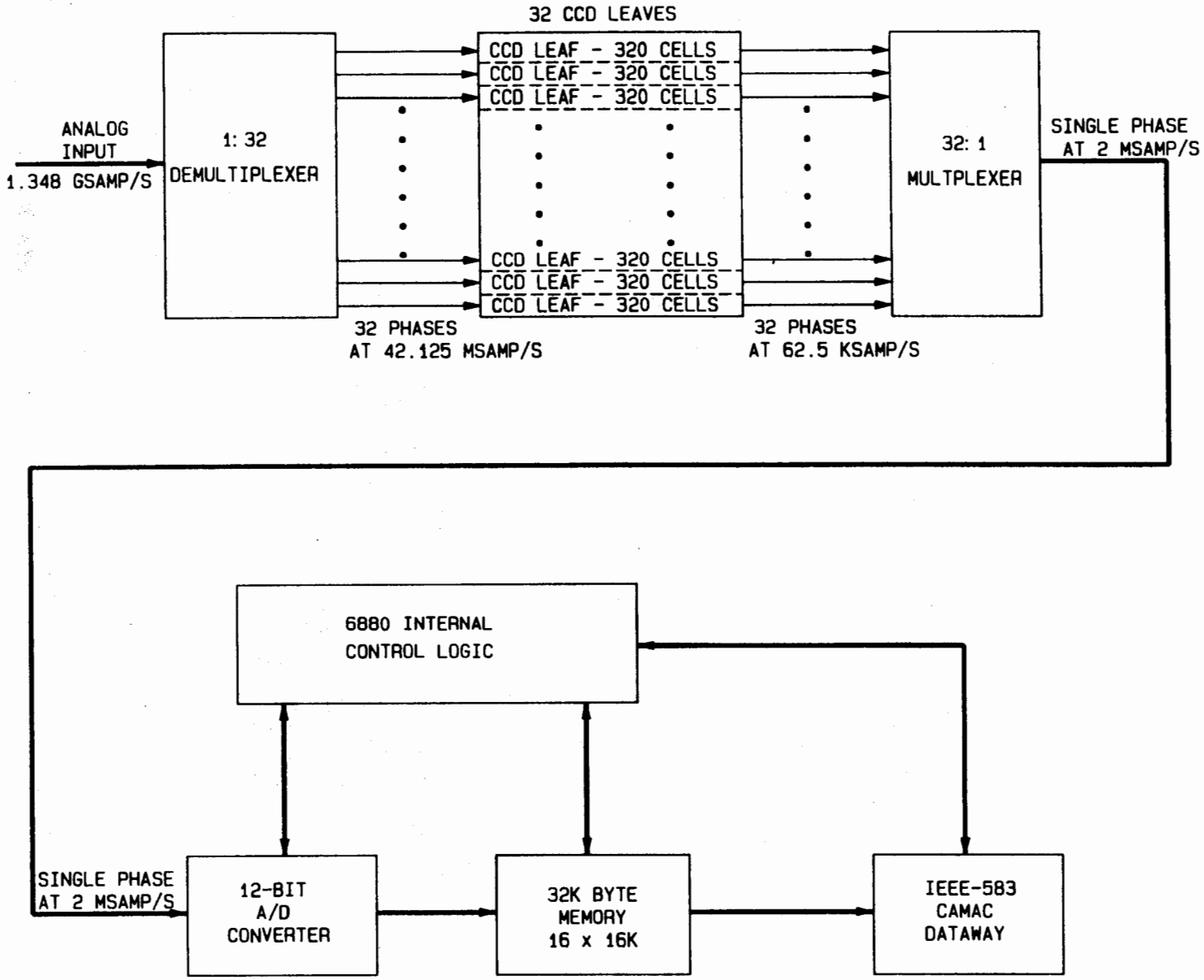

Figure 1

Architecture of the 6880 Digitizer

At present the data acquired from the 6880 has an accuracy of at-least 4 to 6 effective bits; however, this accuracy depends upon the frequency components of the input signal. The number of effective bits can be as much as 8 for some of the lower frequencies which are below 10 megahertz and as low as 4 to 6 effective bits for frequencies nearing 250 megahertz.[1]

Digitizer Operation

The 6880 digitizer is able to acquire data at such a high rate (1.348 gigasamples per second) by utilizing an array of charged-coupled devices (CCDs). The CCDs act as a first in/first out (FIFO) register for the analog data before it is converted to digital data. The CCD array is organized in 32 leaves of 320 CCD cells each. The analog input data is demultiplexed so that each demultiplexed data channel contains a 1/32 phase sample of the input data. By demultiplexing the input data into thirty-two phases, the clocking rate of each of the phases is 1/32 of the sample rate. (With a sample rate of 1.348 MHz, each phase has a clocking rate of 42.125 MHz.) By utilizing the thirty-two phases, LeCroy is able to reduce the rate that the data is clocked into the CCD array. This reduction brings the clocking rate down to a level where the CCDs can be used.

During a typical operation, the digitizer stops clocking samples into the CCD leaves after 10,240 data samples (at 42.125 MHz) and begins to clock the data out of the CCD leaves at 62.5 kilohertz. The data being clocked out of the CCD leaves is multiplexed to have an effective sample rate of 2 megasamples. The 2-megasample data is digitized by a 12-bit analog-to-digital converter and stored in temporal sequence in the data memory. The data memory in the 6880 digitizer module is 16K of 16-bit words. It is battery backed so that the data will remain valid in the digitizer even if power is removed from the CAMAC crate. Only 10,240 words of the 6880 data memory are used for the storage of data. The remainder of the memory in each of the digitizers is used to store information that is used in the post processing of the acquired data.

Once the acquired data is digitized and stored in the 6880 data memory, the raw data is read from the digitizer via the CAMAC dataway. The raw data that is generated by the digitizer has inherent errors. These errors are of such a magnitude that some post processing must be performed before the acquired signal can be recognized in the data (refer to Figure 2).

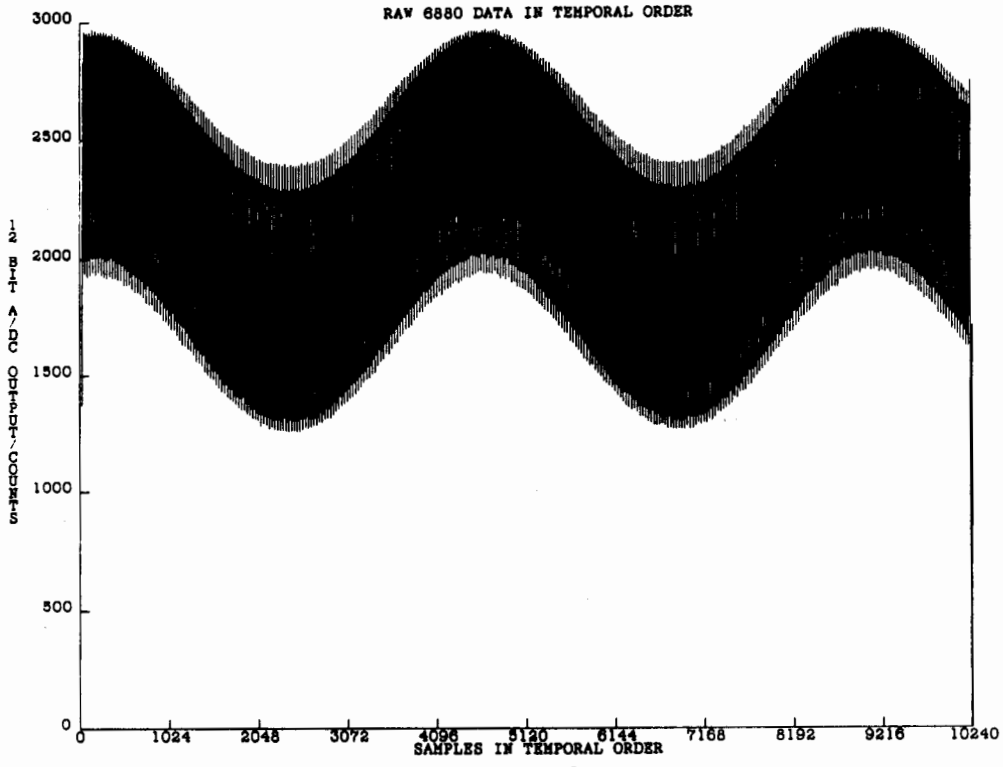

Figure 2

Raw 6880 Data in Temporal Order

[1] A substantial amount of work has been done to characterize the 6880 Digitizer's operation by Mark Dunham, EG&G Energy Measurements in Los Alamos, New Mexico for Los Alamos National Laboratory.

Data Errors

There are several sources for these errors in the data. Among the most prominent are 1) dc offset, 2) dc gain, and 3) dc droop errors. The first error, dc offset, has the most profound affect on the data. (This error is independent of the internal dc offset that can be summed with the input signal and controlled by commands to the digitizer via the CAMAC data bus.) According to LeCroy, this dc offset is generated in the CCDs and their associated drivers. The dc offset error in each of the leaves is relatively constant and does not have any dependence upon the leaf number (0-31) within a digitizer or between digitizers (refer to Figures 3a and 3b).

A second error present in the raw data is generated by a dc gain error. This error, like the dc offset error, is also relatively constant within each CCD leaf. The dc gain error is due to errors in the gains of the CCD's and their associated drivers.

A third error generated by the 6880 during data acquisition is a dc droop error. This error is due to the amount of time that the incoming data is stored in the CCDs. For example, when a sample of data is stored in its analog form in the CCD leaf, a small amount of the stored charge is lost due to leakage; this leakage is similar to the amount of leakage in a capacitor where a charge is stored. Because the data samples are shifted into the CCDs at a faster rate than they are shifted out, each data sample within a leaf spends a different amount of time within the CCD. The first samples that are shifted in are the first to be shifted out of the CCD; the last samples shifted in the data record are the last to be shifted out of the CCD. These latter samples are shifted out of the CCD at the slow rate last, which means that the latter samples spend more time in the CCD array and therefore exhibit more leakage than the earlier samples. This leakage effect appears as droop in the digitized data. Because each sample spends a different amount of time within the CCD leaf, and the amount of time that a sample spends in the CCD leaf depends upon its position within the leaf, the droop remains relatively constant from the first to the last point in the leaf, but is different between CCD leaves.

Beside the dc errors, nonlinearities that are generated in the data by the input and output drivers to the CCDs are also present in the data.

Data Corrections

To correct these errors in the 6880 digitized data, a correction algorithm developed by LeCroy is used. These corrections are performed by using data that parameterizes each of the errors. This parameterized data is collected from the digitizer by using the internal dc offset of the digitizer. The inputs to the 6880 can be disabled internally via commands over the CAMAC bus. To collect parameterized data, the inputs of the 6880 are disabled. The internal dc offset is then set to the desired level, and the digitizer is armed and triggered via the CAMAC bus. Next, selected data points are collected from the data. The data points selected are thirty-two points from near the front of each CCD leaf, but skipping the first ten points in the leaf. There are also thirty-two points selected from the rear of each leaf so that the last point collected is ten points from the end of the leaf. The associated cell numbers for each CCD leaf are listed below.

$$Fmin = 10 \quad (1)$$

$$Fmax = 41 \quad (2)$$

$$Rmin = 278 \quad (3)$$

$$Rmax = 309 \quad (4)$$

Fmin is the cell number of the first point of data taken from the front of the leaf; Fmax is the cell number of last point of data taken from the front of the leaf; Rmin is the cell number of first point of data taken from the rear of the leaf; and Rmax is the cell number of last point of data taken from the rear of the leaf.

These selected data points are used to generate the correction coefficients that are used to correct the raw data in the 6880. The dc offset, dc gain, and dc droop are corrected by setting the internal dc offset to -150 mV. Initially, the digitizer is armed and triggered. Then, thirty-two data points from the beginning of each of the thirty-two leaves are read. This step is accomplished by reading selected data points from the digitizer memory where the position of the data in the memory is directly related to the originating cell and leaf of the data point. The thirty-two points collected from each of the leaves are averaged so that thirty-two numbers are generated that represent an average position of the data at the beginning of each leaf when -150 mV are applied to the input; these averages are stored in the upper portion of the digitizer memory above the 10,240 data memory locations. Next, thirty-two consecutive points from each of the thirty-two leaves are selected from the rear of each CCD leaf. As with the points selected from the front of each leaf, the thirty-two data points from each leaf are averaged, generating a number that represents the position of the data at the end of each of the leaves when -150 mV are applied to the input. These thirty-two averages are stored in the upper portion of the digitizer's memory.

The digitizer's internal dc offset is then set to +150 mV, and with the inputs disabled, the digitizer is armed and triggered via the CAMAC bus. Data is then collected, averaged, and stored from the front and rear of each of the CCD leaves.

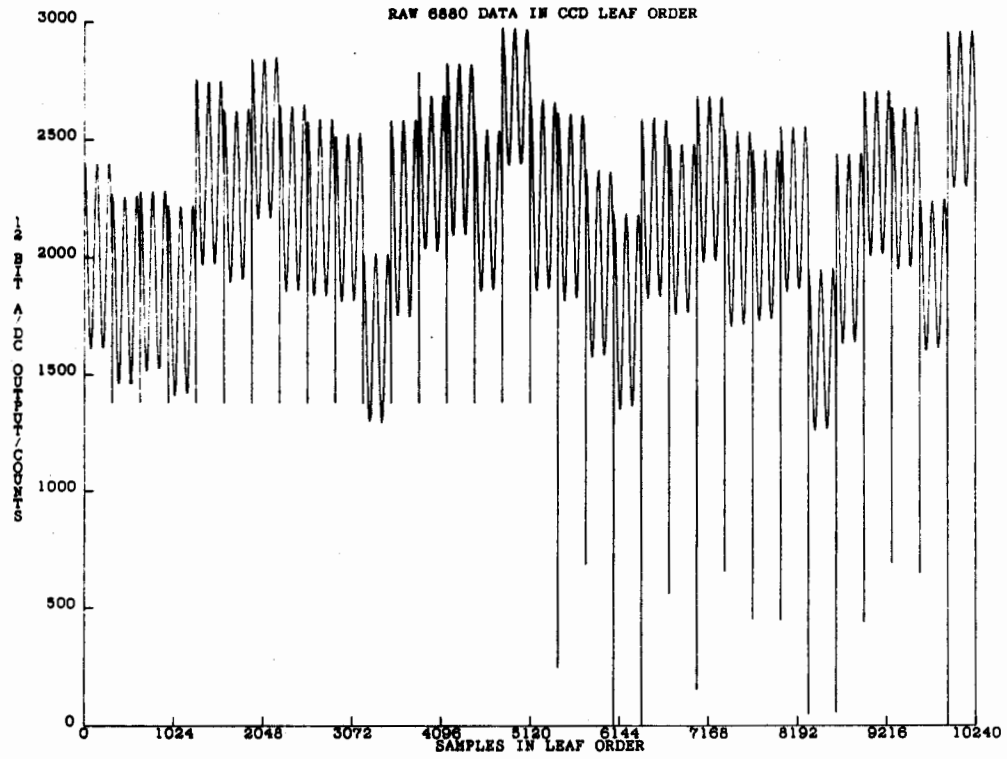

Figure 3a

Raw 6880 Data in CCD Leaf Order

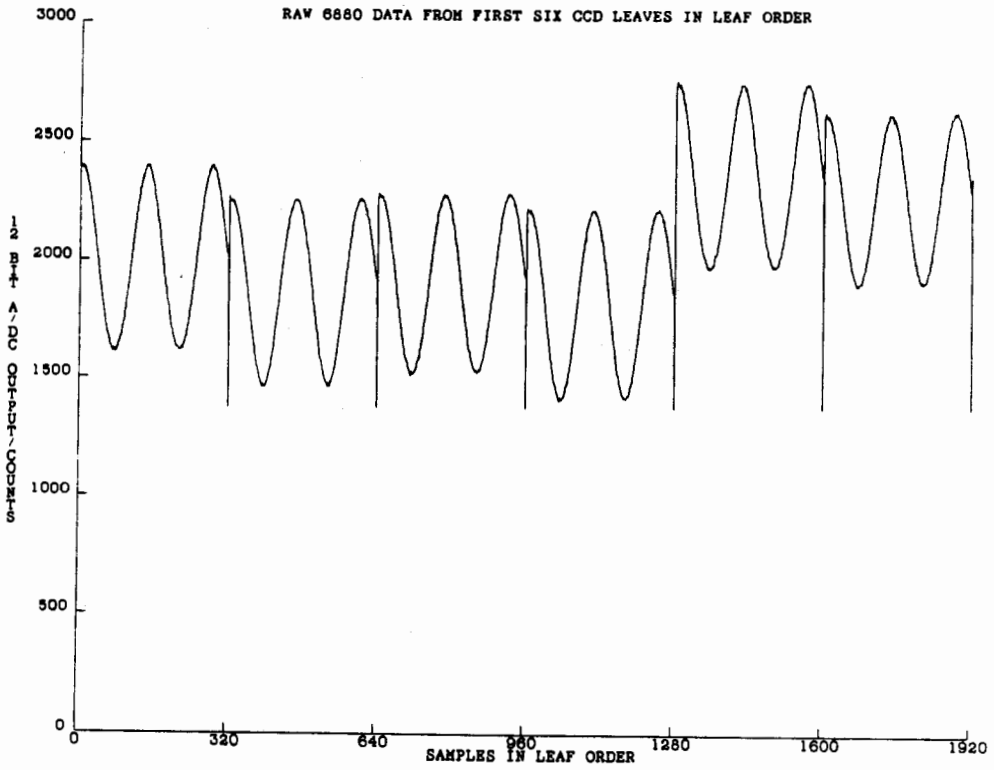

Figure 3b

Raw 6880 Data From Fist Six CCD
Leaves in Leaf Order

The four averages listed below, which represent the data levels read from each of the CCD leaves, are used to generate correction coefficients.

$$PFav = \Sigma PFi + 32 \qquad 10 \leq i \leq 41 \qquad (5)$$

$$PRav = \Sigma PRi + 32 \qquad 278 \leq i \leq 309 \qquad (6)$$

$$NFav = \Sigma NFi + 32 \qquad 10 \leq i \leq 41 \qquad (7)$$

$$NRav = \Sigma NRi + 32 \qquad 278 \leq i \leq 309 \qquad (8)$$

PFav and PRav are the +150 millivolt averages from the front and rear of the CCD leaf, respectively, with PFi and PRi representing the data collected from the leaf at the +150 millivolt level; N is the number of points taken from each of the sections of the CCD leaf. Equations 7 and 8 calculate the averages for the CCD leafs -150 millivolt data.

By drawing a line that intersects the two points designated by the averages, the slope and the y-intercept of the line can be calculated.

$$MP = (PFav - PRav) + (XF - XR) \qquad (9)$$

$$YP = PFav - MP \cdot XF \qquad (10)$$

MP is the slope generated by the +150 millivolt front and rear averages, with XF and XR being the effective location represented by the averaging of the data. YP is the y-intercept of the +150 millivolt data.

The slope and y-intercept is also calculated for the -150 mV averages from each leaf.

$$MN = (NFav - NRav) + (XF - XR) \qquad (11)$$

$$YN = NFav - MN \cdot XF \qquad (12)$$

Using the y intercept from both the -150 mV and the +150 mV, the gain correction coefficient is calculated.

$$Gain = R + (YP - YN) \qquad (13)$$

R is the output range from +150 millivolts to -150 millivolts for an A/D converter with no gain error.

The dc offset and droop can also be calculated using the slope and y-intercept.

$$Offset = (YP - YN) + 2 \qquad (14)$$

$$Droop = MN \qquad (15)$$

These correction coefficients are used to correct the raw 6880 digitized data for the dc offset, dc gain, and dc droop errors.

$$Ci = Di \cdot Gain + Offset + Droop \cdot i \qquad (16)$$
$$0 \leq i \leq 319$$

Ci is the corrected data value, and Di is the raw data value.

Once these errors have been corrected, the information in the 6880 data usually is visible (see Figures 4a and 4b). With these corrections implemented, the data from the 6880 gives about 4 to 5 effective bits. To increase the number of effective bits, additional corrections are implemented.

Among the additional corrections that can be implemented is a correction algorithm used to correct for the nonlinearities and also to expand the effect of the previously implemented corrections. This expansion is necessary because the dc offset, gain, and droop correction are optimized at the plus and minus 150 mV levels. As the input signal varies from these levels, the effect of the correction is minimized because of nonlinearities generated by the CCD drivers. To correct these nonlinearities, a set of data is collected at seventeen dc voltage levels. These seventeen levels are evenly-spaced voltages that range from the minimum to the maximum voltage ranges of the digitizer. Since the input voltage range of the 6880 digitizer is 500 mV, the seventeen voltage steps are separated by 31.25 mV each. At each level, the 6880 digitizer's internal dc offset voltage is set to the desired level (31.25 mV higher than the previous level). The first dc offset level setting is -250 mV. After the dc offset is set, the digitizer is armed and triggered with the inputs disabled. After the digitizer has completed the digitizing, thirty-two points from the beginning of each of the thirty-two leaves are collected. The average of each of the thirty-two points within the leaf is calculated, and the averages for each of the CCD leaves are stored in the upper portion of the memory in the 6880. This process is repeated for each of the seventeen dc levels until the averages for the +250 mV are stored. This data is then used to correct the data that has already been corrected to dc offset, gain, and droop.

The correction of the 6880 data using the calibration data is performed primarily on a VAX-11/750 computer located at a remote data collection facility. The calibration procedures are implemented in the CAMAC crate where the 6880 digitizers and the rest of the FCDNA data acquisition system resides.

EXISTING FCDNA INSTRUMENTATION SYSTEM

The existing FCDNA digital data acquisition system comprises the following equipment:

- a CAMAC Crate
- a KineticSystems 3905 CAMAC Crate Controller
- an EG&G N-EM-101 DES Formatter
- an EG&G N-EM-102 DES Interface Unit

The CAMAC crate and the 3905 Crate Controller are available commercially. The 3905 Crate Controller normally operates in conjunction with a 3885 microcomputer module; however, in the FCDNA systems, a state machine in the DES Formatter module provides local system control.

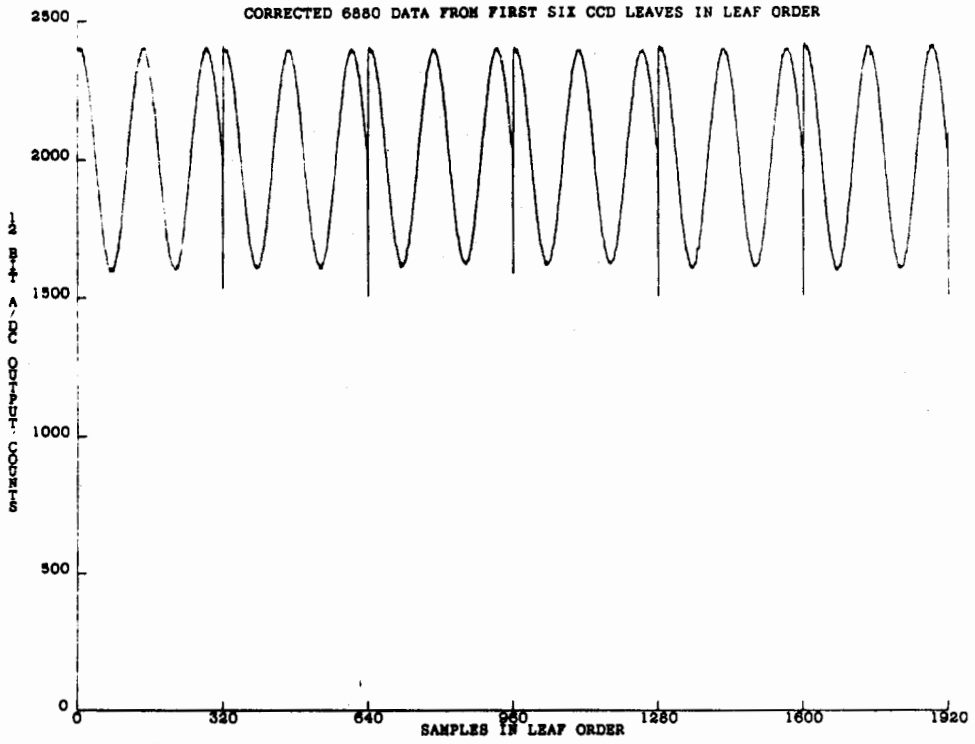

Figure 4a

Corrected 6880 Data From Fist Six
CCD Leaves in Leaf Order

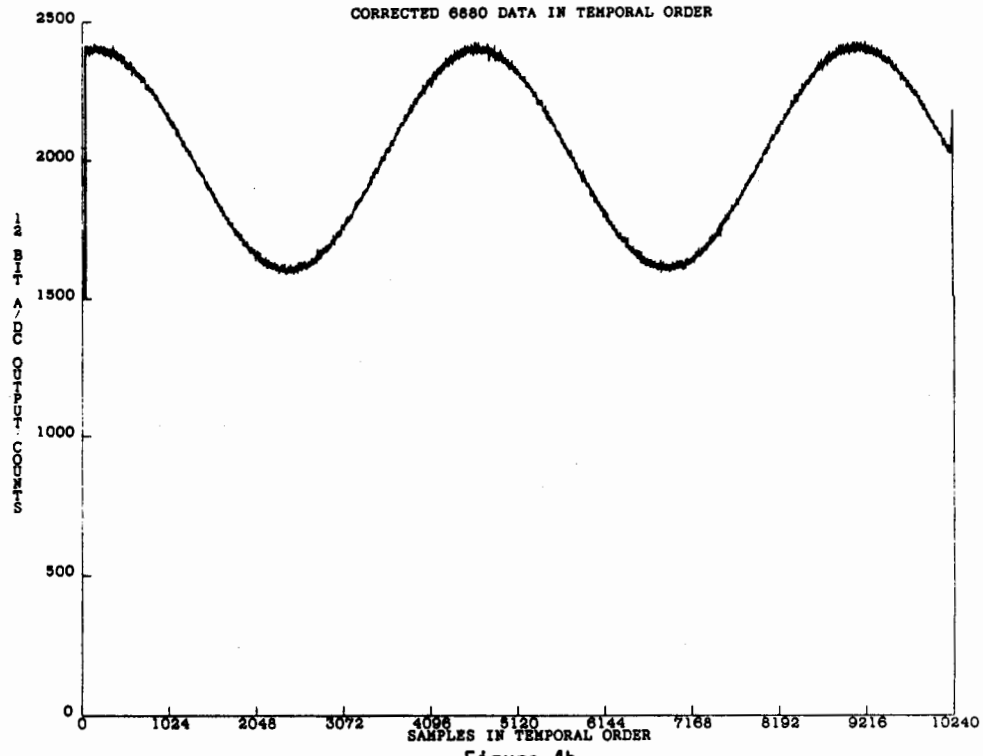

Figure 4b

Corrected 6880 Data in Temporal Order

The DES Formatter is a three-slot wide CAMAC module comprised of two printed circuit boards. The board residing in the left half of the module is the formatter. The circuitry on this board receives data from a rear auxiliary connector and formats it for transmission to a remote data recording facility. The board on the right side of the DES Formatter is the state machine; the state machine is connected via a 50-pin connector to the 3905 Crate Controller. The state machine in the DES Formatter executes a state program that is stored in 2716 EPROMs and sends commands according to the program to the 3905 Crate Controller. The crate controller then executes the commands over the CAMAC bus. Using the state machine, sequences of commands can be executed over the CAMAC bus to control the digitizers that are in the CAMAC crate.

The DES Interface Unit (IFU) provides an interface between the external world and the state machine in the DES Formatter. By way of either front panel switches or sense lines on a rear auxiliary connector, the state machine can receive commands and perform the necessary functions. Also, with a set of front panel LEDs and relay contacts connected to the rear panel auxiliary connector, the IFU can communicate the status of the state machine program.

Problems Integrating the 6880 Digitizer

The integration of the LeCroy 6880 Digitizer into the FCDNA data acquisition system requires more sophisticated control than can be provided by the state machine in the DES Formatter. To perform the droop, offset gain, and linearization corrections, 42 Kbytes are collected from each of the digitizers. With four digitizers in the system, 168 Kbytes of data are collected. Besides storing the calibration data in the CAMAC crate where the digitizers reside, storage must be provided at the remote data collection facility.

At the remote data collection facility, all of the calibration data used to calculate the correction coefficients must be stored in a 64 Kbyte block of memory. The 168 Kbytes of data collected during the calibration of the digitizers exceeds the 64 Kbyte block size for the calibration data in the remote data collection memory. However, if the averages are calculated for each calibration operation in the CAMAC crate, the amount of data changes from 42 Kbytes to 1340 bytes per digitizer. This reduces the total amount of data for four digitizers from 168 Kbytes to 5.36 Kbytes.

The existing FCDNA hardware (the IFU and the DES Formatter with its state machine) cannot provide the averaging function. In addition, the calibration operation is so complex that it cannot be performed reliably in the state machine because of the limited storage capability. The calibration can be performed more simply if the state machine is provided with additional temporary storage registers. This is accomplished using the Auxiliary Formatter module. (The entire DES-7 system including the remote data collection facility are shown in Figure 5a and 5b.)

AUXILIARY FORMATTER MODULE

The Auxiliary Formatter module, a single-wide module with a GPIB interface connector on the front panel, simply enhances the capabilities of the state machine and provides for the necessary storage and calibration process necessary in the CAMAC environment. (A block diagram of the Auxiliary Formatter is shown in Figure 6.) The core of the Auxiliary Formatter is the TMS32010 Digital Signal Processor (DSP). The DSP shares a set of registers with the CAMAC bus, and it is with these registers that the DES Formatter state machine can use the arithmetic and logic functions of the DSP. Among the functions that the Auxiliary Formatter can perform for the state machine are logical functions such as AND, OR and COMPARE and math functions such as add, subtract, multiply, and divide. Also, the Auxiliary Formatter can perform the averaging required for the calibration of the 6880 data. The DSP additionally provides the necessary corrections to the 6880 data so that the corrected data can be transmitted via the GPIB bus for local display. The state machine in the DES Formatter uses the functions in the Auxiliary Formatter by sending commands to it via the CAMAC bus.

Communication between the state machine and the DSP is accomplished using the sixteen 24-bit shared registers. The state machine sets up the shared registers and then sends a command to the Auxiliary Formatter. In the Auxiliary Formatter, the DSP interprets the command, retrieves the necessary data from the shared registers, performs the function, and stores the result back in the shared registers. After the DSP has completed the operation, the state machine can retrieve the results of the function from the shared registers.

The 16 Kword by 16-bit data memory in the Auxiliary Formatter is battery backed. This memory is used by the DSP as a buffer for the GPIB data transfers and communications, as temporary storage of data during the 6880 data correction process, and as work space for the arithmetic and logic functions.

Another function performed by the DSP is the control of the GPIB port. Three types of operations are performed over the GPIB port. These functions include a) receiving CAMAC commands that will be implemented by the state machine, b) transferring data from a module in the CAMAC crate, and c) transferring corrected data to a module in the crate. A provision for plotting in a local environment is also provided for the technician who is installing the DES-7 system. The technician uses the plotting feature to look at data from the digitizers locally and to check the validity of the installation and the operation of the digitizers.

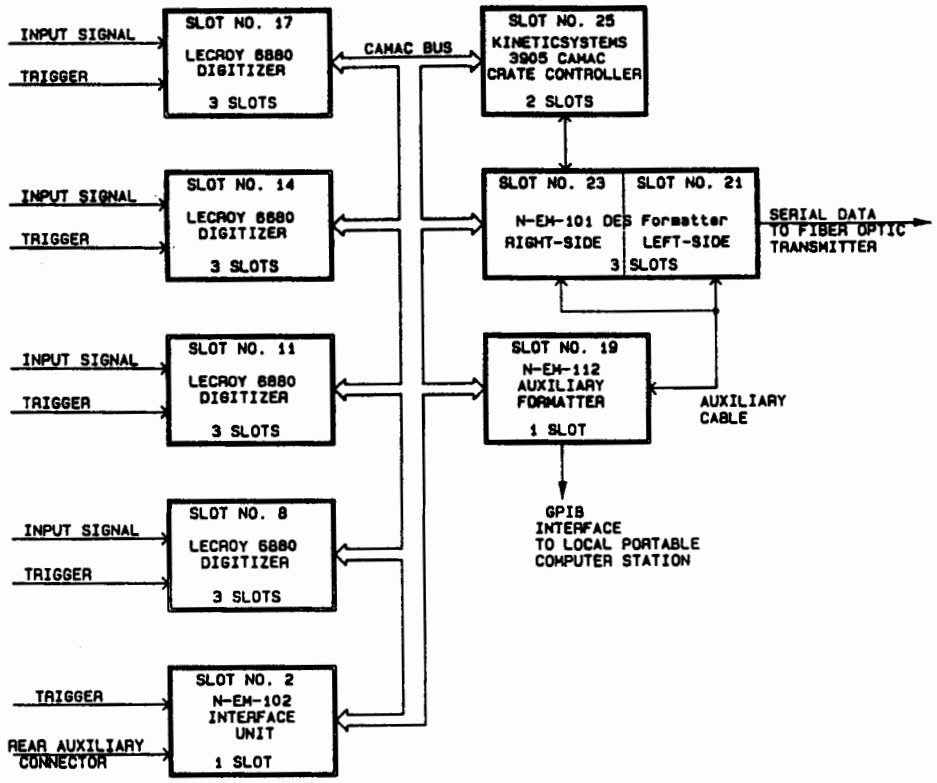

Figure 5a

Functional Block Diagram of the DES-7 System

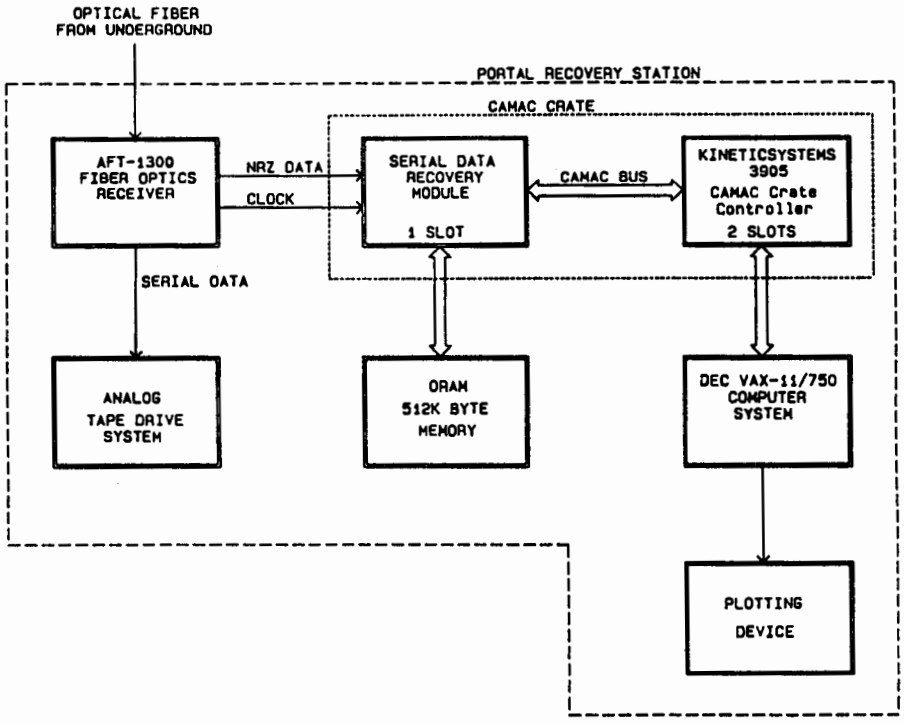

Figure 5b

Functional Block Diagram of the FCDNA System
Remote Data Collection Facility

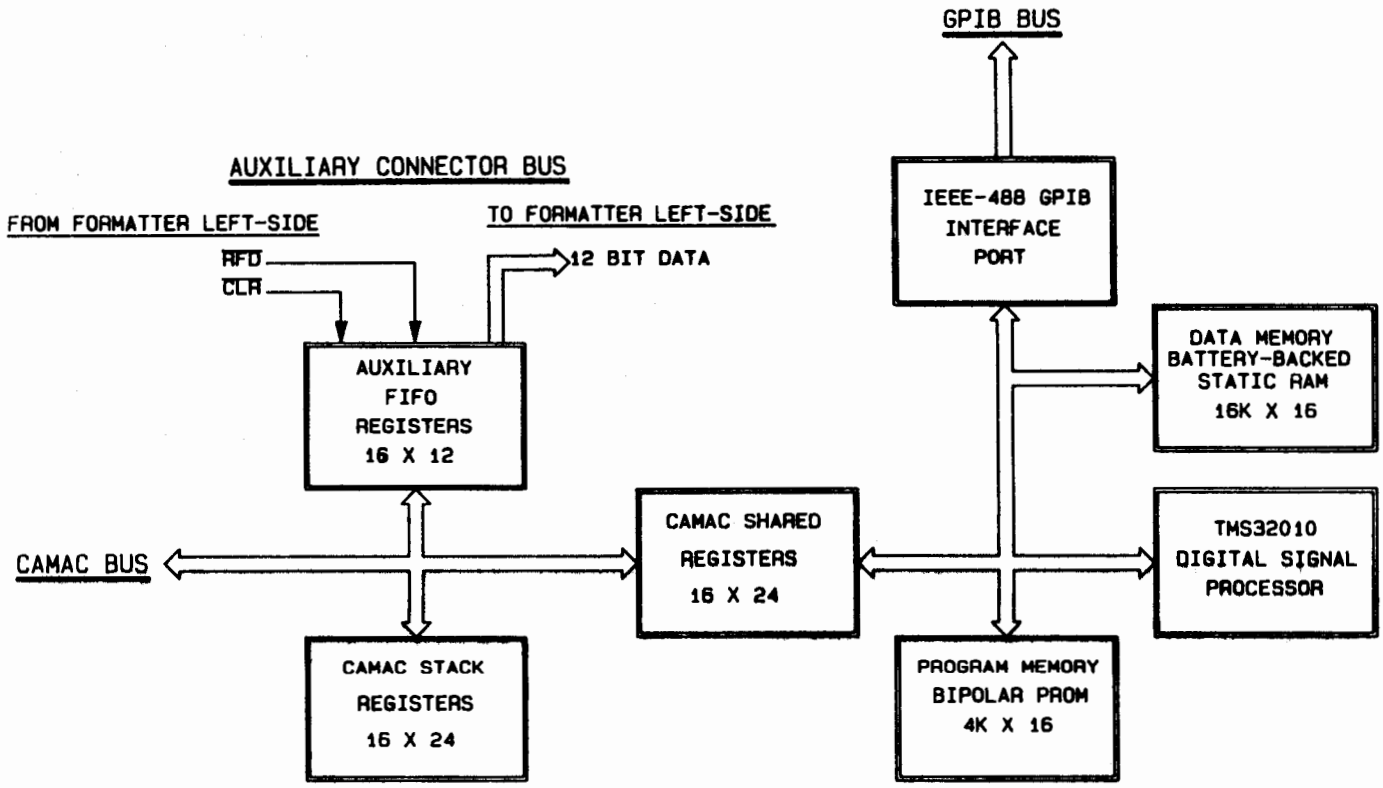

Figure 6

Functional Block Diagram of the Auxiliary Formatter

The auxiliary FIFO register, located in the Auxiliary Formatter, provides an interface between the left-side board of the DES Formatter, which formats the data to be transmitted from the CAMAC crate, and the remote data collection facility and the CAMAC bus. The left side of the DES Formatter retrieves data over an auxiliary rear connector. The Auxiliary Formatter provides the necessary path between the CAMAC bus where the 6880 data is read and the rear auxiliary connector of the DES Formatter. Also, the transfer of data into the left side of the DES Formatter is asynchronous to the operation of the state machine. Its timing is based upon the transfer rate of the serial data being transmitted. Hence, the data read from the 6880s is written into the FIFO by the state machine at a rate which is consistent with the data cycle time of CAMAC instructions and the state machine program. The data is then read out of the FIFO by the left side of the DES Formatter at a rate that is based upon the transmission rate of the data being transmitted to the remote data collection facility. The data is always clocked out of the FIFO at a slower rate than the rate the data is being clocked into the FIFO from the CAMAC bus.

Additionally, one more set of registers, 16-word deep by 24-bits, is available. The state machine uses this set of registers to store data temporarily by pushing it to the stack via the CAMAC data bus and then retrieving the data by popping it off the stack.

DES-7 SYSTEM OPERATION

In the DES-7 system, the state machine program is written to control the sequence of events that occur during a test. First, the state machine sets the digitizers to their initial conditions, which involves setting the dc offset, enabling the inputs, and setting the trigger time delay. Once the initialization is complete, the state machine waits for an indication from the IFU to begin the calibration process. When the signal to start the calibration has been received, the state machine sequences through the steps required to perform the calibration data collection on each 6880 digitizer in the CAMAC crate. During the calibration process, the state machine uses the capabilities of the Auxiliary formatter to collect the points from each leaf and to calculate the average. Each average is then read out of the Auxiliary Formatter and stored in the unused portion of the digitizer memory. Upon completion of the calibration procedure, the state machine begins transmitting the calibration data to the remote data collection facility. The state machine repeatedly transmits the calibration data to the remote data collection facility until it receives the ARM signal from the IFU. When the ARM signal has been received, the state machine quits sending the calibration data to the remote data collection facility, arms the digitizers, and waits for the trigger signal. After the trigger signal has been received, the state machine begins sending the digitized data to the remote data collection facility. The state machine continues sending the digitized data to the remote data collection facility until it is reset.

If the user wants to collect data from the digitizer locally, corrected digitizer data can be retrieved from the system via the GPIB bus. When the system is sitting in the ready state, and a command is received from the GPIB bus requesting corrected 6880 digitizer data, the state machine will be alerted of the request by the Auxiliary Formatter. (This is the state that the system is in when it is waiting for the start calibration signal. The system goes to this state after it has been reset.) The state machine then sends the data from each digitizer to the Auxiliary Formatter where the Auxiliary Formatter corrects the data for droop, offset, and gain before sending the corrected data out over the GPIB bus.

CONCLUSION

The development of the Auxiliary Formatter in the DES-7 system has made possible the integration of the LeCroy 6880 Digitizers into the existing FCDNA data acquisition system without the unnecessary development of a new set of major components. By identifying the portions of the existing system that could not handle the needs of the 6880 Digitizers, and by providing for these capabilities with a single module, the development costs were kept at a reasonable level and the impact to the overall FCDNA system was kept to a minimum. Additionally, the programmability of the digital signal processor used in the Auxiliary Formatter allows for future enhancements to the system without the overhead that would be required by additional hardware changes to the system. The development of better correction algorithms for the 6880 Digitizer still continues. As better methods for correcting the data are developed, the DES-7 system, specifically the Auxiliary Formatter, will be reprogrammed to take advantage of these advancements.

BIBLIOGRAPHY

The Digital Encoding System (DES) Programmer's Manual, EGG-10282-1022. EG&G Energy Measurements, May 1983.

Digital Encoding System (DES) Formatter N-EM-101 Manual, EGG-10282-1027. EG&G Energy Measurements, August 1983.

Digital Encoding System (DES) Interface Unit N-EM-102 Manual, EGG-10282-1028. EG&G Energy Measurements, August 1983.

CAMAC Instrumentation and Interface Standards Manual. Institute of Electrical and Electronic Engineers, Inc., 1975.

Model 3905 Crate Controller Manual. KineticSystems, May 1985.

INTEGRATING THE LECROY 6880 WAVEFORM DIGITIZER INTO AN EXISTING INSTRUMENTATION SYSTEM

Q: Joe Costanza: You mentioned that the IEEE data that comes out of the crate is corrected. What about the bit-stream information that comes out?

A: Jack Carrel (EG&G Energy Measurements, Inc.): It is not corrected there because there isn't time.

IMPLEMENTATION OF DIGITAL SIGNAL PROCESSING FUNCTIONS IN A CAMAC MODULE

Thomas S. Pounds
Electrical Engineer
DoD Engineering/Operations Department
EG&G Energy Measurements

ABSTRACT

A new module has been developed by EG&G Energy Measurements in support of the Field Command Defense Nuclear Agency for use in processing digitized signals and communications via an IEEE-488 General Purpose Interface Bus (GPIB). The module, called the Auxiliary Formatter, is a single-wide Computer Automated Measurement And Control (CAMAC) module that utilizes a TMS32010 Digital Signal Processor Integrated Circuit. The Auxiliary Formatter module is used primarily for correcting digitized data from a LeCroy 6880 Waveform Digitizer, but may also be used for many other DSP applications including active filtering, correlating, and fast Fourier transforming. Additionally, the module can be used as a general interface between the CAMAC and the GPIB bus.

INTRODUCTION

The Auxiliary Formatter module was originally developed for correcting digitized data from a LeCroy 6880 Waveform Digitizer; however, it has enormous possibilities for other functions using the TMS32010 digital signal processor (DSP). The DSP has the capability to perform finite impulse response (FIR) and infinite impulse response (IIR) filters, fast Fourier transformers (FFTs), and correlators. With the hardware in its current configuration, there is also the possibility of transferring some of the functions of EG&G Energy Measurement's N-EM-101 Formatter to the new module, hence the name Auxiliary Formatter. Some of these functions include math and Boolean functions, general-storage registers, and a stack for implementing subroutines in the formatter. CAMAC commands may also be initiated by the Auxiliary Formatter via the GPIB bus.

This paper will describe some of the possible functions of the Auxiliary Formatter using CAMAC and DSP applications. Certain considerations inherent in DSP applications will also be discussed. These considerations encompass 1) filter length vs. speed of filter and their effects on filter accuracy vs. computation time, 2) memory usage problems, and 3) interfacing to a large computer for mass storage and analysis.

HARDWARE DESCRIPTION

The Auxiliary Formatter is a single-wide CAMAC module with three external data paths, a CAMAC bus interface, a GPIB bus interface, an auxiliary connector interface, and a TMS32010 digital signal processor (DSP). The DSP and its associated memory provide the Auxiliary Formatter with the ability to perform signal processing on data, to execute logic and math functions for the CAMAC and GPIB buses, and to control the operations of the GPIB bus interface. Figure 1 shows a functional block diagram of the Auxiliary Formatter.

The CAMAC bus and the DSP communicate via a set of 16-word by 24-bit shared registers. These registers can be individually addressed to perform read or write operations by either the CAMAC bus or the DSP. The Auxiliary Formatter also has a register stack for the CAMAC bus. This register stack of 16 words by 24 bits can be used by the CAMAC bus to store data temporarily, but can only be accessed via the CAMAC bus.

An auxiliary first in/first out (FIFO) register provides a data path and synchronization between the Auxiliary Formatter and the auxiliary rear connector. This interface is used to transfer data to devices that do not have a CAMAC or GPIB data path.

The Auxiliary Formatter is housed in a CAMAC crate containing a digitizer such as the LeCroy TR8828 Digitizer or a data logger such as the LeCroy TR8212A Data Logger, a KineticSystems Model 3905 Crate Controller, and an EG&G N-EM-101 Formatter. The N-EM-101 Formatter is composed of two halves: the left side is a data frame formatter that

*This work was supported by the U.S. Department of Energy under Contract No. DE-AC08-83NV10282.

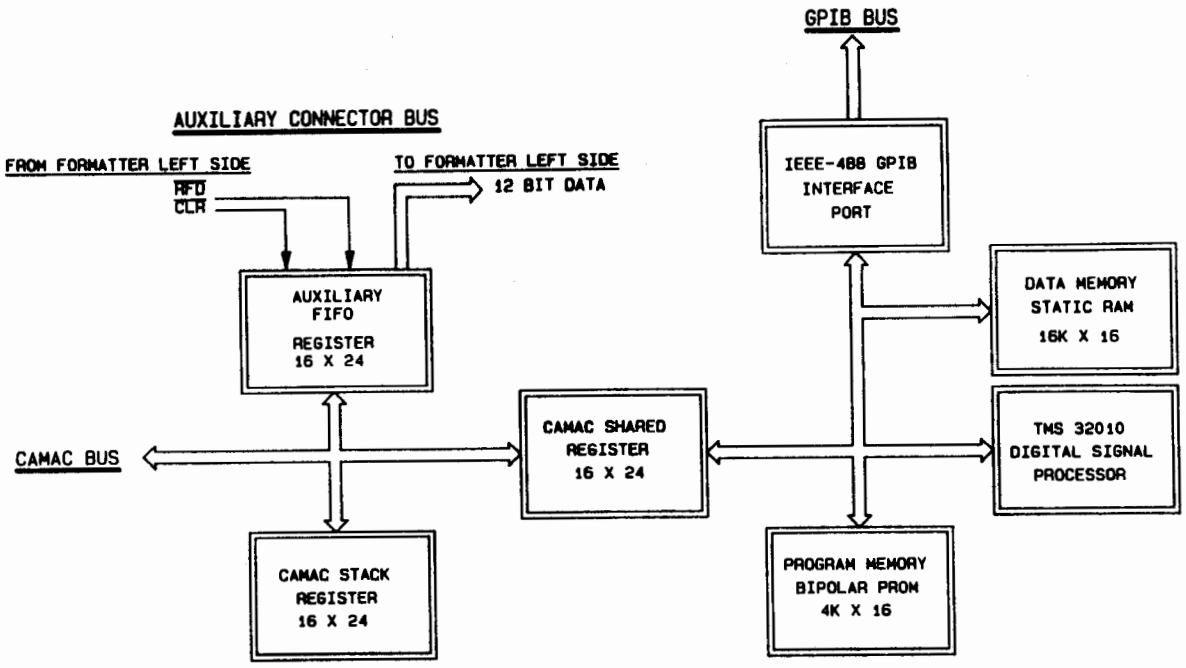

Figure 1

Auxiliary Formatter Functional Block Diagram

converts parallel data into serial frames and transmits either manchester code or NRZ and clock; the right side is a state machine with program memory and a small instruction set for producing CAMAC commands. The formatter right-side must be used with the crate controller for cabling, timing, and protocol requirements.

The formatter state machine has two write-only registers that can be incremented, one data register, and one compare register that doubles as a mode-control register. The crate controller contains two general-purpose registers and the registers for the CAMAC commands: data (read and write), slot (N), subaddress (A), and function (F). The two general-purpose registers are used by the state machine as temporary storage. The state machine has 2K of EPROM program memory and a small instruction set for reading and writing to the various registers. CAMAC commands may be issued to the other modules in the crate by writing to the N, A, and F registers in the crate controller. In addition, the state machine has a jump instruction for programming and a jump-if-compare instruction. There are also two jump instructions that execute a jump if the write-only registers are equal to 0.

The system data flow is diagrammed in Figure 2. Data from the digitizer flows to a buffer or memory and then through the formatter to a data recorder. The data flow is controlled either by CAMAC commands or by timing signals from the formatter and may travel over the CAMAC bus or over an external connector between modules. The Auxiliary Formatter may be placed in line between the digitizer and the formatter to perform DSP functions. If DSP functions are not desired, the Auxiliary Formatter can be placed elsewhere in the crate to act as an interface between the GPIB bus and the CAMAC bus.

CAMAC INTERFACE APPLICATIONS

The Auxiliary Formatter module can be utilized as a general-purpose CAMAC interface in several applications.

GPIB Interface Applications

One CAMAC-GPIB interface application uses a special routine under state machine control to generate CAMAC commands for the GPIB interface. The CAMAC commands are generated by the external GPIB controller for routing through the Auxiliary Formatter to the state machine. To accomplish this process, the state machine periodically polls the Auxiliary Formatter for a command that has been received from the GPIB bus. If a command is present, the state machine then performs the command and continues with its particular process, which includes polling the Auxiliary Formatter.

Another useful application for the Auxiliary Formatter is to act as a router between the CAMAC bus and the GPIB bus. As an example, a GPIB controller, issuing commands via the GPIB bus, sets up a CAMAC-based digitizer for offset, sampling speed, pre-trigger ration, and memory length (each a separate CAMAC command). Next, it triggers the digitizer (another CAMAC command) and reads n words of data (n CAMAC commands). The data is then read into mass storage for further processing or for transfer to a larger computer system.

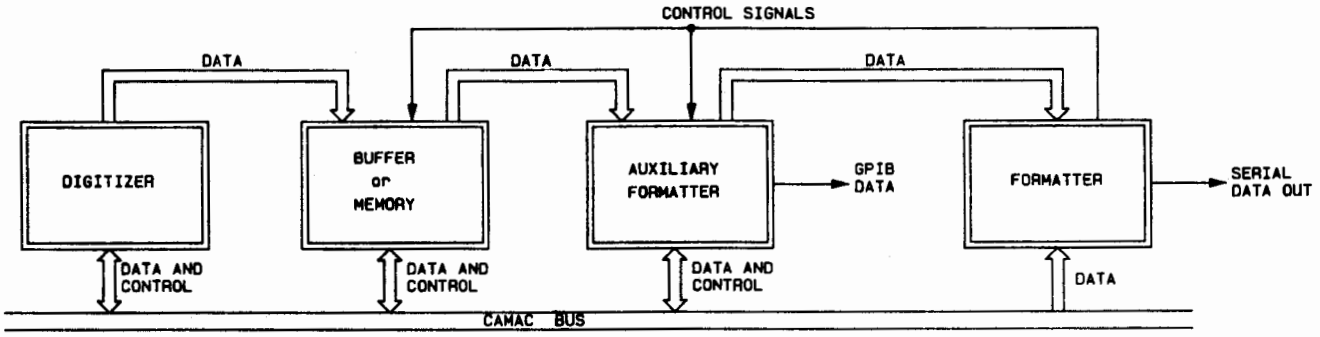

Figure 2

Data Flow Diagram (General)

Formatter State Machine Applications

The Auxiliary Formatter may also be used to augment the capabilities of the state machine using the CAMAC interface. The state machine has a small instruction set, but has no capability to perform math functions; instead, the Auxiliary Formatter performs the math functions such as addition, subtraction, and Boolean logic. Results of these functions are transferred from the Auxiliary Formatter to the state machine to use in its program. The following functions may be performed in the Auxiliary Formatter:

16-bit addition
16-bit subtraction
16-bit compare
16-bit logical and
16-bit logical or
16-bit logical xor
16-bit logical shift left/right
16-bit increment
16-bit decrement
16-bit logical not
16-bit logical and with compare for more than one bit
LeCroy 6880 Digitizer correction functions
GPIB interface functions

The following example illustrates the efficiency of the Auxiliary Formatter in comparison to the state machine: Normally for the state machine to perform a simple bit compare on an 8-bit byte, it must first read the data to compare than load the compare register with every possible combination of bytes in which the bit is set. In general, this is 128 loads and 128 compares (jump-if-compare) or over 256 instructions. By delegating the compare function to the Auxiliary Formatter, the number of instructions in the state machine is reduced to only 20 instructions for data transfer, a small wait loop, and one jump-if-compare instruction.

In addition to these functions, there is also a 16-deep 24-bit word stack in the Auxiliary Formatter for storage use or for implementing subroutines. A push and pop instruction in the Auxiliary Formatter implements the stack function.

DIGITAL SIGNAL PROCESSING APPLICATIONS

Additionally, the Auxiliary Formatter has the capability to use FIR and IIR filters in digital signal processing applications. The general theory and formulas for this use are described in this section followed by several real-time, transient, and frequency domain applications.

Basic Filter Theory

A finite impulse response (FIR) filter may be represented by equation (1) below:

$$y(n) = \sum_{j=0}^{N} b_j x(n - j) \qquad (1)$$

Where (N+1) is the length of the filter.

If the unit sample response of the filter is denoted by h(n) then making the substitution into $h(n) = b$ into equation (1), the results are:

$$y(n) = \sum_{j=0}^{N} h(j)x(n-j) \qquad (2)$$

The previous equation shows that the FIR filter is the finite-length response to the unit sample or the digital equivalent of the unit impulse or dirac delta function. Calculating the h(n) coefficients is fundamental to the filter design process. If the z-transform of y(n), x(n), and h(n) are denoted by Y(z), X(z) and H(z), equation (2) may be written as follows:

$$H(z) = \frac{Y(z)}{X(z)} = \sum_{j=0}^{N} h(j)z^{-j} \qquad (3)$$

Equation (3) shown above may be realized by the diagram in Figure 3 also known as the direct-form FIR filter. Each z represents a delay of one sample and each h(n) represents a multiplication of the x by h. All of the x • h results are added together to make one output point y.

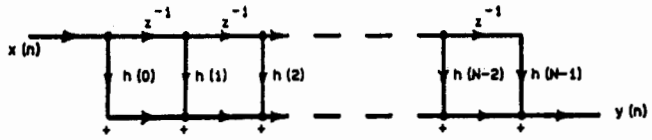

Figure 3

Direct Form FIR Implementation

The DSP makes it simple to implement the direct-form filter using the two powerful instructions: LTD addr and MPY addr. The LTD instruction performs the shifting or delay and the MPY instruction performs the multiplication, the accumulation, and the addition necessary to generate the output points.

Real-time Applications

Figure 4 shows the data flow for a real-time filter application. Data is received from the data logger and input to the Auxiliary Formatter either over the CAMAC bus or via an external connector. The data is then processed and output either on the CAMAC or the GPIB bus. An FIR filter is implemented in the Auxiliary Formatter with the hardware arranged in the data path shown in Figure 4. Sixteen data channels are continuously being sampled by a LeCroy TR8212A Data Logger. When sixteen channels have been sampled, an interrupt is given to the DSP, and it acquires the designated words of data to be filtered. The filter algorithm is then applied and an output word is stored in temporary memory for transfer over a bus. This process is repeated for each of the subsequent data points.

The FIR filter used is an approximation of a 2-pole, low-pass Butterworth filter. The FIR length is 64 points and is selected for speed of computation. The FIR coefficients are derived from equation (4) below, which is the Fourier transform of the transfer function of a 2-pole, low-pass Butterworth filter (1).

$$H(j\omega) = \frac{\omega_0^2}{j\omega^2 + (\omega_0/Q)j\omega + \omega_0^2} \qquad (4)$$

where: ω_0 = the cutoff frequency (20 rad/sec)

Q = 0.7071

The impulse response of this filter is obtained by multiplying equation (4) by the Fourier transform of the dirac delta function (which is 1) and taking the inverse Fourier transform. If the inverse Fourier transform is an inverse FFT, the impulse response is a set of discrete numbers, which is the same as the unit sample response in an inverse z-transform (2).

The impulse response is obtained by computing the inverse FFT of equation (4) for 2048 points. The 2048 points are then depopulated to 64 points and the real value of the complex numbers is taken to reach the resultant FIR coefficients shown in Figure 5.

The length of the filter dictates the maximum speed the data logger can run (2KHz). A shorter length filter will decrease computation time, but reduce accuracy. For a filter with 32 points, the speed will increase to 3.7KHz. A simulation has been done on a DEC VAX-11/750 to show the error and the difference between a 64-point and an analytical-point filter. The results of the simulation are shown in Figure 6.

Figures 7a and 7b show the magnitude and phase response of the filter. Figures 8a and 8b show unfiltered and filtered thermocouple data to illustrate the results of the filter running on the machine.

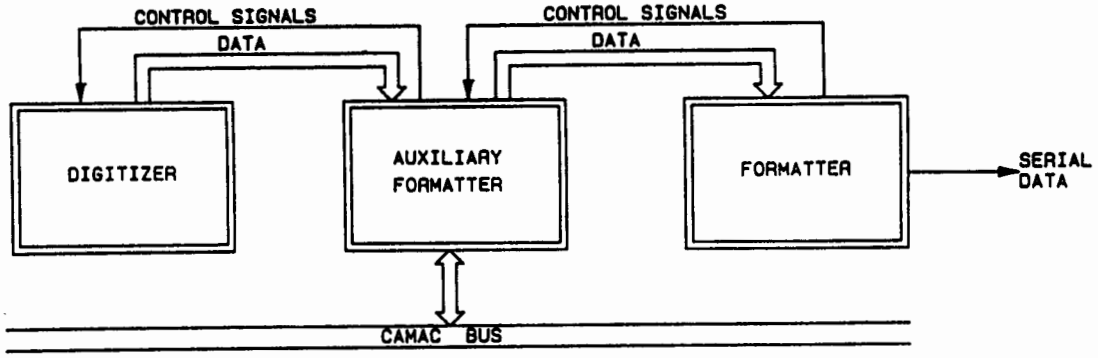

Figure 4

Data Flow Diagram (Real-time)

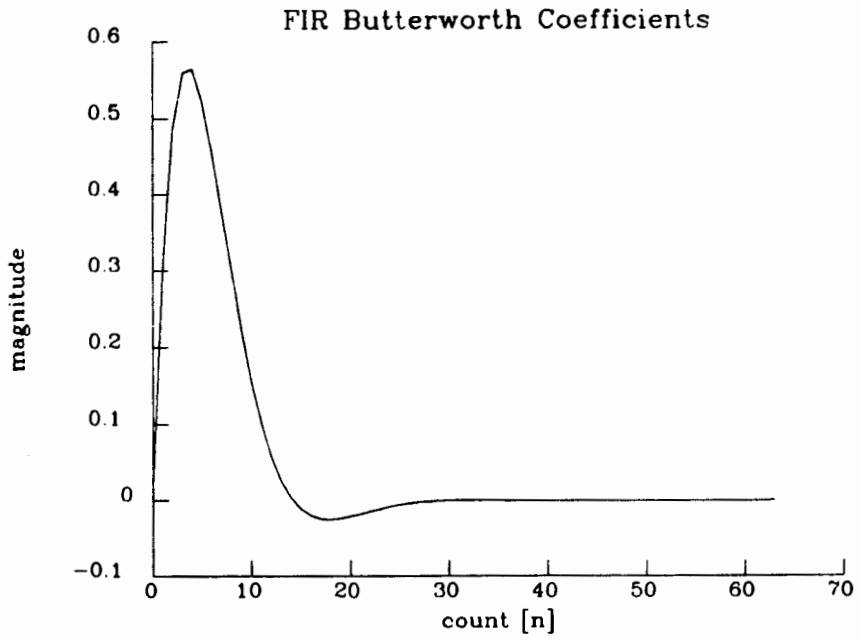

Figure 5

FIR Butterworth Coefficients

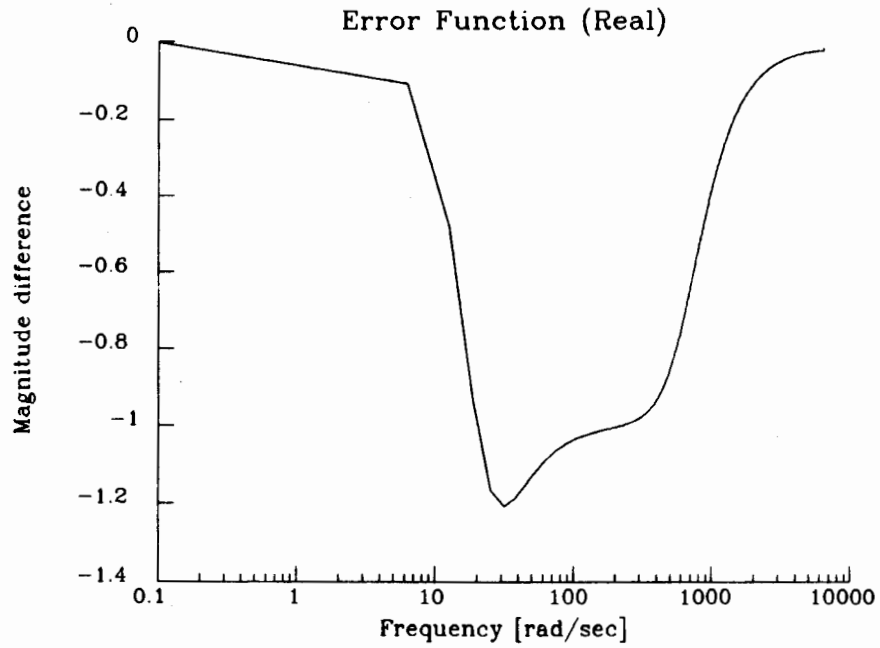

Figure 6

Error Function

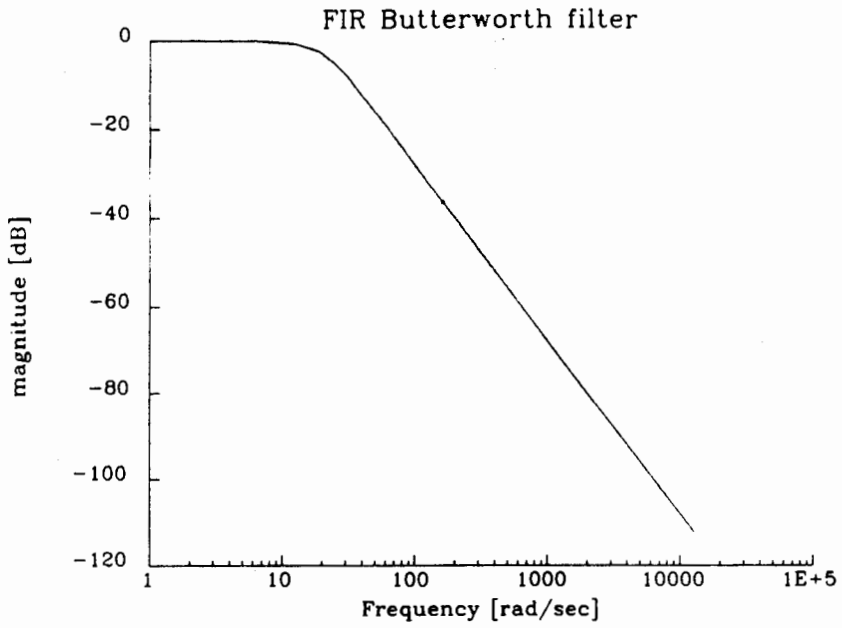

Figure 7a

Magnitude Response

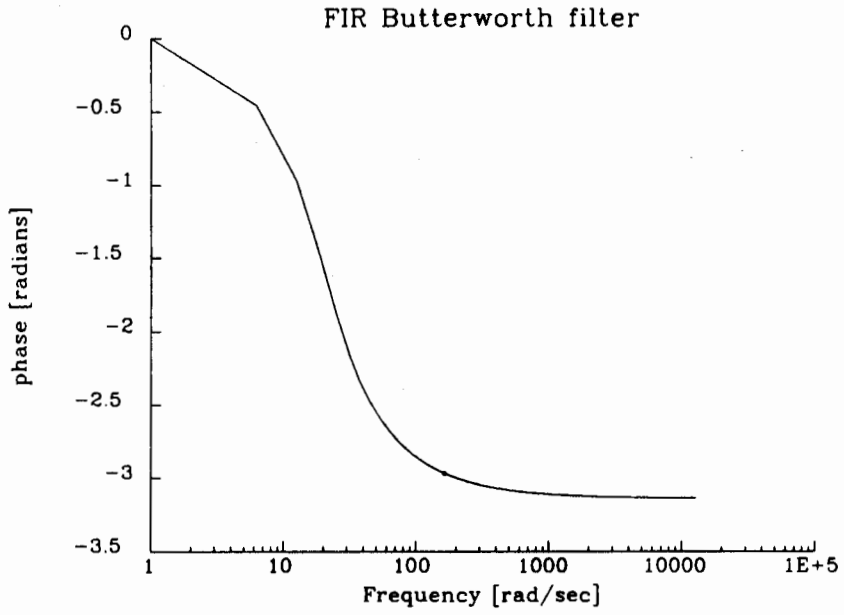

Figure 7b

Phase Response

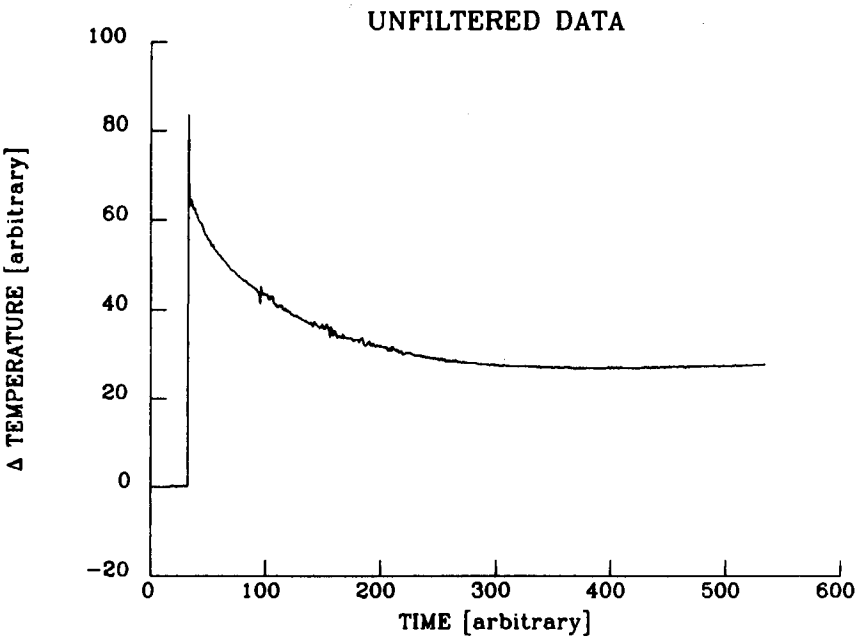

Figure 8a

Unfiltered Data

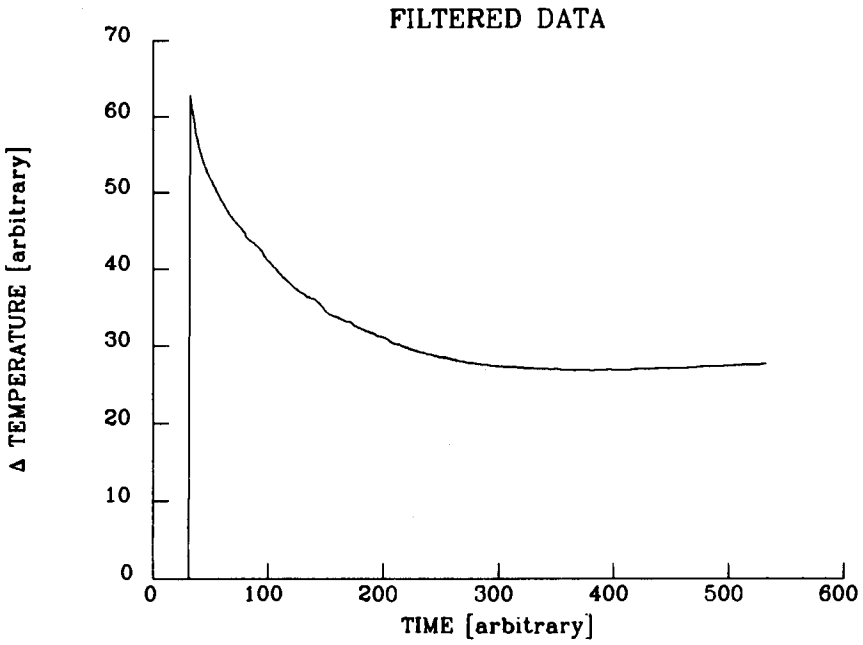

Figure 8b

Filtered Data

Transient Applications

Figure 9 illustrates a captured transient filter application. In this application, data is captured in the digitizer before it flows to the Auxiliary Formatter through the CAMAC bus; the data is then stored temporarily in the Auxiliary Formatter and processed. This processed data is available for transfer over the CAMAC bus or the GPIB bus. For transient applications where a digitizer captures a transient and stores the array in memory, the speed of the filter is not as important as in the real-time application. Hence, larger-sized, more accurate filters may be applied since the captured data is stationary and there are no time constraints for data manipulation. In the current hardware configuration, the main problem is memory space on the Auxiliary Formatter. Many functions other than filtering are assigned to the DSP in the Auxiliary Formatter. Occasionally, these functions require a large amount of program memory already designated for the filter algorithm. Since the amount of program memory is limited, the looping method is used instead of the direct coding method. The DSP has instructions that allow for the implementation of the direct form (3) and the looped method (4).

For the transient application, the hardware is configured to transfer data from a LeCroy TR8828 Digitizer to the DSP memory. A 57-point linear-phase, low-pass FIR filter is calculated using the Remez exchange algorithm. The impulse and frequency responses are shown in Figures 10a and 10b.

CONCLUSION

By utilizing the power of the TMS32010 DSP and the multiple data paths in the Auxiliary Formatter, many complex and powerful functions can be implemented in the CAMAC environment. Namely, the Auxiliary Formatter can provide both real-time and off-line filtering of digitized data. (The filtering techniques presented in this paper comprise just a few of the possible DSP functions that can be performed on data channeled through the Auxiliary Formatter.) In addition, the multiple data paths provided by the Auxiliary Formatter in the CAMAC environment increase the avenues for routing data generated by the CAMAC digitizers. These data paths allow for the sharing of computational capabilities used in reducing data from the digitizers and for transfer of this processed data to another crate or module.

REFERENCES

(1) Standard Handbook for Electrical Engineers, pp. 2-55, 2-57. McGraw Hill, New York, 1978.

(2) Oppenheim, Alan V. and Alan S. Willsky, Signals and Systems, pp. 225, 655. Prentice Hall, New Jersey, 1983.

(3) Digital Signal Processing with the TMS320 Family, pp. 52-56. Texas Instruments, 1986.

(4) Digital Signal Processing with the TMS320 Family, pp. 49-51, Texas Instruments, 1986.

BIBLIOGRAPHY

Digital Encoding System (DES) Formatter N-EM-101 Manual, EGG-10282-1027, August 1983.

Oppenheim, Alan V. And Ronald W. Schafer, Digital Signal Processing, pp. 136-271, 404-464. Prentice-Hall, New Jersey, 1975.

Rabiner, Lawrence R. and Bernard Gold, Theory and Application of Digital Signal Processing, pp. 75-204. Prentice-Hall, New Jersey, 1975.

State Machine Assembler (SMA) Programmer's Manual, EGG-10282-1108. EG&G Energy Measurements, July 1986.

The Digital Encoding System (DES) Programmer's Manual, EGG-10282-1022. EG&G Energy Measurements, May 1983.

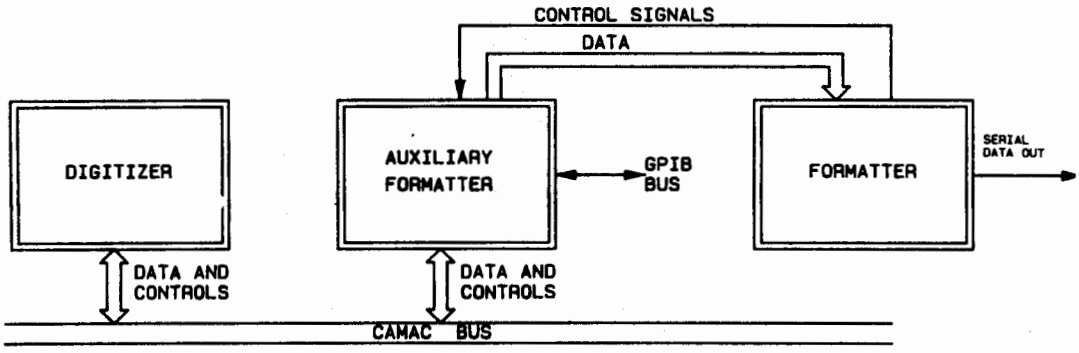

Figure 9

Data Flow Diagram (Transient)

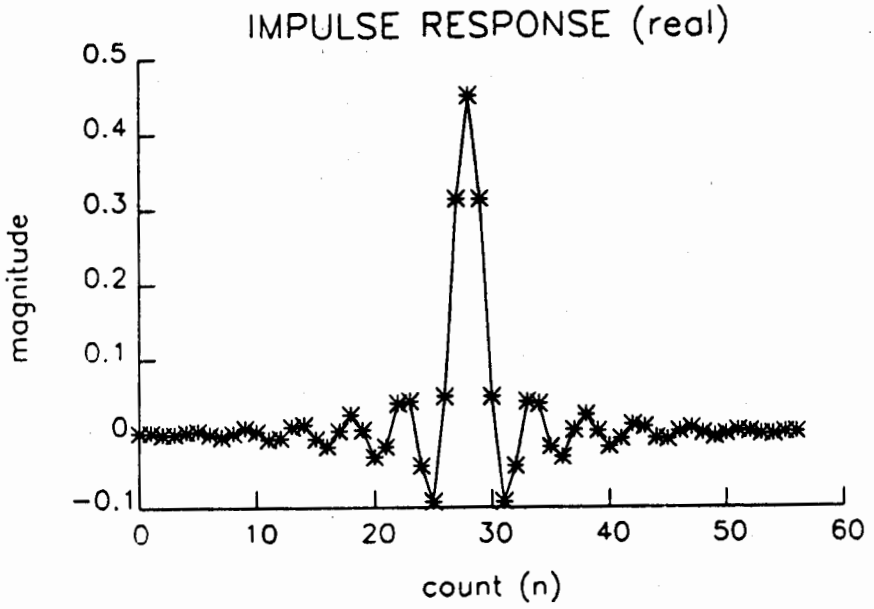

Figure 10a

FIR Coefficients

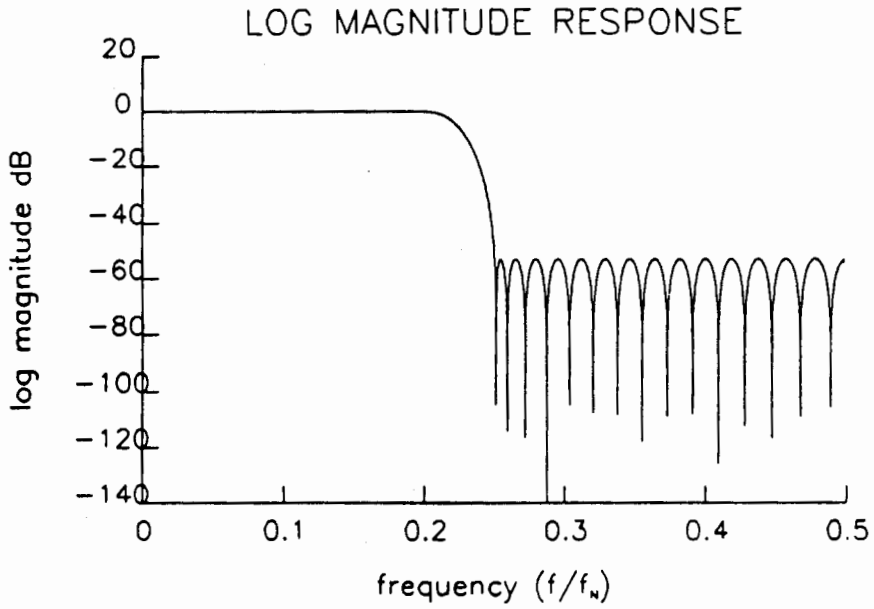

Figure 10b

Magnitude Response